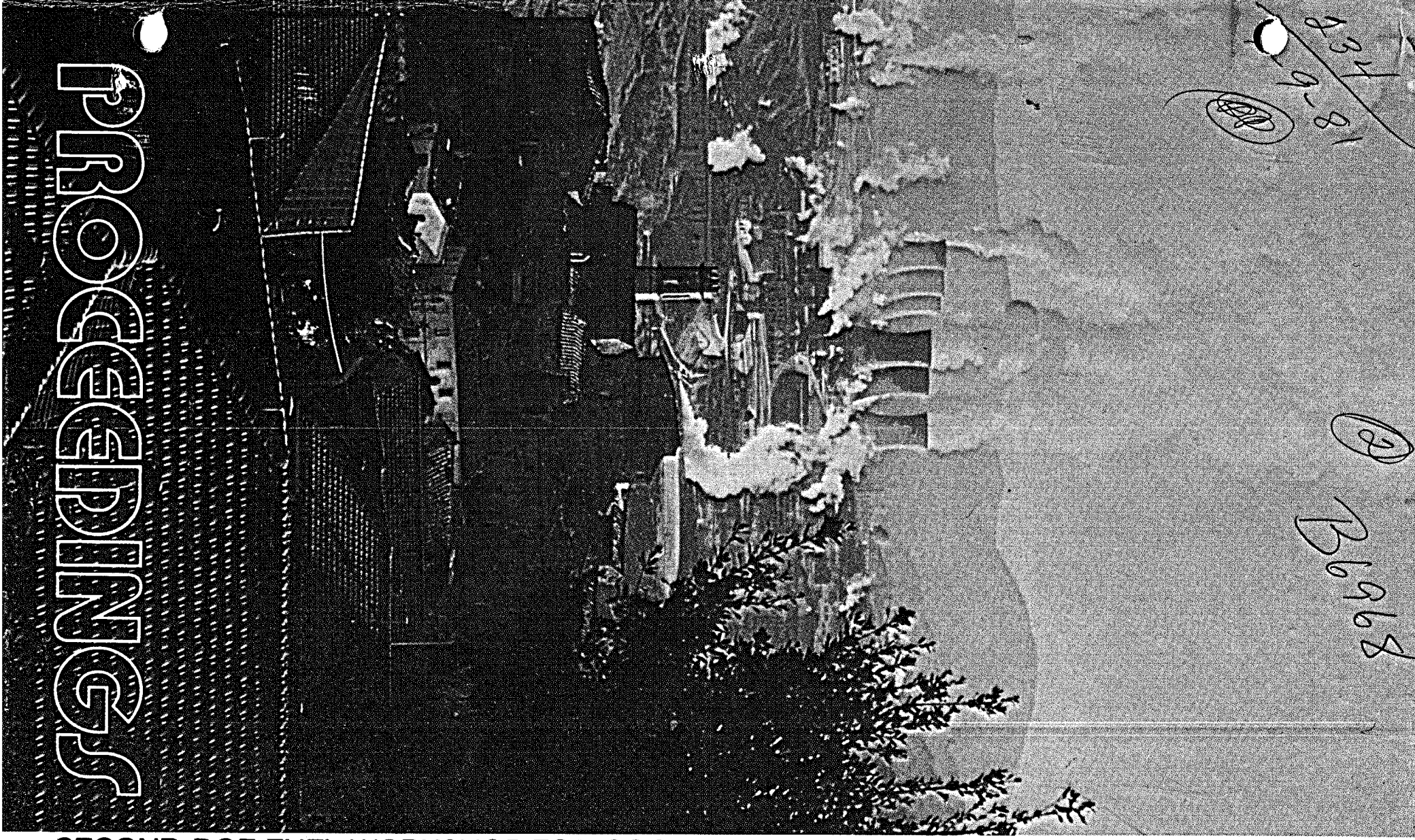

PROCEEDINGS

SECOND DOE-ENEL WORKSHOP FOR COOPERATIVE RESEARCH IN GEOTHERMAL ENERGY

Sponsored by

The United States Department of Energy, Division of Geothermal Energy

October 20 through 23, 1980

LAWRENCE BERKELEY LABORATORY
University of California • Earth Sciences Division
Berkeley, California USA 94720

United States
Department of Energy

This work was supported by the Assistant Secretary for Resource Applications, Office of Industrial and Utility Applications and Operations Division of Geothermal Energy of the U.S. Department of Energy under Contract No. W-7405-ENG-48.

ENEL
Ente Nazionale per l'Energia Elettrica

LBL-11555 UC-66
CONF-801098
January, 1981

#3005

DISCLAIMER

This report was prepared as an account of work sponsored by an agency of the United States Government. Neither the United States Government nor any agency Thereof, nor any of their employees, makes any warranty, express or implied, or assumes any legal liability or responsibility for the accuracy, completeness, or usefulness of any information, apparatus, product, or process disclosed, or represents that its use would not infringe privately owned rights. Reference herein to any specific commercial product, process, or service by trade name, trademark, manufacturer, or otherwise does not necessarily constitute or imply its endorsement, recommendation, or favoring by the United States Government or any agency thereof. The views and opinions of authors expressed herein do not necessarily state or reflect those of the United States Government or any agency thereof.

DISCLAIMER

Portions of this document may be illegible in electronic image products. Images are produced from the best available original document.

LEGAL NOTICE

This book was prepared as an account of work sponsored by an agency of the United States Government. Neither the United States Government nor any agency thereof, nor any of their employees, makes any warranty, express or implied, or assumes any legal liability or responsibility for the accuracy, completeness, or usefulness of any information, apparatus, product, or process disclosed, or represents that its use would not infringe privately owned rights. Reference herein to any specific commercial product, process, or service by trade name, trademark, manufacturer, or otherwise, does not necessarily constitute or imply its endorsement, recommendation, or favoring by the United States Government or any agency thereof. The views and opinions of authors expressed herein do not necessarily state or reflect those of the United States Government or any agency thereof.

Printed in the United States of America
Available from
National Technical Information Service
U.S. Department of Commerce
5285 Port Royal Road
Springfield, VA 22161
Price Code: A22

Lawrence Berkeley Laboratory is an Equal Opportinuty Employer.

MASTER

LBL--11555

DE81 029945

Proceedings

SECOND DOE-ENEL WORKSHOP FOR COOPERATIVE RESEARCH IN GEOTHERMAL ENERGY

October 20-22, 1980
Berkeley, California 94720

Sponsored by:

The United States Department of Energy, Division of Geothermal Energy
in Cooperation with Ente Nazionale per l'Energia Elettrica

Hosted by:

Lawrence Berkeley Laboratory
Earth Sciences Division
University of California
Berkeley, California USA 94720

DISCLAIMER

This book was prepared as an account of work sponsored by an agency of the United States Government. Neither the United States Government nor any agency thereof, nor any of their employees, makes any warranty, express or implied, or assumes any legal liability or responsibility for the accuracy, completeness, or usefulness of any information, apparatus, product, or process disclosed, or represents that its use would not infringe privately owned rights. Reference herein to any specific commercial product, process, or service by trade name, trademark, manufacturer, or otherwise, does not necessarily constitute or imply its endorsement, recommendation, or favoring by the United States Government or any agency thereof. The views and opinions of authors expressed herein do not necessarily state or reflect those of the United States Government or any agency thereof.

This work was supported by the Assistant Secretary for Resource Applications, Office of Industrial and Utility Applications and Operations Division of Geothermal Energy of the U.S. Department of Energy under Contract No. W-7405-ENG-48.

DISTRIBUTION OF THIS DOCUMENT IS UNLIMITED

Contents

Introduction 1
Werner J. Schwarz and Karsten Pruess

The Distribution of Radon and Radon Daughters in the Geothermal Region of Larderello. 3
Andreas C. George, Geovanni Scandiffio, and Alfred J. Breslin

H_2S Abatement for Geothermal Power Plants: Focus at The Geysers, California. 15
Gerald Katz

Seismic Monitoring in Italian Geothermal Areas: I. Seismic Activity in the Larderello Travale Region 20
F. Batini, C. Bufe, G. M. Cameli, R. Console, and A. Fiordelisi

Seismic Monitoring in Italian Geothermal Areas: II. Seismic Activity in the Geothermal Fields During Exploration. 48
F. Batini, G. M. Cameli, E. Carabelli, and A. Fiordelisi

Geothermal Induced Seismicity - Bane or Blessing? 86
Charles G. Bufe and Peter M. Shearer

Selection of Dry Wells in Tuscany for Stimulation Tests 98
P. Baldi, G. Bertini, C. Calore, G. Cappetti, C. Cataldi, R. Celati, and P. Squarci

Fracturing Techniques and Some Applications in Italy. 116
P. Berry, C. Cataldi, and E. M. Dantini

The DOE Geothermal Well Stimulation Program 164
R. J. Hanold, D. A. Campbell, and A. Richard Sinclair

The DOE Hot Dry Rock Program. 173
Gregory J. Nunz

Italian Experience and Problems in Deep Geothermal Drilling 189
U. Cigni

Materials Employed in Deep Geothermal Drilling in Italy 205
P. Del Gaudio

Geothermal Drilling Practices of "The Geysers". 218
Louis E. Capuano, Jr.

Materials Used in Drilling Geothermal Wells in The Geysers 226
Larry Leet

Study on the Equilibria and Properties of Brines. 228
G. Conti, P. Gianni, G. F. Nencetti, L. Petarca, M. R. Tine, and N. Vatistas

Potential Solutions for Geothermal Brine Production Utilization and Reinjection Problems. 245
O. J. Vetter

Production Test Facilities of the Hot Brine of Cesano Geothermal Field 247
R. Corsi and R. Di Falco

Successful Fluid Management of the Salton Sea Reservoir 272
Anthony J. Adduci

Design and Construction of a Pilot Plant for Utilization of Cesano Brine 291
G. Allegrini and G. Nardini

High Salinity Geothermal Energy Conversion Based Upon the Operating Experience at the San Diego Gas & Electric-DOE Geothermal Loop Experimental Facility Located at the Niland Reservoir, Imperial Valley, California, U.S.A.. 311
George Anastas

Cooperative Research and Development in Geothermal Energy. 323
R. Cataldi and P. Witherspoon

Modeling Vapor Dominated Systems - Serrazzano Lumped Parameter Models 328
R. Celati, R. Marconcini, G. Neri, K. Pruess, R. Schroeder, and O. Weres

Performance Matching and Prediction for Serrazzano Geothermal Reservoir by Means of Numerical Simulation 342
K. Pruess, O. Weres, R. Schroeder, R. Marconcini, and G. Neri

Reinjection Studies of Vapor-Dominated Systems. 381
Ronald C. Schroeder, Michael J. O'Sullivan, Karsten Pruess, Romano Celati, and Claudio Ruffilli

A Depletion Model for the Gabbro Zone (Northern Part of Larderello Field) 434
William E. Brigham and Guiseppi Neri

Reservoir Engineering Studies of the Travale-Radicondoli Reservoir 464
A. Barelli, M. Economides, G. Manetti, and F. G. Miller

Study of Water Influx and Fluid Composition in the Bagnore Field 480
Romano Celati, Franco D'Amore, Michael J. Economides, and Giuseppe Neri

Helium Prospecting in Geothermal Areas. 483
R. Bertrami, A. Ceccarelli, I. Friedman, W. Doering, and S. Lombardi

Program 501

List of Participants 505

Name Index 511

Organizational Abbreviations 513

INTRODUCTION

Werner J. Schwarz and Karsten Pruess

Based on a cooperation agreement that was signed in June 1975 in Rome, the U.S. Energy Research and Development Administration (ERDA), now the U.S. Department of Energy (DOE), and the Ente Nazionale per l'Energia Elettrica (ENEL), Italy, have sponsored joint research activities in various areas of geothermal energy over the last five years. As laid out in the original agreement, research was performed in five broad projects:

Project 1. Stimulation of hot dry rocks and hydrothermal reservoirs.

Project 2. Utilization of hot brine resources.

Project 3. Reservoir physics, engineering, and resource assessment.

Project 4. Deep drilling.

Project 5. Environmental control technologies.

Individual tasks within these project areas were defined by engineers in both countries. After approval of funding, the tasks were then carried out in collaboration on an equivalent effort basis.

A first synopsis of ongoing work was presented at a joint U.S.-Italian workshop in September 12-16, 1977, at Larderello, Italy, and was published as the "Proceedings of the Larderello Workshop on Geothermal Resource Assessment and Reservoir Engineering." That meeting was exclusively devoted to Project 3, which was the area in which cooperation was first initiated. Project 3 continued to occupy "center stage" in subsequent years, with most of the joint research activities focused on geothermal reservoir engineering.

The purpose of this second Geothermal Workshop was to summarize the research to date and to discuss future plans for additional cooperative projects between the U.S. Department of Energy and the Ente Nationale per L'Energia of Italy. Invited papers by participants covered on-going programs under the DOE-ENEL Agreement and, in

addition, selected speakers presented the results of their research. The Italian coordinator for this workshop was Dr. Petro Ceron (ENEL) of Pisa, Italy; the American coordinator was Dr. John Salisbury (DOE) of Washington, D.C. The meeting was hosted by the Earth Science Division of the Lawrence Berkeley Laboratory, University of California. All of the papers presented in Project 3 were by Italian and American co-authors. Projects 1, 2, 4 and 5 have received more attention recently, and a half day session was devoted to each at the workshop.

The last five years of cooperative research in geothermal energy have seen a fruitful exchange of information between American and Italian engineers and scientists. This has resulted in better understanding of geothermal resources and in the development of advanced engineering methods for improving geothermal energy recovery. The purpose of these proceedings is to disseminate these achievements to the geothermal community at large.

The workshop was attended by nearly 100 participants from Belgium, Iceland, Italy, Mexico, and the United States.

We wish to thank all participants for making the workshop a success. We gratefully acknowledge the most valuable assistance from ENEL-UNG and the support from the U.S. Department of Energy, DOE which made this workshop possible.

THE DISTRIBUTION OF RADON AND RADON DAUGHTERS IN THE GEOTHERMAL REGION OF LARDERELLO

Andreas C. George*
Giovanni Scandiffio†
Alfred J. Breslin‡

INTRODUCTION

The industrial utilization of steam in the Larderello area results in a continuous release of gaseous effluents to the environment. The plants utilizing geothermal fluids for power generation are distributed over an area of 150 km^2 and are generally near residential areas. Accordingly, the atmospheric distribution and concentration of these effluents and their environmental impact in the area was studied and their relative hazard was evaluated.

One of the most important pollutants released from the Larderello geothermal fluids is radon which is highly concentrated at points of emission, e.g., several thousand picocuries per liter of gas.[1] The overall objective of this study was to determine the distribution of radon and radon daughters, evaluate their impact on the environment at Larderello, and provide a basis against which changes in environmental quality can be assessed. The study was a cooperative investigation by ENEL and by the Environmental Measurements Laboratory (EML), U.S. DOE. Most of the instrumentation and analytical services were provided by EML. ENEL deployed and maintained the instruments in the field and conducted supplementary measurements for radon daughter concentrations.

---

* U.S. DOE, Environmental Measurements Laboratory, New York City

† ENEL - Unita Nazionale Geotermica, Pisa, Italy

‡ At present retired.

Location and Type of Geothermal Plants

The Larderello Geothermal field is about 100 km south of Florence. The first commercial power plant was placed in operation in 1913. Today 27 condensing units are operating in an area of 150 km^2. The fluid from wells generally consists of a mixture of steam and gas. The gas content varies from a minimum of 1% to a maximum of 20% with an average of 5% by weight.

The average chemical composition of the uncondensable gases by volume is as follows: CO_2 95%; H_2S 1.6%; H_2 2.3%; CH_4 and N_2 2%. These gases are released to the atmosphere from condenser gas ejectors and cooling towers. Table 1 lists the quantities of radon and steam released. The distribution of plants and sampling stations is shown in Fig. 1.

Monitoring Procedures

Annual mean concentrations of radon and of working level were determined in each location by periodic two-week-long measurements distributed over the period between October 1977 through November 1978. Time-integrating radon monitors[2] and time-integrating working level monitors[3] were used throughout the study. Both monitors use LiF TLD detectors (LiF-700-1/8x1/8x.015"). Analysis of the TLD detectors was performed at the Environmental Measurements Laboratory (EML) in New York.

For comparison, more than 1500 grab sample measurements for radon daughters were made by ENEL in 1979 and 1980 using the Rolle[4] modified Tsivoglou[5] and Kusnetz[6] methods. ENEL and EML had intercompared instruments used for these measurements during the week of July 11, 1977. The WL obtained by the two laboratories agreed within 10%. Grab samples for radon were also obtained during this week using scintillation flasks.[7]

Radon emanation was measured with charcoal canisters[8] which integrate radon flux over periods of 24 to 48 hours. The measured sites shown in Fig. 2 consisted of several geological formations spread out in the general area of the geothermal fluid. The charcoal

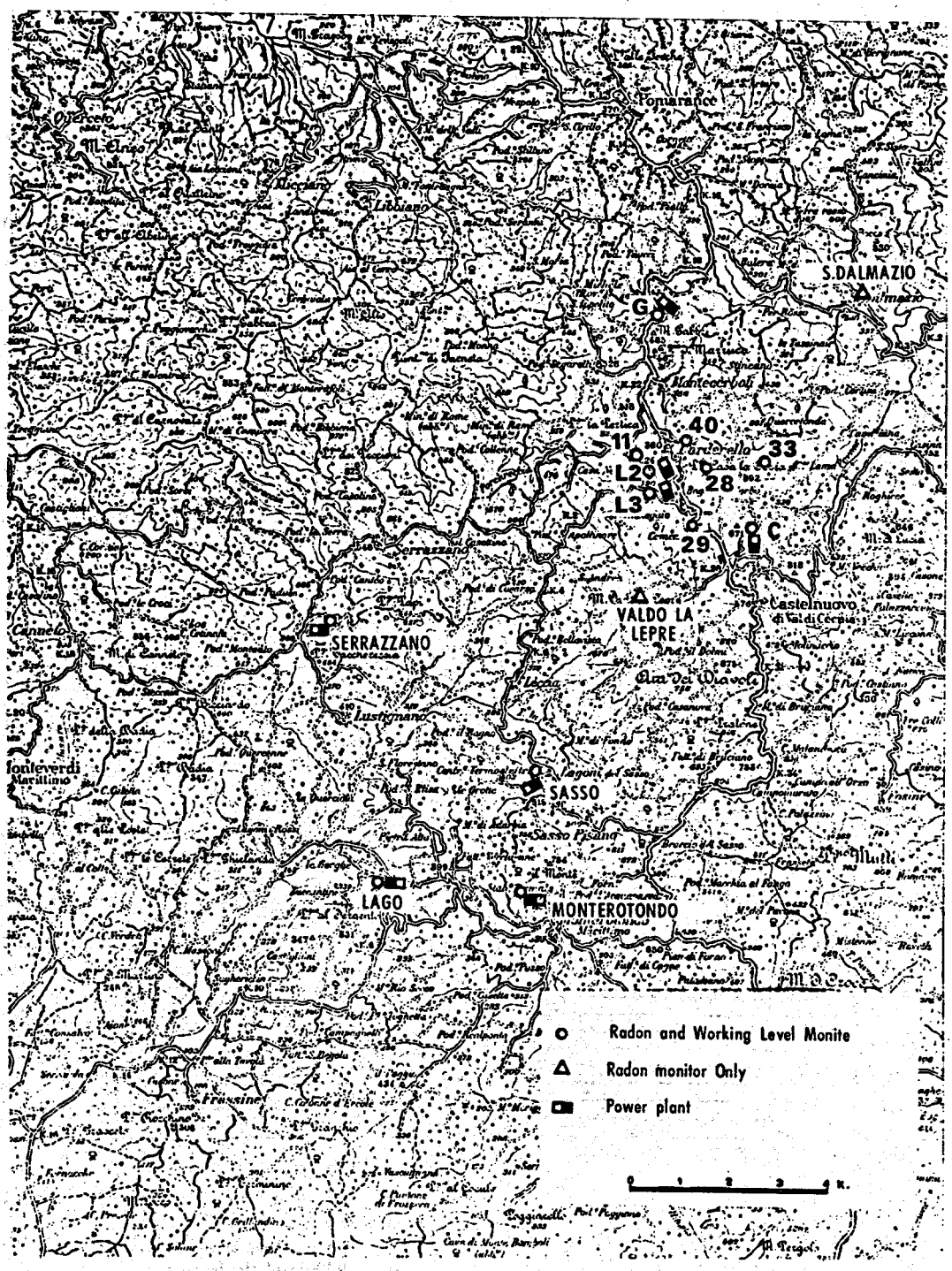

Fig. 1. Geographical distribution of power plants and sampling stations.

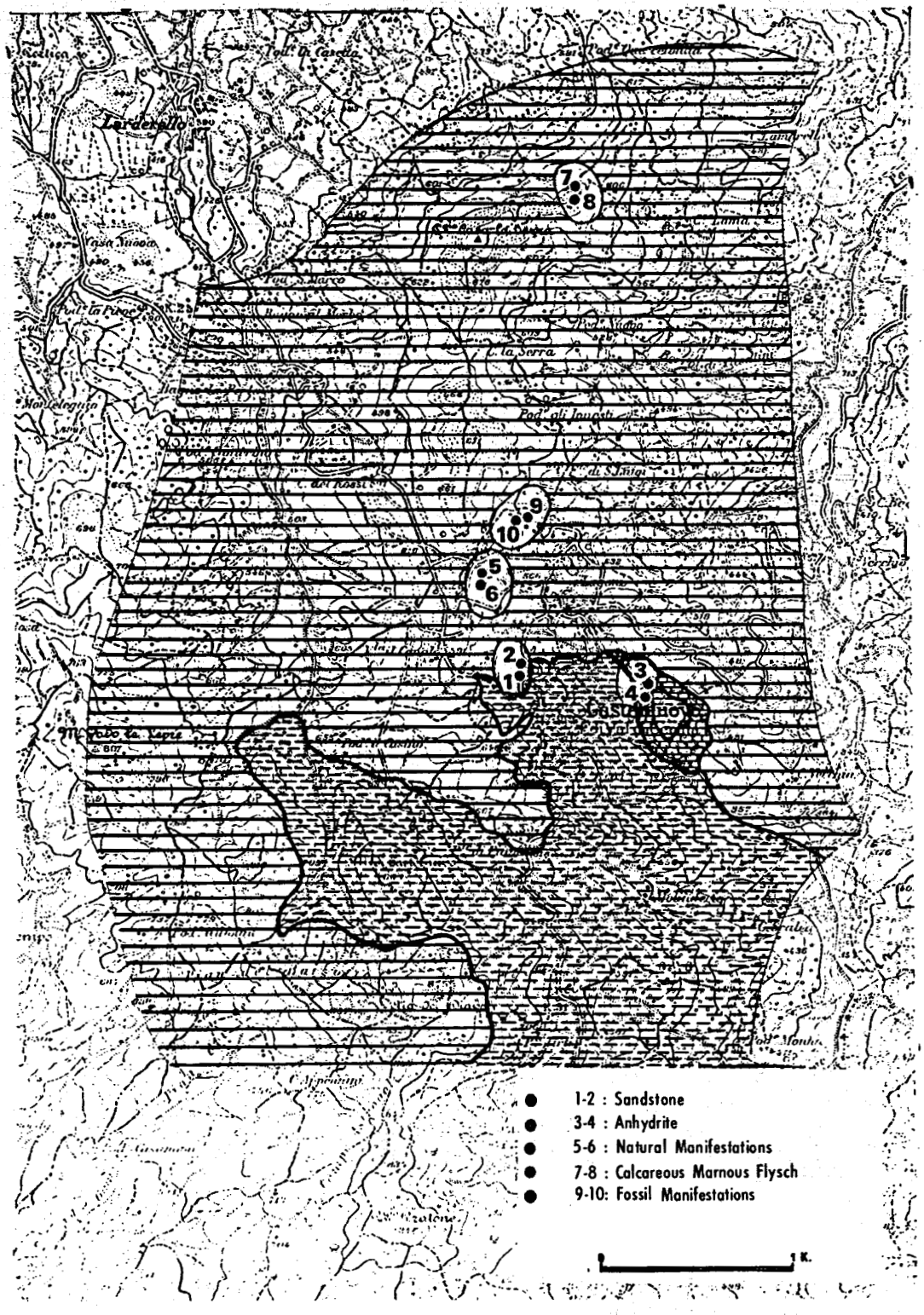

Fig. 2. Location of sampling points for integrated radon flux on main formations of geothermal area.

canisters were analyzed at EML. Samples of soil were collected at the same locations and were analyzed for Ra-226 by gamma spectrometry at EML.

RESULTS

Table 1 lists measurements of radon and steam released from the geothermal plants obtained in an earlier study.[1] The total output of radon is 8 Ci/day. The second most important source of radon in the region is from soil radium. Measurements of radium-226 and radon flux from soils are listed in Table 2. Single soil samples for radium-226 analysis were collected in each location, while measurements of radon flux are the averages of samples collected in triplicate.

The mean radium-226 content of 0.9 pCi/g, usually assumed to be normal background, is nearly equal to 1 pCi/g, the average value measured in New Jersey and New York soils.[9]

The average value of radon flux, 18 pCi m^{-2} is somewhat lower than the world-wide average[10] of 25.5 pCi m^{-2} min^{-1}, and it is comparable to radon flux value obtained in typical residential areas in New Jersey and New York.[11] The natural release of radon into the atmosphere calculated from the measured radon flux, is 3.9 Ci/day, or approximately one-half of the total radon released by all power plants.

Radon concentrations, working levels, and working level ratios from the integrated measurements are summarized in Table 3. The listed mean radon concentrations and working levels are arithmetic means of the two-week-long measurements in each case. The working level ratios were calculated from individual simultaneous measurements of radon and working level in each location. The locations are shown in Fig. 1.

The log-normal distributions of radon and working level calculated from all the measurements obtained in the period from October 1977 through November 1978 (shown in Fig. 3), indicate geometric means of 0.16 pCi/l and 0.001 WL. The concentrations of radon and radon

Table 1 - Radon and Steam from Production Wells

Location	Radon Release PCi/l	Radon Release Ci/day	Steam Tons/Day
Larderello (3 plants)	54,000	3.6	32,000
Castelnuovo	141,000	1.5	7,300
Sasso	57,000	0.5	6,000
Serrazzano	70,000	1.3	7,200
Lagoni Rossi	90,000	0.4	5,300
Lago	163,000	0.7	8,700
Monterotondo	53,000	0.08	2,100
TOTAL OUTPUT		8.0	68,600

Table 2. Sources of Radon near Geothermal Plants

Sample Location*	Radium 226 in soil pCi/g	Radon Flux from soil pCi m^{-2} min^{-1}	Rock Formation
1	1.2	17	Sandstone
2	1.1	20	Sandstone
3	1.2	14	Anhydrite
4	1.1	16	Anhydrite
5	0.5	13	Natural Manifestations
6	0.3	18	Natural Manifestations
7	0.8	19	Calcareous Marnous Flysch
8	0.9	21	Calcareous Marnous Flysch
9	1.0	15	Fossil Manifestations
10	1.1	24	Fossil Manifestations
Average =	0.9	18	

* See Fig. 2

Table 3. Integrated Radon and Working Level Measurements at Larderello, Castelnuovo, and Boraciferous region.

Sampling Station	Measurement Period	RADON (pCi/l) Min.	Max.	Mean	Working Level Min.	Max.	Mean	WL-Ratio*	
11	Oct 1977-Nov 1978	.07	.30	.20	.0007	.003	.0012	.58	
28	"	.08	.37	.21	.0005	.002	.0012	.87	
29	"	.04	.32	.20	.0006	.0023	.0012	.65	Av-0.64
33	"	.07	.24	.11	.0007	.0038	.002	.57	
40	"	.10	.33	.19	.0007	.0032	.002	.72	
Vado la Lepre	"	.09	.23	.17	-	-	-	-	
S. Dalmazio	"	.07	.40	.21	-	-	-	-	
G	March 1980-June 1980	-	-	-	.0004	.0019	.001	-	
C	"	.08	.23	.15	.0005	.002	.0012	.80	
L-2	"	.15	.20	.18	.001	.0014	.001	.70	
L-3	"	.10	.26	.19	.0004	.0022	.001	.51	Av-0.64
Lago	Jan. 1980-March 1980	.18	.50	.29	.001	.0016	.0013	.45	
Sasso	"	.20	.25	.23	.001	.0021	.0016	.71	
Monterotondo	"	-	-	-	.0005	.001	.0008	-	
Serrazzano	"	-	-	.18	.0007	.002	.0012	-	

$$* = \text{WL-Ratio} = \frac{\text{Working Level}}{\text{Radon Conc.pCi/l}} \times 100$$

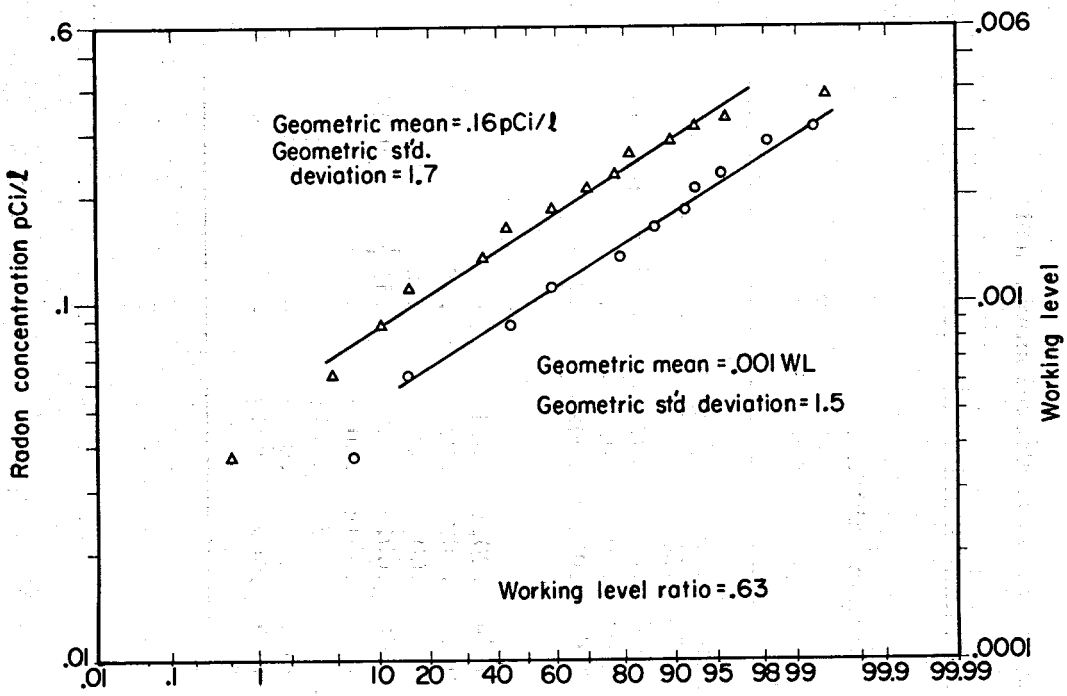

Fig. 3. Distributions of integrated radon and radon daughter concentrations.

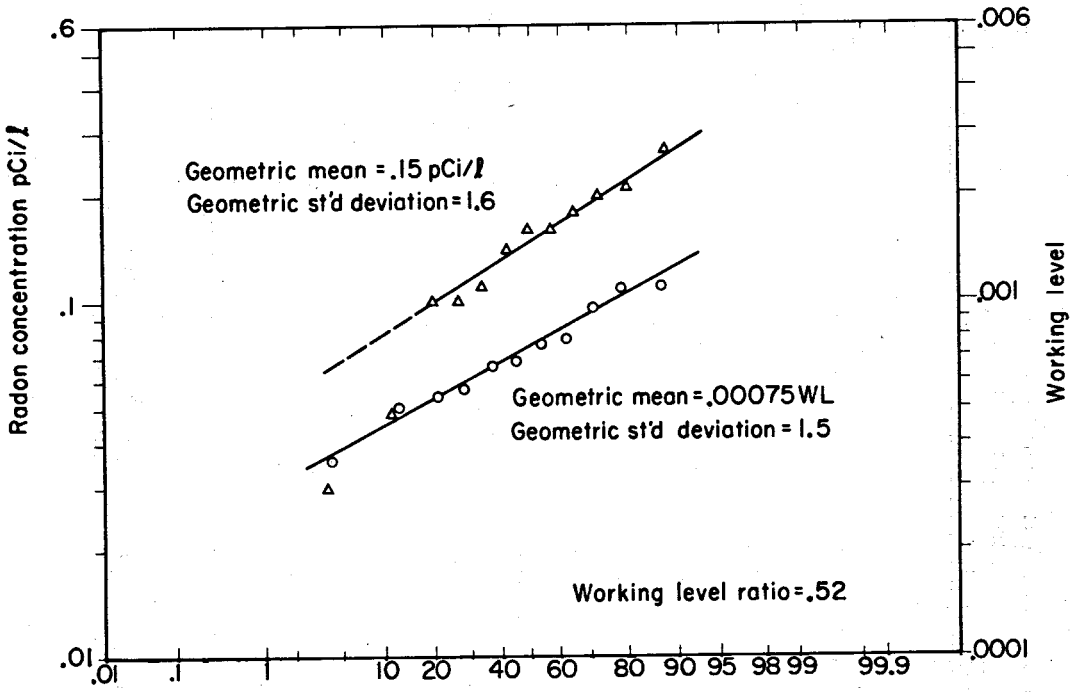

Fig. 4. Distributions of environmental radon and radon daughter concentrations, grab samples (7/11-7/14, 1977).

daughters are within the range that would be considered normal for other geographical areas. For example, the log-normal distributions of outdoor radon and working level measurements in New Jersey and New York[9] exhibited geometric means of 0.18 pCi/l and .0016 WL, respectively, with corresponding geometric standard deviations of 1.5 and 1.6. In a study conducted by Auspaugh et al.[12] at Geysers, similar results were obtained with a working level geometric mean of 0.0012 and geometric standard deviations of 2.07.

The average working level ratio obtained from all the simultaneous integrated measurements and from the geometric means of the distribution shown in Fig. 3 are the same, e.g., 0.64.

The distribution of radon and working level obtained with grab samples are shown in Fig. 4, indicating geometric means of 0.15 pCi/l and .00075 WL. The WL-ratio of 0.52 is somewhat lower than the integrated value. The grab samples were obtained during the day time when concentrations of radon and radon daughters were usually lower.[13] This is more evident from data listed in Table 4 which were obtained with integrated and grab samples during the period from January 1980 through March 1980. Except for the location at Monterotondo, the integrated working level values are about three times higher than those obtained with grab samples.

The monthly average radon concentration and working level values obtained during the period from October 1977 through November 1978, are shown in Fig. 5. The histogram shows a pronounced seasonal variation very similar to the seasonal pattern observed in New Jersey and New York.[13]

CONCLUSIONS

Radon flux from the ground in the Boraciferous region is one half of the total release from cooling towers. However, at present it is impossible to distinguish the environmental impact of the production plants from the natural radon exhalation in the area.

Measurements of radon concentration and working level are within the range that is considered normal for other geological areas.

Table 4. Working Level Values by Integrated Samples and Averaged Grab Samples During the Period Between Jan. 1980 through March 1980 for Some Sampling Stations

Sampling Stations	Period I/8 - I/21 WL		Period I/21 - 2/4 WL		Period 2/18 - 3/3 WL		Period 3/3 - 3/17 WL	
	*	**	*	**	*	**	*	**
Lago	.001	-	.0016	.0004	-	.0006	.002	.0004
Sasso	.002	-	.0021	.0004	.001	.0005	.0007	.0004
Monterotondo	.001	.0008	.0005	.0006	.0006	.0005	.0008	.0004
Serrazzano	.002	.0006	.0007	.0005	.0008	.0005	.0013	.0004

* Integrated Samples

** Averaged Grab Samples

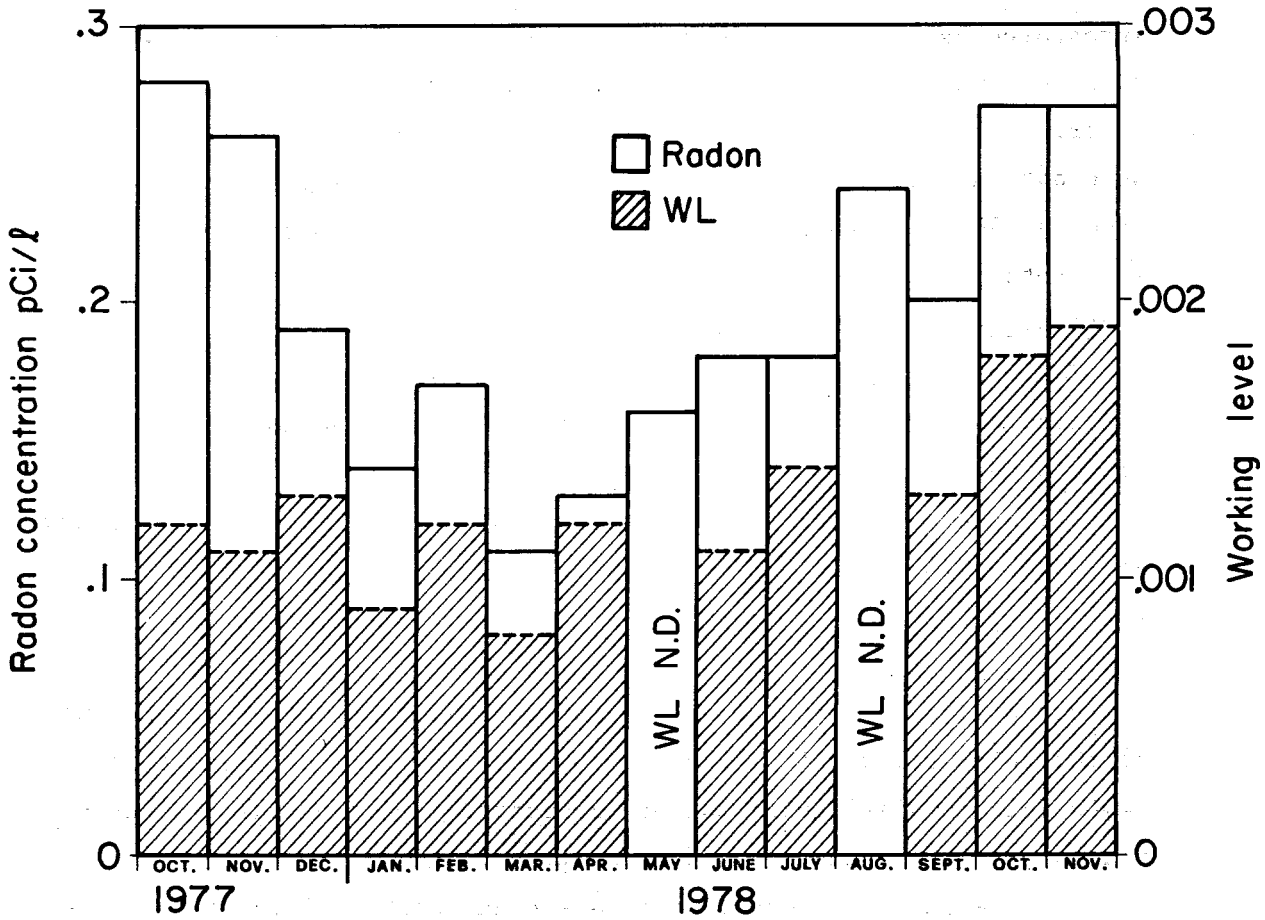

Fig. 5. Average monthly concentrations for seven monitoring locations in Larderello.

The frequency distributions of radon concentration and working level plotted in Fig. 3 appear to follow nearly parallel log normal distributions. The observed seasonal variations are perhaps attributable to change in radon flux from the soil and to local wind forces, and therefore are not a consequence of the geothermal activity in the area.

REFERENCES

1. F. D'Amore - Radon Survey in Larderello Geothermal Field, Italy (Part 1). Geothermics Vol. 4, No. 1-4 (1975).

2. A.C. George and A.J. Breslin - Measurement of Environmental Radon with Integrating Instruments. Workshop of Methods for Measuring Radiation in and Around Uranium Mills, ed. E.D. Harward, Atomic Industrial Forum, Inc. Program Report, Vol. 3 (1977).

3. S.F. Guggenheim, A.C. George, R.T. Graveson and A.J. Breslin - A Time-Integrating Environmental Radon Daughter Monitor. Health Physics 36 457 (1979).

4. R. Rolle - Rapid Working Level Monitoring. Health Physics 22, 233 (1972).

5. J.W. Thomas - Measurement of Radon Daughters in Air. Health Physics 23, 783 (1972).

6. H.L. Kusnetz - Radon Daughters in Mine Atmospheres. A Field Method for Determining Concentrations. Am. Ind. Hyg. Assoc. J., 17, 85 (1956).

7. A.C. George - Scintillation Flasks for the Determination of Low Level Concentrations of Radon. Proceedings of Ninth Midyear Health Physics Symposium, Denver, CO, February 1976.

8. R.J. Countess - Radon Flux Measurement with Charcoal Canisters. Health Physics 31, 456 (1976).

9. A.C. George and A.J. Breslin - The Distribution of Ambient Radon and Radon Daughters in Residential Buildings in the New Jersey New York Area (In Press, Environment III).

10. M.H. Wilkening, et al. - Radon-222 Flux Measurements in Widely Separated Regions. Paper presented at the Second International Symposium on the Natural Radiation Environment, Houston, Texas, August 1972.

11. Personal Communication from A.C. George.

12. L.R. Auspaugh et al. - The Geysers Geothermal Power Plants. Environmental Impact of the Release of Rn-222. UCRL 79038, January 14, 1977.

13. J. H. Harley - Radon-222 Flux Measurement at Chester. EML-367, October 1979.

H_2S ABATEMENT FOR GEOTHERMAL POWER PLANTS FOCUS AT THE GEYSERS, CA

Gerald Katz
Geothermal Energy Division
San Francisco Operations Office
U.S. Department of Energy

Hydrogen sulfide (H_2S) gas is often found associated with geothermal resources. This gas is colorless, has a distinct odor similar to rotten eggs and can be extremely toxic in high concentrations (greater than 400 ppmw for sustained period of time).[1] The Geysers resource contains significant quantities of the H_2S. Since large scale power production has occurred (908 MW on-line) a noticeable amount of H_2S has been released to the environment. The odor of H_2S has prompted local opposition to geothermal development from citizens downwind of the resource. While ambient concentrations have been below toxic levels, local opposition combined with occasional violations of the State Ambient Air Quality Standard of 30 ppb have resulted in strict local air pollution control district regulations. Acceleration of geothermal development is jeopardized by implementation of these regulations which may result in permit delays or even denials. Of all the environmental concerns associated with geothermal development, H_2S emissions are consistently ranked high. In fact H_2S controls for power plants was ranked Number 1 in priority for environmental controls research by the U.S. Interagency Geothermal Coordinating Council Environmental Controls Panel.[2] Abatement technology has been developed to control emissions to acceptable levels. More research and development is needed, however, to economically control H_2S in a safe, reliable and environmentally acceptable manner.

H_2S concentrations found in the resource range from 5 to 1600 ppmw with an average of 222 ppmw.[3] Thus concentrations vary from well-to-well and across the steam field. Recent data indicates that H_2S is less prevalent in the southern portion of the Geysers resource (~50 ppmw). Abatement requirements could be less stringent for power plants located there.

Emission sources at the Geysers include natural fumerols, wells, steam collection system vents, power plant off-gas ejectors and cooling towers, and steam stacking resulting from plant outages (emission source is muffler). Power plant emissions are the most significant source, contributing up to 88% of total estimated emission rates.[4] Steam stacking is felt to be the second largest source. Power plant emission distribution between the off-gas ejectors and cooling towers will depend on how H_2S

partitions in the gas and liquid phases in the power plant condensers. Ideally all the H_2S would be exhausted by the off-gas ejector to a conventional abatement system and no H_2S would dissolve in the condensate. Since dissolved H_2S always appears in the condensate to some degree, abatement has had to be applied in the liquid cooling system. The partitioning is dependent on the pH and condenser design. Ammonia, prevalent in the resource, controls the pH. Higher ammonia concentrations increase the pH and dissolved H_2S found in the cooling water. Steam stacking emissions occur upstream of the power plant during outages. Steam suppliers cannot immediately shut in wells when a plant goes out. Thermal/pressure cycling shock resulting from shut in could result in a loss in well productivity. [5]

Various approaches to controlling H_2S at the Geysers have been tried, some more successfully than others. Pacific Gas and Electric Company (PG&E), the only operating utility at the Geysers, has been involved in developing power plant abatement technology. Steam suppliers at the Geysers are developing controls for steam stacking. The optimal solution to controlling the two largest emission sources is an upstream (of the turbine) system. An upstream process allows continuous abatement whether or not the power plant is on line. An upstream process will also reduce H_2S corrosion of turbine blades. Downstream systems, while not controlling stacking emissions, can be effective for power plant emissions control. Partitioning of H_2S, however, must be understood and predicted to allow proper design of downstream abatement systems.

There are two current power plant H_2S abatement systems in operation at the Geysers: The Iron-Catalyst-Peroxide-Caustic (ICPC) system on existing units and the Stretford-Peroxide-Surface Condenser (SPSC) system on new units. The ICPC is a downstream system that has been retrofitted to existing units with direct contact condensers. Ferrous sulfate added to cooling water oxides H_2S to sulfur and insoluble ferrous sulfide. Caustic is used to scrub H_2S in off-gases back into solution. Peroxide is used to regenerate the iron catalyst. Control efficiencies of 90% have been reported [6] but corrosion, sludge fouling, waste treatment/disposal requirements and high chemical costs have precluded full acceptance of this system by PG&E. [7] The SPSC is also a downstream system. The Stretford Process itself controls H_2S emitted through the off-gas ejector. H_2S is absorbed in an alkaline solution such as sodium bicarbonate or caustic and oxidized to elemental sulfur by sodium vanadium trioxide. [8] The Stretford is conventional technology for H_2S control at oil and gas refineries. It can achieve 99+% removal efficiencies on incoming H_2S. Overall geothermal plant efficiencies are however dependent on the partitioning. H_2S remaining in the condensate will be emitted in the cooling towers. To maximize partitioning of H_2S to the Stretford, PG&E uses surface condensers rather than direct contact condensers. By reducing the amount of steam in contact with condensate, dissolved H_2S is minimized. Unfortunately, this approach has been less than adequate and supplementary peroxide abatement has been required for cooling tower emissions control (small amounts of a non-ICPC iron catalyst improve the reaction). The peroxide loop has brought abatement efficiencies

up to 99+% without the corrosion and sludge problems associated with the ICPC. Reagent chemical costs are very high for this supplementary abatement (~$700K/yr). Elemental sulfur produced by the Stretford is sold, somewhat reducing abatement costs. No solid waste disposal problems result from the overall SPSC system.

Research on another abatement system was initiated in 1976 by the EIC Corporation (now EIC Laboratories, Incorporated) under U.S. Department of Energy (DOE) funding. The EIC Copper Sulfate process (tradename: Cuprosul) controls H_2S by means of the following reactions:[9]

$$H_2S \xrightarrow{CuSO_4} Cu_{1+x}S + H_2SO_4 + S^o$$

$$NH_3 \xrightarrow{H_2SO_4} NH_4HSO_4$$

$$H_3BO_3 \xrightarrow{H_2O} H_3BO_4 \quad (9)$$

The copper sulfides formed are oxidized back to copper sulfate in a regenerator. Cuprosul potentially offers several advantages over the best available control technologies, ICPC and SPSC. First it is an upstream system that controls steam stacking and power plant emissions in total. It can be retrofitted to existing power plants without requiring power plant shutdown as would be required with SPSC (to replace the condenser). Soluble by-products (ammonium sulfate and boric acid) produced can either be reinjected or recovered, separated and sold reducing solid waste disposal problems. Make-up chemical feed rates are low making chemical costs more attractive than ICPC. Ammonia, arsenic and boron are controlled to reasonable degrees. H_2S corrosion of turbine blades is reduced. Recent 1/10 scale pilot field tests at PG&E Geysers Unit 7, under a Cooperative Agreement between PG&E, U.S. DOE and U.S. Environmental Protection Agency, accomplished removal efficiencies up to 99.9%. Regeneration met or exceeded expectations in all respects. Total operating costs for Cuprosul abatement on a 110 mw power plant have been reported to be 3.6 mill/kwh compared to 6.2 for ICPC and 4.2 for SPSC.[10] There were some problems however. Corrosion in the scrubber and auxiliaries, as well as entrainment of chemical compounds in the scrubber exhaust steam marred an almost perfect field test. Neither problem is unresolvable. The first commercial Cuprosul, now being developed for Geysers Unit 7, will use a titanium clad scrubber to resolve corrosion and a more efficient demister system to resolve entrainment problems.

The search goes on as researchers advance the state-of-the-art. DOE is presently funding H_2S abatement research at UOP, Incorporated. Their process utilizes a catalyst to oxidize H_2S in a similar manner to the UOP Sulfox Process.[11] Results thus far have been encouraging. Two approaches are being researched for improving partitioning and thus increasing total performance of a Stretford (or other off-gas treatment) system efficiency.

Research at the Lawrence Berkeley Laboratory (LBL) sponsored by PG&E has resulted in the development of a chemical equilibria and transport model computer code for modeling chemical partitioning and transport in the off-gas ejector, condenser and cooling water loop. This has led to a better understanding of the chemical operating characteristics of geothermal power plants allowing design of more efficient abatement systems. Condenser design modifications to improve abatement have been suggested by LBL.[12] Coury and Associates, Incorporated have developed an upstream technology to separate H_2S and allow conventional treatment. The system, developed with Electric Power Research Institute support, uses a heat exchanger to condense and re-evaporate steam. During field tests at PG&E Unit 7 the system separated 94% of H_2S from the steam with a heat transfer coefficient high enough to indicate favorable economics.[13]

Many other abatement processes can potentially be applied. PG&E has considered all of the following processes and is or will be researching some of the more promising concepts.

Caustic Scrubbing of Steam
Acid Scrubbing of Steam
Dow Iron Chelate Catalyst
Dry Cooling
Intermediate Heat Exchanger
Acid Injection into Condensate
Hydrogen Peroxide/Hydroxyacetic Acid-Iron Catalyst
Vacuum Stripping
Catalytic Air Oxidation
High Temperature
Ozonation
Chlorination
Reverse Osmosis
Takahax
Selectox
Incineration
Fluidized Bed[14]

PG&E and DOE plan to continue research and development on new abatement techniques that will improve the state-of-the art and allow geothermal development at the Geysers to continue.

REFERENCES

1. "Public Health Considerations Relative to the Geyers Power Plant", April 15, 1977, Greenfield, Attaway and Tyler, Inc., A. Hajek, W. Simmons and A. Colucci, pg. 25 and 26.

2. "Status of Environmental Controls for Geothermal Energy Development", Draft Report, April 1980, Interagency Geothermal Coordinating Council Environmental Controls Panel, pg. 42.

3. "An Environmental Overview of Geothermal Development: The Geysers-Calistoga KGRA", Volume 2, Air Quality, July 7, 1978, Lawrence Livermore Laboratory, L. Rosen and C. Molenkamp, pg. 2.

4. "Comprehensive Air Monitoring Plan", Preliminary Draft, February 15, 1980, GRIPS Commission, pg. 47.

5. "Assessment of H_2S Control Technologies for Geothermal Power Plants", Final Report, August 1979, Accurex Corp., M. Angwin and W. Toy, pgs. 5-17.

6. "State-of-the-Art Hydrogen Sulfide Control For Geothermal Energy Systems: 1979", March 1980, Lawrence Livermore Laboratory, F. Stevens, J. Hill and P. Phelps, pg. 67.

7. "Report on H_2S Abatement for Units 1, 2, 7, 8, 9 and 10", June 26, 1980, Geysers Project Office, Pacific Gas and Electric Company, pg. 7-9 and 27-28.

8. "PG&E H_2S Abatement Facilities Operations Manual Unit 15", March 21, 1979, Ralph M. Parsons Company, pg. 6-10.

9. "Control of Hydrogen Sulfide Emission from Geothermal Power Plants," Final Report (Volume 1), EIC Corporation, F. Brown, W. Harvey and R. Warren, pg. 10.

10. "Demonstration of EIC's Copper Sulfate Process for Removal of Hydrogen Sulfide and Other Trace Contaminants from Geothermal Steam at Turbine Inlet Temperatures and Pressures", Final Report, May 1980, PG&E, pg. vii-viii and 5-11.

11. "Sulfide Oxidation: Sulfox System of Pollution Control", December 1975, UOP, Incorporated, R. Rosenwald, R. Hamblin, P. Urban and R. Zimmerman.

12. "Theoretical Study of the Chemistry of Surface Condensers in Geothermal Service", Proposal (and subsequent modification), August 1978, Lawrence Berkeley Laboratory, O. Weres.

13. "Geothermal Power Systems", June 1980, Electric Power Research Institute Journal, pg. 49-50.

14. See Footnote 7 Reference, pg. 3.

SEISMIC MONITORING IN ITALIAN GEOTHERMAL AREAS
I. SEISMIC ACTIVITY IN THE LARDERELLO TRAVALE REGION

F. Batini,* C. Bufe,† G. M. Cameli,*
R. Console,‡ and A. Fiordelisi*

1. INTRODUCTION

Natural seismic activity, characteristic of geothermal fields, may be modified when changes in the fluid-thermodynamic conditions occur in the subsoil, brought about by production and re-injection of fluids. In fact, it has been seen that faults may vary their degree of seismic activity if the pressure of fluids is modified in tectonically active areas and that shallow earthquakes can be generated by a subsequent reduction of the "effective normal stress" (Healy et al. 1968; Teng et al. 1973; Raleigh et al. 1972). In order to measure the effects of variations in the pore pressure on natural seismic activity, a seismic network was installed about four years ago in the Larderello Travale geothermal region and in this report we will discuss the results obtained during the period extending from March 1977 to June 1980.

2. GEOLOGICAL-STRUCTURAL DESCRIPTION OF THE LARDERELLO-TRAVALE REGION

A geological-structural description of the Boraciferous Region has been given in detail by various authors (Lazarotti, 1967; Mazzanti, 1966; Cataldi et al. 1963; Giannini et al., 1970; Batini et al. 1978). The outcropping terrains may be grouped under the following complexes, in order of succession from top to bottom:

---

* ENEL, Unità Nazionale Geotermica, Pisa, Italy

† U.S. Geological Survey, Menlo Park, California, USA.

‡ Instituto Nazaionale Geofisica, Roma, Italy.

1) Neoautocton: consisting of lacustrine and marine and lagoon deposits of the Upper Miocene and Pliocenic marine sediments which are predominantly clayey. It transgresses into almost all of the units below.

2) Nappes of "Liguridi" (a.s.l.): to these belong formations in flysch "facies" and ofiolites of Cretaceous to Eocene age. This unit lies on the tectonic units described below.

3) Tuscan Nappes: this is the well-known Triassic-Oligocenic sequence with predominantly carbonate mesozoic formations in the basal part and terrigenous formations from Cretaceous to Oligocene in the upper part. This tectonic unit is frequently present with an incomplete sequence or with only the "Burano" anhydrite formation. The latter, connected to dolomite and anhydrite breccias, forms the base of the unit. In some areas, the "Tuscan Nappes" are totally absent. Tectonic wedges are present between the Tuscan Nappes and the regional basement mainly in correspondence of Castelnuovo-Larderello and Serrazzano area.

4) "Basement": these formations are present in the upper part of quartzites and phyllites attributed to the pre-carboniferous. In the lower part (over 3000 meters deep) we find mica-schists and gneiss formations. All these tectonic units lie in conformity on a surface of discontinuity which, at a depth of about 4-5 km, has been detected by means of seismic reflection prospecting.

The tectonic is characterized by two styles:

- the first being plicative, has determined a series of folds generally oriented in an appennine direction with an axial dipping toward NW;
- the second being rigid, has led to the formation of a series of faults which cut the folded structures which have previously formed in different directions. The prevailing directions are appennine (NW-SE) and anti-appennine (NE-SW) (Fig. 1).

The structural situation created at the end of the tectonic movements described is represented by "horst" and "graben" structures; the latter have for the most part given rise to sedimentation basins, during the marine invasion of the Miocene and the Pliocene.

3. SEISMOGRAPHIC COVERAGE

Seismographic monitoring in the Larderello-Travale geothermal region was begun in June 1976 with the installation of three permanent seismographic stations (CLSE; NINI and SDAL). Subsequently, seismographic coverage has been increased (Fig. 2), but new stations will have to be set up in order to better control seismic activity in the Larderello-Travale geothermal region which is currently being explored and exploited. Each station consists of a seismometer type Willmore MXIII A/S of 1 sec period and with the generator's constant average > 450 V/m/sec.

The seismic signal, amplified and frequency modulated, is transmitted via radio to multi-channel analogic magnetic tape recorder which records signals with a maximum frequency of 16 Hz.

4. Data Analysis

The determination of the focal co-ordinates of the seismic events recorded by the network is done by means of the Hypoellipse program (Lahr, 1979) based on a model of layered earth which differs from one

SEISMIC MONITORING IN ITALIAN GEOTHERMAL AREAS (1st part)

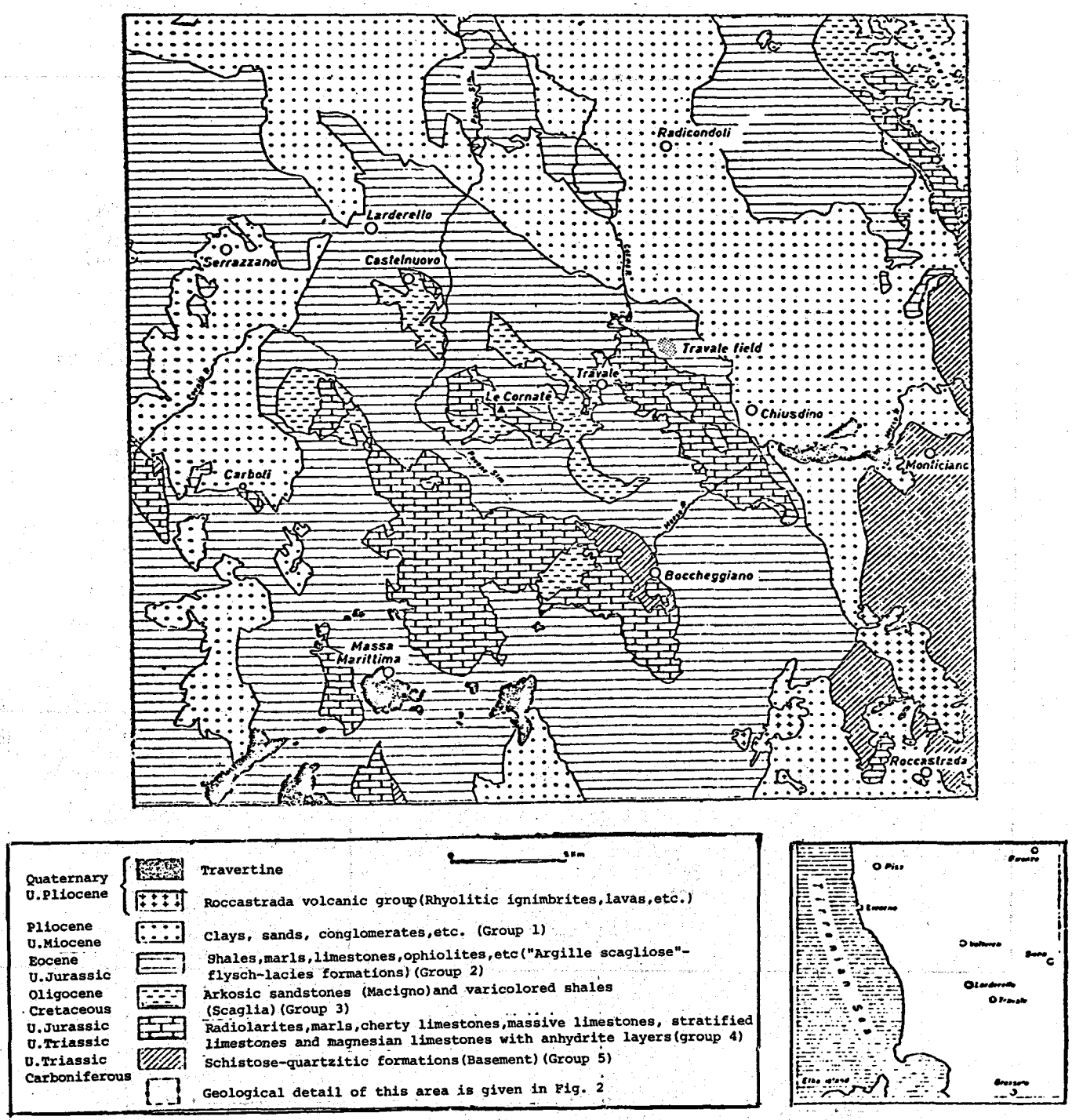

Fig. 1. Location and schematic geological map of the Larderello-Travale region.

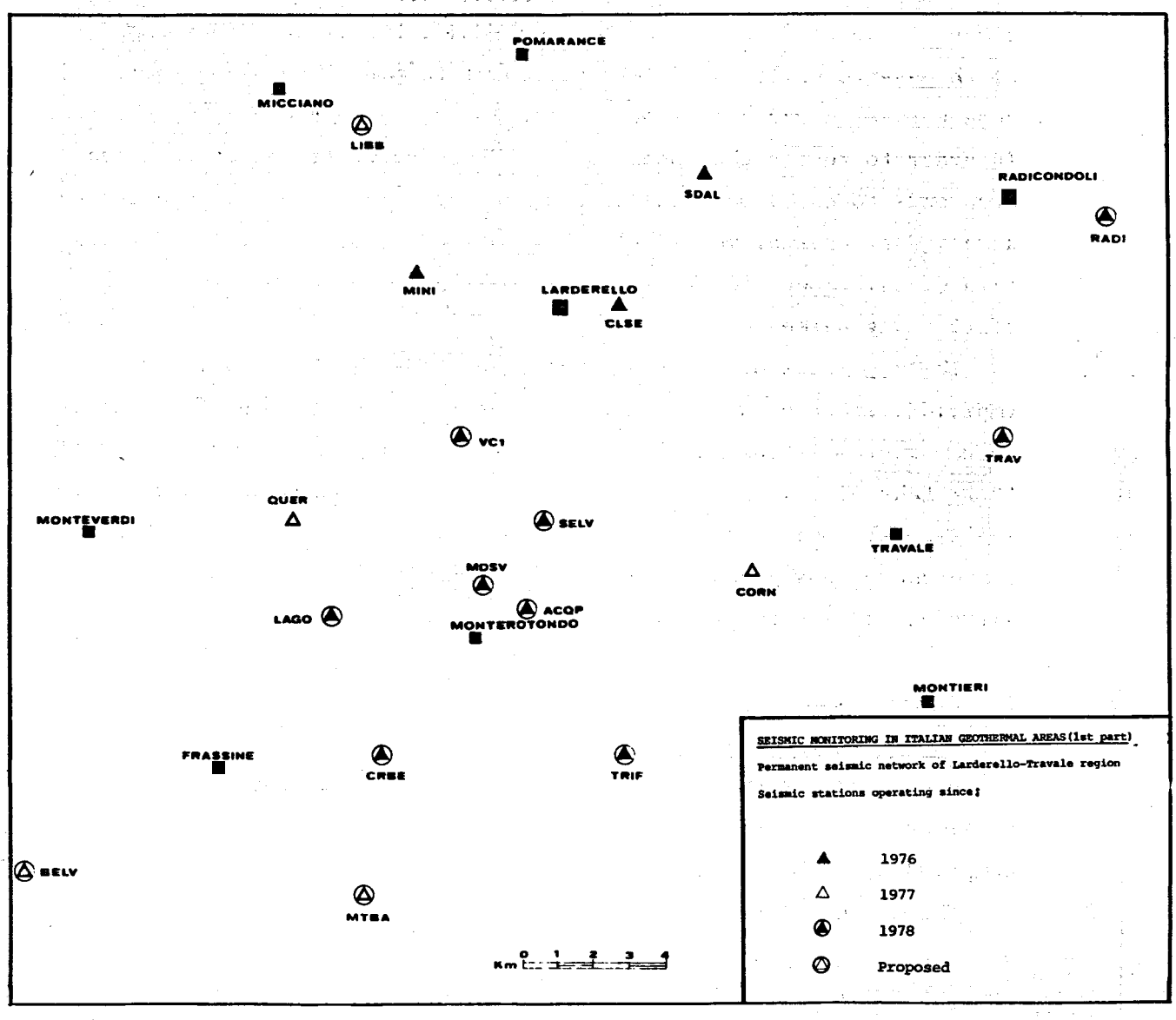

Fig. 2. Permanent seismic network of Larderello-Travale region.

station to another and is reconstructed on the basis of geologic (stratigraphy of the wells) as well as geophysical (seismic refraction and reflection, sonic logs) knowledge (Table 1). The mean square error of the residual travel time is less than 0.1 sec. for over 80% of the events while the determination of the focal co-ordinates is done with an error $\geqslant$ 1 km on the horizontal plane and $\geqslant$ 2 km at depth. In order to render the focal location more accurate, an attempt has been made to use a more advanced computing program, based on a three-dimensional crustal model (Alessandrini - Levato, 1980). The definition of this model for the Larderello-Travale geothermal region is still being worked on.

The magnitude of local seismic events is determined using an empirical equation which ties it to the total duration of the event, to the distance from the epicenter, and to the focal depth (Lee et al. 1972; Lahr et al. 1973). For events of greater magnitude, a comparison has been made between values determined with the method described above and values given by the National Seismic Network, and satisfactory agreement has been found.

5. SEISMIC ACTIVITY

5.1 Historical Seismic Activity

Historical seismic activity has been studied taking into consideration the data contained in the National Seismic Catalogue, compiled by ENEL, for the period 1000 - 1975.

The Larderello-Travale geothermal region is located on the western border of an area with an almost uniform seismic activity which extends towards the center of the Italian peninsula in a NW-SE direction (Fig. 3). The entire (strip) belt between the Tirrenean Sea and the Appennines which runs along the line of Livorno, Massa Marittima, up to Monte Amiata, is an almost aseismic area or one with very moderate seismic activity. In the immediate vicinity of the geothermal area shown in the small square, even though earthquakes of high intensity IX° - X^{o} (prior to 1800) on the Mercalli scale have occurred, seismic activity has remained moderate and in the last few years seems to have decreased.

Table 1 - Crustal Model

STATIONS : MINI - CLSE		STATIONS : SDAL - TRAV - RADI	
Velocity km/sec	Depth. km	Velocity km/sec	Depth. km
3.800	0.	3.000	0.
5.100	0.150	5.100	0.440
6.200	3.900	6.200	4.200

STATIONS : QUER		STATIONS : CRBE	
Velocity km/sec	Depth. km	Velocity km/sec	Depth. km
2.800	0.	3.800	0.
3.800	0.040	5.500	0.100
5.100	0.240	5.100	0.800
6.200	3.500	6.200	3.500

STATIONS : VC/1		STATIONS : MDSV	
Velocity km/sec	Depth. km	Velocity km/sec	Depth. km
3.800	0.	4.200	0.
4.200	0.200	5.500	0.010
5.500	0.800	5.100	0.800
5.100	1.100	6.200	3.000
6.200	3.500		

Table 1. Crustal Mode (Continued)

STATIONS : CORN - TRIF		STATIONS : LAGO	
Velocity km/sec	Depth. km	Velocity km/sec	Depth. km
5.100	0.	3.200	0.
5.500	0.010	5.100	0.300
6.200	4.200	6.200	3.500

STATIONS : SELV		STATIONS : ACQP	
Velocity km/sec	Depth. km	Velocity km/sec	Depth. km
3.800	0.	4.200	0.
4.300	0.100	5.100	0.010
5.100	0.700	6.200	3.100
6.200	3.400		

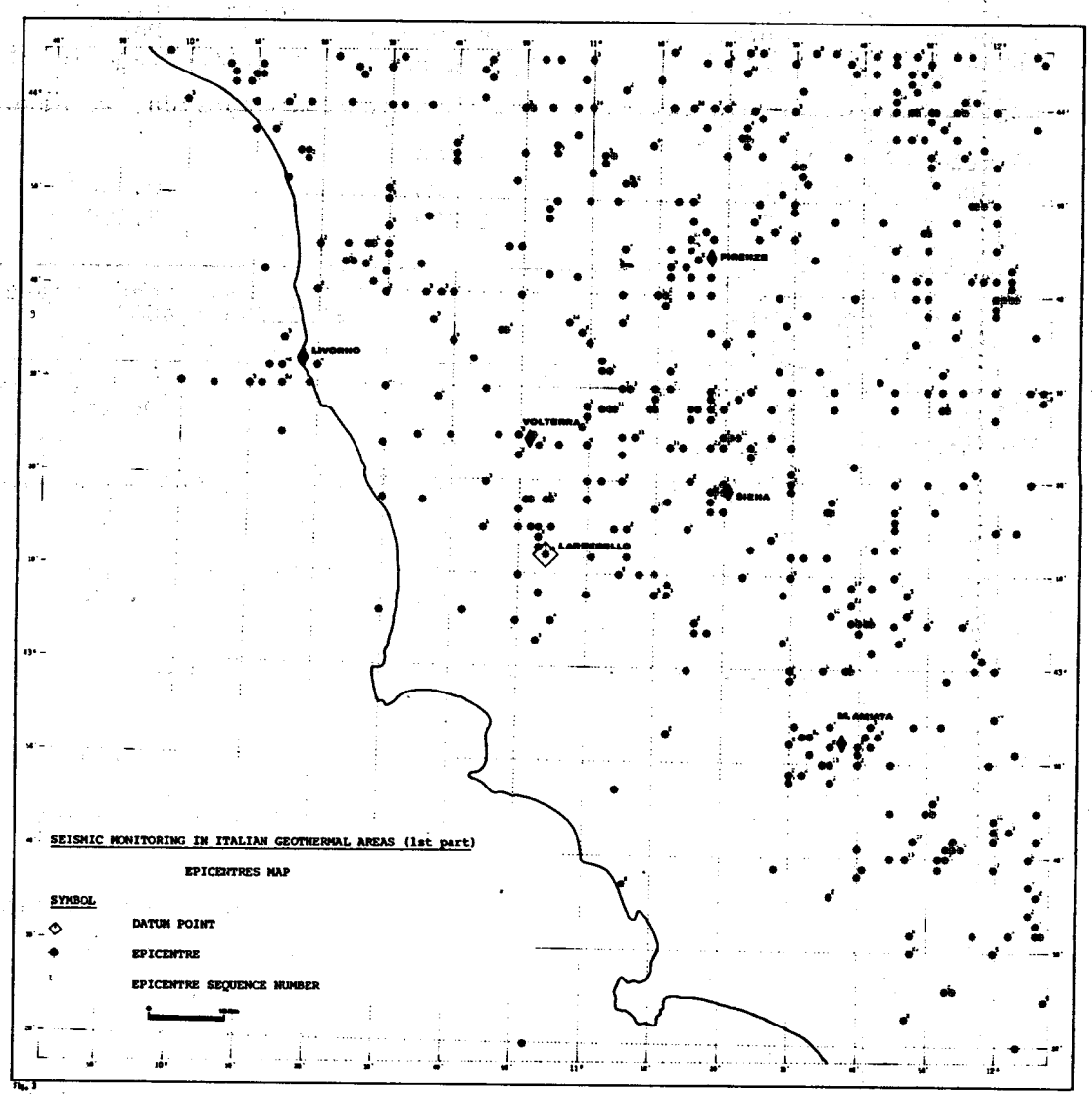

Fig. 3. Epicenters map.

The only noteworthy event verified in recent times is the earthquake at Monterotondo on August 19, 1970 with an intensity of VII° on the Mercalli scale. Since the catalogue appears to be complete from 1880 to 1975 even for earthquakes of low magnitude ($M > 3$), an area which includes the Larderello-Travale geothermal region has been chosen (Fig. 4) in which to attempt to make a statistical table of magnitudes; using the empirical equation of Ishimoto-Iida, we have obtained a value of "b" equal to about 1.5.

5.2 Present Seismic Activity

From March 1977 to July 1980 about 500 events have been located, almost 400 of which fall within the geothermal region. Seismic activity manifests itself by sporadic activity and sequences of events which appear in clusters vary in magnitude and number. These rarely take on the form of typical mainshock aftershock sequences and consist of earthquakes which follow one another in a time range which varies from a few seconds to several hours, with an epicenter which is restricted to a small area.

The maximum magnitude observed during the above mentioned period was 3.8. From the distribution of epicenters (Fig. 5) it may be concluded that seismic activity is present throughout the entire Larderello-Travale geothermal region, but in certain areas there is a greater concentration.

These areas are located at the borders of the geothermal region and coincide with areas whose exploitation has begun in recent times. At any rate, it is noteworthy that only in the Lago area (SW of Larderello) does the release of tension come about in a regular, continuous manner. During the period of observation here considered, it was possible to single out isolated spots of seismicity even in areas not seismically active (i.e., the immediate vicinity of well "Sasso 22" drilled during the period 1978-1979 to a depth of more than 4/km). The projection of the foci on vertical planes running N-S and E-W (Figs. 6-7) demonstrates that earthquakes take place almost totally within 8 km and predominantly at 3-4 km.

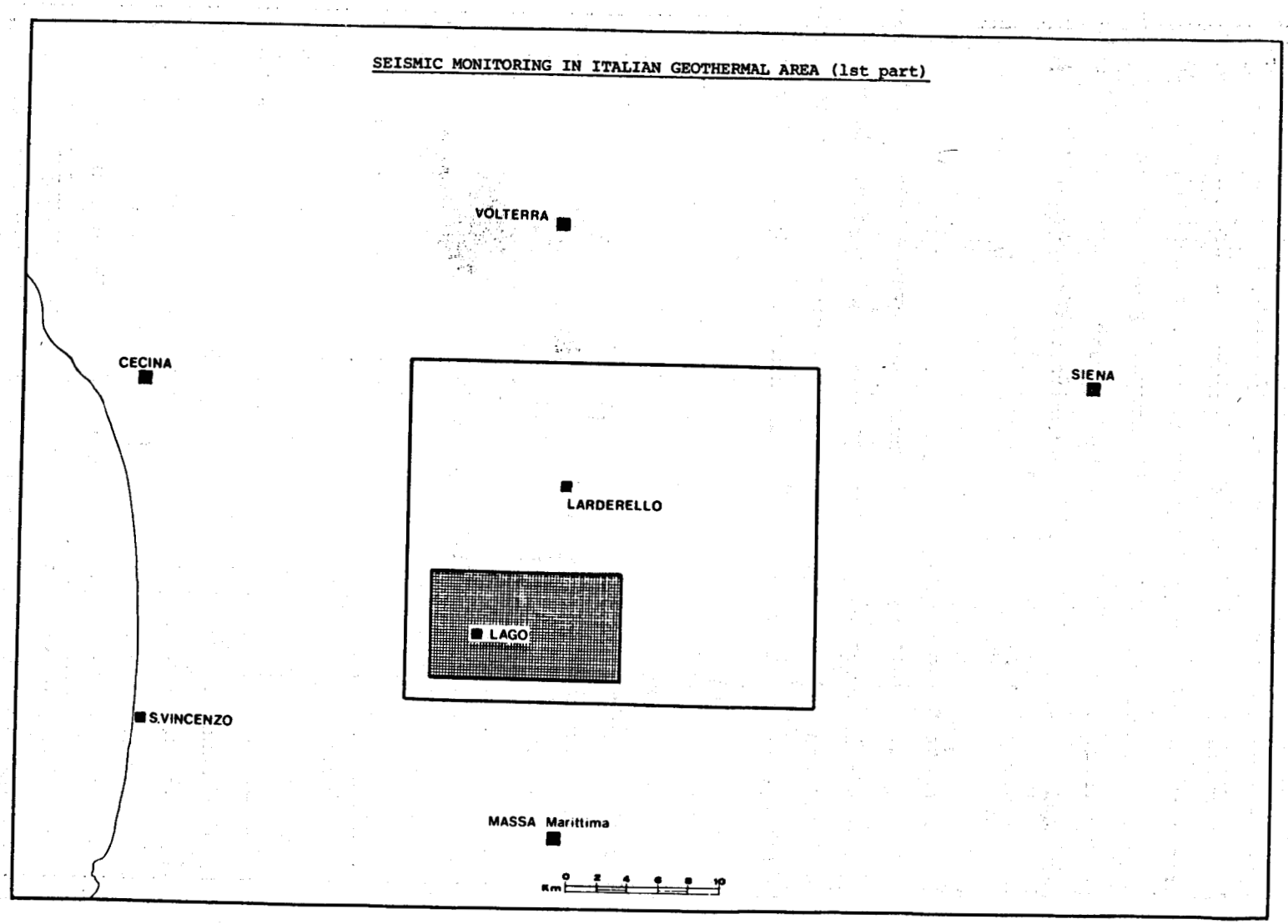

Fig. 4. Index map of historical and actual seismicity.

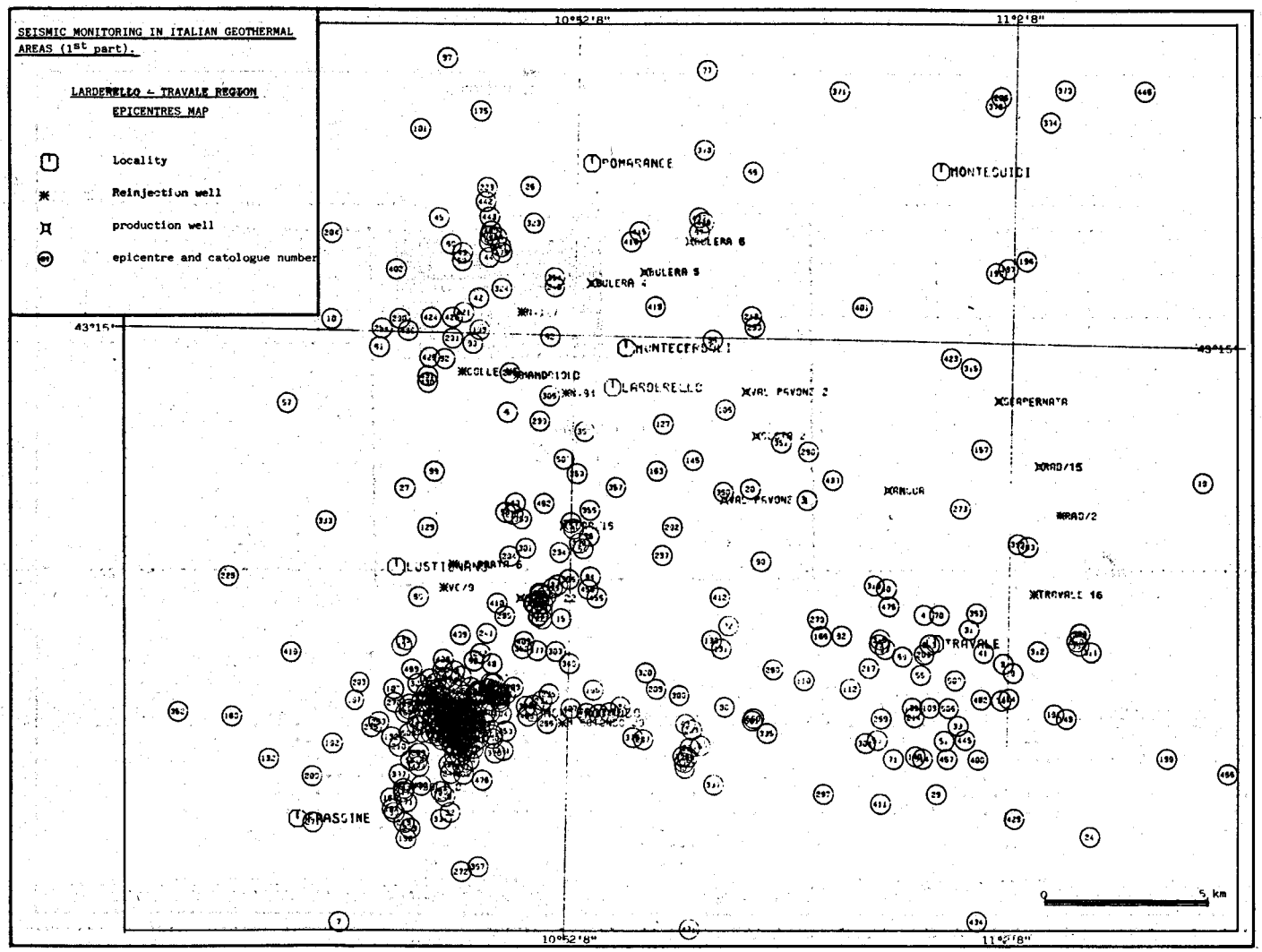

Fig. 5. Larderello-Travale region epicenters map.

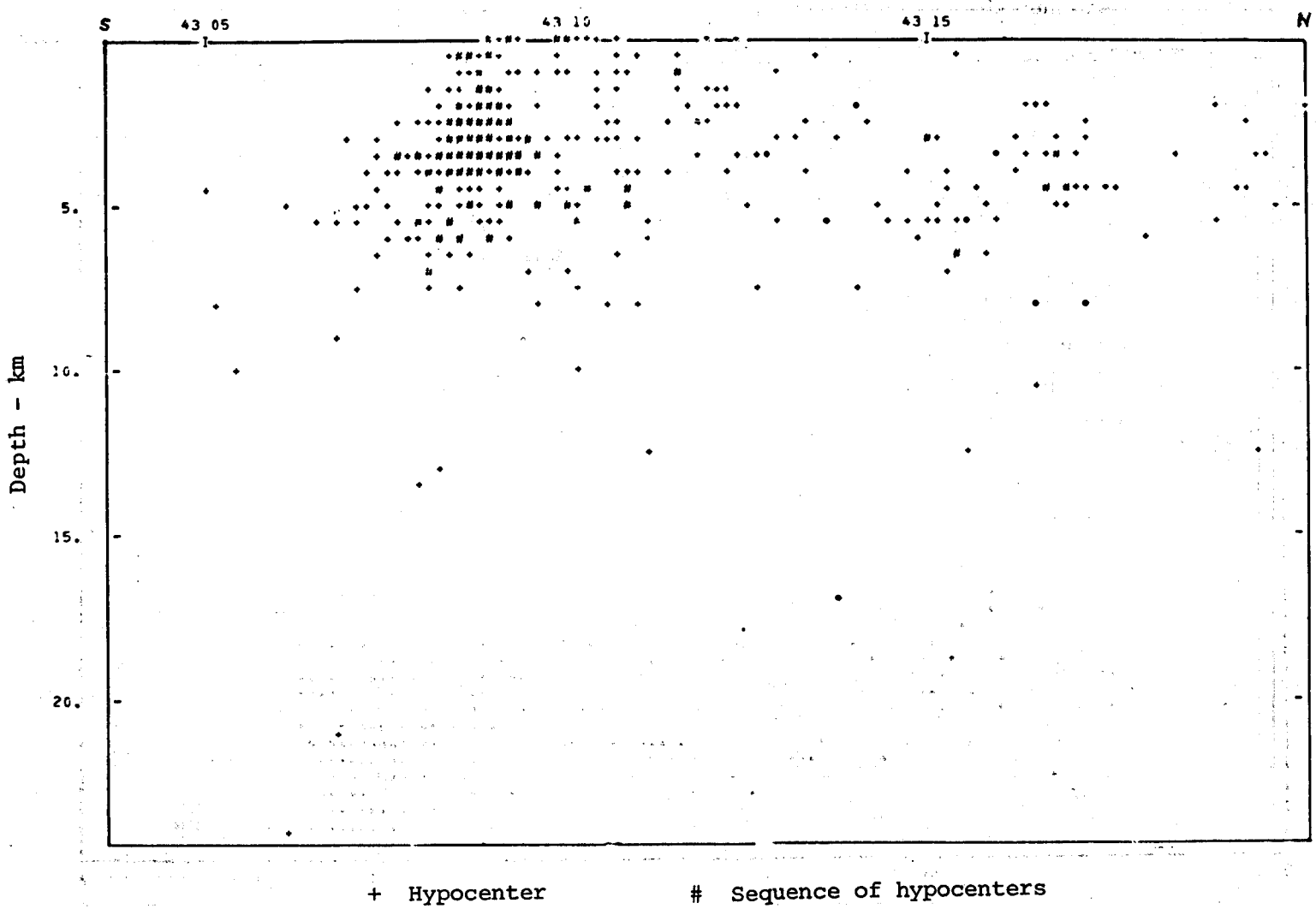

Fig. 6. Hypocenters distribution on N - S section.

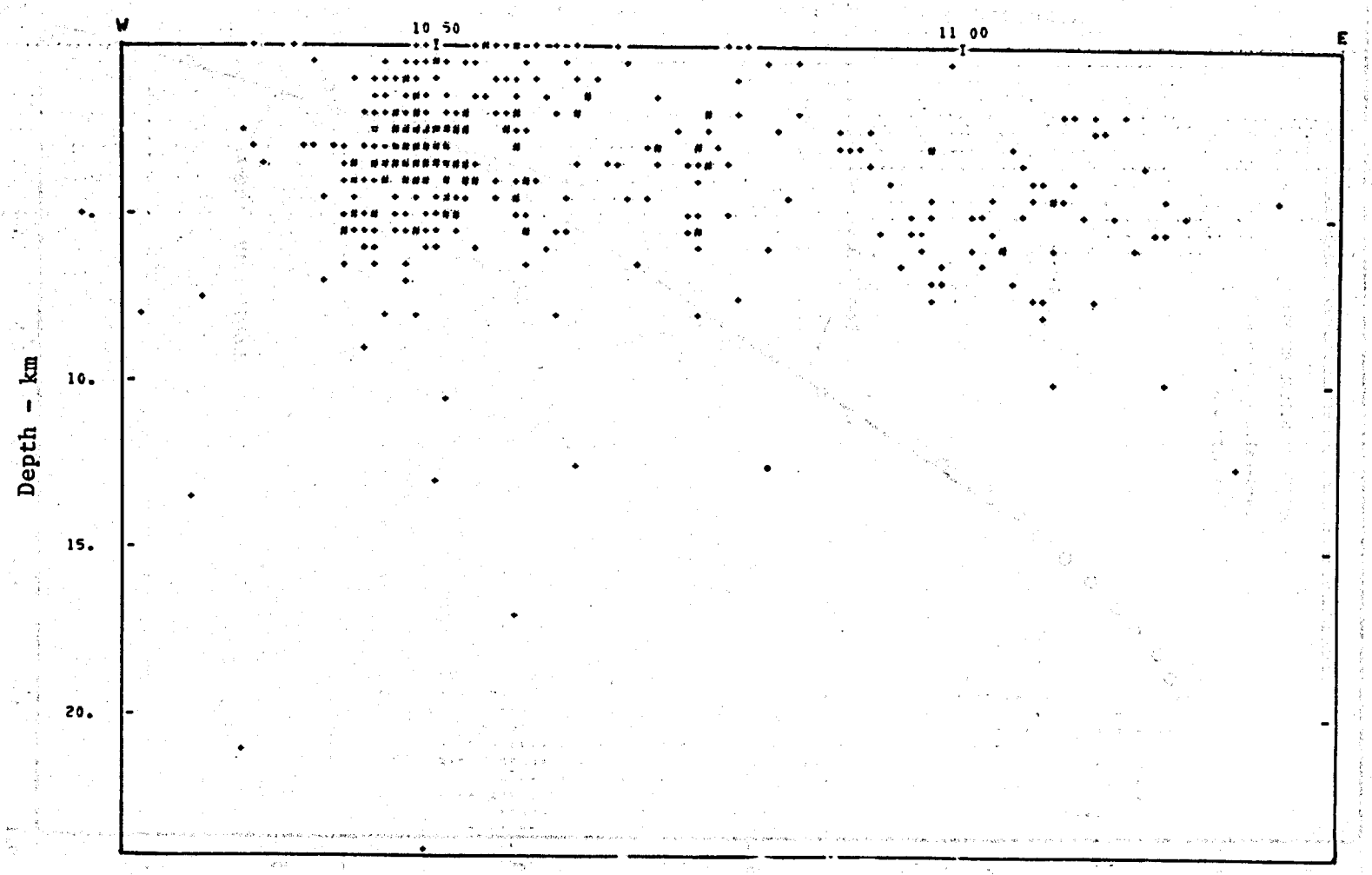

+ Hypocenter # Sequence of hypocenters

Fig. 6A. Hypocenters distribution on E - W section.

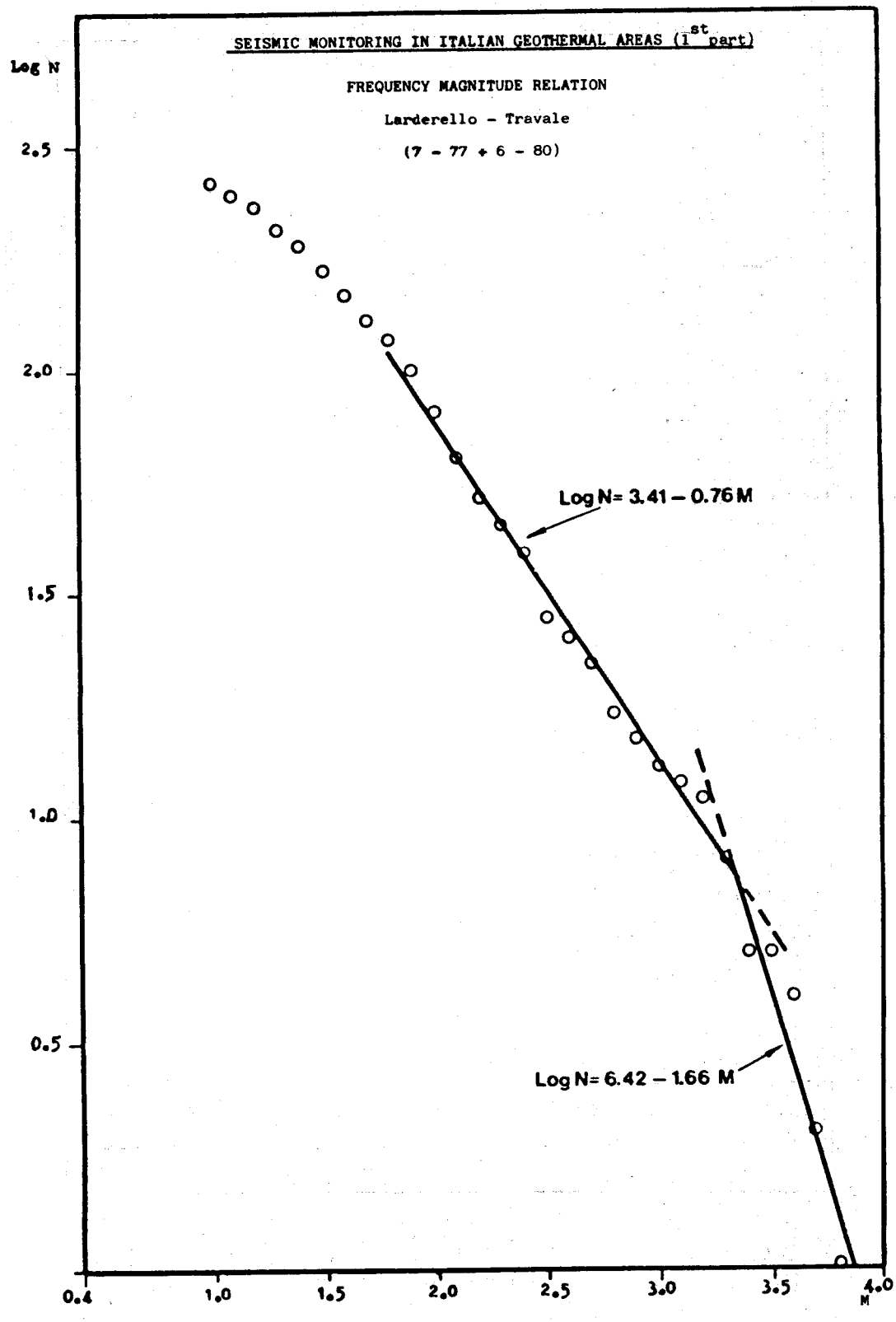

Fig. 7. Frequency magnitude relation Larderello-Travale areas.

It is interesting to note the abrupt interruption in seismicity in correspondence to the W limits of the Larderello geothermal field (Figs. 6-6a) and a progressive deepening of the foci in the eastern zone corresponding to the geothermal field of Travale.

The scarce seismicity observed in the central part of the region may coincide with a less fractured zone which may constitute an eventual barrier between the two geothermal fields.

5.3 Magnitude - Frequency Relationship

The magnitude-frequency histogram has been drawn up for the events localized in the area indicated in the square in Fig. 3 over a three-year period extending from July 1977 to July 1980. The histogram (Fig. 7) presents three distinct slopes: the first for $M > 1.8$ may be attributed at least partly to instrumental detection factors; there is then a stretch which goes from $1.8 > M > 3.3$ which may be approximated by the straight line whose equation is:

$$\text{Log } N = 3.42 - 0.76\ M$$

Finally, for $M > 3.3$ we see an abrupt increase in the slope which corresponds to a "b-value" of about 1.66. Similar lack of linearity has been found in studies done on microseismicity (6 Scalera, 1980, Analysis of the "b" parameter; Seeberg, personal communication). The same type of histogram (Fig. 8) has been constructed from the events which took place during the same period of observation in a more restricted area indicated in Fig. 3, Lago (SW of Larderello).

In this case the stretch which runs from 1.8 — 3.3 may be approximated by the straight line with the following equation:

$$\text{Log } N = 3.97 - 1.19\ M$$

The value of b (1.19) which we find in this last case is notably greater than that relative to the entire region studied.

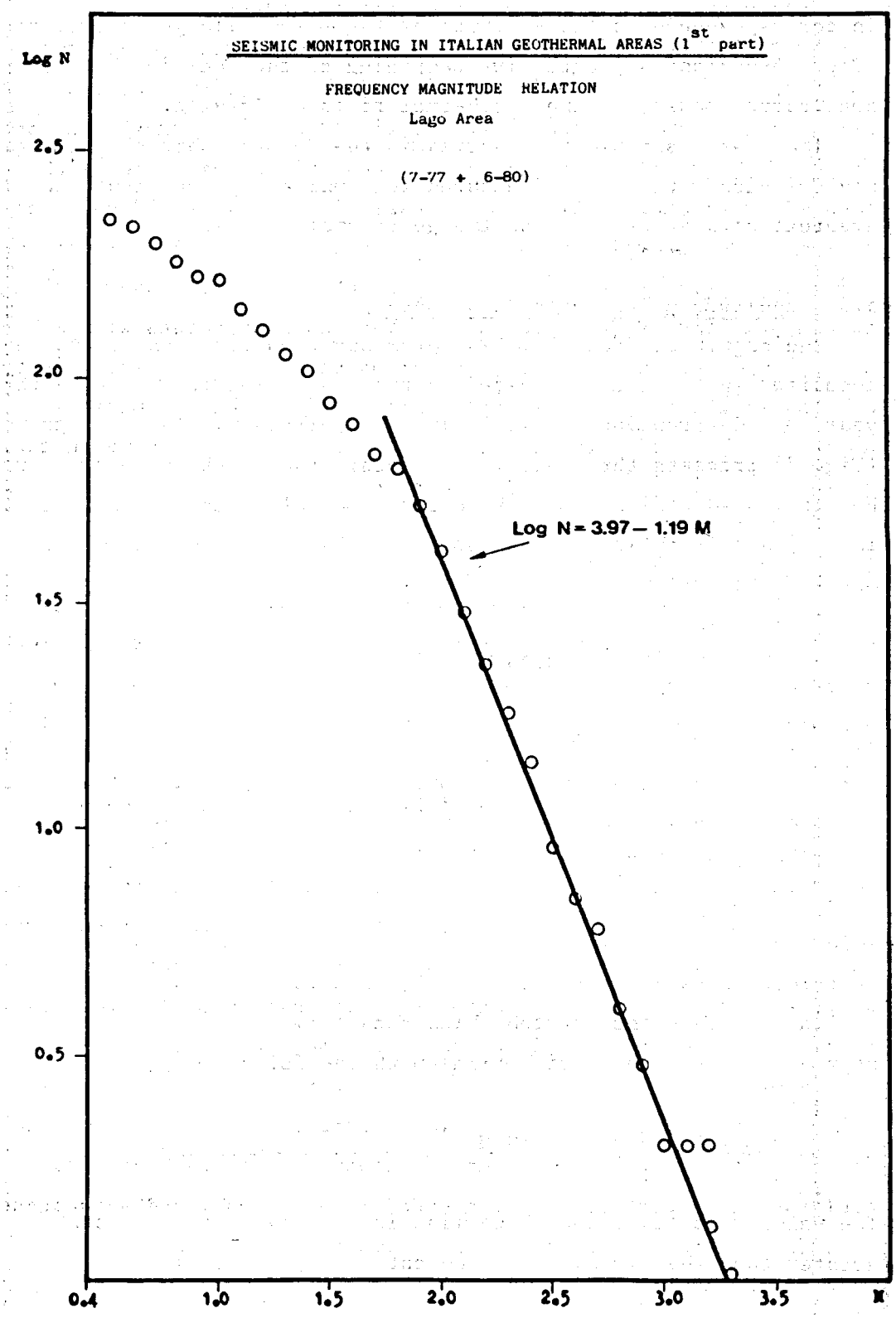

Fig. 8. Frequency magnitude relation Lago area.

This may be connected to a geological situation which is particularly favorable to the release of energy with mechanisms characterized by low tension. This value of "b", characteristic also of other geothermal areas (Marks et al. 1978), is generally associated with a high grade of fracturing of rocks and in some cases with induced seismic activity (Gupta - Rastogi, 1976). A "b" value equal to about 1.5, drawn from data in the National Catalogue of earthquakes which took place from 1880 to the present in the area shown in Fig. 3, is comparable to that calculated on the basis of events with $M > 3.3$ which took place during the observation period (1977 - 1980) in the area shown in the larger square; this confirms the seismically abnormal behaviour with respect to the average value found in the national territory ($b \simeq 0.9$) (Jaccarino, 1968).

6. FOCAL MECHANISMS

The focal mechanism has been determined employing the classical method based on an analysis of the first motion recorded. A computing program has been utilized (Wickens, Hodgson, 1967), adapted to the present problem, which determines the best orientation of nodal planes with relation to the input data.

Given the low energy released by the single seismic events verified in the area studied during the past three years, it has been impossible to utilize, in order to determine focal mechanisms, data from stations which do not belong to the local network at Larderello. The scarce number of available stations and their location with respect to the events has limited the reliability of the results obtainable with an analysis of the first motions of every single earthquake.

In order to obtain more stable solutions of fault planes, the joint fault (or composit) plane solutions method has been used, applying it to earthquakes originated in a well-defined seismogenetic area or even belonging to the same sequence.

The results shown in Fig. 9 are the most representative for the whole region according to the present seismographic coverage. In particular the following features are evidenced:

- frequent mechanisms of normal faults with appennine direction (NW-SE) and antiappennine (NE-SW).

- strike-slips fault mechanisms with the axis of maximum compression trending approximately NW-SE.

7. SEISMICITY - EXPLOITATION OF GEOTHERMAL FIELDS

A comparison between seismicity and activity connected to exploitation of a geothermal field (extraction and injection of fluids at depth, drilling of deep wells in total loss of circulation, stimulation of sterile wells, etc.) has been attempted in order to establish if and how these activities modify the stress release mechanisms of the Larderello-Travale region. The data concerning the quantity of fluids extracted and injected in the subsoil has been compared with the seismic energy which is released every month.

From the histograms reconstructed for the Larderello-Travale geothermal region (Fig. 10) the seismic energy was released as a linear function of time until May 1979, when a sharp increase of seismicity occurred. This increase can not be correlated to either the quantity of fluids injected or to production of fluid or to the average monthly rainfall.

Observing the variations of the same parameter for the Lago area (Fig. 11), we can see that the same pattern in the energy histogram persists throughout the period from May 1979 - June 1980. In this case there are no sure correlations between extraction of injection activities and seismicity. At any rate it is noteworthy that, during the period of March 1978 - January 1980, a deep well was drilled (Sasso 22) in the Lago area; the drilling was performed largely in total loss of circulation injecting large quantities of water into the well. The number of seismic events with a magnitude superior to 1.5

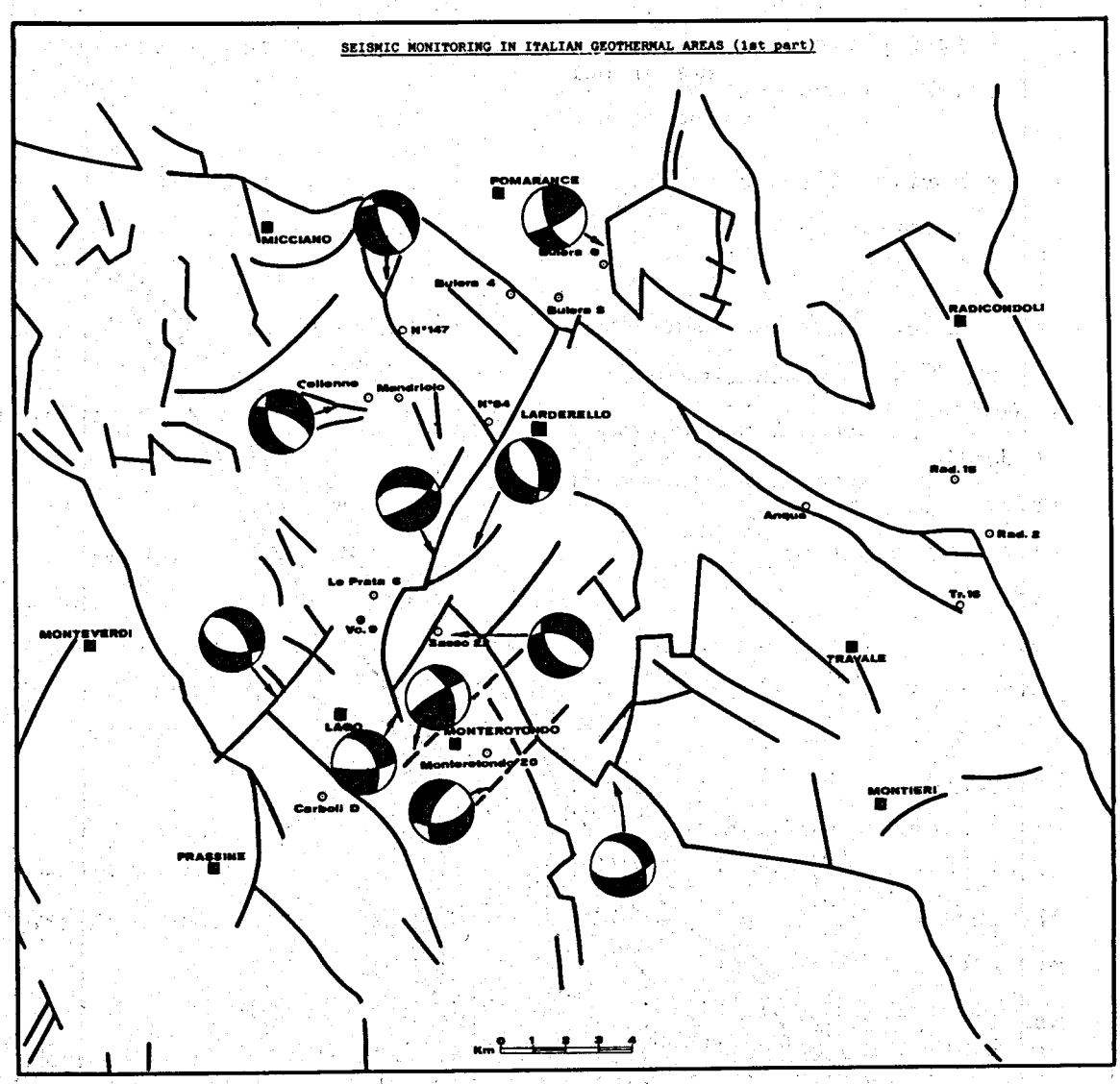

Fig. 9. Representative fault plane solution and main tectonic trends in Larderello-Travale region.

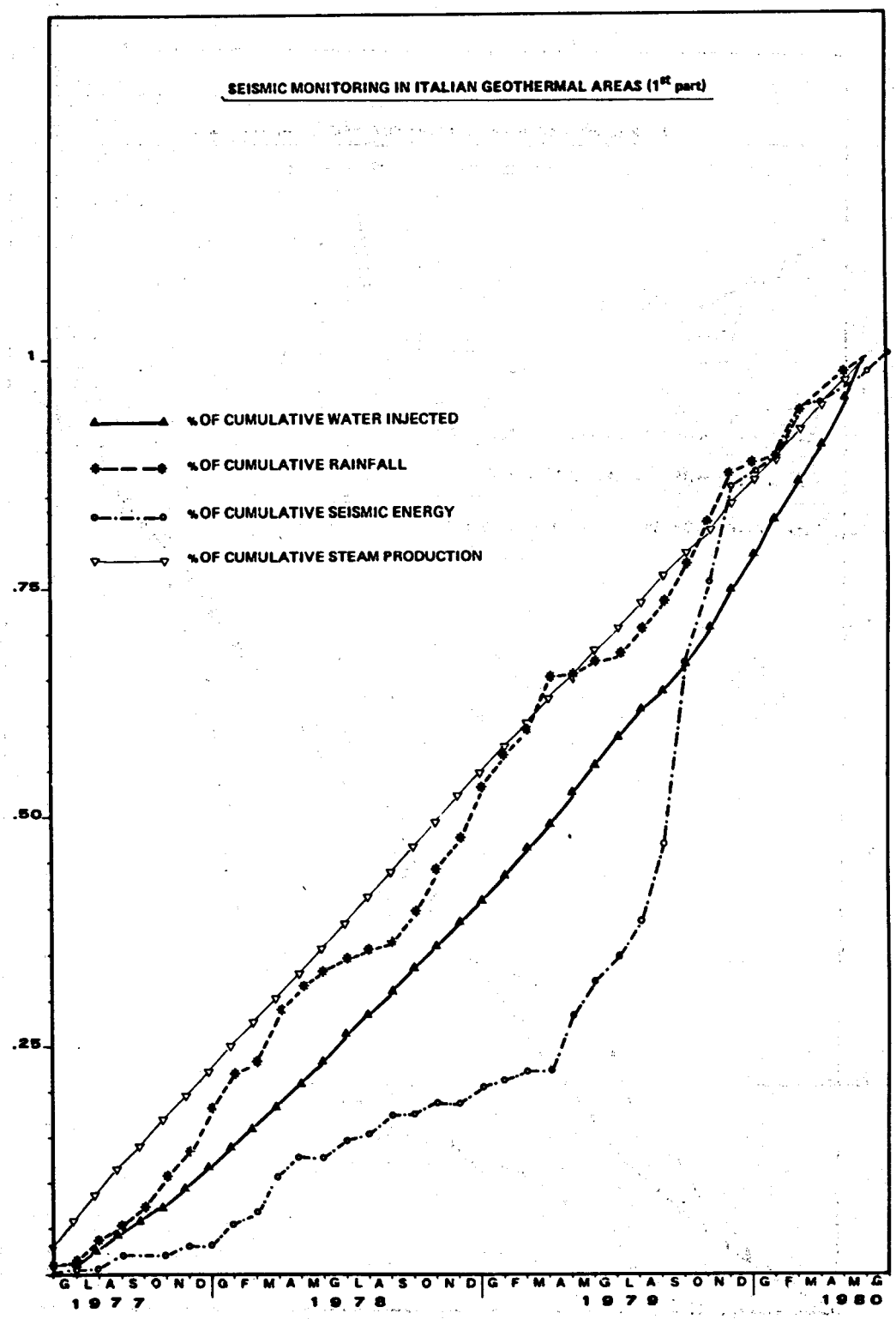

Fig. 10. Temporal distribution of seismic energy released, water injected, rainfall, steam production.

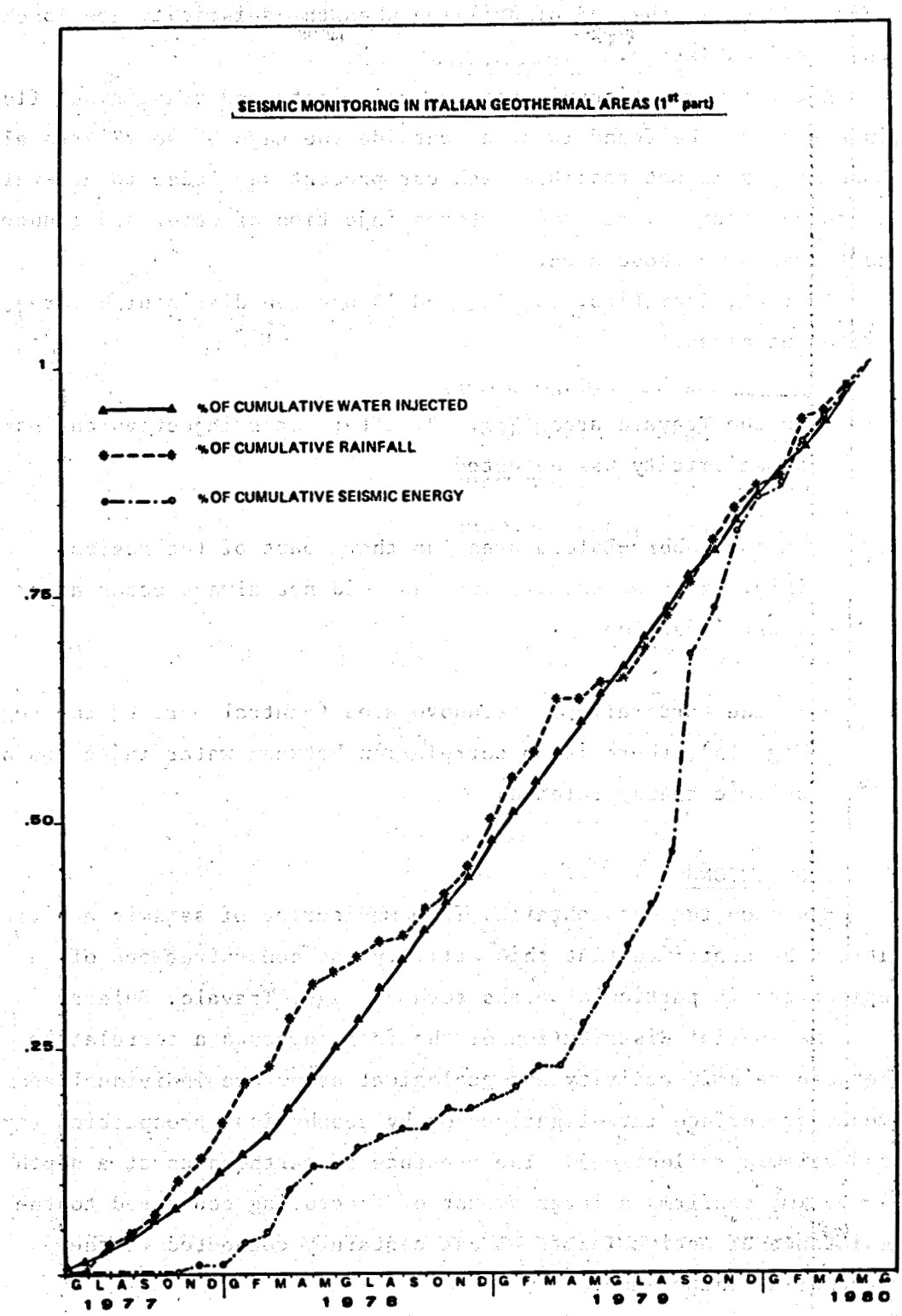

Fig. 11. Temporal distribution of seismic energy released, water injected, rainfall.

increases gradually as the depth of the well reaches about 3000 m (Fig. 12) until the end of drilling when the seismicity goes back to the previous levels.

A certain relationship between seismicity and quantity of fluid injection may be found in areas outside the Lago-Sasso 22 area also. However, it is not possible with our present knowledge to generalize a cause-effect relationship between injection of water and induced earthquakes in those area.

In fact, from Figs. 13, 14, and 15 one can distinguish three different cases:

- in the Travale area (Fig. 13) after water injection an increase of seismicity was detected.

- in the Gabbro-Bulera area (northern part of the region) (Fig. 14) a seismicity increase did not always occur after water injection.

- in the Larderello-Castelnuovo area (central part of the region, Fig. 15), there is no correlation between water injection and seismic energy release.

8. CONCLUSIONS

Based on the data obtained from monitoring of seismic activity, it can be confirmed that this activity has concentrations of epicenters in particular areas such as Lago, Travale, Bulera.

The spatial distribution of the foci suggests a correlation between seismic activity and geological structure individualized by means of surface investigations or by geophysical prospecting (gravity and seismic reflection). The presence of earthquakes at a depth of 4 — 5 km, confirms a large amount of fracturing connected to the existence of active faults almost certainly connected to the geothermal phenomenon.

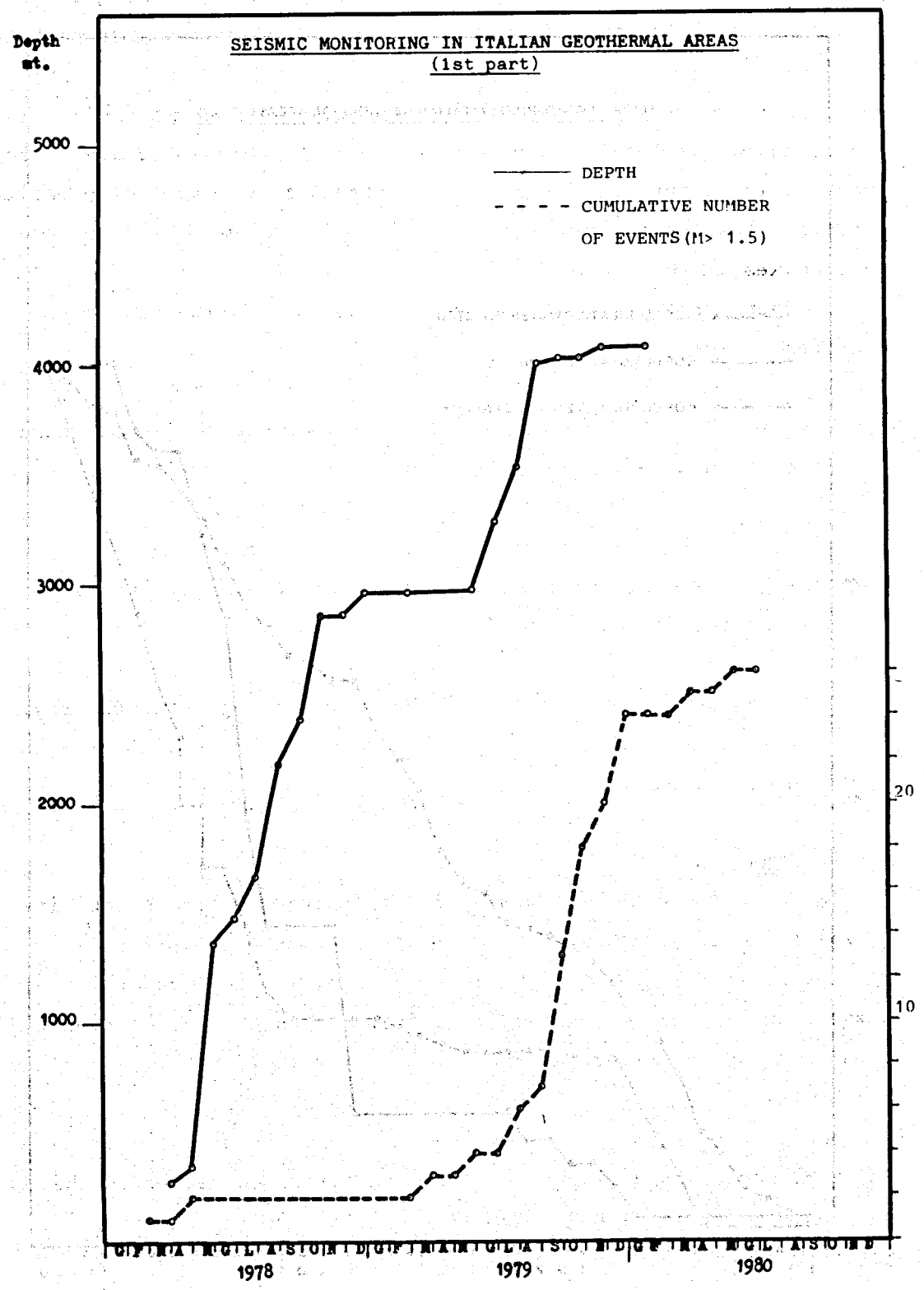

Fig. 12. Sasso 22 deep-well. Depth vs seismicity.

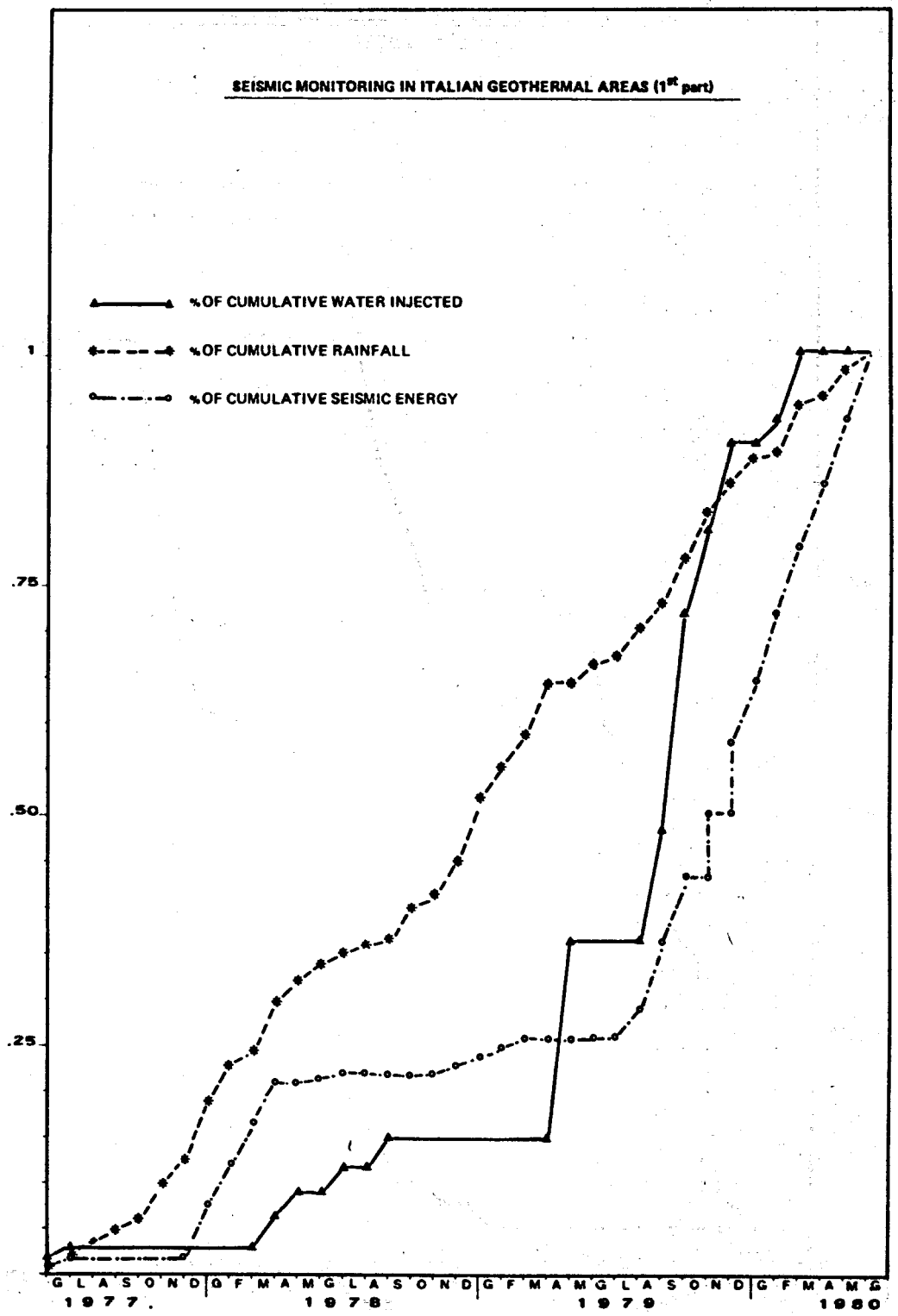

Fig. 13. Temporal distribution of seismic energy released, water injected, rainfall.

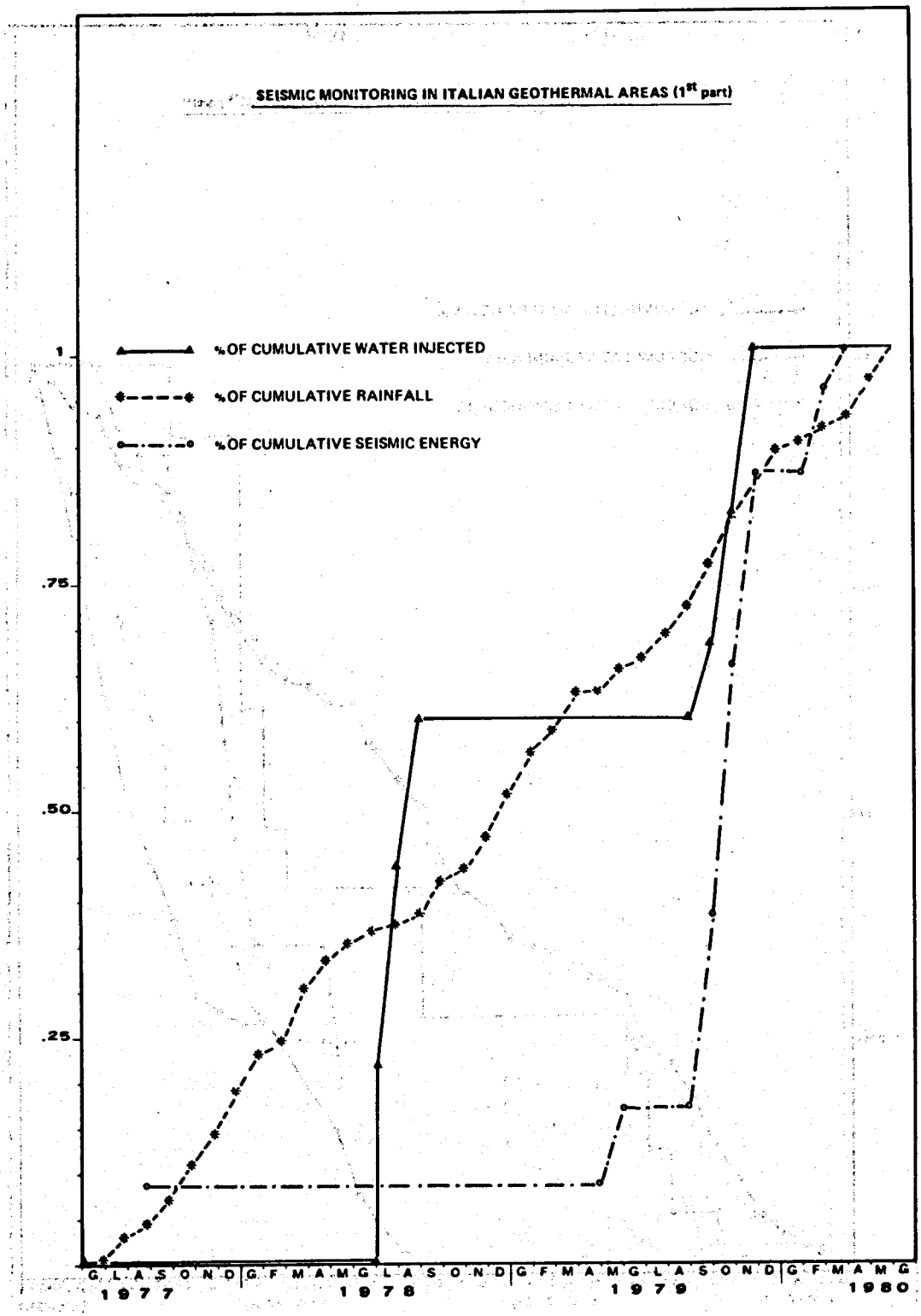

Fig. 14. Temporal distribution of seismic energy released, water injected, rainfall.

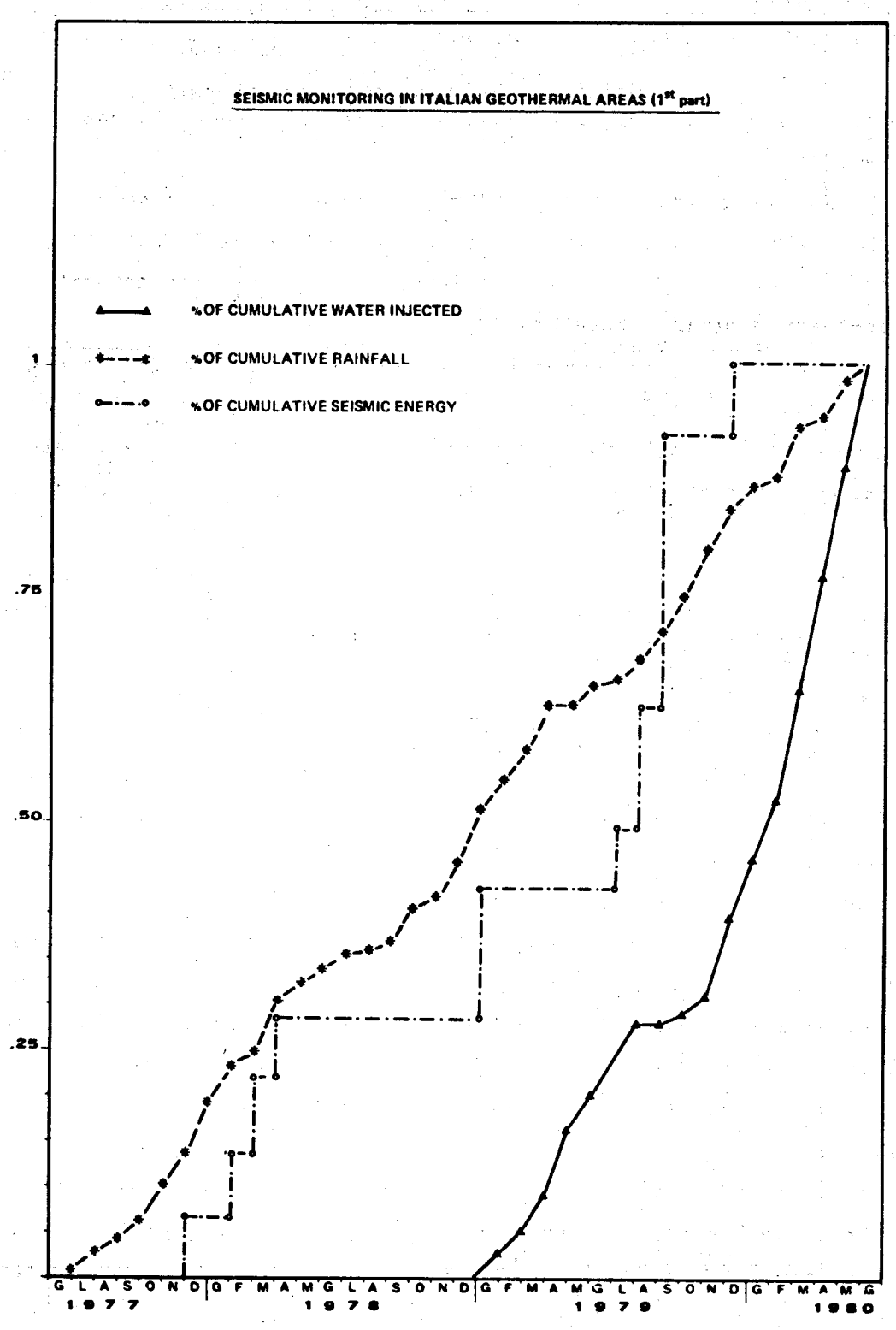

Fig. 15. Temporal distribution of seismic energy released, water injected, rainfall.

The study of focal mechanisms gives us some information on possible directions and inclinations of the faults which agree with the geological-structural data. It has been possible to recognize normal fault mechanisms with sub-vertical inclinations, and, to a lesser degree, strike-slip fault mechanisms from which we can see that the direction of maximum compression is the anti-appennine one (SE-NW).

Given the limited amount of time during which the seismic monitoring has been carried out, it is not yet possible to find a certain relationship of cause and effect between seismic activity and fluid-thermodynamic parameters.

As a matter of fact, even if some phenomena localized in space and time (Sasso 22, Bulera, Travale) allow us to see an influence of the injection of fluids in the subsoil on the seismicity, there is also evidence of no correlation in other parts of the region (Larderello-Travale). These facts lead us to make some hypotheses.

In the Larderello-Castelnuovo area the water, injected in a steam dominated reservoir rapidly passing into a gas phase, does not cause appreciable variations in the hydrodynamic equilibria.

On the contrary in water dominated reservoirs, as in Bulera-Gabbro, Travale, Sasso 22 areas, even small amounts of water injected can cause noticeable pore pressure variations. In particular tectonic conditions, such as variations diminishing the effective normal stress, modify the stress release conditions.

Naturally the results and considerations presented in this report are not definitive; more conclusive results may be obtained when we reach a greater accuracy in the determination of focal co-ordinates, subordinate to a more detailed knowledge of the crustal model. A more accurate determination of focal mechanisms will be possible employing a greater number of seismic stations when more information is available from spectral analysis. Lastly it will be necessary to have a period of observation long enough to get a better knowledge of temporal correlation between seismic activity and parameters connected to the activity of the field.

9. REFERENCES

See the following article for references cited here.

SEISMIC MONITORING IN ITALIAN GEOTHERMAL AREAS
II. SEISMIC ACTIVITY IN THE GEOTHERMAL FIELDS DURING EXPLORATION

F. Batini,* G.M. Cameli,* E. Carabelli,†
and A. Fiordelisi*

1. INTRODUCTION

The Italian areas of geothermal interest are usually located in densely populated zones and very often near centres of historical and artistic renown. Consequently, monitoring of seismic activity induced by exploration and exploitation of these geothermal resources becomes of particular importance, demanding a considerable effort on ENEL's part (Index Map).

Work began a few years ago on setting up a microseismic control network in each of the localities involved in deep exploration for geothermal purposes. Wherever possible the network was installed before drilling began in order to obtain a preliminary picture of the natural background noise.

As the control system had to be put into operation as quickly as possible and create a minimum of operational problems, it was decided to begin with an analogic instrumentation, which is economic, autonomous, and easy to install. The instrumentation, described in the first part of our report, provided a continuous, comprehensive monitoring of all the local and regional seismic activity.

This report will present and discuss the data recorded from the beginning of the survey to June 1980. The data refer to natural seismic activity as well as to events recorded during production and injection tests in some wells.

---

* ENEL - UNG (Pisa)

† ISMES - (Bergamo)

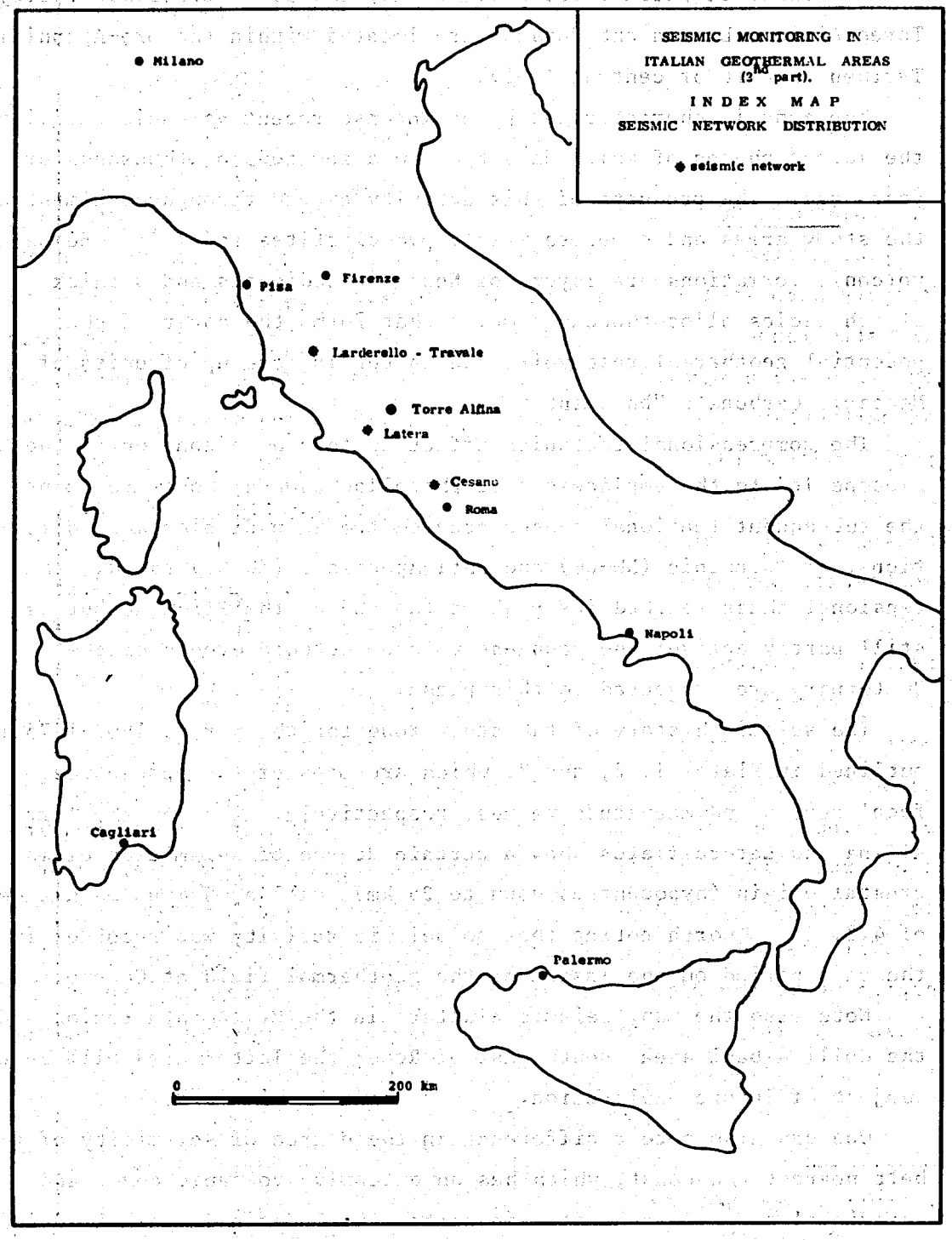

Index Map - Seismic Network Distribution

2. GEOLOGICAL BACKGROUND AND PAST SEISMIC ACTIVITY

The three geothermal areas covered by the passive seismic surveys, Toree Alfina, Latera and Cesano, are located within the pre-Apenninic Tyrrhenian belt of central Italy.

The zone is characterized by an intense recent volcanic activity, the latest phases of which date back to a few tens of thousands of years ago. The products of this activity extend throughout almost all the study areas and comprise mainly pyroclastites and lava. Below the volcanic formations are layers of Neogenic sediments and a thick flysch facies allochthonous complex that forms the cover of the potential geothermal reservoir; the latter is made up of units of Mesozoic carbonate "basement."

The compressional tectonics affecting the whole zone until the Mid Miocene led to the emplacement of the allochthonous cover terrains; the subsequent tensional phases created two main displacement directions, of Apenninic (NW-SE) and anti-Apenninic (SW-NE) trend. The tensional phase reached its peak at the end of the Pliocene but is still partly active; the youngest volcanotectonic events of the Quaternary are connected to this phase.

The seismic history of the study zone for the period 1900-1975 is outlined in Plates 1, 2, and 3, which are maps of the epicentres, focal depths and magnitude values, respectively. Whereas the Torre Alfina and Latera fields show a certain degree of seismicity of mainly crustal origin (hypocentres down to 25 km), with a maximum magnitude of 4.7, it is worth noting that no seismic activity was recorded in the said period on the inside of the geothermal field at Cesano.

Note also the many seismic clusters in the Mt. Amiata region and the Colli Albani area, south-east of Rome; the latter area will be the subject of future exploration.

One can also note a difference in the degree of seismicity of the belt nearest the coast, which has an extensive volcanic cover and seismic clusters concentrated in certain well-defined areas, and that of the Apennine ridge, whose seismic centres have a greater density and are more widely spread.

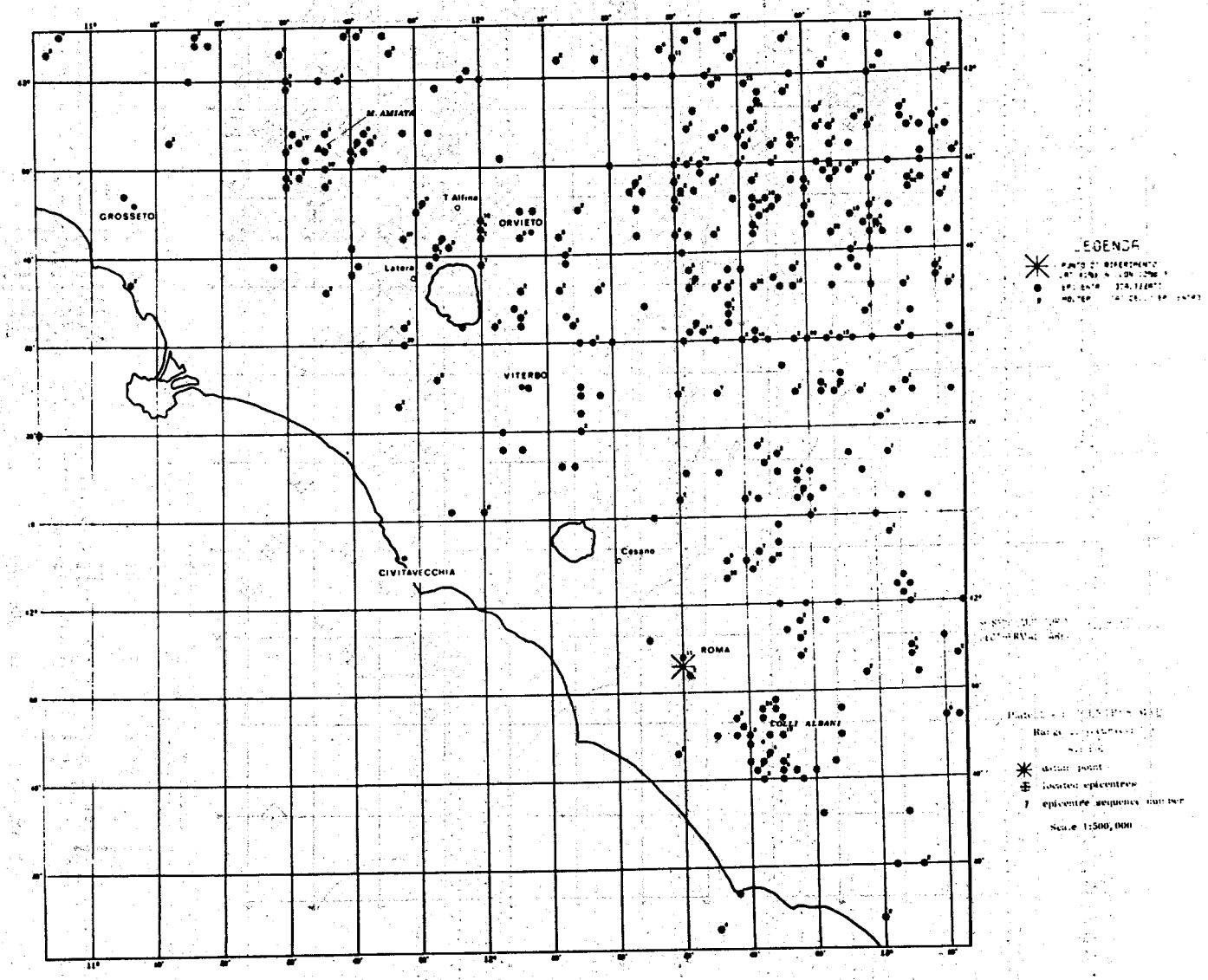

Plate 1. Epicentres.

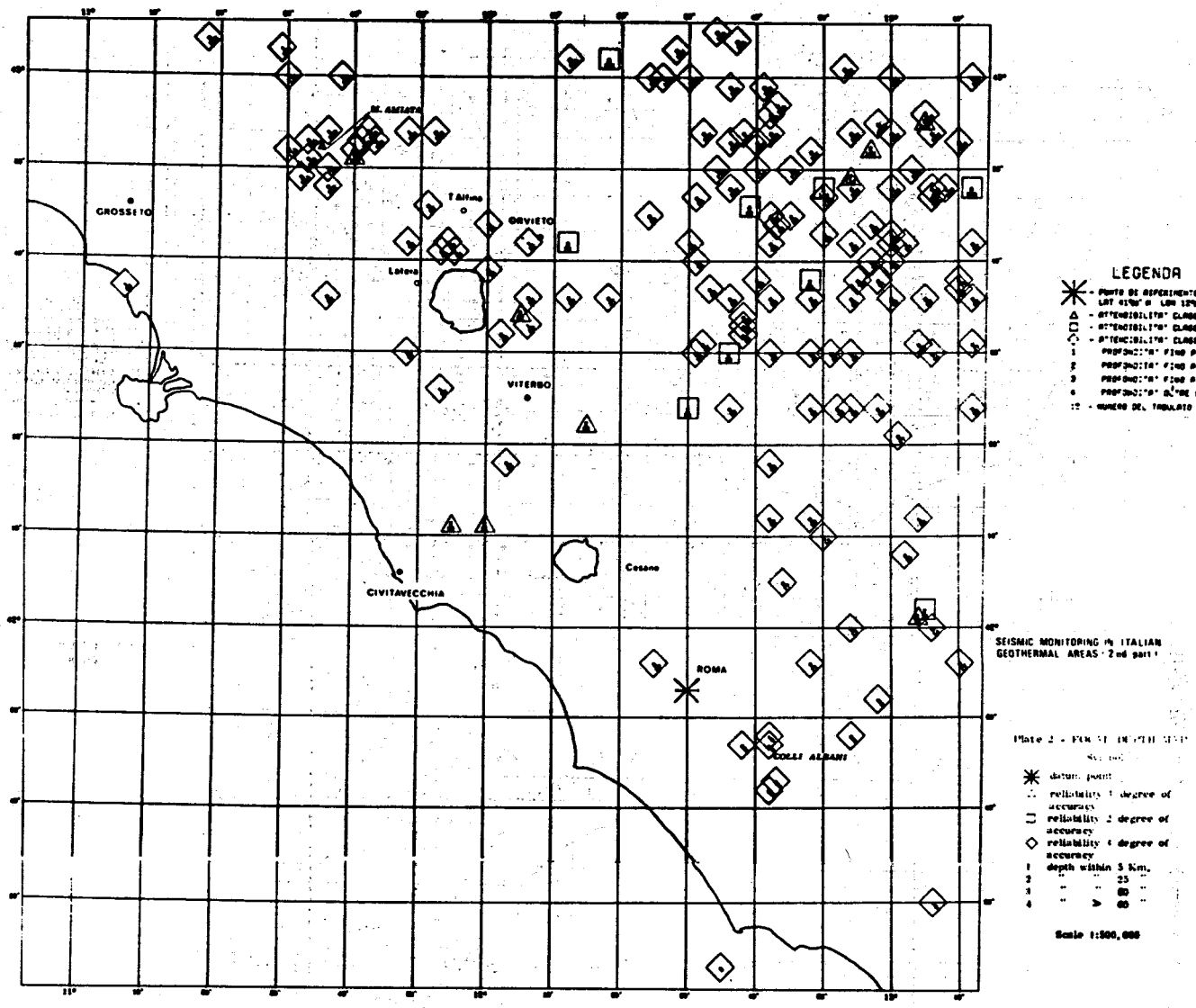

Plate 2. Focal depths.

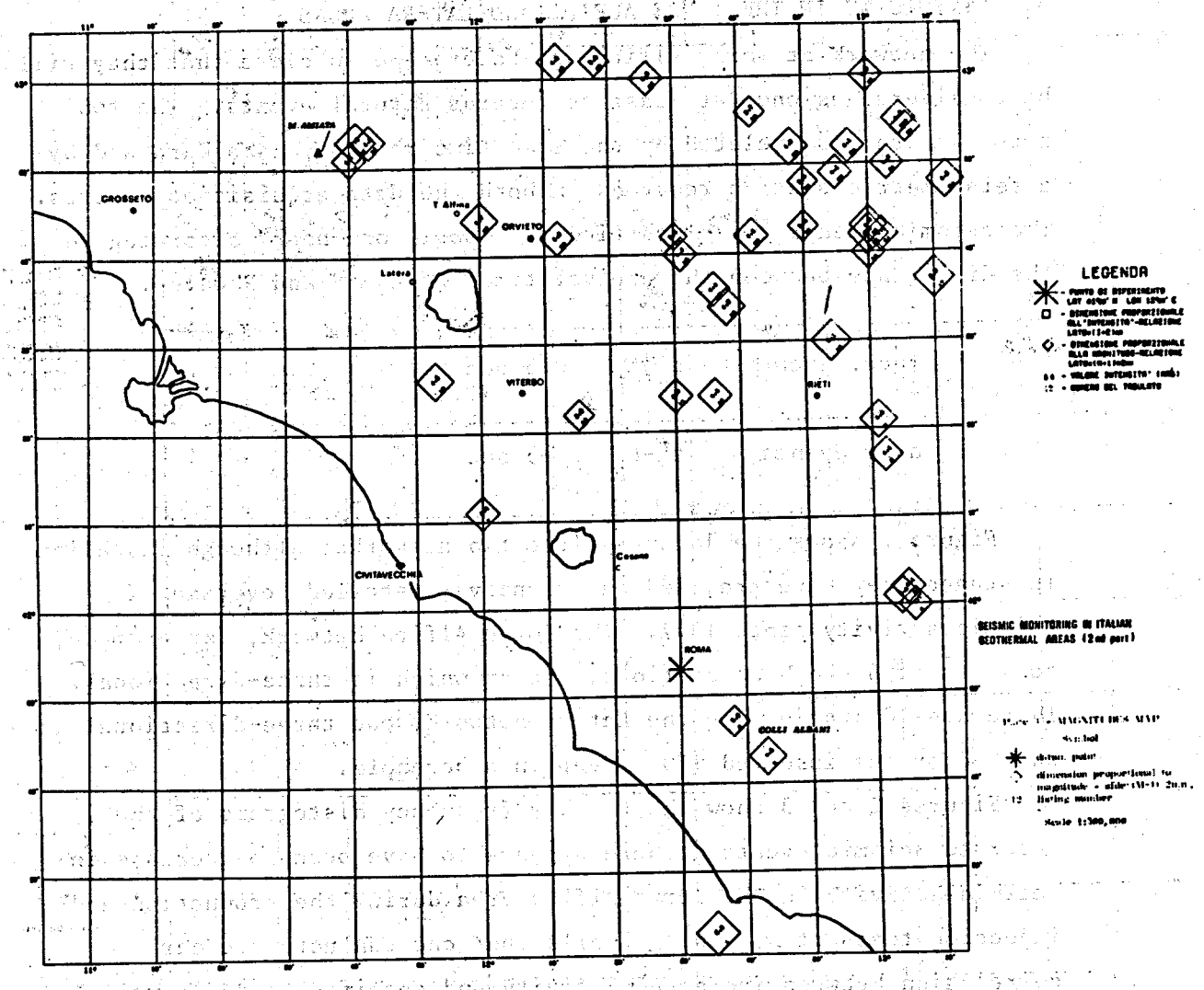

Plate 3. Magnitudes.

3. SEISMICITY IN THE TORRE ALFINA AND LATERA AREAS

The network at Torre Alfina and Latera are so close that they will be considered as one, at least as regards natural events. The two networks are also related by the same time reference standard and by a seismometric station recorded on both the data acquisition centres. The seismic events are classified as "local" or "near" according to the difference between the arrival times of the S and P waves.

local events $t_s - t_p = 0\text{-}3$ sec

near events $t_s - t_p = 3\text{-}5$ sec

Figure 1 shows the layout of the two networks; although installed in stages they have provided an extensive, detailed coverage of seismic activity since 1977. The Torre Alfina network, for example, consists of 6 geophone stations, one of which is three-directional. There are 10 stations on the Latera network, one three-directional and one hydrophone inserted 170 m deep in a borehole.

Figures 2 and 3 show the monthly frequency histograms of the recorded seismic events. There appears to have been no increase in seismic activity in the Torre Alfina area during the production and injection tests at A_{14} and A_4 wells, but one can note a clear correlation between increased activity and specific tests in well L-2 in the Latera area. This aspect will be dealt with later in greater detail.

Not all the recorded events could be processed to determine the focal coordinates as there were some doubts with regard to the first arrivals.

Tables 1 and 2 give the data on the events recorded for the two areas, while Plate 4 presents the distribution of the epicentres, showing magnitude and focal depths projected on a N-S cross-section.

The hypocentres were determined by means of the HYPO 71 computer program, whereas the local magnitude values were calculated with the Cancani-Sieberg equation, valid for Italy:

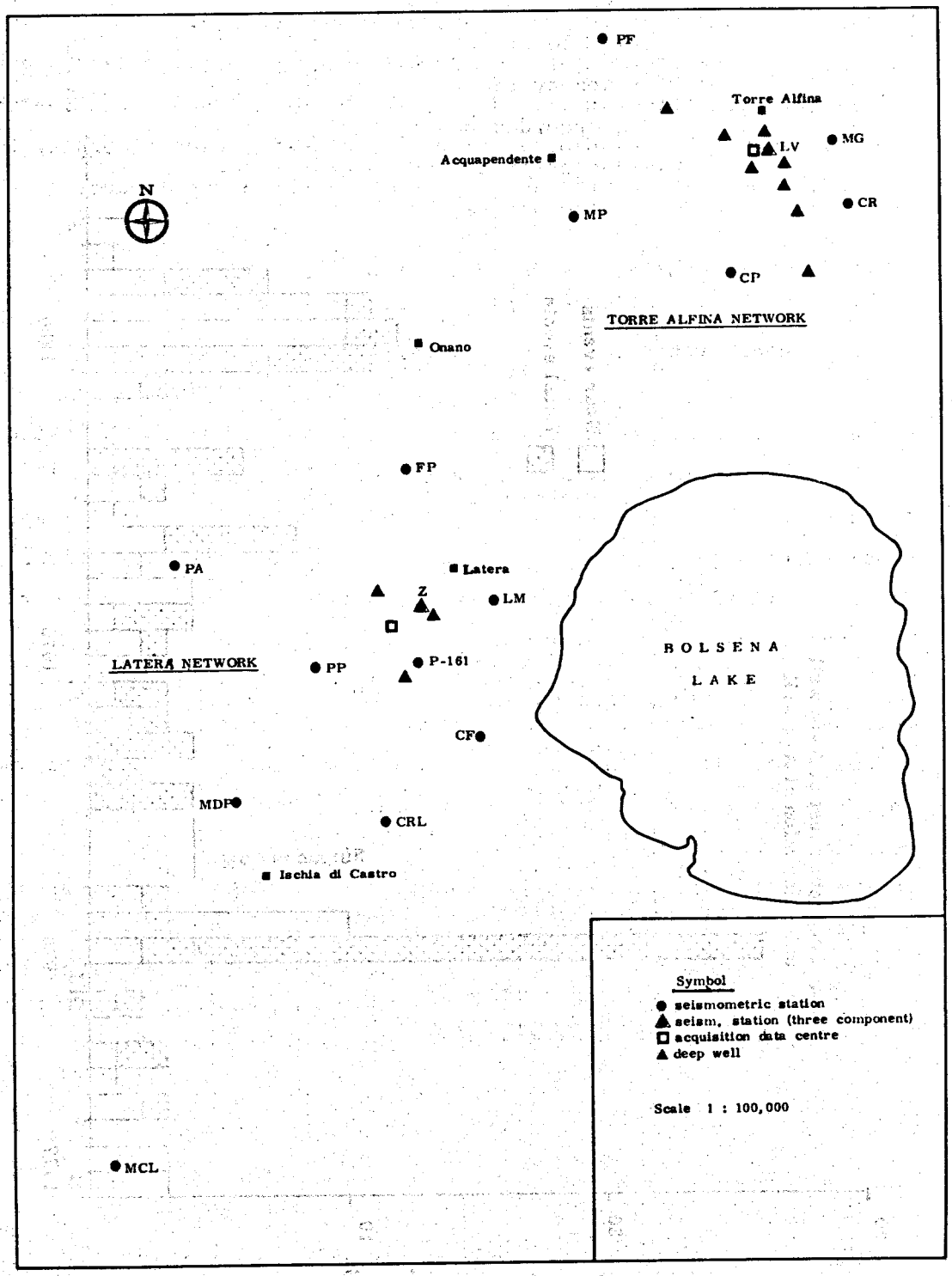

Fig. 1. Torre Alfina and Latera permanent networks.

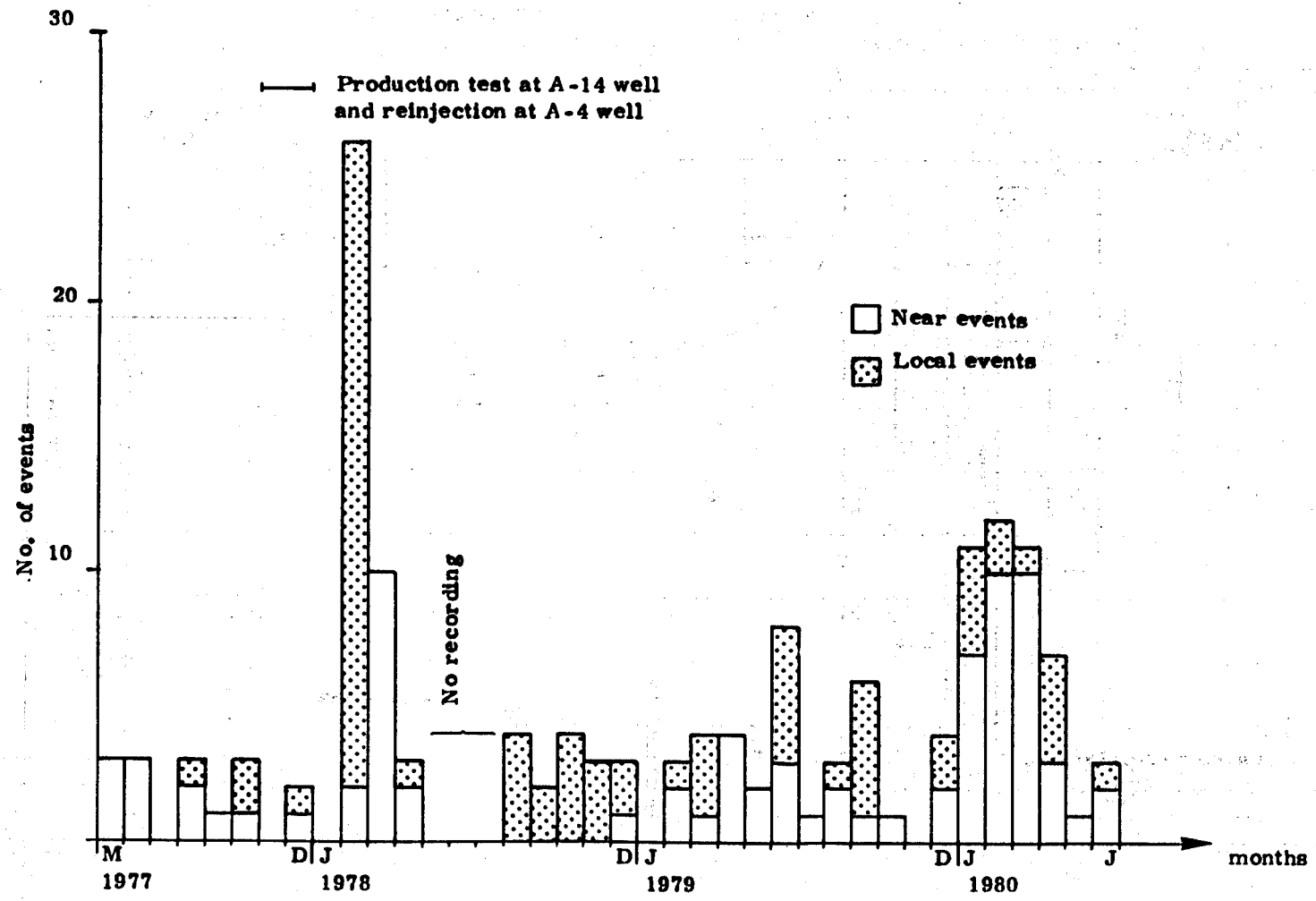

Fig. 2. Torre Alfina area - histogram of seismic events recorded by permanent network.

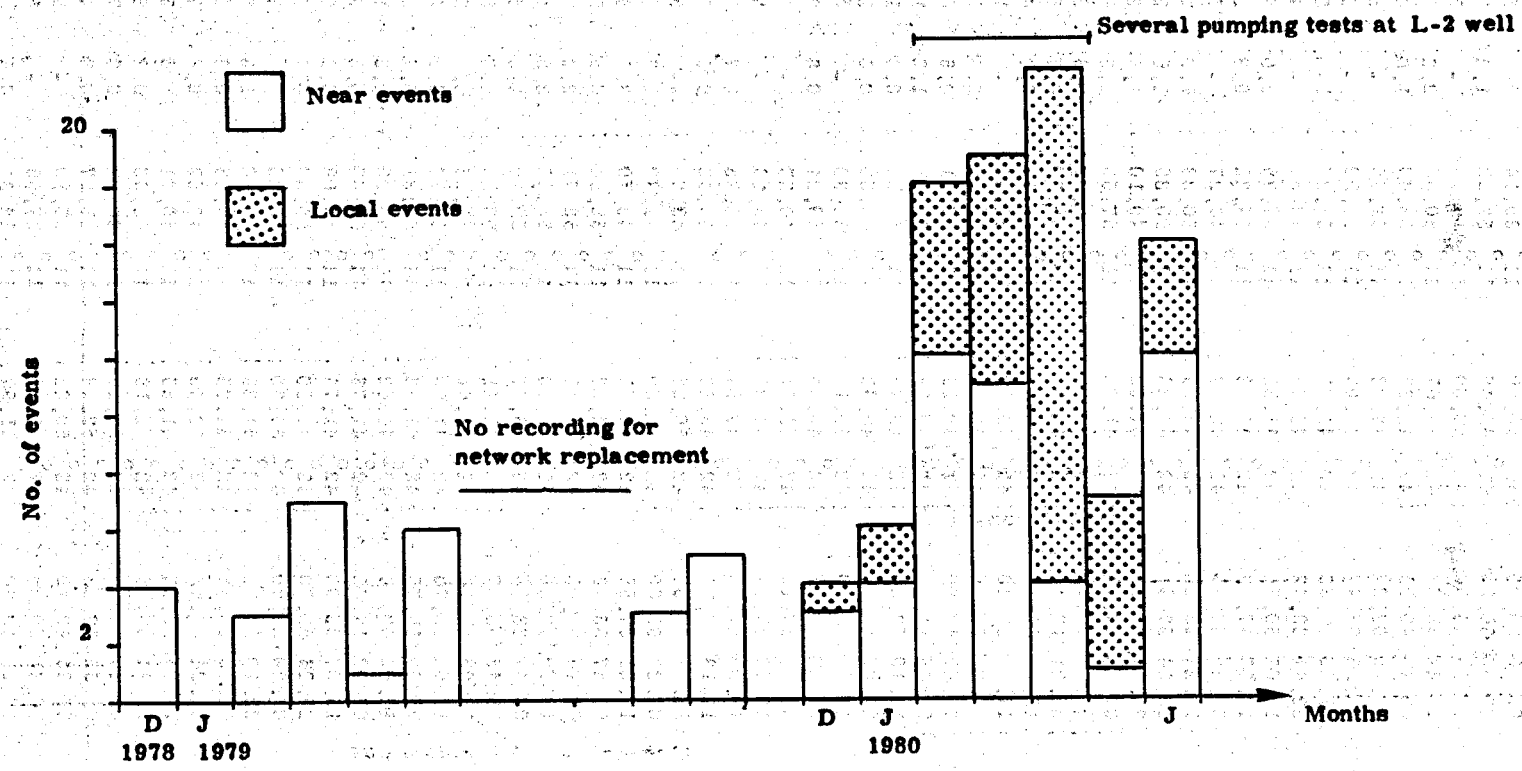

Fig. 3. Latera area - histogram of seismic events recorded by provisional and permanent network.

Table 1. Torre Alfina Earthquakes - Permanent Network.

N°	Date	Origin.	Lat. (N)	Long. (E)	ERH	Z	ERZ	M
11	77.05.25	02.16 20,00	42° 50,00	11° 39,14	-	5,0 *	-	0,0
45	77.08.29	06.30 30,14	42° 48,49	11° 52,62	1,2	2,5	0,1	1,0
55	77.09.21	13.36 45,30	42° 57,00	11° 45,14	-	5,0 *	-	1,4
69	77.10.21	18.44 39,87	42° 43,67	11° 50,66	2,8	3,6	1,5	1,9
81	77.12.06	02.44 40,15	42° 42,38	11° 58,49	1,0	4,5	0,1	0,6
24	78.02.18	01.25 02,82	42° 42,23	11° 51,65	-	5,0	-	1,5
28	78.02.18	01.28 03,47	42° 42,09	11° 51,59	-	5,0	-	2,0
30	78.02.18	01.29 06,65	42° 41,81	11° 51,87	-	5,0	-	2,0
97	78.03.10	22.41 33,42	42° 48,75	11° 42,54	-	4,5	-	-
168	78.04.23	15.07 50,31	42° 41,59	11° 57,35	3,0	4,0	1,7	1,2
230	78.08.05	17.57 47,46	42° 48,43	11° 54,32	0,9	2,9	0,7	0,4
270	78.08.22	21.22 33,29	42° 42,38	11° 47,27	-	5,2	-	0,1
287	78.08.24	13.24 22,32	42° 44,26	11° 50,33	1,9	2,4	0,3	>1,4
288	78.08.24	13.24 57,91	42° 44,36	11° 50,85	1,5	2,7	0,5	0,9
306	78.09.04	20.31 07,84	42° 41,92	11° 49,10	1,4	3,0	0,5	1,7
333	78.09.16	07.23 47,74	42° 41,02	11° 57,63	0,3	6,4	0,4	>1,6
356	78.10.03	02.26 02,79	42° 40,95	11° 55,72	0,6	5,0	0,5	0,2
374	78.10.12	00.21 17,44	42° 40,59	11° 55,89	0,7	5,6	1,0	0,9
378	78.10.15	16.07 36,97	42° 46,71	11° 49,14	0,2	4,1	0,4	>1,6
379	78.10.15	17.47 23,40	42° 46,69	11° 50,43	-	1,2	-	<0,0
416	78.11.10	09.02 26,37	42° 40,91	11° 57,44	0,5	5,5	0,5	>1,6
417	78.11.10	09.02 42,90	42° 40,26	11° 57,91	0,5	6,1	0,6	1,3
423	78.11.14	02.06 11,08	42° 39,38	11° 55,91	1,2	1,6	0,5	0,8
453	78.12.18	11.19 52,30	42° 43,72	11° 57,62	0,8	1,3	0,6	0,3
458	78.12.21	21.02 01,98	42° 45,63	11° 48,59	0,6	2,4	0,2	0,3
467	78.12.27	11.58 04,90	42° 55,15	11° 50,39	-	5,0	-	-
26	79.02.07	11.22 08,27	42° 43,94	11° 59,24	0,8	2,4	0,2	0,4
30	79.02.09	02.29 57,15	42° 55,71	11° 40,55	-	5,0	-	-
46	79.02.28	18.42 29,97	42° 54,33	11° 42,16	-	5,0	-	-
48	79.03.01	12.02 21,73	42° 43,94	11° 58,23	1,7	2,4	2,7	0,4
59	79.03.12	12.13 57,55	42° 43,88	11° 59,42	0,3	2,3	0,0	0,4
62	79.03.14	13.41 37,56	42° 50,26	11° 43,04	-	5,0	-	-
125	79.04.27	07.30 02,60	42° 53,60	11° 41,70	1,5	5,5	0,3	1,1
158	79.05.28	12.21 37,56	42° 51,73	11° 43,70	3,0	6,4	0,7	0,7
169	79.06.01	05.47 38,46	42° 44,27	11° 52,54	0,5	6,0	0,1	1,8
198	79.06.24	02.14 36,06	42° 47,41	11° 58,71	2,2	8,3	1,4	0,7
200	79.06.24	19.29 42,59	42° 48,90	11° 53,55	2,5	1,0	3,0	0,2
202	79.06.25	08.44 38,55	42° 56,77	11° 50,40	1,3	5,0	5,3	1,6
222	79.08.02	06.45 35,97	42° 42,41	11° 58,23	0,2	5,8	0,3	1,8
239	79.09.20	18.03 47,14	42° 41,61	11° 56,35	0,7	2,6	1,0	1,6
240	79.09.20	18.04 22,73	42° 41,63	11° 56,27	0,6	2,9	0,8	0,8
241	79.09.20	18.09 15,75	42° 41,62	11° 56,31	0,7	2,6	1,0	1,0
242	79.09.20	22.09 57,46	42° 41,62	11° 56,29	0,3	1,9	0,6	1,3
243	79.09.23	08.09 19,33	42° 41,76	11° 55,89	0,5	2,6	0,8	1,3
244	79.09.24	15.07 35,39	42° 41,74	11° 56,08	0,2	0,2	0,1	1,1
464	79.12.16	22.26 52,30	42° 41,50	11° 55,89	0,7	5,9	0,8	1,0
467	79.12.17	06.30 33,70	42° 56,39	11° 45,25	-	7,0	-	1,1
505	79.12.25	22.19 13,65	42° 41,88	12° 12,80	1,8	5,5	0,6	0,4
5	80.01.04	02.56 28,35	42° 41,25	11° 46,96	0,3	5,2	0,5	0,9
26	80.01.20	11.24 03,66	42° 52,45	11° 40,92	0,8	7,3	0,5	1,4
27	80.01.20	14.04 13,40	42° 51,86	11° 40,71	1,0	5,0	0,6	1,3
45	80.01.28	11.24 03,66	42° 52,16	11° 48,63	0,8	6,1	0,5	1,7
110	80.03.15	09.25 42,54	42° 52,16	11° 36,02	2,0	7,6	3,3	1,4
119	80.03.16	01.52 46,23	42° 52,18	11° 35,67	0,8	4,4	0,4	1,6
127	80.03.23	07.35 49,49	42° 50,88	11° 37,10	-	5,9	-	0,4
128	80.03.23	10.21 59,98	42° 50,47	11° 37,06	-	5,8	-	1,5
145	80.04.07	19.18 10,30	42° 41,97	11° 58,31	0,6	5,4	0,7	0,9
146	80.04.07	19.32 32,77	42° 41,98	11° 58,64	0,8	5,2	0,9	1,1
152	80.04.19	23.43 25,11	42° 52,12	11° 40,81	1,3	5,0	0,9	0,6
154	80.04.28	20.16 51,12	42° 46,13	11° 50,18	-	1,3	-	0,8
155	80.04.30	00.53 07,99	42° 50,93	11° 40,34	0,1	6,2	0,8	1,6
167	80.06.02	15.46 09,01	42° 51,13	11° 41,24	2,0	5,0	0,9	1,5

* indicates fixed focal depth solution

Table 2. Latera Earthquakes - Permanent Network.

N°	Date	Origin.		Lat. (N)		Long. (E)		ERH	Z	ERZ	M
13	78.12.12	06.33	29,81	42°	28,11	11°	34,76	8,9	5,0	12,4	1,5
14	78.12.12	06.39	39,96	42°	24,13	11°	35,38	9,8	5,0	14,6	1,5
29	79.02.28	18.42	11,78	42°	53,80	11°	46,10	3,8	5,0	33,9	1,3
31	79.03.02	01.17	59,40	42°	37,99	12°	01,04	2,5	5,3	10,0	0,6
51	79.03.18	12.24	50,46	42°	40,09	11°	58,50	2,4	5,0	6,3	1,3
148	79.05.26	11.20	54,27	42°	31,85	11°	47,26	3,2	5,0	50,5	0,6
155	79.05.28	12.21	55,49	42°	51,23	11°	44,94	1,6	5,0	15,7	0,9
171	79.12.10	23.52	15,76	42°	39,90	11°	44,89	1,0	2,0	4,0	1,6
1	80.01.04	02.56	28,35	42°	41,25	11°	46,96	0,3	5,2	0,5	0,9
40	80.02.20	09.03	37,83	42°	31,99	11°	42,22	1,4	5,0	2,4	1,2
42	80.02.22	23.02	21,12	42°	31,85	11°	42,65	1,3	5,0	2,5	1,7
43	80.02.23	03.00	49,60	42°	32,03	11°	42,42	2,3	5,0	2,8	0,9
44	80.02.23	05.33	53,22	42°	31,97	11°	42,60	2,6	5,0	3,2	0,9
87	80.03.15	11.24	04,27	42°	36,66	11°	49,09	-	0,9	-	1,5
88	80.03.15	12.15	26,14	42°	36,75	11°	49,07	0,3	0,8	0,2	1,8
89	80.03.15	13.59	41,14	42°	36,82	11°	49,09	-	1,2	-	1,7
110	80.03.30	08.00	49,67	42°	36,73	11°	49,08	-	1,2	-	1,7
112	80.04.04	20.23	20,68	42°	36,66	11°	49,07	-	1,0	-	1,6
116	80.04.07	09.38	44,08	42°	37,37	11°	49,49	0,4	2,3	0,7	1,6
117	80.04.07	09.39	31,12	42°	37,41	11°	49,52	0,3	2,2	0,5	1,7
118	80.04.07	09.39	52,22	42°	37,35	11°	49,44	1,1	1,7	1,8	1,7
119	80.04.07	09.40	35,53	42°	37,56	11°	49,58	0,4	3,6	0,7	1,7
120	80.04.07	09.41	16,18	42°	37,30	11°	49,84	-	3,0	-	1,7
125	80.04.09	00.39	11,87	42°	37,32	11°	49,82	-	2,7	-	1,3
130	80.04.12	17.02	31,45	42°	36,80	11°	49,34	-	1,0	-	1,8
131	80.04.14	20.44	55,74	42°	48,15	11°	39,53	1,7	5,0	0,8	1,4
132	80.04.15	21.27	05,77	42°	36,72	11°	49,03	-	1,0	-	1,9
133	80.04.15	21.37	35,07	42°	38,84	11°	48,82	0,3	0,9	0,2	1,8
135	80.04.16	03.32	31,66	42°	36,73	11°	49,05	0,3	0,9	0,2	1,8
144	80.05.04	05.16	20,03	42°	32,86	11°	45,30	0,3	5,8	0,4	1,3
146	80.05.05	01.36	04,56	42°	32,13	11°	43,50	0,4	5,0	0,9	1,2
148	80.05.08	23.07	32,09	48°	32,85	11°	45,32	0,4	6,0	0,4	1,7
149	80.05.09	04.54	24,71	42°	32,94	11°	44,71	0,7	5,9	0,5	1,8
205	80.06.27	22.41	05,20	42°	41,45	11°	55,65	0,4	3,8	0,7	0,6

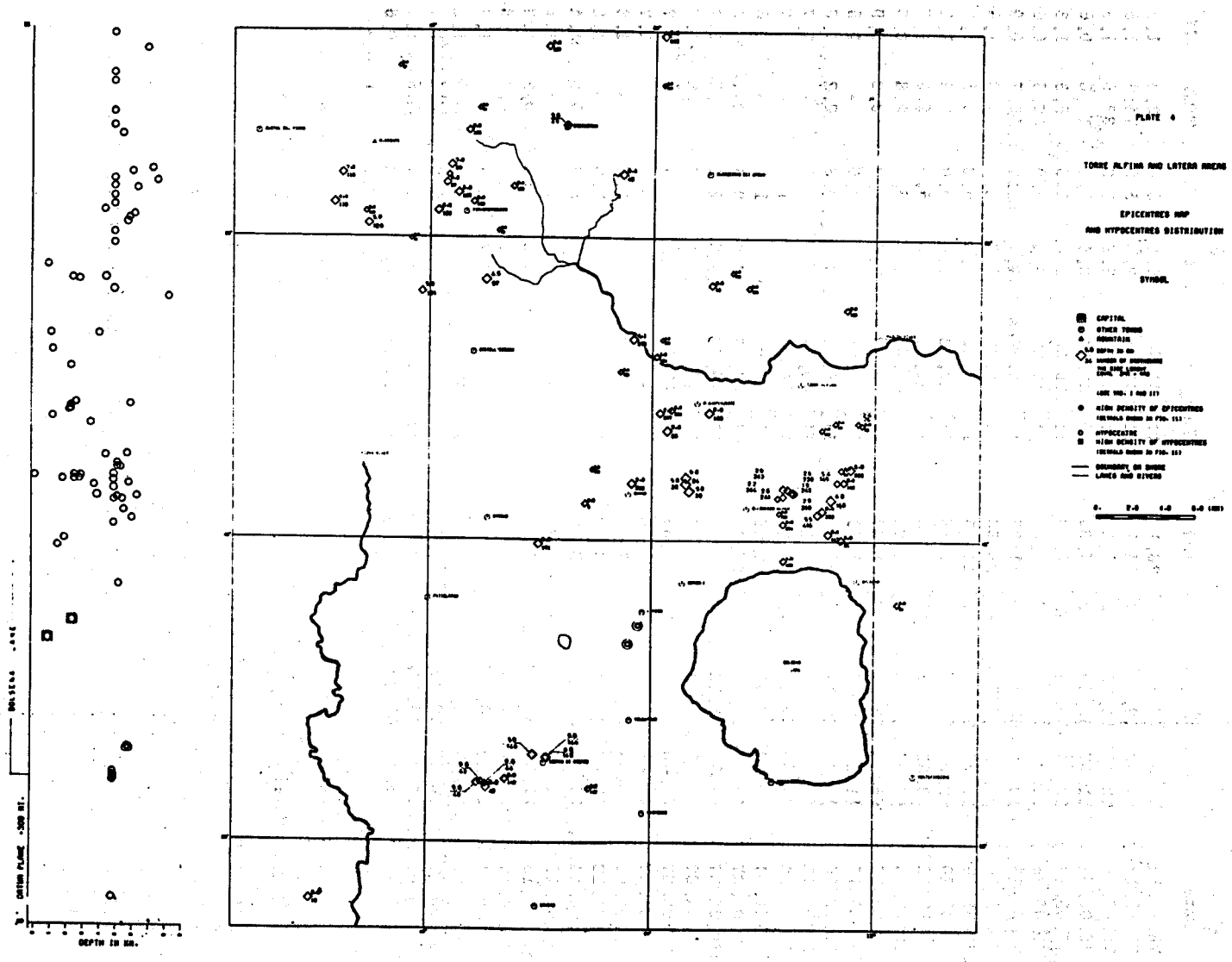

Plate 4. Distribution of epicentres, with magnitude and focal depths projected on N-S cross-section, for Torre Alfina and Latera areas.

$$M = 0.481\ I + 1.407, \text{ for } I\ VII \text{ degree}$$

where $I = 3\ (\log a + 1)$ with a = acceleration.

The thickness and velocity of the geoseismic model used in the hypocentre calculations were obtained from available geological and geophysical data. The delay times at the stations were obtained experimentally, using some events occurring relatively near the networks and having known epicentres.

The models used were:

Torre Alfina			Latera		
Layer	Velocity (km/s)	Thickness	Layer	Velocity (km/s)	Thickness
1°	3.0	1.1	1°	2.5	0.165
2°	5.5	1.9	2°	3.4	0.465
3°	6.0		3°	4.0	1.015
			4°	5.3	7.000
			5°	6.2	

The events recorded on both networks referred to the Latera model only, recalculating the delay-times for the Torre Alfina stations.

The epicentral distribution shown in Plate 4 confirms the existence of many historically known seismic centres, such as Castel Giorgio, San Lorenzo, Onano, Aquapendente, Latera, Ischia di Castro and, further north, the Mt. Amiata region. A certain diffuse activity was noted immediately north-west of the Torre Alfina network and, on a much smaller scale, north-east of Bolsena Lake and south of the Latera network.

The magnitude values are generally low, ranging around an average of 1.5. The cross-section reveals that, as far as focal depth is concerned, these events are nearly all quite shallow, ranging between 0 and about 6 km.

3.1 Torre Alfina - Induced Seismicity?

Before the permanent network was installed the seismic activity was monitored between 21st January and 19th March 1977 on a temporary network, during a series of reinjection tests in well RA-1.

Figure 4 shows the daily distribution of events throughout the period in which this network was in operation. An increase in seismic activity is clearly correlated to the two periods of reinjection tests. Figures 5 and 6 give a detailed picture of hourly distribution of these events during these two periods versus the maxima recorded values for ground movements (μ/sec), correlated with the pressure variation curve recorded at well-head and the flow-rate values of the injected water. In both cases the major density of seismic events occurs in correspondence to the highest pressure values, and affecting the pressure curve, flattening it slightly during both the pumping and the pressure re-establishment.

A total of 177 events were recorded, all being identified as seismic signals; the hypocentral coordinates were attainable for 15 of these, as reported in Table 3. Figure 7 shows the epicentral position for the latter, along with the magnitude values, the hypocentral distribution projected on a N-S profile, and the provisional network configuration. Note that the network had only 4 stations, 3 of which were three-directional and very close to one another. They were also rather off-centre with respect to the well and the calculated epicentres.

Nevertheless, it was possible to define the epicentral coordinates with a certain accuracy and, with a little less precision, the depth values; the data were processed with no surface corrections, using the single Torre Alfina - Latera model and the S phase. As the events in most cases saturated all the stations, the maxima of the magnitude values are not always defined.

One can note the following:

a) the distribution of the epicentres around the well;

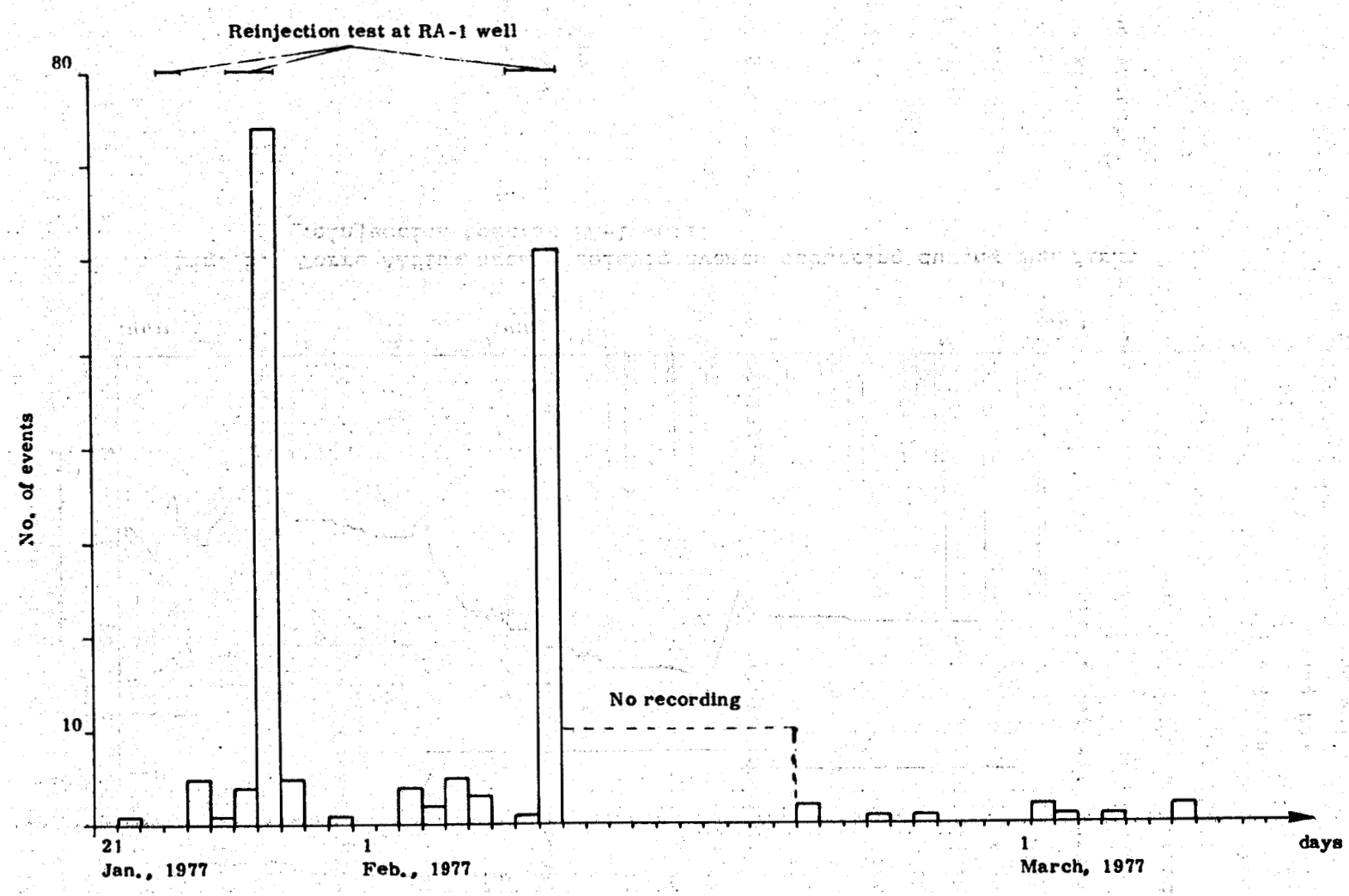

Fig. 4. Torre Alfina area - histogram of seismic events recorded by provisional network during some reinjection tests at RA-1 well.

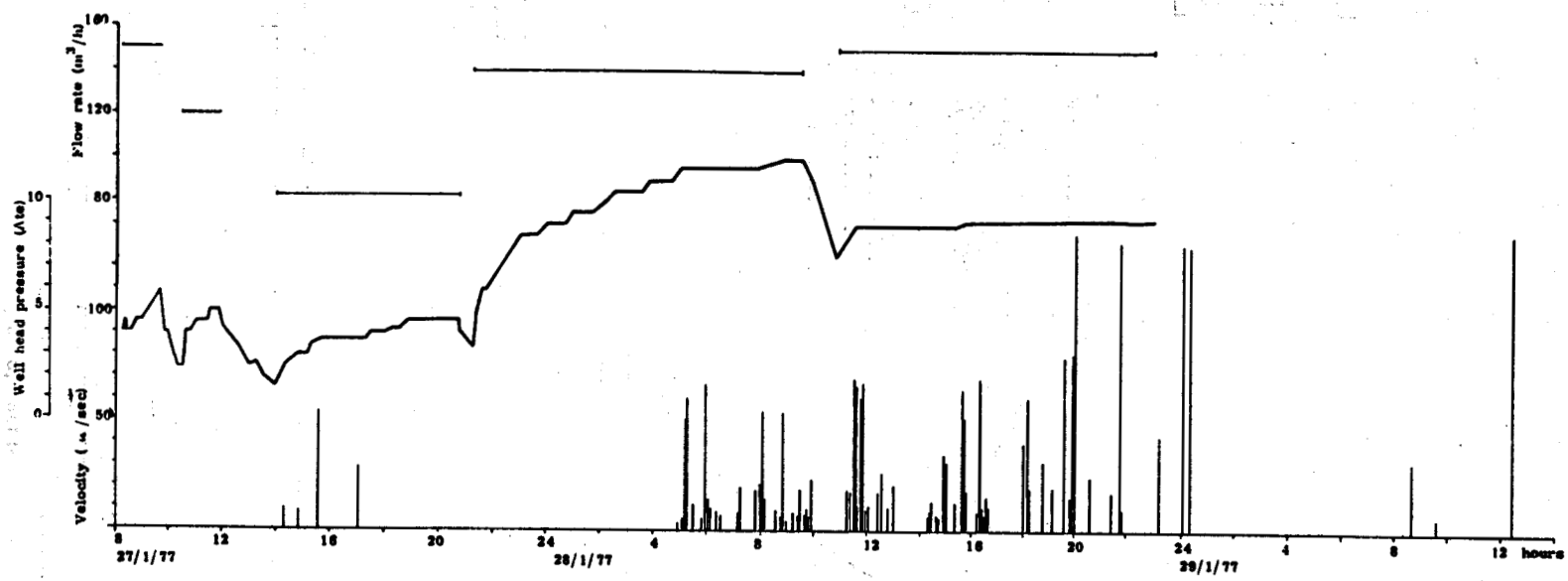

Fig. 5. Torre Alfina area - seismic events occurring during the first reinjection test at RA-1 well.

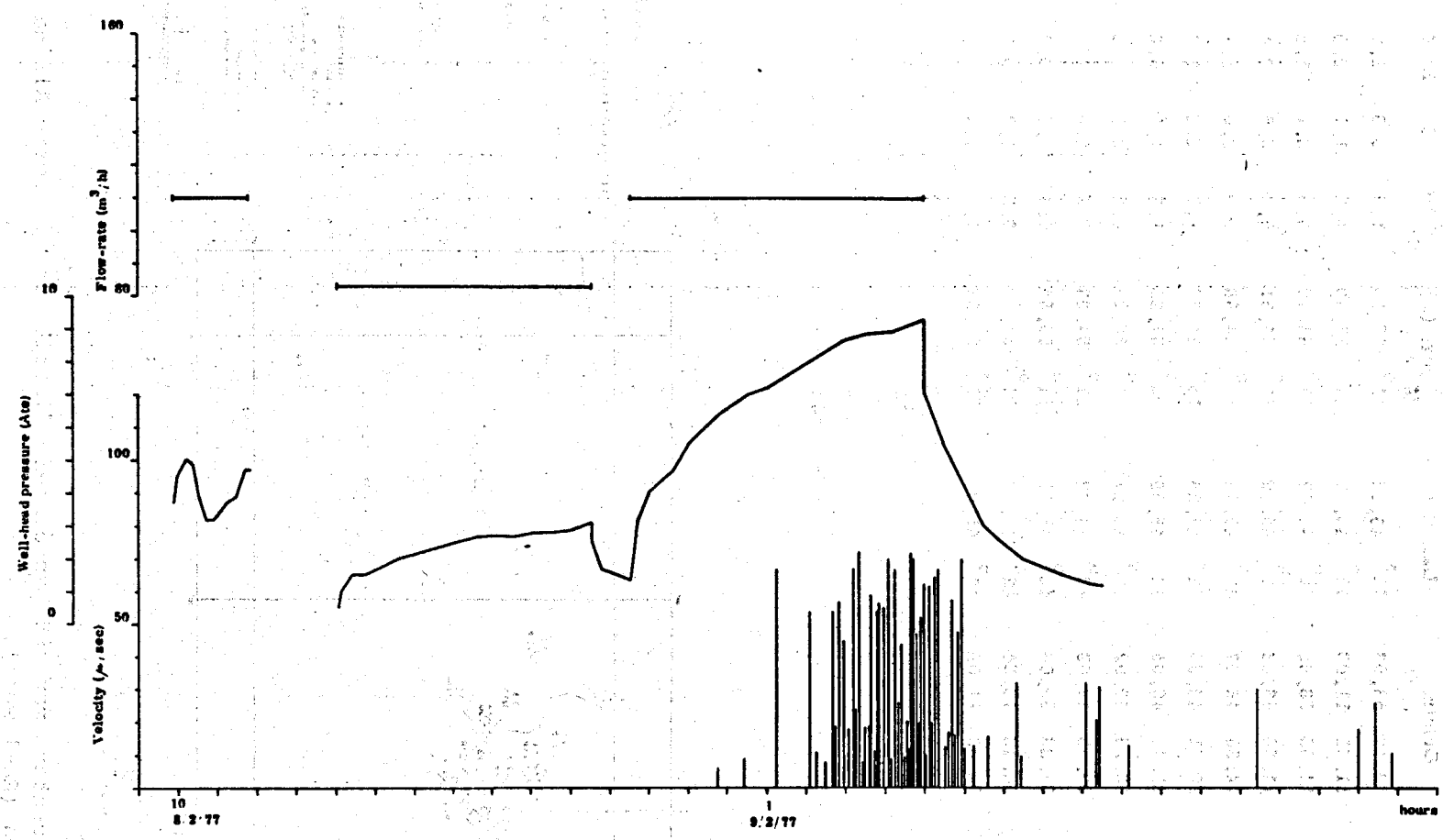

Fig. 6. Torre Alfina area - seismic events occurring during the second reinjection test at RA-1 well.

Table 3. Torre Alfina Earthquakes during Reinjection Test at RA1 Well.

N°	Date	Origin.		Lat. (N)		Long. (E)		ERH	Z	ERZ	M
39/P	77.01.27	09.47	58,98	42°	45,32	11°	55,19	1,8	3,3	1,7	1,1
43/P	77.01.27	11.31	11,00	42°	45,57	11°	54,69	1,2	1,1	9,0	>2,6
44/P	77.01.27	11.35	58,98	42°	45,62	11°	54,70	0,9	2,1	1,8	>2,6
48/P	77.01.27	11.68	46,83	42°	45,59	11°	54,51	0,3	3,6	0,4	1,4
59/P	77.01.27	14.58	46,97	42°	45,42	11°	54,68	0,9	2,6	1,4	2,0
80/P	77.01.27	20.01	45,96	42°	45,25	11°	54,35	1,1	2,2	2,3	>3,0
83/P	77.01.27	21.43	46,95	42°	45,39	11°	54,25	1,2	1,5	6,0	>3,0
119/P	77.02.08	03.23	59,02	42°	45,27	11°	55,04	0,3	3,1	0,2	>2,6
127/P	77.02.08	03.55	47,03	42°	45,32	11°	54,97	0,5	2,8	0,6	2,4
132/P	77.02.08	04.23	59,06	42°	45,61	11°	55,56	0,4	2,9	0,4	2,1
137/P	77.02.08	04.40	46,94	42°	45,23	11°	54,72	0,2	3,3	0,3	>2,5
138/P	77.02.08	04.43	11,09	42°	45,05	11°	54,63	1,0	1,4	4,3	>2,6

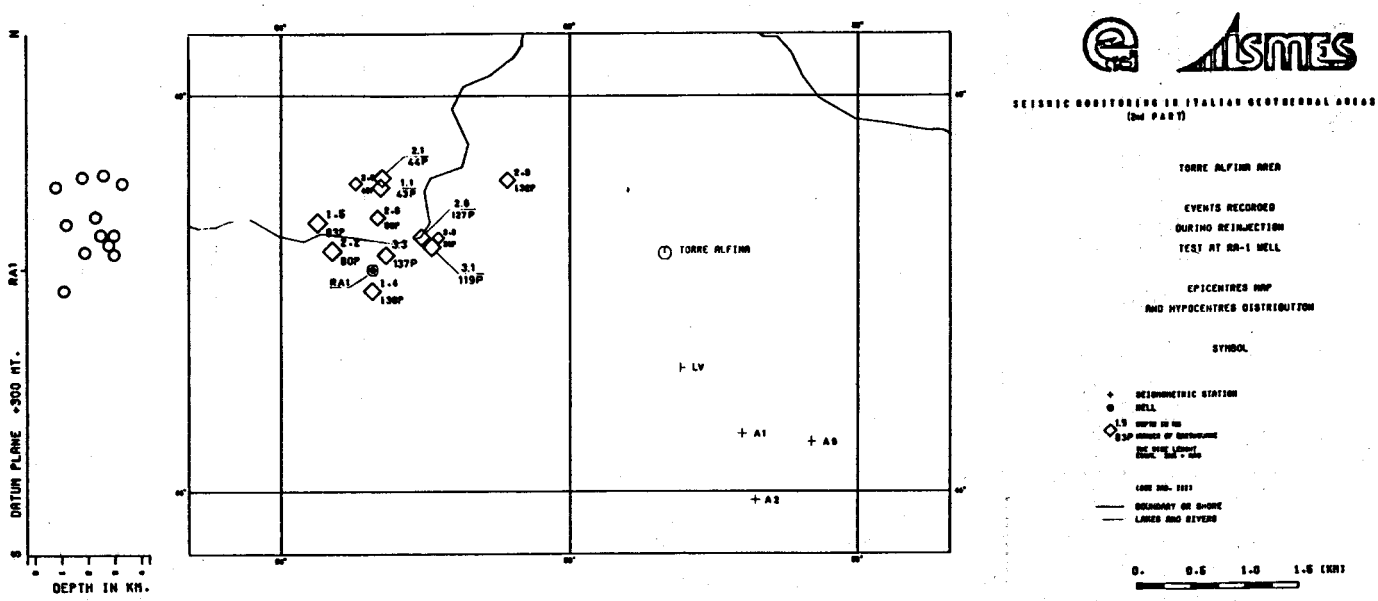

Fig. 7. Epicenters map and hypocenters distribution in Torre Alfina area (RA-1 well).

b) the order of magnitude of the focal depths near the in-hole fractures (2000 m b.s.l.);

c) the maximum magnitude values above even 3.

3.2 Latera - Induced Seismicity?

As mentioned earlier, in reference to Fig. 3, the maximum seismic activity in the Latera area was recorded in well L-2 in March and April 1980, during a series of pumping operations to recover lost equipment.

Figure 8 shows the daily frequency of these seismic events in relation to the cumulative quantities of water injected into the bore. It was impossible to monitor the well-head pressure trend during pumping, except for the initial phase and immediately after operations ended. Figures 9 and 10 give a detailed picture of the events triggered in these two periods, correlating the maximum movement values (μ/sec) with the curve of pressure variation.

These three figures show that an increase in the major seismic activity is connected with the increases in injected volumes of water. In Figs. 9 and 10 in particular the occurrence of the seismic events is clearly accompanied by a flattening of the pressure curve.

Throughout the monitoring period 24 events were recorded, for 15 of which it was possible to determine the focal coordinates (see Table 4). Figure 11 represents the epicentral distribution, with the magnitude values and the hypocentral distribution projected onto a N-S cross-section. This figure indicates that:

a) all the events lie along a NE-SW alignment passing through well L-2;

b) the magnitude values range between 1.5 and 2;

c) the events can be grouped into two well-defined areas of differing focal depth; the first is right next to the well, with a depth of less than 1 km and the second further away with a maximum depth of 2 km.

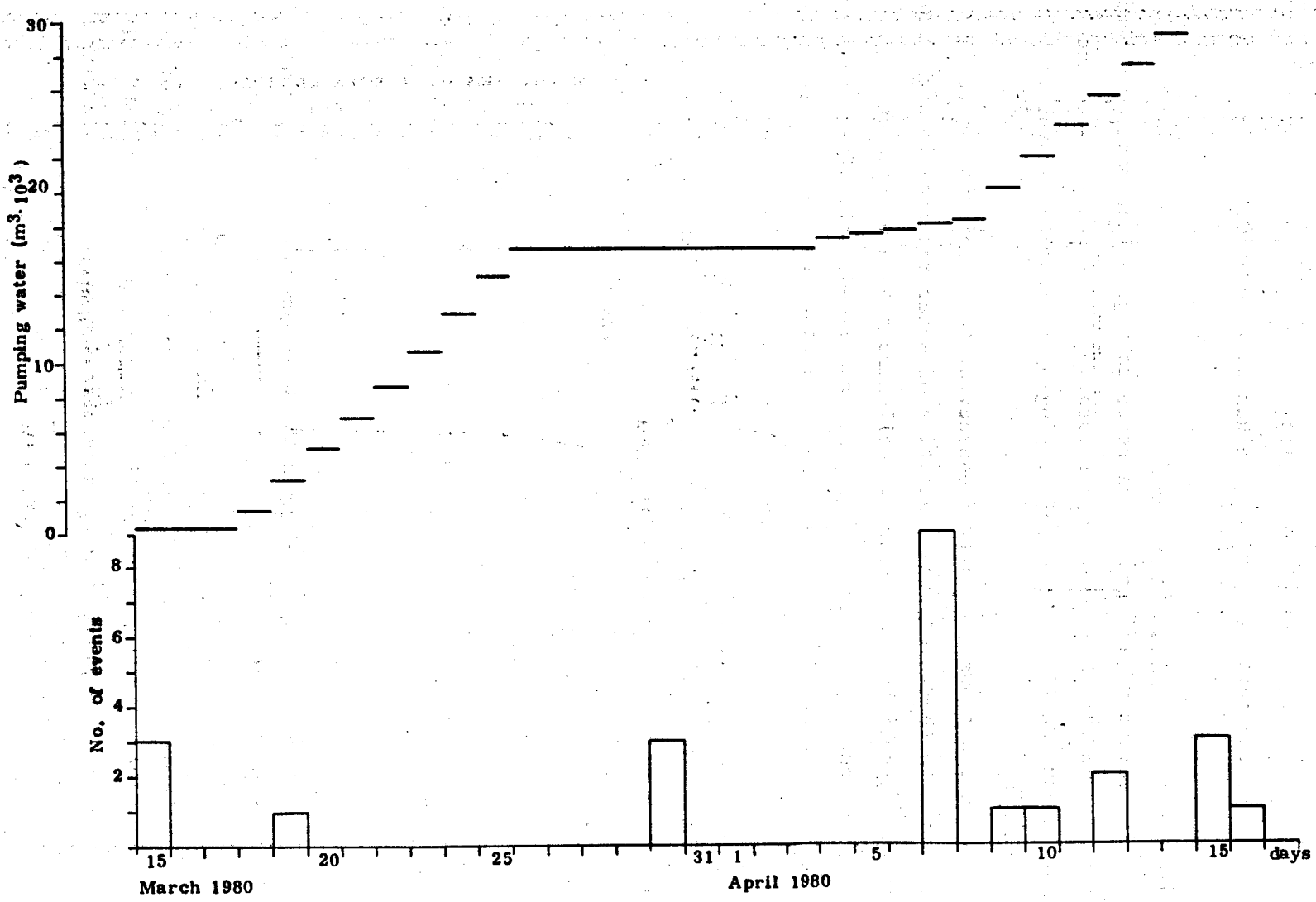

Fig. 8. Latera area - histogram of seismic events recorded by permanent network during pumping operations at L-2 well.

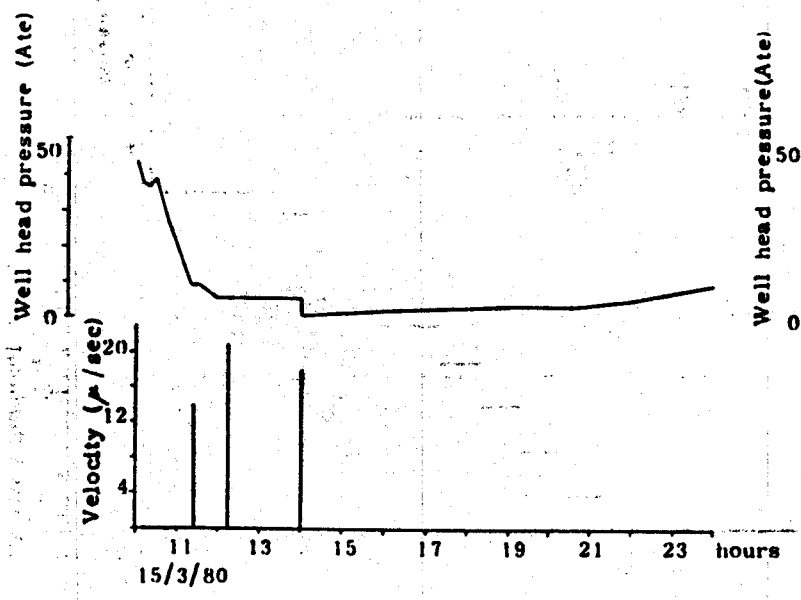

Fig. 9. Latera area - seismic events occuring during the first reinjection phase at L-2 well. (Average flow rate was 100 m^3/h.)

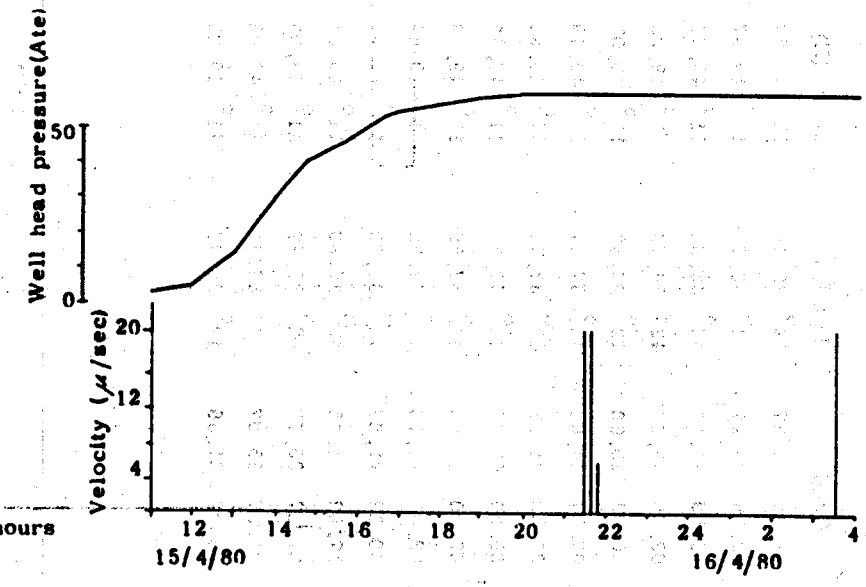

Fig. 10. Latera area - seismic events occurring after shut-in of L-2 well.

Table 4. Latera Earthquakes during Pumping Test at L2 Well.

N°	Date	Origin.	Lat. (N)	Long. (E)	ERH	Z	ERZ	M
87	80.03.15	11.24 04,27	42° 36,66	11° 49,09	-	0,9	-	1,5
88	80.03.15	12.15 26,14	42° 36,75	11° 49,07	0,3	0,8	0,2	1,8
89	80.03.15	13.59 41,14	42° 36,82	11° 49,09	-	1,2	-	1,7
110	80.03.30	08.00 49,67	42° 36,73	11° 49,08	-	1,2	-	1,7
112	80.04.04	20.23 20,68	42° 36,56	11° 49,07	-	1,0	-	1,6
116	80.04.07	09.38 44,08	42° 37,37	11° 49,49	0,4	2,3	0,7	1,6
117	80.04.07	09.39 31,12	42° 37,41	11° 49,52	0,3	2,2	0,5	1,7
118	80.04.07	09.39 52,22	42° 37,35	11° 49,44	1,1	1,7	1,8	1,7
119	80.04.07	09.40 35,53	42° 37,56	11° 49,58	0,4	3,6	0,7	1,7
120	80.04.07	09.41 16,18	42° 37,30	11° 49,84	-	3,0	-	1,7
125	80.04.09	00.39 11,87	42° 37,32	11° 49,82	-	2,7	-	1,3
130	80.04.12	17.02 31,45	42° 36,80	11° 49,34	-	1,0	-	1,8
132	80.04.15	21.27 05,77	42° 36,72	11° 49,03	-	1,0	-	1,9
133	80.04.15	21.37 35,07	42° 38,84	11° 48,82	0,3	0,9	0,2	1,8
135	80.04.16	03.32 31,66	42° 36,73	11° 49,05	0,3	0,9	0,2	1,8

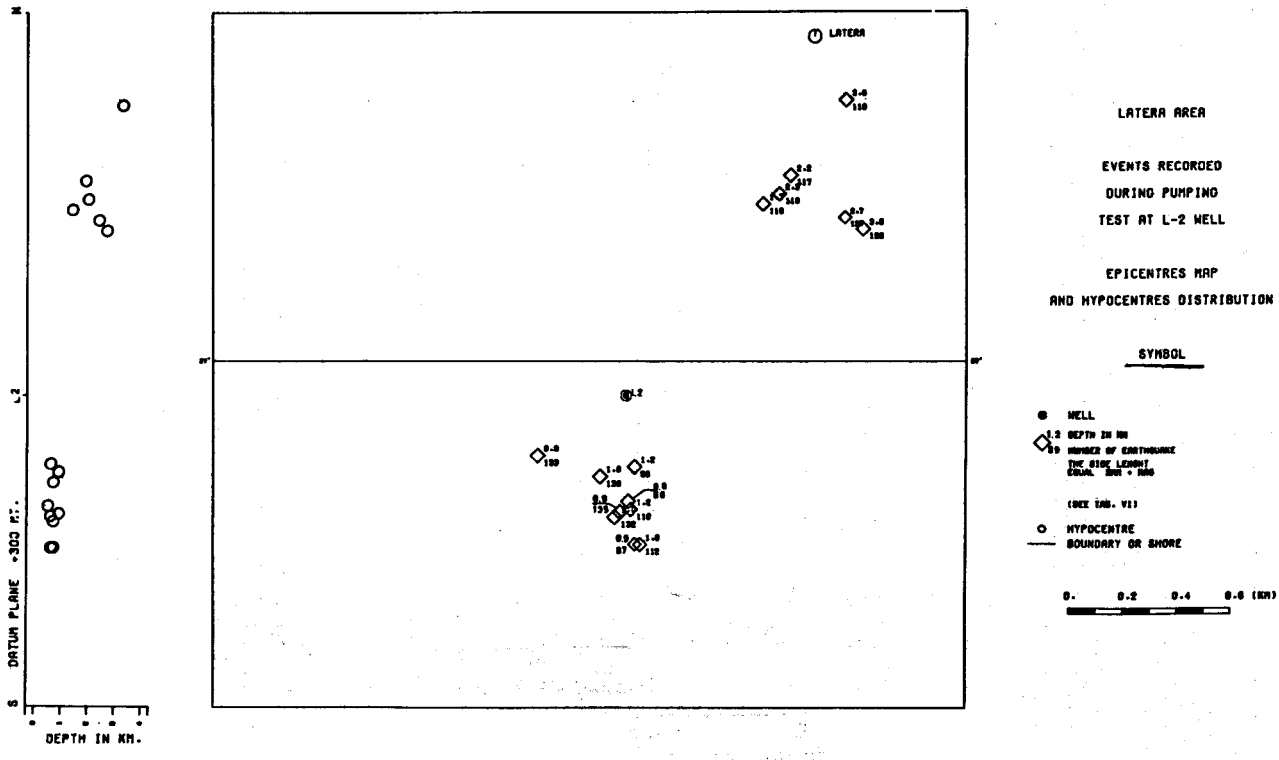

Fig. 11. Latera area - events recorded during pumping test at L-2 well.

4. SEISMIC ACTIVITY AT CESANO

The seismic activity in Cesano area was monitored in two separate phases and on two different networks.

During the first phase, between 5th May and 6th June 1978, a provisional network was used, with 5 seismometric stations connected by cable to the data acquisition centre. This network was installed very near well RC-1 during a series of reinjection tests.

Since 9th March 1979, a permanent telemetered network has been in operation consisting of 7 seismometric stations including one three-component.

4.1 Cesano - Induced Seismicity?

Figure 12 shows the daily frequency of events during operation of the provisional network. The seismic activity clearly intensifies during three periods of injection tests. The triggering of these events during these three periods is shown in Figs. 13 and 14, with the maximum ground movement values (μ/sec) correlated with the curve of pressure variation at well-head.

In the first case (period from 9 to 10 May 1978) the seismic events can be correlated with a certain pressure threshold, while in the second phase the greatest concentration of seismic events occurs during a gradual increase in pressure, about 24 hours after injection began.

Throughout the period a total of 36 seismic events were recorded; the epicentres were determined for 11 of these, as shown in Table 5. This being a densely populated area with a strong background noise of artificial origin during the daytime period, it was somewhat difficult to obtain an accurate estimate of the first arrivals of the P wave, in at least 4 stations. The epicentral coordinates were therefore obtained by a series of calculations, assuming as a fixed hypocentral depth the absorption depth in the well of the injected water.

The geoseismic model used, relative to a depth of 200 m b.s.l., is as follows:

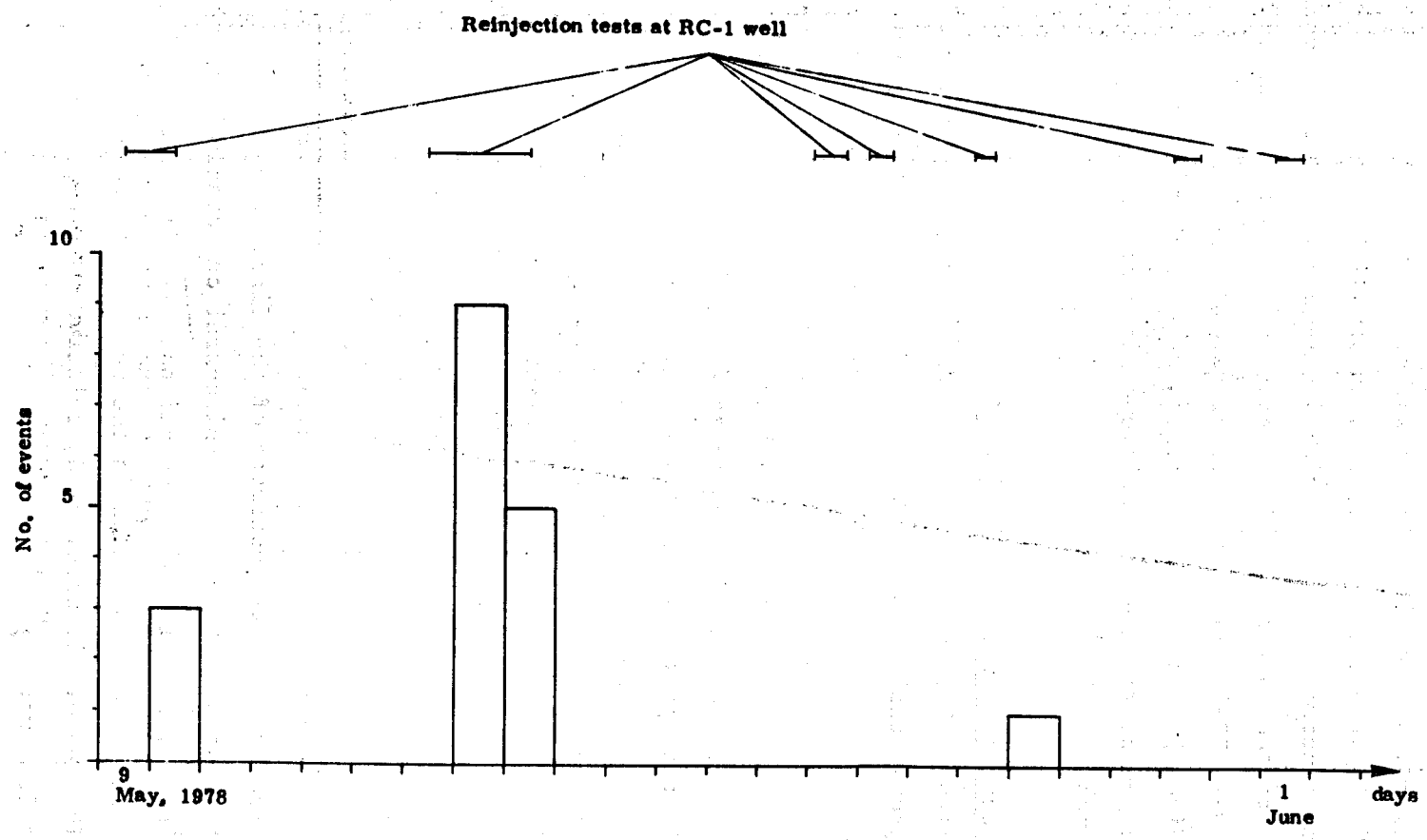

Fig. 12. Cesano area - histogram of seismic events recorded by provisional network during several reinjection tests at RC-1 well.

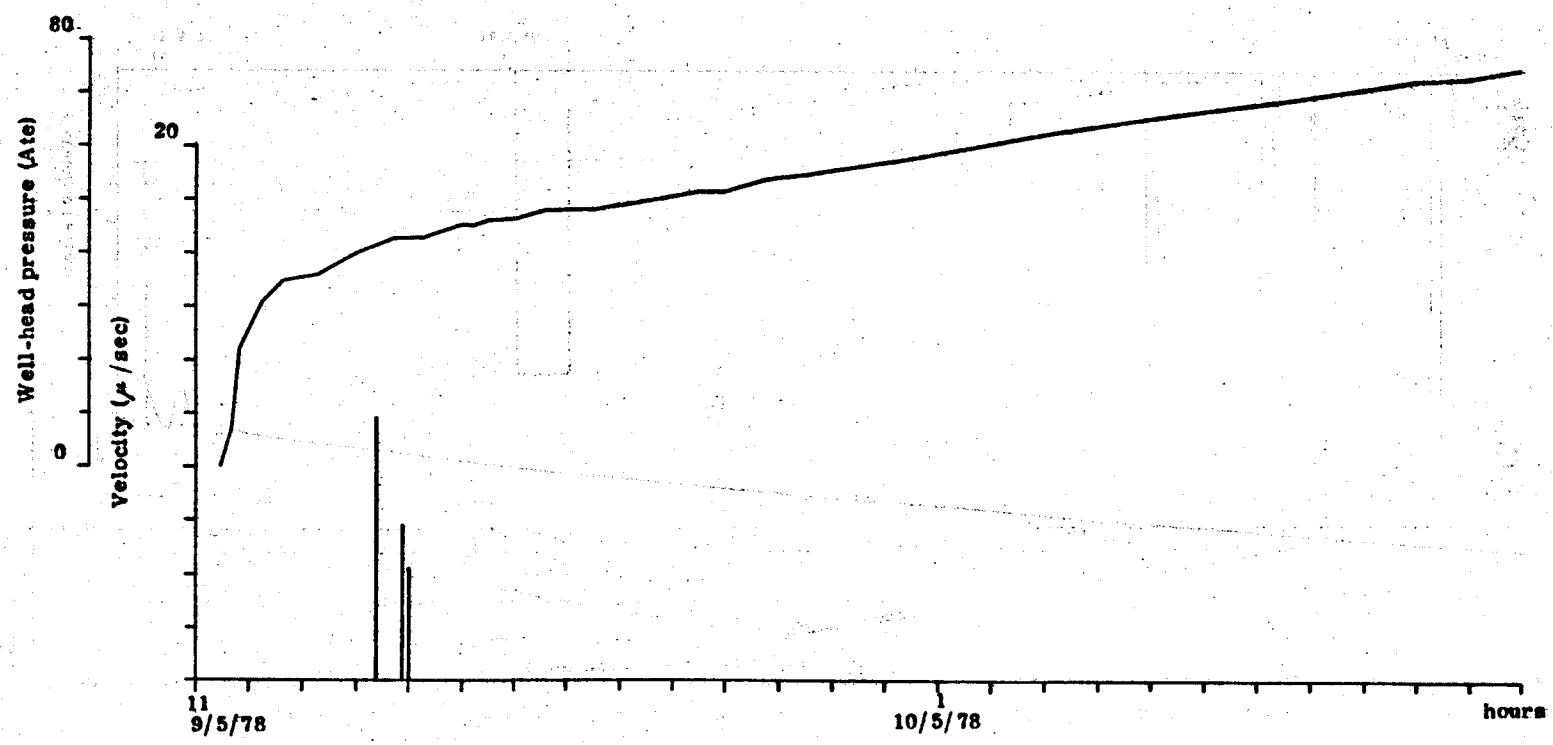

Fig. 13. Cesano area - seismic evnts occurring during first reinjection test at RC-1 well. (Average flow-rate was 100 m^3/h).

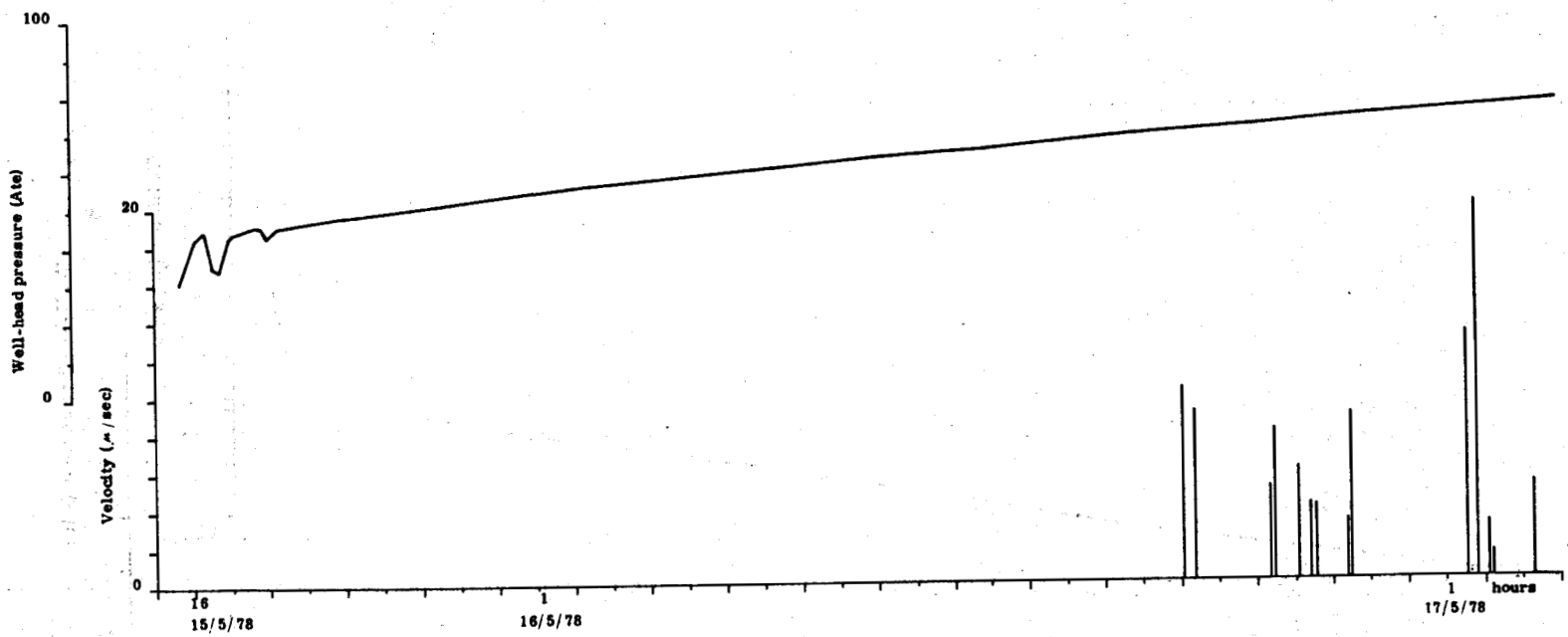

Fig. 14. Cesano area - seismic events occurring during second reinjection test at RC-1 well. (Average flow-rate was 55 m^3/h).

Table 5. Cesano Earthquakes during Reinjection Test at RC1 Well.

N°	Date	Origin.		Lat. (N)		Long. (E)		ERH	Z	ERZ	M
3	78.05.10	14.22	01,18	42°	06,57	12°	22,76	1,7	1,5*	1,9	1,6
5	78.05.10	14.58	59,98	42°	06,63	12°	22,57	-	1,5*	-	1,1
14	78.05.16	18.03	00,06	42°	06,57	12°	22,96	-	1,5*	-	1,8
15	78.05.16	18.22	00,44	42°	06,67	12°	22,57	1,7	1,5*	2,2	1,5
17	78.05.16	20.27	00,55	42°	06,61	12°	22,59	-	1,5*	-	1,5
18	78.05.16	21.05	00,33	42°	06,64	12°	22,76	0,3	1,5*	0,3	1,2
21	78.05.16	22.24	00,11	42°	06,70	12°	22,53	-	1,5*	-	0,9
22	78.05.17	22.28	00,55	42°	06,59	12°	22,54	0,0	1,5*	0,0	1,5
23	78.05.17	01.40	00,38	42°	06,69	12°	22,64	-	1,5*	-	1,8
24	78.05.17	01.52	00,41	42°	06,65	12°	22,60	-	1,5*	-	2,0
25	78.05.17	02.09	00,54	42°	06,62	12°	22,61	-	1,5*	-	0,9

* indicates fixed focal depth solution

Table 6. Cesano Earthquakes - Permanent Network.

N°	Date	Origin.		Lat. (N)		Long. (E)		ERH	Z	ERZ	M
121	79.05.21	16.54	01,82	42°	05,87	12°	27,12	1,5	9,8	1,1	>1,9
122	79.05.21	17.29	52,82	42°	06,32	12°	28,07	1,3	12,4	0,7	>1,6
154	79.06.17	22.41	20,92	42°	03,53	12°	25,52	3,2	13,2	1,9	0,66
200	79.07.07	18.29	07,52	42°	11,37	12°	27,38	1,7	8,1	2,3	>1,4
310	79.09.15	05.19	26,21	42°	04,33	12°	27,07	5,6	10,5	3,1	1,0
315	79.09.30	19.56	02,61	41°	59,83	12°	29,12	3,3	17,6	2,0	0,5
485	79.11.05	22.11	11,61	42°	13,67	12°	30,24	3,9	16,8	3,3	1,2
583	79.11.24	05.27	45,79	42°	05,94	12°	30,28	1,2	10,6	0,9	1,2
584	79.11.24	11.47	05,26	42°	03,15	12°	26,21	2,9	11,6	1,5	1,5
614	79.12.07	05.18	05,72	42°	02,15	12°	26,50	0,8	9,7	0,8	0,9
616	79.12.08	00.50	19,37	42°	04,26	12°	27,24	2,3	14,1	1,0	-0,1
282	80.05.23	17.51	16,11	42°	07,81	12°	25,32	0,4	6,4	0,4	1,6

Layer	Velocity (km/s)	Thickness (km)
1°	3.2	1.5
2°	5.5	

Considering how near the stations are to well RC-1, the model was based on well stratigraphy and the sonic logs. The epicentres vary slightly with a variation in the hypocentral depth from 1.5 to 1.7 km. Figure 15 shows the network configuration, together with the epicentral distribution for both solutions and the magnitude values.

Note that:

a) in the first case, with a focal depth of 1.5 km, the epicentres are concentrated in a small area immediately south-west of well RC-1;
b) in the second case, with a depth of 1.7, they tend to lie along a NW-SE belt passing through the displacement with the same trend, individualized by some surface geophysical and geological surveys;
c) all the events have magnitude values between 1 and 2.

4.2 Cesano - Natural Seismicity

The monthly frequency of the events recorded on the permanent network is shown in the histogram of Fig. 16. The latter shows that in the period in question there was little activity in the area and no particular increase in seismic activity during a production and injection test in well C-5.

As with Torre Alfina and Latera areas, the recorded seismic events were classified as "local" or "near" according to the difference between the arrival times of the S and P waves.

The geoseismic model used for the permanent network is as follows:

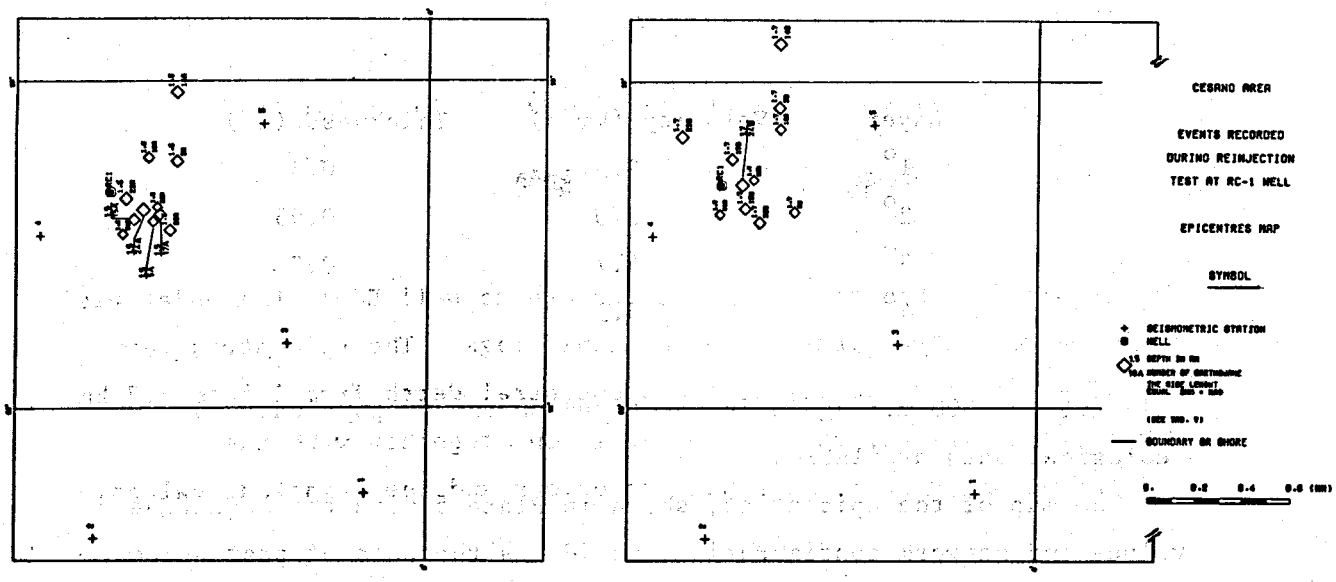

Fig. 15. Cesano area - events recorded during reinjection test at RC-1 well.

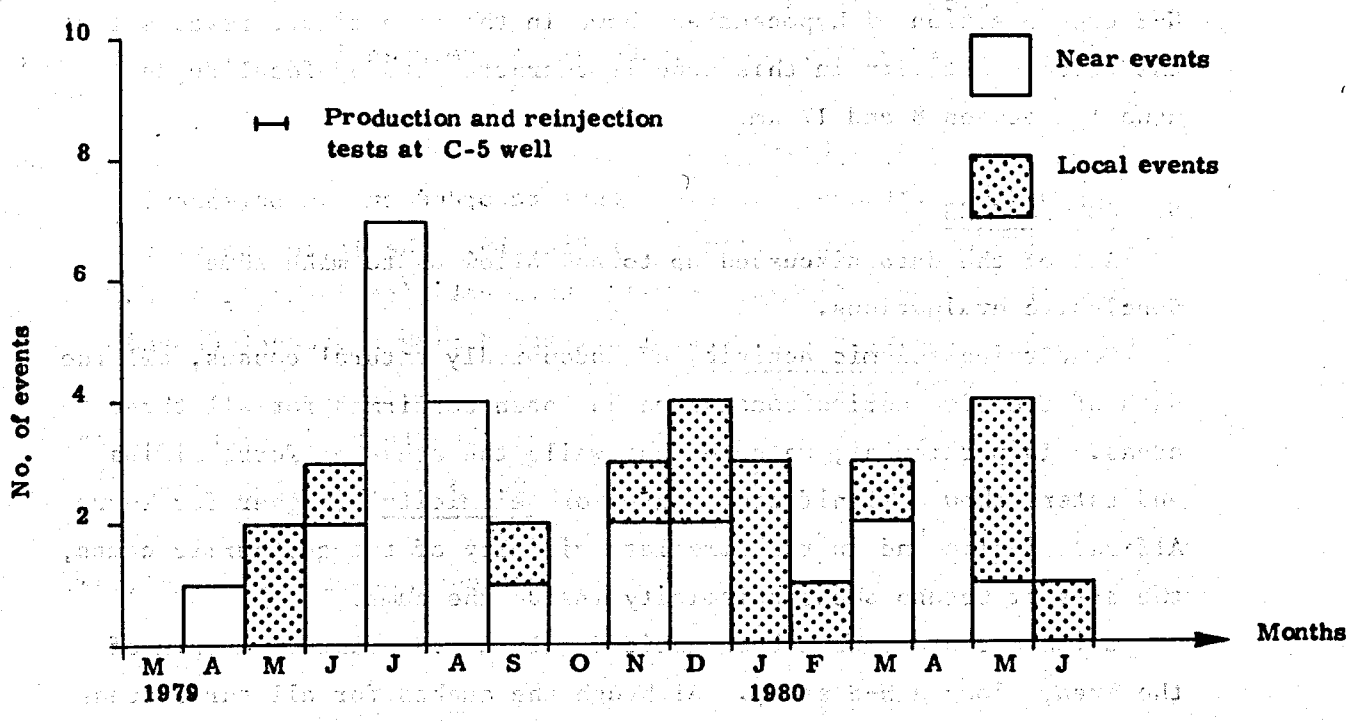

Fig. 16. Cesano area - histogram of seismic events recorded by permanent network.

Layer	Velocity (km/s)	Thickness (km)
1°	2.5	0.4
2°	3.0	0.95
3°	4.7	0.5
4°	5.5	

relative to +300 m.; again it was based on the geophysical and geological data available.

The map of the epicentres, shown in Plate 5 with the magnitude values and network configuration, validates the data of past seismic activity, revealing a low degree of seismicity in the Cesano geothermal area and a cluster of events along a roughly N-S belt east of the area.

The magnitudes, again calculated from the Cancani-Sieberg equation, reach values of more than 1.95.

As all the events were some distance away from the network, the figure shows only those whose coordinates could be determined. The N-S cross-section of hypocentres shown in the same figure reveals that the seismic activity in this zone is characterized by focal depths usually between 8 and 17 km.

5. CONCLUSIONS

All of the data discussed up to now allow us to make some conclusive evaluations.

Concerning seismic activity of undoubtedly natural causes, all the data of the time period considered has been confirmed for all three areas. In particular, we note that while the areas of Torre Alfina and Latera show a significant degree of seismicity, (higher for Torre Alfina), inside and in the immediate vicinity of the geothermic camps, the area of Cesano shows seismicity inside the camp.

Seismic centers have been noticed only at the eastern margin of the area, along a N-S strip. Although the quakes for all three areas have an undoubtedly superficial origin, in Cesano the focal depths are greater.

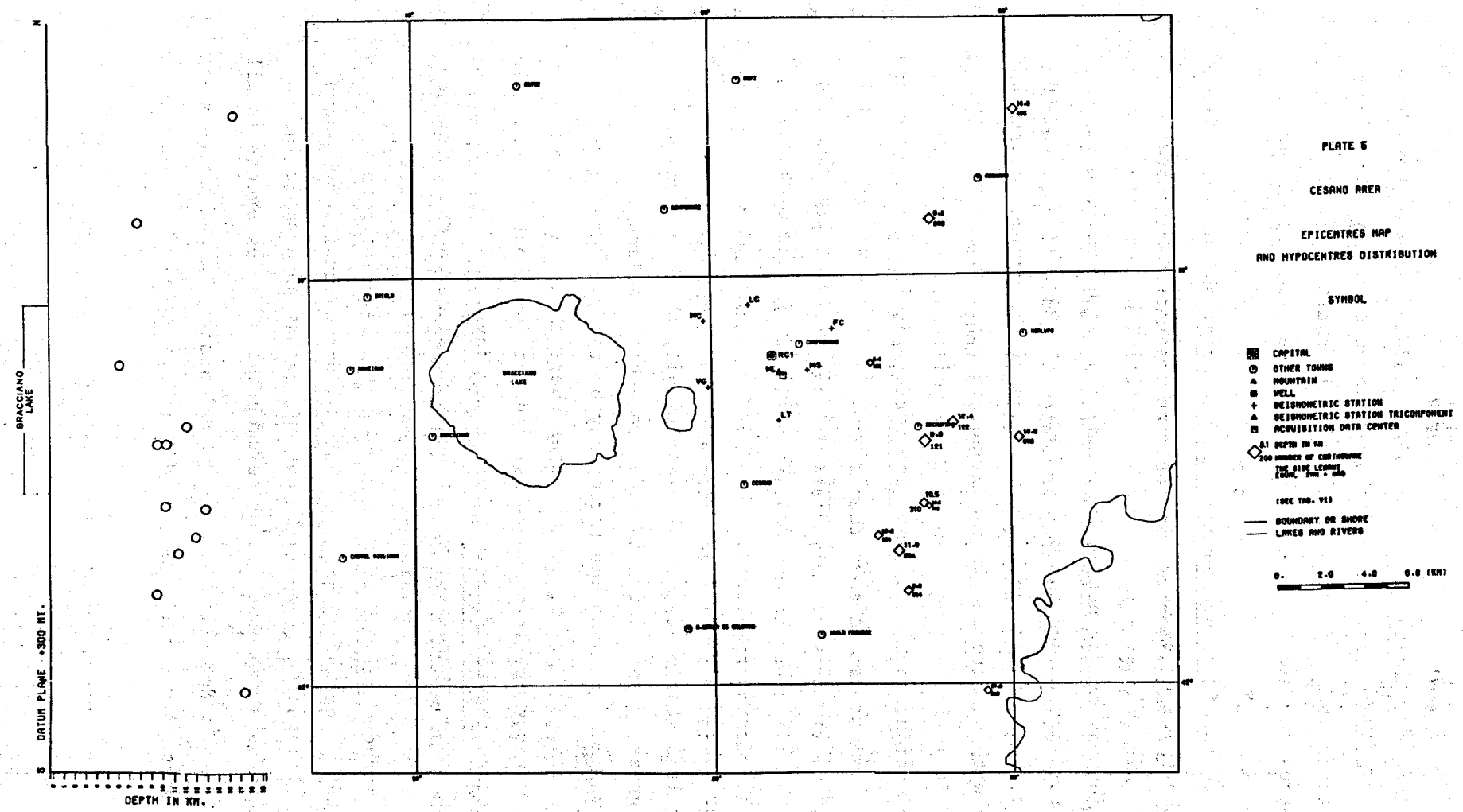

Plate 5. Distribution of epicentres, with magnitude and focal depths projected on N-S cross-section, for Cesano area.

Concerning seismicity of a very likely induced origin there have been contradictory cases. In fact, it has been seen that in connection with tests of reinjection and pumping in shafts RA-I, L-2, and RC-1, numerous seismic events have risen in the vicinity of the shafts.

During tests of production and reinjection at shafts A-14, A-4, and C-5, there was no evidence of any intensification of seismic activity. This triple response may be justified by a multiplicity of factors which may or may not be independent of each other.

The first factor, and the most conditioning one, has to do with the diverse thermo-fluid-dynamic conditions of the various shafts and the second with differences in the manner in which the tests were executed. It is in fact noteworthy that, while in the three cases of seismic induction, the injections were performed with clear water and pressure, in shaft A-4 the fluid extracted from A-14 was injected in a free-flowing manner; the test performed at C-5 consisted first in the emptying of the shaft, followed by injection of the same fluid which had been extracted.

Another factor may be the presence, in the vicinity of the shafts, of more or less stable structural discontinuity which may require varying degrees of soliciting in order to achieve a lack of equilibrium. Finally, another factor may be the time needed to perform the tests; in fact, in the cases where there was a seismic effect the various operations were carried out for about a month. In the other cases the tests covered only a few days.

At this stage, therefore, we can not generalize on the existence of a cause-effect relationship between operations carried out in shafts and induced seismicity. It should also be pointed out that in all areas both types of seismicity, induced and natural, have shown low values of magnitude, generally not over a; as an example in Plate 6 there is a reproduction of seismograms of a few events in all three areas.

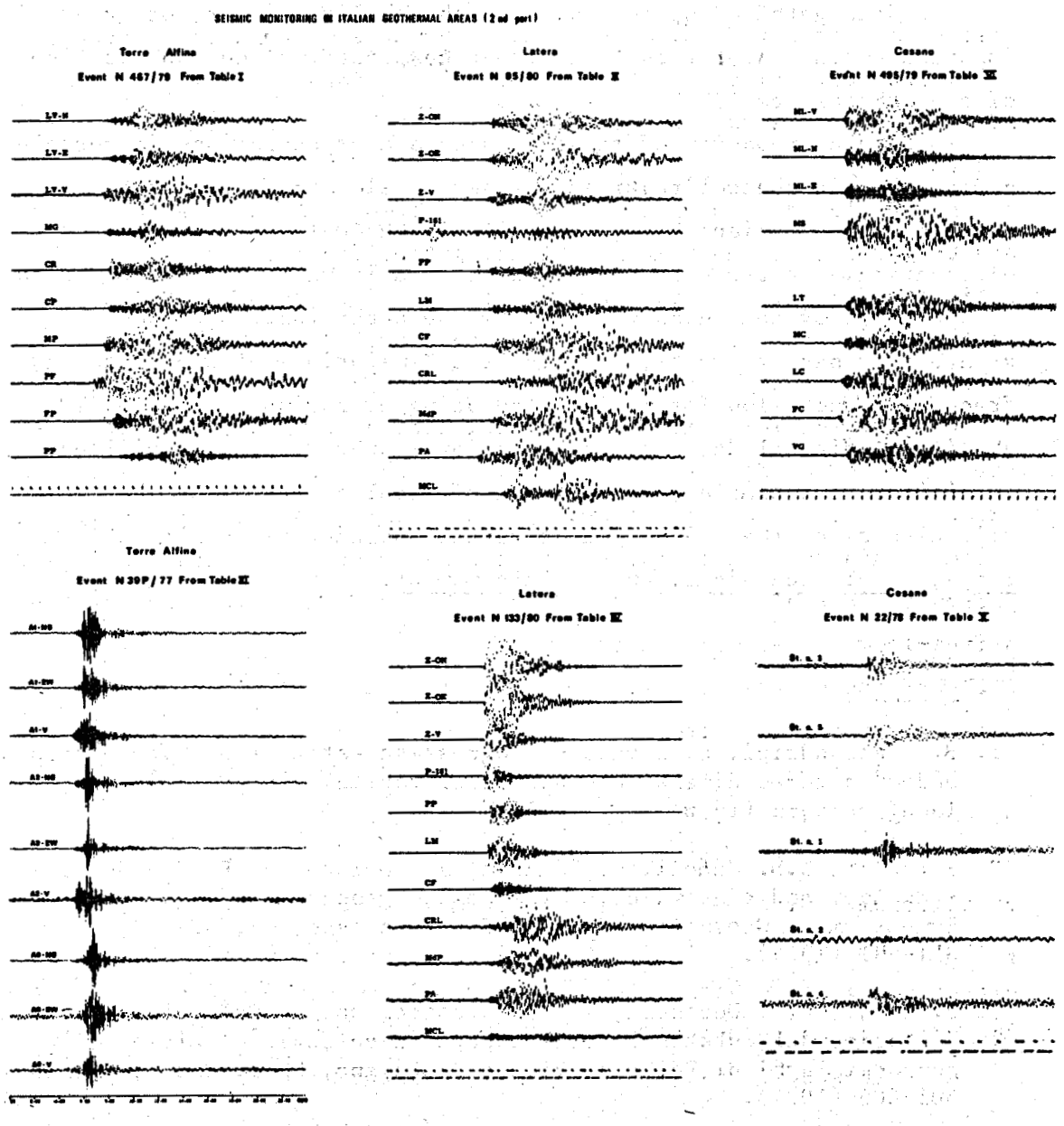

Plate 6. Seismograms of a few events in all three areas.

The data gathered up to now, even though limited, are of great importance since it refers to a situation preceding the exploitation of a geothermic camp.

In future expansion of this research and of operations in certain camps, seismic control requires further development in order to achieve more efficiency in data-collecting as well as in methods of elaboration. Instruments with greater dynamic range are needed, such as a digital system which would allow the determination of the greatest number of events, reducing the limitations of amplitude and frequency, and allow for rapid calculating operations. The availability of digital data is necessary for elaboration which will not be limited to a simple determination of focal co-ordinates, but which will also allow the definition of certain parameters such as signal range, focal mechanisms, and seismic moment.

REFERENCES

1. B. Alessandrini, L. Levato - Progressive estimate of hypocentres and of a three dimension crust model variable in proximity of a local network (in press). (1980).

2. P. Baldi, G.M. Cameli, E. Locardi, J. Mouton, and F. Scandellari - Geology and geophysics of the Cesano geothermal field. U.N. Symposium on Geothermal Energy, San Francisco, CA, USA, 2, 871-881 (1975).

3. P. Baldi, F.A. Decandia, A. Lazzarrotto, and A. Calamai - Studio geologico del substrato della copertura vulcanica laziale nella zona dei laghi di Bolsena, Vico e Bracciano. Mem. Soc. Geol. 13, 505-606 (1974).

4. P. Baldi, R. Funiciello, and E. Locardi - Volcanologic and structural study of the Cesano Geothermal area (Rome, Italy). It. Congr. on Thermal Waters, Geothermal Energy and Volcanism of the Mediterranean Area, Athens, Proc. Geoth. Energy Vol. 1.

5. F. Batini, P.D. Burgassi, G.M. Cameli, Nicolich, and P. Squarci - Study of deep lithospheric profiles: deep reflecting horizons in Larderello-Travale Geothermal Field. 69° Congresso della Societa Geologica Italiana, Perugia (1978).

6. C.G. Bufe, S.M. Marks, K.B. Lowie, and R.S. Ludwin - Seismic monitoring at the Geysers Geothermal Field, California. U.S.G.S. - U.S. Department of Energy, Menlo Park (1979).

7. K.E. Bullen - An introduction to the theory of seismology. Cambridge University (1963).

8. A. Calamai, R. Cataldi, E. Locardi, and A. Praturlon - Distribuzione delle anomalie geotermiche nella fascia preappenninica tosco-laziale. Symp. Int. sobre Energia Geotermica en America Latina, Citta del Guatemala 16/23 Ottobre 1976, pp. 189-229 (1977).

9. G.M. Cameli - Experience from Geothermal Exploration: the role of geophysical investigation in the discovery of the Latera geothermal field. 3rd Course on Geophysics of Geothermal Areas (Erice, May 1980) - Editors Rapolla and Keller - Plenum Press - London (in press) (1980).

10. G.M. Cameli and E. Carabelli - Seismic control during a reinjection experiment in the Viterbo Region (Central Italy). 2nd U.N. Symposium on the Development and Use of Geothermal Resources, San Francisco, CA, USA, 20/29 May 1975, Vol. 2, pp. 1329-1334 (1975).

11. G.M. Cameli, J. Mouton, and B. Toro - Contribution of geophysical surveying in the discovery of Cesano Geothermal Field (Northern Latium, Central Italy). Int. Congr. on Thermal Waters, Geothermal Energy and Volcanism of the Mediterranean Area, Athens, Proc. Geoth. Energy, Vol. 1, pp. 130-143 (1976).

12. R. Cataldi, G.C. Stefani, and Tongiorgi - Geology of Larderello region (Tuscany)-Contribution to the study of geothermal basins. Laboratorio Nucleare, Pisa (1963).

13. R. Cataldi and M. Rendina - Recent discovery of a new geothermal field in Italy: Alfina. Geothermics, Vol. 2, n. 3 e 4 (1973).

14. Combs and Hadley - Microearthquake investigation of the Mesa Geothermal anomaly, Imperial Valley, California. Geophysics, Vol. 42, 1 (1977).

15. Di Filippo and Macelli - Magnitudo ed energia dei terremoti in Italia. Pubblicazioni dell'Istituto Nazionale di Geofisica - Roma (1950).

16. R. Funiciello, E. Locardi and M. Parotto - Lineamenti geologici dell'area sebatina orientale. Bull. Soc. Geol. It. 95, pp. 831-849 (1976).

17. R. Funiciello and M. Parotto - Il substrato sedimentario nell'area dei Colli Albani: considerazioni geodinamiche e paleogeografiche del margine tirrenico dell'Appennino Centrale (Vulcano Laziale). Geologica Romana 17, pp. 233-278 (1978).

18. Giannini, Lazzarotto, and G.C. Stefani - Studio strutturale del tetto del basamento filladico-quarzitico (Verrucano) nella Tosacana a Sud dell'Arno. Mem. Soc. Geol. It. Vol. IX (1970).

19. Lee, Gilpin - A Microearthquake study in the Salton Sea Geothermal Area, California. BSSA Vol. 68, N. 2 (1978).

20. Gupta, Rastogi - Dams and earthquakes, Elsevier, North Holland Publishing Company, Amsterdam (1976).

21. Hamilton, Muffler - Microearthquakes at the Geysers Geothermal Area, California. Journ. of Geophy. Res. vol. 77, N. 1 (1972).

22. Healy, Hubert et al. - The Denver Earthquakes. Science 1301, 161 (1968).

23. Kissingler - A review of the theories of mechanisms of induced seismicity. Engin. Geology 10 (1976).

24. Iaccarino - Attivita sismica in Italia dal 1863 al 1965. RT/GEO (68) 14 (1968).

25. J.C. Lahr - Hypoellipse: A computer program for determining local earthquakes hypocentral parameters, magnitude and first motion pattern. Open - File Report U.S.G.S., Menlo Park (1979).

26. Lazzarrotto - Geologia della zona compresa fra l'alta valle del fiume Cornia e il fiume Pavone (Provincia di Pisa e Grosseto). Mem. Soc. Geol. It., Vol. VI (1967).

27. W.H.K. Lee, R.E. Bennett, and K.L. Meagher - A method of estimating magnitude of local earthquakes from signal duration. Open File Report, U.S.G.S. (1972).

28. W.H.K. Lee and J.C. Lahr - Hypo 71 (revised) - A computer program for determining hypocenter, magnitude and first motion pattern of local earthquakes U.S.G.S. Open - File Report (1975).

29. E.L. Majer and T.V. McEvilly - Seismological investigations at the Geysers Geothermal Field. Geophysics Vol. 44 N. 2, February 1979 (1979).

30. P.P. Mattias and U. Ventriglia - La regione vulcanica dei Monti Sabatini e Cimini. Mem. Soc. Geol. It. 9, 331-384 (1970).

31. Mazzanti - Geologia della zona di Pomarance-Larderello (Provincia di Pisa). Mem. Soc. Geol. It. 5 (1966).

32. Parotto M. and A. Praturlon - Geological summary of central Appennines - Structural Model of Italy-Maps and Exploratory Notes. Ric. Sci. 90, pp. 257-311 (1975).

33. W. Peppin and C.G. Bufe - Induced versus natural earthquakes: search for a seismic discriminant. Bulletin of the Seismology Society of America Vol. 70 N. 1, February 1980 (1980).

34. C.B. Raleigh - Earthquakes and fluid injection. American Association of Petroleum Geologists, 1972 (1972).

35. Richter - Elementary seismology. Freeman and Company, San Francisco (1958).

36. G. Scalera - Analisi del parametro "b" nella sequenza di Norcia. In Press (1980).

37. L.T. Teng, C.R. Real and T.L. Henyey - Microearthquakes and water flooding in Los Angeles basin. BSSA V. 63 (1973).

38. A.J. Wickens and J.H. Hodgson - Computer revolution of earthquake mechanism solution 1922-1962. Dominion observatory XXIII, 1 (1967).

39. Word, Bjornsson - Microearthquake swarms and the Geothermal Area of Iceland. Journal of Geoph. (1976).

40. Word, Jacob - Microearthquakes in the Ahuachapan Geothermal Field. Science 173 (1971).

41. Catalogo dei terremoti avvenuti in Italia dal 1000 al 1975. ENEL.

42. Seminario sui metodi di localizzazione ipocentrale. Progetto Finalizzato "Geodinalica" - CNR. Milano 1978.

GEOTHERMAL INDUCED SEISMICITY - BANE OR BLESSING?

Charles G. Bufe *
Peter M. Shearer †

Abstract

Production of steam or hot water from a geothermal reservoir and disposal of geothermal fluids by injection can be expected to disrupt hydrologic and tectonic equilibria in and around the reservoir, possibly producing instabilities leading to increased seismicity. As in well-documented cases of seismicity associated with reservoir impoundment (earthquakes as large as magnitude 6.5) or fluid injection (events as large as magnitude 5), the mechanisms of earthquakes induced by geothermal production and injection seem to reflect the regional tectonic stress orientation. Most probably the events are triggered by reduction in effective normal stress brought about by non-uniform pore pressure changes and thermal cooling. Although earthquakes induced by geothermal operations may very likely result in enhanced local seismicity and possibly damaging earthquakes, concern over this possible increase in seismicity has not been a barrier to geothermal development. At the world's largest geothermal development, The Geysers, thousands of earthquakes have been detected and located by the U.S. Geological Survey/Department of Energy network. The larger (magnitude 2.0 to 3.8) of these events are felt on a weekly basis, and some are disruptive in that temporary plant shutdowns result from the response of machinery-protective devices the earthquake-induced vibration. The largest events to date have occurred at injection wells.

On the positive side, earthquakes induced by cooling or fluid pressure changes provide unique information on the location of fracture zones within the reservoir by mapping the paths of fluids being withdrawn or injected. This information can be invaluable for geothermal reservoir definition and operations management.

Induced seismicity may also generate new fractures in the rock and serve to maintain existing fracture permeability in the presence of cementation and compaction processes which decrease permeability in the reservoir.

* U.S. Geological Survey, Reston, VA
† U.S. Geological Survey, Menlo Park, CA

Introduction

When man modifies the hydrologic regime by fluid withdrawal or injection, he runs the risk of releasing stored elastic shear strain, often in the form of earthquakes. This phenomenon of induced seismicity has been demonstrated in the case of reservoir impoundment resulting from construction of dams (Gupta and Rastogi, 1976) and in the case of fluid injection in boreholes (Healy and others, 1968). The largest induced earthquakes to date have had magnitudes near 6.5, but there is no reason to believe that larger earthquakes could not be triggered. The principal factor in triggering earthquakes is believed to be increased fluid pressure which reduces the effective normal stress on faults. This is the stress which inhibits fault movement. The same effect can be achieved by thermal cooling (Denlinger and Bufe, 1981).

Since techniques for extraction of geothermal heat generally involve both fluid withdrawal and injection, geothermal operations can be expected to trigger earthquakes in regions of stored elastic shear strain. Most hydrothermal regions are tectonically active; thus one might expect induced seismicity to result from geothermal production activities in these regions. Hot dry rock sites may or may not be in tectonically active regions, but the high fluid pressures required to hold fractures open can be expected to release shear stresses which might exist across other preexisting fractures, and induced seismicity is likely.

To date earthquakes triggered by geothermal production activities have been too small to result in property damage or loss of life, and thus have not posed a barrier to geothermal development. Geothermal induced seismicity has not been considered a high priority environmental concern by the Interagency Geothermal Coordinating Committee (IGCC).

Steam production and condensate injection at The Geysers

The only large-scale geothermal power development in the United States is at The Geysers steam field in northern California. Power production at The Geysers reached 900 megawatts with the addition of Plant No. 14 this year. When the plants are operating at full capacity, over 6 million kilograms of steam are removed and nearly 2 million kilograms of condensate injected each hour. Although the mass of water injected is less than that withdrawn, the rate of fluid injection is nevertheless great and is, we believe, responsible for triggering the larger earthquakes at The Geysers.

The rate of fluid injection at The Geysers complements the rate of evaporation, which is higher (80% of produced steam) during the dry, sunny months than during the rainy, overcast winter period (60%). Significantly, most of the larger ($M \geq 2.5$) earthquakes at The Geysers occur during the rainy season when injection rates are highest.

Injection wells are in several instances distant enough from producing wells to permit isolation of the effects of fluid injection on earthquake activity. The two largest earthquakes to occur at The

Geysers (December 22, 1976, magnitude 3.5; September 22, 1977, magnitude 3.8) were located within a few hundred meters of isolated injection wells (DX-7 and LF-3, respectively) outside the regions of steam extraction.

Maximum injection rates in single wells at The Geysers are on the order of 300,000 kg/hr. The table below compares this rate with injection rates at other sites of geothermal interest or where induced seismicity has occurred.

Table 1

Site	Maximum Sustained Injection Rate (kg/hr)
The Geysers (field)	2×10^6
The Geysers (single well)	3×10^5
Larderello, Italy (field)	1×10^5
Larderello (Sasso 22, water loss rate during drilling at depth of 4 km)	1×10^5
Fenton Hill (LASL)	1×10^5
Rocky Mountain Arsenal (single well)	8×10^4
Rangeley Oil Field, Colo. (field)	2×10^6

From Table 1 it is apparent that the fluid injection program at The Geysers is massive. Although the injection pressures are subhydrostatic, the pressure gradients between injection wells and production wells are large, as the reservoir is severely underpressured. The temperature contrast between the injected

condensate and the reservoir rock is also large and thermal stresses must be high in the vicinity of the injection wells.

Because The Geysers is a steam field, one might expect that problems such as subsidence normally associated with withdrawal of oil or water would not occur here. However, Lofgren's (1980) data indicated a subsidence rate of 3 cm/year over the production zone. The combined effects of steam withdrawal and condensate injection have resulted in a consistently high level of shallow (0 to 4 km) earthquake activity at The Geysers, and perhaps the greatest frequency of felt events in the United States. The Pacific Gas and Electric Company, operator of the power plants at The Geysers, reports that earthquakes are felt weekly and some are intense enough to temporarily shut down power plants.

Characterization of induced seismicity at The Geysers

Since 1975 the U.S. Geological Survey has operated a network of seismographs in The Geysers-Clear Lake region. The present configuration of the network is shown in Figure 1. Marks and others (1978) have documented the existence of two clusters of earthquake activity at The Geysers. These clusters are spatially correlated with two separate zones of decreased fluid pressure resulting from steam production described by Lipman and others (1977). Marks and others (1978) also examined pre-1975 earthquake data and conclude that the seismicity level at The Geysers has increased since production began. The earthquakes at The Geysers resemble those in the surrounding region with regard to focal mechanism (Bufe and

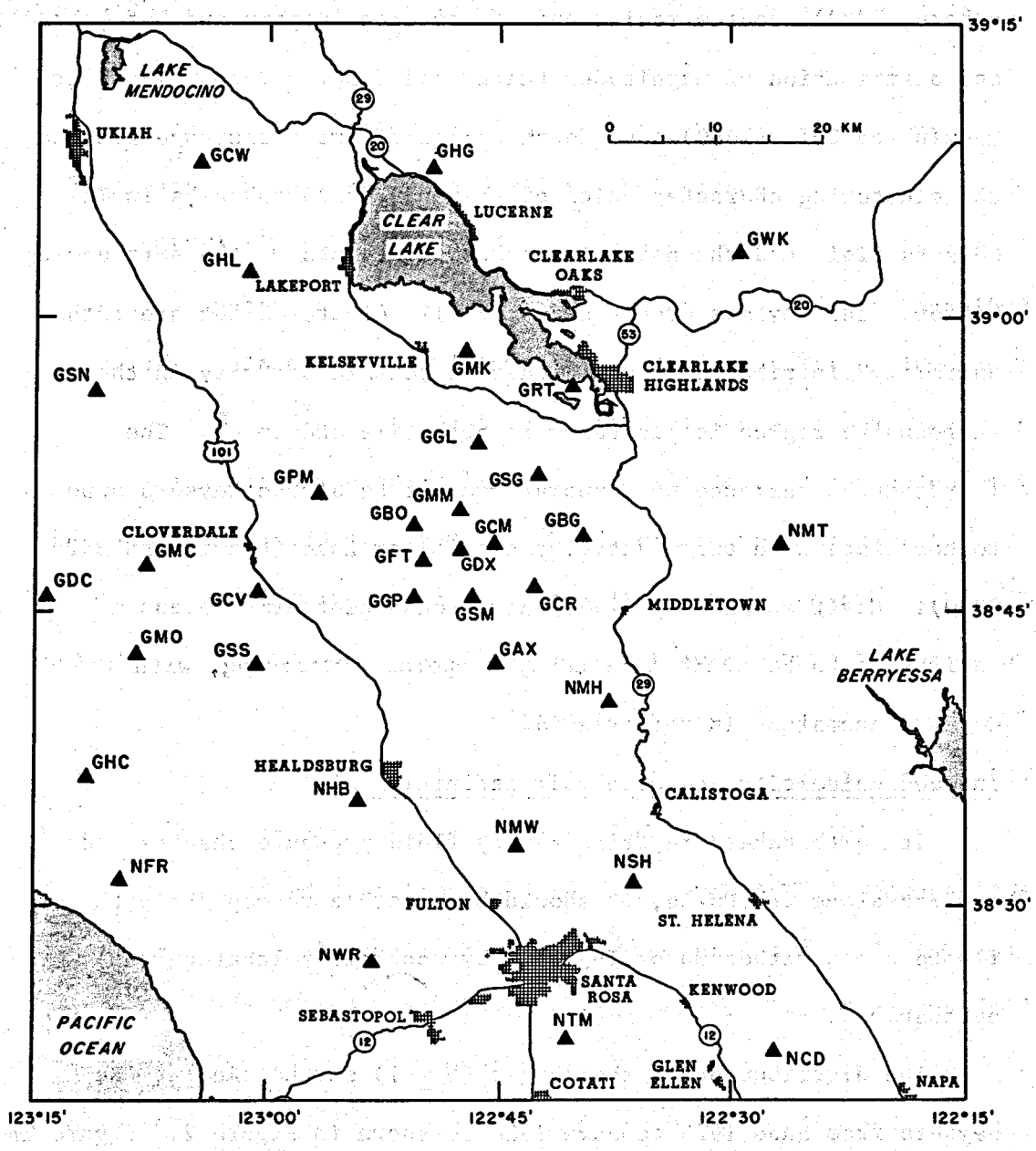

Fig. 1. Seismographic stations operated by USGS in and around the Geysers KGRA known geothermal resource area. Data are telemetered to Menlo Park for analysis. Stations GDX, GBO, GMM, GFT, GSM, GCR, GCM are in the steam production area at The Geysers.

others, 1980), source radius and stress drop (Peppin and Bufe, 1980), and distribution of magnitudes (Marks and others, 1978). However Ludwin and Bufe (1980) have found a significant difference between the clustering characteristics of the induced earthquakes in The Geysers field and the naturally occurring events in the surrounding region. The Geysers events are spatially clustered but are rather uniformly distributed in time, whereas seismic activity in the surrounding region is clustered in both time and space. The infrequent occurrence of temporal clustering at The Geysers appears to correlate with swarm activity near Clear Lake (Ludwin and Bufe, 1980). Cavit and Hadley (1980) have found geothermal areas in California to be characterized by temporal clustering, with The Geysers anomalous in this regard.

Induced seismicity and reservoir definition

If earthquakes are triggered by fluid pressure changes and cooling along fractures, it should be possible to map the paths of fluids being withdrawn or injected by accurately locating the earthquakes.

The distribution of the larger ($M \geq 1$) earthquakes at The Geysers from June 1975 to June 1980 is shown in Figure 2. Figure 2A shows the shallow activity in the field, while Figure 2B shows events below a depth of 2 km. The shallow earthquakes are concentrated in the zones of maximum pressure decline (Lipman and others, 1977) in the shallow reservoir. The deeper events of Figure 2B follow quite a different pattern, possibly defining the reservoir at depth.

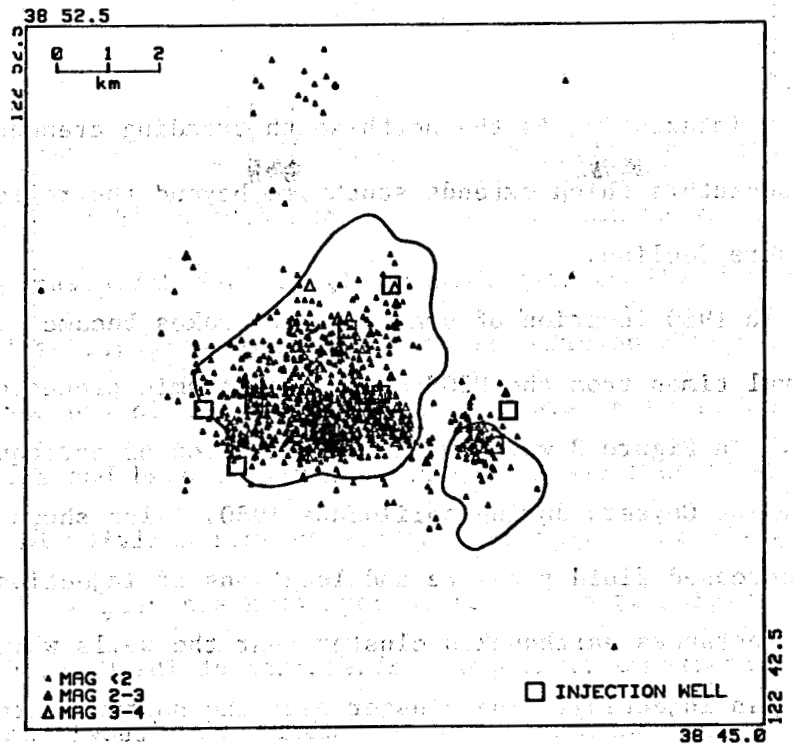

Fig. 2A. Distribution of larger (M $\geq$ 1) shallow (depth less than 2 km) earthquakes at The Geysers. Wells presently and previously used as injectors are also shown. The zones of fluid pressure decrease associated with steam production are outlined by the 500 psi isobar of Lipman and others (1977).

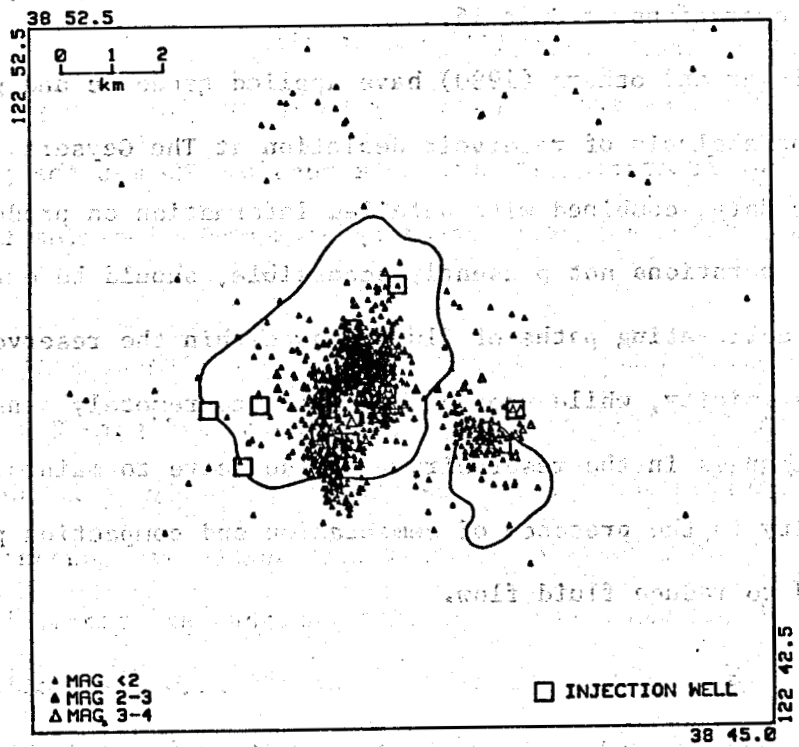

Fig. 2B. Distribution of larger (M $\geq$ 1), deeper (depth range 2 to 5 km) earthquakes at The Geysers. Injection wells are also shown. The zones of fluid pressure decrease associated with steam production are outlined by the 500 psi isobar of Lipman and others (1977).

Particularly interesting is the north-south trending crescent-shaped zone of hypocenters which extends southward beyond the region of known pressure decline.

Early in 1980 location of smaller earthquakes became feasible using arrival times from the USGS automatic seismic processor in Menlo Park. In Figure 3 we show the distribution of earthquakes ($M \geq 0.5$) at The Geysers during April-June 1980. Also shown are the zones of decreased fluid pressure and locations of injection wells. In several instances earthquakes cluster near the wells which most recently began injecting. The cluster near the southwesternmost injection well is new and lies outside the zone of previous seismicity, although within the boundaries of the pressure sink. This new cluster is believed to be the result of production and injection operations at Unit 15.

Denlinger and others (1980) have applied geodetic and gravity data to the analysis of reservoir depletion at The Geysers. Earthquake data, combined with detailed information on production and injection operations not presently accessible, should be extremely useful in delineating paths of fluid flow within the reservoir. Induced seismicity, while providing a means to remotely sense physical changes in the reservoir, may also serve to maintain permeability in the presence of cementation and compaction processes which tend to reduce fluid flow.

Acknowledgment

This work was supported by the Induced Seismicity Program of the Division of Geothermal Energy, Department of Energy.

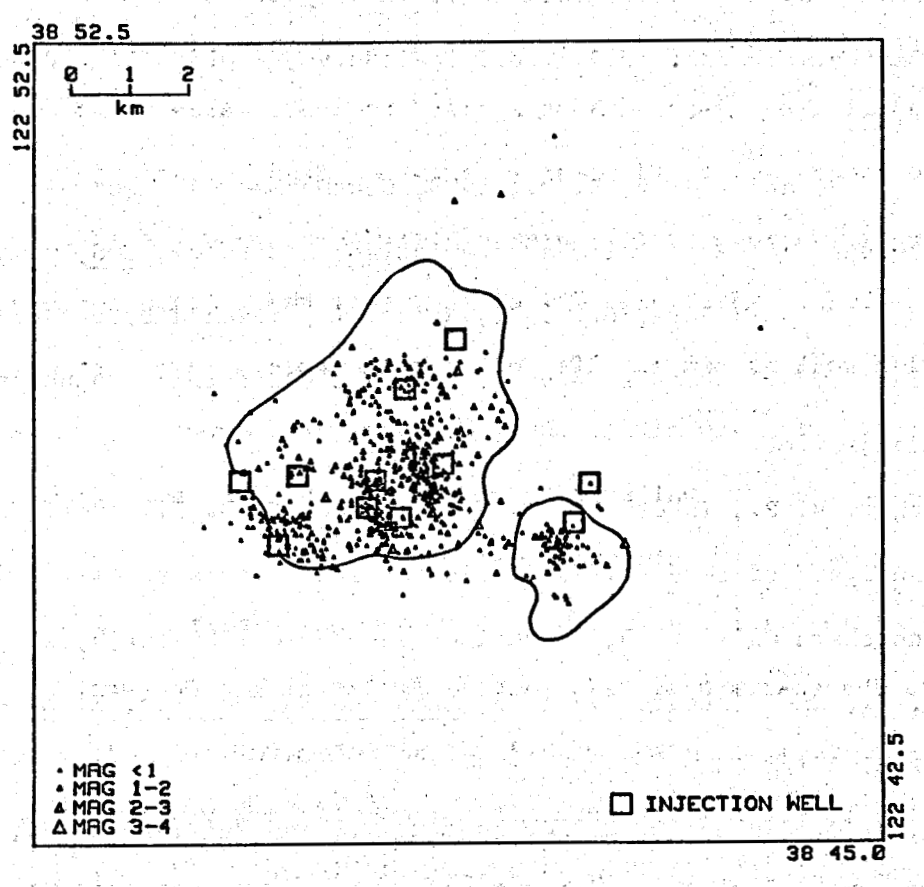

Fig. 3. Distribution of earthquakes ($M \geq 0$), at The Geysers, April-June 1980. Locations are based on arrivals picked automatically by USGS real-time seismic processor. During this period injection had been suspended at the northernmost injection well and the easternmost injection well. The zones of fluid pressure decrease associated with steam production are outlined by the 500 psi isobar of Lipman and others (1977).

References

Bufe, C. G., Marks, S. M., Lester, F. W., Ludwin, R. S., and Stickney, M. C., 1980, Seismicity of The Geysers-Clear Lake geothermal area, California, in McLaughlin, R. J., and Donnelly-Nolan, J. M., eds., Research in The Geysers-Clear Lake geothermal area: U.S. Geological Survey Professional Paper 1141.

Cavit, D. S. and Hadley, D. M., 1980, Geothermal earthquakes: temporal and spatial characteristics (abstract), EOS, in press.

Denlinger, R. and Bufe, C., 1981, Seismicity induced by production at The Geysers steam reservoir, northern California, unpublished manuscript.

Denlinger, R. P., Isherwood, W. F., and Kovach, R. L., 1981, Geodetic analysis of reservoir depletion at The Geysers steam field in northern California, Journal of Geophysical Research, in press.

Gupta, H., and Rastogi, B., 1976, Dams and Earthquakes, Elsevier Publishing Company, Amsterdam.

Healy, J. H., Rubey, W. W., Griggs, D. T., and Raleigh, C. B., 1968, The Denver Earthquakes, Science, v. 161, p. 1301-1310.

Lipman, S. C., Strobel, C. J., and Gulati, M. S., 1977, Reservoir performance of The Geysers field, in Proceedings of the Larderello Workshop on Geothermal Resource Assessment and Reservoir Engineering, Larderello, Italy, September 12-16, 1977, pp. 19-22.

Lofgren, B. E., 1980, Monitoring crustal deformation in The Geysers-Clear Lake region, in McLaughlin, R. J., and Donnelly-Nolan, J. M., eds., Research in The Geysers-Clear Lake geothermal area, U.S. Geological Survey Professional Paper 1141.

Ludwin, R. S., and Bufe, C. G., 1980, Induced seismicity at The Geysers geothermal field, California: U.S. Geological Survey Open-File Report 80-1060.

Marks, S. M., Ludwin, R. S., Louie, K. B., and Bufe, C. G., 1978, Seismic monitoring at The Geysers geothermal field, California: U.S. Geological Survey Open-File Report 78-798, 26 p., 1 plate.

Peppin, W. A., and Bufe, C. G., 1980, Induced versus natural earthquakes: Search for a seismic discriminant, Seismological Society of America Bulletin, v. 70, pp. 269-281.

SELECTION OF DRY WELLS IN TUSCANY FOR STIMULATION TESTS

P. Baldi,* G. Bertini,* C. Calore,† G. Cappetti,*
C. Cataldi,* R. Celati,† and P. Squarci

1. NON-PRODUCING WELLS IN THE LARDERELLO AND TRAVALE FIELDS

Of the 570-odd wells drilled during the last 50 years in the geothermal fields of Larderello and Travale, little more than 220 are now producing.

Excluding a few wells that are not exploited because of the chemical characteristics of the fluid, the productive wells can be classified as follows:

a) Wells that were once productive but are now exhausted (meaning that they are no longer capable of economic production at the working pressure of the power plant).

Apart from a few examples of an unexpected halt in production caused by collapse of the wellbore walls, exhaustion occurred in densely drilled zones in which reservoir pressure decreased to a few tens of atmosphere above the turbine inlet pressure (the reservoir pressure value was measured in shut-in wells during field production). The flow-rate drawdown in these wells (at nearly constant pressure) is generally characterized by a series of sharp decreases that occur with the entry-into-production of new

---

* ENEL - Unità Nazionale Geotermica, Pisa, Italy.

† CNR - Instituto Internazionale per le Ricerche Geotermiche, Pisa, Italy.

Work conducted as part of the Finalized Energy Program of the Italian National Research Council.

wells. Pressure build-up tests, conducted in some wells showing a strong depletion, revealed that transmissivity was still high and skin factors generally negative. The lowering of flow-rate was therefore considered to be attributable neither to an important variation in formation permeability nor to local permeability reduction around the borehole.

These wells are clearly of no interest as far as stimulation is concerned.

Figure 1 shows the location of the non-productive wells in the Larderello field. The exhausted wells are nearly all located in the densely drilled zones.

b) Another group of wells of no interest to stimulation are those lying in peripheral areas, where the temperature in the upper layers of the reservoir is too low, even with a good permeability, to produce fluids exploitable for electricity generation (Figs. 1, 2 and 3).

Note that the low temperature in the top of the reservoir is of no interest to stimulation when dealing with shallow wells only. Temperatures of 250°-300°C have been recorded at depths of about 3 km in various areas that have low temperature values at the top of the reservoir.

c) Dry or low productivity wells, owing to a lack of permeability. Most of these wells are in areas in which the reservoir temperature, at depths between 500 and 1500 m, exceeds 200° and frequently even 250°C, with pressure above 20 atm. The deeper wells are of some interest even though they lie within areas with relatively low pressures in the top of the reservoir. It has, in fact, been noted that reservoir pressure increases with depth[1,2] and values of more than 20 atm were found between 1000 and 1500 m depth in zones with pressures below 5 atm in the uppermost layers of the reservoir.

Our attention was concentrated on hot, low permeability wells in the selection of a few wells with the most favorable characteristics for stimulation. The wells were selected on the basis of their technical characteristics, their state of conservation, the rocks crossed

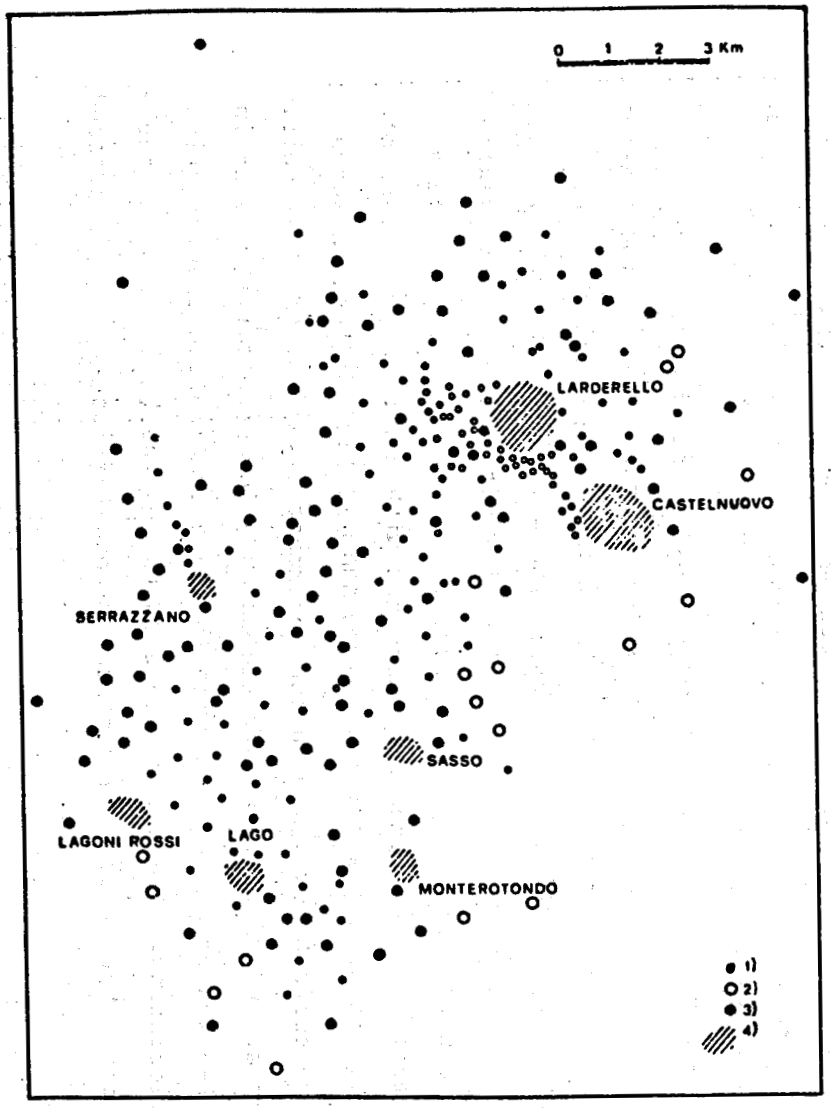

Fig. 1. Location of the wells in the Larderello geothermal field.
1) Productive wells; 2) Non-productive (low temperature) wells; 3) Dry or low productive wells (lack of permeability); 4) Densely drilled areas.

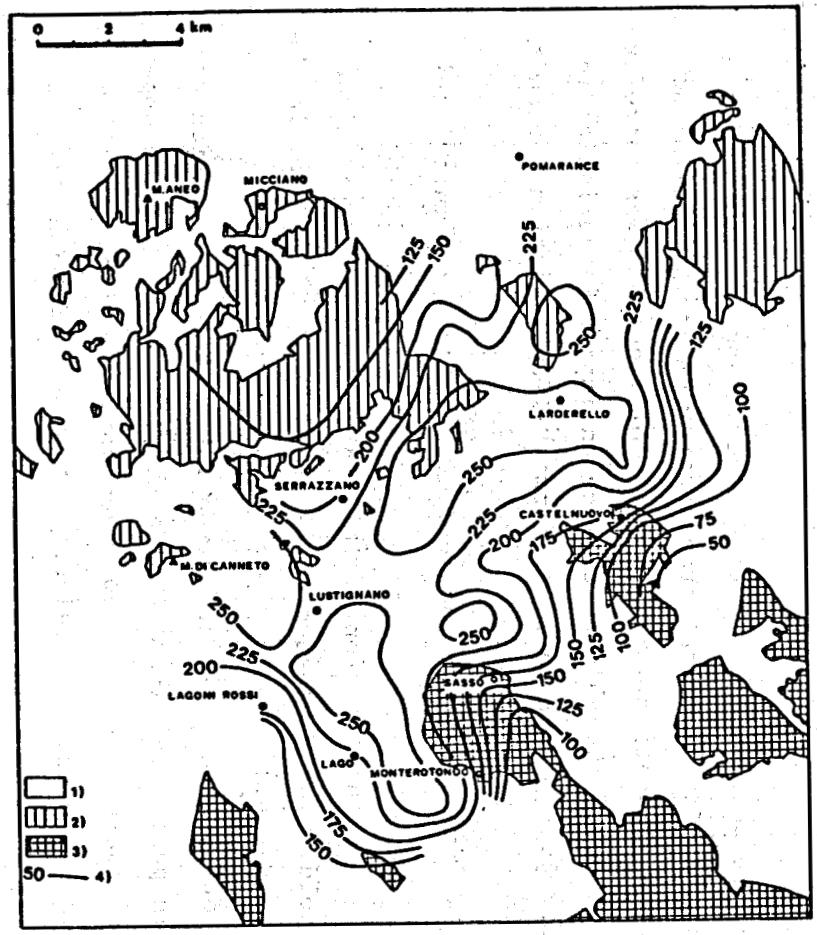

Fig. 2. Temperature distribution at the top of the reservoir in the Larderello geothermal field.
1) Cover formations; 2)Ophiolites and associated sedimentary breccias; 3)Reservoir rocks (including "Macigno" sandstone); 4) Isotherms (°C).

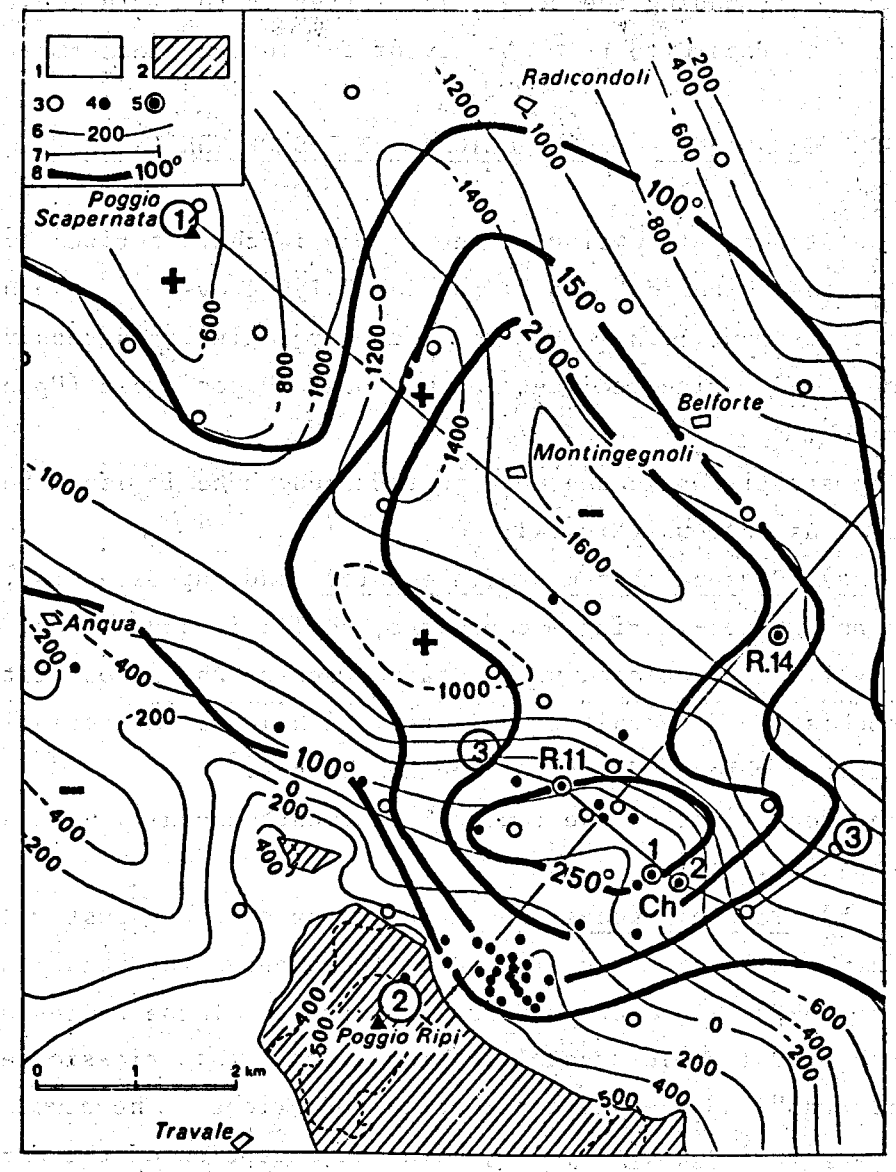

Fig. 3. Structural setting and temperature distribution at the reservoir top in the Travale geothermal field.
1) Cover formations; 2) Outcrops of the mesozoic carbonate formations (reservoir); 3) Geothermal boreholes; 4) Deep wells; 5) Selected wells; 6) Isobaths of reservoir top; 7) Traces of the cross-sections; 8) Isotherms at the reservoir top.

in the open-hole section and, especially, the structural setting in the area surrounding the bore. The latter is the main controlling factor with regard to permeability of the Tuscan geothermal areas.

2. GEOLOGICAL AND HYDROGEOLOGICAL OUTLINE OF THE LARDERELLO-TRAVALE ZONE

The structural setting of the region is characterized by overlying nappes, the "Ligurids" and "Tuscanids," lying over a regional metamorphic basement. These complexes are overlain transgressively by the lagoonal and marine sediments of a neoautochthon cycle (Upper Miocene-Pliocene).

The stratigraphic sequence in the study area is, from bottom upwards, as follows (Fig. 4):

a) Regional basement (Paleozoic), made up of gneiss, plagioclase and garnet-bearing micaschists, phyllitic quartzites, quartzites and phyllites associated with metagreywackes, chloritoschists, calceschists and graphitic phyllites, with local intercalations of dolomitic marbles and crystalline anhydrites.[3]

The formations of the regional basement generally have a low permeability.

b) Tectonic wedge zone, consisting of overthrust wedges (maximum total thickness of 1400 m) found above the "basement" in the Larderello-Castelnuovo and Serrazzano areas. These wedges are made up both of Paleozoic crystalline formations, the Triassic terrigenous ("Verrucano") and mesozoic carbonate formations. The permeability of this complex is generally low, with the exception of the carbonate and quartzitic layers, which may have a good secondary permeability.

c) Tuscan nappe, whose base comprises green phyllite (Verrucano) overlain by evaporitic and carbonate deposits (Burano Formation) of the Upper Trias, followed upwards by a group of mainly carbonate Jurassic formations and, finally, by varicoloured shale ("Scaglia") of the Cretaceous-Eocene and the arenaceous flysch "Macigno" of the Oligocene.

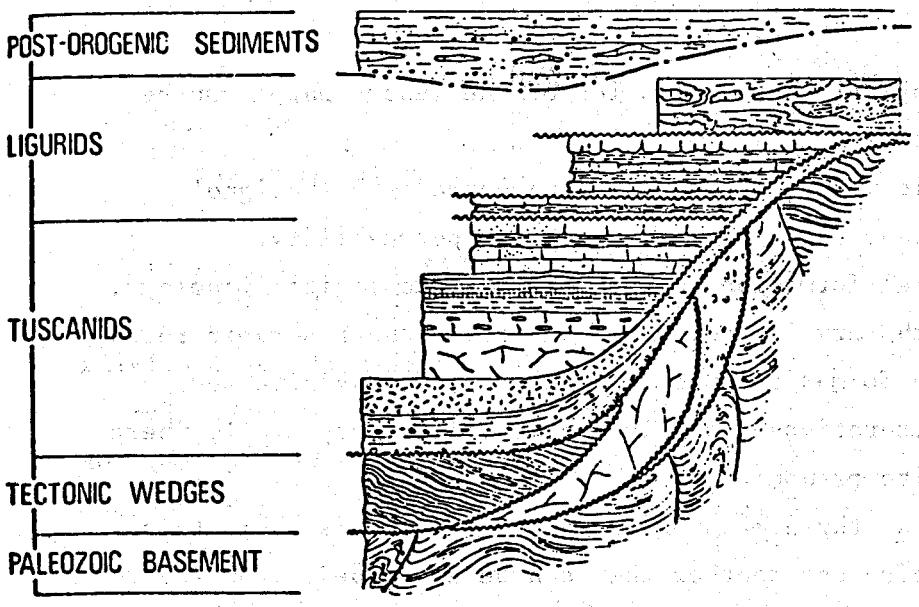

Fig. 4. Relationship between the main stratigraphic units in Larderello-Travale region.

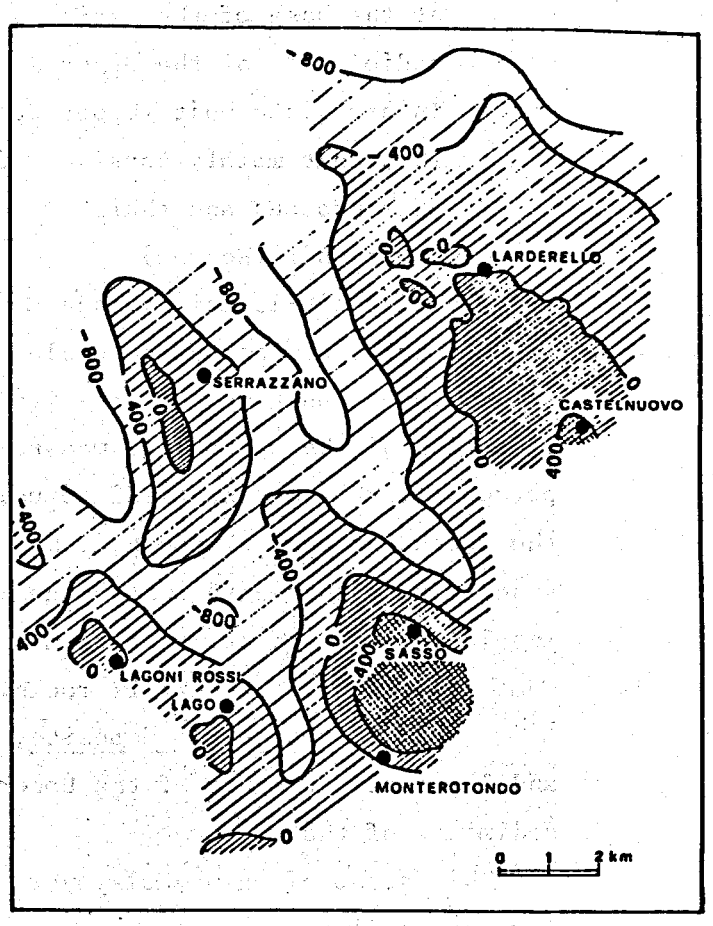

Fig. 5. Isobaths of the top of the geothermal reservoir formations (m.a.s.l.)

The hydrogeological characteristics of the Tuscan nappe can be summarized as follows:

- The Jurassic mainly carbonate sequence and the 'Macigno' formation have a good fracture-derived permeability;
- the 'Scaglia' formation (mainly shale), due to its lithology, a layer with very low permeability within the reservoir rocks;
- the 'Burano formation' which is made up of anhydrite and dolomite alterations has a low permeability, especially where the anhydrite predominates.

d) Ligurids, three main units can be distinguished in this complex. Overlapping one another they can be described, from the top downwards, as:

- Upper unit (Lower Cretaceous)
  This unit consists of shale and siliceous stratified limestone; at the base of the series are masses of ophiolitic rocks and radiolarite of the Upper Jurassic.
- Intermediate unit (Upper Cretaceous)
  This unit mainly consists of marly layers with interbeddings of sandstone and shale.
- Lower unit (Eocene)
  This unit is mainly made up of marly limestone interbedded in marly, sandstone and shaley layers.

The upper unit is characterized by very low permeability, with the exception of the ophiolitic masses that have average fracture-derived permeability. The intermediate unit is similar hydrogeologically to the preceding one, although it has more frequent marly limestone and sandy layers that have an average fracture-dependent permeability. The lower unit has at its base mainly limestone layers that may, in some cases, act as reservoir rocks.

e) Post-orogenic deposits, these consist of lacustrine, marine and lagoonal sediments of the Upper Niocene (Messinian) and marine sediments of the Pliocene.

This group of mainly clayey formations has, on the whole, a very low permeability.

3. INFLUENCE OF GEOLOGICAL-STRUCTURAL FACTORS ON PERMEABILITY

In order to define the main structural parameters that, along with lithostratigraphy, have an effect on permeability and, hence, on well productivity, a systematic analysis was made of the geostructural and hydrogeological conditions of all the wells, productive and non-productive.

This analysis revealed that permeability distribution is greatly influenced by geostructural factors and by related tectonic events. The latter can be attributed to three main phases: the first of these, the Hercynian, affected the Paleozoic metamorphic basement only; the second, Alpine phase of compressional and gravitational tectonics controlled the emplacement and folding of the Tuscan and Ligurid units and led to tectonic shearing within the Tuscan formations, and probably within the regional basement as well, with reduction of the series and creation of the main structural features. A third, tensional phase gave rise to the main horst and graben structures existing in the area. The formation of these structures had the following effects on permeability.

The Alpine compressional tectonics created a series of overthrust planes between the Ligurids and Tuscanids and within the latter. A thin belt of fractures was formed along these planes, especially if the contact involved the carbonate formations, increasing permeability considerably.

The main overthrust planes, from the bottom upwards, are:

- that between the Tuscan nappe and the underlying complexes. In some areas (Serrazzano and Larderello-Castelnuovo) tectonic wedges have formed between the Tuscan nappe and the Paleozoic basement increasing the permeability of the formations involved;
- that between the Ligurid units and the underlying complexes. In some cases strong shearing has carried the Tuscanids off and placed the Ligurids in contact with the Paleozoic basement. Intense fracturation can also occur in correspondence to this plane. In other cases this phenomenon has transformed the

Burano Formation into a breccia of fragments of dolostones, anhydrites and limestones with a very high permeability.

Considering the areal distribution of the dry and noncommercial wells, the structural characteristics of the different areas, drilling data, geophysical logs, in-hole measurements and the production tests from the various geothermal wells, it can be concluded that:

a) the dry wells are generally concentrated in areas (Fig. 1) in which almost all the wells have a low productivity. Consequently, low permeability of the reservoir formations would appear to be a wide spread phenomenon throughout these areas.

b) The reservoir formations show the highest productivity in zones of structural highs.[4,5] Figures 5 and 6 clearly reveal this areal correspondence. Of all the factors responsible for intense fracturation in these zones the most important seems to be the folding undergone by the rocks during the orogenic phases; the fractures are particularly concentrated along the main axes of these structures.

c) The fracturation of the anhydritic carbonate formation (Burano Formation) becomes more intense in its thinner layers. This can be noted in Fig. 7, which shows the thickness distribution of the "Burano Formation" for the wells crossing it and the ratio between productive and unproductive wells* for each thickness interval.

d) The overthrust planes are of great importance in the fracturation of the reservoir rocks. Tied to this overthrusting is the large number of productive fractures found near the contact between the cover and the reservoir formations. Figure 8 shows the frequency distribution of the distance between the fractures crossed by the wells and the tectonic contact. The fractures (or groups of fractures located in small depth intervals) were individualized from drilling data, in-hole measurements and geophysical logs. The data on older wells consist of drilling data only and are therefore less

---

* Whenever there are only few elements in a class, this ratio was calculated considering the nearby classes, using a moving average.

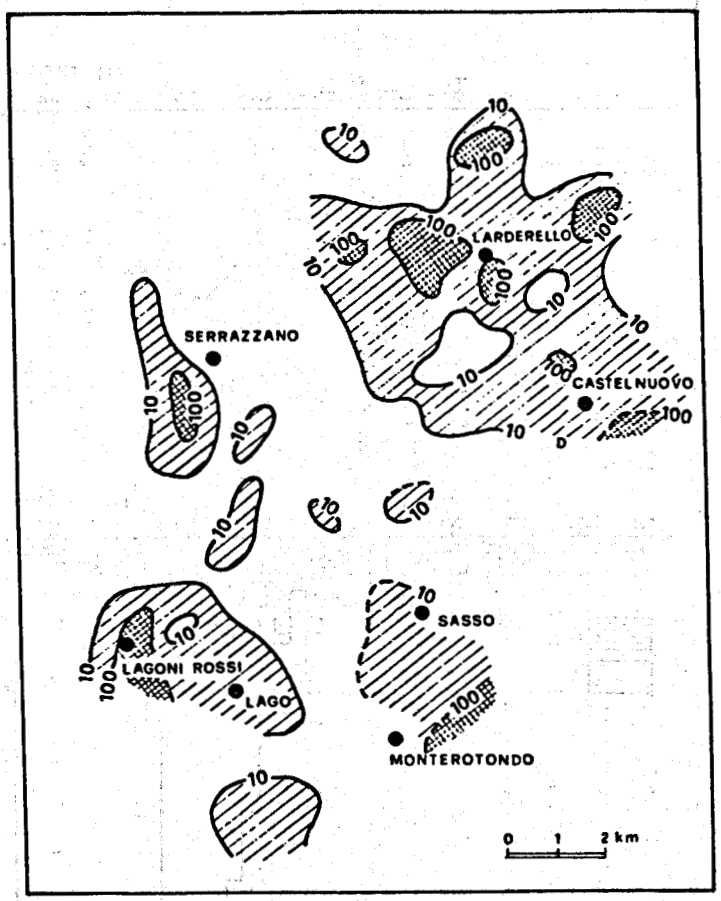

Fig. 6. Distribution of the kh values (Darcy-meters in Larderello geothermal field.

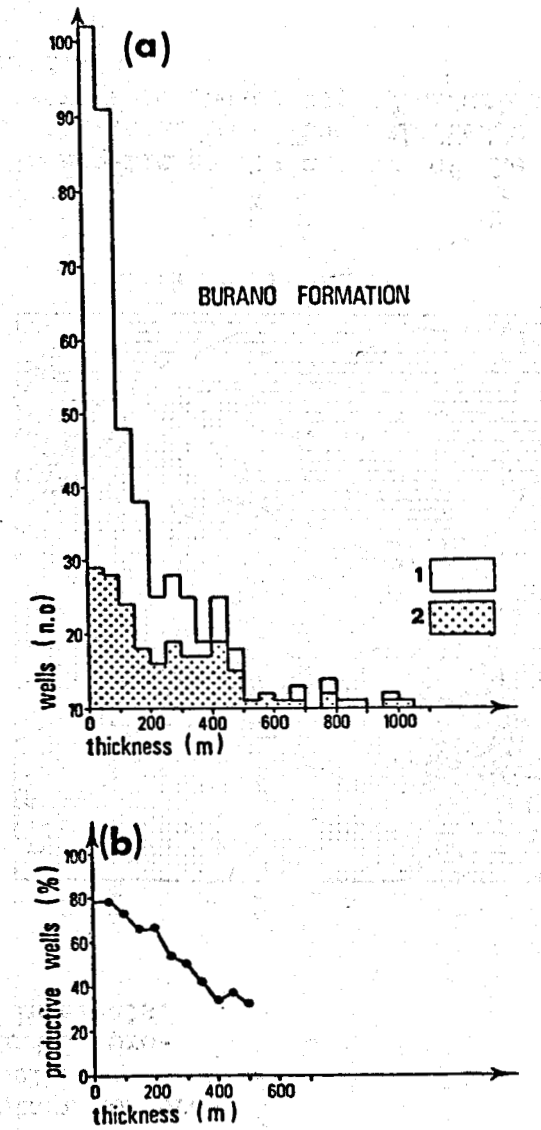

Fig. 7. a) Distribution of the "Burano Formation" thickness for productive (1) and non productive (2) wells.

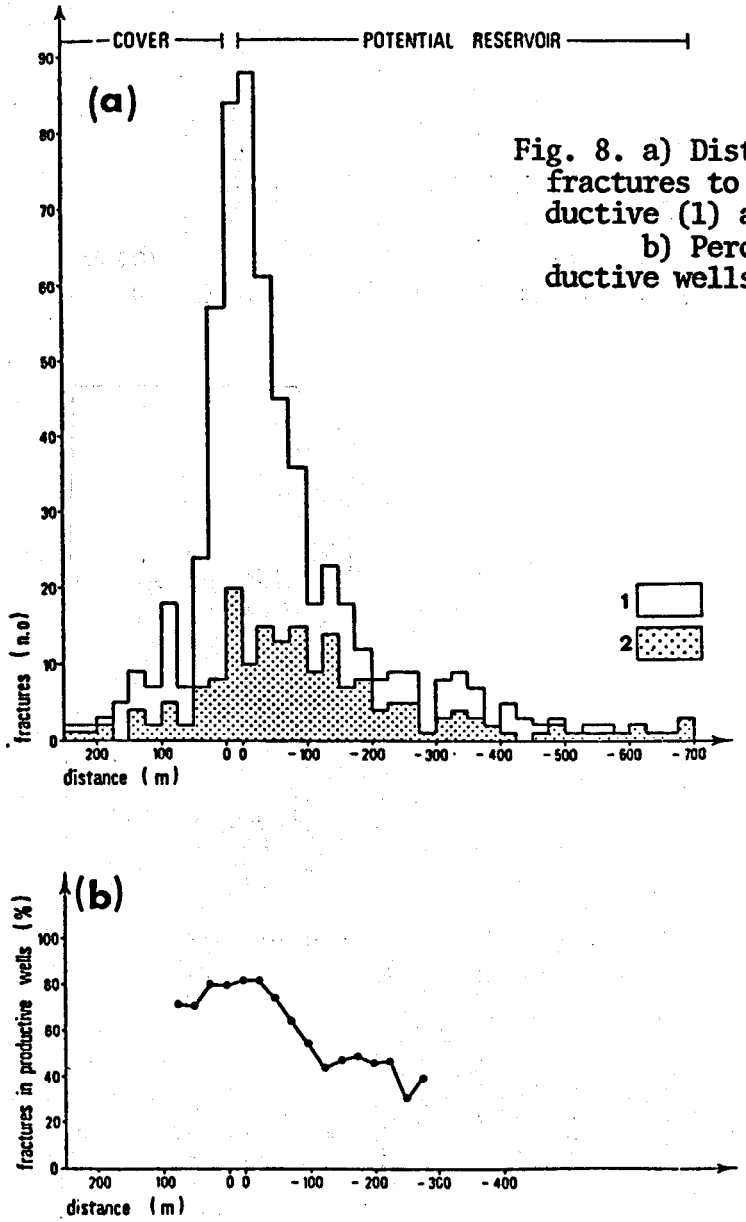

Fig. 8. a) Distribution of the distance from the fractures to the cover-reservoir contact for productive (1) and non productive (2) wells.
b) Percentage of fractures found in productive wells in different distance intervals.

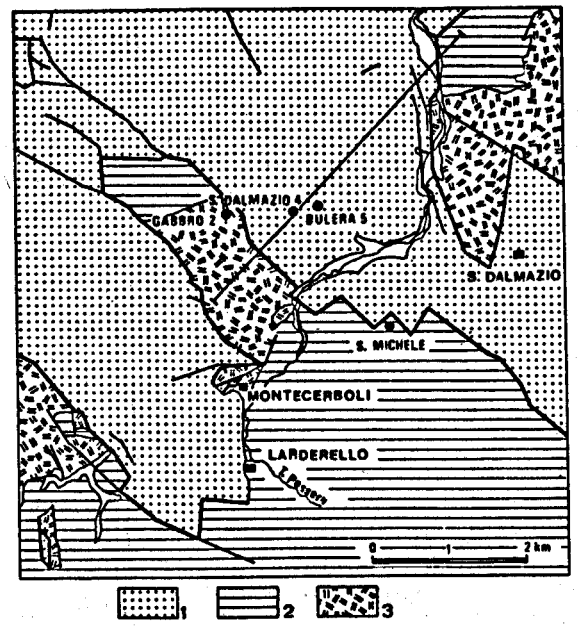

Fig. 9. Schematic geological map of the zone of Gabbro with location of the selected wells.
1) Post-orogenic sediments; 2) Ligurids; and 3) Ophiolites.

reliable than the other data. Class (0,0) of nil width has been added to represent the fractures lying right on the contact.

The distribution shows a clear concentration of fractures near the tectonic contact. The fractures within the cover complex usually lie in correspondence to calcareous or arenaceous layers at the base of the Ligurids. The percentage of productive wells also peaks in correspondence to the contact.

Similar observations could also be made for the contact between the "Burano formation" and the underlying Triassic or Paleozoic terrigenous formations.

e) The influence of the Neogenic tensional tectonics on reservoir permeability is still not clear. The fault systems created during this phase appear to have played an important role in providing connections between permeable horizons at different depths so that the permeable layers of the reservoir can collect fluids from large masses of low permeability rock.

4. SELECTED WELLS

Based on the preceding analysis and on examination of all available data (thermodynamic and technical), 13 dry or low permeability wells were considered suitable for tests and logs, prior to possible stimulation experiments.

Nine of these wells are sited in the Larderello geothermal field and four in the Travale field. Their main geological and thermodynamic characteristics can be summarized as follows.

Part of the wells in the Larderello field lie on the western margin of the Era graben, near the faults bordering this graben with a regional NW-SE trend (Fig. 9). Below the cover formations (Neogene and Liguirids) these wells meet the "Burano Formation" and/or the Triassic-Paleozoic terrigenous complex (Fig. 10).

In addition to reducing the thickness of the Burano formation, this fault may also have created fractures in the Triassic-Paleozoic phyllitic-quartzitic formations. These fractures are probably nearly

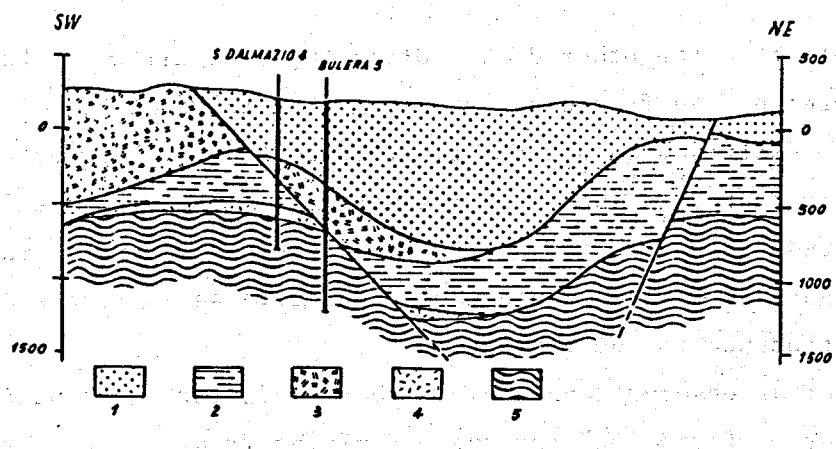

Fig. 10. Schematic geological cross-section of the zone of Gabbro. 1) Post-orogenic sediments; 2) Ligurids; 3) Ophiolites; 4) Burano Formations; 5) Triassic-Paleozoic terrigenous formations.

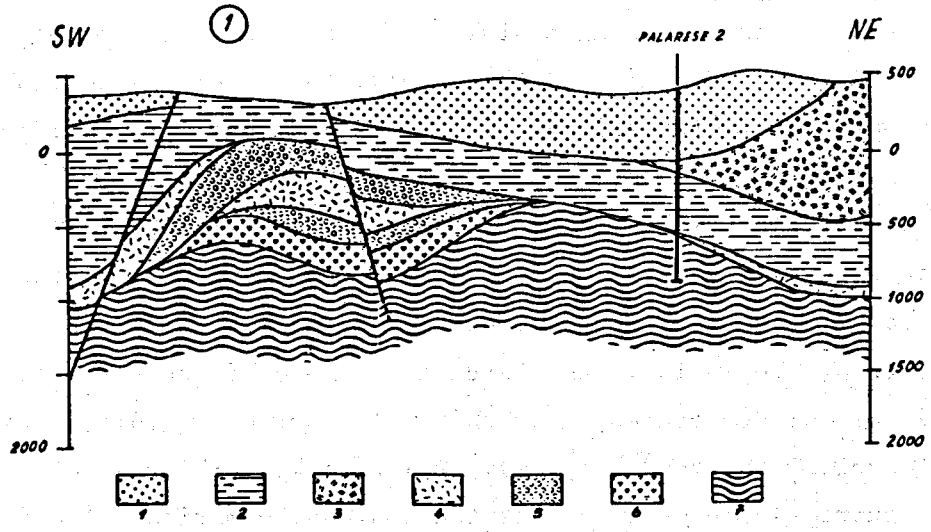

Fig. 11. Schematic geological cross-section of the Serrazzano structure. 1) Post-orogenic sediments; 2) Ligurids; 3) Ophiolites; 4) Burano formation; 5) Quartz conglomerates (Verrucano); 6) Quartzites (Verrucano); 7) Triassic-Paleozoic terrigenous formations.

vertically oriented and irregularly distributed throughout the area, being more concentrated in a belt along the fault. One of the main reasons for selecting these wells was the inferred possibility of connecting them to the fracture system.

A second group of selected wells lies within the northern part of the Cornia River basin, south-west of Larderello.

These bores are sited on the flanks of two main positive structures of the potential reservoir formations: the Serrazzano and Lagoni Rossi structures.

The Serrazzano structure (Fig. 11) extends N-S and is made up of a complex of tectonic wedges of Triassic formations (anhydrites, anagenites, quartzites).[3]

The Lagoni Rossi positive structure trends NW-SE and is formed by Triassic-Paleozoic metamorphic terrigenous formations and Jurassic carbonate formations of the Tuscan Series. Towards the north this structure is separated from that of Serrazzano by a wide NW-SE trending (regional) tectonic depression.

This second group of wells crosses thin layers of the "Burano Formation" and/or the underlying metamorphic terrigenous formations (Figs. 12 and 13). Although some of these wells are dry, they lie in a zone containing other highly productive wells. The low permeability of the reservoir is, therefore, a local phenomenon and there is the possibility of connecting the wells to fractures tied to faults and tectonic laminations.

Other boreholes, on the contrary, are sited in zones with a more general low permeability. In these zones, drastic changes in productivity after stimulation are not expected. However, there are a few wells which could become economically viable with only a relatively small increase in productivity. An even larger number of wells could be used for injection purposes immediately or when stimulation achieves only a limited success. The exploitation of reservoirs which have uniformly low permeability throughout most of their area is a problem. In fact, these characteristics are presented by large areas of the known fields and the majority of deep hot rocks reached by

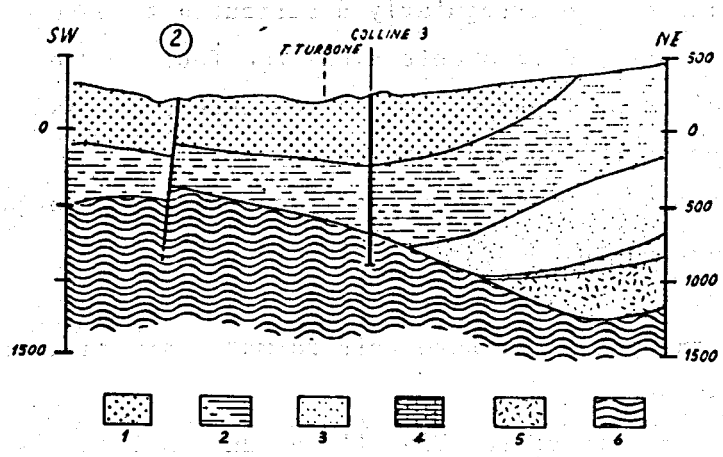

Fig. 12. Schematic geological cross-section of the zone East of the Serrazzano structure. 1) Post-orogenic sediment; 2) Ligurids; 3) "Macigno sandstone"; 4) Mainly carbonate formations of the Tuscan unit; 5) Burano formation; 6) Paleozoic formations.

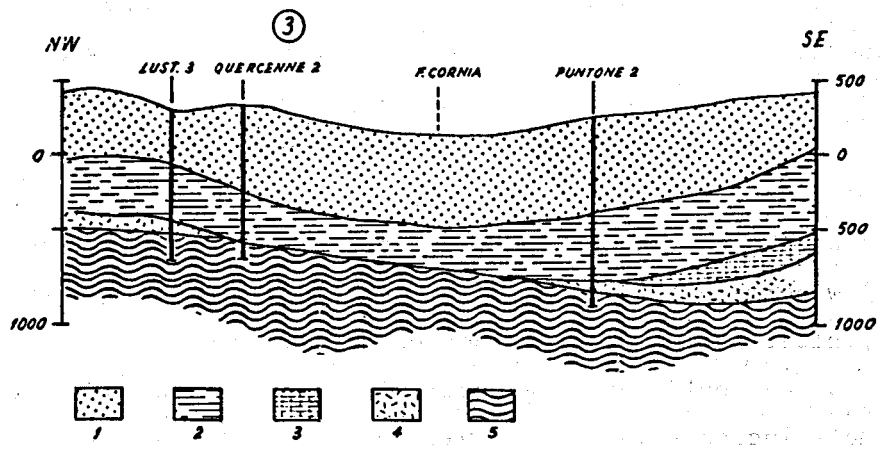

Fig. 13. Schematic geological section of the zone NE of the structure of Lagoni Rossi. 1) Post-orogenic sediments; 2) Ligurids; 3) Mainly carbonate formations of the Tuscan Unit; 4) Burano formation; 5) Triassic-Paleozoic terrigenous formations.

wells. Permeability is too low to permit economic production, too uniformly low to expect positive results from well stimulation attempts, but too high for hot dry rock type exploitation. The injection of large amounts of water into groups of wells in the low permeability area and the production of a flow from the injection zone to the high permeability, depleted areas of the field is now being considered. Feasibility projects based on this idea are now being studied.

Three of the Travale wells are sited over a positive structure of the potential reservoir, on the margin of a graben and near productive or exploited wells (Fig. 14).

This structure is cut by a group of NW-SE trending direct faults in three main steps.

The boreholes have generally crossed rather thick layers of the Burano formation and the metamorphic basement (phyllites and quartzites, followed by alternations of anhydrites and crystalline dolostones).

Again it may be possible to connect these wells to a fracture system tied to the faults bordering the graben.

The fourth well selected in the Travale zone lies in the central part of this graben (Fig. 15). It appears to have been drilled on the E-NE extension of the positive structure characterizing the productive area. The well was chosen because even a small productivity would be of extreme interest for the study of the geothermal reservoir in this zone.

From the thermodynamic point of view, the group of wells in the Larderello geothermal field show temperatures between ~200 and 270°C in the potential reservoir and reservoir pressures between 17 minimum and 36 atm maximum. The Travale group of wells has temperatures of 250-260°C in the potential reservoir and reservoir pressures around 50 atm.

The stimulation methods which can be employed on the 13 selected wells depend on the geostructural situation around the well and on the

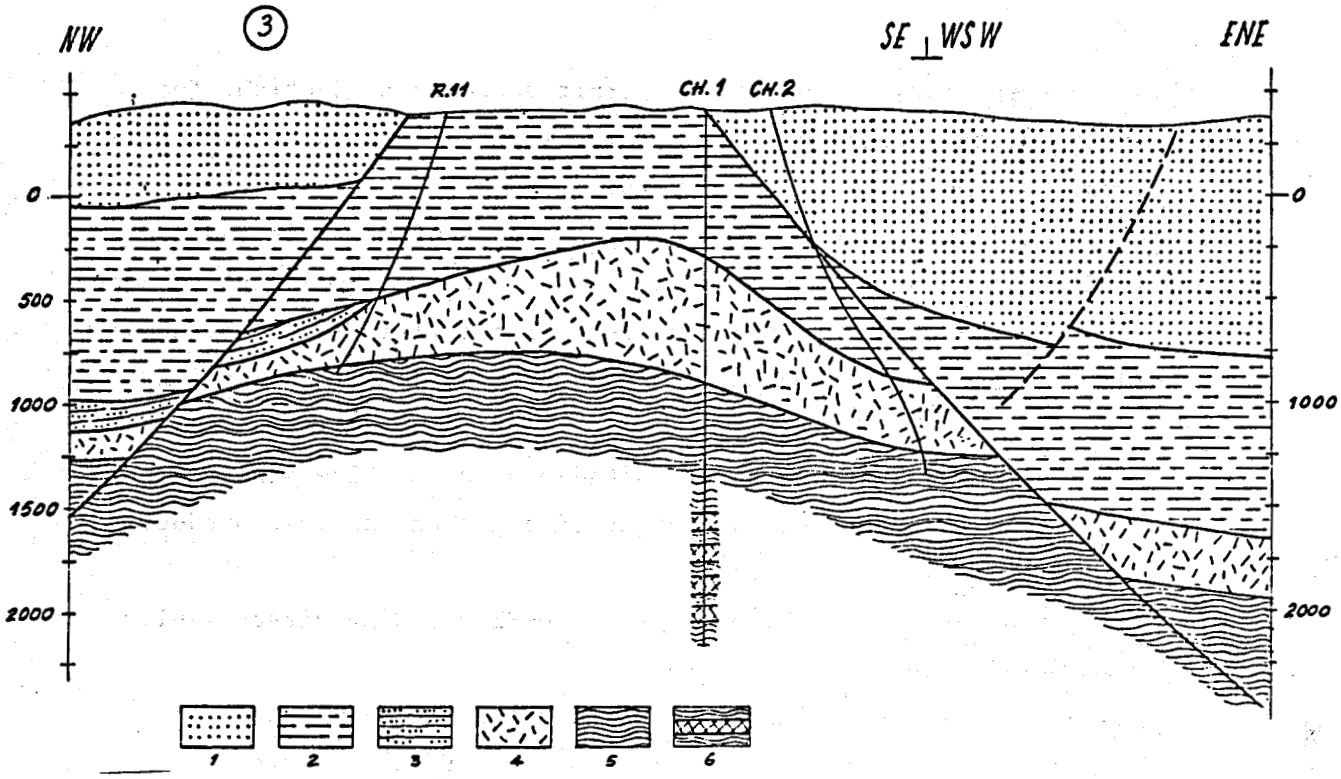

Fig. 14. Schematic geological cross-section of the new field of Travale. 1) Post-orogenic sediment; 2) Ligurids; 3) "Macigno sandstone"; 4) Burano formation; 5) Paleozoic phyllites and quartzites; 6) Paleozoic phyllites, quartzites, anhydrotes, and crystalline dolostones.

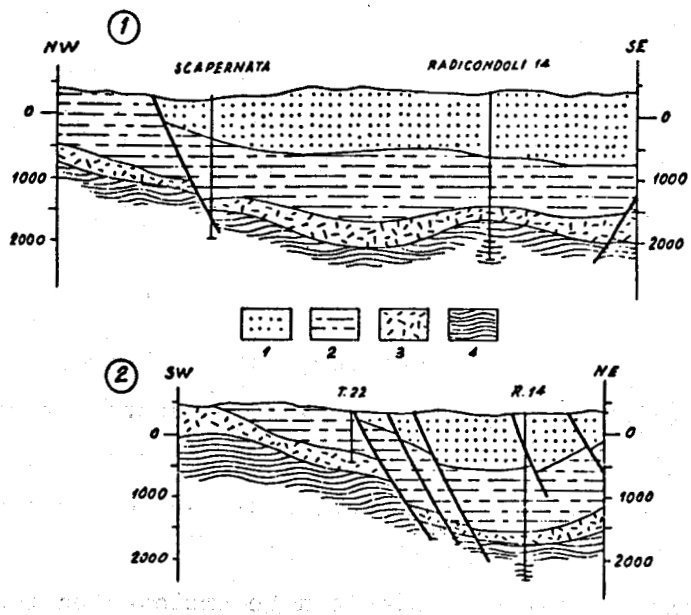

Fig. 15. Schematic geological cross-section of the Travale zone. 1) Post-orogenic sediments; 2) Ligurids; 3) Burano formation; 4) Paleozoic phyllites and quartzites.

type of rock formations involved. In order to define the geomechanical and hydraulic characteristics of the formations, to establish whether stimulation is feasible and to be able to plan the treatment program, permeability tests will be made.

REFERENCES

1. R. Celati, P. Squarci, L. Taffi, and G.C. Stefani - Analysis of water levels and reservoir pressure measurements in geothermal wells. Proc. 2nd U.N. Symposium on the Development and Use of Geothermal Resources, San Francisco, Vol. 3 (1975).

2. R. Celati, P. Squarci, G.C. Stefani, and L. Taffi - Study of water levels in Larderello region geothermal wells for reconstruction of reservoir pressure trend. Simposio Internacional sobre energia geotermica in America Latina, IILA, Roma (1977).

3. G. Gianelli, M. Puxeddu, and P. Squarci - Structural setting of the Larderello-Travale geothermal region. Mem. Soc. Geol. It., 19 (1978).

4. R. Cataldi, G. Stefani, and M. Tongiorgi - Geology of Larderello region (Tuscany); contribution to the study of the geothermal basins. Nuclear geology on geothermal areas. Laboratorio di Geologia Nucleare, Pisa (1963).

5. R. Celati, G. Neri, P. Perusini, and P. Squarci - An attempt to correlate kh distribution with geological structure of Larderello geothermal field. Geothermal Reservoir Engineering, Stanford University, Stanford, pp. 37-41 (1975).

FRACTURING TECHNIQUES AND SOME APPLICATIONS IN ITALY

P.BERRY [1] C.CATALDI [2] E.M.DANTINI [1]

ABSTRACT

Problems connected to stimulation processes are analysed as critical parameters that must be taken into account from the research stage through to exploitation.

Such an approach is of prime importance for the optimization of the project, for achieving more efficient results during the implementation stage, and finally, for making the best choice of the stimulation technique to be adopted.

The relationship between the stimulation treatments and the geostructural and geomechanical characteristics of the reservoir have been analysed also in the light of some recent experiences in Italy.

1 - INTRODUCTION

For many years now the Oil Industry has been implementing technological operations (stimulation processes) that make it possible to intensify production and to control the exploitation of reservoirs. The way to proceed is decided individually for each case at the end of a drilling program and on the basis of the ensuing results.

The design criteria of the stimulation processes are therefore based on the experience acquired through drillings that do not always turn out to be relevant to the particular case being dealt with. Since, within this context it is not possible to quantify most of the numerous parameters that condition the outcome of the stimulation treatment, the ensuing effects are often disappointing.

A statistical analysis |1| correlating the design data with the results obtained through stimulation can provide the means for a

[1] University of Rome

[2] ENEL, National Geothermal Unit

better choice of the method, of the relevant parameters, and furthermore, it can offer a more accurate forecast of the results that can be obtained through stimulation.

The analysis of problems related to the investigation and exploitation of geothermal fields demands an approach making the most of the geostructural characteristics, of the physical and mechanical parameters of the reservoir, and of the complex laws governing its behaviour as concerns the mass and heat flow problems. An appropriate approach should make use of all of these data to solve all the planning and design-related problems.

Indeed, each stimulation generally produces a deep variation in the mechanical and hydraulic characteristics of the surrounding rock mass following an input of energy either in static or in dynamic conditions.

Such processes are however, initially conditioned by the geometry of the hole and by the characteristics of the formation.

As the process gradually spreads out, there are close interactions between the effects of the energy introduced (fractures) and the characteristics of the rock mass, that affect the final outcome of the operation. Keeping account of this close interdependence, the investigation programs for the research and study of geothermal fields should be worked out on the basis of criteria that consider the stimulation techniques as a means of investigation capable of providing useful information on the most important parameters that characterize the reservoir.

Furthermore, the exploitation program should also consider the various solutions provided by the stimulation techniques in relation to the geostructural and geomechanical characteristics of the rock mass.

This paper briefly discusses the problems relating to the correct determination of some of the fundamental parameters that govern the mechanical behaviour of the reservoir rock;the limits of the simplifications usually adopted,will be analysed for the cases in which two of the most widespread stilumation techniques are adopted:hydraulic fracturing and explosive fracturing.

2 - BASIC CHARACTERISTICS OF THE ROCK MASS THAT INFLUENCE STIMULATION

In order to optimize any type of intervention in a reservoir it is necessary to have an exhaustive knowledge of the parameters and

laws that govern its behaviour in all the possible situations that could occur.

In particular, during the design and implementation stages, and when analysing the results obtained after stimulation, it is necessary to keep account of the following fundamental parameters.

2.1 Original and induced state of stress

In engineering practice, the values and the directions of the three principal stresses are determined by means of well-founded methods that provide both sufficiently accurate data and a reliable interpretation of the results.

As regards Geothermy, attempts to make in situ measurements cannot be made due to the great depths and high temperatures involved. This drawback is usually overcome by assuming that one of the components is vertical and its value is inferred from the density of the formation (γ - logs). Since also this measurement is hampered by the high temperatures of the well, the trend of the values must be extrapolated down to the required depth.

Furthermore, it is virtually impossible to predict the horizontal state of stress merely on the basis of the theoretical considerations. In large areas, experimental measurements have pointed out the presence of higher horizontal stresses than the vertical ones, this being probably due to the tectonic events.

In areas where high temperatures are not involved, the experimental technique based on "hydraulic fracturing" provides useful indications as to the minimal principal stress for wells that are even very deep |2|. The obstacle set up by the high temperatures can be avoided by interrupting the measurements where the temperature starts to be too high, and then the values can be extrapolated down to the required depth.

The results obtained through this technique together with its limits will be analysed in one of the next paragraphs; such results must, however, be interrupted with caution and account must be kept of the mechanical behaviour of the formation.

The original state of stress is deeply modified near the walls of the well. Further variations are due to the static or dynamic pressurization of the borehole (hydraulic or explosive fracturing), or to the mass and heat flow (injection and production).

An analysis of the induced state of stress is rather complex since it is generally characterized by a point distribution of the

principal values and of the principal directions. Furthermore, variations in the hydrostatic stresses exerted by the fluid in the pores (i.e. after an explosion in the blasthole), or the flow that gives rise to hydrodinamic actions in correspondence to the walls of the fractures (i.e. after injections, production or hydraulic fracturing), modify the state of stress.

Experimental results have provided the possibility to check the validity of the law of effective stresses, as far as rocks are concerned, by using the same expression which applies to soft soils. The state of total stress $\bar{\sigma}$ acting simultaneously with the pore pressure P_o can be broken down into an effective state of stress and a hydrostatic state of stress, and therefore, the following equation can be written |3| :

$$\bar{\sigma}' = \bar{\sigma} - P_o \qquad (1)$$

2.2 Deformability and strength

2.2.1 Deformability

The assumption generally made for solving "reservoir engineering" problems (i.e. that rocks are characterized by an isotropic, homogeneous, linear and elastic behaviour) is not true in practice.

Indeed, the mere presence of oriented microfissures causes the rock to show a decidedly anisotropic behaviour. Even for the rocks consisting of minerals having a marked orientation, the anisotropic behaviour is partially to be attributed to the latter, whereas the influence of the microfissures appears to prevail.

The progressive closing of the microfractures brings about evident changes in the linear behaviour (Fig.1) and in the elastic behaviour, and as the stress increases, the deformability tends towards that of the rock matrix, thus entailing a decrease in the anisotropic degree (Fig.2).

When the rock matrix is assumed as being homogeneous and isotropic within the range of investigated pressures, and neglecting the influence of the temperature, the compressibility of the rock matrix C_r can be taken as constant. The compressibility of the rock C_b depends not only on the overall volume of the voids but also on the form of the pores (Fig.3) |5,6,7| and it varies with the effective stress |8,9,10|.

In particular for some types of rocks, a variation of the C_b value can be noted both with the direction and with the level of the applied stress |5| that can be ascribed to the closing of the microfissures. At low loads, for rocks such as granite, gneiss, quartzite,

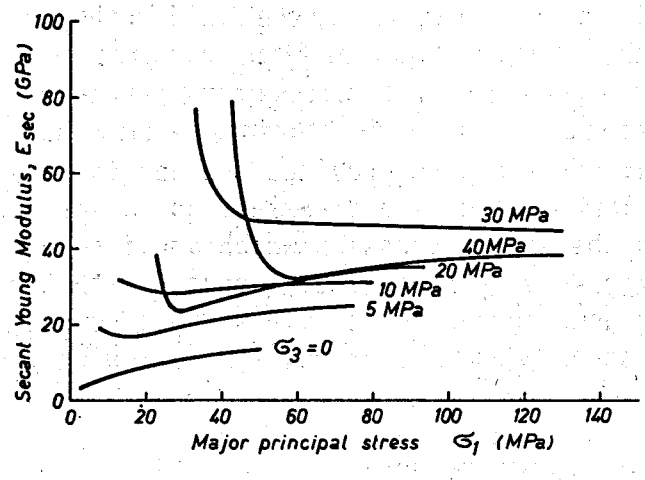

Fig.1 - Secant Young Modulus versus the major principal stress (phyllites from the Larderello field)

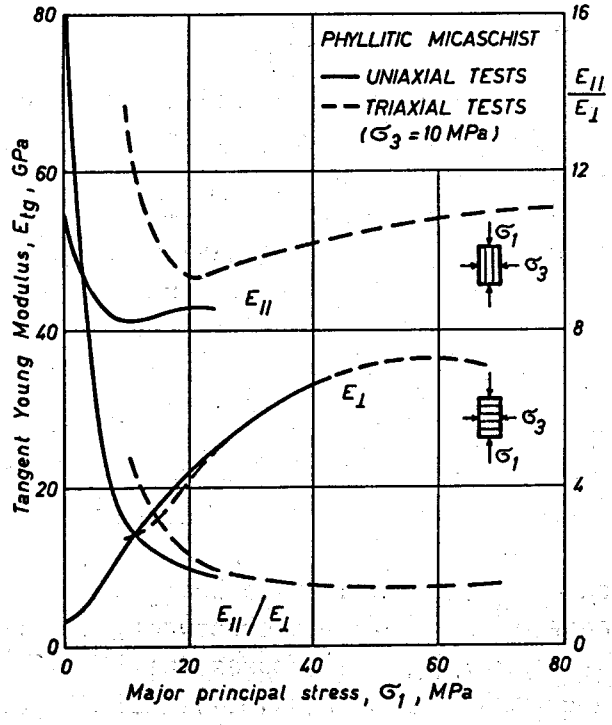

Fig.2 - Tangent Young Modulus versus the major principal stress. At high stresses the deformability of the rock tends to be similar to that of the rock matrix with ensuing decrease in the anisotropy degree |4|

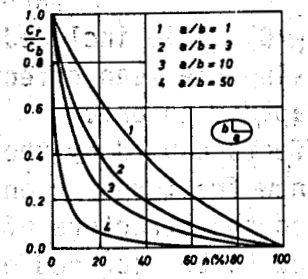

Fig.3 - The compressibility of the rock C_b depends not only on the overall volume of the voids but also on the form of the pores |7|

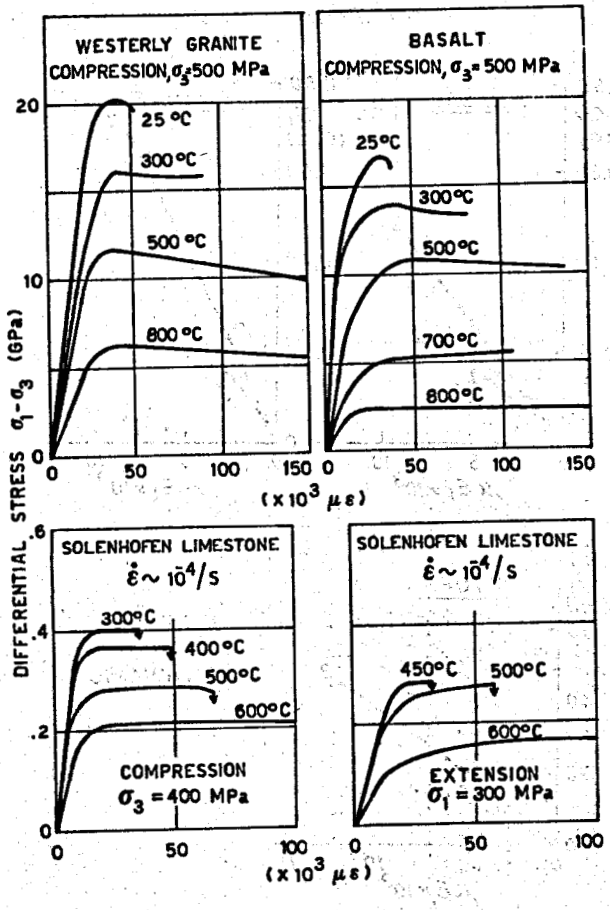

Fig.4 - Stress-strain curves relating to some samples of granite, basalt and limestone for triaxial compression and extension tests. Notice the variation in the mechanical behaviour of the rocks (deformability and strength) when submitted to temperature variations |11|

and marbles, values of the C_b/C_r ratio included between 7 and 3 were measured, whereas, by increasing the mean effective stress, such values all tend more or less rapidly to one.

If the extent of the effects caused by the temperature variations upon the initiation of new fractures or on the extension of pre-existing discontinuities or on the structure of the composing minerals is changed, the causes are to be ascribed essentially to the type of rock involved and to the way in which the temperature variations are produced.

Laboratory tests |11| have pointed out a progressive increase in the values of the elastic characteristics and a variation of the

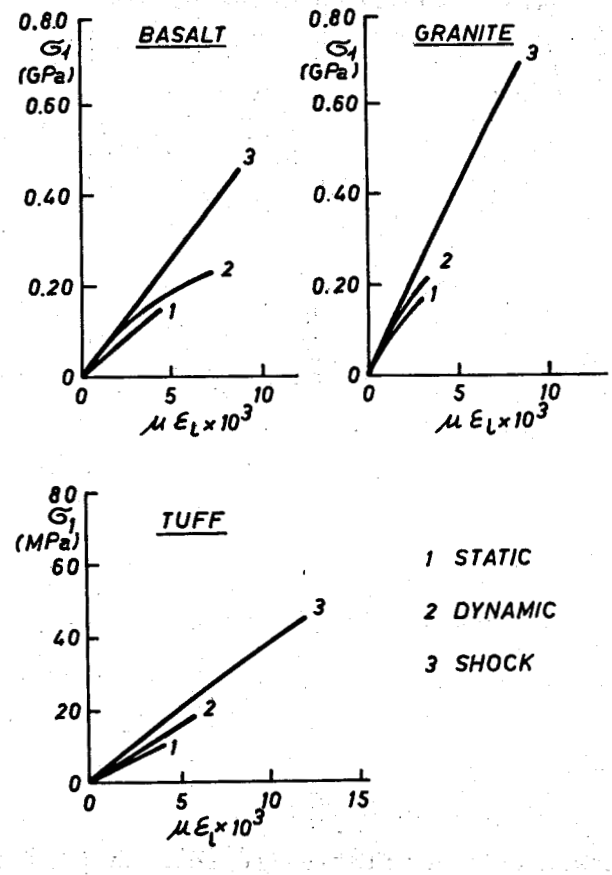

Fig.5 - Stress-strain curves relating to some samples of granite, basalt and tuff for uniaxial compression tests. Notice the variation in the mechanical behaviour of the rock materials (deformability and strength) when they are submitted to different load rates (static, dynamic, shock) |14|

stress-strain curves as the temperature slowly increases (Fig.4).

Also the temperature decrease (due to the injections in geothermal wells) brings about a concentration of stresses caused by the differential deformations of the minerals forming the rock and therefore, a progressive decrease of the stiffness due to thermal cycles is to be expected.

Generally the axial and transversal deformability tends to increase with the load rate depending upon the type of imposed stress and on the characteristics of the rock |12,13| . As regards problems related to explosive stimulations,some laboratory tests provide interesting indications |14| which compare the elastic characteristic of the materials with static and dynamic loads and with shocks (Fig.5).

2.2.2 Strength

As previously mentioned even the strength of rocks having brittle behaviour is a function of the effective stresses |15| and in general the strength values grow smaller as the fluid pressure in the microfissures increases.

Even though an adequate number of experimental tests are not available, it may however be assumed that the presence of a fluid in the pores does influence the strength of materials submitted to dynamic stresses produced by explosives. A greater development of the crushed zone and of the radial fractures produced by explosive stimulation is therefore to be expected.

The influence of temperature has been the object of extensive theoretical and experimental research and investigation|11,16| also for stimulation treatments in oil wells |17,18|.

With the gradual increase of the temperature values,a considerable decrease in the strength value related to the applied stress can be noticed (Fig.4), and generally the behaviour of the material deeply changes in terms of failure, passing from brittle to perfectly plastic.

The effect of temperature decreases on strength values can turn out to be the same as that noticed for temperature increases. Even in this case rock fracturing is caused by induced stresses in the rock.

The way in which the rock is stressed causes considerable variations in the strength values. In particular when the load rate is close to that obtained by the explosion of a charge in a blast-hole, a considerable strength increase is to be expected (Fig.5).

2.3. Flow in continuous porous media

In poorly fractured rock masses having a brittle behaviour and in fractured rock masses (in transitory flow conditions), the motion of the fluid in the matrix which is virtually made possible by the presence of communicating microfissures and pores, becomes considerably important.

The experimental relationships that link the porosity values to the permeability values, as suggested by some authors |19|, cannot be applied on a general basis since permeability is a function of many other factors.

Extensive laboratory investigations have pointed out that the pore structure can condition the distribution of the permeability values|20|.

Variations in the effective state of stress or in the pore pressure or in the temperature, entail changes in the porosity values.

Fig. 6 shows that porosity decreases as the effective hydrostatic stresses increase for some typical rocks of the Larderello field.

High temperature values cause an extension of the discontinuity network probably because of the differential dilatation of the solid matrix that brings about a concentration of stresses.

For some types of rocks, as temperature increases initially there is a decrease in the porosity, problably caused by the dilatation of the minerals forming the rock. Beyond a certain temperature value, at which new fractures are initiated |12|, the porosity gradually increases.

The increase of effective stresses causes the closing of the microfissures and as a consequence a decrease in the permeability values. The extent of such variations depends merely on the form and on the orientation of the pores and microfissures with respect to the applied state of stress and it varies as the latter varies.

For the case of some sedimentary rocks (Fig.7) that are homogeneous, not fractured and compact with equidimensional pores, permeability generally varies only slightly with the direction and with the intensity of the state of stress |22|.

On the other hand for fissured rocks having a rigid behaviour there is a considerable decrease of permeability as the effective stress increases|23 , 24| and quite often an anisotropic flow develops.

Fig.8 shows the results of permeability tests performed on

samples of phyllites, recrystallized micaschists and gneiss in the Lardarello reservoir.

Fig. 9 shows the permeability values of the four samples in Fig.8, obtained for different values of the effective hydrostatic stress versus the corresponding differing porosity values. A first analysis has shown that the two parameters appear to be correlated by an exponential law.

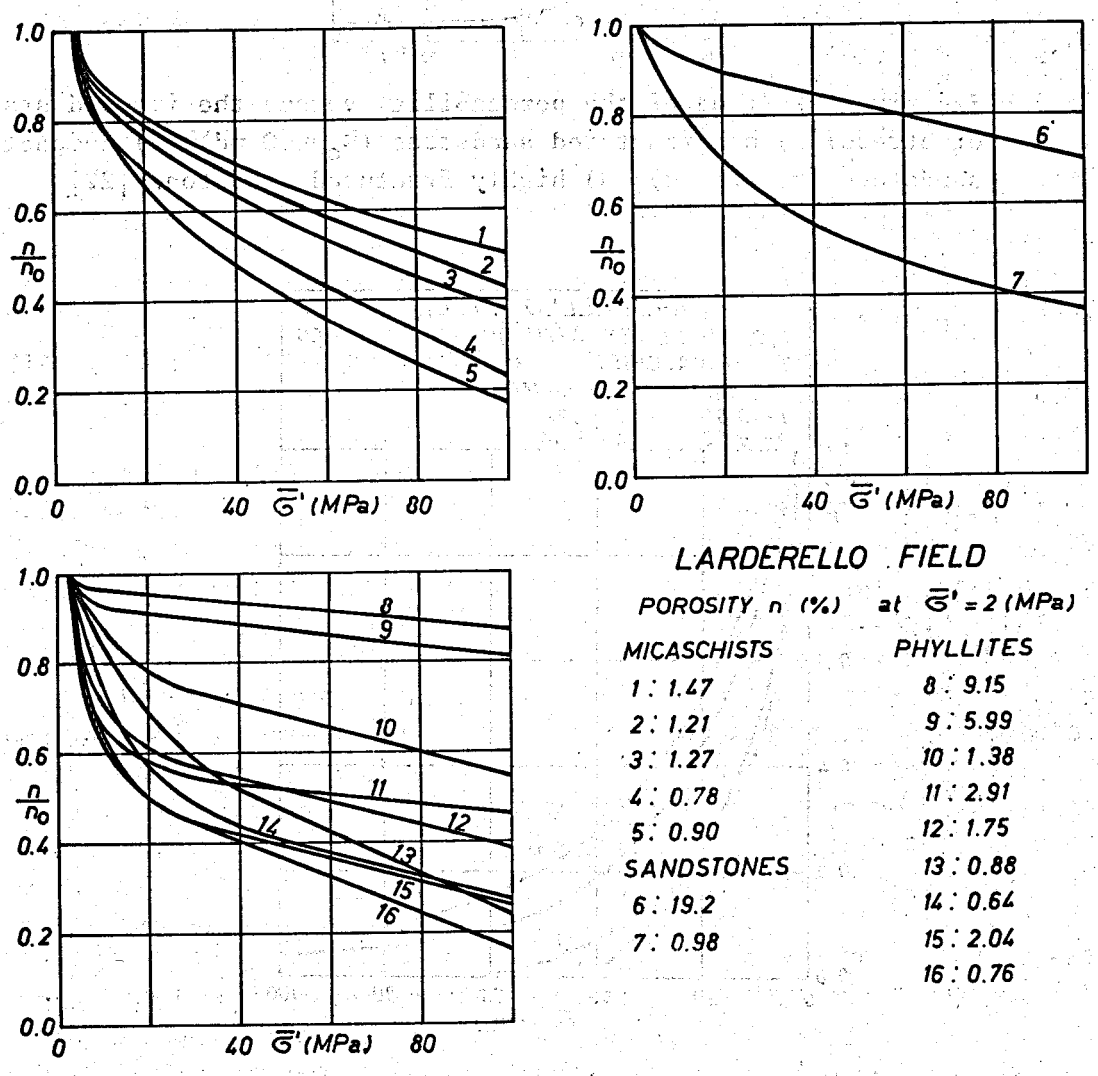

Fig.6 - Experimental trend of the permeability versus the effective hydrostatic state of stress (Larderello field)

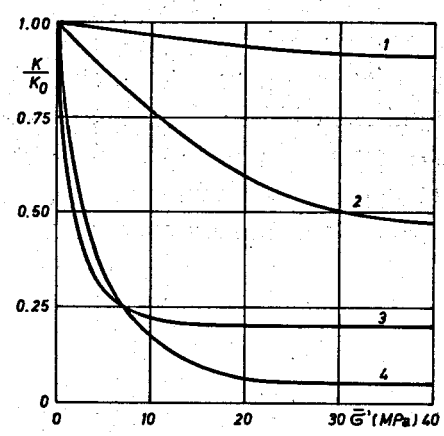

Fig.7 - Experimental trend of the permeability versus the imposed state of stress: 1) non-fractured sandstone (k_o = 60 md); 2) compact sandstone (k_o = 25 md); 3) highly fractured sandstone |22|

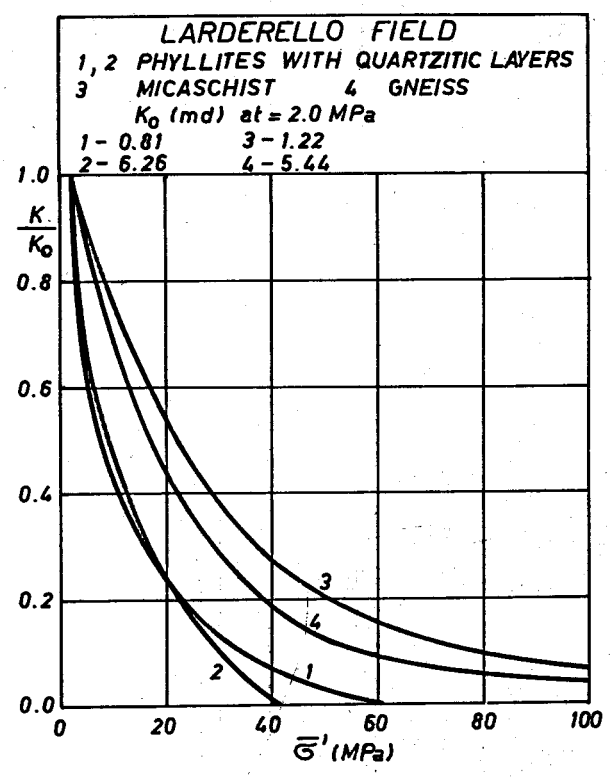

Fig.8 - Experimental trend of the permeability for specimens submitted to hydrostatic effective stresses varying from 2 to 100 MPa (Larderello field)

However , further data are required in order to make a final evaluation as to the general validity of the law.

For rocks having a homogeneous and isotropic hydraulic behaviour,when they are hydrostatically stressed and by assuming that the permeability values depend exclusively on the acting mean effective stress, Morgenstern |26|suggested the following empirical relationship between the permeability and the mean effective stress:

$$k = \frac{A_o}{(\bar{\sigma}' + A_1)^m} \qquad (2)$$

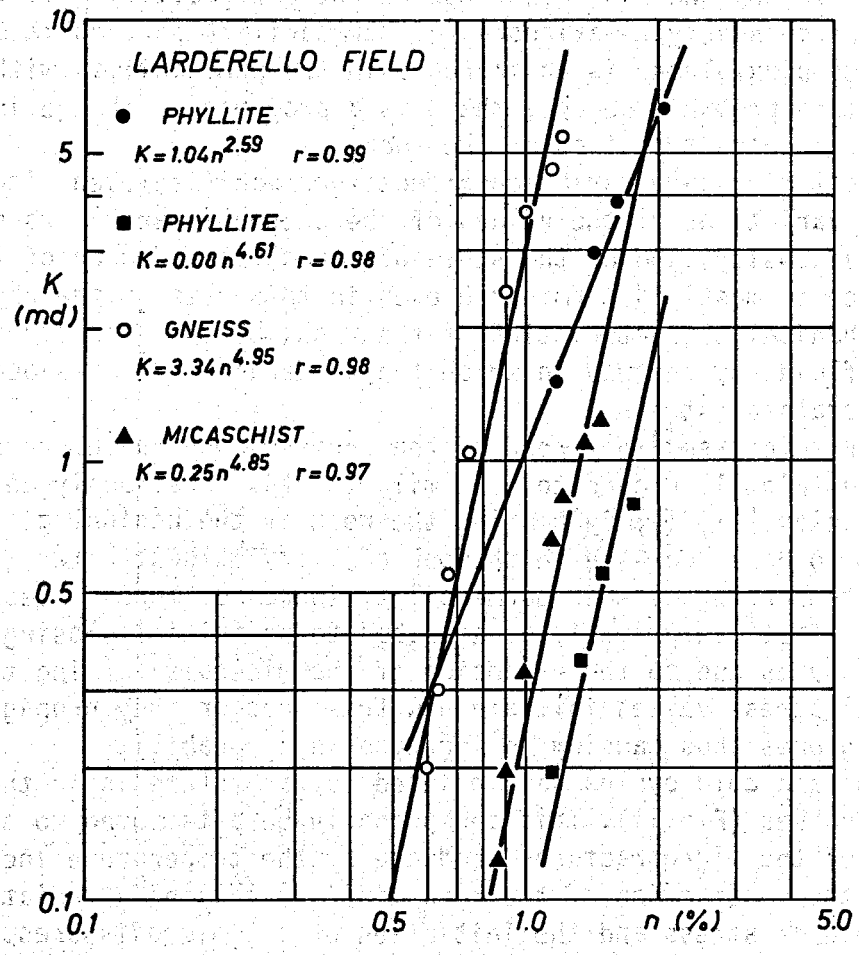

Fig.9 - Relationship between porosity and permeability (Larderello field)

By plotting the permeability values obtained for the samples of the Larderello reservoir in a log-log diagram the curves shown in Fig. 10 are obtained. The trend is a typically curvilinear trend that has been noticed also for other types of rocks having microfissures and a brittle behaviour|23,24,26|, and it points out that the values of the coefficients of the empirical relationship depend also on the range of the imposed effective stresses.

Loading and unloading cycles emphasize the irreversible behaviour of the flow |27,28| and this is probably due to the irreversible closing of a part of the microfissures present in the samples.

For very high stress values it is possible to determine the propagation and the coalescence of the microfractures which are emphasized|12| by the rapid increase of the permeability values|29,30|.

The dependency relationship of permeability on temperature is rather complex. There is an increase in the permeability with the temperature probably because there is a progressive change in the structural characteristics of the rock.

The temperature variation affects permeability even indirectly through variations of the values of the physical parameters of the fluid (viscosity) and of the state of stress. The degree of the influence is mostly determinated even in this case by the physical and mechanical characteristics of the rock, by the characteristics of the fluid, by the way in which the temperature changes occur, and by the state of stress.

For some cases the trend of the permeability values versus temperature (Fig.11) proved to be similar to that previously described for porosity |21,31|. By heating the rock at the beginning, there appears to be a decrease in the permeability values. Later, for higher temperature values permeability increases more or less rapidly. This fact can probably be ascribed to an initial closing of the microfissures due to the expansion of the minerals forming the rock; critical stress values initiate new fractures or they propagate the existing ones thus causing an increase in permeability.

Hot and cold cycles have pointed out a hysteresis in the permeability values (Fig.11). This can probably be attributed to the propagation of the microfractures produced by the temperature increase and by the contraction of the rock minerals causing a variation in the state of stress and the initiation of new microfissures.

All the aspects that have been illustrated are made more complex in situ because all the various effects that have been analyzed sepa-

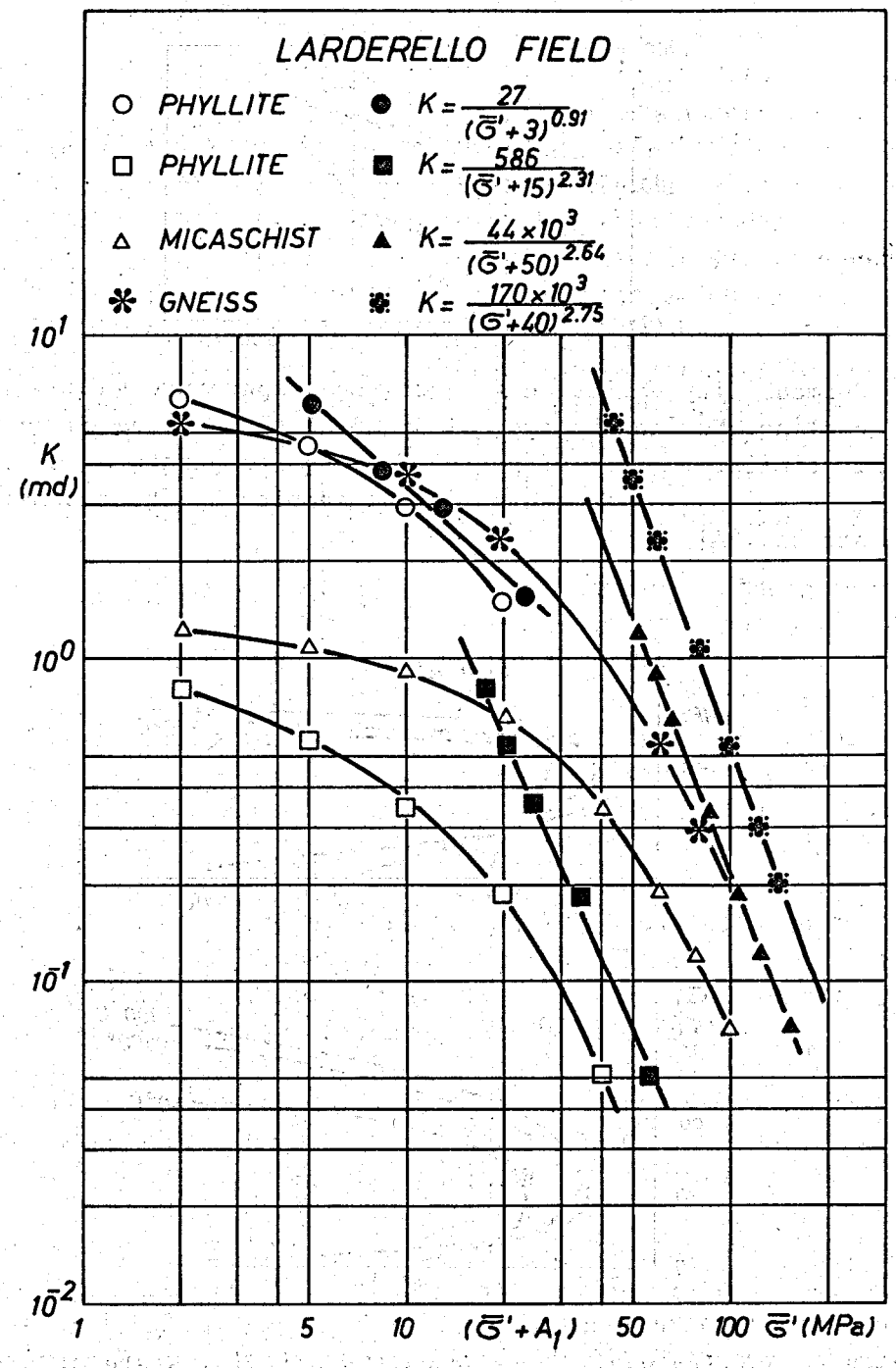

Fig.10 - Experimental trend of the permeability for specimens submitted to hydrostatic effective stresses and experimental data fitted by equation (2) (Larderello field)

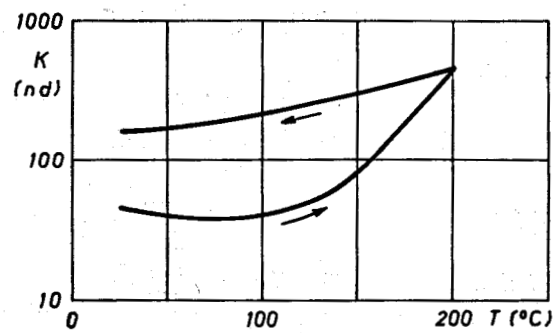

Fig.11 - Permeability variation for growing temperature values and for cooling. Notice the typical trend of the heating curve which is similar to that of porosity versus temperature and the increase in porosity caused in the samples by the thermal stress |24|

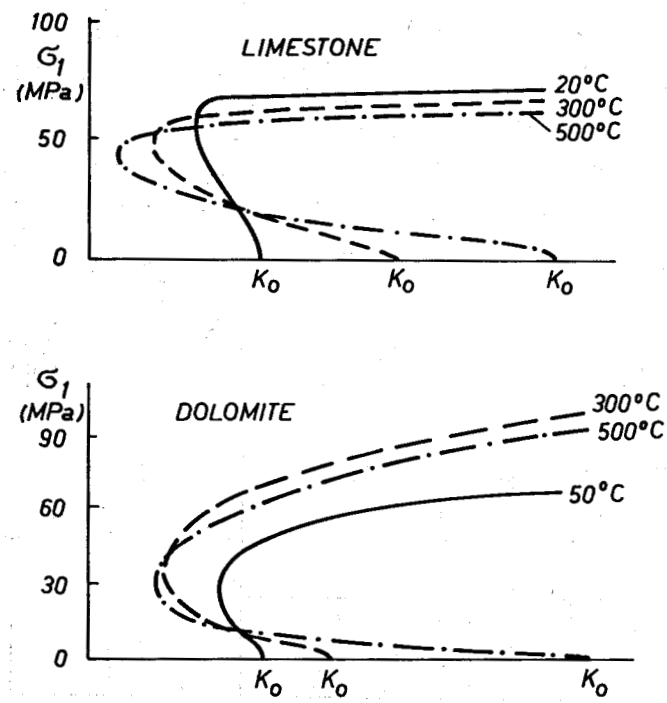

Fig.12 - Permeability variation versus the uniaxial state of stress and the temperature variations. The typical trend is caused by the initial closing of the microfractures and the increase in porosity brought about by the induced stresses |21|

rately obviously overlap.

As an example, Fig. 12 shows the effects on permeability both of the pressure and temperature variations. The curves prove that it is not possible to expect the phenomenon univocally. Indeed, in some cases, temperature appears to play a marginal role as compared with the imposed stress, in other cases thermal stresses have a greater influence. This difference is probably due to the different types of rock and to the type of imposed stress.

2.2. Mass flow in fractured rocks

In most geothermal wells the flow under standard conditions occurs through the discontinuities present and is due to the great difference between the permeability values of the rock mass and of the rock material. Some permeability value ranges of a few common rocks are given |32|:

Table 1 : In situ and laboratory permeability values k(cm/s)

ROCK MATERIAL	
Sandstone	$1\ 10^{-10} - 2.2\ 10^{-5}$
Granite	$5\ 10^{-11} - 2.0\ 10^{-10}$
Limestone and Dolomite	$7\ 10^{-10} - 1.2\ 10^{-7}$
ROCK MASS	
Sandstone	$1.0\ 10^{-2}$
Granite	$0.6\ 10^{-3}$
Limestone	$1.0\ 10^{-4} - 10^{-2}$
Gneiss	$1.2\ 10^{-3} - 1.9\ 10^{-3}$

The following table provides the reservoir formation for some of the most important Italian Geothermal Reservoirs.

The hydraulic characteristics of the fractures condition the flow of the fluid in these reservoirs, and the mechanical behaviour of the rock mass depends mainly on the geomechanical characteristics of the joints.

Experience has shown that in geothermal fields conditions of flow

Table 2 - Italian Geothermal Reservoirs

FIELDS	RESERVOIR FORMATION
Larderello	Quartzites, Phyllites and Anhydrites
Travale	" " "
Monte Amiata	" " "
Piancastagnaio	" " "
Torre Alfina	Limestone
Latera	"
Cesano	"
Lago Patria	Tuffs

anisotropy, dishomogeneity may be found, according to the geometrical characteristics of the fractures (spacing, opening, state of surfaces), to their orientation and distribution, to the extent to which they are filled as brought about by the settling of salts, to the state of stress.

A typical example |32| of dishomogeneous distribution of the flow is found in the Larderello reservoir that represents a reliable means for exploring the details of this problem due to the high number of wells that have been driven.

Another example is the Cesano Reservoir (Fig. 13) where the orientation of the fractures, that are mainly sub-vertical, plays an important role. In the upper part of the reservoir, these fractures are partially closed due to the settling of salts, and besides, intense recrystallization occurs due to the high temperatures. Furthermore, in these reservoirs the inter-section of a high number of discontinuities and their dishomogeneous filling originates canals where the flow runs; these canals could even have led to surface manifestations (volcanic chimneys).

In order to theoretically analyse in a straightforward way the reservoir engineering problems, the rock mass can be schematized as a porous and continuous medium having an anisotropic permeability with,on average, the same characteristics as the real rock mass |33|

In this manner, the value of the average rate can be defined for each point and the proportionality relationship between the velocity vector and the potential gradient vector is defined by means of a symmetric matrix of the permeability |31|.

If the objective is that of studying the surrounding of a well inside a reservoir (for example when the well crosses an important dis-

continuity surface or when dealing with stimulation problems), it is preferable to assume a perfectly impermeable continuum crossed by several systems of joints that, more or less, intercommunicate. In this case, the solution to the flow problems can be found by studying in detail, the motion of the fluid through such discontinuities.

Experimental tests |34| carried out on a rough natural fissure in a porphyry specimen in which the joints had different opening conditions, have pointed to a clear non-linear relationship between the flow-rate and the hydraulic gradient. For very low hydraulic gradients

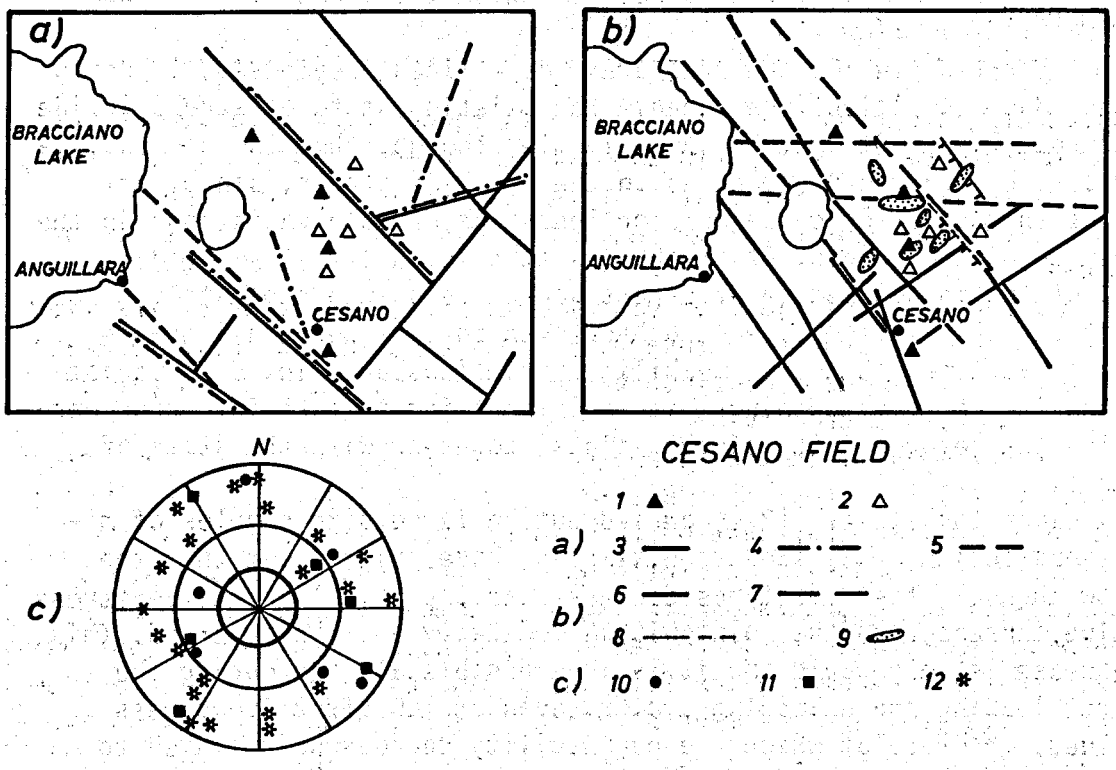

Fig.13 - Structural scheme. Cesano field: a and b show: 1) productive wells; 2) dry wells; 3) electric discontinuities; 4) magnetotelluric discontinuities; 5) gravity anomalies; 6) main regional tectonic lines inferred from photo-geological surveys; 7) alignment of volcanic chimneys; 8) faults; 9) volcanic chimneys Schmidt's net in c shows the directions of the principal faults in outcrops near the Cesano field in the following formations: 9) siliceous limestone ("Corniola"); 10) Dolomite limestone; 11) Limestone ("Calcare massiccio")

there is a progression towards a non-linear laminar condition and finally to a turbulent flow (which is typical in the case of a fracture crossed by a well). On the basis of these results a power law was proposed between the effective mean flow rate of the joint and the opening "e" with an exponent that varies according to the flow rate:

$$q \propto e^{m} \qquad (3)$$

The exponent is 2 for a linear laminar flow; 1.2 for a fully turbulent flow, and it ranges between these two values for the non-linear laminar flow.

Water flow inside the fractures, as noticed previously, leads to hydro-dynamic actions that change the existing state of stress inside the rock mass. It must be borne in mind though, that the permeability inside the fracture depends on the state of stress, since variations in the latter cause more or less considerable variations in the opening of the joints. It is obvious that the water flow problems and of the induced state of stress cannot be solved separately since they mutually influence each other, even in a rather considerable manner at times. Since permeability variations are linked to variattions in the joint openings, it is interesting to take into consideration the deformability of the joints, together with the state of stress.

Laboratory tests |27|,carried out on large-size samples of micaceous schist or on sandstone samples, have pointed out that the flow through the fractures decreases as the normal effective stress value increases on the joint with a decidedly non-linear trend. This decrease is very rapid and it is irreversible already during the first loading and unloading cycles, even at low effective stress values. The rate at which the permeability decreases is linked to the opening of the fractures. For closed fractures there is a rapid decrease at the low effective stress values, whereas as the stress increases, the permeability value remains constant. For fractures having a larger opening, the constant permeability value is reached at higher imposed effective stress values. Permeability does not markedly vary with parallel stresses at the joints whereas, it decreases considerably and irreversibly with the shear stresses due to dilatation that occurs close to the limit strength conditions of the joint.

Theoretical analyses show that the permeability of the joints varies markedly with the temperature |35|. It must be noted that probably most of the permeability variations must be attributed to the

variations in the state of stress induced by temperature variations.

It must be borne in mind that much caution is necessary when making an evaluation of the hydraulic characteristics of fractures on the basis of results provided by the permeability tests conducted on rock samples because, this evaluation can differ from that inferred on the basis of the in situ measurements. This difference is greater the higher the fracture control on the flow inside the reservoir (as generally occurs in Italian reservoirs).

Indeed, while it is possible to make sufficiently good laboratory simulations of the pressure conditions of the fluid and of the state of stress (when studying the permeability) it is very difficult to obtain a meaningful representation of the fractured medium by using small samples.

Observations made in some fields confirm the fact that permeability and state of stress are mutually interdependent. For the reseroirs where permeability depends almost exclusively on fractures, the decrease in the production of the wells is to be attributed to a decrease in the pressure of the fluid (increase of the effective stress). Conversely, in the reservoirs where matrix permeability prevails, the effective stress appears to have less influence on the latter.

The curves obtained for production and injection tests do not differ much for the reservoirs where matrix permeability prevails, whereas it was pointed out that the injection rate is much higher than the output rate for reservoirs where permeability is due to fractures. Increasing flow values during production lead to an increase in the effective stress that tends to close the fractures. Whereas, for the case of injections, as the flow rate increases the effective stress that acts on the walls of the fractures decreases.

3 - HYDRAULIC FRACTURING

As known this technique consists in using a fluid to pressurize a borehole section isolated by packers in order to lead to the failure of the walls of the hole and to a propagation of the fracture. The fracture clearly entails an increase in permeability due to a decrease in the effective stresses.

By analysing the results of "hydraulic fracturing" performed in sandstones and dolomites (Fig. 14) |22| the flow - pressure curves are characterized by three more or less well defined curve portions depending on the permeability characteristics, on the viscosity of the fluid used, and on the injection conditions. The OA interval repre-

sents the initial pressurization of the hole; AB corresponds to the opening of some fractures in the pressurized part of the hole which have a favourable orientation; BC corresponds to the propagation of the preferential fracture.

The curves show a marked linear trend both when very permeable formations are involved (since the fluid can be injected and it is not possible to induce considerable permeability variations in the rock mass) and for formations having an impermeable matrix and scarce structural discontinuities and therefore, the flow is confined to the fracture.

It is possible to make global analyses |22| of the evolution of the permeability of the reservoir versus the effective stresses both during the extraction of the fluid (already discussed previously) and during"hydraulic fracturing" (Fig.15). Figure 15 points out that in

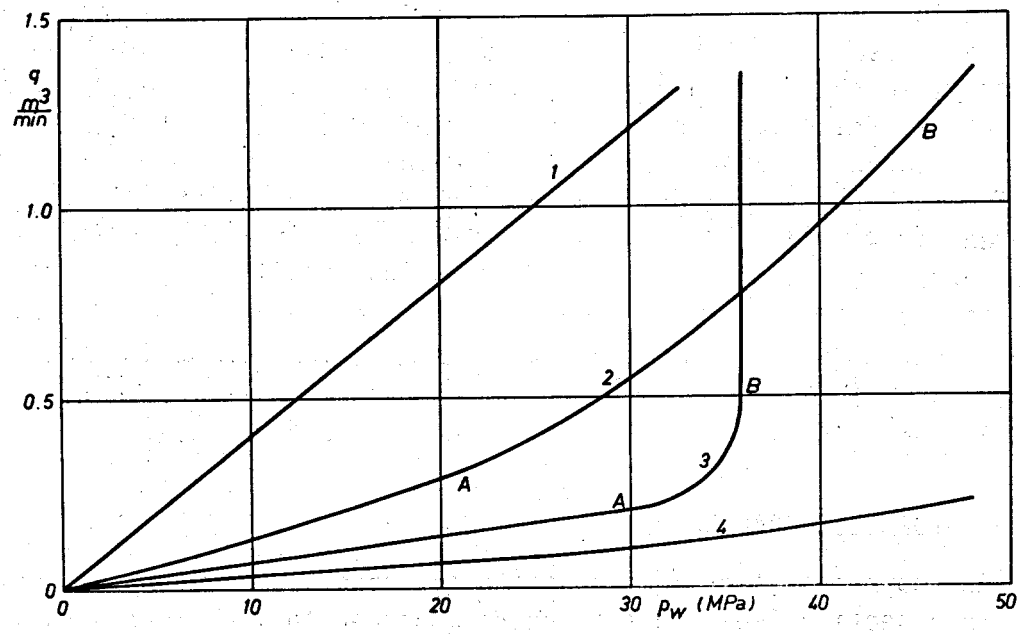

Fig.14 - Hydraulic stimulation in reservoirs having different structural characteristics: 1) permeable sandstone (50-100 md); 2) medium permeability sandstone having slightly permeable fractures (10-50 md); 3) low permeability sandstone (10 md) having very permeable fractures; 4) dolomite reservoirs having very low permeability (<< 1 md) where a hydraulic fracturing treatment does not cause considerable effects |22|

highly fractured formations the hydraulic fracturing operation merely turns out to be an opening of natural pre-existing fractures. In scarcely fractured reservoirs, the effectiveness of the hydraulic fracturing treatment will depend on the ratio (Kh) fracture/(Kh) formation, that is a function of the initial permeability and of the possibility of keeping the fractures open. Quite obviously, a high ratio can annul the effectiveness of the treatment if the permeability of the formation is close to zero.

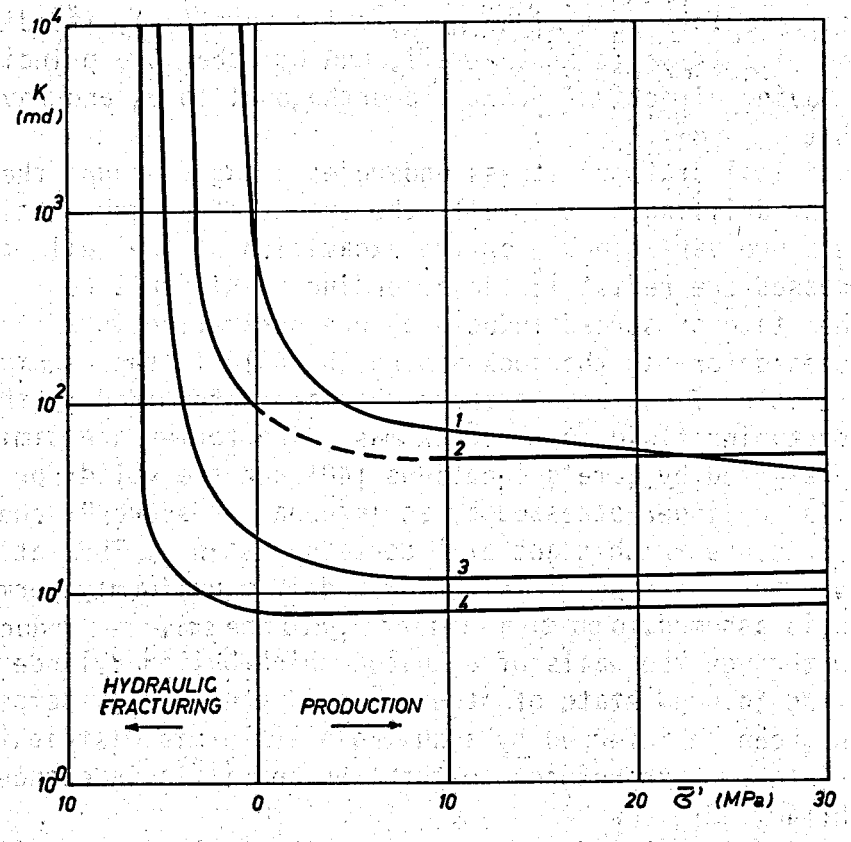

Fig.15 - Permeability versus effective state of stress in hydraulic fracturing. 1) highly fractured reservoir; 2) slightly fractured, average permeability reservoir; 3) and 4) non-fractured low-permeability reservoirs. It must be pointed out that in highly fractured reservoirs permeability depends greatly on the effective stresses, both during the hydraulic fracturing and during production |22|

3.1 Fracturing pressure

The induced state of stress around the well and the analysis of the failure phenomena have been dealt with by many authors |36, 37|. The effect of the penetration of the pressurization fluid into the rock has also been recently the object of investigation |38| by assuming that the rock is porous (with fluid in the pores at pressure P_0), homogeneous and isotropic and that it has a linearly elastic brittle behaviour. The flow of the fluid caused by the pressurization of the hole at the pressure P_W follows Darcy's law.

The induced stresses were written for an original state of stress defined by a maximum or minimum principal stress (σ_3), its direction coinciding with the axis of the well, and by other two principal stresses having directions that are orthogonal to σ_3 and having such values that $\sigma_{H1} > \sigma_{H2}$.

The original state of stress undergoes changes around the hole because of the drilling of the well, the effect of pressurization and the temperature variations. For the excavation of the well, the original stresses are redistributed according to Kirsch's relationships |40| . The state of stress induced by pressurization is a result of the stresses deforming the rock around the hole in the assumption that there is no flow, and of those that are determined by the flow of the fracturing fluid in the rock mass. The former are similar to those represented by Lame's equations |40| and are valid for a hollow thick-walled cylinder stressed by an internal pressure P_W and by an external pressure P_0 that act at a certain distance. The latter can be obtained for an axi-symmetric flow and if a uniformly permeable formation is assumed, in quite a similar way to the stresses induced by the heat flow through the walls of a hollow thick-walled cylinder |41|. Finally, the induced state of stress around the hole by temperature variations, can be inferred by assuming a symmetric distribution of the temperatures with respect to the axes and it is independent from the depth |40, 42| .

By overlapping all of these effects, the following relationships are obtained that give the effective radial, tangential and axial stresses to the walls of the well:

$$\sigma'_v = 0 \tag{4}$$

$$\sigma'_\theta = \sigma'_{H_1}(1-2\cos 2\theta)+\sigma'_{H_2}(1+2\cos 2\theta)-p_w\left(2-\alpha\frac{1-2\nu}{1-\nu}\right)+\frac{\beta E\Delta T}{1-\nu} \tag{5}$$

$$\sigma'_z = \sigma'_v - 2\nu\,(\sigma'_{H_1} - \sigma'_{H_2})\cos 2\theta - p_w\left(1-\alpha\frac{1-2\nu}{1-\nu}\right) + \frac{\beta E\Delta T}{1-\nu} \qquad (6)$$

In these relationships the overpressure that determines the flow is provided by:

$$p_w = P_w - P_o \qquad (7)$$

where ν is Poisson's coefficient that in most cases takes on values from 0.2 to 0.3; α is a parameter that keeps account of the mechanical response of the rock in relation to the flow |8,41,42|. It is expressed by:

$$\alpha = 1 - \frac{C_r}{C_b} \qquad (8)$$

and it can be determined by laboratory tests |9|.

On the basis of the foregoing it can be stated that microfissures bring about a clearly non-linear behaviour, especially at low pressures where the α values for the most common rocks range from 0.9 to 0.7, whereas, as the effective stresses increase, α tends to values ranging between 0.04 and 0.06.

The relationships point out that as overpressures P_w increase, the axial and tangential stresses tend to become tensile stresses. The minimum value of a pressure necessary for inducing tensile stresses along the walls of the well is obtained when $\theta = 0$ and so the relationships are as follows:

$$\sigma'_\theta = 3\sigma'_{H_2} - \sigma'_{H_1} - P_w\left(2 - \alpha\frac{1-2\nu}{1-\nu}\right) + \frac{\beta E\Delta T}{1-\nu} \qquad (9)$$

$$\sigma'_z = \sigma'_v - 2\nu(\sigma'_{H_1} - \sigma'_{H_2}) - P_w\left(1 - \alpha\frac{1-2\nu}{1-\nu}\right) + \frac{\beta E\Delta T}{1-\nu} \qquad (10)$$

So, one might conclude that if, as often occurs in practice, σ'_v is the maximum principal stress or, if it is the minimum principal stress, but the difference $(\sigma'_{H_1} - \sigma'_{H_2})$ is not very high, a vertical fracture will be induced along the wall of the well.

The limit value of the pressure at which failure occurs is expressed by the following relationship:

$$p_w^c = \frac{\sigma_t + 3\sigma'_{H_2} - \sigma'_{H_1} + \beta E\Delta T / (1-\nu)}{2 - \alpha\,(1 - 2\nu / 1 - \nu)} \qquad (11)$$

where if the ν and α values are as previously indicated, the denominator generally ranges between the limits:

$$1.3 \leq 2 - \alpha \frac{1-2\nu}{1-\nu} \leq 1.9 \qquad (12)$$

and for the same rock it varies as the pressure varies. The lower limit can be applied for impermeable rocks, whereas the upper limit can be applied for permeable rocks.

Relationship (11) points out that the distribution law of the pressures, as determined by the injected fluid, does not influence the state of stress in correspondence to the walls of the well, and therefore it does not affect the value of the fracturing pressure. Vice versa, the experimental results (Fig.16) obtained in the laboratory |44,45| and in situ |46|, have pointed out that the strength values obtained by controlling the rate of pressurization, are different from those obtained by controlling the value of the flow. Whereas, by means of the latter procedure, the increment rate of the load does not affect the strength,in the former case the strength increases as

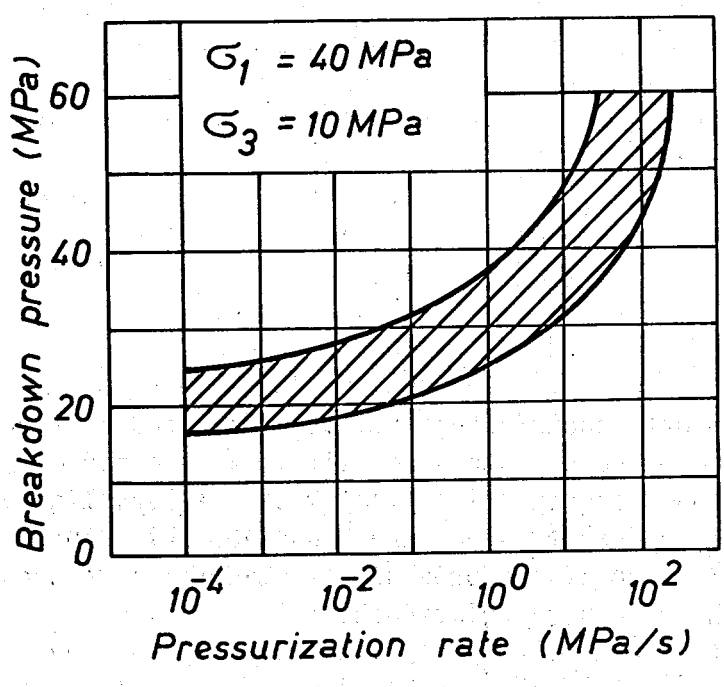

Fig.16 - Hydraulic fracturing: influence of the pressurization rate on the strength of the rock samples |44|

the rate increases, as one might expect. This must probably be attributed to the greater probability of failure occurring as the rock volume increases around the pressurized hole interval. Indeed, experimental measurements have shown that strength decreases even as the diameter of the pressurized interval increases |45|.

Laboratory results |47| show that for scarcely permeable rocks, the value of the breakdown pressure versus the confining horizontal pressure differs considerably from the linear trend expected by expression (11). In particular, for increasing values of σ_H, the values of p_W^c tend to decrease progressively down to the critical values obtained for permeable rocks (lower limit of relationship (12)). This trend could correspond to a permeability increase as previously discussed, brought about by high stresses, that allow a higher penetration of the fluid. Indeed, it must be borne in mind that, at the beginning, the denominator of the relationship assumes a value that is close to one when the load values are zero, whereas, it tends to the typical maximum limit of scarcely permeable rocks as the stresses increase.

The experimental analysis has pointed out that anisotropy has a high influence |48| on the p_W^c values. Under the same confining stresses where $\sigma_V > \sigma_H$ and independently from the σ_V / σ_H ratio, the p_W^c values are higher when the injection hole is orthogonal to the schistosity planes and it gradually decreases down to the minimum value when schistosity is parallel to the axis of the well.

If the hole is crossed by joints, the values of the breakdown pressures can prove to be independent from the tensile strength of the rock σ_t. This independence is a function of the geometrical and hydraulic characteristics of the fracture, of the state of stress and of the pressurization methods, as already described. According to the foregoing paragraph, in these cases, the fluid merely flows through pre-existing fractures, and it enlarges them.

A typical example is provided by Fig. 17, which relates to an acidifying process carried out in the Torre Alfina Reservoir |49|. It can be noticed that during the first instance the pressure increases with the flow (in order to reach a pressure value of about 16 MPa, a flow of about 40 m^3/h is necessary), subsequently, the pressure increases up to 18 MPa and fluid is injected for a constant flow; the rapid and irregular decrease of the pressure values would represent the interconnection of the pre-existing fractures. The subsequent increase of the flow up to about 90 m^3/h is not sufficient to raise the pressure to the maximum values and furthermore, even though the flow

is maintained around this value, there is a corresponding progressive and irregular decrease of the pressure. The latter pressure decrease is probably related to the pressure increase measured inside the annulus between the casing and the drill pipes, determined by the extension of the rock volume involved in the fracturing treatment. Indeed, it is quite probable that treatment has also affected the walls of the open hole beyond the packers.

The volume of the rock mass affected by the fracturing processes increases during the second phase of the stimulation treatment. In fact, from the very first instant, the pressure in the annulus increases regularly with the flow. Subsequently, with a considerable flow increase the annulus pressure decreases down to values close to zero and this seems to indicate that the open hole is connected with a wider zone of the rock mass.

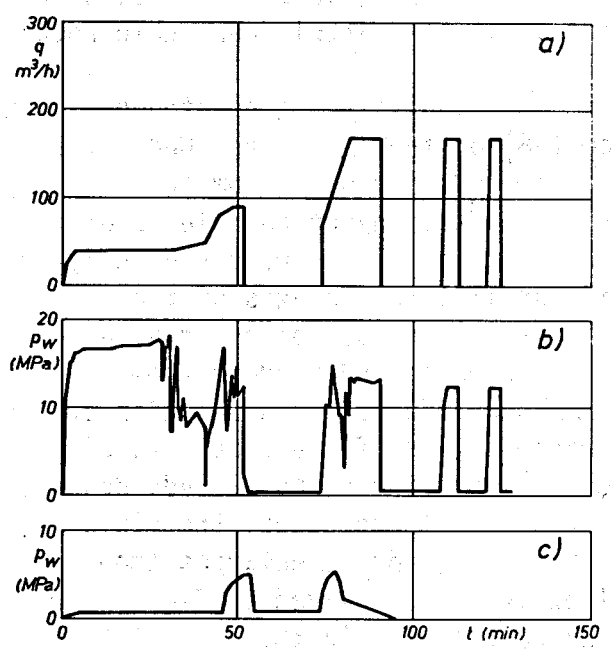

Fig.17 - Hydraulic stimulation at the Torre Alfina well: a) flow versus time; b) pressure in the pressurized interval measured at well head versus time; c) pressure in the annulus measured at well head versus time. The three diagrams relate to the phases: 1) injection of about 10 m^3 of water solution containing about 4% HCl; 2) injection of 40 m^3 of the water solution containing 15% HCl; 3) and 4) injections of 12 m^3 of water each

a wider zone of the rock mass.

During the last two phases, when the flow exceeds 150 m^3/h, the pressure values are slightly over 12 MPa at the well head and no overpressure is noticed inside the open hole.

3.2 Orientation, propagation and geometry of the induced fractures

Under the simplifying assumptions made, the induced fracture should have a vertical direction. Laboratory and in situ tests have pointed out that even horizontal or inclined fractures can be induced because of the inevitable irregularities that are present in the walls of the pressurized interval |46|. The probability of obtaining horizontal fractures increases when one of the ends of the pressurized interval is the bottom of the well. In this case the horizontal fractures are helped by the concentration of stresses linked to the geometry of the well bottom. Similarly, horizontal or inclined fractures can be initiated near rigid packers due to the high value of the vertical tensile stresses |37| which is clearly greater than that of the tangential stresses, whereas, the utilization of rubber packers maintains higher tangential stress values than the vertical ones along the entire length of the pressurized interval.

Fractures having an anomalous direction as compared with those to be expected on the basis of the foregoing theory, for ideal material, should generally deviate at a distance from the walls of the hole, down to the vertical direction. In particular for the case in which a pre-existing fracture were to cross the well, according to the theory based on the concepts of "Fracture Mechanics", for a non hydrostatic principal state of stress, the propagation of a fracture inside a medium having a linear elastic behaviour follows a route in which the deformation energy density assumes a minimum value. Therefore as it lengthens, the pre-existing fracture tends to assume an orientation that is perpendicular to the minimum principal stress |50|. It must be pointed out that the state of stress induced around the edges of the fractures produces a concentration of stresses that aim at plasticizing a part of the rock. Furthermore, the fractures that are present at a distance from the hole having appropriate geometric characteristics could sensitively deviate the propagating fracture (Fig.18), that would thus assume a configuration that virtually could not be predicted.

The calculation methods for the propagation and geometry of the fractures induced by hydraulic fracturing are all based on the

assumption that the rock is homogeneous, isotropic and characterized by an elastic behaviour.

Two fundamental calculation techniques were developed: one keeps account of the mechanical characteristics of the rock that is assumed to be impermeable |51| , the other method keeps account of the flow through the walls |52|. An overall analysis of the various methods allows an evaluation of the geometrical parameters of the fractures as the various fundamental parameters involved vary |53|.

According to such theories, an induced vertical fracture is a

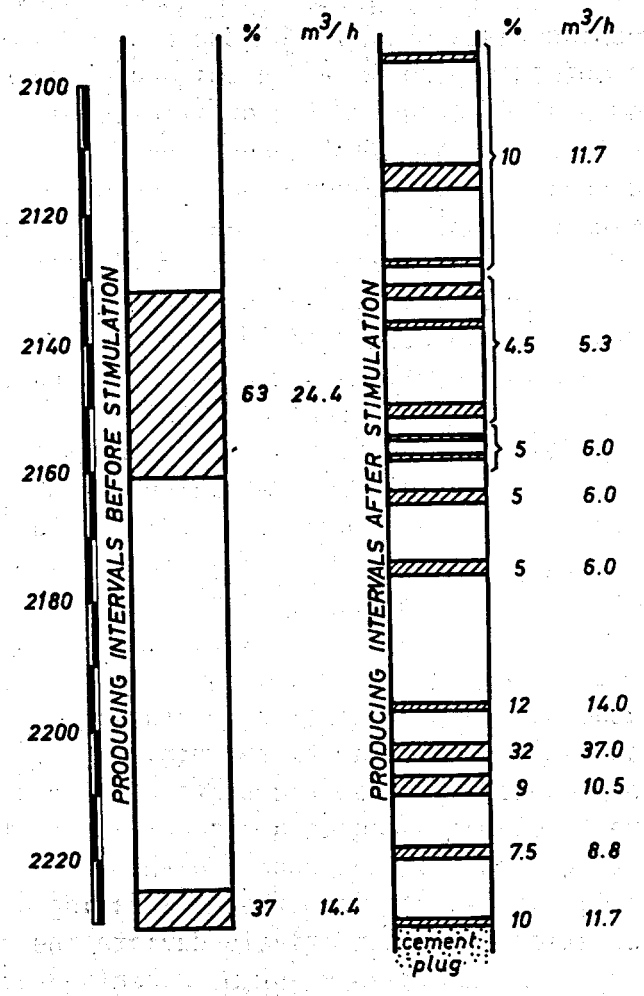

Fig.18 - Hydraulic stimulation at the Torre Alfina well. The Figure points out the height of the formation near the well involved in the stimulation and the opening and connection of pre-existing fractures

few millimeters wide and can propagate for several hundreds of metres. It is obvious that these results derive from the solution of mathematical models that do not keep account of the actual geological and structural complexities, and of the laws that govern its actual mechanical behaviour. The flow and the mutual influence between flow and state of stress.

4 - CHEMICAL EXPLOSIVE STIMULATION

4.1 - Propagation of the crushed zone and of the radial fractures

The system of fractures induced by a "camouflet explosion" and their propagation are conditioned by the characteristic parameters of the explosive and of the rock mass, by the geometry of the explosive and by the decoupling.

The maximum extension of the crushed zone and of the radial cracking zone that can be obtained in homogeneous and isotropic rock masses can be calculated by |54|:

crushed zone	spherical	$\phi_{cr} = A_2 W^{1/3}$	(13)
	cylindrical	$\phi_{cr} = A_3 Q^{0.5}$	(14)
radial cracking zone	spherical	$\phi_r = 1.6 A_4 W^{1/3} (0.48 B_c^{0.5} + 1)$	(15)
	cylindrical	$\phi_r = 2.5 A_5 Q^{0.5} (0.32 B_c^{0.67} + 1)$	(16)

The coefficients A_2 and A_3 can be estimated on the basis of the relationship between the extension of the crushed zone versus the characteristic impedence of the rock (Fig.19). The coefficient A_4 and A_5 are respectively equal to 0.24 and 0.11 for rocks having the same characteristics as the Lithonia Granite and for an explosive having a mean detonation velocity.

Relationships have been worked out |55| on the basis of the results obtained with nuclear explosives:

crushed zone $\phi_{cr} = 0.20 W^{1/3}$ (17)

radial zone $\phi_r = 0.52 W^{1/3}$ (18)

It must be pointed out that the coefficients are constant under

the simplified assumption that the result of the explosion is independent from the mechanical characteristics of the rock mass. Furthermore, it must be pointed out that there is only a slight difference between these coefficients and those obtained with the results of conventional explosions in spite of the fact that the quantity used is many orders of magnitude smaller than the nuclear explosives.

Figure 20 shows the empirical relationships proposed |56| on the basis of the experimental results provided by explosions of conventional spherical charges. However, the trend proposed, appears to disagree with the physical and mechanical phenomena that govern the fracturing processes. With reference to the maximum experimental values, the coefficients of the relationships indicating the extension of the crushed zone are obtained:

$$\phi_{cr} = 0.47\ W^{1/3} \tag{19}$$

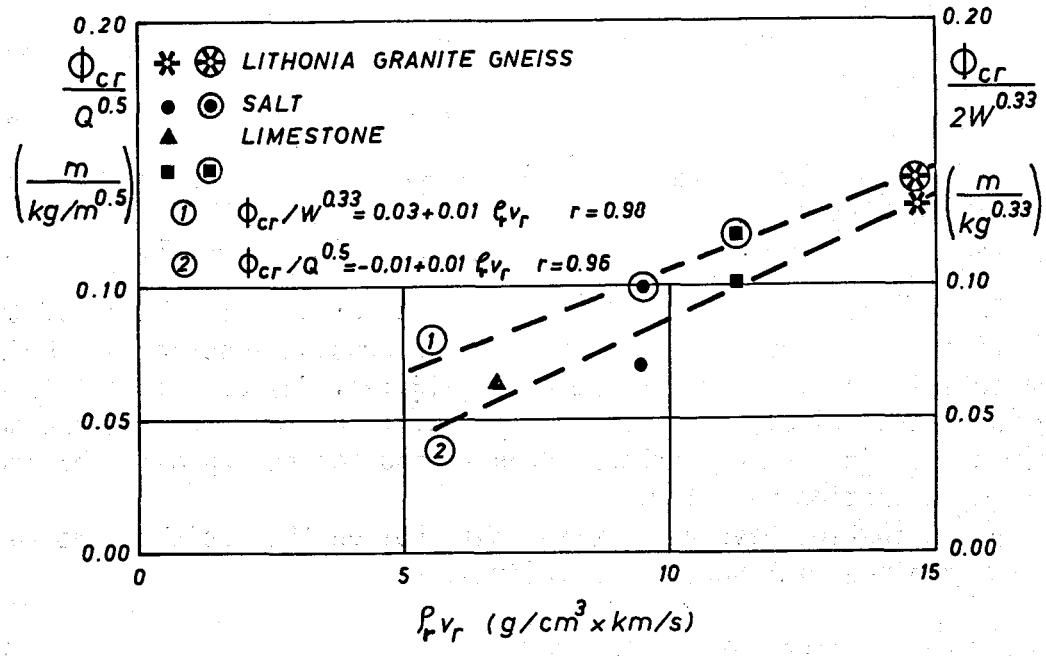

Fig.19 - Influence of the mechanical characteristics of the rock on the extension of the crushed zone. The analysis was carried out for spherical and cylindrical charges. The values shown represent the average of the results obtained by using various types of explosive |54|

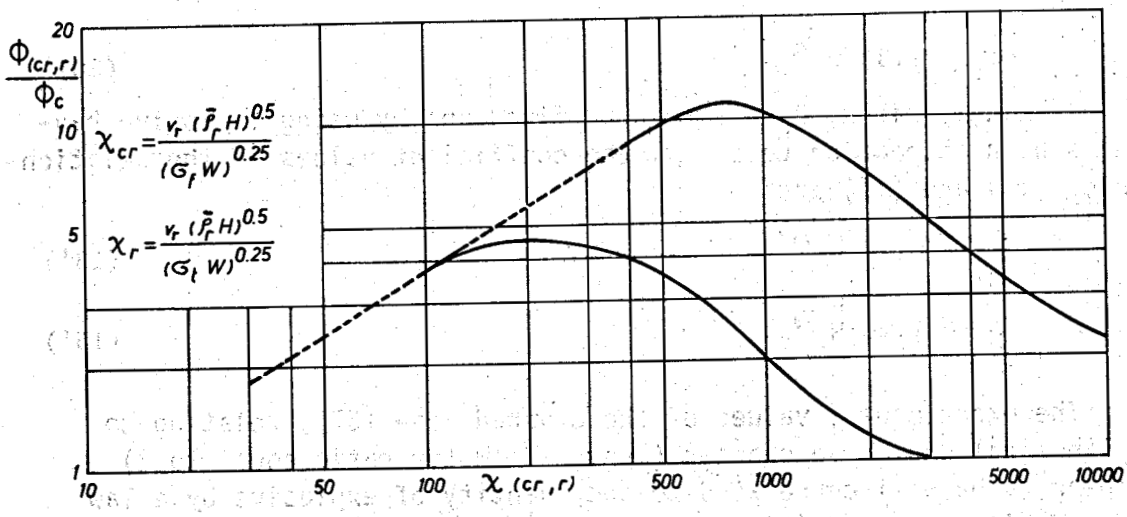

Fig.20 - Extension of the radial crack (upper curve) and of the crushed zone versus adimensional groups that keep account of the characteristics of the explosive, of the rock and of the vertical state of stress |56|

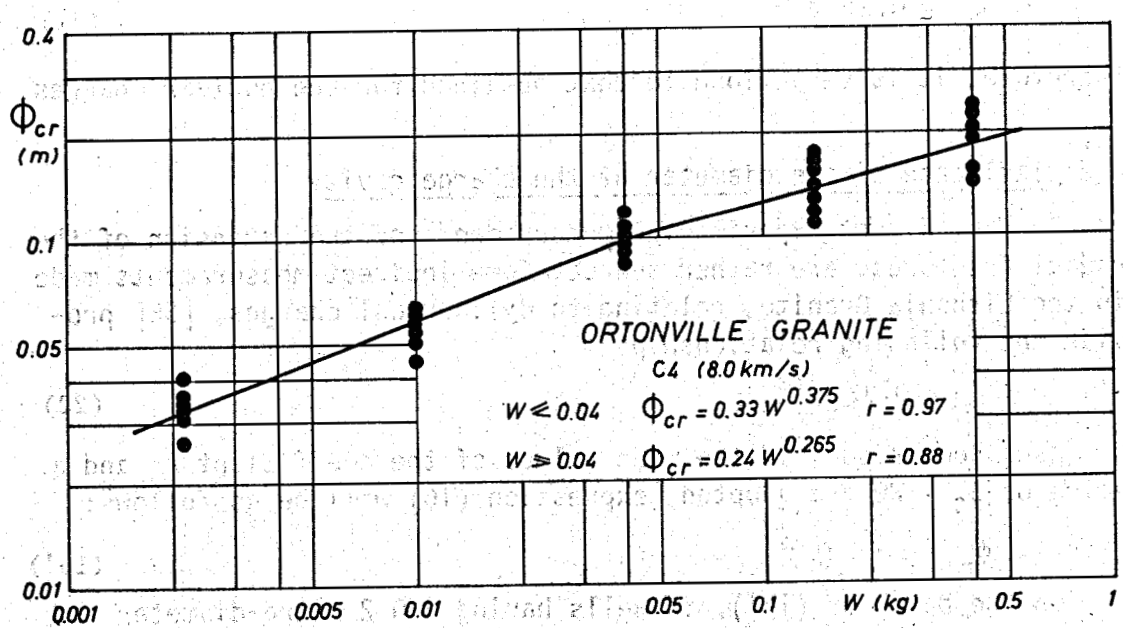

Fig.21 - Extension of the crushed zone versus the quantity of explosive. The correlation analysis is based on the experimental results obtained through the explosión of cylindrical charges (the height-diam. ratio being equal to 2) |57|

$$\phi_r = 1.36\ W^{1/3} \tag{20}$$

As a comparison, $B_c = 20$ can be fixed and by using explosive having a high detonation velocity, the coefficient values of the relationships (13) and (15) are:

$$\phi_{cr} = 0.28\ W^{1/3} \tag{13'}$$

$$\phi_r = 1.20\ W^{1/3} \tag{15'}$$

The experimental values of the crushed zone |57|, relating to cylindrical explosive charges (length-diameter ratio equal to 2) appear to be well correlated to the quantity of explosive by a law of the bilinear type (Fig.21). This result appears to suggest the variability of the coefficients and of the exponents of the relationships used to evaluate the extension of the crushed zone.

By carrying out a correlation analysis of the linear type and by imposing that the geometry of the explosive charge must be spherical, the value of the coefficient is:

$$\phi_{cr} = 0.24\ W^{1/3} \tag{21}$$

therefore, it is very close to that obtained for the nuclear charges.

4.2 Influence of the diameter of the charge cavity

So far, direct experimental measurements of the extension of the radial fractures, are rather scarce. Some indirect measurements made in the Lithonia Granite, relating to cylindrical charges, |58| provide the following relationship:

$$\phi_r = 0.37\ Q^{0.5} \tag{22}$$

As a comparison, if the mean values of the coefficient A_5 and a value of $B_c = 20$ are adopted, expression (16) will be as follows:

$$\phi_r = 1.0\ Q^{0.5} \tag{16'}$$

On the basis of (16'), in wells having a 0.2 metre-diameter and by assuming a charge density of 1.4 kg/dm^3, the radial cracking zone would extend to a diameter of 7 metres.

The development of the radial cracks and of the crushed zone increases linearly, the charges being the same, as the diameter of the

hole increases. A calculation example is given in Fig. 22 where (14) and (16') were used and a charge density of 1.4 kg/dm^3 and a mean value of coefficient A_5 were considered. This example suggests that in a homogeneous material having appropriate mechanical characteristics it is possible to obtain a greater extension of the crushed zone by means of a succession of explosions in the same well, each utilizing the crushed zone of the previous explosion as charge cavity. The upper limit of the extension is obviously conditioned by the technical problems involved in removing the rubble that obstructs the new charge cavity.

Figs. 23, 24 and 25 show an example of the size of the new volumes that can be used as charge cavities. The calculation was made by analysing the experimental results obtained |59,60| through single and multiple explosions performed in rocks having different mechanical and physical characteristics; explosives having varying "power" were used and the charges were spherical.

The different influence of the type of rock and of the type of explosive on the extension of the crushed zone emerges clearly. Indeed, while in the salt and limestone the extension of the crushed zone does not depend on the type of explosive used, in granite the latter is critical |54| . However, as to granite, this dependence tends to decrease in the explosions following the first one; this might probably be due to the drop in the peak and residual values of the mechanical characteristics of the medium, at the radial cracking zone.

As a preliminary indication, it must be pointed out that the tests carried out in the same rock |61| with explosives having different characteristics and decoupling varying between 1.2 and 1.26, seem to show that the extension of the crushed zone is independent from the type of explosive used if decoupling is kept greater than one (Fig.26).

Expression (16) provides an evaluation of the extension of the radial cracking brought about by a succession of explosions in the same hole, but the volume of the charge cavity increases progressively. Under the assumption that the sequence of explosions does not initiate new fractures but merely propagates the existing ones induced by the previous explosions, expression (16) will thus read:

$$\phi_r^{(N)} = 2.5\, A_5 \cdot Q^{0.5} \left[1 + 0.37\, B_c^{0.67} + \sum_{a=1}^{N} (A_5 N)^{a-1} \right] \qquad (16'')$$

The evolution of radial cracks according to (16'') for explosions

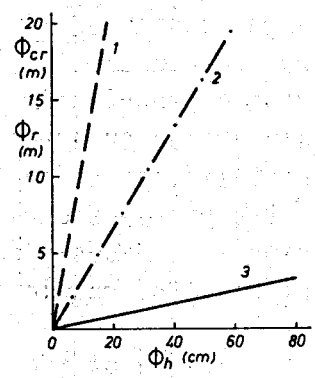

Fig.22 - Extension of the crushed zone (curve 3) and of the radial cracks (curve 2) in the rock mass which is similar to the Lithonia Granite, versus the diam. of the hole. The values are based on explosions where decoupling was equal to 1. Curve 1 provides the extension of the radial fractures in the presence of discontinuities.

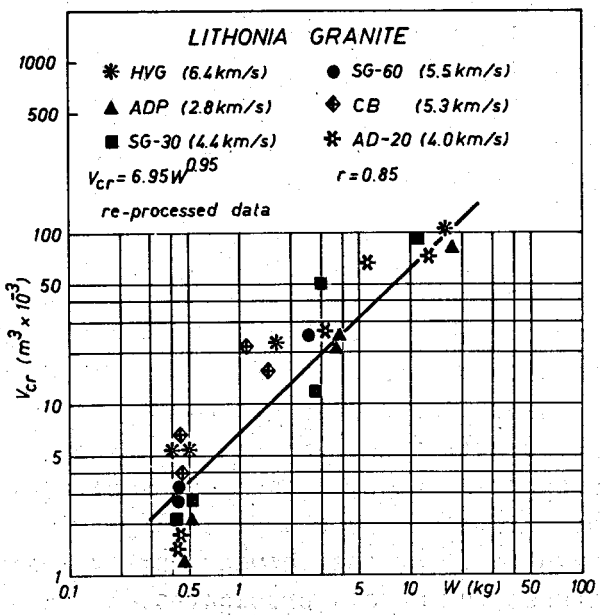

Fig.23 - Correlation and analysis between the extension of the crushed zone and the quantity of explosive. The values analysed are based on multiple successive explosions performed in the same blasthole. As regards the first explosions the marked influence of the type of explosive on the extension of the crushed zone must be noticed. This influence appears to decrease for the explosions following the first one |60|

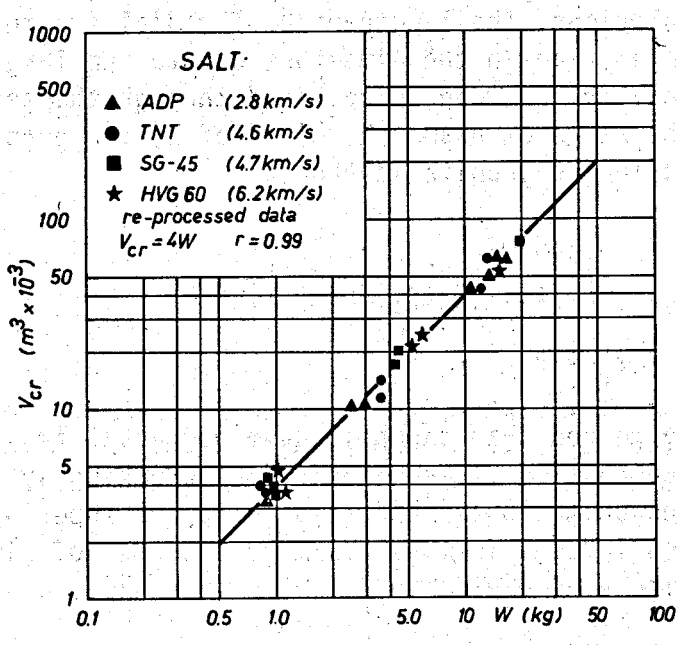

Fig.24 - Correlation analysis between the extension of the crushed zone and the quantity of explosive. The values are based on multiple successive explosions performed in the same borehole. In this rock mass the extension of the crushed zone is not influenced by the type of explosive used |59|

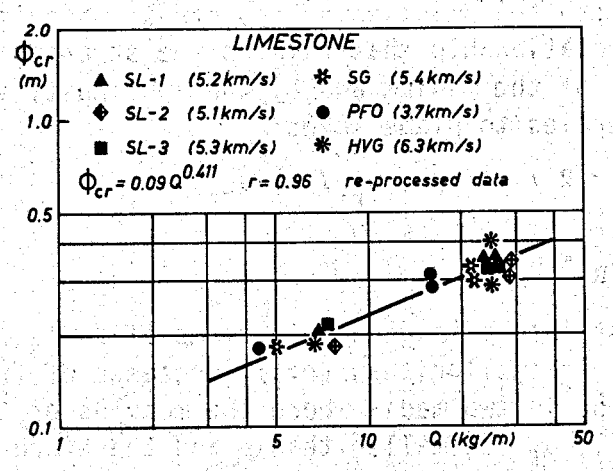

Fig.25 - Extension of the crushed zone versus the quantity of explosive contained in a 1-m hole. For this rock material the diameter is not influenced by the explosive used

in granite rocks and limestone |62| is shown in Fig. 27 versus the number N of explosions. The lengthening of radial fractures in the granite is greater than in the limestone due to the larger volumes of the charge cavity that can be obtained through the sequence of explosions. In the range of examined values of N, the propagation that can be obtained in the granite is about:

$$\phi_r^{(N)} / \phi_r = 5 \tag{23}$$

whereas for the limestone it is:

$$\phi_r^{(N)} / \phi_r = 2 \tag{24}$$

A different method that can help develop radial fractures and guarantee the connection between the radial cracking systems |63, 64, 65, 66| is based on the phenomena related to the superimposition of the stress waves induced in the medium by a number of simultaneous or nearly simultaneous explosions.

4.3 Influence of natural discontinuities on the propagation of radial cracks

The presence of natural discontinuities that cross the rock mass, and more generally, the dishomogeneity of the elastic characteristics of the medium influence the transmission of the stress wave induced in the rock mass by the explosion. The way in which the discontinuities influence the trasnmission of the stress wave is governed by the following relationship that relates the stresses to the elastic characteristics of the medium and by the continuity equation. This relationship applies to plane waves:

$$\sigma_T/\sigma_I = 2 / (1 + \rho_1 v_{r1} / \rho_2 v_{r2}) \tag{25}$$

$$\sigma_I + \sigma_R = \sigma_T \tag{26}$$

For the most interesting case in terms of radial crack extension, in which $(\rho v_r)_2$ is smaller than $(\rho v_r)_1$(presence of fractures with or without fluid, or in two media where the modulus of elasticity E_2 is smaller than E_1), σ_T is smaller than σ_I and therefore for a σ_I of compression, a reflection stress wave in medium 1 is obtained.

The reflection processes are furthermore conditioned, for the case of joints, by the characteristics of the fluid that fills them

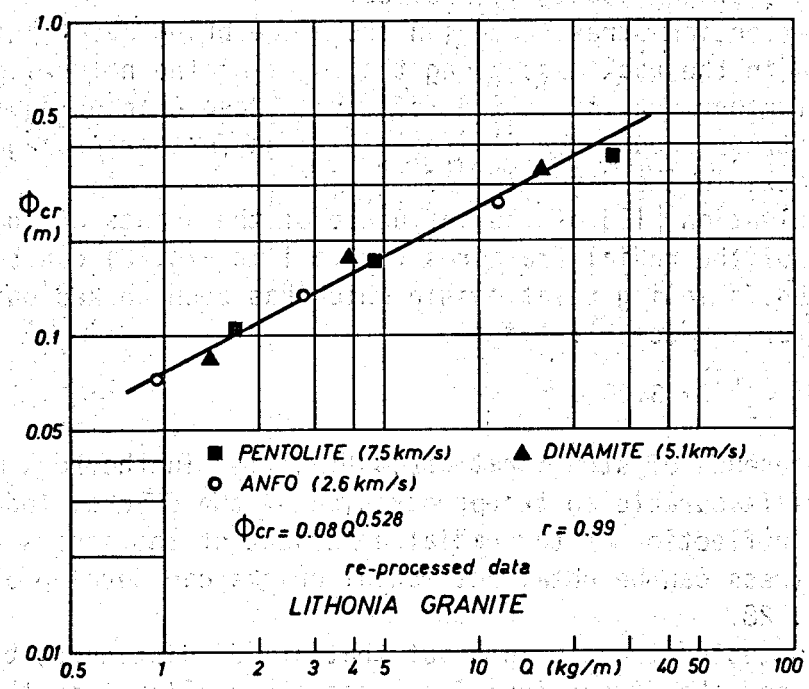

Fig.26 - Extension of the crushed zone versus the quantity of explosive contained in a 1-m hole. The experimental values |61| are based on explosions performed with different types of explosive and with decoupling between 1.2 and 1.26. The analysis of the results shows that the extension of the crushed zone appears to be independent from the explosive used

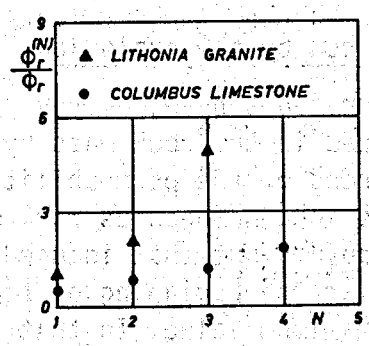

Fig.27 - Length of the radial cracks versus the number of explosions N carried out successively in the same blasthole. The explosions following the first one use explosion cavities that grow gradually larger proportionally with the diameter of the crushed zone produced by each previous explosion

and by those of the joints themselves.

The reflection stress wave can therefore bring about a further fracturing in the rock mass along the edges of the natural discontinuities; furthermore, since the reflection wave changes again the state of stress around the blasthole, it can further propagate the radial cracks in the direction of the joint.

An evaluation |11| of the influence of the joints on the maximum extension of the radial fractures (curve 1 in Fig.22) can be obtained through the following relationship which has been worked out from the one used for surface blasting:

$$\Phi_r^{(d)} = 3.28\ Q^{0.5} \qquad (27)$$

The presence of structural discontinuities in the rock mass is not always favourable to the propagation of the cracks. Indeed, if the total reflection of the radial component of the stress wave as tensile stress can be obtained, radial cracks can develop as indicated in Fig. 28.

The suggested trend points out that at "d" distances, between the blasthole and the discontinuities, that are smaller than the maximum radial extension of the cracks that can be obtained in a homogenous rock medium, the development of the fractures would be interrupted by the discontinuities. As the distance increases, the cracks propagate to a maximum value that can be approximately calculated by means of expression (27). For greater distances, the influence of the discontinuities decreases rapidly down to values where they are ineffective.

4.4 Permeability induced by the explosion

Experimental measurements have, only very seldom, been made of the permeability induced in the rock mass by explosions.

The qualitative trend of the permeability induced by the explosion of cylindrical charges in a homogenous rock mass is illustrated in Fig. 29. The diagram points out that induced permeability is lower in the crushed zone than at the beginning of the radial fractured zone where it reaches its maximum value. In that latter zone it decreases gradually until it reaches the permeability values of the rock mass |66, 68, 69|.

The loss of permeability in the radial fracturing zone can be expressed as a function of the distance from the axis of the blasthole

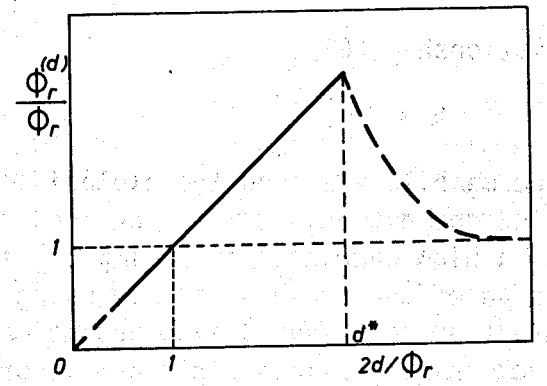

Fig.28 - Qualitative development of the radial cracks induced in a medium by structural discontinuities near the explosion cavity. The extension of the radial cracks induced by the explosion and influenced by the discontinuities (ϕ_r^d) is scaled from the extension that would be obtained under the same conditions in a homogeneous medium. If the discontinuity is near the hole, the radial fractures are interrupted by the joint and the value of ϕ_r^d coincides with d. As the joint-hole distance increases, ϕ_r^d reaches a maximum value which is close to the critical distance. By further increasing the distance, the length decreases rapidly and it comes close to the values obtained for homogeneous rock masses

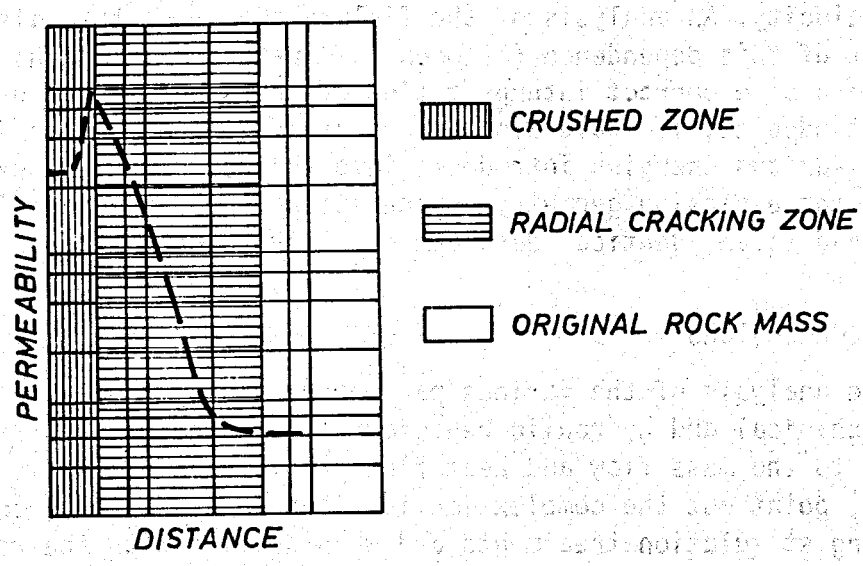

Fig.29 - Qualitative trend of the permeability induced by the explosions around a hole

by the following relationship |68| :

$$k \propto d^{-4} \tag{28}$$

An increase in permeability around the explosion cavity could be obtained by decreasing the extension of the crushed zone.

For rocks having a high characteristic impedence it is possible to reduce the extension of the crushed zone by using low detonation-rate explosives |54|; they do however, also produce a smaller radial cracking zone. In rocks having a less rigid behaviour, the extension of the crushed zone does not appear to be influenced by the type of explosive used |54|.

If decoupling greater than one is used at a first approach, it can be stated that the development of the crushed zone does not appear to be influenced by the explosive used (Fig. 26) even in rocks having a high characteristic impedence. On the contrary, the stresses induced in the medium scaled by the extension of the crushed zone, vary with the explosive used. A detailed and complete analysis appears to be very complex for the time being. It can, however, be pointed out that the limits of the crushed zone are usually calculated by assuming that the induced dynamic stresses are equal to the dynamic strength of the medium. On the other hand it has already been emphasized that the strength varies considerably with the load rate (Fig. 5) and therefore also with the type of explosive and with the detonation velocity. An analysis of the fialure phenomena that also keeps account of this dependence (between load rate and strength) could lead to a more correct interpretation of the experimental data. From this standpoint, it would also be necessary to analyse the influence of the various energies introduced into the medium by the explosives and by the explosion geometry on the extension of the radial cracks that lead to an identical development of the crushed zone.

5 - CONCLUSIONS

The analysis of the various parameters and of the laws that govern the mechanical and hydraulic behaviour of a geothermal reservoir in relation to the mass flow and heat flow problems and to stimulation processes, point out the complex implications that are involved when planning stimulation treatments and when dealing with the results obtained.

The models developed so far appear to be inadequate at large,

especially for Italian geothermal reservoirs that, in most cases, are structurally complex. Such drawbacks can be overcome by introducing into the mathematical model used, a greater number of parameters keeping account of the complexities of the reservoirs. This must be matched with more thorough and extensive theoretical and experimental research providing greater understanding of the events that are involved in the stimulation processes and that make the interpretation of the data obtained more reliable.

ACKNOWLEDGEMENTS

This research was partially financed by the National Research Council (CNR) of Italy (Contract n°. 79.01649.92).

REFERENCES

| 1| Vakhitov G.G. et al.: "Selection of Efficient Methods Applied for the Increase in Well Productivity Based on the Probability and Statistic Models" - 10th World Petr.Congr.,P.D.7,Bucharest, 1979

| 2| Haimson B.C.: "Recent in Situ Stress Measurements Using the Hydrofracturing Technique" - 18th U.S.Symp.on Rock Mech., Keystone, Colorado, 1977

| 3| Stagg K.G.,Zienkiewicz O.C.: "Rock Mechanics in Engineering Practice" - pp. 55-97, Wiley and S., London, 1968

| 4| Berry P. et al.: "The Influence of Fabric on the Deformability of Anisotropic Rocks" - 3rd Congr.of the ISRM, Vol. IIA, pp. 105-110, Denver, Colorado, 1974

| 5| Brace W.F.: "Some New Measurements of Linear Compressibility of Rocks" - J.Geoph.Res., Vol. 70, pp. 391-398, 1965

| 6| Walsh J.B.: "The Effect of Cracks on the Compressibility of Rock" J.Geoph.Res., Vol. 70, pp. 381-389, 1965

| 7| Warren M.: "Theoretical Calculation of the Compressibility of Porous Media" - J.Geoph.Res., Vol. 78, pp. 352-362, 1973

| 8| Geertsma J.: "The Effect of Fluid Pressure Decline on Volumetric Changes of Porous Rocks" - AIME Trans.SPE, Vol. 210, pp. 331-340, 1957

| 9| Mann R.L.,Fatt I.: "Effect of Pore Fluids on the Elastic Properties of Sandstone" - Geoph., Vol. XXV, n° 2, pp. 433-444, 1960

|10| Knutson C.F.,Bohor B.F.: "Reservoir Rock Behaviour Under Moderate Confining Pressure" - 5th U.S.Symp.Rock Mech.,Minnesota, 1963

|11| Heard H.C.: "The Influence of Environment on the Brittle Failure of Rocks" - 8th U.S.Symp. Rock Mech., Minnesota, 1966

|12| Logan J.M.,Handin J.: "Triaxial Testing at Intermediate Strain Rates" - 12th U.S.Symp. Rock Mech., Rolla, Missouri, 1970

|13| Perkins R.D. et al.: "Uniaxial Stress Behaviour of Porphyritic Tonalite at Strain Rates to 10^3 s^{-1}" - Int.J.Rock Mech.Min.Sci., Vol. 7, pp. 527-535, 1970

|14| Stowe R.L.,Ainsworth D.L.: "Effect of Rate of Loading on Strength" 10th U.S.Symp.Rock Mech., Austin, Texas, 1968

|15| Schwartz A.E.: "Failure of Rock in the Triaxial Shear Test" - 1st Congr.ISRM, Vol. 1, pp. 109-151, Lisbon, 1966

|16| Lehnoff T.F.,Scheller J.D.: "The Influence of Temperature Depend Properties on Thermal Rock Fragmentation" - Int.J.Rock Mech.Min. Sci.,Vol. 12, pp. 255-260, 1975

|17| Clark K.K.,Somerton W.H.: "Laboratory Investigation of Reduction of Fracture Pressures of Rocks by Intensive Borehole Heating" - AIME Trans.SPEJ, Vol. 234, pp. 225-228, 1965

|18| Whitsitt N.F.,Dysart G.R.: "The Effect of Temperature on Stimulation Design" - AIME Trans.SPE, Vol. 249, pp. 493-502, 1970

|19| Hawle H. et al.: "Reservoir Geology of the Carbonate Oil and Gas Reservoir of the Vienna Basin" - 7th World Petr.Congr., Vol. 2, pp. 371-395, 1967

|20| Wible D.O.: "Effect of Applied Pressure on the Conductivity,Porosity and Permeability of Sandstones" - AIME Trans.SPE, Vol.213, pp. 430-432, 1958

|21| Perami R.: "Microfessuration of Rocks under Homogeneous Thermic Variations" - ISRM Symp.on Rock Fracture, Nancy, 1971

|22| Le Tirant P.,Baron G.: "Flow in Fissured Rocks and Effective Stresses.Application to Hydrocarbon Production" - ISRM Symp. Percolation through Fissured Rock, Stuttgard, 1972

|23| Brace W.F. et al.: "Permeability of Granite under High Pressure" J.Geoph.Res., Vol. 73, pp. 2225-2236, 1968

|24| Fisher H.N.: "Interpretation of the Pressure and Flow Date" - Proc.II NATO-CCMS Inf.Meet.on D.H.R.Geothermal Energy,Los Alamos, N.Mexico, 1977

|25| Pomeroy C.D.,Robinson D.J.: "The Effect of Applied Stresses on the Permeability of a Middle Rank Coal to Water" - Int.J.Rock Mech. Min.Sci., Vol. 4, pp. 329-343, 1967

|26| Morgenstern N.R.,Guther H.: "Seepage into a Excavation in a Medium Possessing Stress Dependent Permeability" - ISRM Symp.Percolation

|27| Jouanna P.: "Laboratory Tests on the Permeability of Micaschist Samples under Applied Stress" - ISRM Symp.Percolation through Fissured Rock, Stuttgard, 1972

|28| Mordecai M.,Morris L.H.: "An Investigation into the Changes of Permeability Occurring in a Sandstone when Failed under Triaxial Stress Conditions" - 12th U.S.Symp.Rock Mech.,Rolla,Missouri,1970

|29| Jager C.: "Rock Mechanics and Engineering" - Cambridge University Press, 1972

|30| Potter J. "Laboratory Studies of Permeability" - Proc.II NATO - CCMS Inf. Meeting H.D.R.Geothermal Energy, Los Alamos,N.Mexico, 1977

|31| Serafim J.L.; "Influence of Interstitial Water on the Behaviour of Rock Masses" - Rock Mechanics in Engineering Practice, Stagg K.G.,Zienkiewicz O.C.,Wiley J.and Sons, pp. 55-97, London, 1968

|32| Baldi P. et al.: "Selection of Dry Wells in Tuscany for Stimulation Tests" - II Workshop for Coop.Res.in Geothermal Energy,Berkeley, California, 1980

|33| Castillo E.: "Mathematical Model for Two-Dimensional Percolation throught Fissured Rock" - ISRM Symp.Percolation through Fissured Rock, Stuttgard, 1972

|34| Sharp J.C.,Maini Y.N.T.: "Fundamental Considerations on the Hydraulic Characteristics of Joints in Rock" - ISRM Symp.Percolation through Fissured Rock, Stuttgard, 1972

|35| Rayneav C.,Jouanna P.: "Temperature Influence on Seepage through Fissured Media" - ISRM Rock Fracture, Nancy, 1971

|36| Hubbert M.K.,Willis D.G.: "Mechanics of Hydraulic Fracturing" - AIME Trans. SPE, Vol. 210, pp. 153-168, 1957

|37| Kehle R.O.: "Determination of Tectonic Stresses through Analysis of Hydraulic Well Fracturing" - J.Geoph.Res., Vol. 69, p.259,1964

|38| Haimson B.C.,Fairhurst C.: "Initiation and Extension of Hydraulic Fractures in Rocks" - AIME Trans. SPE, Vol. 240, pp. 310-318,1967

|39| Daneshy A.A.: "Principles of Hydraulic Fracturing" - Proc.Symp. 103rd AIME Annual Meeting, Dallas, Texas, 1974

|40| Timoshenko S.,Goodier J.N.: "Théorie de l'elasticité" - Librairie polytechnique Ch.Béranger, Paris, 1961

|41| Lubinski A.: "The Theory of Elasticity for Porous Bodies Displaying a Strong Pore Structure" - Proc.II U.S. N.Congr.Appl.mech., pp. 247-256, 1954

|42| Murphy H.D.: "Thermal Stress Cracking and the Enhancement of Heat Extraction from Fractured Geothermal Reservoirs" - Informal Report

LA-7235-MS, Los Alamos, N.Mexico, 1978

|43| Wong H.Y.,Farmer I.W.: "Hydrofracture Mechanisms in Rock During Pressure Grouting" - Rock Mech., Vol. 5, pp. 21-41, 1973

|44| Zoback M.D. et al.: "Laboratory Hydraulic Fracturing Experiments in Intact and Pre-Fractured Rock" - Int.J.Rock Mech.Min.Sci.,Vol. 14, pp. 49-58, 1977

|45| Haimson B.C.,Fairhurst C.: "In-Situ Stress Determination at Great Depth by Means of Hydraulic Fracturing" - 11th U.S.Symp.Rock Mech. Berkeley, California, 1969

|46| Von Schonfeldt H.,Fairhurst C.: "Field Experiments on Hydraulic Fracturing" - AIME Trans.SPEJ,Vol. 249, pp. 69-77, 1970

|47| Haimson B.C.: "A Simple Method for Estimating in Situ Stresses at Great Depths" - 76th Annual Meeting ASTM, Philadelphia, 1973

|48| Haimson B.C.,Avasthi J.M.: "Stress Measurements in Anisotropic Rock by Hydraulic Fracturing" - 15th U.S.Symp.Rock Mech., South Dakota School of Mines and Technology, 1973

|49| Berry P.,Cataldi C.: "Geothermal well Stimulation at Torre Alfina" - ENEL-DSR, Relazione di Studio e Ricerca n° 355, 1978

|50| Abou-Sayer A.S.: "In Situ Stress Determination by Hydrofracturing: A Fracture Mechanics Approach" - J.Geoph.Res., Vol. 83, pp. 2851-2862, 1978

|51| Perkins T.K.,Kern L.R.: "Widths of Hydraulic Fractures" - AIME Trans. SPE, Vol. 222, pp. 937-949, 1961

|52| Geertsma J.,De Klerk F.: "A Rapid Method of Predicting Width and Extent of Hydraulically Induced Fractures" - AIME Trans.SPE, Vol. 246, pp. 1571-1581, 1969

|53| Le Tirant P., Dupuy M.: "Dimensions des fractures obtenie par fracturation hydraulique des couches pétroliferes" - Revue de l'Institute Français du Pétrole, Vol. XXII, n° 1, 1967

|54| Berry P. et al.: "Geothermal Stimulation with chemical Explosives" - Energy Technology Conference & Exhibition, Houston,Texas 1978

|55| Siskind D.E. et al.: "Fracturing in the Zone around a Blasthole" R.I. 7753, USBM, 1973

|56| Diadkin Y.D. et al.: "Theoretical and experimental Grounds for Utilization of Dry Rock Geothermal Resources in the Mining Industry" - 2° U.N.Symp.Dev.Use Geothermal Resources, S.Francisco, 1975

|57| D'Andrea D.V. et al.: "Crater Scaling in Granite for Small Charges" - R.I. 7409, USBM, 1970

|58| Atchison T.C.: "Explosive Fragmentation Principles" - Abattage des roches a l'explosif - Rev.Industrie Minérale, num.spec.,1971

|59| Nicholls H.R. et al.: "Comparative Studies of Explosives in Salt" R.I. 6041, USBM, 1962

|60| Nicholls H.R. et al.: "Comparative Studies of Explosives in Granite" - R.I. 6693, USBM, 1965

|61| Nicholls H.R. et al.: "Effect of Charge Diameter on Explosive Performance" - R.I. 6806, USBM, 1966

|62| Atchison T.C. et al.: "Comparative Studies of Explosives in Limestone" R.I. 6395; USBM, 1964

|63| Berry P. et al.: "Aumento della permeabilità di serbatoi geotermici mediante tecniche di stimolazione" - Energia Geotermica, I Seminario informativo, PEG, Roma, 1979

|64| Weber P. et al.: "Calcul de la propagation d'une onde de contrainte à symetrie sphérique au cylindrique.Application ou tir d'explosif" - Rev.Ind.Min., num.spec., 1971

|65| Berry P. et al.: "Gli esplosivi nella coltivazione delle pietre ornamentali ed il controllo della fratturazione indotta" - Int. Days on the Quarrying Technologies of Ornamental Stones, Carrara, 1980

|66| Mc Kee C.R. et al.: "Permeability from Single and Multiple Detonations of Explosive Charges" - Joint MMIJ-AIME Meet., Denver, 1976

|67| Langefors U. et al.: "The Modern Technique of Rock Blasting" - Almqvist and Wiksell,Stockholm, 1967

|68| Schmidt R.A. et al.: "A New Perspective on Well Shooting. The Behaviour of Contained Explosions and Deflagrations" - 54th Annual Tech.Conf.Exh.SPE-AIME, Las Vegas, Nevada, 1979

|69| Batchelor A.S. et al.: "Preliminary Studies of Dry Rock Geothermal Exploitation in Southwest England" - I.M.M., Vol. 88, Sect. B, pp. 51-56, 1979

NOMENCLATURE

A_n = constants

B_c = blastability coefficient σ_{fd}/σ_{td}

C_b = rock bulk compressibility

C_r = rock matrix compressibility

d = distance blasthole-discontinuity , distance

E_{sec} = Young Modulus (secant)

E_{tg} = Young Modulus (tangent)
e = opening fissure
H = depth
k = permeability
k_o = initial permeability
m = exponents
N = number of explosions in the same hole
n = porosity
n_o = initial porosity
P_o = initial pore fluid pressure
P_w = borehole pressure
p_w^c = $P_w^c - P_o$ critical borehole (break down) pressure
Q = explosive quantity contained in a 1 metre lenght of the hole
q = flow rate
$\bar{R}_1$ = $\phi(r, cr)/\phi_c$
t = time
T = temperature
V_{cr} = crushed zone volume
v_r = seismic velocity
v_d = detonation velocity
W = explosive quantity
α = $1 - C_r/C_b$ porous - elastic parameter of the rock
β = linear thermal expansion coefficient
δ = charge density
ε_1 = axial strain
$\dot{\varepsilon}$ = strain rate
ϕ_{cr} = crushed zone diameter
ϕ_r = radial fracturing zone diameter
$\phi_r^{(d)}$ = radial fracturing zone in a medium by structural discontinuities
$\phi_r^{(N)}$ = radial fracturing zone diameter induced by a sequence of explosions in the same hole

ϕ_c = equivalent diameter of TNT explosive charge
ϕ_h = blasthole diameter
ρ_r = rock density
$\bar{\rho}_r$ = mean density of the overlying rock massif
σ_{fd} = dynamic compressive strenght
σ_f = compressive strenght
σ_{td} = dynamic tensile strenght
σ_t = tensile strenght
$\sigma'_{r,\theta,z}$ = principal effective stresses at the borehole wall
σ'_{H1} = larger horizontal effective original stress
σ'_{H2} = smaller horizontal effective original stress
σ'_v = vertical effective original stress
$\bar{\sigma}'$, $\bar{\sigma}$ = mean effective stress, mean state of total stress
σ_I = incident stress wave
σ_T = transmitted stress wave
σ_R = reflected stress wave
σ_1 = major principal stress (axial)
σ_3 = minor principal stress (confining)
θ = angle measured counterclockwise from the radius in the direction of σ_{H1}
$X_{(cr,r)}$ = dimensionless values
ν = Poisson's ratio

THE DOE GEOTHERMAL WELL STIMULATION PROGRAM

R. J. Hanold[1], D. A. Campbell[2], and A. Richard Sinclair[3]

(1) Los Alamos Scientific Laboratory - Los Alamos, NM
(2) Republic Geothermal Inc. - Santa Fe Springs, CA
(3) Maurer Engineering, Inc. - Houston, TX

INTRODUCTION

The stimulation of geothermal wells presents some new and challenging problems. Formation temperatures in the 300-500°F range can be expected. The behavior of frac fluids and proppants at these temperatures in a hostile brine environment must be carefully evaluated before performance expectations can be determined. In order to avoid possible damage to the producing horizon of the formation, the high-temperature chemical compatibility between the in situ materials and the frac fluids, fluid additives, and proppants must be verified. Perhaps most significant of all, in geothermal wells the required techniques must be capable of bringing about the production of very large amounts of fluid. This necessity for high flow rates represents a significant departure from conventional oil field stimulation and demands the creation of fractures with very high flow conductivity or large fracture surface areas in the case of matrix permeability dominated formations.

Stimulation treatments have been conducted in formations which produce hot water as a result of both matrix permeability and from natural existing fracture systems. The following targets of opportunity are of particular interest to this program:

- Wells that require additional drainage area because of insufficient formation permeability.
- Wells that did not intersect nearby major fracture systems.
- Wells that suffered man-made damage during drilling or completion operations including mud or cement invasion.
- Wells that require periodic remedial treatment as a result of fluid production related damage.

Although numerous criteria have been established for the selection of candidate wells, the most significant is definite proof of a good producing reservoir. These data are normally obtained from offset well production.

PROPPANTS

Although sand is generally used as a proppant today and it has been the most widely used in the past, it is not strong enough to withstand the conditions in geothermal wells at elevated temperatures. Sand is definitely affected by temperature, particularly when tested in hot water or brine at various closure stresses. Figure 1 shows the effect of temperature on common frac sand (20/40 mesh). These results are short term results and only suggest the severity of long term field results.

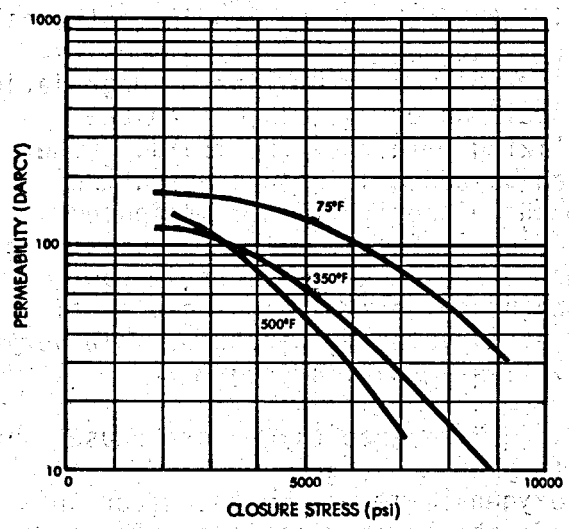

Fig. 1. Temperature Effects on 20/40 Brady Texas Sand.

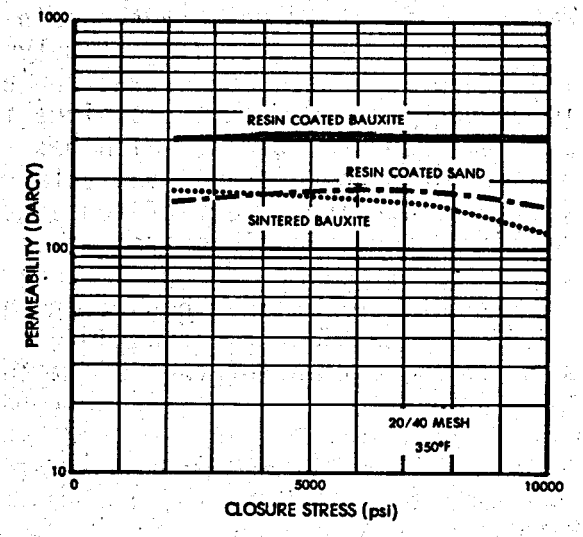

Fig. 2. Permeability vs. Closure Stress for Temperature Insensitive Proppants.

There are several mechanisms that can destroy sand grains in the fracture. First, the sand is brittle and point-to-point loading can cause brittle failure. Second, sand is full of microfractures and faults which weaken the sand. Finally, when sand is stressed in a corrosive medium like hot water, stress corrosion cracking appears to destroy the sand at low closure stresses. High temperatures and high stresses combine to bring out the worst properties of sand and tend to emphasize the fact that sand is inadequate as an effective proppant under high-temperature conditions.

The strongest proppant tested to date is Resin Coated Bauxite. It shows no temperature sensitivity or permeability decrease under load. The Resin Coated Sand is not temperature or load sensitive but does have a slightly lower permeability at any closure stress due to a slightly different distribution of particle sizes. Figure 2 shows the permeability of Resin Coated Bauxite and Resin Coated Sand under varying closure stress to 10,000 psi at 350°F. No temperature differences or sensitivities were found so tests at all temperatures gave the same results shown in Fig. 2 within experimental scatter. One important point is that the resin coated materials are cohesive; therefore, once emplaced in the fracture, flowback is reduced during production. Although slightly crushable, the Sintered Bauxite is much stronger than sand and effectively inert in hot brines. Figure 2 shows how Sintered Bauxite permeability behaves under increasing closure stress. It exceeds Resin Coated Sand at lower closure stress but drops below Resin Coated Sand at 10,000 psi.

FLUIDS

Many fluids and fluid systems have been tested for geothermal wells. Water soluble polymers are the main viscosifiers for application in geothermal wells. Above 250°F almost all polymer systems show a decline in viscosity. There are many techniques that can be used to delay this decline or degradation in properties. One such technique is the addition of 5% methanol to the polymer water solutions, which has a stabilizing effect on the fluid. Other proprietary products are available which can be added as high-temperature stabilizers. The effect of temperature on the viscosity of some proposed polymer-water frac fluid systems is illustrated in Fig. 3. The rapid decline in viscosity of polymer "A" at temperatures above 200°F could result in poor proppant placement in a high-temperature geothermal stimulation treatment. Laboratory testing of proposed frac fluids at elevated temperatures is a very significant element of the DOE geothermal well stimulation program.

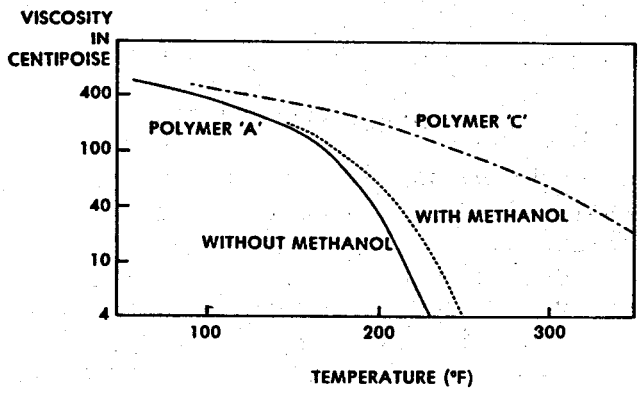

Fig. 3. Polymer-Water Frac Fluid Viscosity vs Temperature.

Dissolved oxygen can cause polymer degradation but by adding an oxygen scavenger to the water this effect can be minimized. The type and amount of polymer determines the speed and extent of degradation. Polymers used in fracturing are of these basic types: polysaccharides, modified celluloses and polyacrylamides. These particular polymers were chosen because of their unique ability to viscosify water, and at the same time to reduce tubular friction and have a good tolerance to brine. An ideal frac fluid would have the properties of high viscosity for proppant carrying, low pumping friction, wide chemical compatibility, and low cost. In the case of geothermal wells, an ideal frac fluid would retain its desirable properties at the high temperature until it has done its job of placing the proppant in the fracture.

PLANAR AND DENDRITIC FRACTURING

Conventional fracturing is an attempt to make a planar, vertical fracture in the producing formation. This occurs when the pressure and fluid flow is sufficient to break the formation in its plane of weakness. After the planar fracture is created, a proppant is carried into the fracture to keep it open and conductive for subsequent production. In geothermal wells, large tubular goods are available and the producing formations are reasonably shallow so that high flow rates can be used to create the planar fractures. Along with efficient fracture creation, convective cooling can be achieved to keep the working fluid cooler than the ambient formation temperature. Fluid systems that complement the high flow rate fracs are chosen for each particular application. Each formation's permeability, porosity and temperature also

affects the selection of the fluid system's physical properties such as its viscosity. The complex chemistry caused by the high-temperature water requires complete chemical compatibility testing.

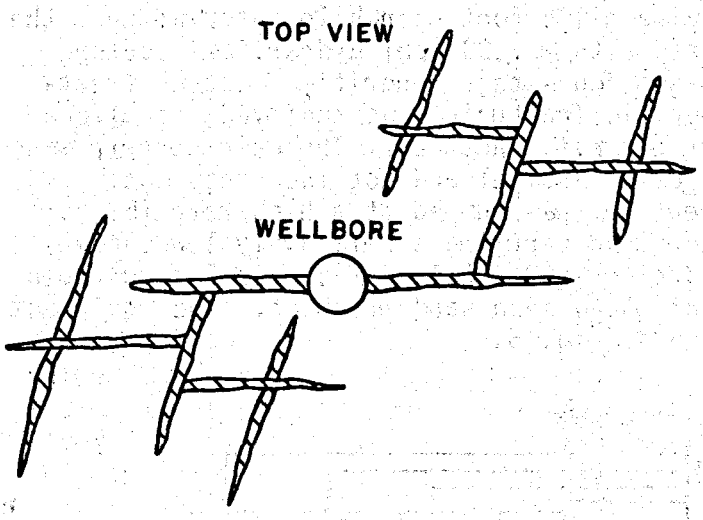

Fig. 4. Idealized Schematic of a Dendritic Fracture (after Kiel).

The main proponent of branched or dendritic fracturing has been Kiel. An estimated 750 Kiel fracs have been run to date. Dendritic fractures are caused by pulsing the formation which causes formation spalling and diversion of the fracture wings by downhole stress modification. Methods to predict the extent and direction of the fractures are still being worked upon; however, the best results have been reported in naturally fractured formations where major and minor fracture systems already exist but may not have flow capability. Usually 5 or more stages are used with each stage utilizing a low-viscosity fluid, sand slugs, and several flow-back periods. High flow rates and friction reduction are used to advantage on these treatments. An idealized schematic of a dendritic fracture system is depicted in Fig. 4.

STIMULATION TREATMENTS AT RAFT RIVER

Raft River is a moderately low-temperature (260-290°F) hydrothermal resource. Wells RRGP-1 and RRGP-2 are the best producing wells in the field and appear to intersect a natural fracture zone with high transmissibility, having a permeability thickness (kh) of greater than 50 Darcy-feet. Wells RRGP-3, RRGP-4, and RRGP-5 are less productive and were all considered for stimulation. Wells RRGP-4 and RRGP-5 were chosen as the best two candidates because RRGP-3 is further from the best producing wells and its mechanical configuration is very complex. There are two major faults running through the field. The Narrows Fault lies between Wells RRGP-1 and RRGP-2, and trends roughly east-west. Well RRGP-4 is approximately 1/2 mile south of RRGP-1 and the Narrows Fault. The Bridge Fault is on the east side of the field and trends northeast-southwest. Well RRGP-5 lies between the two faults, near their intersection.

Before stimulation, RRGP-4 was essentially non-productive. RRGP-5, however, was capable of flowing at a stabilized rate of 140 gpm and produced more than 600 gpm with a pump. This is adequate productivity, but the production came from the upper portion of the completion interval, and the produced fluid temperature of 255°F was undesirably low. Based on the performance of the better wells in the field and the proximity of Wells RRGP-4 and RRGP-5 to the Bridge and Narrows Faults, it was considered likely that highly productive fractures existed near the wells. Hydraulic fracture treatments in the deeper intervals were

chosen as the best means to connect the wells with major productive fractures and to achieve the desired produced fluid temperatures of 270°F or greater. Although on the upper temperature margins of conventional oil field fracturing technology, no special techniques or materials were thought to be necessary for Raft River.

Well RRGP-4 was recompleted leaving a 195 foot open-hole interval near the bottom of the well which was stimulated with a 7,900 bbl hydraulic fracture treatment. The technique employed was a four-stage dendritic fracture treatment. It was chosen because, if dendritic fracturing was achieved, it offered the best chance of intersecting major natural fractures. The main concern was that a single, planar fracture might only parallel and not intersect the principal natural fractures. The treatment was pumped at a high rate (50 bpm) and utilized a light polymer gel frac fluid carrying a relatively low concentration of proppant. The treatment included 50,400 lbs of 100-mesh sand added for leak-off control and 58,000 lbs of 20-40 mesh sand proppant. The equipment layout for the frac treatment is shown in Fig. 5.

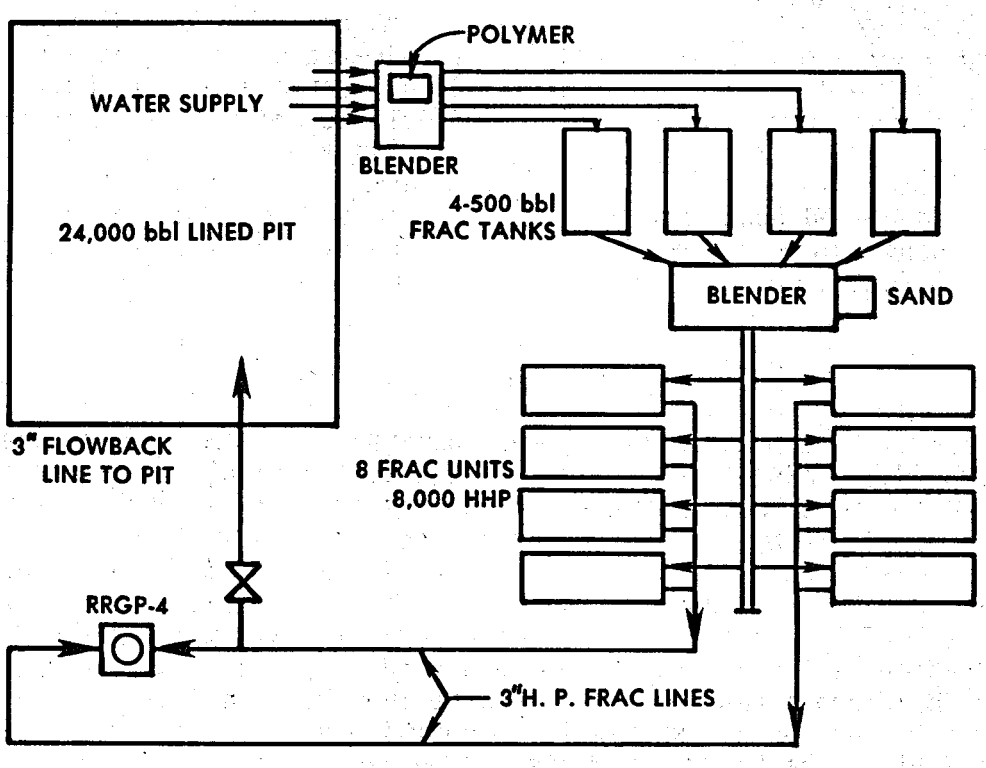

Fig. 5. Equipment Layout for RRGP-4 Frac Treatment.

Following the treatment, the U.S. Geological Survey ran their high-temperature acoustic borehole televiewer and observed that the created fracture extended the full 195-foot height of the open interval and was oriented approximately east-west, parallel to the Narrows Fault. In the post-stimulation flow test, the well produced at a stabilized rate of 60 gpm with a downhole fluid temperature of 270°F. This rate represented at least a five-fold increase over the pre-stimulation rate, but was still sub-commercial. The produced fluid temperature is significantly higher than past measurements.

This fact suggests that the new artificial fracture is producing fluid from a deep reservoir zone not open in the original hole. The chemical data further support this interpretation. The extent of polymer degradation determined chemically is consistent with fluid production from a higher temperature zone.

Conventional fracture type curve analysis (log-log plot) yields a fracture length of approximatlely 335 feet and a kh of 800 millidarcy-feet. The Horner plot of the same pressure buildup data has two straight line segments, one during early time (less than 15 hours) and one during later time (greater than 15 hours). These two segments give kh values of 1,070 millidarcy-feet and 85,000 millidarcy-feet, and suggest the presence of more than one permeability zone in the vicinity of the wellbore. Also, a negative skin factor (minus 6.0) indicates a stimulated zone close to the wellbore.

Well RRGP-5 originally had good productivity from the upper portion of the completion interval. The goal of the treatment for this well was a similar or higher productivity, but from a deeper, hotter interval. The well was recompleted similar to RRGP-4 in preparation for this stimulation treatment. The recompletion consisted of cementing 7 in. casing which excluded the existing producing interval and left a 216-ft open-hole interval near the bottom of the well. A more conventional, large fracture treatment designed to create a single propped fracture was selected for RRGP-5. The treatment consisted of 7,600 bbl of a relatively low viscosity polymer gel with 84,000 lbs of 100-mesh sand for leak-off control and 347,000 lbs of 20-40 mesh sand proppant. Near the end of the treatment, the pumping rate was gradually reduced in an effort to sand the well out and leave the fracture well-propped near the wellbore. As the rate approached zero, the wellhead pressure dropped to zero psi indicating that communication with the reservoir fractures had been achieved. Also, a significant pressure response was noted in RRGP-1.

Following the treatment the USGS borehole televiewer showed that the created fracture spanned the upper 135 feet of the open interval. The fracture was oriented northeast-southwest, parallel to the Bridge Fault. In the post-stimulation production test, the well stabilized very rapidly at a 200 gpm rate with a 30 psia wellhead pressure. The produced fluid temperature was unchanged from the pre-stimulation flow. Following the natural flow test, a pump was installed in the well and it produced more than 650 gpm. Chemical analysis of the produced fluid indicated a relatively low rate of polymer degradation in the reservoir, confirming that the frac fluid traveled upward into a cooler portion of the reservoir.

Pressure buildup and temperature data also suggest strongly that the fracture treatment went upward to the original producing interval. The Horner plot of the pressure buildup data shows only a short transition phase between the fracture dominated period and the late time constant pressure period. Estimates of the late time formation kh were large--greater than 100 Darcy feet. The Horner analysis indicates a very large positive skin factor. This skin factor is not due to formation damage but rather to the limited entry nature of the completion.

In summary, RRGP-4 and RRGP-5 were successfully recompleted and fracture treated, although the desired stimulation results were not achieved. Well RRGP-4 was stimulated from a PI of essentially 0 to 0.6 gpm per psi. Well

RRGP-5 has a post-stimulation PI of 2.0 gpm per psi and no significant increase in productivity or temperature was achieved. The artificially created fracture probably intersected existing natural fractures near the wellbore. Summaries of the stimulation treatments are presented in Tables I and II.

TABLE I

RRGP-4

4-STAGE KIEL FRAC 8/20/79

FRAC FLUID:	7900 BBLS 10 LBS H.P. GUAR/1000 GAL 2 LBS XC POLYMER/1000 GAL
SAND:	50,400 LBS 100 MESH 58,000 LBS 20/40 MESH PROPPANT
RATE:	50 BPM
INTERVAL:	4705'-4900'
FRAC HEIGHT:	200'

TABLE II

RRGP-5

CONVENTIONAL (PLANAR) FRAC 11/12/79

FRAC FLUID:	7600 BBLS 30 LBS H.P. GUAR/1000 GAL
SAND:	84,000 LBS 100 MESH 347,000 LBS 20/40 MESH PROPPANT
RATE:	50 BPM
INTERVAL:	4587'-4803'
FRAC HEIGHT:	135'

STIMULATION TREATMENTS AT EAST MESA

Two hydraulic fracture stimulation treatments were successfully performed in Republic Geothermal East Mesa well 58-30. East Mesa is located in an area of anomalously high heat flow on the east flank of the Salton Trough, at the southeast corner of the Imperial Valley of California. East Mesa is a moderate temperature reservoir producing from a sandstone and siltstone rock matrix. Several features of the East Mesa field made it an excellent choice for the next field experiments. The reservoir is known in more detail than most other geothermal reservoirs. This in-depth knowledge provides a sound basis for designing and evaluating stimulation treatments. This moderate geothermal reservoir temperature range (320°-350°F) is the next step in the evaluation of the fracture fluids, proppants and mechanical equipment. The selection of a matrix type reservoir is also important at this stage of the program. Fracture geometry has been successfully predicted in matrix type reservoirs in the petroleum industry, and the existing interpretive techiques should transfer to geothermal reservoirs. Furthermore, the reservoir fluids, with a total dissolved solids content of about 2000 mg/l are not expected to chemically interfere with the stimulation fluids or tracers.

Well 58-30, selected for these experiments, is ideally suited mechanically. Unlike many other geothermal wells at East Mesa and elsewhere, it is completed with a cemented, jet perforated liner. This affords an opportunity to isolate zones of a size that can be effectively treated and evaluated. The first treatment was a conventional planar type hydraulic fracture of a 250 foot low permeabilty sandstone interval near the bottom of

the well. This zone has good sand development, but the permeability has been severely reduced because of authigenic cementation by carbonate minerals. Porosity is still high enough, however, to provide good storage capacity. A fracture treatment of this zone is intended to create a much larger effective drainage area surrounding the well in a manner similar to conventional oil and gas well stimulations, and thereby enhance the flow capacity. The treatment consisted of 2,800 bbl of a viscous crosslinked polymer frac fluid and 163,000 lbs of sand. The fluid was pumped at an average rate of 40 bpm during the treatment with B-J Hughes as the service company.

The second treatment was a dendritic fracture treatment in a more shallow, higher permeability, 300 ft interval of the same well. This upper zone, drilled with a predominantly bentonitic mud system, has good sands (high porosity and permeability) which show permeability impairment near the wellbore. A mini-frac of these zones will break through the mud and cement damage near the wellbore such that fluid can more easily flow into the well from the formation. The treatment consisted of 10,300 bbl of low viscosity frac fluid and 44,000 lb of 100-mesh sand pumped in 5 stages at an average rate of 48 bpm. The job was terminated before the planned 8 stages and 15,600 bbl because the rate/pressure history of the job indicated there was little to be gained by pumping the last three stages. The 100 mesh sand was used as fluid-loss control agent in the 50 md permeable sandstone interval that was fractured.

From July 25 to August 2, 1980 the well was production tested to evaluate the fracture experiment on the upper zone. The lower section of the well, from 6,547 to TD, was sanded back to prevent flow from the lower frac zone. The well flowed an average of 135,000 lbs per hour with a wellhead pressure of 33 psig. A wireline unit was utilized to monitor the reservoir pressure buildup. Reservoir pressure buildup data show the total open interval permeability-thickness was 9,881 md-ft, or approximately a 2.5 fold increase in productivity for the upper frac zone. This analysis indicates the shallow hydraulic stimulation treatment of the high permeability, upper interval was very successful. The upper zone treatment to correct near wellbore damage is of particular importance because such mud and cement damage is believed to be a common cause of impairment in Imperial Valley wells.

Well clean-out operations were initiated in August to remove the sand covering the lower frac zone. The coil tubing (used to inject nitrogen) parted and left approximately 5,170 ft of tubing in the hole. Fishing and clean-out operations are in progress. A production test of the entire wellbore will then be performed to evaluate the lower frac job. Summaries of the stimulation treatments are presented in Tables III and IV.

TABLE III

EAST MESA 58-30 (DEEP ZONE)
CONVENTIONAL (PLANAR) FRAC 7/3/80

FRAC FLUID:	2800 BBLS CROSSLINKED POLYMER GEL 20 LBS CALCIUM CARBONATE/1000 GAL (FLUID LOSS ADDITIVE IN PREPAD AND PAD)
SAND:	44,500 LBS 100 MESH 59,200 LBS 20/40 MESH 60,000 LBS 20/40 MESH "SUPERSAND"
RATE:	40 BPM
INTERVAL:	6587'-6834' (247')
FORMATION:	350°F-15md

TABLE IV

EAST MESA 58-30 (SHALLOW ZONE)
5-STAGE KIEL FRAC 7/6/80

FRAC FLUID:	10,300 BBLS 10 LBS H.P. GUAR/1000 GAL 2 LBS XC POLYMER/1000 GAL 20 LBS CALCIUM CARBONATE/1000 GAL (FLUID LOSS ADDITIVE)
SAND:	44,000 LBS 100 MESH
RATE:	48 BPM
INTERVAL:	4952'-5256' (304')
FORMATION:	325°F-50md

CONCLUSIONS

An effective stimulation treatment requires the interaction of four separate items.

- Frac fluids
- Proppants
- Equipment
- Planned and Properly Engineered Schedules

While there are good fluid systems and proppants, only judicious combinations and a well thought out schedule which uses all of these materials and available equipment to best advantage is an optimum stimulation treatment. Generally, high flow rates and convective cooling can be used either with conventional (planar) fracturing or with a dendritic fracturing technique. Many of todays fluid systems have been tested to above 400°F. Some fluids have survived quite well. Current tests on proppants have shown temperature sensitivities in sand; however, there are resin coated materials and sintered bauxite which are not temperature sensitive. Much more work is required in the specific application of fluid systems and proppants to the actual hydrothermal wells since the temperature, water chemistry and formation properties vary greatly.

THE D.O.E. HOT DRY ROCK PROGRAM*

by

Gregory J. Nunz
Los Alamos Scientific Laboratory
The University of California
Los Alamos, New Mexico 87545

ABSTRACT

Hydraulic fracturing has been used to create and subsequently to enlarge the first hot dry rock heat-extraction loop at Fenton Hill, New Mexico. Encouraging results prompted the DOE to expand this project into a program of national scope. The elements of that Program and their present status are discussed.

Emphasis is given the ongoing Fenton Hill Project where techniques and information developed in the existing research system will soon be used to produce a multiply-fractured engineering system in hotter rock at the same site. Recent results from research loop operation and progress in constructing the engineering system are reported.

Although acoustic mapping and system geometry indicate that the primary hydraulic fractures are essentially vertical, relatively low fracturing pressure and absence of a sharp breakdown suggest that at Fenton Hill fracture initiation occurs by reopening of old natural fractures rather than by initiation of new ones. Flow patterns and temperature behavior suggest opening of additional old fractures as the loop is operated. Except where the hot fluid leaves the crack system to enter the production well, flow impedances are very low without either artificial propping or inflation by pressurization.

INTRODUCTION

In September 1977, researchers at the Los Alamos Scientific Laboratory (LASL) demonstrated the successful establishment of the first hot dry rock

* Work performed under the auspices of the U.S. Dept. of Energy, Division of Geothermal Energy.

(HDR) geothermal energy-extraction loop at their Fenton Hill test site in northern New Mexico. Results of testing this system over the ensuing year were extremely encouraging and motivated the DOE Division of Geothermal Energy (DOE/DGE) to expand the Fenton Hill HDR Project into a program of national scope — the "Hot Dry Rock Geothermal Energy Development Program" (HDR Program"). This paper presents the current status and recent results of the various elements of the HDR Program, with emphasis on the continuing Fenton Hill Project.

ENERGY-EXTRACTION CONCEPT

In its broadest sense, hot "dry" rock is crustal rock containing heat energy at temperatures of commercial interest but which will not spontaneously produce indigenous fluid at a rate adequate for economic energy extraction. The basic HDR concept is therefore to "mine" the heat energy from such rock by artificially introducing the heat transport fluid from the surface and, when required, artificially creating or increasing the effective permeability of the rock to provide the required subterranean heat-exchange area. A spectrum of engineering implementations is thus possible. For any given site, the specific approach to energy extraction will depend upon the temperature and nature of the formation, its permeability and porosity, its capability (if any) to self-produce, local availability of water, and other factors.

OBJECTIVE AND SCOPE OF THE PROGRAM

The overall objective of DOE's HDR Program is to demonstrate the commercial feasibility of geothermal energy derived from hot dry rock resources. It is DOE's intent to attain this objective within the 1980's decade subject, of course, to meeting the anticipated rate of technological progress and to the appropriation of requisite funds. The program is field-managed by the LASL, in conjunction with DOE's Albuquerque Operations Office as associate program manager, under the aegis of the DOE/DGE.

The scope of the program presently encompasses application of the concept only to formations of very low permeability (i.e. a few microdarcies, or less). The approach for this application, as illustrated conceptually in Figure 1, consists of: (a) drilling two wells — an injection well and a production well — through the sedimentary cover into the relatively impermeable formation of interest; (b) connecting these wells through a man-made fracture system of appropriate size, created by hydraulic, pneumatic, or other means; and (c) forming a closed circulation loop by connecting the two wells at the surface through a suitable heat exchanger and conversion system.

PROGRAM STRUCTURE AND PLAN

The HDR Program consists of four major elements which derive logically from the Program's objective:

- Resource Evaluation
- Technology Development
- Institutional Issues Analyses
- Commercial Feasibility Assessment

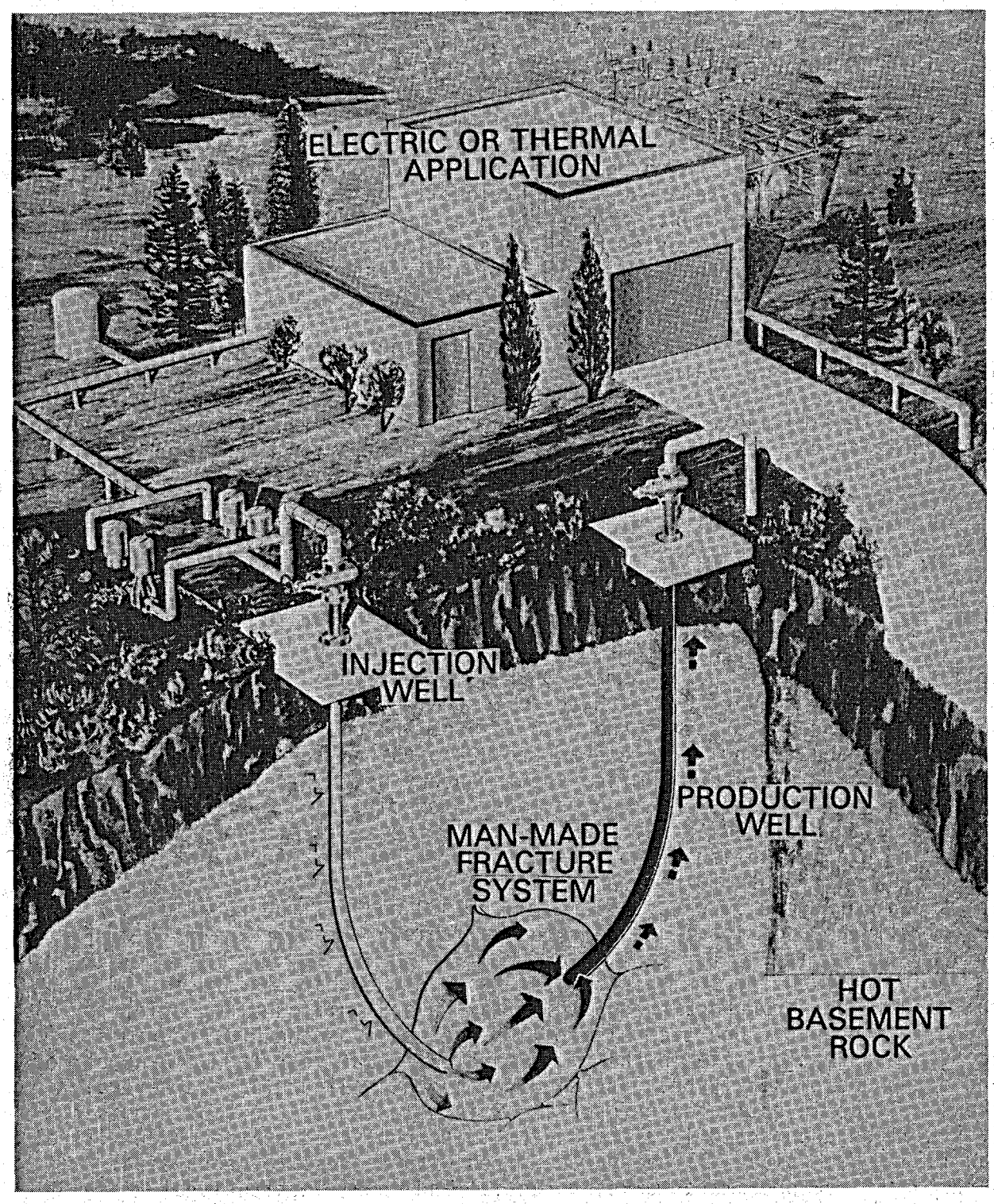

Fig. 1. Hot Dry Rock Geothermal Energy Extraction Concept

The resource evaluation element is aimed at better identifying the accessible US resource base and estimating the fraction thereof that constitutes an economic resource. The dominant element, both in priority and in allocated funding, is technology development which includes the establishment of HDR systems at two reservoir-demonstration sites. Analysis of institutional issues which bear upon the economics, or constrain the development, of HDR systems — either nationally or regionally — forms an important supportive element. These three elements then interact in the fourth where economically-oriented studies, culminating in a detailed commercial feasibility analysis, will ultimately assess the commercial potential of HDR-derived electricity and space/process heat.

The current program schedule is given in Figure 2. By fiscal year 1987, with a final resource evaluation completed as well as the testing of the two demonstration reservoirs, adequate data will be available to complete the commercial feasibility analysis. The results will enable the DOE to make a final decision on whether or not to proceed with a commercialization program for this technology.

The status and results to date in each of the program's elements are discussed in the following sections.

RESOURCE EVALUATION

The objective of this element, as noted previously, is to obtain a realistic estimate of the economic HDR resource of the United States. The work is a coordinated effort with the U.S. Geological Survey (USGS) which has the primary charter to assess the resources of the country. The program is compiling and analyzing data relevant to HDR obtained largely from the USGS, state, and other sources. Limited supplementary geophysical measurements are being sponsored by the program in regions of specific interest for HDR. These data are being provided to the USGS as well. The early products will be a series of jointly published geophysical maps: geothermal gradient, regional rock properties, depth to basement, etc. A preliminary geothermal gradient map, shown in Figure 3, was published in FY1980 and will be updated periodically as additional data become available.

A derivative effort within this element is the characterization of promising sites throughout the US which may have significant potential for future development. One such site will be selected as the HDR Program's second demonstration site in the first part of fiscal year 1982. A number of candidates are presently being studied, as shown in Figure 4, and several others will be investigated before Site 2 is selected. A host of promising sites will be documented in a compendium to be published at the end of fiscal year 1985. Each site will be characterized with respect to geophysical characteristics, proximate market potential and local institutional constraints.

TECHNOLOGY DEVELOPMENT

(A) FENTON HILL PROJECT

At present, the only operational HDR energy-extraction system is LASL's research system at the Fenton Hill, NM site (Figure 5). The downhole portion

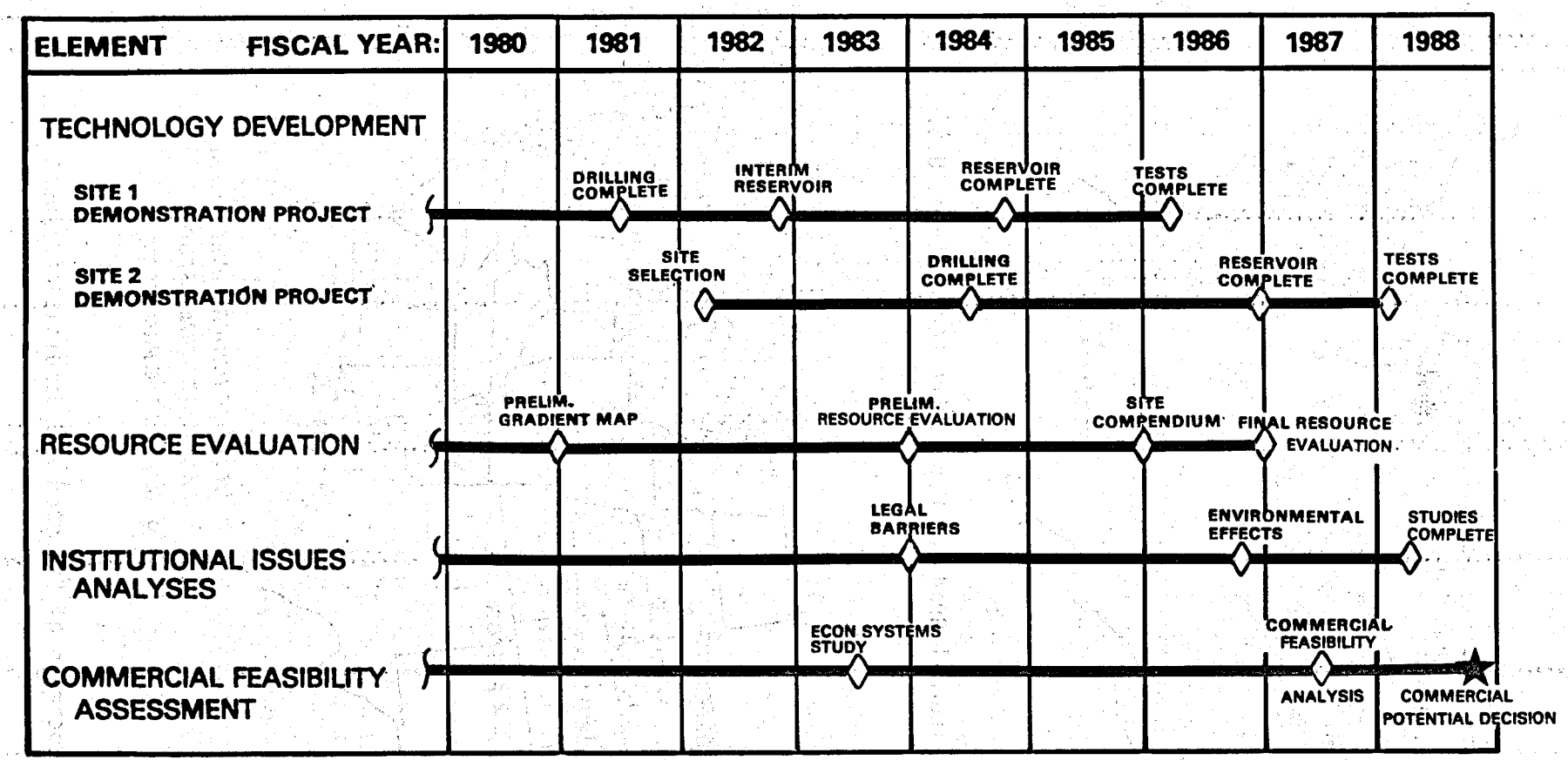

Fig. 2. Hot Dry Rock Program Milestone Schedule

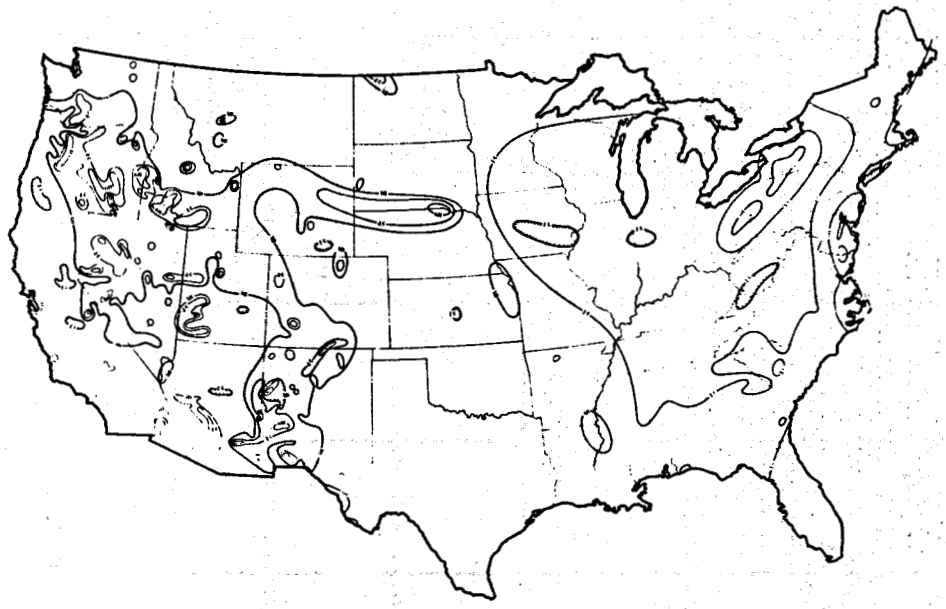

Fig. 3. Thermal Gradient Map of the Conterminous U.S.

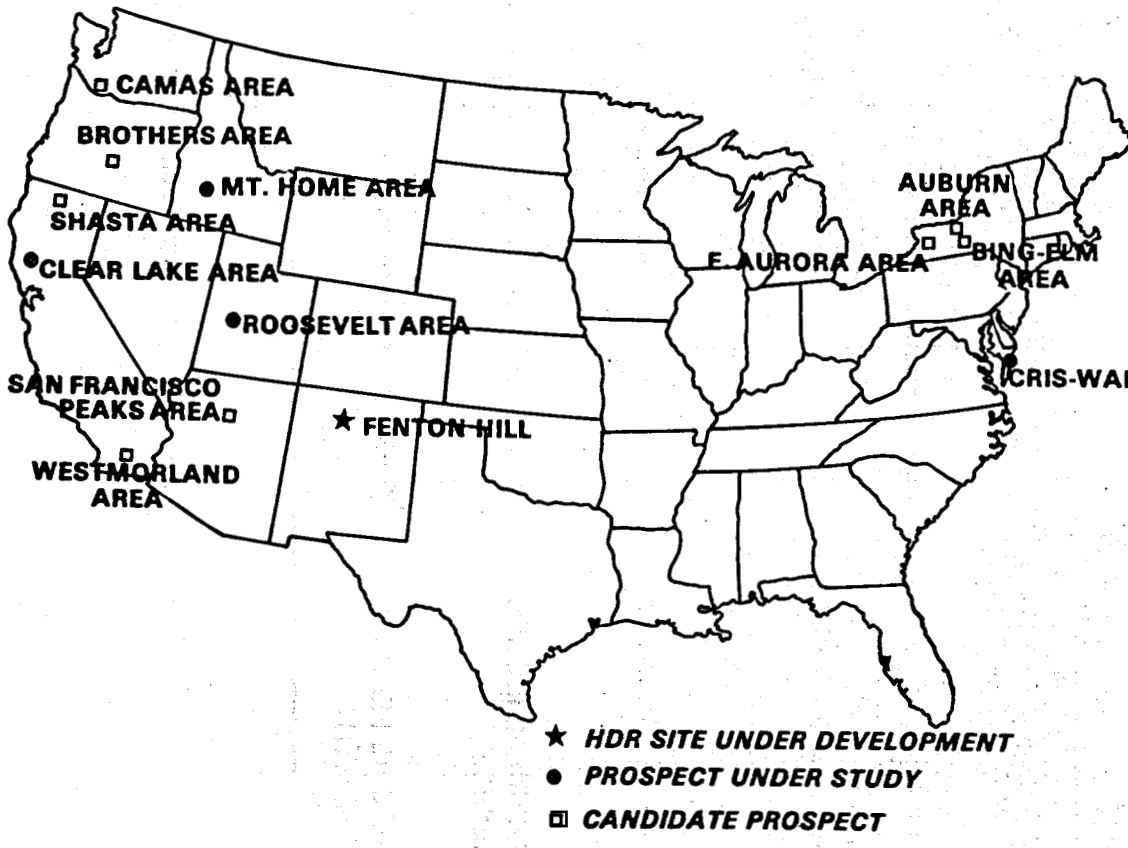

Fig. 4. Location of Selected and Candidate Prospect Areas

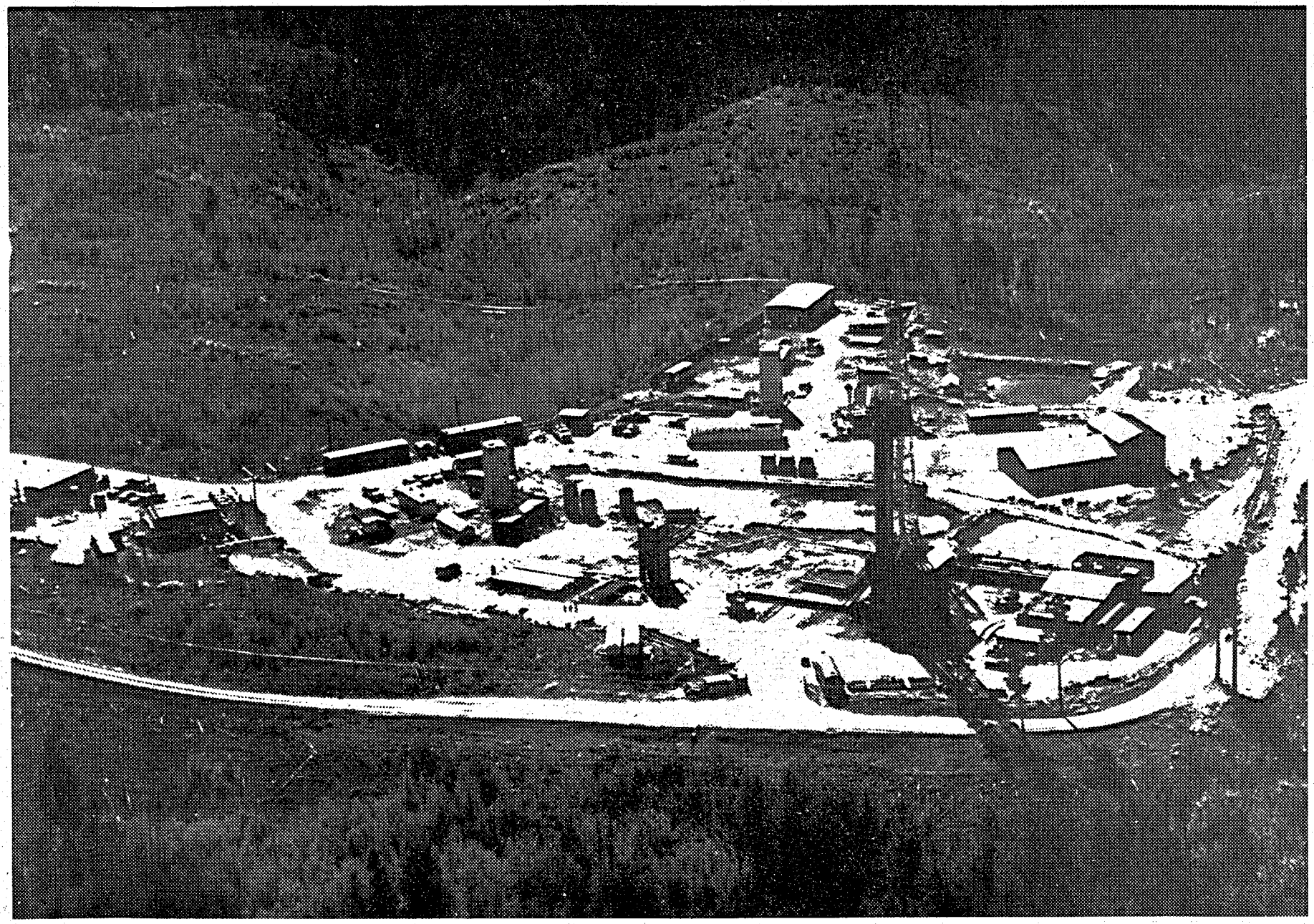

Fig. 5. Fenton Hill, New Mexico Site

of this research system, as originally established, consisted of a relatively small (circa 8000 m^2) fracture complex which connected the injection well, EE-1, and production well, GT-2, through a series of high-angle natural joints, as shown in Figure 6(a). The essentials of this geometry have been established through numerous well logs, downhole interwellbore acoustic transmission experiments and extended flow tests. The smooth and continuous form of the pressure history curve generated during fracturing indicates that an old sealed fracture was probably reopened (and possibly extended) rather than virgin rock matrix having been fractured. Three operational runs were conducted on this original research reservoir. Run Segment 1, a 100-h initial check-out and feasibility demonstration test was conducted in September 1977. In Run Segment 2 - a 75-day accelerated drawdown test conducted between January and April 1978 - preliminary answers were obtained, on an accelerated time scale, to questions concerning what would have been long-term effects in a commercial-size reservoir. Those preliminary answers were both enlightening and very encouraging:

- DRAWDOWN PREDICTABILITY - The somewhat simplified model of the downhole fracture system used in LASL's computations is mathematically adequate to represent drawdown. Specifically, the original research system behaved like a simply-fractured reservoir with an effective heat transfer area of about 8000 m^2 as shown by the lower curve and data of Figure 7. Whereas the numbers are particular to this system, the results indicate that the modeling methodology should be applicable to both the next (engineering) system at Fenton Hill and other sites.

- MAKEUP WATER REQUIREMENTS - Water loss to permeation quickly declined to less than 1-1/2% of the circulation rate (under 0.2ℓ/s), once the initial pore field saturation was achieved. This result, although obtained specifically for the Fenton Hill formation, is tentatively extrapolable to other sites where matrix permeability is in the units-to-tens of microdarcies range and indicates that makeup water requirement will not be a major constraint in such formations.

- GEOFLUID CHEMISTRY - A near-equilibrium composition was achieved in the circulating water, which remained at less than 2000 ppm total dissolved solids. Except for a slightly high terminal fluoride concentration (∿9 ppm), this is virtually drinking water and scarcely deserves to be called a "brine" compared to the hydrothermal brines. No evidence of corrosion or scaling was detected in the flow loop. Although these compositional data are highly Fenton Hill specific, they lend credence to the qualitative prognosis that HDR geofluid chemistry should generally be manageable.

- OPERATIONAL CONSTRAINTS - A number of stop/start transients were imposed on the system, many of them inadvertent, because of brief power outages on the local utility. Although no major operational constraints were indicated, some minor freezing problems were encountered, which pointed to the need for careful attention to surface system design at HDR sites with similar moderate-to-severe winter climate and comparatively pure water geofluid.

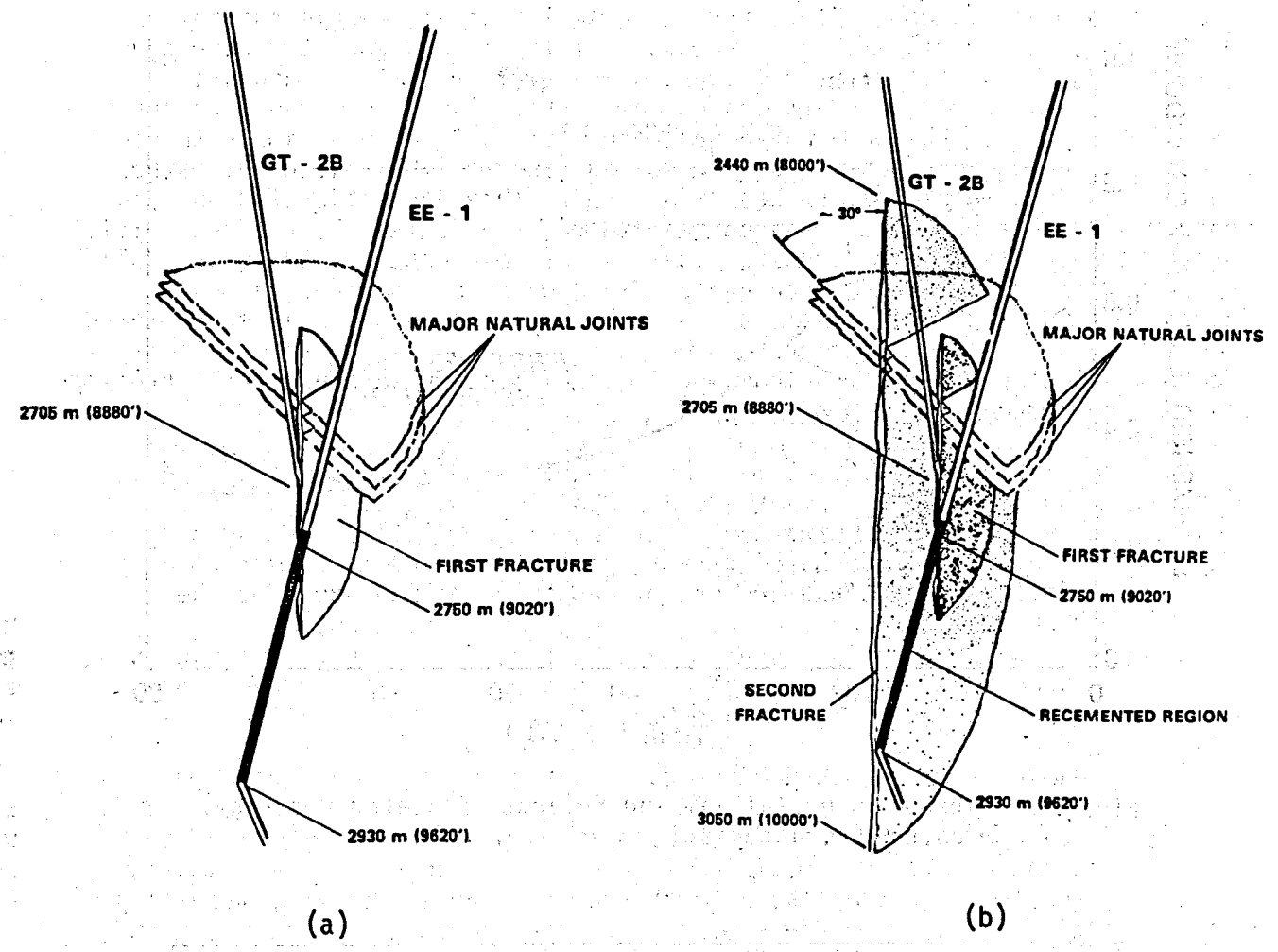

Fig. 6. Initial (a) and Enlarged (b) Research Reservoir Configuration

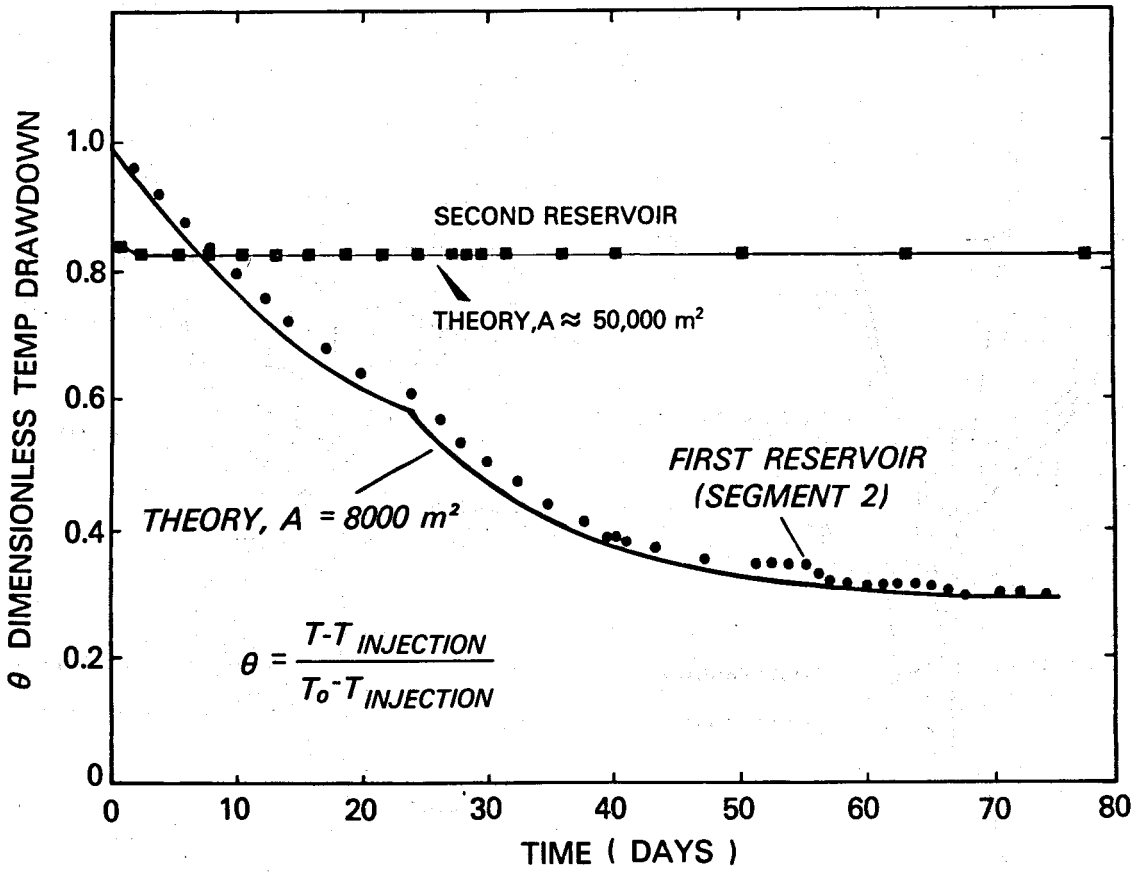

Fig. 7. Comparison of Initial and Enlarged Research Reservoir Drawdown Characteristics

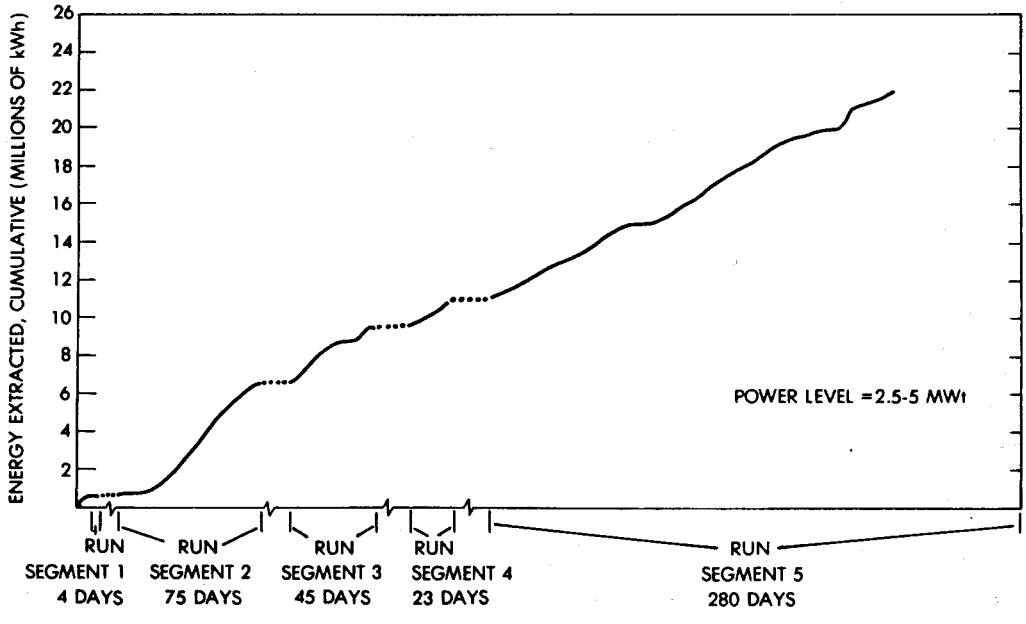

Fig. 8. Thermal Energy Extracted from Fenton Hill HDR Research Reservoir

- ENVIRONMENTAL EFFECTS - Perhaps most encouraging, no detrimental environmental effects were observed. In particular, under extremely careful monitoring, there was absolutely no evidence of affecting the composition of local aquifers or other hydrological effects and there was no detectable induced seismicity.

After some minor modifications to the surface plumbing to permit higher flow rates, Run Segment 3 was conducted during the period September to October 1978. In this segment, comprising about 786 operating hours, three distinct flow experiments were conducted back-to-back. The first of these was a series of transient flow-dependent impedance measurements; the second consisted of interwellbore acoustic attenuation surveys under shut-in conditions; and the third (and longest) was a continuous-flow experiment under high back pressure. This run segment was terminated prematurely because of the development of a major ($\sim$3.5ℓ/s) leak behind the casing in the injection well. In the high-back-pressure operation it was observed that reservoir flow impedance declined significantly, from over 200 kPa-s/ℓ to about 55 kPa-s/ℓ.

The leak observed at the end of Run Segment 3 was due to final degradation of already degenerate cement in the annular space behind the casing of the injection well. Recementing was necessary and, in the process, access to the vertical fracture emanating from the EE-1 wellbore at 2750 meters was shut off. A new and much larger fracture was initiated (probably also a reopening of an old, sealed fracture) further down the wellbore and extended upward until it too communicated with the GT-2 well through the same system of natural joints, as seen in Figure 6(b).

Since the enlargement of the research reservoir was effected, two extended heat-extraction runs have been made. Run Segment 4 was conducted during October and November of 1979 for a total operating duration of 551 hours. The thermal drawdown data — or rather lack thereof — indicated that the effective heat transfer area had been increased by not less than a factor of 6. The second test, Run Segment 5, began near the end of February 1980, is presently in progress, and is scheduled to conclude about 15 December 1980. The enlargement of the reservoir is confirmed by the very gradual thermal drawdown, indicated by the upper data in Figure 7, and the effective heat transfer area of the research reservoir is now believed to be of the order of 50,000 m^2.

To date, over 20 million kilowatt-hours of thermal energy have been extracted from the Fenton Hill research reservoir at power levels ranging from 2.3 to 5.0 MW_t, as shown in Figure 8. Recently, a small on-line electric generation experiment has been added as part of Run Segment 5. The generating unit is a 60kVA (net) binary cycle turboalternator package using R-114 halocarbon as the working fluid. It is driven by a fraction of the superheated water produced from the research system and is connected into the site electric mains, providing a part of the base load.

In parallel with evaluation of the research system, planning and construction of an engineering system has been proceeding. Although the research system demonstrated initial technical feasibility of the concept and provided encouraging preliminary answers to some issues of concern, the establishment of a reservoir of more nearly commercial size and (even more important) longevity remains to be demonstrated in the engineering system.

A schematic comparison of the enlarged research system with the engineering system is given in Figure 9. As noted, the former now consists of two nearly vertical wells connected by a 50,000 m^2 fracture system in 200°C rock at about 3 km depth. The new engineering system will be both larger and hotter, consisting of two deeper wells -- EE-2, the injection well, and EE-3, the production well -- to a depth of about 4.5 km with their working sections inclined at 35° to the vertical. These wells will be connected by a multiple fracture system in the 300°C rock with a nominal effective area of 1.5×10^6 m^2. This engineering system, when completed, will be capable of producing 20-50 thermal megawatts with not more than 20% thermal drawdown in 10 years, and could be suitable for possible commercial use when the DOE-sponsored demonstration of the reservoir is complete.

The injection well, EE-2, is now complete to a depth of 4450 m with a bottomhole temperature of 320°C and the production well, EE-3, is being drilled. Establishment of the fracture system is scheduled to begin in 1981.

(B) PLANS FOR SITE 2 PROJECT

A key program activity is the selection of a second experimental HDR site. Development of such a site is necessary to establish: (a) that the reservoir techniques utilized at Fenton Hill or modifications thereof, are applicable in a different formation; and (b) an expanded data base for assessing the commercial feasibility of HDR energy. Survey of the existing data continued through 1978, culminating in the nomination of a number of candidate prospect areas throughout the US. From this listing, the most promising prospect areas were selected for detailed geophysical investigation. Conduct of this field work is now in progress. The anticipated outcome is sufficiently positive characterization to permit selection of a specific site early in 1982.

(C) INSTRUMENTATION AND EQUIPMENT DEVELOPMENT

Another major area of technology development, which directly supports experimental operations at Fenton Hill (and will, subsequently, at Site 2), is directed toward providing the specialized instrumentation and downhole equipment needs of the HDR Program, which are commercially unavailable. Whenever possible, development is accomplished through subcontracts with industry, thereby effecting immediate technology transfer as well. In addition, these developments are coordinated with those of Sandia's Geothermal Instrument Development and Drilling Technology programs, as well as the needs of USGS, to avoid duplication of effort.

During 1978-79, Maurer Engineering proceeded with development of the turbodrill, a high-temperature downhole drilling motor, sponsored jointly by DOE/DGE and the DOE/Division of Fossil Energy Extraction (DFEE). It was successfully field tested in the drilling of well EE-2 and is now being used in the drilling of EE-3 at Fenton Hill. LASL also sponsored improvements in open-hole packer and shock-sub temperature capability. These high-temperature units are being tried in the same drilling program.

Development work also continues on a high-temperature multiconductor instrument cable. Testing is currently in progress of 1000-foot evaluation specimens from several sources.

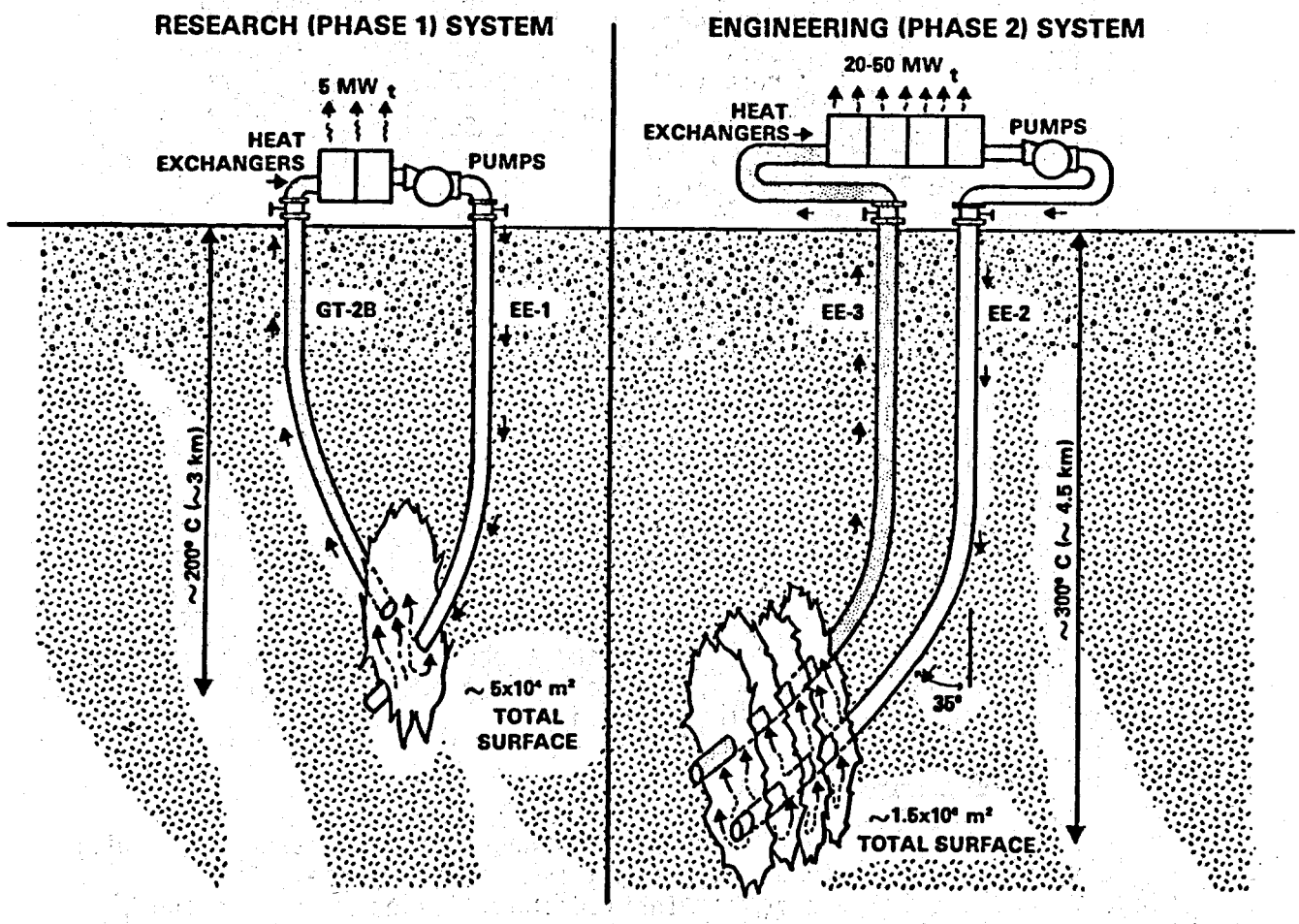

Fig. 9. Comparison of Fenton Hill Research and Engineering Systems

TABLE I

HIGH-TEMPERATURE INSTRUMENTS AND EQUIPMENT DEVELOPED TO DATE

Item	Developer/Vendor(s)
Temp./Pressure Probe (260°C)	LASL/Bell & Howell
Wellbore Fluid Sampler	LASL/Globe
3-Axis Fluid Sampler	LASL/Mark Products
Mechanical Acoustic Source	LASL/Globe
Multidetonator Acoustic Source	LASL/Reynolds/Vacuum Barrier
Fluid Sample Downhole Injector	LASL/Globe
Self Potential Probe	LASL
Temp./Conductivity Probe (275°C)	LASL
3-Indep.-Arm Caliper/Contour Probe	LASL/Dale Electronics
Wellbore Fluid Velocity Meter	Worthwell-LASL
Radiotracer Injector/Monitor Tool	Worthwell

Major LASL-internal developments are listed in Table I. With the exception of the first item listed, all of these instruments have a temperature capability of at least 275°C. Those recently completed included improved downhole temperature- and velocity-measuring units and a temperature hardened 3-independent-arm caliper tool for borehole gaging. Subcontracted work on fracture-mapping instruments includes: feasibility studies and preliminary design for a radar-based far-field mapping tool and in situ stress measurement device; fabrication of a prototype downhole acoustic transceiver unit utilizing a magnetostrictive driver; and a phased program to develop a high-temperature downhole video system which will produce real-time monochrome images under visible and ultraviolet illumination.

INSTITUTIONAL ISSUES ANALYSES

There are a number of quasitechnical and non-technical issues that will affect the suitability of HDR as an alternative energy source. For convenience, they are categorized as Institutional Issues. They include: (1) legal aspects of HDR development; (2) regulatory issues; (3) environmental effects of intensive development; (4) water availability; and (5) public awareness. The program is examining the extent to which these issues may impact HDR development.

Institutional aspects of HDR development typically differ from one locale to another and depend on subjective factors as well as objective considerations. For instance, the legal definition of "geothermal resource" varies widely among the States. The variance in this case is due largely to differences in the public's perception of geothermal resources rather than a real physical difference among resources.

Similarly, regulatory controls are subject to differing degrees of interpretation and enforcement. As the perception of HDR and its technology varies from one place to another, so will the extent to which HDR development is accepted.

Activities involving institutional issues include environmental studies, legal/regulatory studies, and public relations. Environmental studies are directed at obtaining more definitive information about the effects of commercial-scale HDR development. Although much experience from hydrothermal projects is directly applicable because the effects are similar to those expected from HDR, other environmental aspects of HDR are unique to its application. Careful and continuous environmental monitoring is being done in conjunction with the program's demonstration projects. This operational experience will clarify the environmental issues and help to place them in perspective for the regulatory authorities. A detailed Environmental Analysis Report and an Environmental Impact Assessment have been published for the Fenton Hill Site.

Studies of laws and regulations at both the Federal and State levels are identifying potential barriers to HDR development. Where possible, developmental routes to avoid or eliminate barriers will be suggested. A preliminary legal study was published in 1979 discussing the differences from state-to-state in the definition of the "resource" under which the ownership question would be adjudicated. The study proposed a more consistent sui generis definition.

The interested public, including the geothermal industry, financial community, and regulatory agencies, is being kept informed of the program's progress and findings. This information is being disseminated through discussions and presentations, press releases, a quarterly newsletter, educational materials, brochures, technical reports, and annual conferences.

COMMERCIAL FEASIBILITY ASSESSMENT

Commercial feasibility can best be proven by demonstration combined with appropriate economic analyses; both are deemed essential to reaching the program's goal. Demonstration is implicit in the Technology Development element. Economic analysis, which involves a synthesis of all critical factors affecting the cost of HDR systems, is conducted in this Program element.

Economically-oriented studies have been an ongoing activity in the Program since its inception. Preliminary studies, done by LASL in concert with the University of New Mexico and (at this stage of development) subject to a great many assumptions, have shown that HDR-derived energy costs can be of the right order of magnitude to be competitive with other energy sources in the post-1990 time frame.

A more comprehensive economic systems study is now underway, focusing on the modeling of reservoir establishment and management strategies. The overall study will examine drilling costs, conversion costs and so forth. Sensitivity analyses will identify cost-sensitive factors and through a feedback mechanism, technology improvements which reduce costs will be pursued. The study will include institutional and other factors that influence development costs. As more field data become available, the study will be updated.

The ultimate question to be answered is: Can energy produced through HDR technology compete with that from other energy production technologies in the

private marketplace? The answer will come from a final commercial feasibility analysis that accounts not only for technology costs and benefits, but for the availability of resources, market needs, and regulatory requirements.

SUMMARY

The HDR Program is a multifaceted long-range program of national scope aimed at establishing an energy-producing industry. It is a combined development and demonstration program whose elements include: characterizing the resource; cataloging promising sites; developing the reservoir technology, and required tools and instruments; attacking the institutional problems and assessing the commercial feasibility of the concept in the near future.

ITALIAN EXPERIENCE AND PROBLEMS IN DEEP GEOTHERMAL DRILLING

U. Cigni

1. INTRODUCTION

Geothermal activity in Italy is now directed partly at exploring new areas and partly at recovering fluids with better thermodynamic characteristics from the traditional geothermal areas. For the latter reason the Tuscan geothermal areas are now the subject of a deep drilling program which is aimed at individuating, below the reservoir exploited at present, geological horizons whose lithological characteristics are such as to guarantee the presence of hydrothermal circuits.

A seismic survey of the Larderello area indicated a deep reflecting horizon that varies between 3500 and 7000 m depth. At the moment, however, "deep research and exploration" is used in reference to wells that are 3000-5000 m deep. The objectives set for these wells are:

1) to verify whether, at technically feasible depths, there are permeable horizons capable of forming a second reservoir of industrially exploitable endogenous fluids;
2) to improve the hydrogeological model of the field for a more rational exploitation of the resource;
3) to evaluate the geothermal potential in terms of "resource" and "reserve," to a depth of 5 km;
4) to study the possibility of recharging the field artificially by injecting water to great depths.

These objectives are attainable if the deep wells can guarantee:

- exploration of the deep horizons with wide diameters capable of providing significant data on their productive capacity;
- isolation of any reservoirs encountered in shallower horizons.

The stratigraphic sequence expected in these wells in the Larderello zone is, approximately:

from 0 - 500 m:	cover formations, comprising Neogenic sediments and flysch facies allochthonous complexes of a mainly clayey-carbonate composition.
from 500 - 1000 m:	complex forming the so-called "first reservoir," consisting of limestones and the Mesozoic Anhydritic Series. These are highly fractured formations.
below 1000 m:	Triassic-Paleozoic schistose-quartzitic basement, made up of schists, quartzites, micaschists, amphibolites and gneisses. These rocks are also rather fractured.

In view of the objectives of the program and the geological situation in the area, the technical profile of these deep wells is usually that shown in Fig. 1. That is, the cover formations are lined with an 18"5/8 casing; the first reservoir is isolated with the 13"3/8 casing to 1500 m; the first part of the schistose-quartzitic basement is lined with a 9"5/8 casing to 3000 m. The last stretch of the bore remains uncased, with a diameter of 8"3/8. Depending on well conditions a 7" liner can be inserted in the last sector of the bore and joined to the 9"5/8 casing with a hanger.

2. RIG MACHINERY AND EQUIPMENT

Special machinery and equipment had to be used for these wells.

For the drilling in the Larderello area, the first rig was electric-driven so as to take advantage of the electricity produced by Larderello's own power-plants. The drilling rig, whose nominal drill capacity is 5000 m, consists of the following main elements (Fig. 2).

- 142 foot cantilever mast with a Gross Nominal Capacity of 1.025.000 lbs and storage capacity of 5000 m for 5" diam. D.P.; the tilt-up sub-structure is 7.60 m high with a set-back capacity of 227 tons and 363 ton casing capacity;

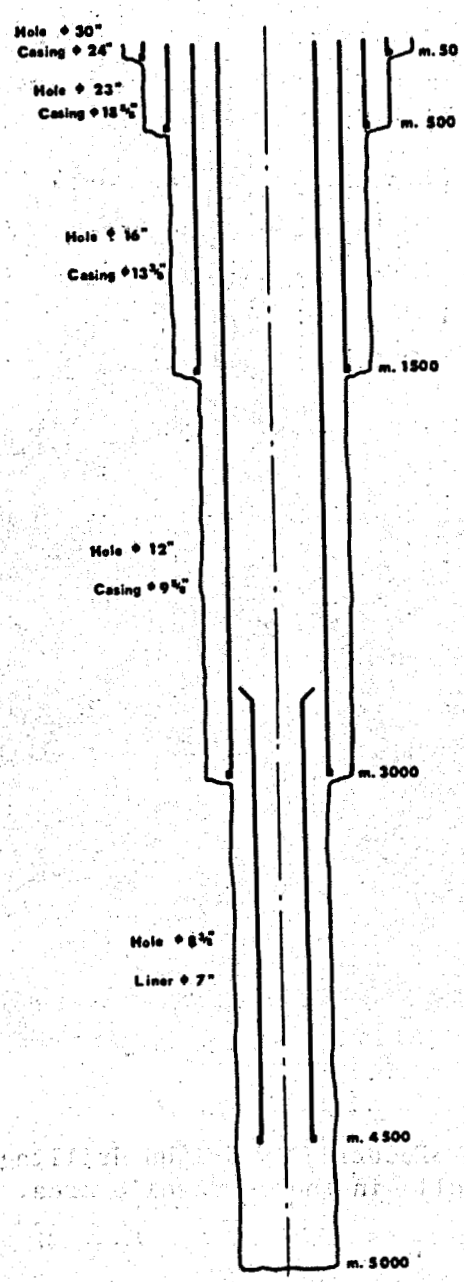

Fig. 1. Typical technical profile of the Larderello deep wells. These are used at Larderello to explore the layers between 3000 and 5000 m.

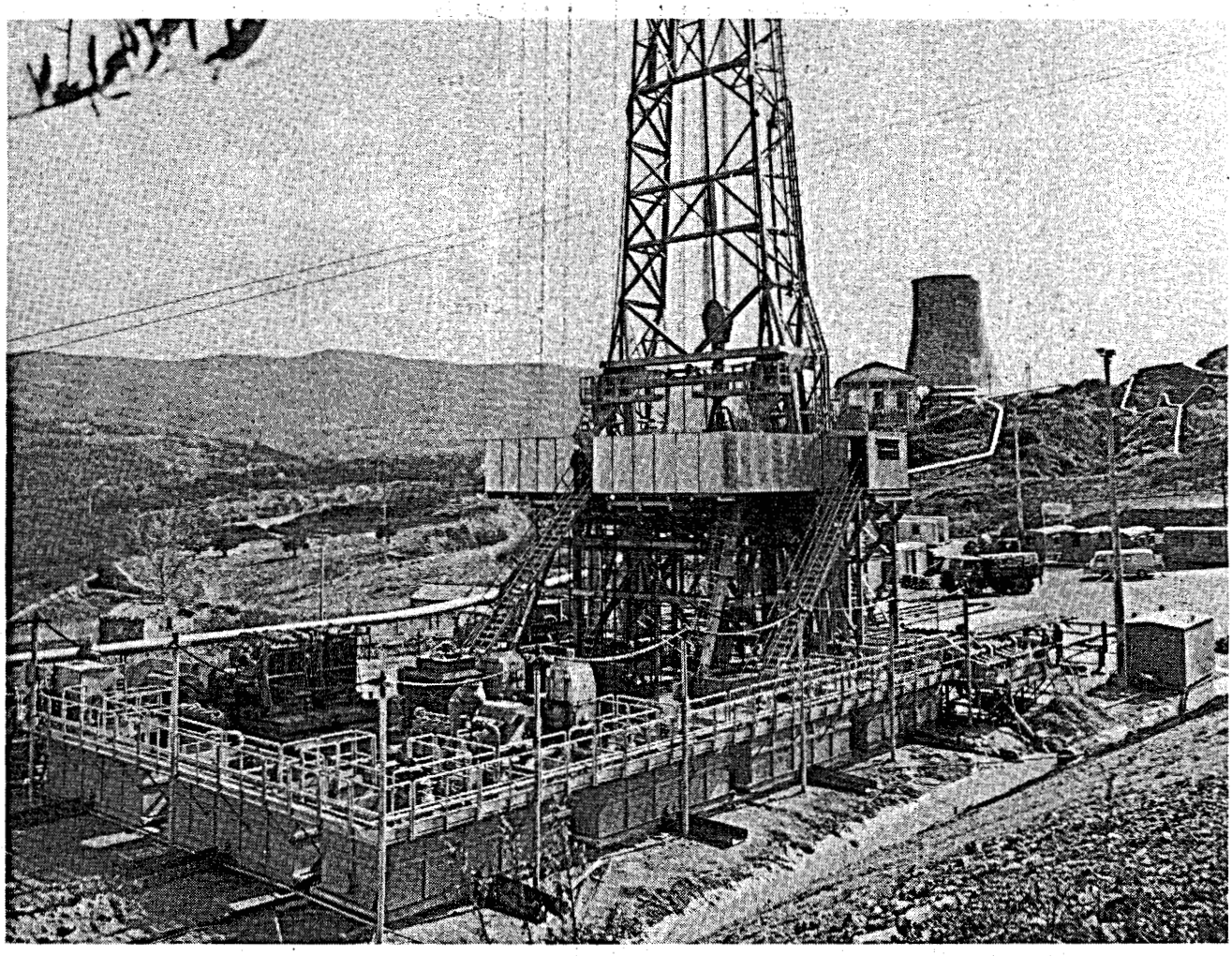

Fig. 2a. View of electrically driven drilling rig used for deep geothermal wells in the Larderello area. Capacity is 5000 m.

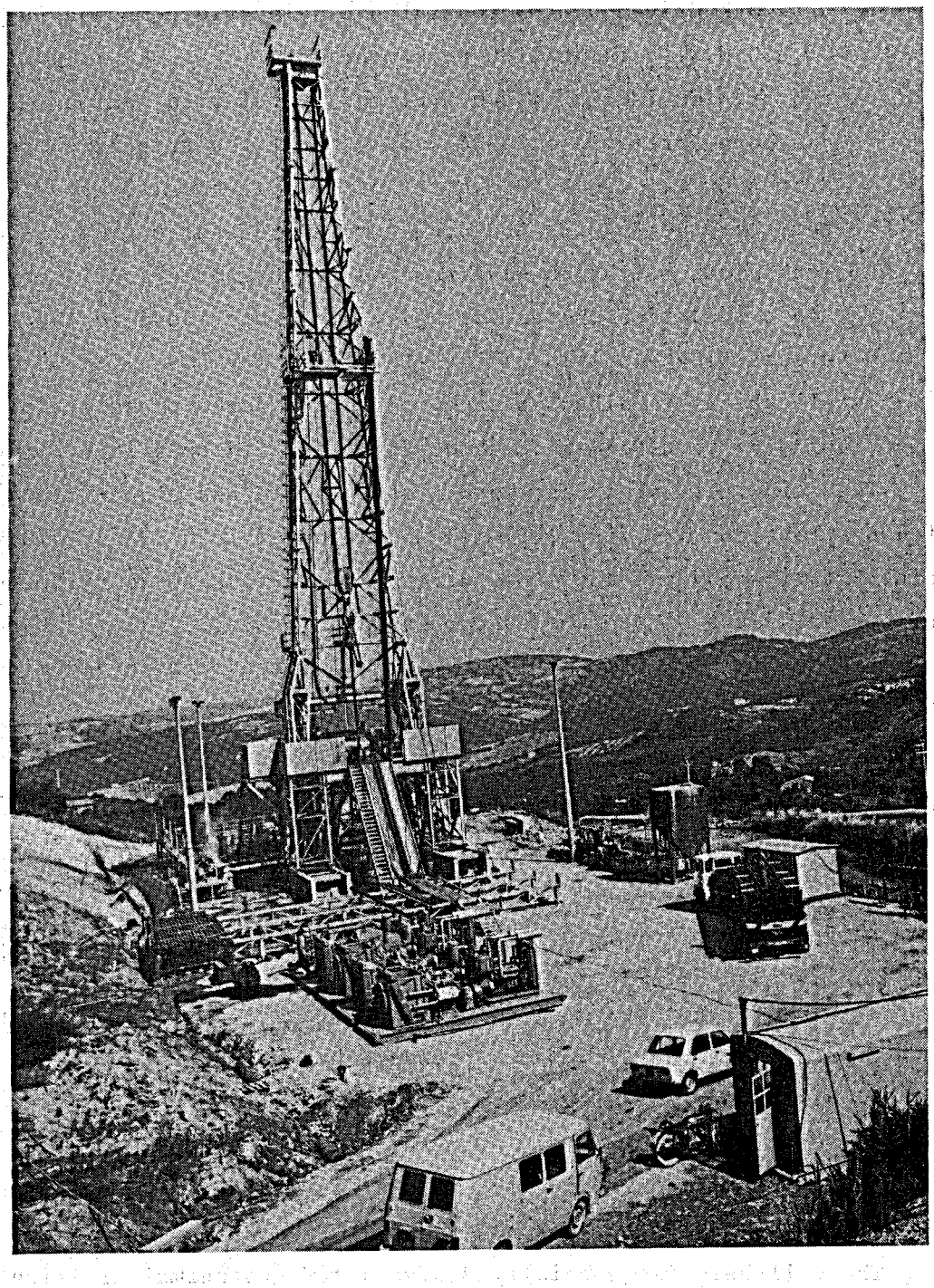

Fig. 2b. Another view of drilling rig as in Fig. 2a.

- drawwork driven by two coaxial d.c. electric compound engines, of 600 H.P. each at 1100 revs/min;
- two triplex 7" x 9", 1000 H.P. mud pumps, with maximum discharge pressure of 5300 psi. One of the triplex pumps is driven by two 600 H.P. d.c. electric engines, 1100 revs/min, and the other by two 600 H.P. compound diesel engines. Mechanical operation was provided to guarantee continuity of the circulation system during eventual breakdown in the electricity supply;
- electrical feeding system comprising a three-phase, triple-winding transtormer of about 2000 KVA, fed by a 16 KV line.

The main facilities (drawwork, rotary table and electric pump) are fed by the secondary circuit, with an output of 1850 KVA at 570 V, after static conversion of the current from alternate to direct through a system of controlled diodes (thyristors).

The tertiary circuit of 150 KVA at 380 V feeds the other minor facilities and auxiliary equipment.

The drilling yard is fitted with an air-drilling plant, ready for use in deep geothermal wells. This plant consists of four parts:

1) compressed air production from four two-stage 10"1/4 x 7" x 6" compressors, with an effective capacity of about 22 Nmc/min each and maximum delivery pressure of 18 kg/cm^2; a booster is also provided for raising the pressure to 106 kg/cm^2;
2) stand-pipe containing the instrumentation for measuring and recording the flow-rate, pressure and temperature of the air;
3) discharge line with dust separators, silencer and air-water separator;
4) system for dosing chemical additives, injecting foaming agents and corrosion inhibitors.

The well-head was specially designed for geothermal drilling (Fig. 3) and consists of API 3000 valves and spool capable of operating at a working pressure of up to 192 kg/cm^2 at 232°C. Beyond the kill-line are two 10" lateral flow lines for high fluid flow-rates

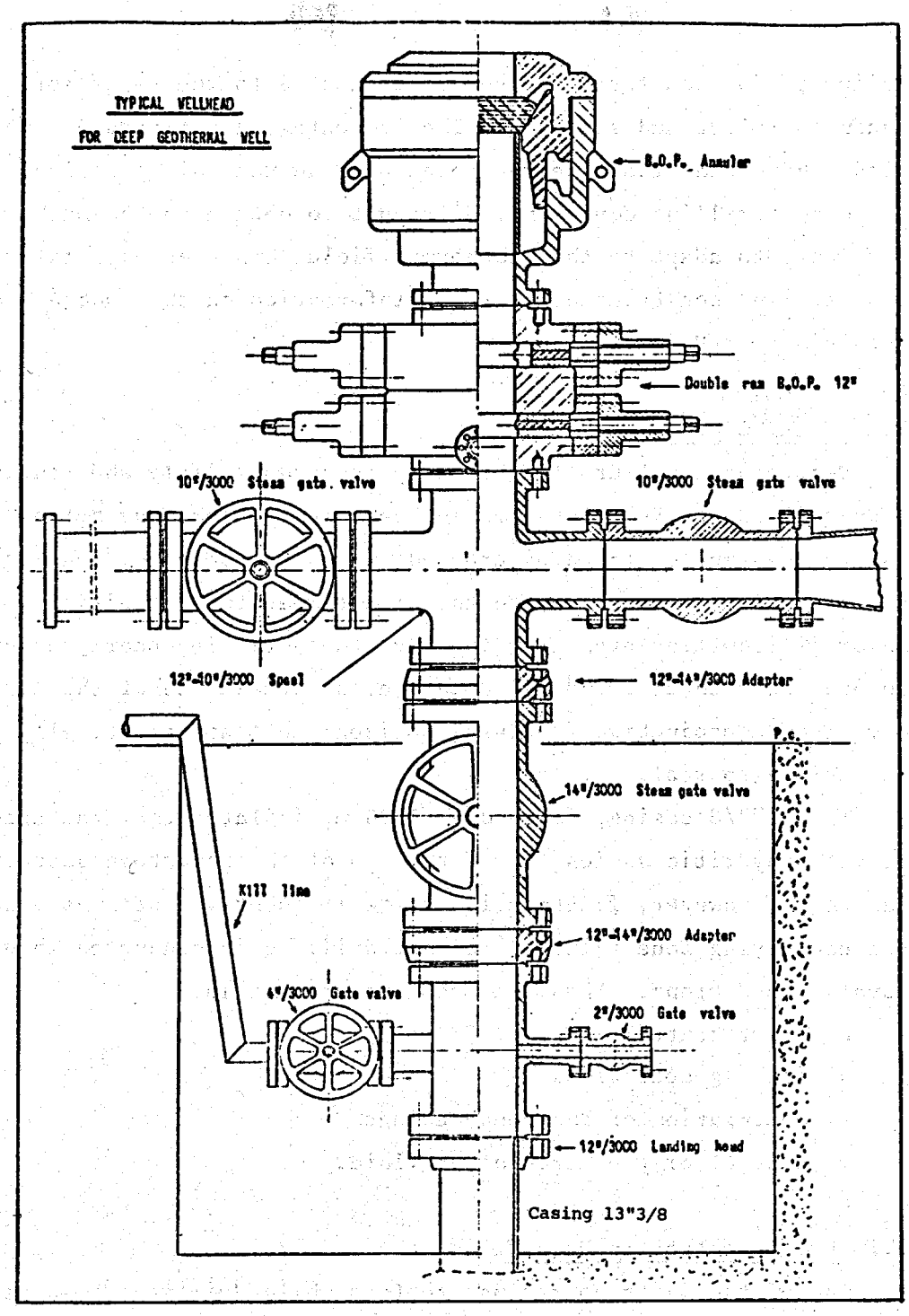

Fig. 3. Typical wellhead for deep geothermal wells.

during production tests; these are connected to the separator, measuring plant and silencer. The preventers are fitted on the well-head, which can also take the rotating-head when air-drilling.

Other drilling equipment, difficult to obtain on the market or difficult to adapt to the geothermal field, has been especially designed and constructed. Further information on this subject can be obtained from Ref. 1.

3. DRILLING PRACTICE

Deep geothermal drilling usually proceeds swiftly and routinely down to 3000 m. Beyond this point certain problems may arise, either due to the type of terrains crossed, which may be hard, unhomogeneous or of complex attitude, or to the high temperature conditions. The major difficulties stem from the fact that drilling nearly always has to proceed without return circulation, a consequence of the large number of unproductive fractured horizons that are practically impossible to seal.

The 13"3/8 casing, lowered at 1500 m, isolates the fractured zones of the anhydritic series and of the top of the schistose-quartzitic basement. However, fracturation quite frequently continues down into the underlying zone (Fig. 4) so that drilling is conducted in very adverse conditions. The main problems are met in:

- drift control
- fishing operations
- cementation of the deep casings
- control of the circulation fluid.

3.1 Drift Control in Deep Wells

One of the major operating problems while drilling these wells is controlling their drift, as they are extremely prone to deviation and the formation of terrible dog-legs.

The geological formations are responsible for this phenomenon. The terrains of the schistose-quartzitic basement vary in lithotype from schists to quartzites and gneiss. These rocks have undergone

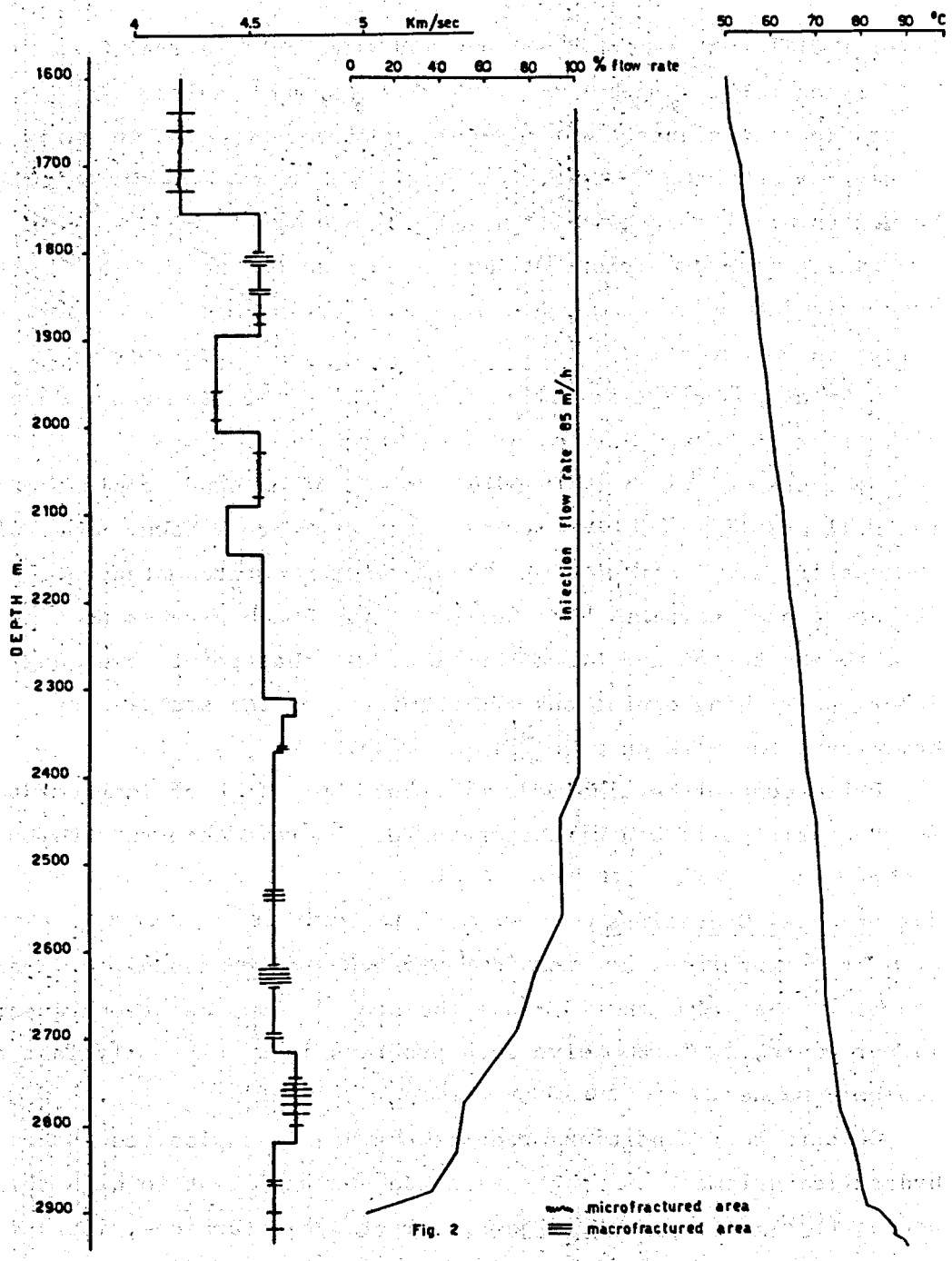

Fig. 4. Diagram 1: Sonic log of the layers forming the exploited reservoir. Diagram 2: Injectivity log of the layers forming the exploited reservoir (injected flow - rate: 85 m^3/hr). Diagram 3: Temperature log run during the injection test of diagram 2. Note the extent of the fractured zones that are so difficult to isolate.

several different tectonic events that have created fractures, filled to varying degrees with secondary minerals, and faults. The stratification planes are consequently tilted by a few to a few tens of degrees. A sample of these rocks taken from a core was shown to have a uniaxial compressive strength of 800 kg/cm^2.

Under these conditions even a small load on the rock bit in attempting to drill at a reasonable rate of 1-2 m/h has a negative effect on bore verticality.

Only a very rigid stabilization of the drill-stem can reduce the risk of drift and doglegs.

An extremely rigid drill-stem, on the other hand, could endanger the well itself should some part of the stem break down, especially when water is the circulation fluid. In these circumstances the water is such a poor carrier that the debris in the bore takes no time to fall to the bottom and block the fish. At that point some long, laborious fishing operations are required, as the stabilizers complicate the work on cleaning the fish.

Drift control is also made difficult by a lack of instrumentation for measuring tilt and direction in very extreme temperatures.

3.2 Fishing Operations

These operations are considerably hindered by the high temperatures in the wells that exclude the use of classical techniques; the latter would, in fact, solve such problems in a relatively fast and economic manner.

Certain well conditions require the use of explosives and hydraulic equipment, or parts that are not resistant to high temperatures (back-off, hydraulic jars, bumper subs, turbines, impression block, etc.). In these circumstances one must fall back on more simplified and less efficient mechanical devices or, for example, undertake time-consuming, hazardous unscrewing of the pipes within the bore, using a left-hand drill-string.

When, as sometimes happens, it is no longer economically worthwhile recovering a fish, the side-track technique is used to unblock

the well. However, the high temperature conditions may preclude the traditional system for this technique, which consists of a support cement plug and turbine with bent sub. Our alternative in this type of operation, used at a depth of 4028 m and with an in-hole temperature of about 380°C, was to design and construct a special permanent whipstock (Fig. 5), diameter 7"3/4. This was lowered into a 8"3/8 diam. open-hole, fitted with a stalk of seven 7" casings, so as to join the equipment to the underlying 3"1/2 pipes of the fish. The whipstock was blocked by pumping barite bentonitic mud of 1800 gr/l density. After the mud had set, with the help of the high temperatures, the deviation was successfully brought to completion.

Technical measures of this type are frequently resorted to when the specialized market is unable to provide the necessary equipment and material for geothermal drilling.

3.3 Cementation of Deep Casings

Cementation of the casings in deep geothermal wells is one of the most complicated drilling operations. Intense rock fracturation causes serious problems in filling the annulus, added to which are the temperatures that affect the behaviour of the slurry.

Various methods have been developed for attaining the good cementation required in deep wells only partly filled with water as a result of circulation losses.

The first step is to cement the casing from the bottom up to the fracture, injecting large quantities of partly thixotropic slurry of low density from the bottom upwards. A duplex casing shoe is used, for operating with a stinger and drill-pipe.

The second stage can be approached in various ways. The annular space from the fracture to the surface can be filled by placing a full opening multistage cementer above the fracture, isolating the latter with an external casing packer. Where there is more than one fracture this operation can be repeated, perhaps even shooting into the casing to create injection holes for the slurry; the top of the previous cementation is individuated beforehand by means of a log. The slurry

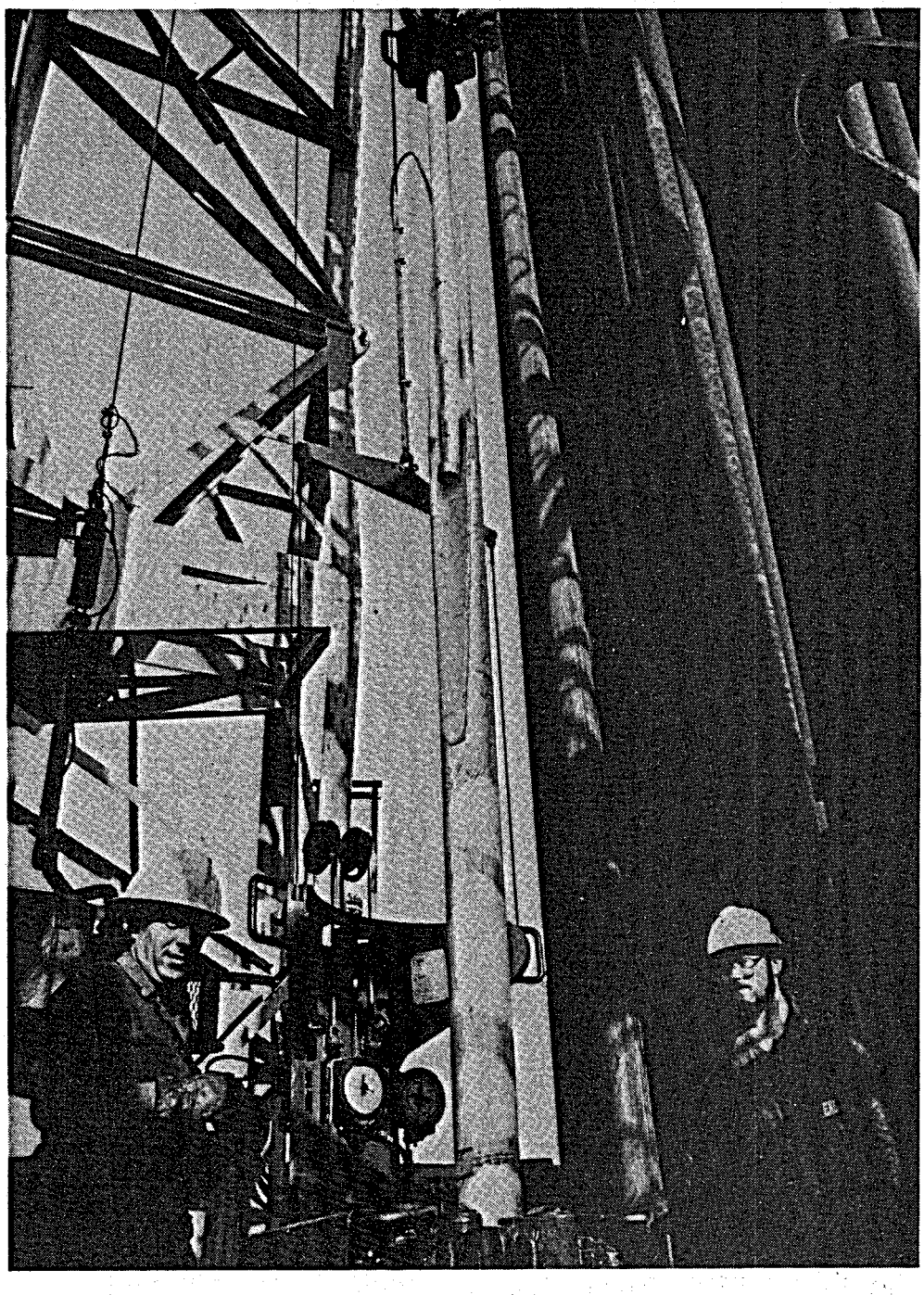

Fig. 5. Whipstock made in Larderello for side track operation in a deep geothermal well.

used for these operations must be specially prepared each time, adding silica flour, retarders, filtrate reducers and lightening materials as necessary.

In place of the external casing packer one could inject an extremely clogging mixture through the full opening multistage cement (sodium silicate in brine environment); this mixture will temporarily plug the fracture and keep the slurry within the overlying annulus.

In other situations the second step will consist of injecting down into the empty annulus, in various stages if necessary. The slurry in this case is preceded by a given thixotropic volume spacer which, due to the load loss from pumping this mixture, slows the slurry down and creates a more uniform distribution.

3.4 Control of the Circulation Fluids

As an alternative of drilling with water and no return circulation in the schistose-quartzitic formations of the basement we have sometimes conducted tests with air as circulation fluid. The advantage in this case is the avoidance of the problem of finding the immense quantities of water (up to 100 m^3/h) needed during drilling without return circulation.

However, the well must be very dry for drilling with air only. The circulation system could be assisted by a contribution of dry steam. The steam flow-rate must, at all events, be rather small, or problems will arise during extraction and insertion of the drill-stem.

We have very rarely encountered optimum conditions for air-drilling in the deep geothermal well. The intensely fractured formations cause a reduction in the rising velocity of the air, thus reducing the system's flow capacity. On other occasions a very small quantity of water or wet steam may come from the fractured formations. In such cases the debris produced by the bit is not removed fast enough and accumulates at well-bottom in a slushy phase, preventing the bit from cutting into the virgin rock. The foam agents used in such high temperature environments are not always able to solve this problem.

When a total loss of circulation occurs in routine drilling with mud or water a certain hydrostatic level stabilizes in the well. This must be removed before air-drilling is begun. When this water is being removed, however, there is sometimes a strong and continuous flow of water from the surrounding formations, so that the operation cannot be completed immediately. Drilling must then continue with the air-water circulation system, regulated to varying ratios.

The well conditions, however, are not always suited to drilling with lightened fluid, especially as regards depth, diameter, elevation of the hydrostatic level and the fracturation system. In order to use this fluid, its density must be reduced until the level reaches the surface. So much air must be injected to attain this that, instead of having one lighter fluid only, we produce two dynamically unstable phases (water and air) that may lead to a loss of the air phase along the fracturations and even to uncontrolled blow-outs. For example, we conducted a test at about 3200 m in an 8"3/8 well with a hydrostatic level at about 2300 m and flow of water. Despite the jet subs placed in critical points along the drill-stem, the circulation fluid was not homogeneous enough to make drilling a success.

Where mud drilling is possible or advisable the fluids used must have a rheological stability and filtration characteristics that guarantee optimum operating conditions in high temperature environments.

The muds that have proved successful in prolonged working conditions of up to 200°C have a bentonitic base dosed with a synthetic resin and chromolignite. The resistance can be improved, especially for higher temperatures, by adding products such as a synergesic blend of selected polymers.

Good results up to 250°C were obtained with bentonitic and asbestos-based mud, activated with chromolignite and polycrylates, with or without the polymeric products, and with synthetic resin and caustic soda.

A similar success was also attained with the sepiolite and bentonite-based muds, using a small amount of the bentonite and the same additives mentioned above, although they do tend to develop rather strong gels in static, high temperature conditions.

Finally, oil or a colloidal suspension of sized asphaltic solids in water or in diesel-oil can further improve stability, even in higher temperatures than those described above.

The efficiency of the above mud systems can, of course, be improved by attending to a few practical matters, such as replacing any water lost by evaporation, cooling the fluid in special towers, stirring the fluids continually in tanks fitted with electric agitators and guns.

4. CONCLUSIONS

The deep exploration program for the Larderello area is now in its first stage of development. The activity carried out so far has presented us with new problems in terms of operating methods and equipment.

It became immediately clear that the first priority was to devise an adequate technology for deep drilling, with the result that this is now one of the objectives of the deep drilling program itself. The solution to the problems outlined above lies in the construction of equipment and instruments designed specifically for the geothermal field.

Particular attention is paid in this respect to perfecting the methods and materials for controlling drift, for a more extensive use of air as a circulation fluid and for alleviating any eventual fishing operations.

The casings and drill-pipes of the geothermal wells are subjected to extreme mechanical stress and corrosion. The studies and research being undertaken in this sector should contribute greatly to the success of the deep exploration.

It is clear from what we have just said that the work times and costs involved in this first phase cannot be held representative. However, there is no doubt that this type of research is a heavy financial commitment. At the moment the unit cost ratio between traditional geothermal wells and the deep bores in the Larderello area is 1:1.4.

Nevertheless, the objective remains that of optimizing the technical aspects of drilling and minimizing as much as possible the difference between these two factors.

REFERENCES

1. P. Del Gaudio - "Materials employed in deep geothermal drilling in Italy," 2nd ENEL-DOE Workshop, October 20-22, 1980. Lawrence Berkeley Laboratory, Berkeley, CA (1980).

2. U. Cigni, F. Fabbri, and A. Giovannoni - "Advancement in cementation technique in the Italian geothermal wells," 2nd Geothermal Symposium, United Nations, San Francisco, CA (1975).

3. F. Fabbri and R. Ricciardulli - "Relazione finale delle operazioni di cementazione sondaggio Sasso 22, Piancastagnaio 26." Internal Report ENEL, UNG, Perforazioni (1979).

4. U. Cigni - "Machinery and Equipment for harnessing of endogenous fluid," U.N. Symposium on the Development and Utilization of Geothermal Resources, Pisa Italy (1970).

MATERIALS EMPLOYED IN DEEP GEOTHERMAL DRILLING IN ITALY

P. Del Gaudio

1. DEEP GEOTHERMAL DRILLING IN ITALY

ENEL is now carrying out a systematic study in the Larderello area, directed at ascertaining whether geothermal fluids can be recovered from the layers underlying the 'reservoir' exploited at present.

The research program also includes the drilling of deep wells ranging from a minimum of 3000 m to a maximum of 5000 m. Some of these wells have already been completed. The technical profile of these wells is generally that shown in Fig. 1.

Drilling is a complicated operation (Fig. 2) because:

- the layers forming the present reservoir, which lies between 1000 and 3000 m, are not easy to isolate;
- the zones below 3000 m are characterized by very high temperatures and chemical aggressiveness.

Further information on deep geothermal drilling in Italy and on the problems involved can be found in Cigni (1980).

Considering the operative problems encountered so far, the perfecting of an ideal 'deep geothermal drilling technology' could, in itself, be said to represent one of the objectives of deep exploration at Larderello.

The technological research now consists of a market survey to procure drilling equipment suited for use in the operative conditions peculiar to deep geothermal wells. As the standard equipment used in oil research cannot always be used directly, a study must sometimes be made of the modifications required and adequate operative methodologies developed for using this equipment. Certain operations carried out in deep geothermal wells, on the other hand, require specially designed equipment.

This paper will outline the main equipment and methodologies now used in drilling deep geothermal wells. Attention is paid in

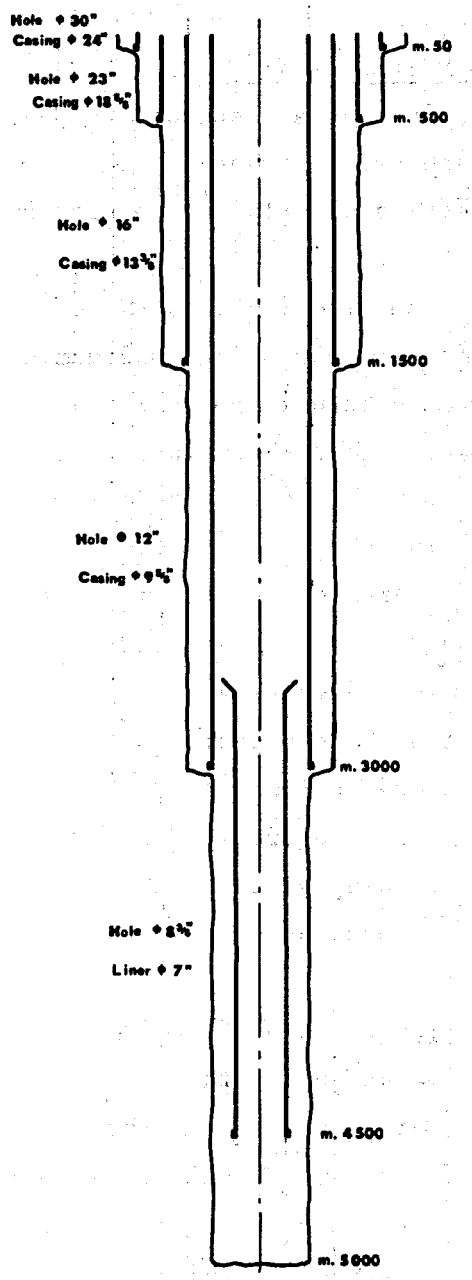

Fig. 1. Typical technical profile of the Larderello deep wells. These are used at Larderello to explore the layers between 3000 and 5000 m.

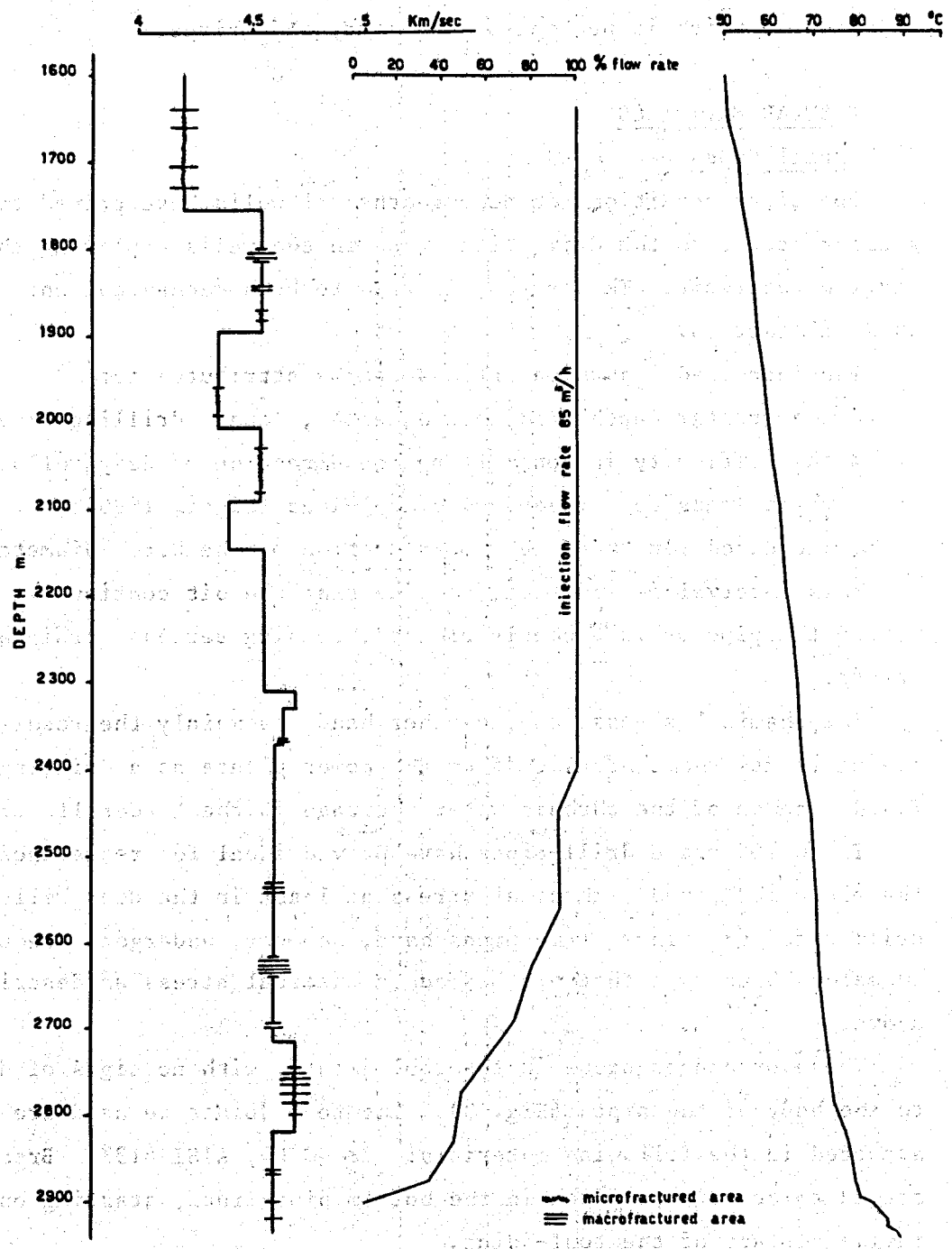

Fig. 2. Diagram 1: Sonic log of the layers forming the exploited reservoir. Diagram 2: Injectivity log of the layers forming the exploited reservoir (injected flow-rate: 85 m^3/hr). Diagram 3: Temperature log run during the injection test of diagram 2. Note the extent of the fractured zones that are so difficult to isolate.

particular to the problems arising during the drilling operations, a solution to which is now one of our study objectives.

2. TUBULAR MATERIALS

2.1 Drill Pipes

Operative conditions in deep geothermal wells have proved to cause greater stress to the drill-pipes than in the wells exploring the shallow reservoir. This stress is tied to both mechanical and chemical factors.

The increased mechanical stress can be attributed to:

- the greater depths and, consequently, longer drilling times;
- the difficulty in controlling the direction of deep wells, which leads to a frequency of dog-legs (Cigni, 1980);
- increased length of the upper section of the bore, diameter 16".

This interval is, in fact, so wide that the bit continually jumps within the pipe or is suddenly blocked, causing serious torsional stress.

The chemical stress, on the other hand, is mainly the result of having to use the condensate from the power plants as a drilling fluid because of the chronic water shortage in the Larderello area.

The G 105 grade drill-pipes have proved ideal for resistance to the above-mentioned mechanical stress at least in the deep wells drilled so far. These same pipes have, however, undergone frequent anomalous breakages that are blamed on chemical stress as described above.

These breakages occur in the tool-joints, with no signs of damage to the body of the pipes (Fig. 3). The tool joints we used are constructed in the following materials: 38 NC D4, AISI 4137. Breakage seemed to occur more often in the bottom pipe-lines, starting on the inside surface of the tool-joint.

These phenomena were so serious it was decided to run a series of tests simulating well conditions to define the phenomenology of the attack and attempt a solution to the problem. The preliminary results confirm that the chemical attack is further aggravated by the existing

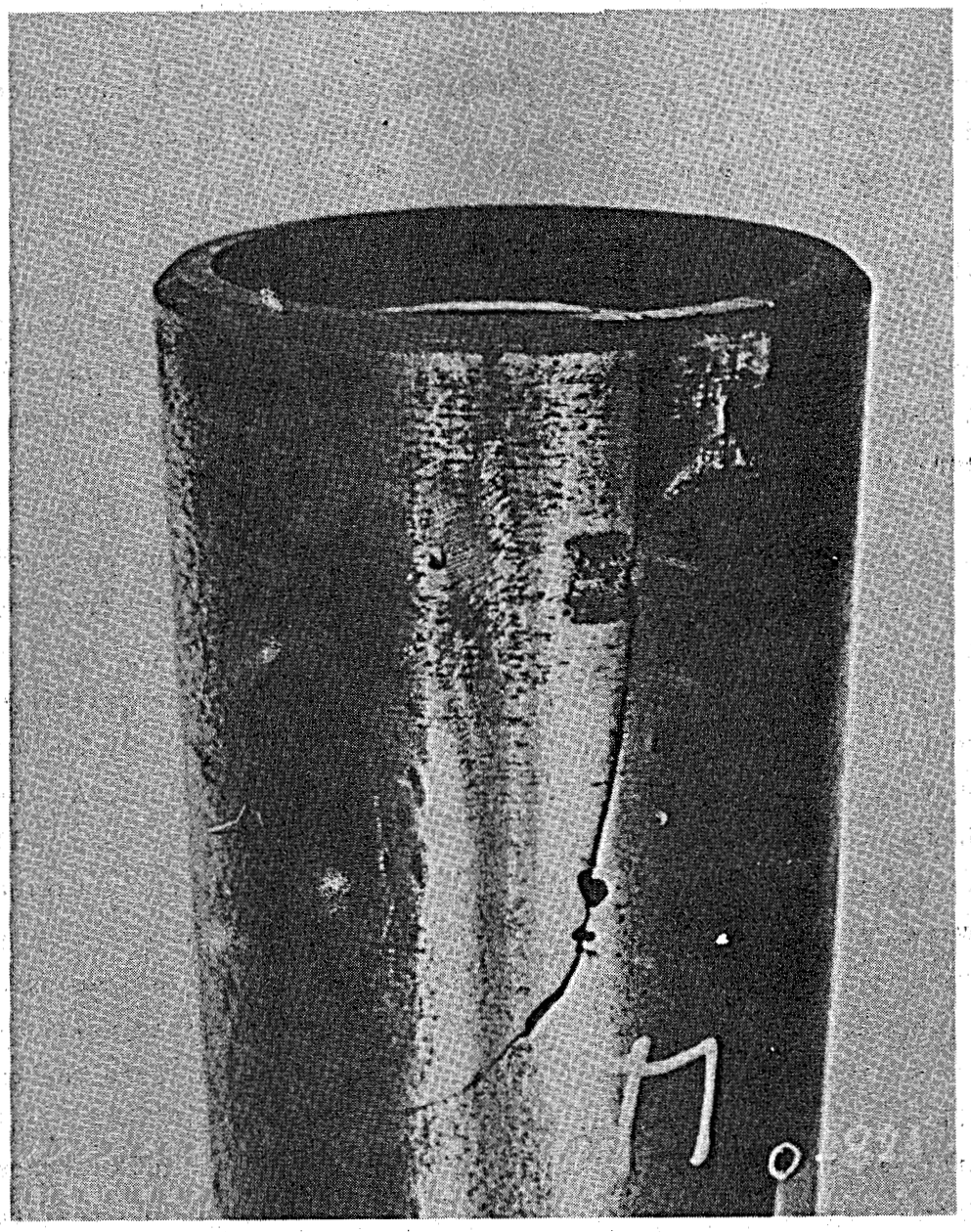

Fig. 3. Breakage of a tool-joint.

temperatures. An attempt is now being made to solve the problem either by using other materials for the pipes or by dosing the drilling fluid.

2.2 Casing

The criteria followed in designing the deep geothermal wells at Larderello were that the diameters used to explore the deep reservoir should be wide enough to attain satisfactory productivity values despite the greater depth of borehold required.

The various casings were lowered not only to strengthen the bore walls but also to isolate the formations of the shallow reservoir. Cementation of the column was therefore an arduous operation and not always an absolute success (details will be given later).

This outcome had been foreseen when drawing up the drilling program, and it was felt that the best results would only be achieved by adopting ideal criteria for the design of the casing. At the same time we were aware that the higher temperatures of the deep wells and their relatively longer drilling times would create quite serious thermal stress to the casing.

Consequently, great care was taken in designing the casing to avoid breakages that would compromise completion of the well.

The results of the first drillings appear to validate the criteria chosen. These criteria include the use of API drill-pipes with buttress joints. The thickness and grade of the steel were chosen after detailed analysis of the thermal stress and of the resistance of the materials.

Casing design was based on the results of lab tests to determine the tensile strength of J55, C75, N80 and P110 steels, cited in the American Petroleum Institute standards, at temperatures of 200°C, 250°C, 300°C and 350°C.

These results (Fig. 4 shows those for the N80 steel) were used to introduce a 'reduction factor of the tensile properties' in the project design of the casing. This factor was used empirically to evaluate, as a function of the maximum foreseeable temperature, the

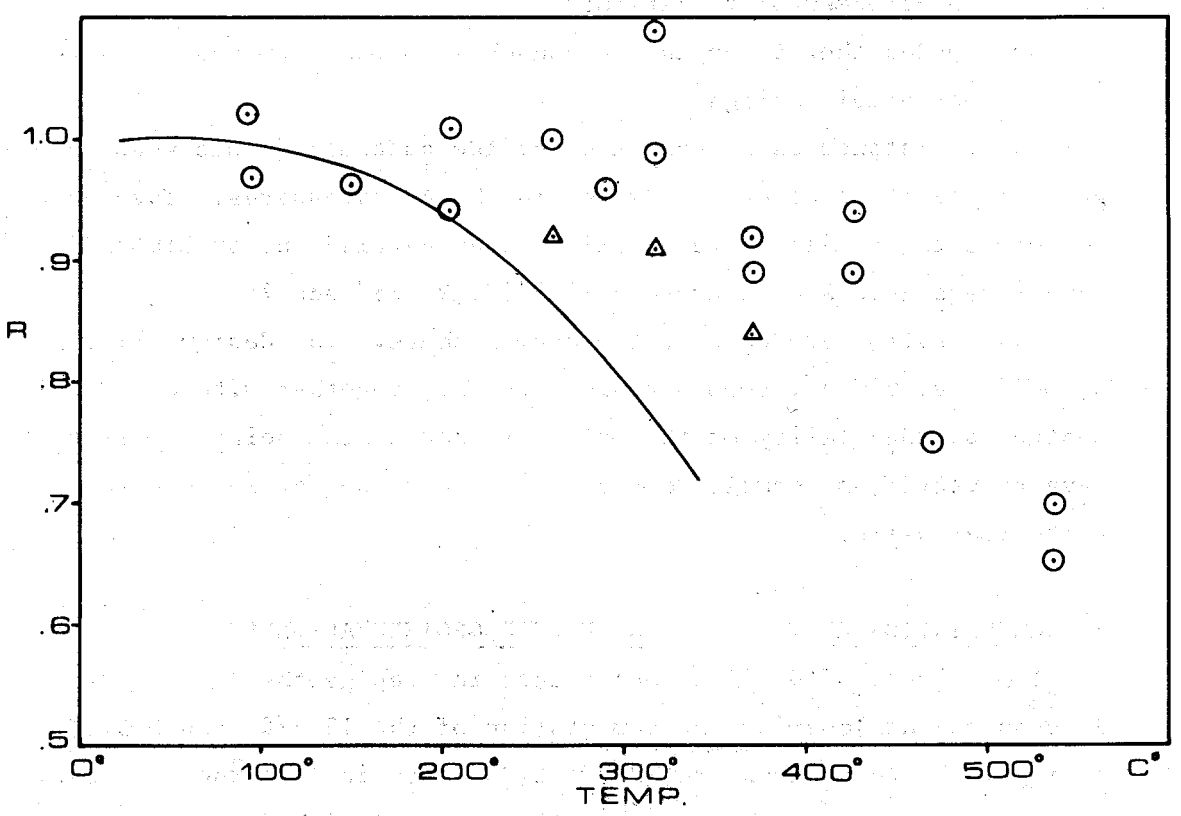

Fig. 4. Values of the R ratio between the yield point of the N80 steel at high temperature and the recorded value at environmental temperature.

collapsing and crushing strength of the casing, beginning with the API data for environmental temperatures.

An impeded thermal expansion causes anomalous compressive stress to the geothermal casings.

The resistance characteristics of the buttress joints when undergoing these stresses are not given in the API standards. They were therefore the subject of a specific study carried out by ENEL (Fig. 5) on buttress joints of diameters 13 3/8", 9 5/8" and 7".

The results were used in the design phase. The design criteria, as mentioned before, seem satisfactory and, together with a careful control of the quality of the materials and of the joint - make up, have prevented any damage to the casings used so far in the deep geothermal wells.

3. CEMENTATION OF THE CASINGS IN DEEP GEOTHERMAL WELLS

The success of drilling operations in deep geothermal wells depends on the lowering and cementation of the 13 3/8" and 9 5/8" casings. These casings are, in fact, used to isolate the layers of the shallow reservoir and are usually cemented with no return circulation.

Cementation is consequently a laborious task carried out in several phases, using the inner string cementing method, or F.O. multiple stage cementer, or pumping slurry down into the upper annulus. The problems arising during this operation and the reasons that led to the choice of methodology are described in Cigni (1980).

A description will now be given of the composition of the various slurries (Cigni 1975).

3.1 Slurries Used for Primary Cementation by the Inner String Cementing Method

These slurries are used to cement the final section of the casing, using the drill-pipes and a stab-in float collar.

The slurry consists of a class G cement with 35% silica flour. Density is about 1.850 kg/l. One percent of filtrate reducer is

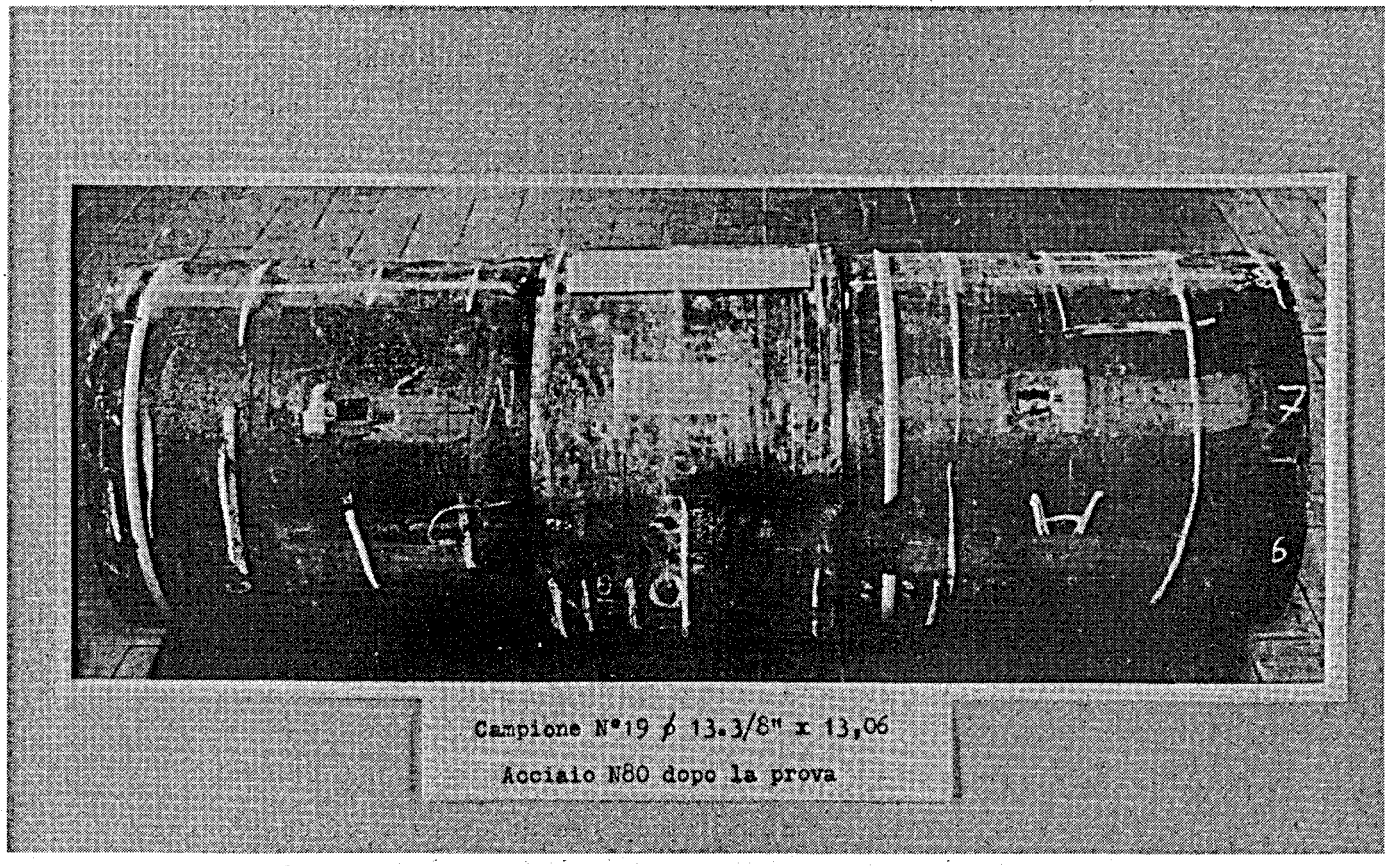

Fig. 5. Buttress joint of diameter 13 3/8" x .72 N80 steel, subjected to axial compression.

added to achieve a low filtration. As water sometimes has to be used as a drilling fluid, the reducer is added to prevent dehydration of the slurry because of the lack of an adequate mud cake.

The casings are at such great depths (3000-4000 m), and the temperatures so high, that the pumping times have to be guaranteed by a retarder, which is added in the ratio of 0.5% in weight of the cement.

The composition of the slurry is studied in the laboratory by means of simulation tests, not scheduled in API standards, reproducing the setting conditions of the slurry in the bore. This applies to both the setting pressure and the increase in temperature with time.

On the site the slurry is prepared in tanks beforehand to ensure the mixture is homogeneous. A cooling circulation at well-bottom during setting of the slurry prevents excessive retrogradation of the mechanical properties which occur when slurry sets in high temperature environment (Fig. 6).

3.2 Slurries Used in Secondary Cementation

These slurries are used to cement the upper part of the casing, circulating them through an F.O. multiple stage cementer inserted in the drill-pipe (Fabbri and Ricciardulli, 1979). A class G cement with 35% silica flour is generally used in this case.

Where circumstances so require the density can be reduced to about 1.650 kg/l by adding diatomite. However, the latter can lead to marked retrogradation, as well as sedimentation and contraction. The setting times are also much longer, so that chemical extenders, such as the D79 by Dowell, are generally preferred to the diatomite. Slurry prepared in this way does not create the problems mentioned above and results are equally satisfactory.

3.3 Slurries Used in Cementation with Pumping from Above

These slurries are used to fill the annulus by injecting the cement from ground-level. Before pumping the cement a special viscous solution is injected, either SPACER 1000 or equivalent. This product

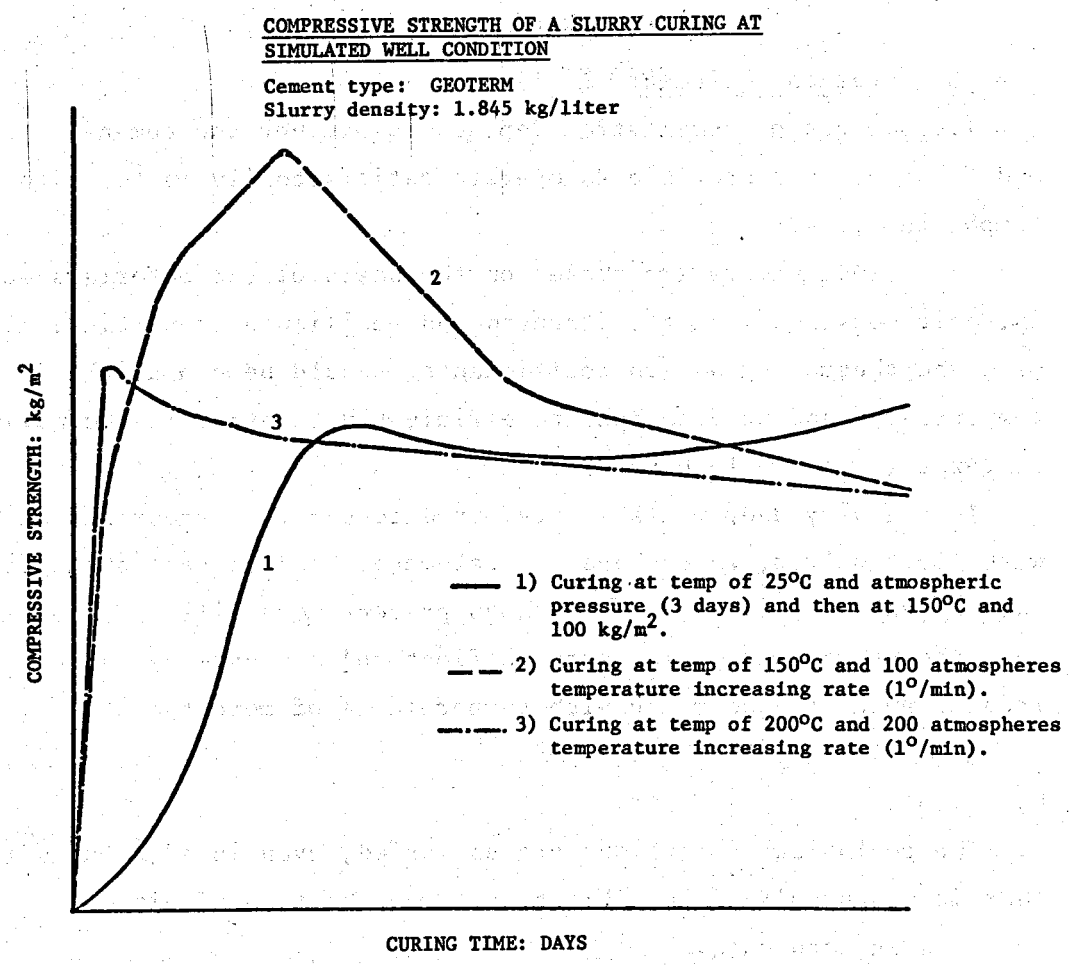

Fig. 6. Trends with time of the mechanical strength of the slurry as a function of setting conditions.

provides a slower and more uniform distribution of the cement into the annulus. Several cement units are used at one time to ensure high flow-rates and a continual flow.

3.4 Cementation Equipment

The success of cementation depends on whether the cementing shoes and float collars are able to operate satisfactorily in the high temperature environments.

These instruments are chosen on the basis of the materials used in their construction; the strength and resilience properties, along with the thermal expansion coefficients, should be compatible in high temperatures and able to operate efficiently together in the maximum temperatures of well-bottom.

In the very deep wells we preferred to use the cementing shoes with float valves, which have a metal-metal contact seal and cast-iron back-up valve. However, these shoes present more milling problems than the other types. The stab-in float collars gave excellent results even at 3000 m and with temperatures of more than 200°C.

4. BITS

The geological conditions are so varied, even in adjacent wells, that it was usually impossible to program the type of bit most suitable in each case.

The data obtained on site so far are greatly influenced by the working conditions of the bits (with or without return circulation, drilling capacity of the formations, temperatures). It is thus difficult to establish fixed criteria for the choice of bits. Some encouraging results were obtained from the use of diamond bits in intervals with high temperatures and no return circulation.

5. LOGGING INSTRUMENTS

One of the problems in deep geothermal drilling (Cigni, 1980) is that of obtaining ready-made equipment for directional drilling in high temperature conditions. Suitable turbines and instruments for

continuous monitoring of direction and inclination are particularly difficult to find in the specialized market.

ENEL has now decided to solve the problem by designing and constructing its own instrumentation for measuring inclination and direction in the presence of temperatures of 250°C and pressures of 500 bar. These studies will be based on past experience in constructing similar instrumentation for measuring temperature and bore diameter.

REFERENCES

1. U. Cigni - "Italian Experience and Problems in Deep Drilling (< 3000 m)." 2nd ENEL-DOE Workshop, October 20-22, 1980. Lawrence Berkeley Laboratory, Berkeley, CA (1980).

2. ENEL-Unita Nazionale Geotermica - Esami su giunti ed aste di perforazione. Internal Report, ENEL-D CO, Laboratorio Centrale, Piacenza (1980).

3. U. Cigni, F. Fabbri and A. Giovannoni - "Advancement in cementation technique in the Italian geothermal well," 2nd Geothermal Symposium, United Nations, San Francisco, CA (1975).

4. F. Fabbri and R. Ricciardulli - Relazione finale delle operazioni di cementazione sondaggi Sasso 22 - Piancastagnaio 26. Internal Report, ENEL-UNG-Perforazioni (1979).

GEOTHERMAL DRILLING PRACTICES OF "THE GEYSERS"

Louis E. Capuano, Jr.

Introduction

Geothermal energy has quickly become recognized both domestically and internationallly as a supplement to fossil fuels and nuclear power for the purpose of electric power generation. There are four basic types of geothermal development in the United States today and they are: dry steam, liquid dominated or hot water, dry hot rock and geopressured fluids. This paper will concern itself specifically with the drilling and completion of dry steam wells.

Only a few geothermal systems, including the important Larderello Field of Italy (which has produced since 1913) and The Geysers of California, contain dry or superheated steam produced with no associated liquids. The largest dry steam production in the world is located in The Geysers area of Northern California, some 80 miles north of San Francisco. Drilling for geothermal energy began in The Geysers in the early 1920's with the first turbine (12,500 kilowatts) installed in 1960. Pacific Gas and Electric started commercial electrical generation with geothermal energy by purchasing steam from producers and generating it with their own condensing turbines. Presently Pacific Gas and Electric is generating approximately 900 megawatts from steam supplied by Union Oil of California, Magma Power Company, Aminoil U.S.A. and Thermogenics, Inc. Another 400 megawatts will come on line within the next 3 years with steam supplied by Aminoil U.S.A., Inc., Union Oil of California, Shell Oil Co. and McCullough Oil Corp.

It requires approximately 20#/hr. of steam to generate 1 kilowatt of electricity. Electricity is currently produced from geothermal energy at a cost of 25 to 30% less than that of coal, oil or nuclear. The steam produced in The Geysers normally occurs at approximately 450°F and a pore pressure of 480 psi. The producing interval ranges in depth from 4000' to 9000'.

Geology

A brief description of The Geysers geology is necessary to better understand the steam system. The geology of The Geysers is extremely complex with many periods of faulting, superimposed by recent vulcanism. This complexity makes it almost impossible to correlate from one well to another.

At The Geysers, steam is found in fracture systems located in graywacke and metagraywacke of the Cretaceous age. The graywacke is a tight

metamorphosed sandstone with hardness and densities varying over a wide range. Argillite is interbedded with the graywacke in thicknesses from a few inches to several tens of feet. This unit contains water at depths less than 4000' and will cause difficulty if encountered while drilling with air.

Other rocks drilled in the area include volcanics, serpentinite, periodite and a melange of chert, greenstone, and blueschist. The serpentinite can be a problem when it is encountered in thicknesses larger than 2000' because it behaves plastically and will slough into the hole. Therefore, to obtain the best results the serpentinite must be drilled with mud.

Predrilling Planning

After a location has been selected and approved by county, state, or federal agencies, construction begins on the drill pad, access road and drilling fluid sump. The drill site is a flat rectangular shaped area usually 300' by 500' with a sump of a capacity of 1.0 to 1.3 million gallons. Sites for pads and sumps are carefully selected to avoid landslide areas. Stability studies are performed on each location, prior to its approval by the governmental agencies involved. Due to rugged terrain the construction costs contribute approximately 15 to 25% of the total well cost. The total cost of construction and drilling of a typical geothermal well is running between $850,000 to $1,600,000 depending upon the location and depth of the well.

Many wells in The Geysers area are directionally drilled. This is done for two reasons. First, drill sites are difficult to locate because of the steep topography and the high incidence of a landslide prone area. Second, many geologists now believe that a majority of the steam bearing fractures are vertical or nearly vertical. Drilling within steam producing areas may result in little or no steam production, therefore, the well must be kicked up to three times to insure the highest probability of intersecting these fractures.

Drilling

Drill rigs used in The Geysers Field must be able to withstand rough drilling and have the capability of drilling a dry hole from 10,000 to 12,000'. The typical rig has a rated horsepower of between 800 to 1000 and has a minimum derreck capacity of 500,000# and must be equipped with two large horsepower mud pumps.

The first problem encountered in drilling for dry steam in The Geysers is the formation. The producing zone, as previously mentioned, is the tight graywacke sandstone of the Franciscan formation. The porosity in the graywacke ranges from 1 to 3% and is fracture porosity rather than interstitial. In drilling, these fractures cause some of the largest problems. The steam in these fractures is at a maximum reservoir pressure of 500 psi and ones that do not contain steam may

be connected to a vast system of fractured voids. Therefore, drilling in the graywacke with mud is very slow and prone to zones of lost circulation. Since the steam reservoir pressure is quite low, drilling through a steam bearing fracture with mud may go completely unnoticed.

The casing, cementing and blow-out-preventer programs presently being used by Thermogenics in both our development and exploratory wells is as follows: (See Figure 1)

1) Prior to the large rotary drilling rig moving onto location, a 30" hole is drilled to 50-80' with a small rat hole digger and 26" O.D. conductor casing is cemented to total depth.

2) After the large rotary drilling rig is in place over the conductor pipe, a 26" hole is spudded with a simple gel and water mud system. In some cases the 26" hole drills so slow that it may be reduced to 17 1/2" for better penetration rates, and drilled to a total depth of approximately 300', and later opened to 26". 20" casing is then cemented from surface to total depth. This 20" string of casing can be eliminated if the well is drilled in a known field in which no ground waters have been encountered. The 20" is cemented using a Class G cement mixed with 3% $CaCl_2$. A single gate blow-out-preventer is installed on top of the 20" casing.

3) Through the 20" casing a 17 1/2" hole is drilled with mud to a total depth between 2000 and 2800'. It is very important at this point to set the next casing string, which normally is 13 3/8", in a consolidated, non-water bearing formation; hopefully a graywacke. The reasoning behind this is, after the 13 3/8" casing is set and a 12 1/4" hole is to be drilled it is entirely possible to drill with air. The 17 1/2" hole should be drilled straight to reduce any wear in the casing strings during steam production. The 17 1/2" hole is very prone to lost circulation and some argillite swelling which can slough and stick pipe. The most important point in completing a geothermal steam well is to get a good primary cement job on all casing strings. To leave a water filled void between casing strings and cement could be a source of corrosion which could ultimately result in collapsed and/or burst casing. The 13 3/8" casing is cemented with Class G cement and perlite blended on a ratio of one to one, to reduce the hydrostatic pressure of the cement column. It is also blended with 40% silica flour to aid this lightened cement column in compressive strength.

4) After the 13 3/8" casing is set and cemented, the blow-out-preventers are installed and tested. The blow-out-preventer stack from the casing upward is as follows: (See Figure 2)

   a) A wellhead with two 3" flanged outlets is welded internally and externally to the casing then tested to 2000 psi.

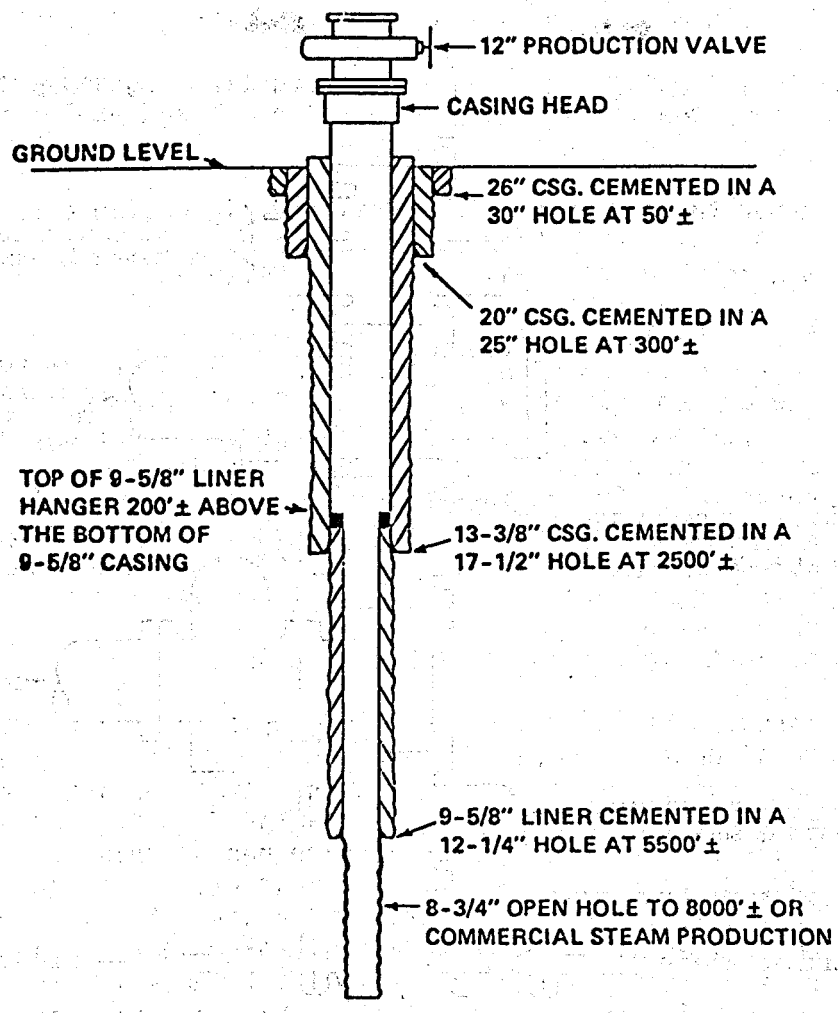

Fig. 1. Typical completion profile.

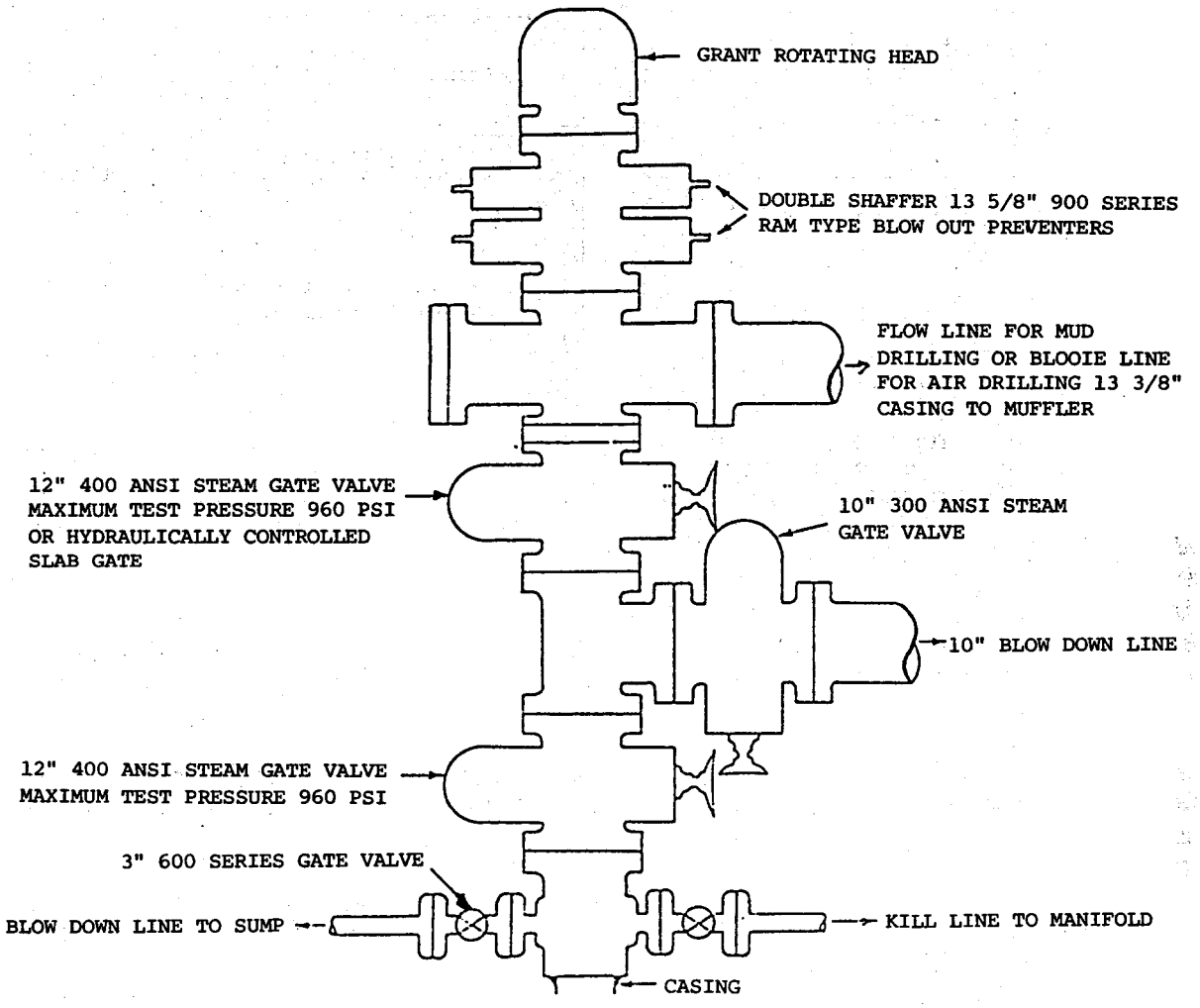

Fig. 2. Blow-out-preventer stack.

b) A 12" slab gate valve with a working pressure of 960 psi at 500°F is bolted to the wellhead. This is the master production valve which is closed upon completion of the well and produced through.

c) A 12" 400 ANSI by a 12" ANSI spool with a 10" 400 ANSI bypass is then installed. This bypass is used to allow the well to bleed while bits are changed.

d) Above the spool is installed another slab gate valve which can be either manually or hydraulically controlled.

e) A Banjo Box, which is nothing more than a flow line for both mud and air drilling, is installed next.

f) Above the Banjo Box is a double hydraulic ram type blow-out-preventer, one with pipe rams and one with blind rams.

g) A Grant Oil Tool rotating head tops the stack.

5) After the blow-out-preventers are tested, a 12 1/4" hole is drilled to approximately 4500 to 6000'. This string should be anchored firmly in the graywacke formation. This hole can also be drilled directionally, all directional work being done with mud and locked in to maintain desired angle and direction. Once the direction and angle is obtained, and the formations do not produce water or slough, the hole can be blown dry. On the average it requires approximately 3500 to 4200 SCFM of air to drill the 12 1/4" hole depending on the particle size being removed and the presence of fluid. Penetration rates with air are as much as five times faster than with mud and you have the opportunity to test each fracture as it is drilled.

6) Once the 12 1/4" hole is drilled to the desired depth the hole is filled with water and a 9 5/8" liner is hung from 200' in the 13 3/8" to total depth. This casing is cemented with a cement very similar to the cement used on the 13 3/8" casing with the addition of a retarder to withstand the higher temperatures encountered.

7) Through the 9 5/8" casing an 8 3/4" hole is drilled to commercial production or total depth. The 8 3/4" hole requires between 2600 and 3600 SCFM of air to adequately clean the hole.

Completion

In The Geysers area, the wells are drilled to a depth where steam production appears commercial. The well is then tested for approximate flow rate by installing an orifice plate in the blooie or flow line and measuring pressure upstream and downstream of the orifice while the well is allowed to blow through the muffler. These measured pressures

indicate a flow capacity. If at this point, the capacity is sufficient the well is completed, if not, it is drilled deeper in anticipation of increased production capacities.

When the flow capacity reaches a point where it is too high to continue drilling, the drill pipe and drilling assembly are pulled out of the hole. The bottom production valve is then closed and a 1/2" bleed line is installed at the casing head. The drilling rig is removed from the well site. The well will be retested to determine a more precise flow rate and allowed to bleed while awaiting production facilities.

Upon completion, it may be desireable to run an additional string of 10 3/4" tie-back casing from the top of the 9 5/8" liner back to surface. (See Figure 3) This can be done by killing the well with water and setting a drillable mechanical packer at the shoe of the 9 5/8" casing and filling the hole with water. After the 10 3/4" casing is set, the cement and plug are drilled out to return the well to production.

If the well is converted to injection, a string of 7" casing is run to the top of the steam zones and cemented back to surface. All cement plugs are then drilled out of the 8 3/4" and a 5" slotted liner hung across the steam zone. The best injectors are marginal producers as the water can be forced back into the production zone. Of all the steam utilized at the power plant, approximately 80% is evaporated at the cooling tower and 20% condensed and returned to the operator for reinjection.

ACKNOWLEDGMENTS

Cromling, J., Geothermal Drilling Technology of California, SPE of AIME, California Regional Meeting, Bakersfield, CA. 1972.

Dorfman, Myron H., "Drilling in The Geysers Field," The Drilling Contractor, November-December. 1973.

Otte, Carel & Kruger, Paul, Geothermal Energy "Resources, Production, Stimulation." Stanford University Press, 1978. Stanford, CA.

Wahl, Edward F., Geothermal Energy Utilization (A Wiley - Interscience publication) by John Wiley & Sons, Inc. 1977, Canada.

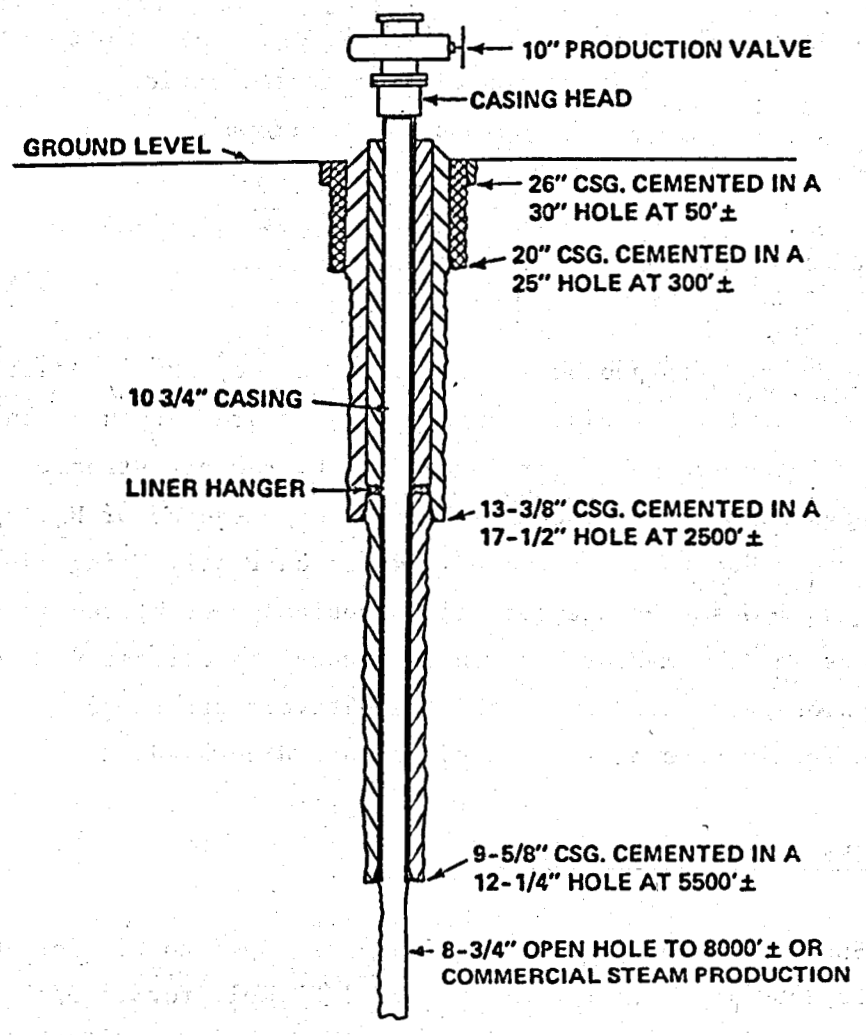

Fig. 3. Typical completion profile with 10 3/4" tie-back.

MATERIALS USED IN DRILLING GEOTHERMAL WELLS IN THE GEYSERS

Larry Leet
Magcobar
Division of Dresser Industries
Healdsburg, California

ABSTRACT

Drilling deep geothermal wells in the Geysers is usually done with air as a drilling fluid. Corrosion rates are very high unless the proper corrosion inhibitors are added to the air stream. Because of the high temperature encountered and the presence of H_2, special inhibitors had to be developed and are currently being used. This paper will describe the corrosion problems encountered in drilling the Geysers and the measures taken to reduce the corrosion rates. Corrosion rates with and without inhibitors are compared and the cost and effectiveness of the inhibitors are discussed.

GEYSERS DRILLING MUD PROGRAM

Spud mud to 500'±	17 1/2" Open to 26" for 20" casing
to 2500'±	17 1/2" hole for 13 3/8" casing
to 5000'±	12 1/4" hole for 9 5/8" liner

Lightly treated lignite/bentonite drilling fluid: bentonite; lignite; caustic. Loss circulation zones treated with cottonseed hulls and/or cement as required. Corrosion problems can be severe, so film forming amines and oxygen scavengers are used to minimize drill pipe losses. Described as follows:

Inhibitor 202 is a formulated, persistent film type, water and oil dispersible corrosion inhibitor designed to protect the drill

string during drilling operations. It functions effectively in air stiff foam, mud misting, aerated mud or conventional mud drilling fluids. It may be painted or sprayed on the drill pipe or it may be used as a slug treatment. 55 gallon drum, density of 7.7 lb/gal.

OS-1 liquid is a liquid oxygen scavenger of the ammonium bisulfite type. It is used by diluting one part in ten parts water. The diluted solution is added at the pump suction at 1-1/2" to 2-1/2 gallons per hour. 55 gallon drum-density 11.16 lb/gal.

SI 1000 is an organic phosphate type scale inhibitor for tubular goods. It may be added to fresh water or brine systems to prevent deposition of alkaline earth metal scale. 55 gallon drum-density of 9.37 lb/gal.

STUDY ON THE EQUILIBRIA AND PROPERTIES OF BRINES

G.Conti[+], P.Gianni[+], G.F.Nencetti[†], L.Petarca[†], M.R.Tinè[+], N.Vatistas[†]

[+] Institute of Physical Chemistry, University of Pisa, Italy

[†] Institute of Industrial and Applied Chemistry, University of Pisa, Italy

Brines at high temperatures and with a high salt content can, in principle, be exploited for many purposes including the production of electric energy, the supply of district heating and the recovery of those chemical compounds which are of commercial interest.

Obviously, in order to examine the different exploitation possibilities of such brines to determine the best alternatives and consequently the most suitable technological cycles for the complete utilization of the resource, it is essential that sufficient information on the characteristics of the salt composition of the system and, in particular, on the equilibria in solution is available. This information must refer to all the thermodynamic properties, e.g. heat capacity, latent heat, vapour pressure, etc.

The problem of obtaining such information arises whenever a new geothermal resource is discovered as one manifestation can vary considerably from another. This is shown by the data given in Table I which refer to some Italian geothermal areas.

The complexity of the systems involved means that it is unrealistic to attempt a theoretical approach to this problem. It was, therefore, decided to initiate an experimental research program in order to obtain data which could be compared with the data already published and could be used to determine the

values which are still lacking in the literature.

Although the development of theoretical prediction methods had been excluded a priori, the reliability of certain semi-empirical relations for the extrapolation of the available da

TABLE I

Chemical Composition of Brines from some Italian geothermal fields.

	Cesano 5 (1)	Cesano RC1 (2)	Latera 2 (3)	Latera 2 (4)	Piancastagnaio 20 (5)	Cesano 1 (6)
Total Salinity (mg/l)	101,000	167,376	8,595	7,563	15,242	350,000
Ca^{++} "	9.5	60.36	10.8	289	-	110
Mg^{++} "	6.0	10.69	3.2	10.45	-	15
Na^{+} "	22,000	52,142	2,450	1950.0	1,400	57,000
K^{+} "	15,800	33,833	351	286.0	282	77,000
Li^{+} "	80	-	10	9.3	-	180
Cs^{+} "	62	-	3	-	-	50
Rb^{++} "	116	-	2.5	0.74	-	350
$Fe^{++}+Fe^{+++}$ "	7.2	-	-	3.0	-	0.7
NH_4^{+} "	206	31.17	24.8	67.84	136.4	100
Al^{+++} "	-	-	-	-	-	-
As^{+++} "	440	-	147	77.0	60	5.0
Cl^{-} "	26,530	17,313	2,815	2,292	2,325	27,000
SO_4^{--} "	24,450	76,638	415	347	-	180,000
NH_3 (total) "	-	29.41	23.4	64	129	-
CO_2 (total) "	3,365	2,520	849	1,418	44	1500
H_2S (total) "	194	-	40	12	12	trace
CO_2 (gas) "	-	-	370	390	44	-
Boron as H_3BO_3 "	11,265	7,892	1,600	1,271	13,958	7,000
SiO_2 "	133	140	440	247	1,350	130
pH	7.95	8.35	7.94	7.2	7.1	7.5

(1) Sample taken 14-15 May 1979.
(2) Sample extracted with airlift, 12/8/77.
(3) Mean values of five samples taken during delivery.
(4) Water taken using sampler (total fluid), 12/6/80.
(5) Analyses of samples of entrained water, 12/10/80.
(6) Mean values for analyses of water delivered.

ta was analysed with reference to at least some of the properties to be recognized. The priority of the properties to be recognized changes according to the particular application of the geothermal resource. The various aspects of this problem are listed in the following points.

a) Chemical exploitation of the resource.

This type of exploitation can be employed directly on brines at temperatures which are considered unsuitable for energy or heat production. It can also be applied to brines at high temperatures after they have been first exploited for electric energy production.
Examining the compositions reported in Table I, it can be seen that the brines appear particularly interesting for the recovery of potassium salts and boric acid and also of sodium sulfate, even if it is rather doubtful whether this last salt is of any real commercial interest.

It should be remembered that although the recovery of salts may be economically advantageous it also gives rise to many minor problems and difficulties connected with the disposal of the exhausted brines.

A number of processes for the recovery of potassium salts from brines have been described in the literature, e.g. precipitation as perchlorate (1) (2) or potassium salt of dipicrylamine (3-8) or in the form of double salts such as synginite or alum or recovery using high selectivity ionic exchange resins (9-13). The most practical process from the operational viewpoint, however, seems to be the utilization of fractional crystallisation. This has been confirmed by technical and economical analyses of different processes. In order to use this method, it is essential to have a full knowledge of the equilibria in solution in the system in addition to the other thermodynamic properties.

b) Thermal exploitation of the resource.

When there is no interest in the recovery of the saline products, the main information necessary is the total solubility curve. This curve represents the separation of the salts as the temperature of the brine decreases. Obviously, all the other thermodynamic properties must also be known.

c) Exploitation of the resource to produce electric power.

The observations made above in point b) are also valid for this.

In order to study the most suitable process to be used for the exploitation of the resource it is important to have as complete a picture as possible of the salt equilibria in the aqueous phase and also of the gas solution equilibria as these have a direct bearing on the possibility of corrosion or scaling during the delivery.

In the experimental research program described in this paper all these factors have been considered and the first results are given here.

As the research program has been conducted from a practical rather than a theoretical stance, the measurements have often been performed adopting standards of precision and accuracy which, while completely acceptable on the technical level, would certainly be inadequate if judged from a scientific view-point. However, as the program has progressed, equipment has been designed,developed and tested so that it will be possible in the near future to achieve results which are completely satisfactory also on the scientific level.

COMPLEX EQUILIBRIA IN SOLUTION

Studies, described in detail elsewhere (4), have been conducted to examine the quaternary system Na_2SO_4-K_2SO_4-KCl-NaCl; these are the predominating salts in the brine of Cesano 1 well. Data on this system, limited to temperatures below 100°C, have already been published. Our experience so far is limited to verifying the data reported in the literature for this system and to investigating the influence of the other species such as boric acid.

We used a very simple apparatus, represented in Fig.1, consisting of a container of pyrex glass composed of a central piece with a syntherized glass filter (G1 porosity) and two 100 ml flasks connected by means of spherical joints.

The water and an excess of the predicted solid phases were loaded into the lower part of the apparatus and the system was stir

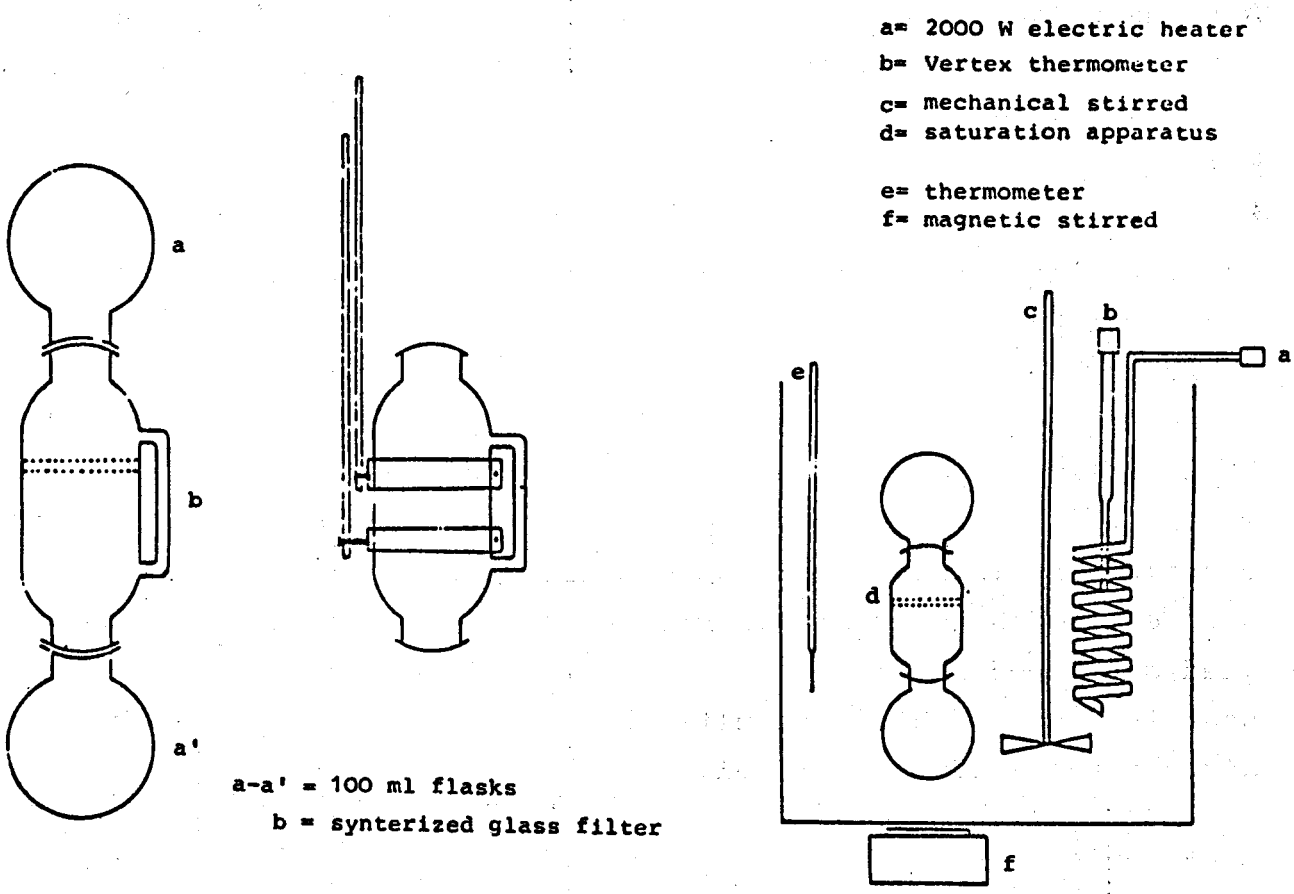

Fig. 1. Apparatus for solubility measurements.

red by a magnetic stirrer. The device was placed inside a thermostatic bath which maintained a chosen temperature within $\pm$ 0.05°C. When sufficient time had elapsed to ensure that equilibrium had been reached, the equipment was reversed without removing it from the bath. The clear solution was separated from the residual solid phase by filtration through the septum and then chemically analysed in order to determine the concentrations. Fig.2 plots the path of our experimental points against that derived from the published data. The influence of the presence of other chemical species is, however, of great relevance. In fact, if boric acid is present in the system the diagram changes considerably. This is shown by Fig.3 which illustrates a Jänecke diagram at 100°C and shows the shifting in position of the point of equilibrium of glaserite, sodium chloride and potassium chloride. The presence of boric acid causes the point to shift towards zones with higher sulfate and potassium ion concentrations, particularly at higher temperatures. In addition, there is a strong increase in the solubility of both the species of the system Na^+-K^+-SO_4^{--}-Cl^- and of the boric acid, see Fig.4.

From our experience with simplified systems, we have concluded that although such systems can be to some extent indicative of general behaviour, they may well be inadequate for a complete understanding of the real system. Furthermore, the problem of studying the system at higher temperatures is still unresolved and the implementation of a first autoclave has not proved satisfactory.

INTEGRAL SOLUBILITY DATA

In addition to the composition and nature of the separated solid phase, the main parameters which should be known are the temperature at which the separation of the solid phase begins and the total amount of solids separated from the brine as the temperature decreases. As apparatus has not yet been developed which is capable of operating at elevated temperatures and pressures, we

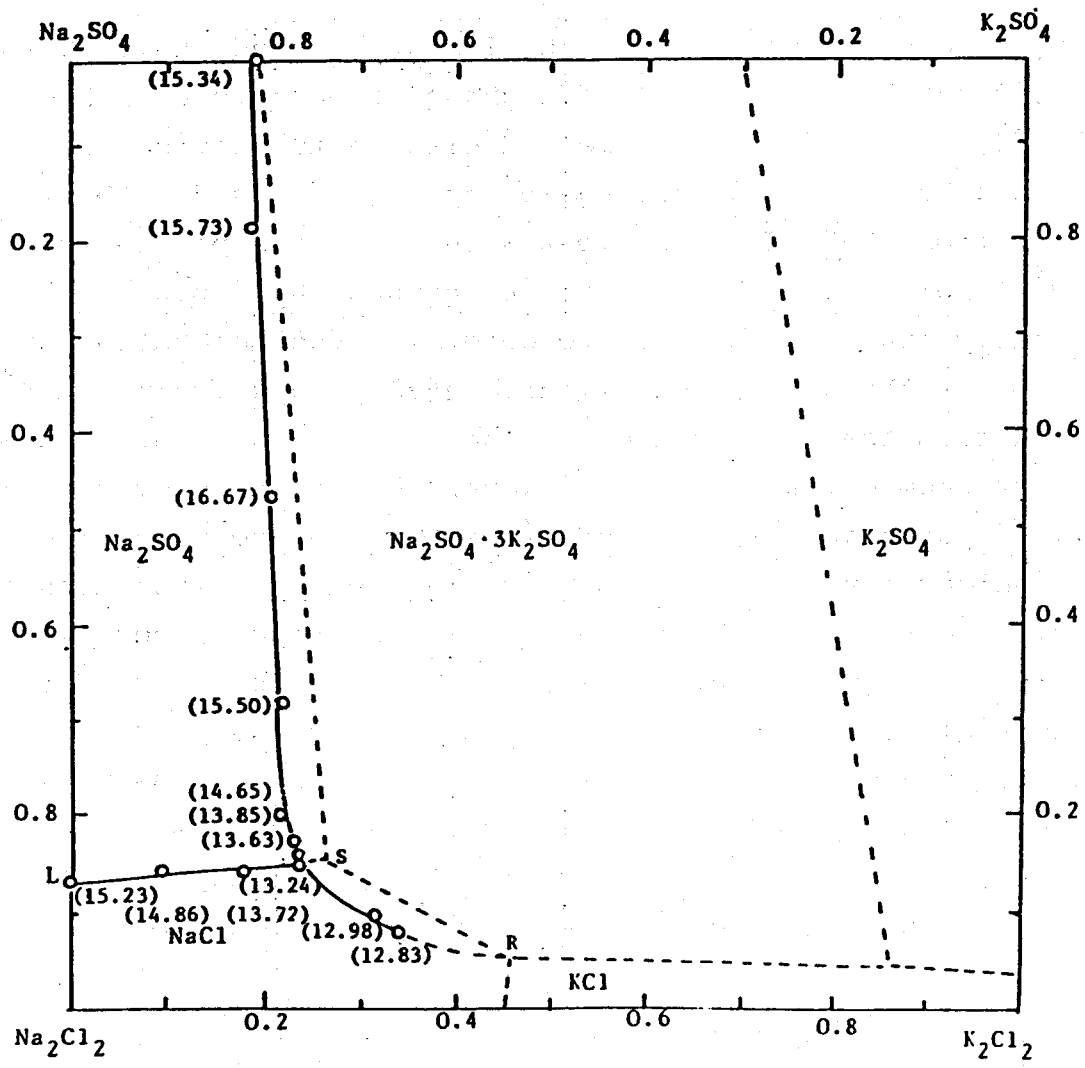

Fig. 2. Janecke diagram at T = 75°C.

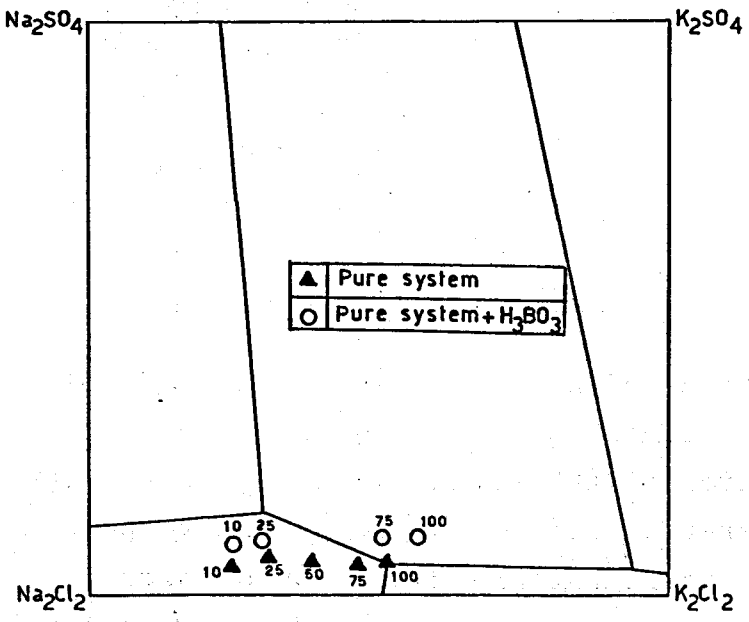

Fig. 3. Janecke diagram at 100°C; influence of the presence of boric acid.

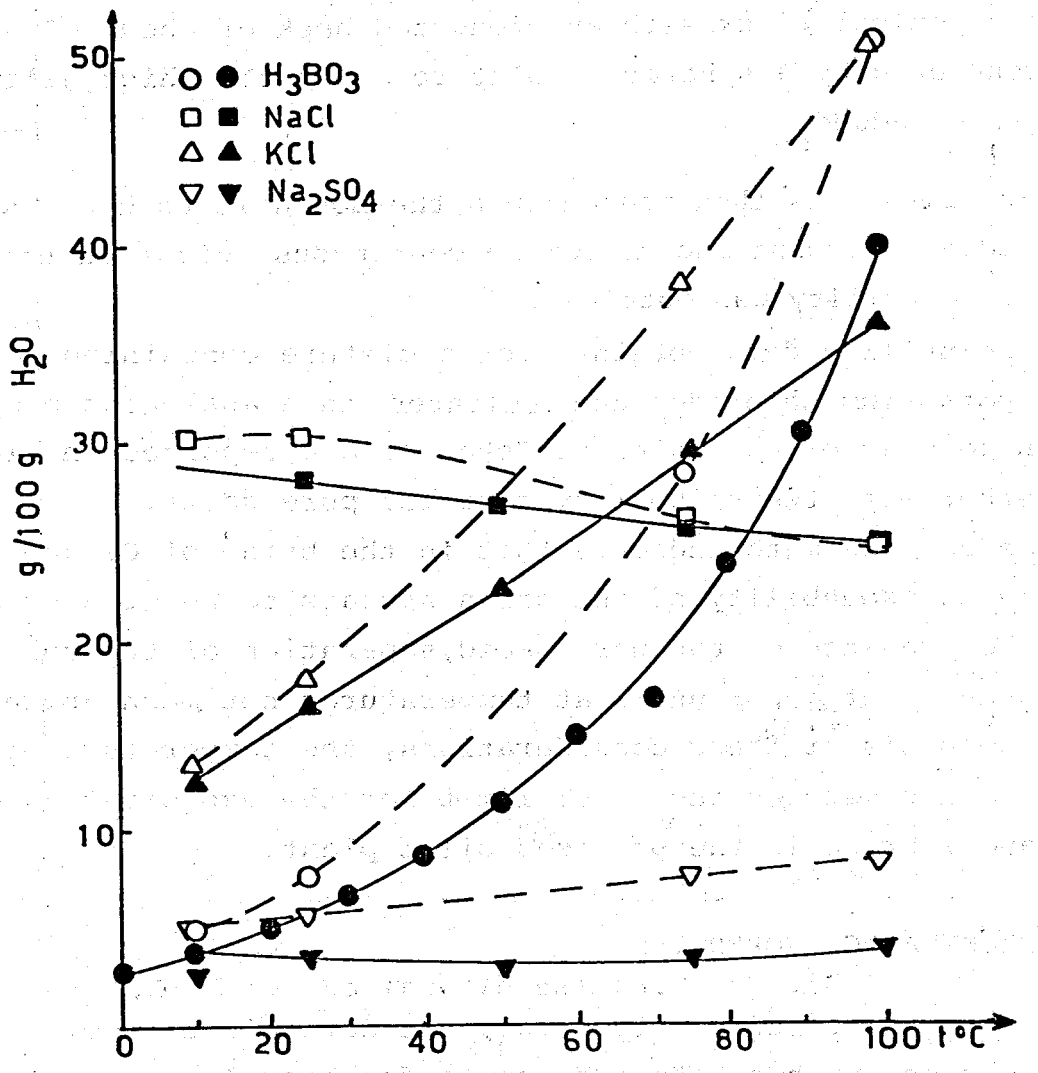

Fig. 4. Solubility vs temperature of Na_2SO_4, KCl, NaCl and H_3BO_3 when boric acid is absent (black points) or present (white points) in the system.

have performed measurements below 100°C by using a simple apparatus. The desired salt composition was weighed and introduced into a conical flask with an elongated neck of about 20 cm which is connected by a spherical joint to a burette which allows water to be added.

The flask was then placed in a thermostatic bath and water was added, keeping the system in continuous agitation until total solubility was obtained.
The solubility data obtained for a mixture containing sodium and potassium chlorides and sulfates in a analogous proportion to that of the brine of Cesano 1 are reported in Fig. 5 together with the solubility data for pure salts.
These data seem to indicate that in the brine of Cesano 1, where the solubility of the salts appears to be greater owing to the presence of the boric acid, separation of the solid phase should not occur until at temperatures not much above 100°C. On the basis of these considerations, the temperature of 125°C has been chosen as the lower limit for the exploitation of the Cesano 1 brine in the proposed pilot plant.

THERMODYNAMIC PROPERTIES

From the experimental viewpoint, the determination of certain properties, such as steam pressure for example, presents no particular difficulties as long as suitable equipment is available. The theoretical prediction is obviously far more complex. Neither are there any particular problems, from the practical side in measuring the latent heat of the evaporation of water as this is influenced very little by the salt concentration. The measurement of the heat capacity is a much more important and complex problem.
There is a notable lack of published data concerning brines at elevated temperatures and concentrations. Bromley (15), Silvester and Pitzer (16), and Tanner and Lamb (17) have measured the dependence of the heat capacity on the concentration. These authors, however, were working with a limited range of tempera

tures and concentrations and generally restricted their studies to simple systems.

From these considerations, there emerges a clear necessity for the collection of an extensive body of experimental data.

The work began by measuring the heat capacity of a series of multi-component salt mixtures and of all the single electrolyte solutions contained in them in order to find suitable correlations which could be used to predict the heat capacity of such mixtures over a much wider range of temperatures and total con

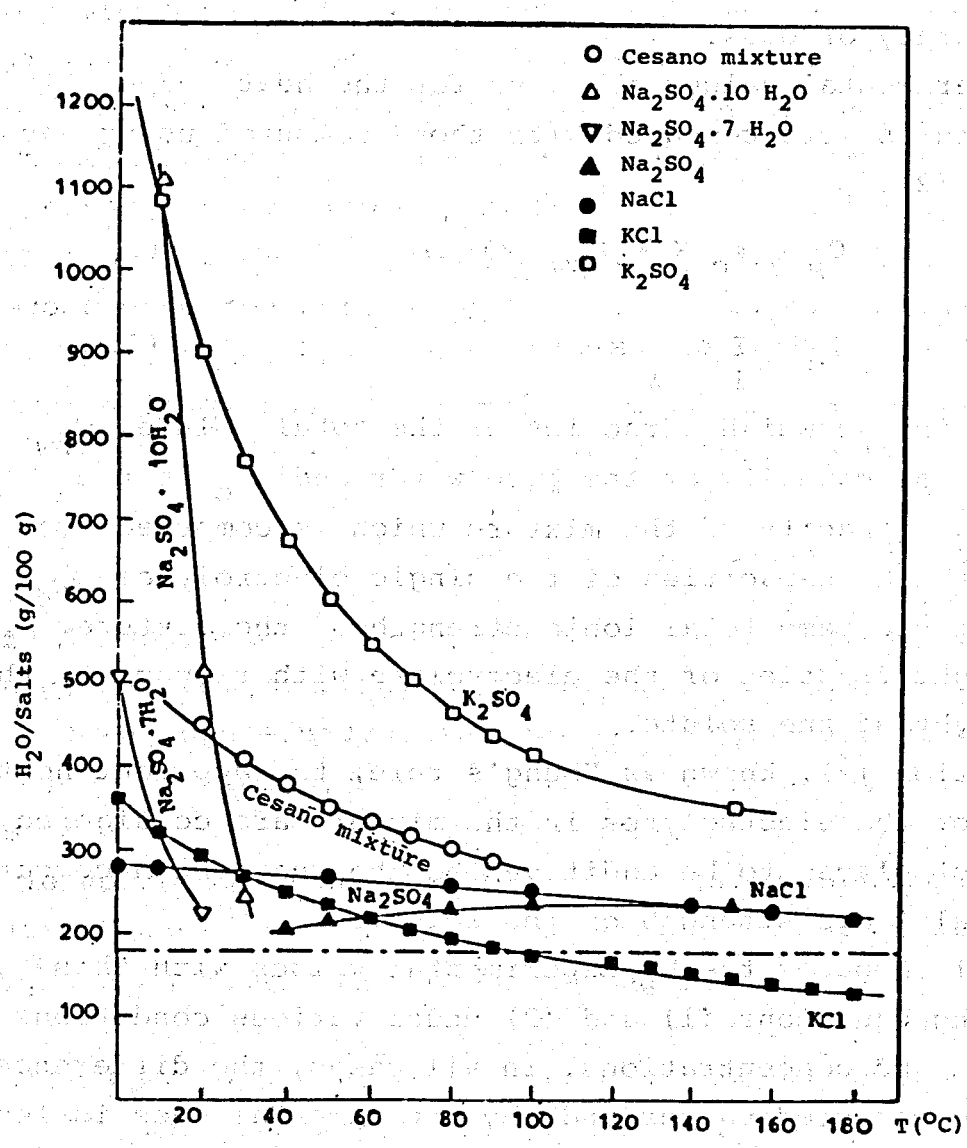

Fig. 5. Integral solubility of pure sodium amd potassium chlorides and sulfates and their mixtures in proportion analogous to Cesano-1 brine vs temperature.

centrations and at different ratios between their components. In this study, the heat capacities between 30°C and 80°C have been measured for salt water solutions of NaCl, KCl, Na_2SO_4 and K_2SO_4 and for some of their mixtures for different component ratios and using a CALVET type calorimeter and the "continous heating" method. The range of temperatures and concentrations studied was limited both by the fact that it was impossible to agitate the mixture while measurements were being made and by other special characteristics of the experimental apparatus. The heat capacities were measured within an estimated accuracy of 0.5%.

The experimental values obtained for the heat capacities of the mixtures were compared with those computed using equations (1) and (2).

$$C_p = \phi_c X + C_{pw} (1-X) \qquad (1)$$

$$\phi_c = \sum_i \phi_{c_i} x_i \qquad (2)$$

where X is the weight fraction of the total solute, C_{pw} is the heat capacity of the pure water and ϕ_c is the apparent heat capacity of the mixture which is computed from the apparent heat capacities of the single electrolytes ϕ_{c_i} measured at the same total ionic strength of the mixture. x_i is the weight fraction of the electrolyte with respect to the total weight of the solute.

In equation (2), known as Young's rule, the apparent heat capacities of the electrolytes in the mixture are considered, in the first place, to be additives as they have been computed for the total ionic strength of the solution.

Table II compares the C_p experimental values with those computed using equations (1) and (2) under various conditions of temperature and concentrations. In all cases, the difference between the computed values and the experimental ones is less than 1%.

We now plan to check the validity of Young's rule for higher concentrations and temperatures and to eventually attempt other correlations. In order to be able to extend the measurements to

TABLE II

Comparison between experimental C_p values and those calculated following Young's rule for selected binary mixtures.

1 a): Temperature dependence at selected ionic strengths I $(I = 1/2\ \Sigma\, m_i z_i^2)$

NaCl/KCl = 1/1 at I = 4			Na_2SO_4/K_2SO_4 = 1/3 (Glaserite) at I = 1.5			$NaCl/K_2SO_4$ = 2/1 at I = 1		
T°C	C_p (calc.)	C_p (exp.)	T°C	C_p (calc.)	C_p (exp.)	T°C	C_p (calc.)	C_p (exp.)
30	0.7819	0.7817	30	0.9109	0.9124	30	0.9347	0.9366
40	0.7835	0.7835	40	0.9135	0.9140	40	0.9363	0.9379
50	0.7851	0.7842	50	0.9158	0.9159	50	0.9378	0.9390
60	0.7864	0.7840	60	0.9179	0.9178	60	0.9391	0.9402
70	0.7873	0.7832	70	0.9196	0.9197	70	0.9406	0.9416
80	0.7880	0.7820	80	0.9213	0.9216	80	0.9422	0.9435

1 b): Concentration dependence at Fixed Temperatures T = 50°C

NaCl/KCl = 1/1				Na_2SO_4/K_2SO_4 = 1/3 (Glaserite)				$NaCl/K_2SO_4$ = 2/1			
I	Weight %	C_p(calc.)	C_p(exp.)	I	Weight %	C_p(calc.)	C_p(exp.)	I	Weight %	C_p(calc.)	C_p(exp.)
1.0	6.24	0.9275	0.9254	0.6	3.22	0.9626	0.9608	0.33	1.90	0.9759	0.9767
2.0	11.74	0.8700	0.8671	0.9	4.75	0.9470	0.9452	0.67	3.74	0.9561	0.9574
3.0	16.63	0.8231	0.8208	1.2	6.23	0.9315	0.9303	1.00	5.50	0.9378	0.9390
4.0	21.01	0.7851	0.7842	1.5	7.67	0.9158	0.9159	1.33	7.21	0.9196	0.9214

a wider range of temperatures and concentrations, a calorimeter has been constructed and tested to measure the thermal capacity of salt water solutions in the temperature range 50°-250°C and at the relative equilibrium pressures. The sample can be agitated while measurements are being made and saturated solutions in the lower temperature range can, thus, also be analysed. The calorimeter is of the drop calorimeter type and is illustrated in the diagram in Fig.6. The cell of the calorimeter is composed of a cylindrical container in stainless steel with the internal walls completely lined with gold at 1000/1000. The capacity of the cylinder is - 5 cm^3. This apparatus makes it possible to obtain the mean heat capacity of the cell and its content between the furnace temperature T_i and the temperature T_f of as underlying calorimeter C, of adiabatic type, where the cell has been dropped.
The ratio between the heat capacity of the cell and the calorimeter is approximately 1:50. If, in a series of experiments at various temperatures, T_i, the values cf T_f vary little from a mean value $\overline{T}_f$, it can be demonstrated that the heat capacity C_T at a temperature T, within the range of the analysed temperatures, can be computed from the following expression:

$$C_T = \overline{C}_T + (T - \overline{T}_f) \frac{d\,\overline{C}_T}{d\,T} \qquad (3)$$

The values of $\overline{C}_T$ and of the derivative $\frac{d\,\overline{C}_T}{d\,T}$ are obtained from a best fitting of the values $\overline{C}_{T_i}$ using polynomial equations of the type:

$$\overline{C}_T = \sum_{j=0}^{n} a_j\, T^j$$

The following type of expression can thus be obtained for C_T

$$C_T = \sum_{j=0}^{n} a_j\, T^j + (T - \overline{T}_f) \sum_{j=0}^{n} j\, a_j\, T^{j-1}$$

A = Cell releasing device
Sh = Adiabatic shield
B_C = Calorimetric aluminium block
B_F = Furnace aluminium block
C = Calorimeter
F = Furnace
G = Brass tube
R = Electrical calibration heater
H_F = Furnace heating
H_S = Adiabatic shield heating
I = Thermal insulation
K = Sample receiver
M = Motor for sample revolution
Pt_1, Pt_2 = Platinum resistance thermometers
QT = Quartz thermometer probe
S_f = Position of the sample inside the calorimeter
S_i = Position of the sample inside the furnace
T = Circulating water thermostat
TH = Thermocouples

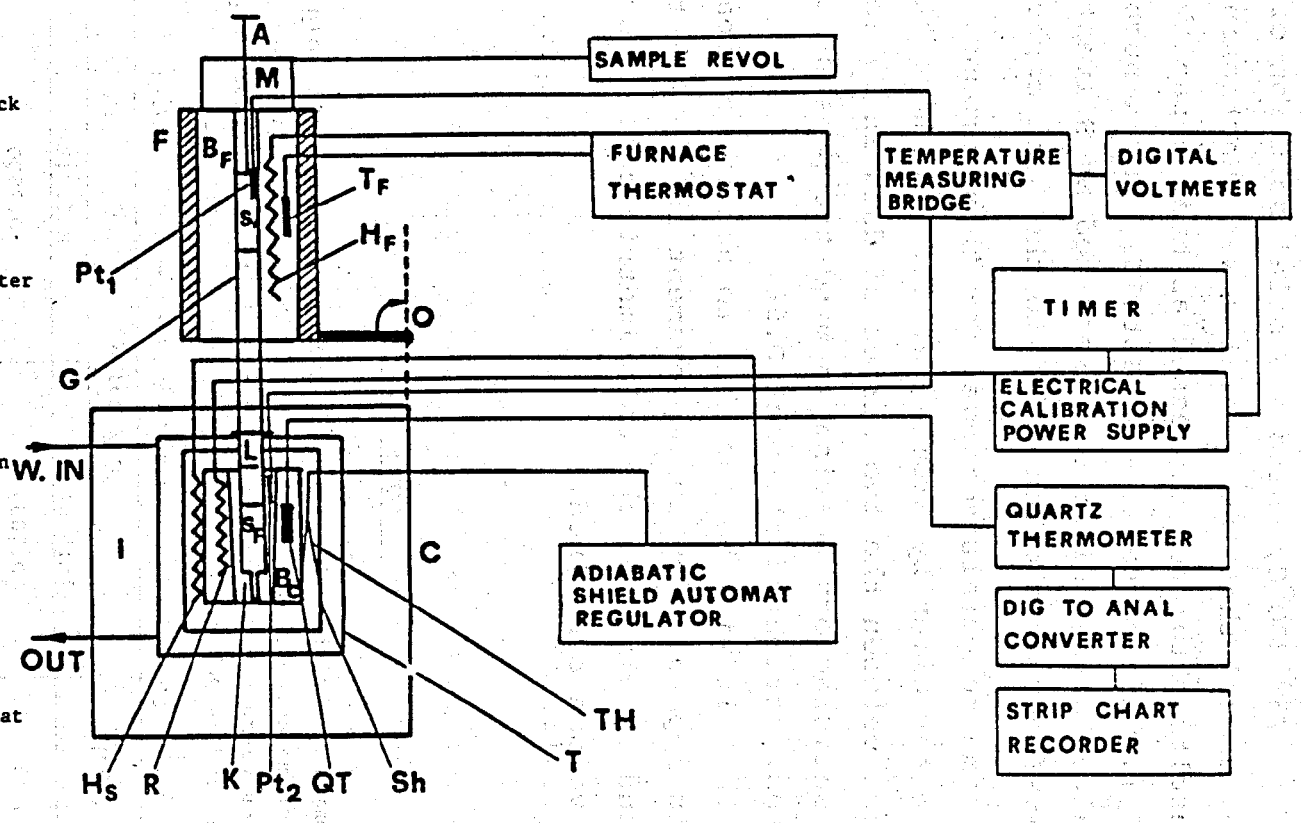

Fig. 6. Scheme of the drop calorimeter.

A first series of experiments has been performed over the temperature range 75°-200°C, using a 6 molal solution of sodium chloride to control that the apparatus was functioning correctly. The results obtained, expressed as heat capacity at constant pressure (C_p), were compared (see Tab.III) for a number of temperature values with similar data reported by Silvester and Pitzer (16). The values given refer to the heat capacity of water in the same temperature range. For this purpose, the values of C_p for water given by Bromley et al. (18) have been used. The agreement between the two series of data in Table III can be considered satisfactory bearing in mind the present accuracy of our apparatus, estimated at about 0.5%.
We believe that it will be possible to achieve a greater precision in this apparatus by an improvement in the treatment of the data and by altering the calorimetric cell in order to increase the volume contained.

TABLE III

Comparison of some heat capacity values of a 6 m NaCl solution measured during this study and the corresponding values taken from Silvester and Pitzer in the temperature range 75°C - 200°C.

T (°C)	C_p/ cal g^{-1} $°C^{-1}$	
	This study	Ref. (2)
75	0.7837	0.7800
100	0.7791	0.7776
125	0.7754	0.7715
150	0.7729	0.7644
175	0.7722	0.7614
200	0.7766	0.7739

CONCLUSIONS

The initial stage of our experimental research program to study the equilibria and properties of brines has now been completed and we hope to have at our disposal, in the near future, an extensive body of data.

From the results obtained so far it appears unrealistic to think in terms of a theoretical approach; at the present moment, a development in the experimental research methods is necessary if reasonably reliable correlations are to be obtained on the technical level.

LITERATURE CITED

1) D.R.George et al., Chem.Eng.Progr. 64, 96 (1968).

2) D.R.George et al., U.S.Patent 3,424.657 (2/9/1966).

3) W.F.Linke, A.Seidell, Solubilities of inorganic and metal-organic compounds, American Chemical Society , Washington 1965, 4th Ed. V.II pg.59

4) G.Marshall, Tourn.Ind.Eng.Chem. 12, 336 (1920).

5) La Chimica e l'Industria (Milano) 1, 23 (1941).

6) F.Massazza et al., Annali Chim.(Roma) 42, 664 (1958).

7) F.Massazza et al., Annali Chim., 51, 645 (1961).

8) S.K.Chu, C.T.Liaw, Hua Hsueh 4, 106 (1969).

9) S.Inao et al., Japan Patent 7212322 (22/12/1968).

10) F.L.D.Cleets, Ion.Exch.Process Ind., Pap.Conf.182 (1969).

11) H.Matsushita, Japan Patent 7323269 (12/9/1969).

12) V.I.Gorshkov, U.R.S.S. Patent 376322 (24/6/1971).

13) V.I.Gorshkov, Vestn.Mosk.Univ.Khim. 14, 41 (1973).

14) F.Giovannini, F.Nasti, Thesis University of Pisa (1977).

15) S.Likke, L.A.Bromley, J.Chem.Eng.Data 18, 189 (1973).

16) L.F.Silvester, K.S.Pitzer, "Thermodynamics of Geothermal Brines", LBL-4456 Lawrence Berkeley Laboratory - University of California (1976),(Nat.Tech.Inf.Serv., Springfield, Virginia 22161).

17) J.E.Tanner, F.W.Lamb, J.Sol.Chem. 7, 303 (1978).

18) L.A.Bromley, A.E.Diamond, E.Salami, D.G.Wilkins, J.Chem. Eng. Data 15, 246 (1970).

POTENTIAL SOLUTIONS FOR GEOTHERMAL BRINE PRODUCTION UTILIZATION AND REINJECTION PROBLEMS

O. J. Vetter, Vetter Research Inc.
Costa Mesa, California

ABSTRACT

The geothermal industry is presently confronted with a large number of technical problems related to geothermal brine production, utilization and reinjection processes. The United States Department of Energy/Division of Geothermal Energy realizes these problems and is funding large efforts to help overcome them.

The joint efforts by private industry and DOE/DGE have still not solved, in a satisfactory manner, the following most critical problems:

1. Scale and corrosion problems in subsurface and surface equipment.
2. Removal of silica and other suspended particles from the reinjected brine; these particles cause severe damage to the injection wells.
3. Proper gas handling (noncondensables) to ensure optimum power plant efficiency.
4. Mineral recovery through utilization of brine constituents.
5. Maximum reservoir heat recovery and avoidance of subsidence through reinjection of heat depleted brine and injection of aqueous fluids which are not native to the reservoir.

Many papers dealing with various aspects of these problems have been published. These papers describe attempts to attack these problems through theoretical evaluations and/or through bench scale experiments. Unfortunately, very little is published about full-scale field experiments to find solutions to these problems.

Recently, a number of private geothermal operators have commissioned us to conduct some of these large scale experiments in actual field tests. A large scale test unit was built and operated at

various sites. This unit is capable of handling up to 1,000,000 lbs/hr total flow at a maximum temperature of 515°F.

DOE/DGE joined forces with these operators by providng funds through its research program on reinjection problems. In return, all data obtained through these field experiments will be published whether or not they are directly funded by DOE/DGE.

The following tasks are included in this work:

1. Experiments to determine the practical feasibility of brine clarification by various processes including reactor-clarification and flocculation.
2. Extensive documentation of actually measured data and precise identification of problems based on these actually measured field data.
3. High temperature/high pressure test loop experiments to determine:
   a. Practical aspects of mineral recovery.
   b. Optimization of gas and liquid handling processes.
   c. Scale deposition rates.

Of particular interest are the types of instrumentation used to identify problems and to monitor the gas and liquid quality in large-scale field experiments. Theoretical evaluations using the field data to determine various chemical aspects of foreign brine injection are also given.

PRODUCTION TEST FACILITIES OF THE HOT BRINE OF CESANO GEOTHERMAL FIELD

R. Corsi and R. Di Falco
ENEL

1. - INTRODUCTION

Since 1968 ENEL has developed a prospecting program for geothermal fluid research in the Vulsini and Sabatini mountains regions. The data acquired from these investigations enabled ENEL to site the first exploratory well and discover the Cesano Geothermal Field (1).
This field is located approximately 15 Km north of Rome, (Fig. 1).
So far nine deep wells (1400 - 3000 m) have been drilled in this area. Bottom-hole temperatures range from a minimum of 145°C (C 5 well) at 1800 m of depth to a maximum of 300°C (C 4 well at 3080 m of depth).
Production characteristics of these wells are quite different : five are sterile or scarcely productive, four produce very high saline brines but with different physio-chemical characteristics. The pressures of productive wells at the same elevation above sea-level are also quite different. These facts prevent us from formulating hypotheses on the geothermal reservoir for the moment.
This paper describes the results obtained with a small measuring plant in the first exploratory well C1, which began production in 1975.
C 1 well is located approximately 15 Km north of Rome, near the southern edge of the Baccano Valley (Fig. 2).
Its characteristics (technical profile, depth, hydrogeology, thermal profile) are summarized in Fig. 3.

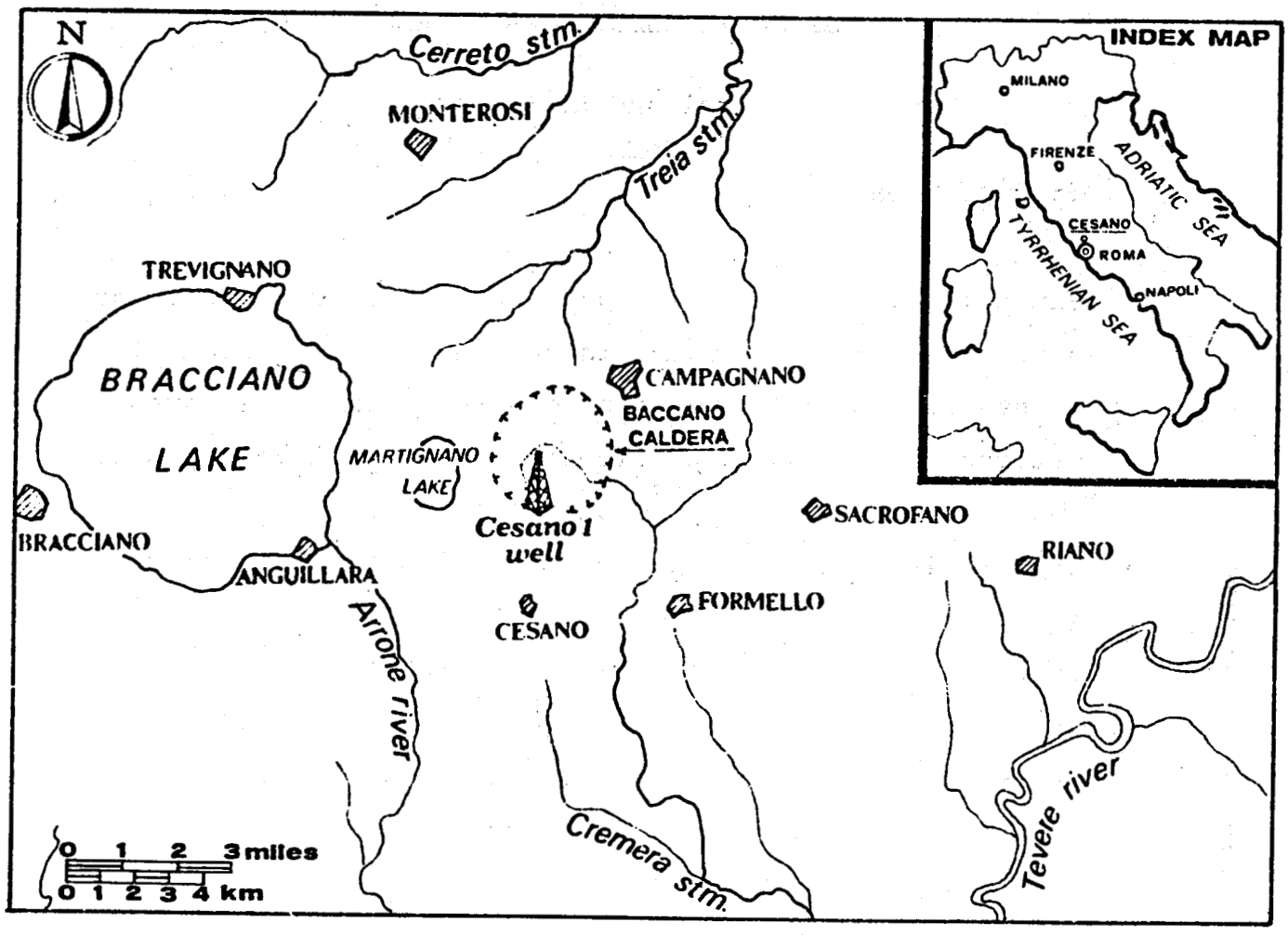

Fig. 1. Location of the Cesano area.

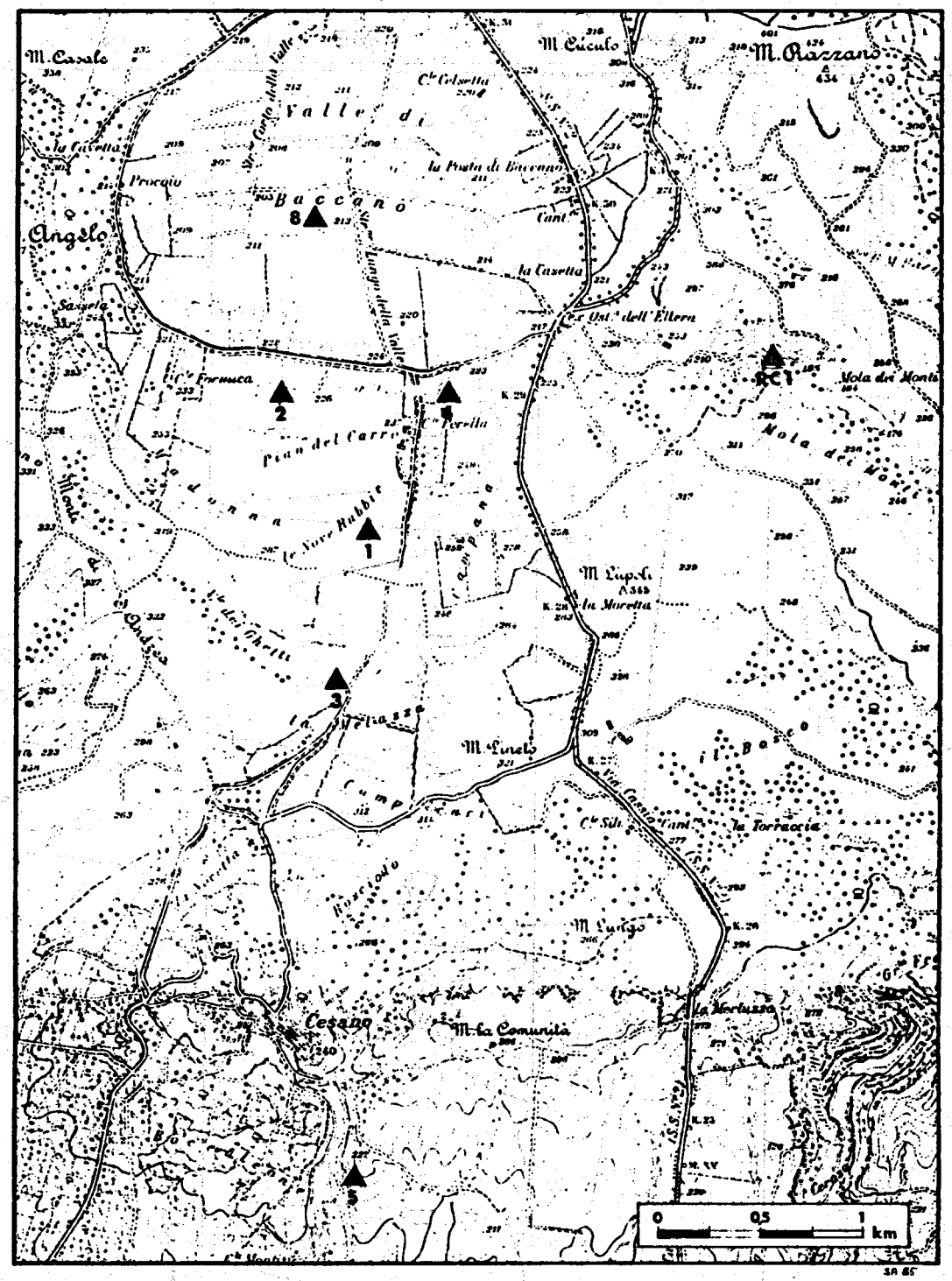

Fig. 2. Location of wells of Cesano area.

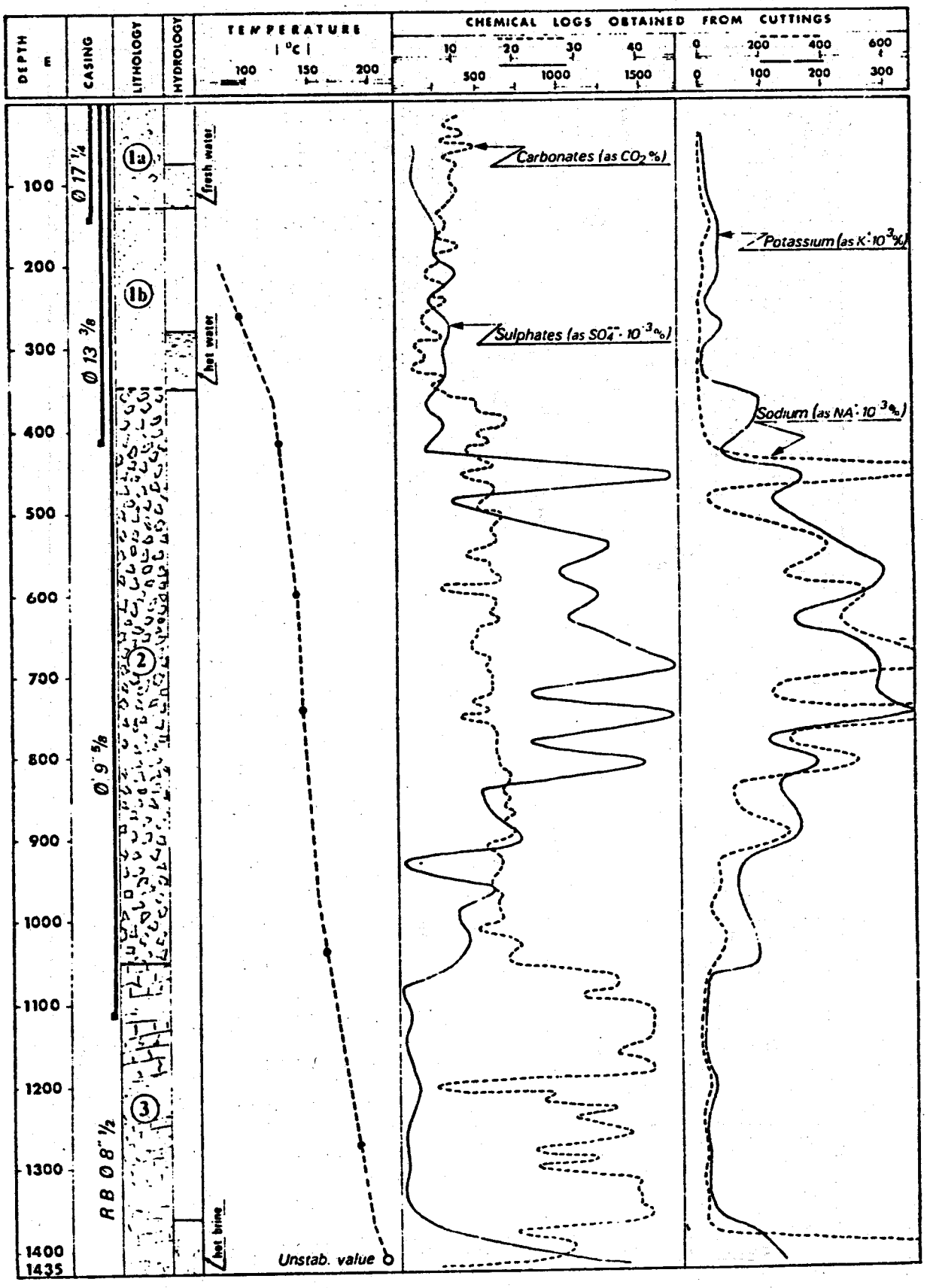

Fig. 3. Summary of geohydrological, thermal, and geochemical data.

2. - CESANO 1 TEST FACILITY

This well went into production for the first time in 1975 (1) when the drill-rig was still on the well.
As the water produced was a hot brine with an elevated salt concentration, the well-head equipment was rapidly affected by incrustation so that, after about 10 hours production, the well was shut-in. From this first production period, however, some data were gathered on the chemical composition of the brine (1).
Since no re-injection well was available for waste disposal, a steel-lined basin was built to collected the brine produced from the well, and a small separation plant assembled to measure flow conditions and the physio-chemical characteristics of the brine.
A sketch of this plant is shown in Figs. 4 , 5 and 6.The hydrostatic level being at a depth of ∿ 105 m from the well-head gas lift stimulation is required to put the well into production.
A 230 m tubing was lowered into the well to perform this gas lift.
Flashing in the well causes the dissolved salts to precipitate and give rise to scaling phenomena in the well-head equipment (Fig. 7 and 8). A water pipeline was then inserted to flush water into the hot brine pipeline. The salt concentration thus dropped and it was possible to prevent sulphate incrustation on the pipes.
Three different types of materials and coatings were used down stream of the cyclon in an attempt at avoiding scaling.

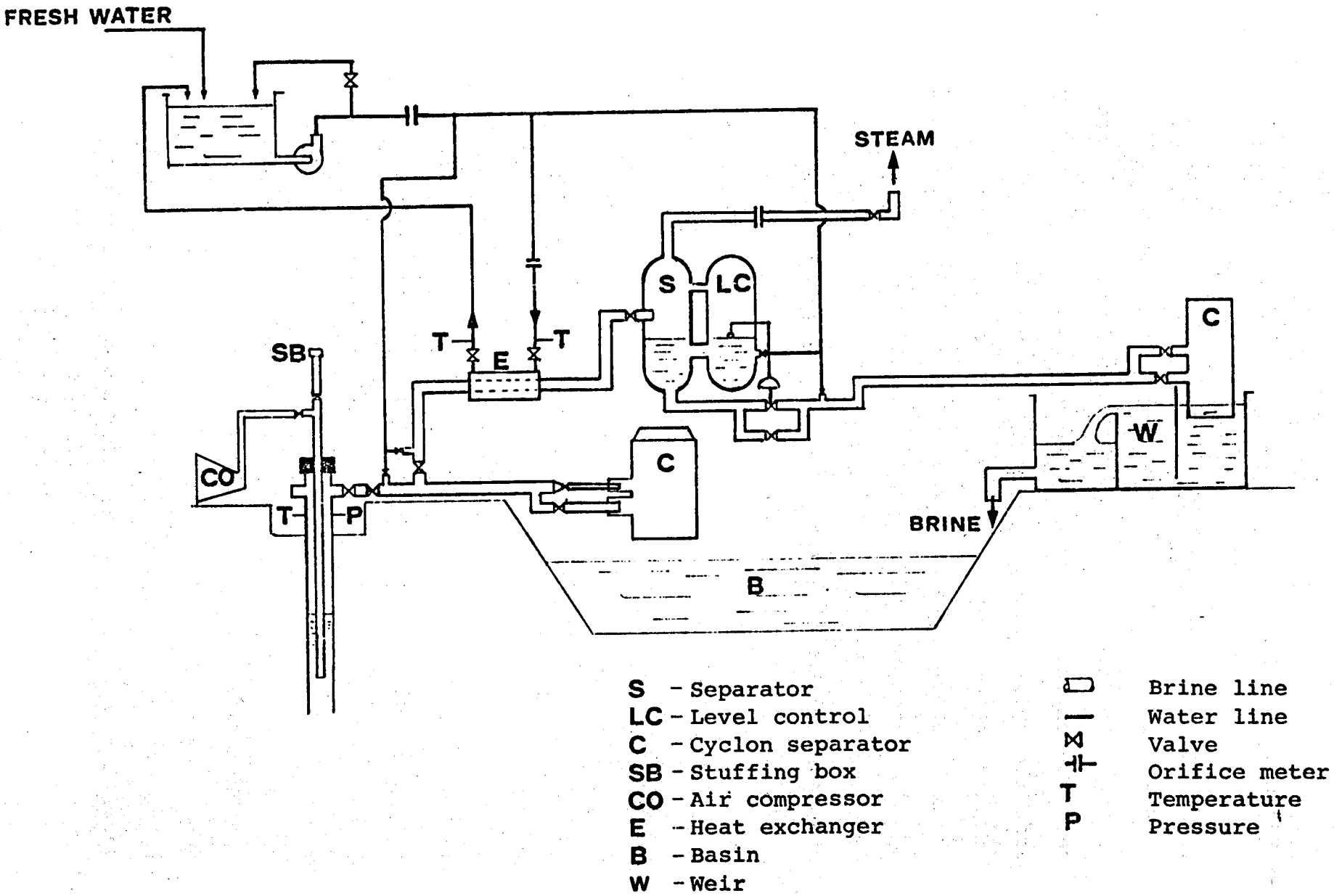

Fig. 4. Schematic diagram of separator assembly.

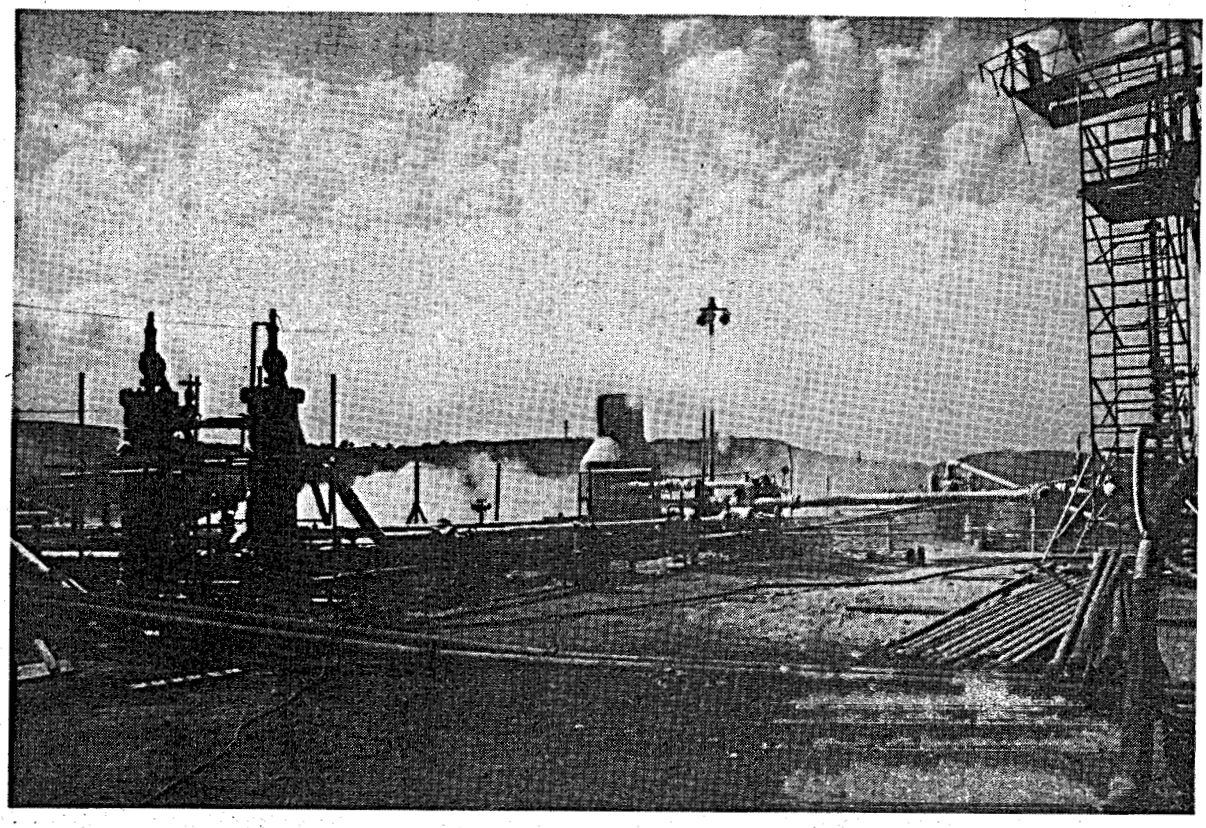

Fig. 5. View of separator.

Fig. 6. View of the basin for collecting the brine.

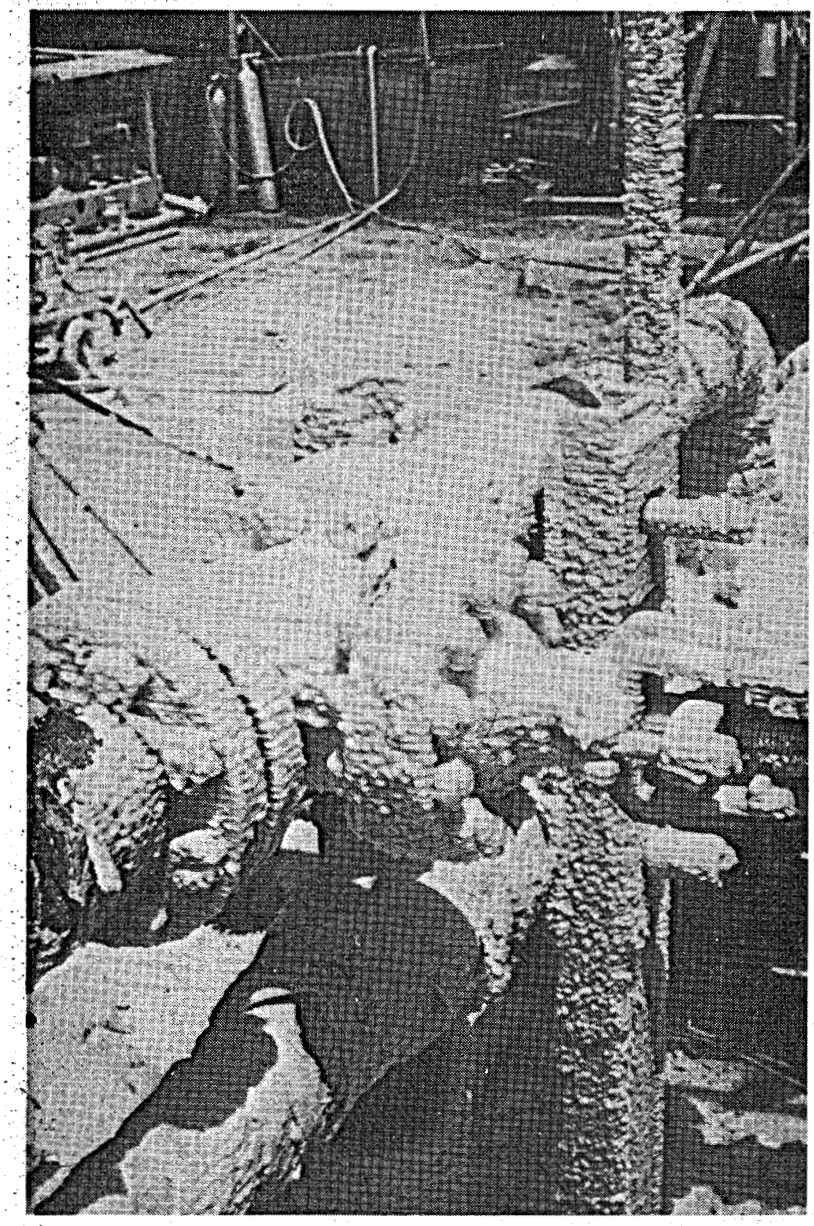

Fig. 7. View of scaling on outside of pipeline.

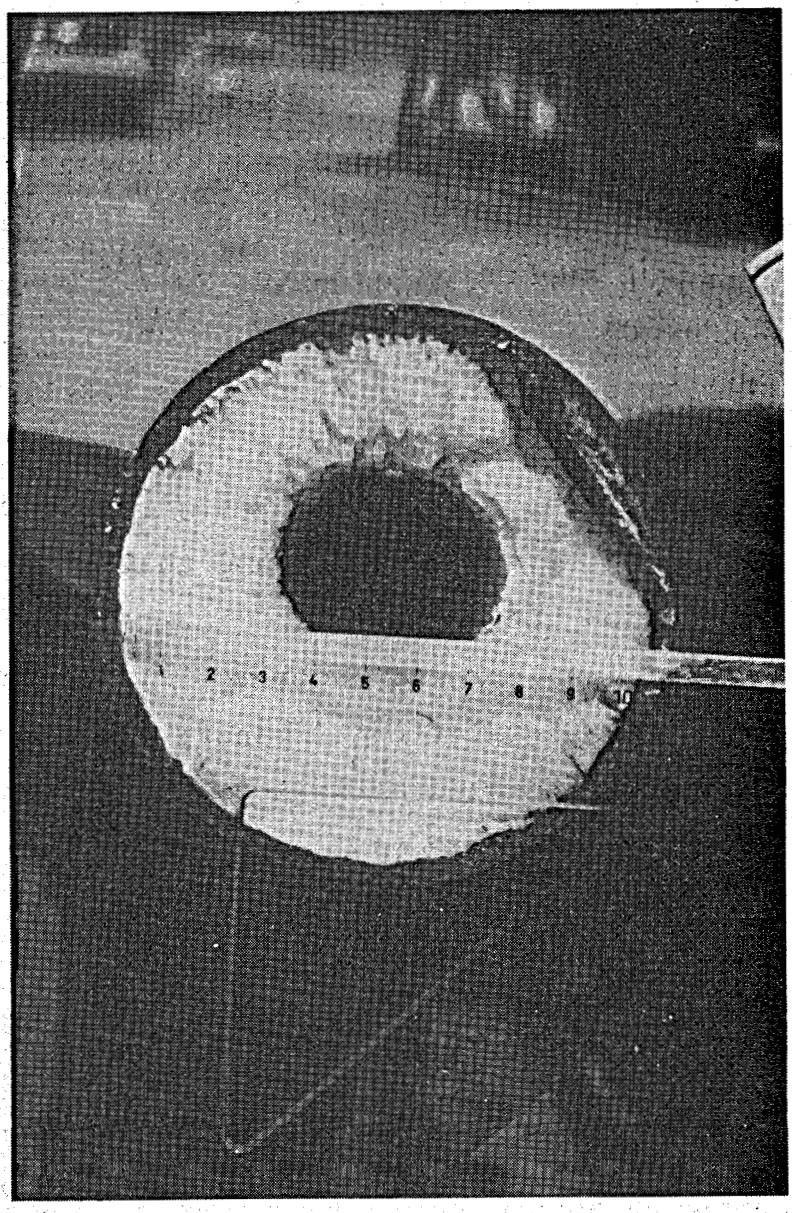

Fig. 8. View of scaling on inside of pipeline.

Figures 9 , 10 and 11 show the incrustations on these materials.
The first is stainless steel AISI 316, the second steel coated with zinc, the third steel coated with teflon. The thickness of scaling was respectively 6 mm, 6 mm and 4.2 mm after about 75 hours of production. The smaller thickness on steel coated with teflon is likely due to the fact that crystal formation takes longer on teflon. The materials examined did not show signs of corrosion after scaling was removed. We presume that scaling prevented a corrosion attack.
A small double-pipe heat exchanger was also installed to measure the brine-water heat transfer coefficient.
A stuffing-box was mounted at well-head to lower measuring instruments during production. As shown in Fig. 4, the mixture was passed into a separator and the discrete phases measured with an orifice meter.
Although no difficulty was involved in measuring the steam phase, the water phase presented some problems on leaving the separator, as it contained a small percentage of steam carried over from the separator along with the water phase. Even a very small quantity of the order of 1/2% would cause a relatively large error in the estimated flow (2). Hence water was introduced in the level control tank both to reduce incrustation in the automatic valve and to condense part of the steam entrained in the liquid phase.
A weir was mounted down stream of the separator to verify whether the orifice measurements were correct.
Taps were left in different parts of the plant and at well head for sampling purposes.

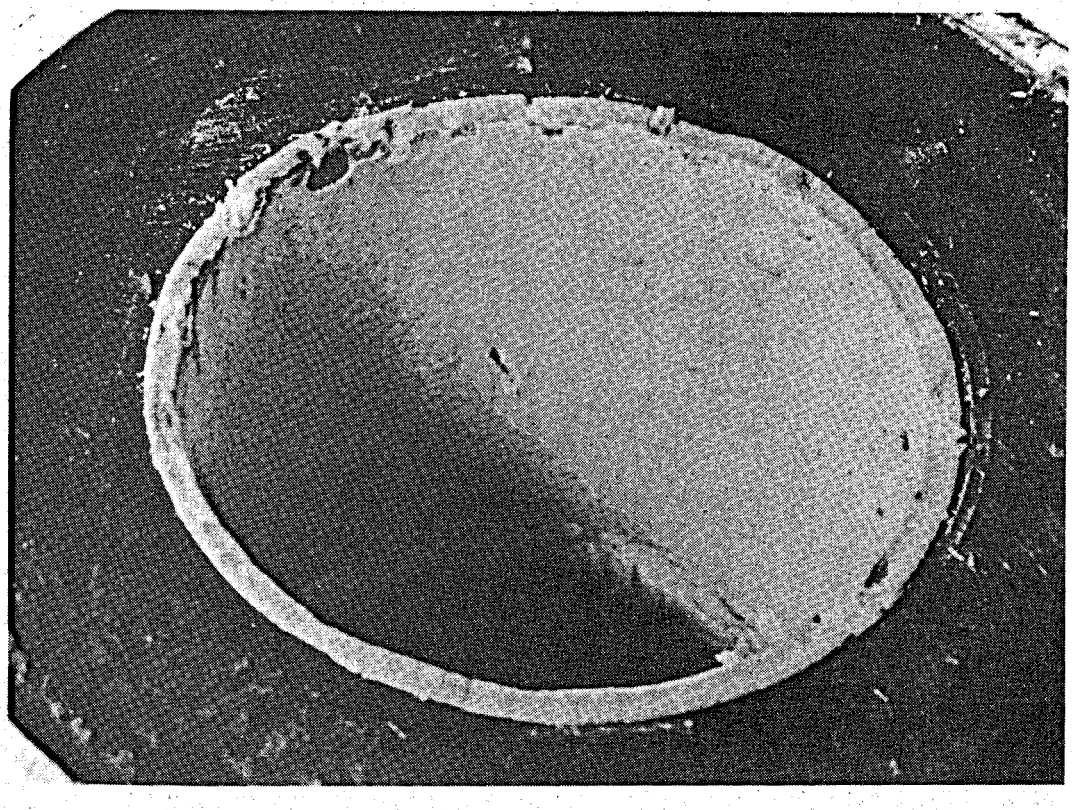

Fig. 9. Incrustation on stainless steel AISI 316.

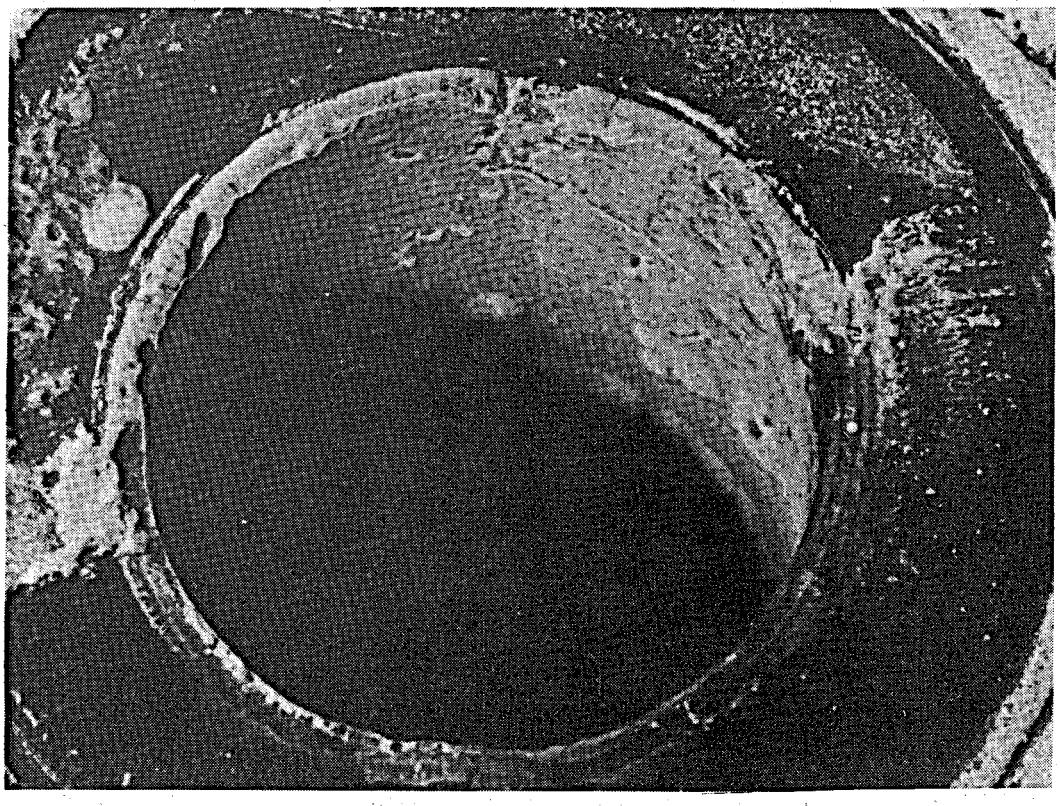

Fig. 10. Incrustation on steel coated with zinc.

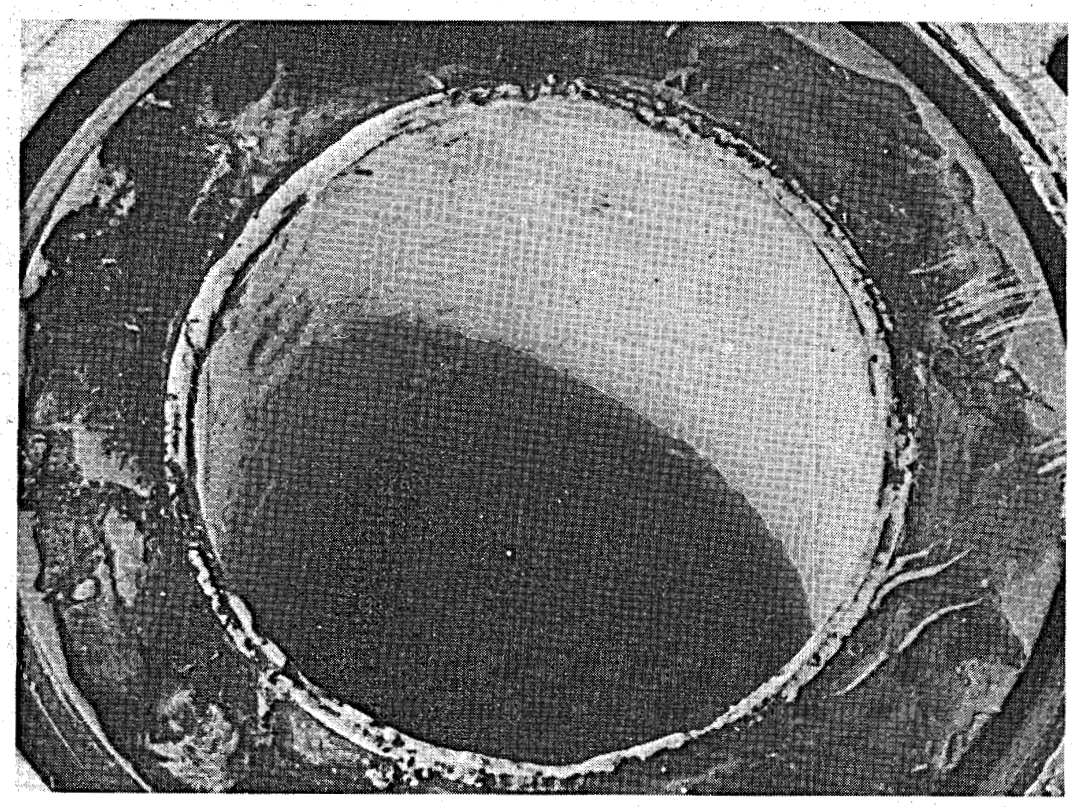

Fig. 11. Incrustation on steel coated with Teflon.

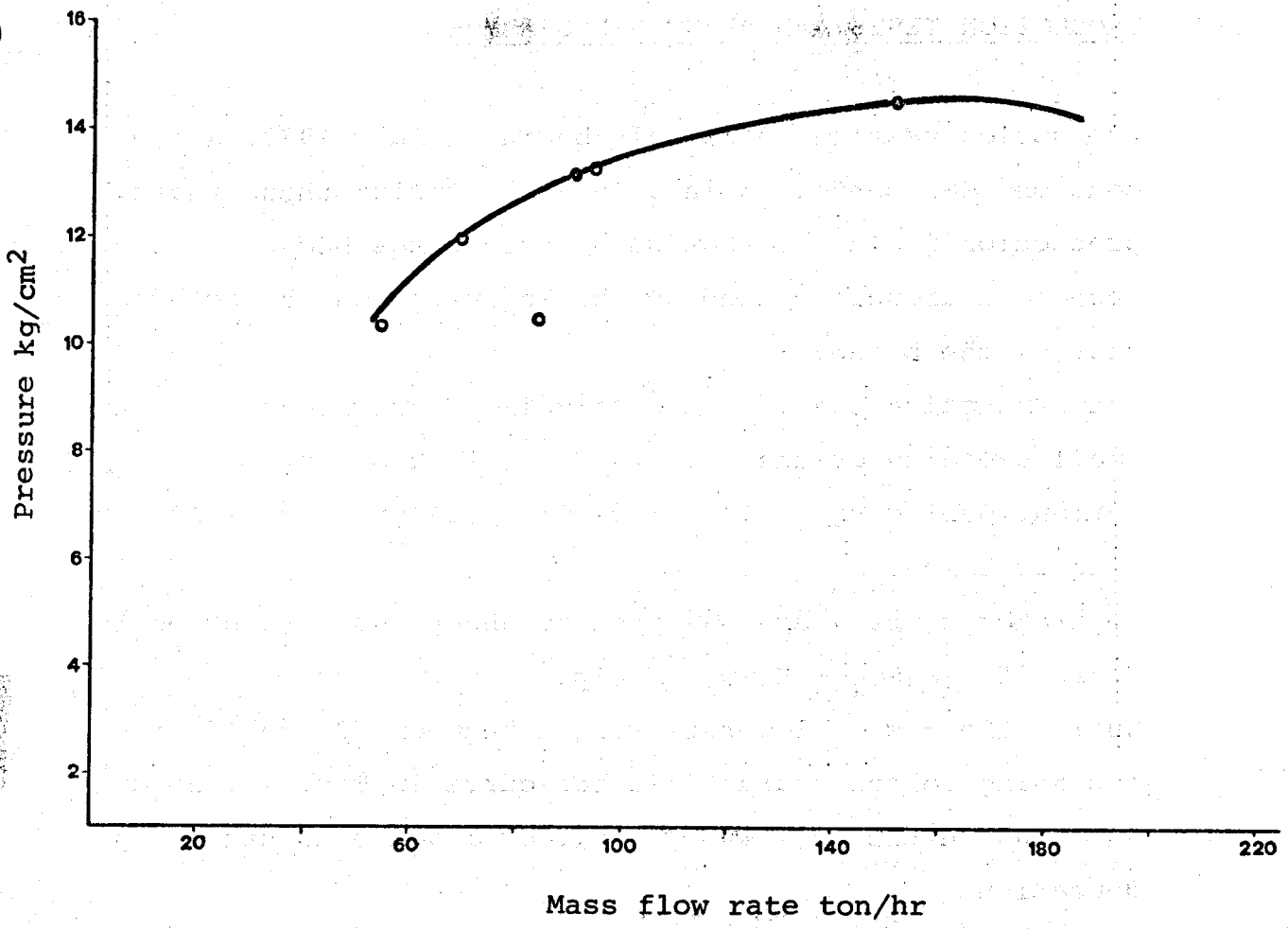

Fig. 12. Characteristic curve of Cl well.

3. - PRODUCTION TESTS AND PLANT PERFORMANCE

Production testing could only begin in July 1977. A second one was performed in July 1978. During these tests, production had to be shut-down three times because of technical trouble caused by the incrustation characteristics of the brine.

The production tests lasted only 135 hours because of the small capacity of the basin and the lack of water for dilution. During these 135 hours the well produced ∿ 10.000 tons of brine.

Separator temperature was kept at about 140°C to prevent Glaserite $Na_2SO_4 \cdot K_2SO_4$ precipitation.

During the test, flow-rate ranged between 70 and 150 t/h, according to the characteristics curve in Fig. 12. Below 50 - 60 t/h the well stopped producing due to steam condensation.

The separator ran regularly during all the period of production but during the last hours,the bypass valve had to be opened because of partial obstruction of the automatic valve.

At the end of the production tests, the inner part of the cyclon was covered with a uniform $CaCO_3$ incrustation of about 20 mm of thickness, whereas the inner part of the steam pipe was quite clean. This is due to the fact that during the production a water valve was periodically opened to wash the steam pipe inside the cyclon.

The dilution of brine allowed us to maintain production for 75 hours continuously. Unfortunately scaling prevented us from obtaining accurate measurements.

The pressure top were regularly obstructed so that pressure, and flow rate measurements were discontinuous. Scaling on the thermometer well may have altered the temperature measurements.
The flow rate measurements in the weir was the most reliable as it was unaffected by scaling.
At the end of production water was flushed into the plant and well to avoid salt precipitation.
Recently a borehole geometry log was made to see if there were incrustations in the well. The results of this measure are shown in Figure 13.
It is clear from the figure that the thickness of the scaling increases with depth and then diminishes. At a depth of about 350 m (at flash level) the well was obstructed.
The discontinuties in the figure are probably due to the glaserite crystals that grew when the temperature of the brine dropped below about 120°C, as will be discussed later.

4. - CHEMICAL CHARACTERISTICS OF THE BRINE

Many samples were collected in order to estimate the physio-chemical characteristics of the brine.
Five types of sampling are used :

1) - in bottle set up at well-head to collect the brine under pressure conditions;

2) - collecting brine downstream of the weir, after dilution of the brine;

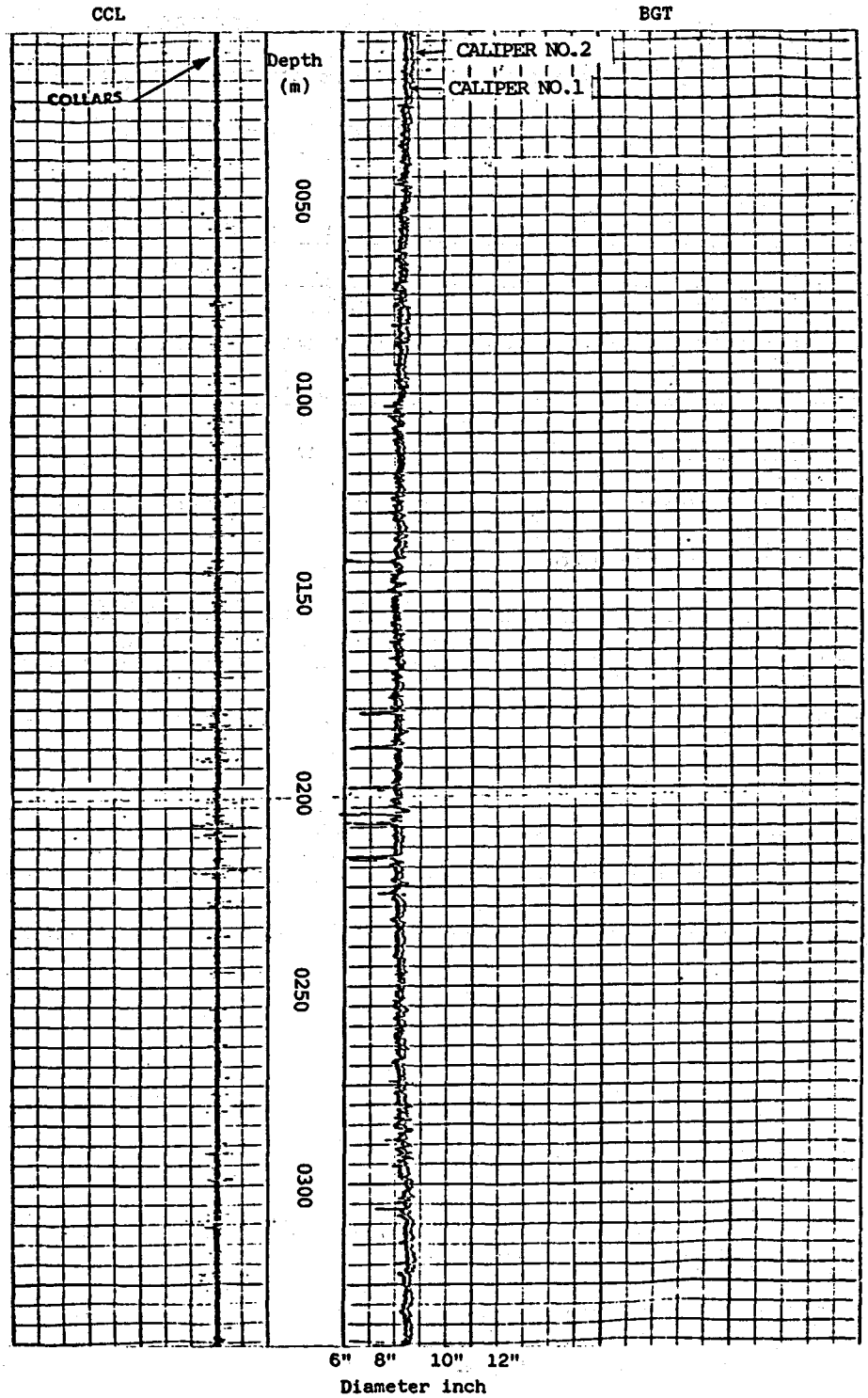

Fig. 13. Borehole geometry log.

3) - using an in-hole Küster sampler;

4) - collecting scaling samples inside and outside the pipes;

5) - deviating the two phase flow on a bypass and closing at the same time two valves.

The results of the chemical analyses are very different, depending on the type of sampling used. It must be remembered that the well produced a two-phase mixture of steam, brine and gas. For example, the samples collected with the bottle method of 1) did not always reflect the real conditions in the pipeline, as in some cases the gas phase was predominant in the sample and in others the liquid phases.
Downhole sampling, as in 3), was difficult because the high temperatures destroyed the o-ring seals of the sampler. Hence , the most reliable samples were those collected downstream of the weir, 2), although the total concentration were affected by evaporation and by inaccurate measurements of the flow-rate of the diluting water.
The unreliable results of the fifth method may be due to the fact that the valves were not shut at the exact same time.
The results of the chemical analysis of the two productions tests are quite different, the main uncertainty lying in the Na/K ratio determination.
However the average composition of the brine can be represented as shown in table 1.

TABLE 1

CHEMICAL COMPOSITION OF BRINE IN mg/l

Ca^{++}	∿ 200	Cs^{+}	∿ 30
Mg^{++}	∿ 20	As^{+++}	∿ 15
Na^{+}	∿ 60000	Cl^{-}	∿ 27500
K^{+}	∿ 80000	SO_4^{--}	∿ 186000
Li^{+}	∿ 220	HCO_3^{-}	∿ 2500
$Fe^{+2/+3}$	∿ 1.5	H_3BO_3	∿ 7500
NH_4^{+}	∿ 30	SiO_2	∿ 120
Rb^{+}	∿ 400	TDS	∿ 364000

The gas produced from the well was sampled downstream of the separator on steam line and was mainly carbon dioxide, whereas H_2S was absent (see Table 2).

TABLE 2

CHEMICAL COMPOSITION OF GAS (WEIGHT PERCENTAGE)

H_2S	—	N_2	0.5
CO_2	99.5	CH_4	traces
H_2	traces		

The scaling samples inside the pipes and separator were analyzed and revealed that the incrustations consist

mainly of $CaCO_3$.
However sodium and potassium sulphate precipitation begins whenever the brine temperature drops below ∿ 110°C. Scaling samples were collected inside the basin where temperature was ∿ 70°C. These were analyzed chemically and crystallographically. The results reveal that the incrustation consists mainly of glaserite $Na_2SO_4 \cdot 3K_2SO_4$
The figures given in Table 1 suggest that the hot brine discovered at Cesano has a particular composition, characterized by a prevalent sodium and potassium sulphate chemism and by its non-reducing property.
From these results it is clear that Cesano hot brine differs significantly from all the other thermal brines discovered to date in other parts of the world.
If we leave aside the constituents present in small quantities, the hot brine composition can be represented on a Jänecke diagram as shown in Fig. 14 (3). This diagram is drawn from published data. Using it we can easily explain the difference between the chemical analyses of the first production period, reported in (1), and the present results.
The composition of Table 1 could be represented by point A in the diagram of Fig. 14, whereas the results of the analyses reported in (2) could be represented by point B. The two point can be seen to lie on the same straight line as point G, which represents the composition of the glaserite. When a solid phase separates from a solution, the composition of the latter varies according to a straight line joining the point representing its initial composition and that of the solid phase. Hence, the solution of

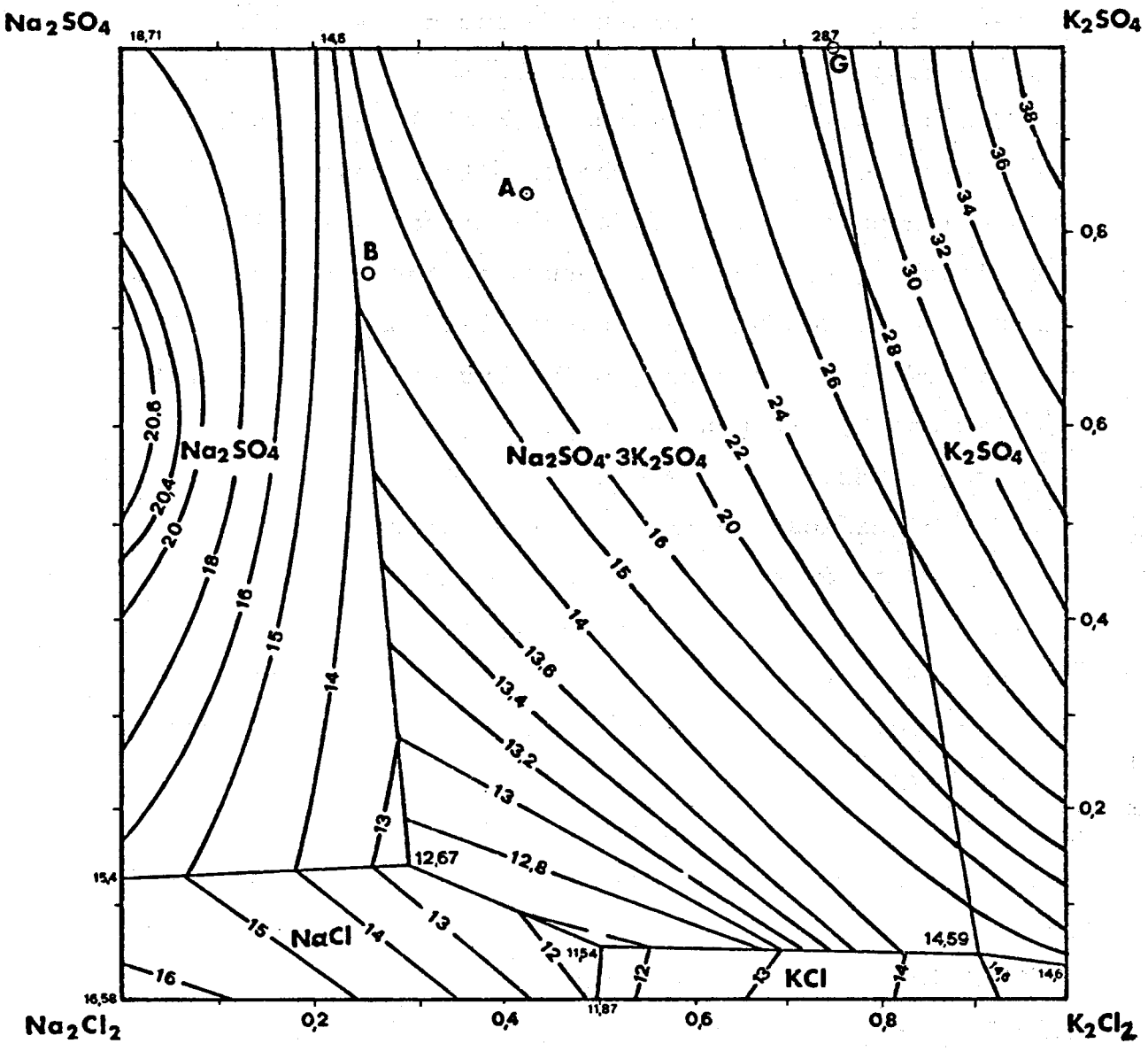

Fig. 14. Janecke's diagram at 100° C.

composition B can derive from a solution of composition A, after the glaserite has precipitated. The liquid samples of the 1975 production period were collected at atmospheric pressure when they obviously had lost most of their glaserite content. Their representative point on Jänecke's diagram thus shifted from a point A to point B. Solubility tests were also conducted on brine samples reconstructed in the laboratory. The boric acid was seen to increase the total solubility of the sodium and potassium salts (3) (4).

Finally, it should be noted that dissolved CO_2 forms about 2% of the total brine, as revealed by the gas/steam ratios measured in samples taken downstream of the separator.

5. - IN-HOLE PRESSURE AND TEMPERATURE MEASUREMENTS

In-hole pressure and temperature trends versus depth during production are given in Figs. 15 and 16.

These figures clearly show the level at which fluid evaporation begins for flow-rates of about 110 t/h.

Note that the pressure at the evaporating level is about 40 atm for a temperature of about 203°C. That is, this pressure is much higher than the steam vapour pressure as that temperature.

This phenomenon is due to the release of CO_2 from the solution and the gradual enrichment in steam of the gas phase.

Values of bottom hole static pressure were taken and plotted versus total mass produced from the well to investi-

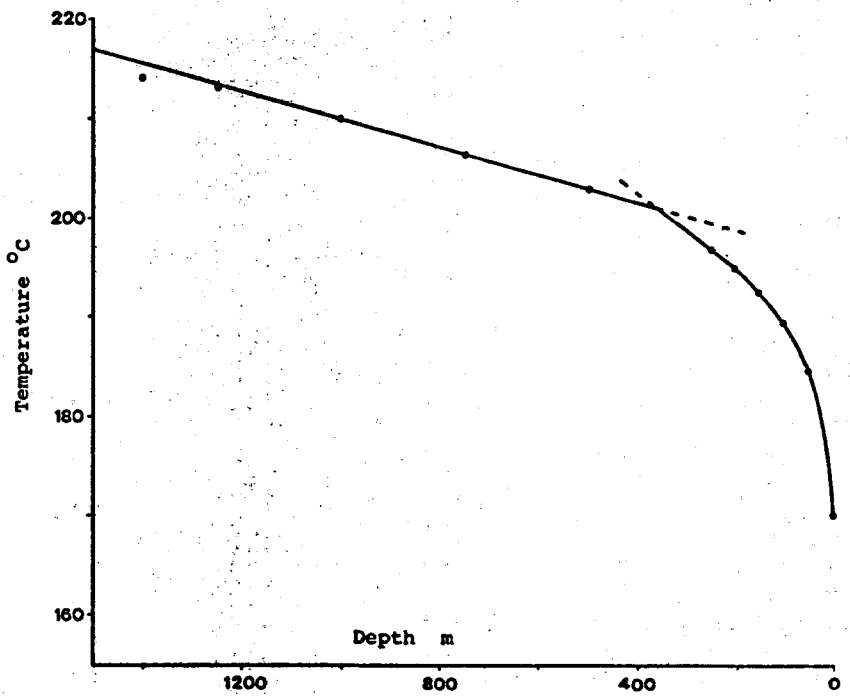

Fig. 15. In-hole temperature vs depth.

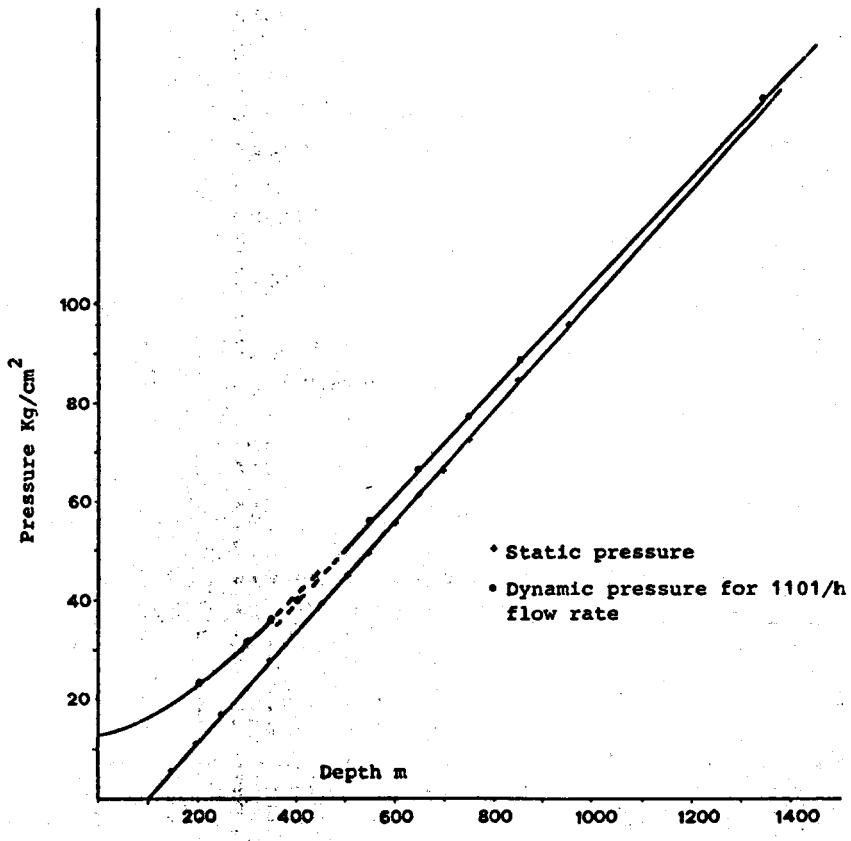

Fig. 16. In-hole pressure vs depth.

gate reservoir dimensions.

The results of the measurements indicate only that pressure drawdown is small, but, because of the inaccuracy of the instrumentation, no definitive conclusion can be drawn.

The interpretation of two pressure build-up tests after well shut-in did not add further information.

Maximum pressure build up was in fact smaller than 2 Kg/cm^2 for a mass flow-rate of ∿ 80 t/h and then comparable with instrument accuracy; however, this pressure variation is not due to skin effect after shut-in as, botton-hole pressure increases slowly.

In future these measurements are expected to improve.

At the moment no definitive conclusion can be drawn on geothermal reservoir geometry and dimension.

6. - CONCLUSION

The production tests, although short, did provide, at a low cost, an indication of the chemio-physical characteristics of the brine and production conditions.

Nevertheless the operations of this small pilot plant were made very difficult because of the incrustations and work will be required in future to improve the reliability of the measurements and to solve production problems (scaling inside the well and in the surface equipments).

However production and laboratory tests have shown that glaserite precipitation may be controlled by modifying

production conditions and diluting the brine with water. Finally, well Cesano 5 has provided a means of disposing of the waste from Cesano 1. Using the experience of past production tests, some studies have been made of the feasibility of exploiting the Cesano field for generating electricity or its potassic salts. Agronomic tests by the ANIC Company have shown that the glaserite could be used in fertilizers.

The plant, which will be described in detail in a separate report, will permit :

- long-term production from the well, by recurring to techniques for preventing scaling;
- flash steam production through special separators capable of operating in the presence of incrusting fluids;
- control of the Helical Screw Expander with concentrated brines;
- production of glaserite salt using a special crystallizyer.

Meanwhile measurements and tests will also be carried out directed at acquiring further information on Cesano reservoir.

REFERENCES

(1) - Calamai A., Cataldi R., Dall'Aglio M., Ferrara G.C., 1975 Preliminary report on the Cesano hot brine deposit (Northern Latium, Italy) - 2nd U.N. Symposium on the Development and Use of Geothermal Resources, San Francisco. Proceedings, V.1, pp. 305-313.

(2) - James R., 1970 - Factors controlling borehole performance. 1st U.N. Symposium on the Development and Utilization of Geothermal Resources, Geothermics, Sp. Iss. 2, v. 2, pt. 2, pp. 1502-1515.

(3) - Giovannini F., Nasti F., 1977 - Studio di processi di recupero di sali da salamoie naturali. Chemical Engineering Thesis, Pisa University.

SUCCESSFUL FLUID MANAGEMENT OF THE SALTON SEA RESERVOIR

Anthony J. Adduci
U. S. Department of Energy
San Francisco Operations Office

Introduction

This paper has been extracted from several reports including the final report on the Geothermal Loop Experimental Facility and discussions with several persons currently in the process of managing geothermal fluid production utilization and disposal at the Salton Sea Geothermal Reservoir.

Background

The Salton Sea Geothermal Reservoir has been known to exist for at least 15 years. It was first produced by Southern Pacific Land Co., Phillips Petroleum, Morton Salt and other firms for various reasons, one of which was the extraction of heat.

All of these original explorers found the production unprofitable due to well plugging, high total dissolved solids in the fluid and other reasons. The South Salton Sea area still has abandoned sites as evidence of these attempts.

In 1975-1976 San Diego Gas & Electric and the U.S. Department of Energy (at that time (ERDA) began a 50-50 shared cost venture on the geothermal loop experimental facility. The initial objective was to show a multi-stage (4-stage) flash binary system would extract the heat from the geothermal fluid, utilize it to make electricity and dispose of the waste water and solids.

The Magma Power Company, the geothermal resource owner, agreed to provide fluid to GLEF under a special contract with SDG&E. Magma also supplied labor, data and self funded experiments which contributed greatly to the success of the GLEF.

Initially the system would be operated to assure sufficient vapor quantities to support a 10 MW design capacity turbine generator and then the turbine-generator would be added to produce power.

In the ensuing months it was obvious that "fluid management" would become the overall objective of the GLEF.

The Salton Sea geothermal reservoir (referred to as the reservoir) yields a fluid of 375°F (190°C) at a pressure of 150 psig (11.2 atm) and a flow of 324,000 lbs/hr (146,934 Kg/hr) liquid, 64,000 lbs/hr (29,024 Kg/hr) vapor, 12,000 lbs/hr (5,442 Kg/hr) gases and 200,000 parts per million of dissolved solids (see Figure No. 1 for solids and gas details).

The facility was initially to use flow from two wells (800,000 lbs/hr or 362,800 Kg/hr) for fluid production and one well for fluid injection.

ELEMENTAL RANGE FOR WELLHEAD BRINE

	MAC-MAX NO. 1 WELL			WOOLSEY NO. 1 WELL		
ELEMENT	HIGH	LOW	AVERAGE	HIGH	LOW	AVERAGE
CI	126,000	107,000	112,800	146,000	94,000	121,000
Na	46,500	39,000	41,700	54,600	29,600	42,700
Ca	21,400	16,300	19,400	28,300	16,700	22,900
K	8,130	6,500	7,350	14,100	5,830	10,200
Mn	563	462	520	903	498	718
Sr	430	370	393	472	292	382
Zn	229	184	203	313	172	256
Si	243	159	213	236	152	204
Ba	154	111	130	195	79	142
Li	175	146	156	197	122	162
Fe	145	117	126	320	152	236
Mg	106	88.2	96.7	116	67	87
Pb	38.7	8.0	21.0	68	24	49

Note: All measurements are ppm

(NON CONDENSIBLE GASES AT WELLHEAD
DATA GENERALLY SAME FOR BOTH WELLS)

	DECEMBER 1976 % OF TOTAL GAS	AUGUST 1979 %OF TOTAL GAS
CO_2	98.14	98.92
CH_4	0.68	0.51
N_2	0.02	0.57
O_2	*ND	*ND
H_2	*ND	*ND

*ND implies none detected

Fig. 1.

The surface plant was a 4 stage flash/binary system See Fig. 2 where fluid would be flash 4 times: at 370°F (187.6°C), 165 psia (11.2 atm); 308°F (153°C), 60 psia (4.08 atm); 262°F (127.6°C), 28.3 psia (1.92 atm); and finally 221°F (104.9°C), 13.3 psia (0.90 atm). After each flash the steam was scrubbed with vertical plate steam scrubbers and then the steam (vapor) was passed through normal shell and tube heat exchangers.

The "working fluid" (fluid to be vaporized and to drive the turbine; flowed from exchanger No. 4 to exchanger No. 1 to establish the counter flow process.

The non-vaporized geothermal fluid (the liquid) was injected back into the ground and the condensate was used for cooling water make up.

During initial operation of the 4 stage flash/binary system distilled water would be the "working fluid."

The vaporized distilled water would then be replaced with a hydrocarbon prior to turbine-generator installation.

All of this planning and design was based upon preliminary testing and analysis which took place from 1973 through 1974.

Initial system start-up on 3 May 1976 encountered problems with well flow and from that point on the 4 stage flash/binary system achieved a less than 40% plant availability time.

Problems: The basic problem was poor chemical data on which the design was based; because of this a series of problems occurred, all of which are chemical in cause.

a. Scaling up of pipes, tanks, thermal wells, fluid extraction ports, valves and injection the wells

b. Materials failures and degradation in the "working fluid" heat exchangers, injection pump bearings, and in the fluid system in general

These problems were so bad that the actual heat and mass balance for the plant could not be calculated because accurate data collection was impossible due to instrument failure.

The injection of fluid though initially easy became very difficult. In order to maintain liquid disposal injection pressures were raised and formation fractures were opened. The injection pressure was then dropped until these fractures were plugged, and then the process was repeated. This practice is not acceptable since fracturing of unknown direction has many potential catastrophes associated with it.

Pipe plugging and valve inoperation was the cause of great concern at times, plus it resulted in unstable system operation at certain times.

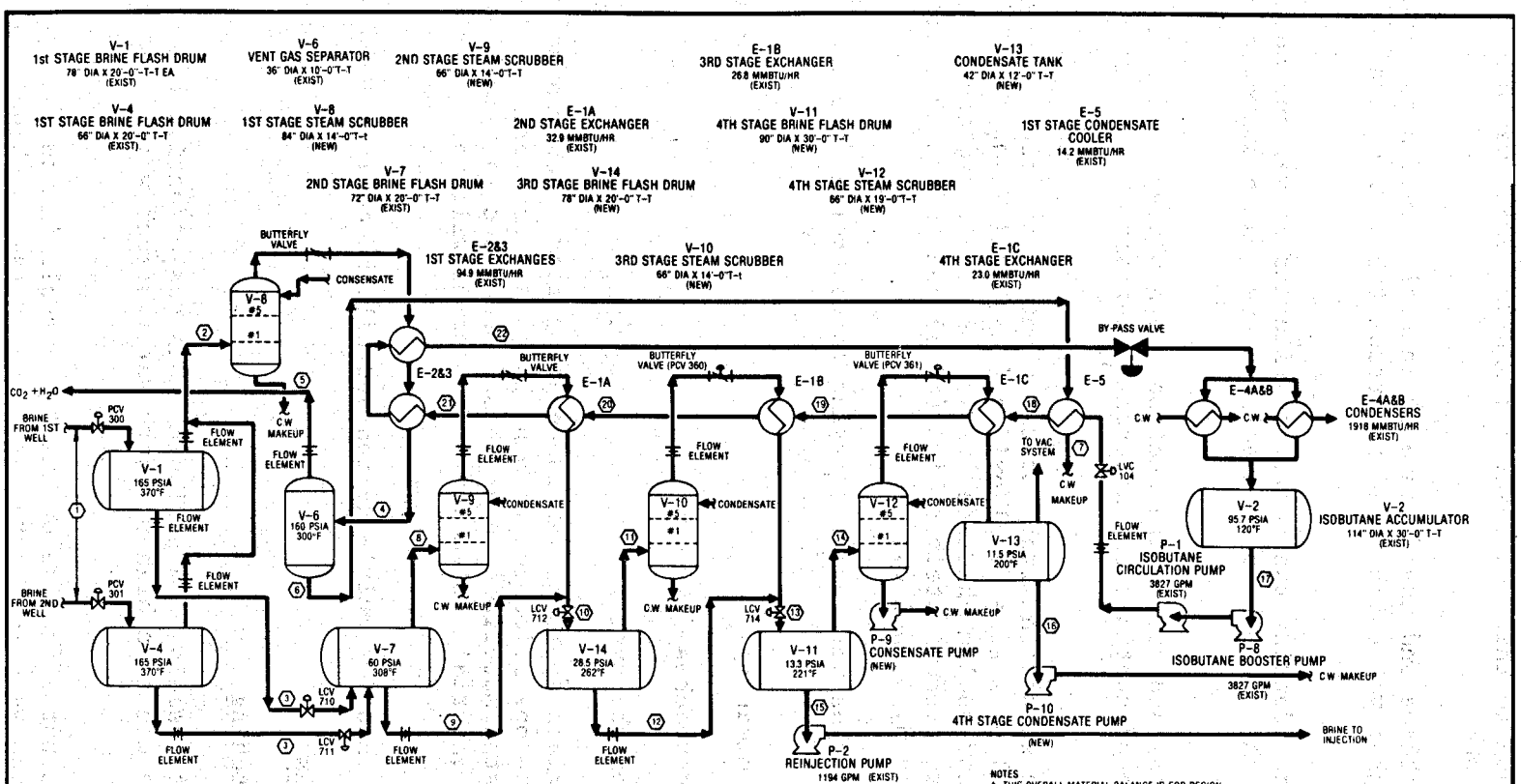

	1	2	3	4	5	6	7	8	9	10	11	12	13	14	15	16	17	18	19	20	21	22
FLUID	[illegible]	STEAM +CO_2	BRINE	COND + CO_2+H_2O	CO_2+H_2O	COND	COND	STEAM	BRINE	BRINE	STEAM	BRINE	BRINE	STEAM	BRINE	COND	i C_4	i C_4	i C_4	i C_4	i C_4	i C_4
M #/HR	800	132	668	132	307	101.3	101.3	35.9	632.1	668	28.3	639.7	668	23.6	644.4	23.6	1000	1000	1000	1000	1000	1000
GPM (ACFM)	1544	(5882)	1289	—	(786)	220	207	(4219)	1205	1250	(6852)	1197	1237	(12501)	1194	491	3827	3974	4261	4732	5755	(2884)
°F	370	370	370	300	300	300	160	293	308	262	297	262	221	207	221	200	120	143	176	211	246	300
PSIA	165	165	165	160	160	160	150	60	60	28.3	28.3	28.3	13.3	13.3	12.3	11.5	95.7	540	530	520	510	500
P_1 #/FT^3	64.6	374	64.6	—	656	57.3	61.0	142	65.4	66.8	0688	66.6	67.3	0315	67.3	68.0	32.6	31.4	29.3	26.3	21.7	5.78
MMBTU/HR	—	—	—	—	—	27.2	13.0	—	—	—	—	—	—	—	—	—	0	14.2	37.2	64.0	96.9	191.8

NOTES
1 THIS OVERALL MATERIAL BALANCE IS FOR DESIGN PURPOSE ONLY AND DO NOT NECESSARILY REPRESENT ACTUAL OPERATING CONDITIONS
2 THIS IS A PROPRIETORY PROCESS FOR WHICH A PATENT WAS APPLIED FOR

A	ISSUED FOR CUSTOMER APPROVAL	TC	IS
0	ISSUED FOR CONSTRUCTION	GEO	IS
3	INSTALLED TURBINE GEN & BY PASS VAL	DA	GL
4	REMOVED TURBINE GEN	DA	GL

NILAND TEST FACILITY
PROCESS FLOW DIAGRAM
SAN DIEGO GAS & ELECTRIC CO.
MORA
JRB
9-16-74
7429-0 3201
0

Fig. 2. GLEF process schematic four stage flash/Binary cycle.

Along with the fluid problems there were chemistry problems with the cooling water which caused corrosion of the shell and tube condensers. This problem however was not unique to this sea reservoir and therefore was considered as of secondary importance.

Because of these problems and the failure of initial solution to solve these problems a test program was established to attack the scaling and the materials problems.

The first item was to identify the scale constituents at various points in the plant to define the methods to be used in a systematic approach to solving the problem.

Also, material coupons and small pipe sections were placed in the system to determine if the use of coatings or different materials would reduce scaling and/or corrosion.

The scaling analysis showed the front of the plant to contain a heavy metal sulfide (FeS and PbS) plus some metal oxides (Fe_2O_3 and Fe_3O_4) plus silica (SiO_2) and sodium chloride (NaCl). As the fluid ended its journey the scale was predominately silica (SiO_2) and sodium chloride (NaCl). (See Figures 3, 4, 5 & 6.)

Three separate approaches were used in trying to control/manage the scaling problem.

a. Mechanical cleaning

b. Chemical approaches

c. Re-design of the system

(The alternate materials approach was an on-going test which was not to be incorporated into the operation due to many factors. However, the data on the worth of the tested materials under these conditions is valuable to future plant design materials selection. This paper will not cover materials test results.)

Each of these approaches was multi-faceted and will be handled separately.

Mechanical Approaches

Hydroblasting & etching

The hydroblasting of vessels on a periodic basis was effective but costly. Hydroblasting is the use of a high pressure water stream which physically removes the scale.

The initial test was not effective on the tough scale in the 1st and 2nd stage steam separation vessels. After acid and/or base etching of the scale the hydroblasting was effective. The expense of hydroblasting was high, and therefore the frequent use of this procedure was not recommended.

Date	5/23/77	5/23/77	5/23/77
Location	Below Fluid Level	Floor Debris	Venturi On Outlet
Thickness	0.3-0.5 cm	0.1-2 cm	0.2-0.5 cm
General Appearance Color	redish-brown black porous	black formed by particle conglomeration	black very hard
	Wt%	Wt%	Wt%
Fe	25.25	24.20	22.55
Cu	0.18	0.30	0.21
Zn	0.07	0.15	0.09
Mn	1.53	1.07	1.78
Pb	0.91	8.25	5.60
Ca	1.50	0.85	1.10
Al	0.89	1.64	1.15
Si	16.65	16.65	16.10
Ba	0.13	0.08	1.60
Mg	0.11	0.12	0.08
Na	2.50	0.46	0.78
Co_3	*ND	*ND	*ND
S as $S^{=}$	0.25	1.55	0.97

*ND implies none detected

Fig. 3. First stage separator scale.

Date	5/23/77	5/23/77	5/23/77
Location	Well below Fluid Level	Floor Debris	Venturi On Outlet
Thickness	0.18-1.8 cm	to 2.5 cm	0.7 mm
General Appearance Color	black multi-layered	porous grains built on central portion black	hard black
	Wt%	Wt%	Wt%
Fe	25.55	23.85	21.25
Cu	0.13	0.10	0.50
Zn	0.14	0.22	0.10
Mn	1.10	1.23	2.37
Pb	0.08	.52	0.05
Ca	2.10	1.15	1.15
Al	0.85	0.75	1.15
Si	17.85	19.20	19.65
Ba	1.04	0.81	0.42
Mg	0.05	0.65	0.43
Na	3.25	1.40	2.05
Co_3	*ND	*ND	*ND
S	0.45	0.51	0.23

*ND implies none detected

Fig. 4. Second stage separator scale.

Date	5/23/77	5/23/77	5/23/77
Location	Well below Fluid Level	Floor Debris	Venturi On Outlet
Thickness	0.5-1 cm	to 2 cm	1.5 cm
General Appearance Color	porous yet hard	porous black	hard multi-layered black, green
	Wt%	Wt%	Wt%
Fe	16.65	21.60	3.10
Cu	0.16	0.74	0.41
Zn	0.26	0.16	0.06
Mn	1.07	1.45	0.36
Pb	0.51	0.93	0.26
Ca	1.45	0.95	1.55
Al	0.61	0.87	0.24
Si	18.30	18.70	34.15
Ba	1.20	1.10	0.18
Mg	0.31	0.37	0.12
Na	2.95	1.00	2.60
Co_3	*ND	*ND	*ND
S	1.26	1.55	0.18

*ND implies none detected

Fig. 5. Third stage separator scale.

Date	5/27/77	5/27/77	5/27/77
Location	Flash Vessel Wall	P-2 Suction Inlet to First Impeller	P-2 Casing
Thickness	0.5 cm	0.6-1 cm	
General Appearance Color	light olive soft	hard black ochre film	soft porous gray
	Wt%	Wt%	Wt%
Fe	2.95	1.70	2.10
Cu	0.21	19.80	0.24
Zn	0.09	0.09	0.10
Mn	0.24	0.25	0.30
Pb	0.22	0.63	0.18
Ca	0.85	0.55	0.40
Al	0.13	0.28	0.41
Si	31.80	28.70	38.75
Ba	4.10	0.60	1.25
Mg	0.26	0.27	0.47
Na	0.55	0.26	0.20
Co_3	*ND	*ND	*ND
S	1.20	0.40	0.77

*ND implies none detected

Fig. 6. Fourth stage separator and injection pump scale.

(After the plant re-design, however, the scale was not as well attached to the metal surface and thus the need for acid or base etching was eliminated.)

In conclusion, hydroblasting is the most effective method of scale removal during scheduled maintenance down times.

On Line Hydroblasting or Cavitation Cleaning

This is a system where high pressure water is forced through a nozzle. The water has air bubbles which expand past the nozzle; the bubbles burst at the surface of the scale setting up a shock wave and dislodge the scale from the surface on which it formed.

Cavitation cleaning was performed periodically while the plant was operating to remove scale buildup. The procedure was to connect a high pressure water line to the nozzle connection exterior to the geothermal fluid system and flow the high pressure water thru the nozzle to perform the cavitation cleaning.

Three types of removals were tried. The first was in a straight pipe, the second was on valve seats and the third was in a thermal well.

The first two tests were inconclusive as to results due to technical problems with the support equipment. Specifically, the water pressure required for adequate cleaning was not available due to lighter than required hoses and connectors; before this could be corrected the GLEF operation was terminated.

The thermal well test had excellent results. The thermal well was cleaned at 7 day intervals. The temperature instrument reading was higher after each cleaning. Upon plant shutdown, the examination of the thermal well showed definite effects of cavitation cleaning. The scale was gone at the cleaning points and approximately 1 cm. thick in other areas of the well.

In conclusion, even though on-line cavitation cleaning had marginal results it does have potential for being an effective scale removal process. (In my opinion, cavitation cleaning efficiency is a function of the distance of the nozzle from the surface to be cleaned and the water pressure applied. In the reported results, as the distance increases the pressure to the nozzle increases exponentially. This pressure increase causes high support equipment costs to clean components where the nozzles have long distances from the nozzle tip to the surface where the scale is formed.)

"Pigging" of lines for Off Line Plant Cleaning

The operation of "pigging" is the forcing of a projectile through a pipe in order to scrape the sides of the pipe and remove the scale.

The "pigging" process was successful when using a wire brush pig (See Fig. 7) against moist silca scale deposits. However, when the silica scale dries and hardens the pigging operation is not effective.

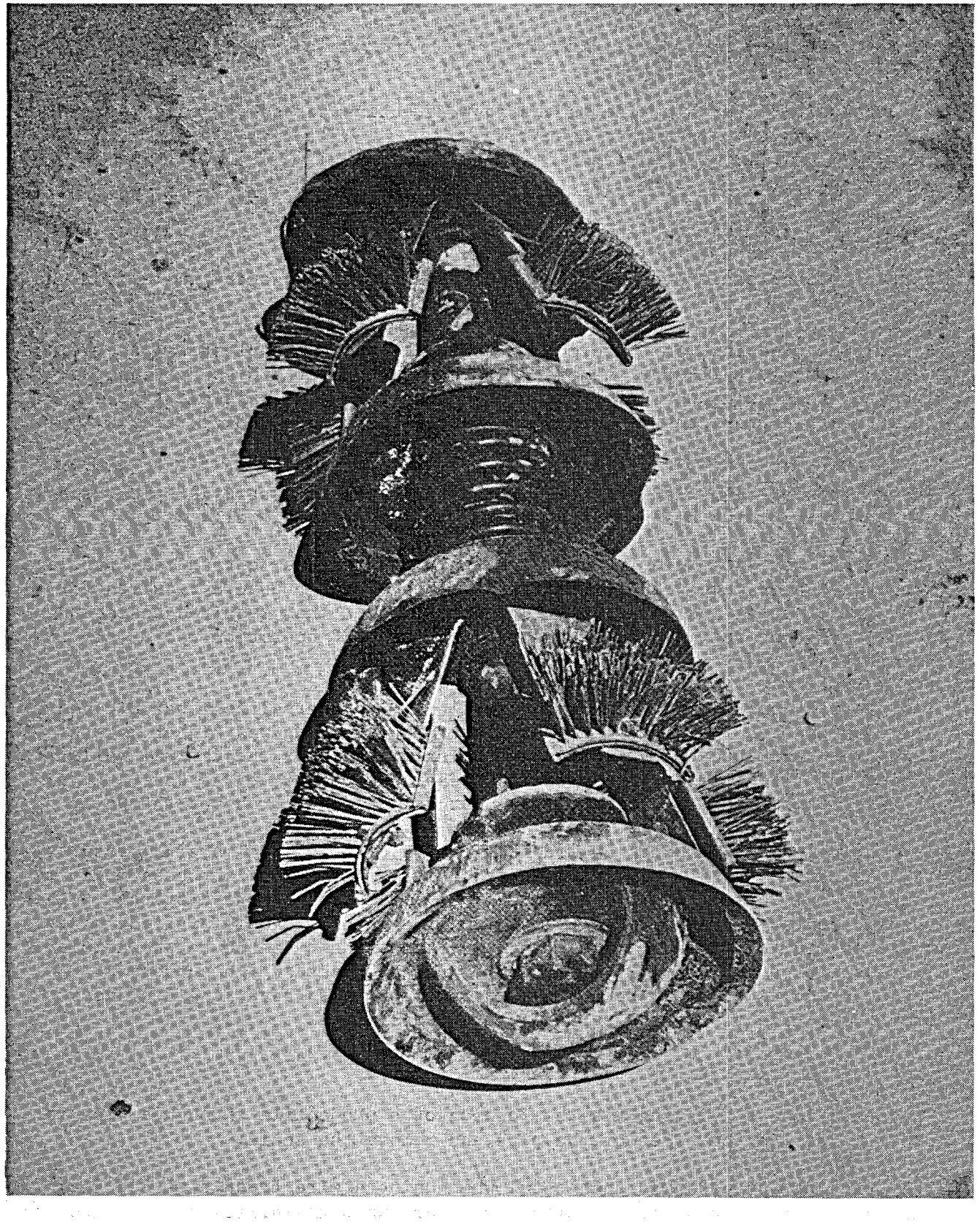

Fig. 7. T.D. Williamson wire brush pig (used).

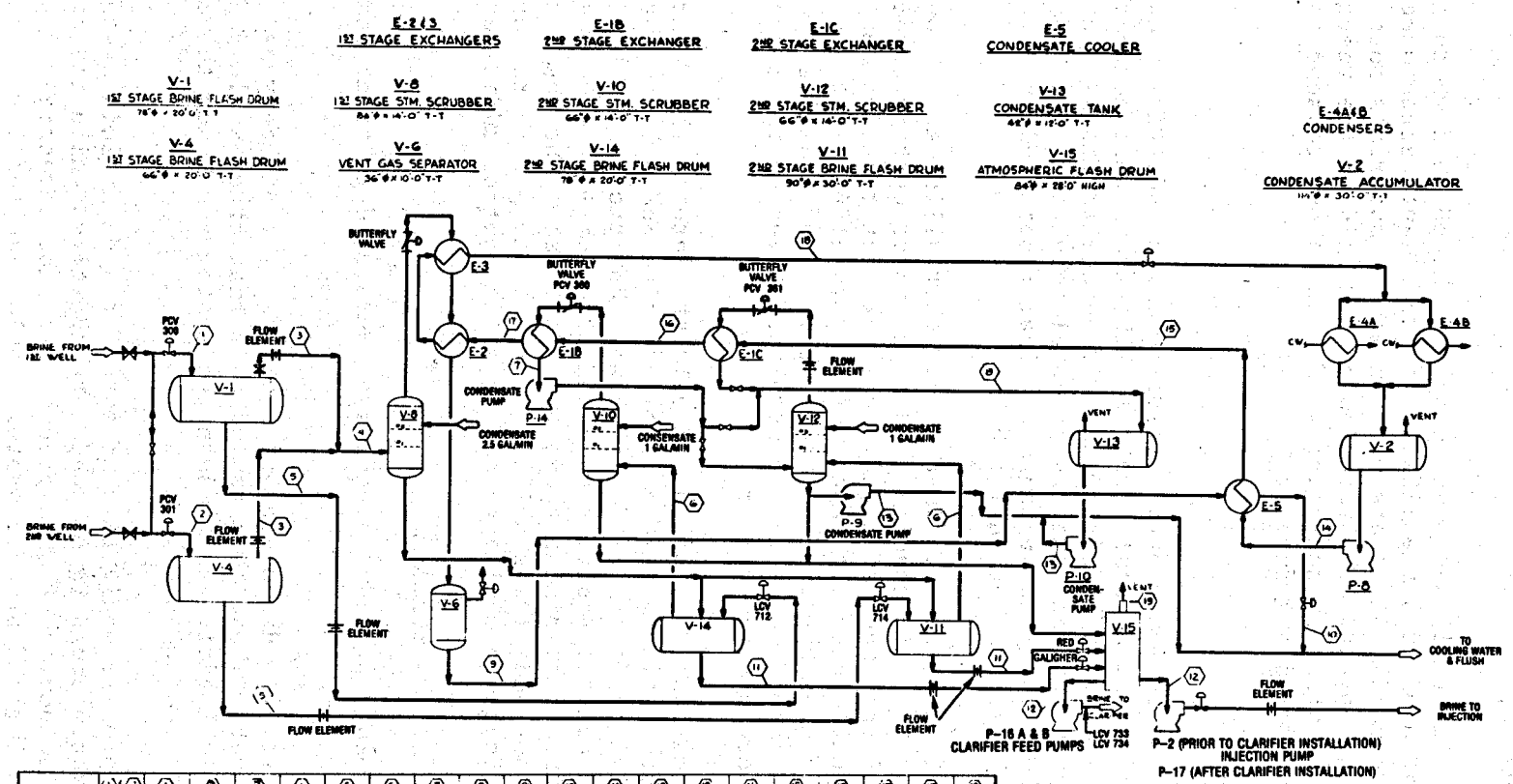

	(1)(4)	(7)	(8)	(3)	(6)	(5)	(6)	(7)	(8)	(9)	(10)	(11)	(12)	(13)	(14)	(15)	(16)	(17)	(18)	(19)
FLUID	TOTAL BRINE	BRINE	BRINE	STEAM	STEAM	BRINE	STEAM	STEAM CONDENSATE	STEAM CONDENSATE	STEAM CONDENSATE	STEAM CONDENSATE	BRINE	BRINE	STEAM CONDENSATE	WATER	WATER	WATER	WATER	WATER	STEAM
M LBS/HR	800	400	400	51.6	103.2	349.4	35.9	35.9	35.9	103.2	103.2	312.5	218	71.8	800	800	800	800	800	7.1
GPM (6)	1266	633	633	-		553		71.8	71.8	206	206	565	1117	144	1600	600	600	600	445	
STEAM M LBS/HR	103.2	51.6	51.6	51.6	103.2		35.9							(6)					77.600	
°F	363	363	363	363	363	363	232	212	212	340	110	242	228	212	90	121	98	206	228	228
PSIA	130	130	130	130	130	130	21	20	ATMOS	125	115	20	ATMOS	150					20	ATMOS
MM BTU/HR	1198	154.9	154.9	61.5	123.0	93.4	41.9	6.5	6.5	32.2	5.0	52.6	37.0	12.9	46.4	70.6	105.8	140.7	231.6	8.7

A	ISSUED FOR CUSTOMER APPROVAL
B	REVISED & REISSUED FOR APPROVAL
C	RE. SEQ & REVISED FOR APPROVAL
D	ADD STEAM TAPS & REVISED
E	REVISED STEAM TAPS AS INDICATED,

Fig. 8. GLEF two stage flash binary process flow diagram.

Chemical Scale Control

Acidification of the fluid: Fluid acidification was successful but had many disadvantages.

First, hydrochloric acid (HCl) was used to adjust the pH to 3 which is not economic. Second, at a pH of 3 the lifetime of the plant carbon steel piping is severely reduced. Alternate very expensive materials must be utilized in the surface plant. The reaction of the acid on the reservoir and injection well was also not acceptable. For the above reasons this solution was not considered any further.

Chemical Additives

Under a long and comprehensive program several chemical additives (over 65 in all) were tested for silica scale control. The tests were conducted at different temperatures and at differing additive concentrations. The details of these experiments and the experimental results are too numerous to mention here. They are given in the GLEF final report and in several reports by Lawrence Livermore National Lab.

Conclusions reached from these experiments were that silica scale control could be achieved with certain chemical additives under certain conditions. However, since all of the successful additives were not tested under all conditions (due to GLEF closure in Sept. 1979) it is difficult to totally assess the worthiness of a specific additive or group of additives. The question of the effects of these scale control additives on the injection well and reservoir were not investigated.

As a matter of information: one of the experiments late in the Program was to combine a successful silica scale control additive and a known carbonate scale control additive to determine if there were any problems with interference of one scale control additive with the other or if there were any other detrimental affects by mixing these two additives. The results showed no difference in either additive's ability to function, and there were no other detrimental effects in mixing these two scale control additives.

Chemical Leaching to Remove Scale

Using standard minerology procedures additives were used to treat scale already in place.

The results showed definite dissolving of scales almost directly as minerology texts direct. These results indicate that after scale deposition the use of minerological additives to wash the system and leach the metals will loosen and dissolve the scale.

Conclusion: Such a process would be successful if a dual fluid system was built so that one system could be flushed with additives while the other loop operated. The economics of this process were not investigated but it would appear that dual fluid process systems would make the idea uneconomic. However, if the metal recovery were to be profitable an entirely new economic picture would need study.

Mechanical Re-Design

This was accomplished to decrease scale especially in the lower temperature process areas and to decrease the complexity of a 4 stage flash/binary system.

Rather than treating this under the scaling treatment section it will be covered under the next sections.

2 Stage Flash/Binary System

In 1978 the plant was redesigned from the 4 stage flash/binary system to 2, 2 stage flash/binary systems (named train A and train B) both capable of 400,000 gal/min flow each. The steam separator, scrubber, heat exchanger scheme was kept intact. (See Fig. 8)

The first stage flash was at 363° F (183.7° C) and a pressure of 130 psia (8.84 atm), the second stage flash was at 242° F (116.5° C) at a pressure of 20 psia (1.37 atm). There were two additions to the system, the first was an atmospheric flash tank where the un-flash liquid constituent was brought to atmospheric pressure. The second addition was a clarifier/sand filter system for processing the unflushed liquid effluent prior to injection. (The clarifier system will be discussed under injection fluid treatment.)

The result of the re-design was a slight loss of heat extraction efficiency but a plant availablility factor of over 60%. This was an increase of over 20% in plant availability over the 4 stage flash/binary system.

As stated before another reason why the 2 stage flash/binary system was installed was to reduce or aid in scale control. The new system did have that effect. First it reduced the tenacity of the scale in the first stage steam separator tanks by making it more brittle and susceptible to hydro-blasting without etching as mentioned earlier.

Second, it reduced the quantity of scale in the 2nd stage flash tank and transferred most of the (silica) scale to the atmospheric flash tank and downstream piping leading to the Clarifier system. This positioning of the scale made it much easier to manage than when it was spread through the last two stages of the 4 stage flash/binary system.

Conclusion: The 2 stage flash/binary system appears to be the most acceptable plant scheme for this type of high salinity - high dissolved solid type of reservoir.

INJECTION TREATMENT AND OPERATION

As stated earlier liquid injection was at best troublesome and erratic. In order to keep the plant in operation waste liquid on occasion had to be stored while an injection well was overhauled so that it would again accept fluid.

In investigating this problem it was found that silica was the cause of the problem.

Silica precipitation is a sluggish reaction. As the temperature declines for a silica laden solution the silica is slow to come to a saturation equilibrium and therefore appears as a super-saturated liquid for a period of time.

In the injection process a silica laden solution has been dropped in temperature relatively quickly going through the plant system. Silica has precipitated, but the injection liquid is still super-saturated with silica. When the super-saturated liquid is injected and meets the reservoir face in the injection well the silica precipitates to achieve a saturated solution state. The silica precipitate blocks the reservoir pores from accepting liquid and causes the rise in injection pressure.

The solution to the problem was obvious. Treat the injection liquid so that silica saturation and not super saturation is present prior to injection.

Detention and settling was the first idea tried but the resulting injection liquid was still super-saturated (although not to as great an extent) with silica and the settling tanks were difficult to keep clean on a continuous process basis.

Flocculation with chemical additives was tried but the experimental results showed that the best flocking agent was precipitated silica.

In early 1978, the Magma Power Co. and the Envirotech Corps. began pilot experiments using a sewage sludge type reactor/clarifier to remove silica. The results were very successful bringing the suspended solids from 180 p.p.m. (parts per million) to 100 p.p.m. The silica in solution was also dropped from 390 p.p.m. to 200 p.p.m. The clarifier effluent was then filtered through a dual media filter and an injection liquid of 4-10 p.p.m. and a suspended silica content of 192 p.p.m. was ready for injection.

Based upon these results a system was designed using a reactor clarifier, a dual media sand filter, a thickener, a filter press and a holding tank for filter back wash. The construction was begun in late 1978, but the system was not started up until May 1979 due to several construction delays. (Fig. 9)

The theory on why the clarifier system operates is as follows:

Silica is a slow precipitator as mentioned before.

Also, as found in the flocking tests, silica is its own best flocking agent because the precipitated silica provides nucleation sites for further silica precipitation.

The reactor clarifier takes in account both of these phenomena by the use of 3 concentric tubes within the clarifier/reactor tank (Fig. 10). The center tube is the reactor where the precipitated silica is pulled up from the tank

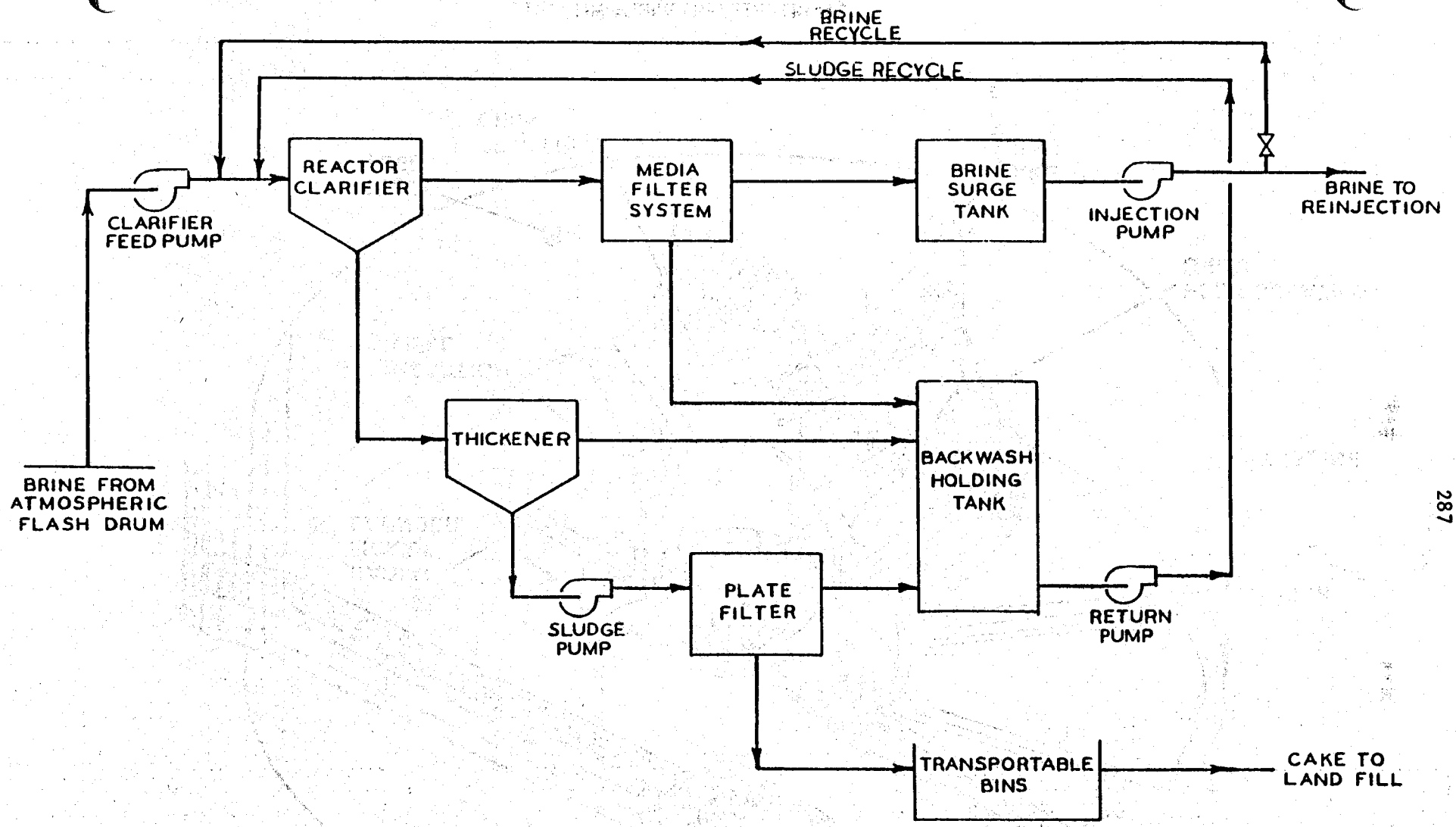

Fig. 9. Clarifier/filter installation process flow diagram.

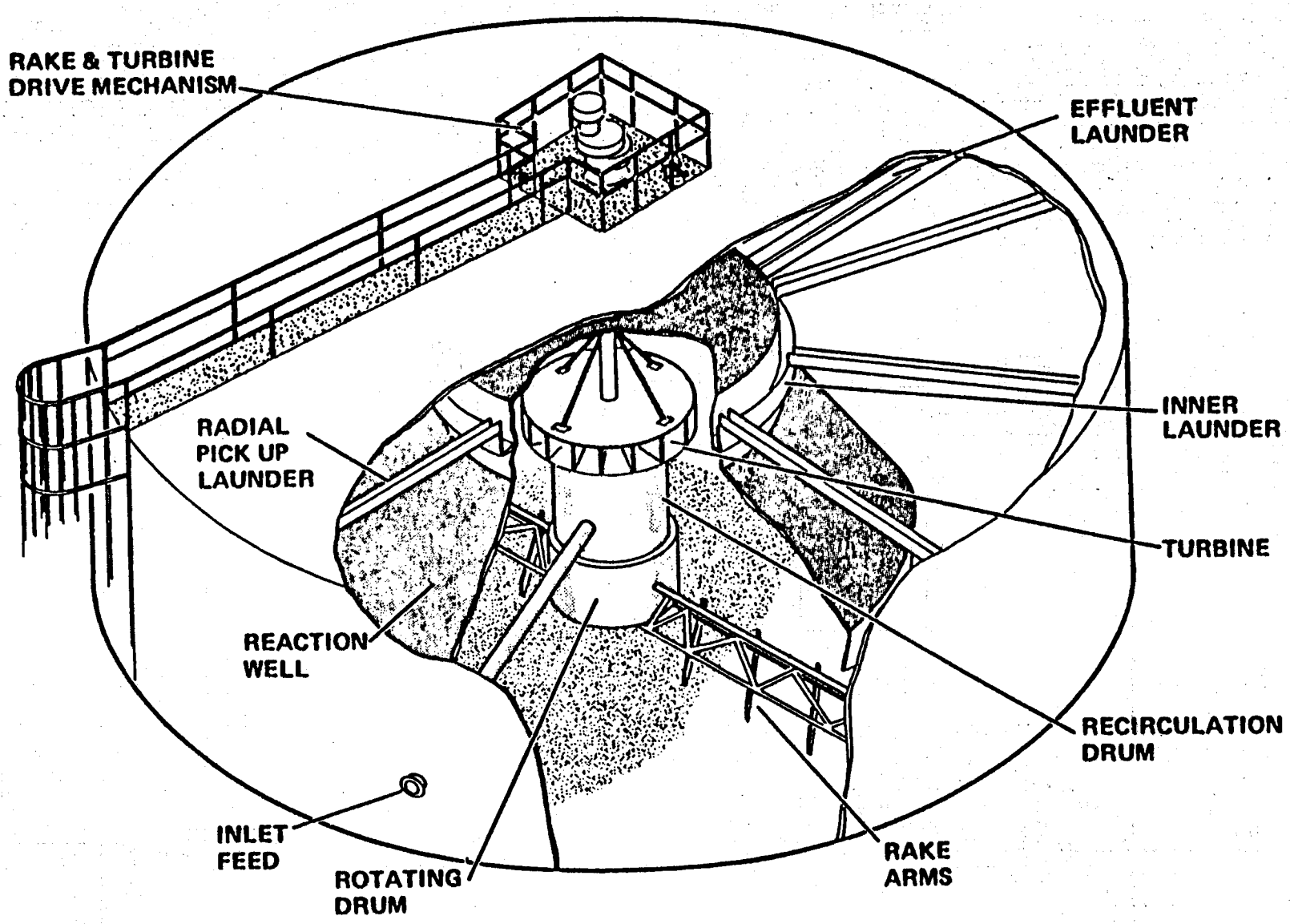

Fig. 10. Reactor/clarifier.

bottom and mixed with the new discharge liquid. The mixture then flows over the top of the first tube into the second tube where now the reaction of the silica in solution and the solid takes place. The precipitated silica slowly settles to the bottom. In the third tube the liquid rises leaving the solid silica on the bottom of the tank to be used for further precipitation. The excess solid silica is extracted for de-watering by a thickener and prepared for disposal by a filter press.

The other system components such as the sand filter and filter back wash holding tank are self explanatory. Also the liquid from the thickener & filter press are placed in the back wash holding tank.

The liquid in the back wash holding tank is returned to the clairifier/ reactor for processing.

As usual, there were problems in system start up. The first was poor instrumentation and control, the next was optimizing the time the liquid spent in the reaction and clarification zones to assure complete reaction and adequate settling. Upon resolution of these problems the clarifier worked as designed.

The next problem to arise was the identification of heavy metal oxides in the injection liquid. The cause was air leakage into the clarifier thus allowing reaction with the metal ions not precipitated before in the system. The sealing of air intrusion to the feed back loop and clarifier remedied this problem.

The entire clarifier system operated from June '79 to Mid Sept. '79 and totaled less than 1000 hrs. of operation. This system proved its ability to clean the injection liquid as preliminary experiments had indicated. However, due to this short operating time of the system the long term capability of the system is still questionable. If the experiment had operated for 6 to 9 months without problems then the clarifier system would be a proven entity, but because of this short operation there is nothing which can be said about the system life with any confidence.

After the Sept. '79 shutdown the clarifier/reactor system was examined. There was no scale of any type on any of the system parts. The only apparent wear was some corrosion on the interior walls of the clarifier tank. This is easily remedied by coating the vessel inside.

As a matter of information, a silica scale control additive was tested in the operating clarifier system. The results showed the additives worked upstream of the clarifier and yet had no effect on the function of the clarifier/reactor system.

There are other injection liquid clean up schemes or methods to circumvent the silica precipitation problem which were not tried at the GLEF.

One of these methods which was not tried was "hot injection".

Hot injection involves taking only a portion of the available heat out of the produced fluid and then injecting it in order to keep silica in solution.

GLEF did not try this scheme for two reasons. First, it did not appear reasonable to give away this heat which was difficult to get; and second, it appeared that the precipitates which appear at higher temperatures (heavy metal sulfides) would cause injection plugging if the silica did not.

Other firms working with this reservoir have tried "hot injection" and have had injection well plugging problems for the reason mentioned above.

The conclusion reached therefore at the GLEF and by other firms trying to produce the Salton Sea reservoir is that the only method of cleaning liquid for injection into this reservoir is a reactor clarifier sand filter type system.

There are ,at the present time, firms in the process of expanding the use of the reactor clarifier principles to apply it to flash vessels. Also other firms are investigating methods of accelerating clarification by using new flocculating chemicals. If this is achieved the capital cost of the clarifier system can be reduced. Both of these experiments are on going and privately funded.

At this point I would like to conclude this paper since all of the major items leading to the success of the GLEF have been discussed.

CONCLUSION

In summary, the following items have been accomplished by GLEF:

a. The use of a 2 stage flash/binary system is best for this reservoir and others of similar chemistry. Although it is not as thermodynamically efficient, it is in operation 20% more of the time than the more thermally efficient 4 stage flash/binary system.

b. Off line cleaning can be accomplished within economic bounds by using hydroblasting or chemical leaching with a dual fluid system.

c. On line cleaning and scale control chemicals still require development before they are ready for operational use.

d. Injection liquid processing of a silica dominated reservoir is practically and economically accomplished by using a clarifier/sand filter system.

Based upon the GLEF work the Salton Sea reservoir will give rise to at least 170 MW of power in the next seven years.

This means that high salinity, high total dissolved solids silica dominated reservoirs can operate economically.

DESIGN AND CONSTRUCTION OF A PILOT PLANT FOR UTILIZATION OF CESANO BRINE

G.Allegrini and G. Nardini

Introduction

On the base of conclusions obtained from a preceding study and experimental runs carried out on Cesano 1 well, a pilot plant has been designed and its assembly is foreseen to be accomplished in the present year.

A brief description of two possible processes for chemical and energetical exploitation of the resource is given.

Afterwards the type of flow of the brine has been characterized (annular and dispersed flow) and consequently choice criteria for separators have been given.

An equipment flow diagram, including regulation and control systems, is reported; choice criteria for instrumentation and regulation valves are suggested.

Geofluid characteristics

For a better comprehension of the following considerations, the chemical characteristics of Cesano 1 brine are given in Table 1.

As the ions present in the solution are mainly Na^+, K^+, Cl^-, SO_4^{--}, the saline system can be considered as a system of four reciprocate salts: NaCl, KCl, Na_2SO_4, K_2SO_4. In such a way it is possible to use literature data for system K^+, Na^+, Cl^-, SO_4^{--}, H_2O and to utilise Janecke diagrams for studying the path of different processes which can be proposed.

The Janecke diagram at 75°C is reported in Fig. 1.

Point A represents initial composition of brine and number associates with each point gives "H_2O moles/Salt moles" ratio at saturation conditions.

Table 1

Chemical Characteristics of Cesano 1 brine

Chemical constituents		p.p.m.	Dissolved gases		p.p.m.
Calcium	Ca^{++}	208	Ammonia	NH_3	86
Magnesium	Mg^{++}	27,1	Hydrogen sulfide	H_2S	Ass.
Sodium	Na^{+}	51000	Carbon dioxide	CO_2	1650
Potassium	K^{+}	64000	Boric Acid	H_3BO_3	+5800
Lithium	Li^{+}	165	Cesium	Cs	42
Iron	Fe^{++} + $+Fe^{+++}$	4,5	Arsenic	As	4,3
Ammonium	NH_4^{+}	90			
Rubidium	Rb^{+}	280			
Mercury	Hg	0,0030			
Bicarbonate	HCO_3^{-}	2290			
Metaboric acid	BO_2^{-}	4000			
Chloride	Cl	20000			
Sulfate	SO_4	140000			
Silica	SIO_2	113			
	F^{-}	55			

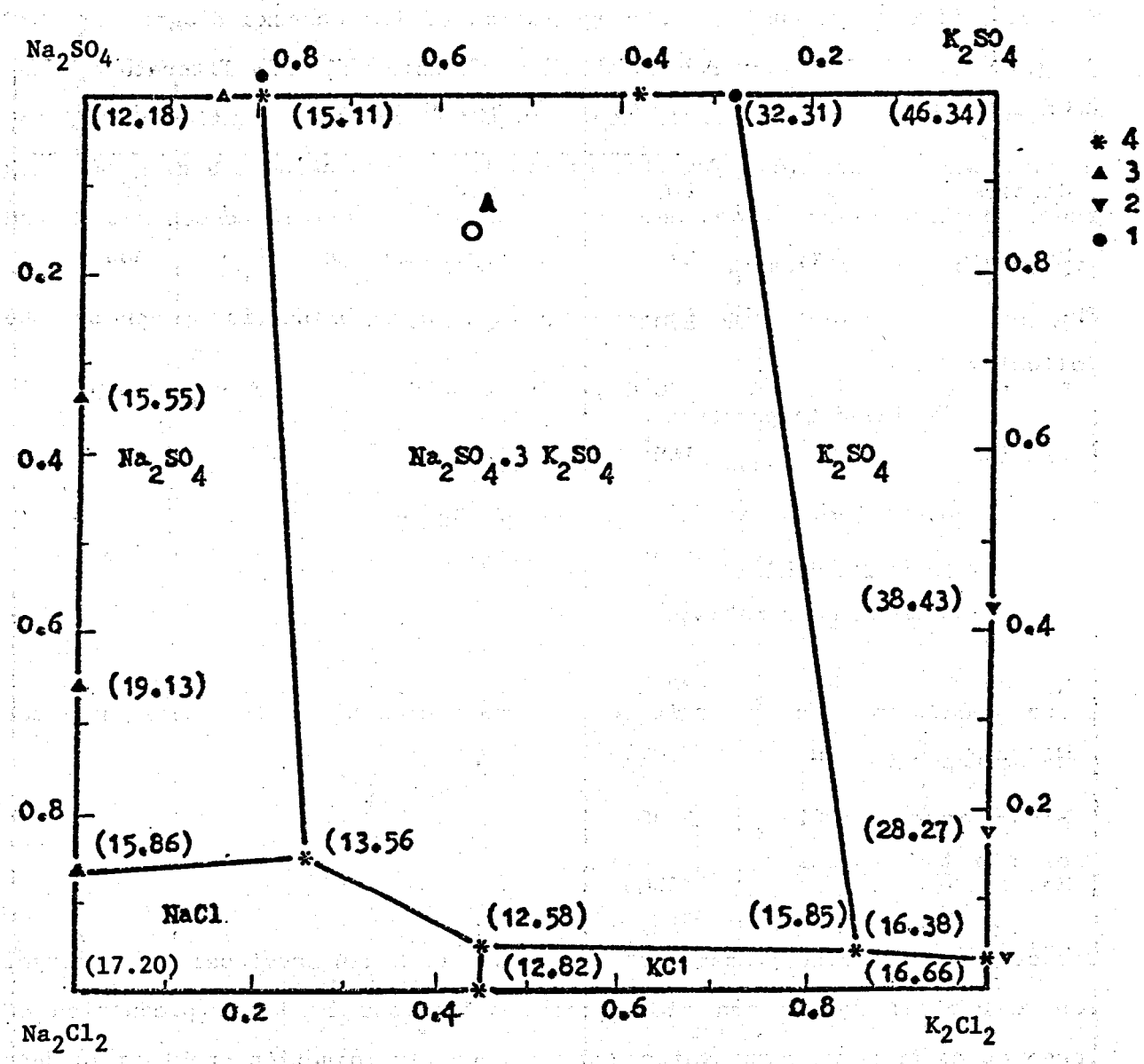

Fig. 1. Janecke diagram at 75°C.

In Table 2 data relative to considered Janecke diagram are given. Other data on the Na - K - SO_4 - Cl system equilibria are given in literature (4-12).
A qualitative tridimensional representation of the Janecke diagram at 75°C is given in Fig. 2; such representation was obtained from literature data, knowing the water content present in the saturated solution along the diagram borders and in a few characteristic points inside the diagram. This representation gives a good help to the comprehension of concentration and crystallisation processes.
The physical characterisation of the Cesano 1 brine is given by the following data

Wellhead temperature	185°C
" pressure	125 bar
Overall mass rate	27 Kg/sec.
Vapor mass rate / Overall mass rate	0,51

These conditions can be assumed as input conditions for designing the process apparatus.

Choice of the process

Use of Cesano 1 brine, whose chemical composition has previously been given, for electrical and/or non electrical applications leads to production of large quantities of waste water and consequently injection problems in deep wells arise.
As a large quantity of salts crystallizes after cooling due to brine energetical exploitation, addition of fresh water shall have to be provided. A process which allows a salts recovery together with a reduction of waste water should offer many advantages for integral use of this resource.
Many alternative processes for salts recovery have been considered (13-14),

Table 2

Data relative to Janecke diagram at 75°C

References	Solid phase	grams for 100 grams of saturated solution				Molar Ratio				H_2O moles / Salt moles	$\sum Na_2^{++}$	$\sum K_2^{++}$	$\sum Cl_2^{=}$	$\sum SO_4^{=}$
		NaCl	KCl	Na_2SO_4	K_2SO_4	Na_2Cl_2	K_2Cl_2	Na_2SO_4	K_2SO_4					
1	N+G			27.84	7.38			0.822	0.178	15.11	0.822	0.178		1
"	K+G			5.64	16.43			0.296	0.704	32.31	0.296	0.704		1
2	K		10.00		8.77		0.571		0.429	38.43		1	0.571	0.429
"	K		18.70		4.47		0.830		0.170	28.27		1	0.830	0.170
"	Ka+K		32.30		1.42		0.964		0.036	16.39		1	0.964	0.036
3	N+Na	25.3		4.95		0.861		0.139		15.42	1		0.861	0.139
"	N	16.5		10.2		0.663		0.337		19.13	1		0.663	0.337
"	N	7.76		19.7		0.324		0.676		19.65	1		0.324	0.676

N=Na_2SO_4; K=K_2SO_4; Na=NaCl; Ka=KCl; G=$Na_2SO_4 \cdot 3K_2SO_4$

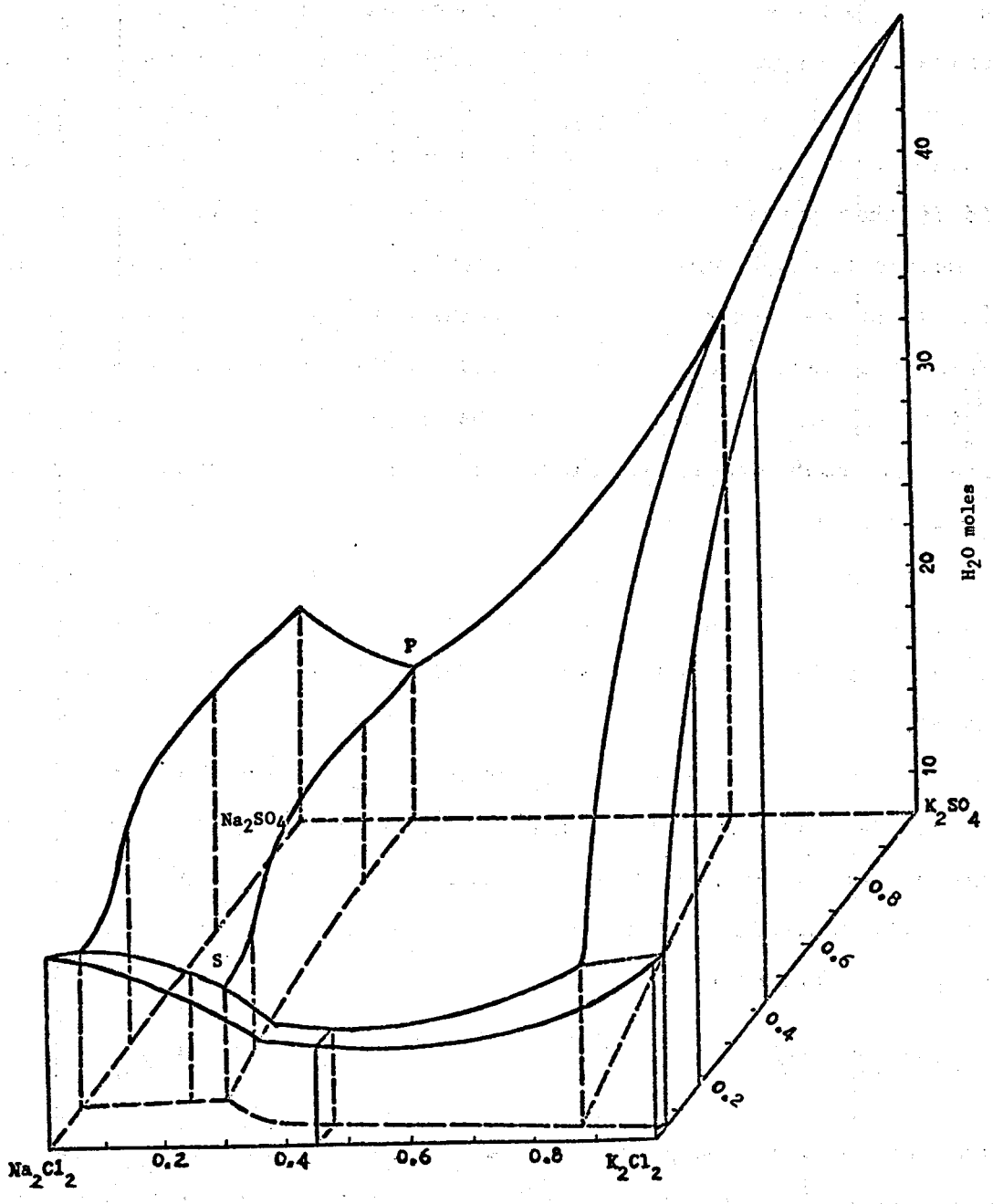

Fig. 2. Tridimensional representation of Janecke diagram at 75°C.

but a few of these were not compatible with energetical use of the brine. The two taken into consideration for practical application are shown in Figures 3 and 4. The flow diagram illustrated in Fig. 3 could be suggested whether the boric acid recovery were economically convenient.

The brine (stream 1) goes to the first high pressure separator; steam is fed to a turbine while liquid to a low pressure separator; the steam rising up from this second separator is fed to an intermediate section of turbine, liquid is than passed to a crystallizer for obtaining glaserite (Na_2SO_4 . 3 K_2S_4) Mother liquors coming out of centrifuge are pumped to a countercurrent double effect which performs as a crystallizer. From these two stages mixed crystals are obtained: glaserite and Na_2SO_4 from the first one and glaserite, Na Cl and Na_2 SO_4 from the second one. In Table 3 a material balance for each stream is given as a result of detailed calculations referred in (15).

The 17th stream contains theoretically a solution of H_3BO_3 from which it is possible to try a recovery. But this process is too complicated for a first trial pilot plant and the opportunity of H_3BO_3 recovery must be carefully evaluated.

The flow diagram of the second process, that assumed for the pilot plant designing, is given in Fig. 4. This scheme which is quite a simplification of the preceding one, must be utilized when boric acid recovery is not economically convenient. Mother liquors after crystallization of glaserite are pumped to reinjection well.

Pilot plant targets

Design, construction and performance of the pilot plant are aimed at

1) execution of long term runs with sufficient flow rate in order to allow a correct resource evaluation.
2) Verification of design methods of apparatus such as control and sampling systems.
3) Evaluation of quantity of steam produced by flash and its characteristics

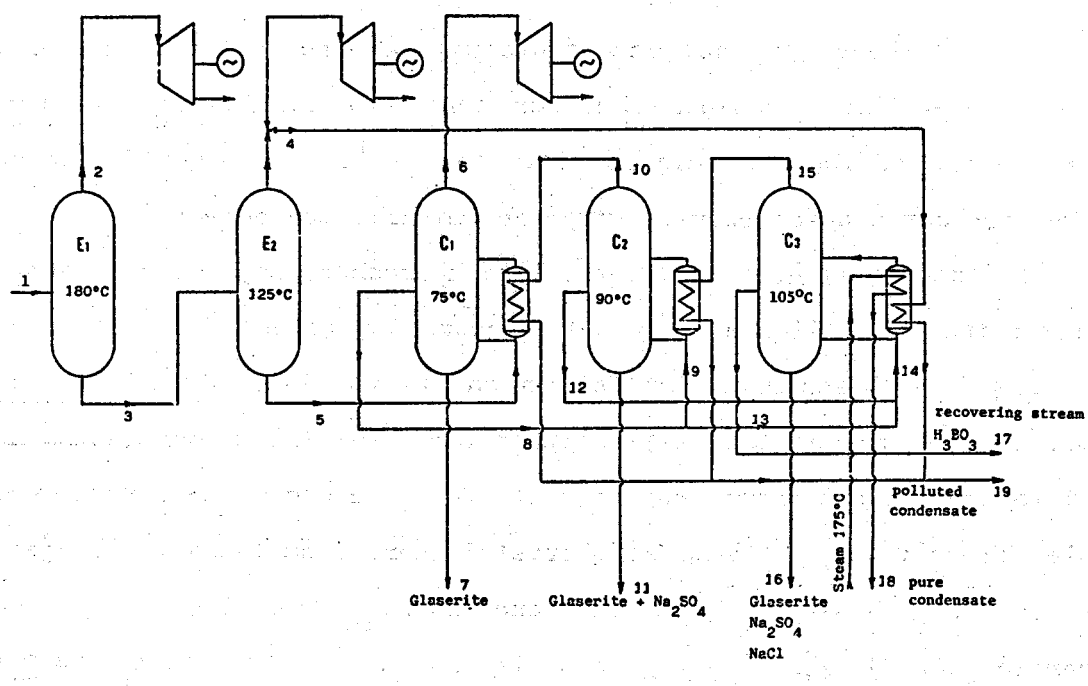

Fig. 3. Flow diagram for energetical exploitation of the resource coupled with salts recovery.

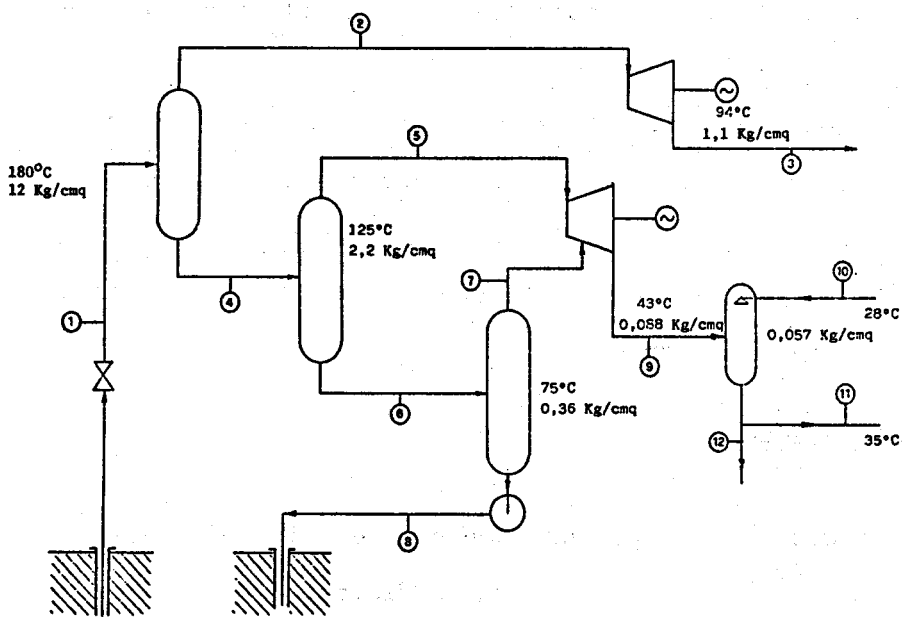

Fig. 4. Flow diagram for energetical exploitation of the resource coupled with partial salts recovery.

Table 3. Material balance for Fig. 3 flow diagram.

STREAM	Temp. °C	Press. Kg/cm^2	Na^+ tonn/hr	K^+ tonn/hr	$SO_4^=$ tonn/hr	Cl^- tonn/hr	H_3BO_3 tonn/hr	H_2O tonn/hr	STEAM tonn/hr	GAS tonn/hr	TOTAL tonn/hr
1	180	12	9,59(s)	12,02(s)	29,15(s)	4,20(s)	1,10(s)	132,8(s)	6,6	4,5	200,00
2	180	12	-	-	-	-	-	-	6,6	4,5	11,1
3	180	12	9,59(s)	12,02(s)	29,15(s)	4,20(s)	1,10(s)	132,8(s)	-	-	188,9
4	125	2,2	2,2	-	-	-	-	-	15,7	-	15,7
5	125	2,2	9,59(s)	12,02(s)	29,15(s)	4,20(s)	1,10(s)	117,1(s)	-	-	173,2
6	75	0,36	-	-	-	-	-	-	47,9	-	47,9.
7	75	0,36	1,69(c)	8,60(c)	14,10(c)	-	-	-	-	-	24,4
8	75	0,36	7,91(s)	3,42(s)	15,04(s)	4,20(s)	1,10(s)	69,2(s)	-	-	100,9
9	75	-	4,04(s)	1,75(s)	7,68(s)	2,14(s)	0,56(s)	35,3(s)	-	-	51,5
10	90	0,66	-	-	-	-	-	-	27,0	-	27,0
11	90	0,66	2,82(c)	1,03(c)	7,16(c)	-	-	-	-	-	11,0
12	90	0,66	1,21(s)	0,72(s)	0,52(s)	2,14(s)	0,56(s)	8,3(s)	-	-	13,5
13	75	-	3,87(s)	1,68(s)	7,36(s)	2,05(s)	0,54(s)	33,9(s)	-	-	49,5
14	78	-	5,08(s)	2,39(s)	7,88(s)	4,02(s)	1,10(s)	42,2(s)	-	-	62,9
15	105	1,1	-	-	-	-	-	-	28,8	-	28,8
16	105	1,1	3,19(c)	1,01(c)	7,09(c)	0,59(c)	-	-	-	-	11,9
17	105	1,1	1,89(s)	1,39(s)	0,79(s)	3,61(s)	1,10(s)	13,4(s)	-	-	22,2
18	125	2,4	-	-	-	-	-	-	16,5	-	16,5
19	103	-	-	-	-	-	-	-	71,5	-	71,5

(c) crystals
(s) solution

4) Possibility of evaluating a helical screw expander performance.
5) Estimate of corrosion, erosion and scale problems.
6) Determination of the chemical consistency of resource in order to produce glaserite as chemical fertilizer.
7) Study of exhaust brines by deep well reinjection.
8) In a second time, if of interest, can be examined the possibility of heat recovery with new type heat exchangers.

Choice of operative conditions

The choice of operative conditions must be made considering

1) Temperature, pressure and flow rates of the brine at wellhead;
2) Well characteristic curve;
3) Presence of CO_2 in the brine;
4) $CaCO_3$ deposition due to CO_2 stripping, caused by pressure reduction while brine is rising up;
5) Solubility of glaserite and other salts at different temperature.

From examination of characteristic curve an overall mass rate of about 100 t/h has been chosen because performance of well around this value of mass rate should be stable enough. Primary separator works at a pressure as close as possible to that of wellhead; consequently its operative conditions are approximatively p = 12 bar, t = 180°C. In this apparatus carbon dioxide saturated with steam is separated from the brine. This part of the plant, including first separator, is subjected to calcium carbonate scaling. Secondary separator works at a pressure of 2,2 bar and temperature of 125°C; at these conditions crystallization of glaserite or other salts does not occur because the solution is under the saturation conditions in respect of these salts.

Crystallization of glaserite is expected to occur just in the crystallizer whose operative conditions are 0,36 bar and 75°C.

Under these conditions, according with Janecke diagram and a few preliminary

data obtained during a brief erogation run, practically pure glaserite is obtained.

Material balances relating to the process are summarized in Table 4.

Choice of the separators

Liquid-vapor separators can be roughly classified in three types listed below:

- gravitational separators
- centrifugal separators
- inertial separators

The choice among these ones depends on the type of two phase flow and on the characteristics of the entrained liquid. A method based on the use of Baker's parameters has been used for a quick evaluation of the flow region. In Fig. 5 Baker's diagram is given; the obtained results with our input data are summarized in Table 5. The operating field is therefore located on the border between annular and dispersed flow region.

The type of flow suggests the choice of cyclone separators. As the input flow rate can oscillate, the bottom hold-up of the separator must be sufficiently large in order to prevent possible flooding of the apparatus.

Small diameter drops are undoubtedly entrained by the rising up steam and gas and therefore it needs to wash such stream by fresh water; moreover a demister is put an the top of the separator for removing the smallest drop still present in the steam before its entering into a turbine. Details of the primary and secondary separators design are given in (15); the schemes of such apparatus are given in Figs. 6 and 7.

Choice of crystrallizer

For obtaining crystals of same size a Kristal-Oslo crystallizer has been

Table 4: Material balance for Fig. 4 flow diagram (tonn/h)

Stream	Liquid	Steam	Gas	Total
1	188,9	6,6	4,5	200,0
2	-	6,6	4,5	11,1
3	1,0	5,6	4,5	11,1
4	188,9	-	-	188,9
5	-	15,7	-	15,7
6	173,2	-	-	173,2
7	-	11,7	-	11,7
8	161,5	-	-	161,5
9	3,4	24	-	27,4
10	2000	-	-	2000
11	2000	-	-	2000
12	27,4	-	-	27,4

Table 5

Bx	By	Ø mm	Flow
50	13600	200	annular
50	20500	125	annular
50	31000	90	dispersed

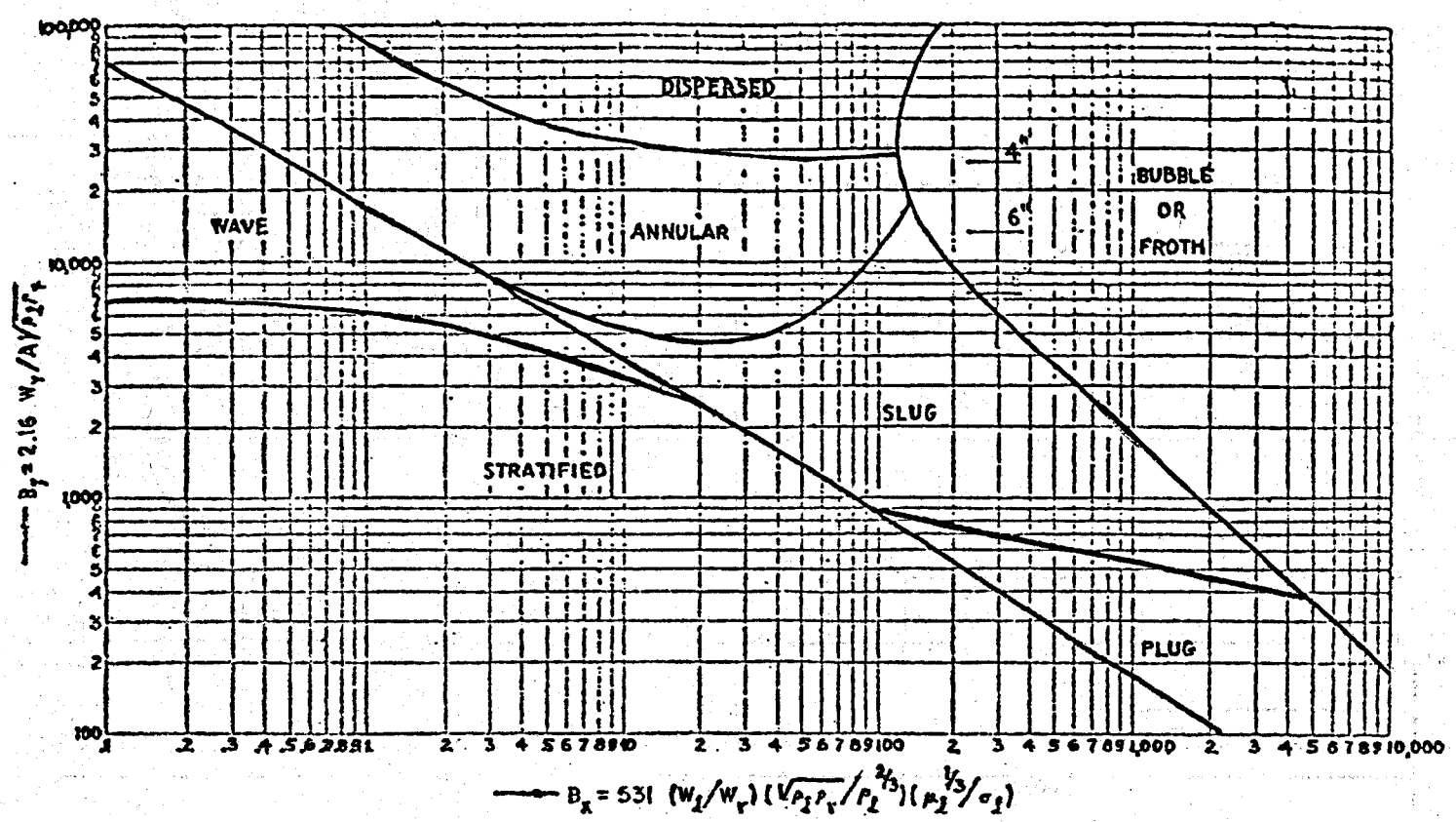

Fig. 5. Type of two phase flow as a function of Baker's parameter.

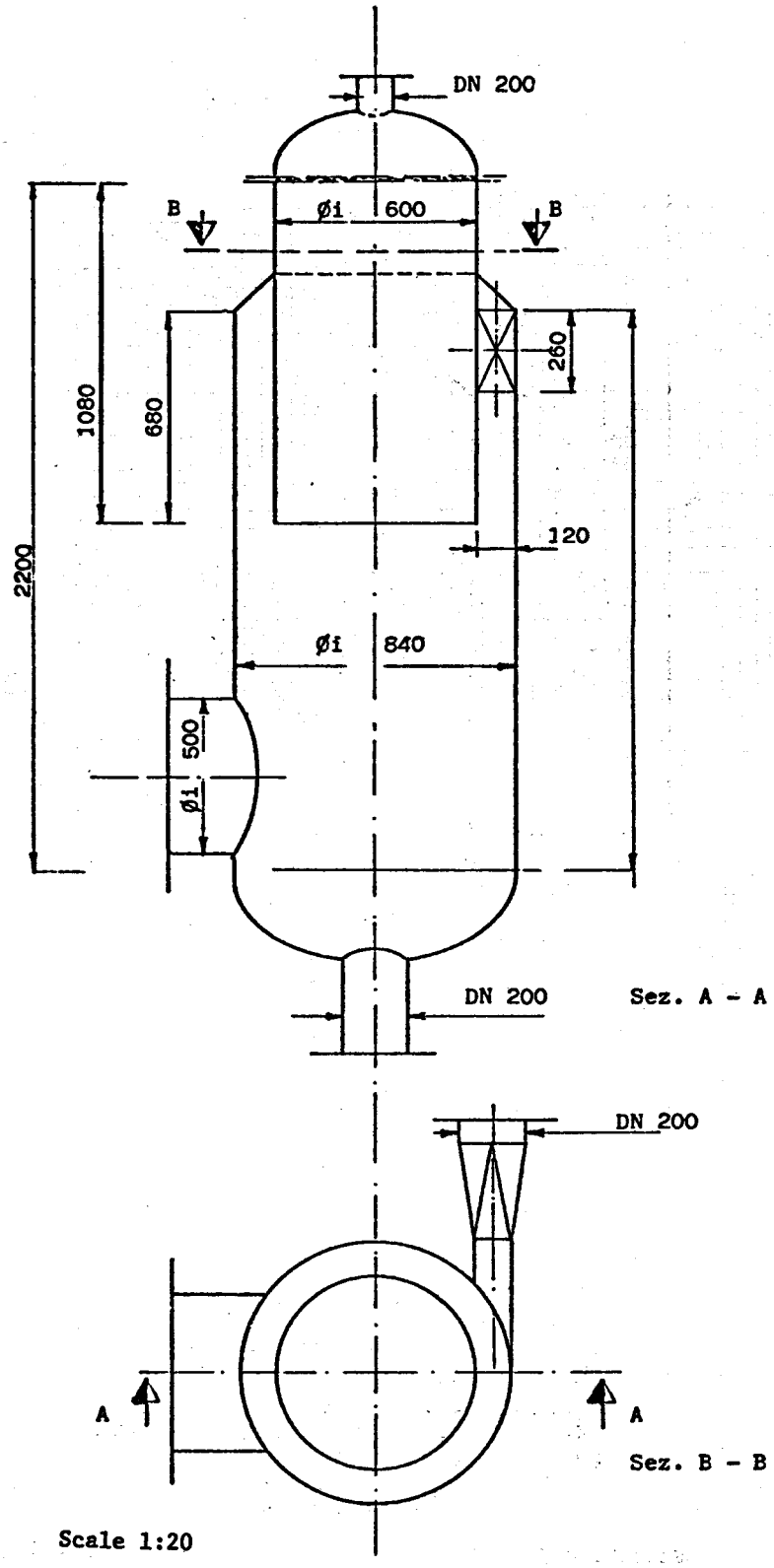

Fig. 6. Primary separator.

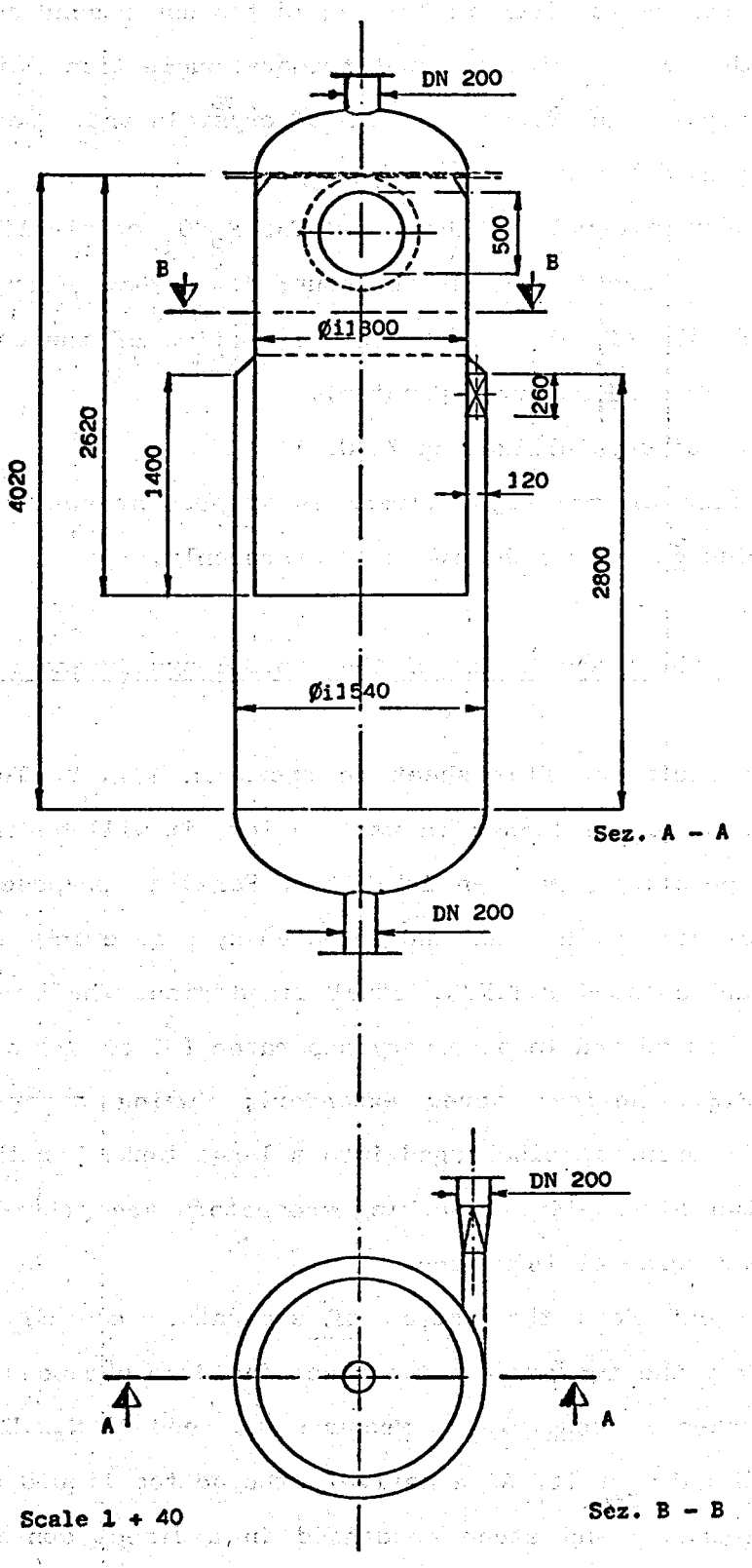

Fig. 7. Secondary separator.

chosen. Its scheme is given in Fig. 8; in the upper zone evaporation occurs together with supersaturation and primary nucleation while in the lower zone it has growing and classification of crystals and secondary nucleation. The designing hypothesis are

1) Griffith number equal to that used for K_2SO_4 crystallization (P/V = 30 Kg/hm^3; P = produced crystals for hour; V = Volume of crystallizer).
2) Feed flow rate of 5000 Kg/h (only a portion of the concentrated brine discharged from secondary separator).
3) Temperature of crystallization 75°C.

The construction of the crystallizer is at present suspended and the runs will be carried out using the two separators only.

Equipment flow sheet and choice of the control system and regulation valves

A simplified equipment flow sheet is shown in Fig. 9. To reduce troubles with calcium carbonate scales in well casing, it will be tried to introduce below the vaporating level an inhibitor. For this purpose the additive is previously diluted with water and injected by a metering pump into the well through an articulated P.T.F.E. steel lined pipe. The brine coming out of the wellhead can be fed to a primary separator (S1 or S2) or to a total flow turbine (H.S.E., helical screw expander); during start-up or blow-down operations the brine is discharged into a large tank. For the first stage of separation two alternatively working separators are provided because heavy scale problems arise at this step.

Liquid drawn out from the bottom of separators can be mixed with steam flowing up from the top and the two phase fluid so produced is fed to H.S.E. Such a way makes it possible to measure the feed to H.S.E. and to vary the ratio steam/liquid in it. Alternatively the bottom liquid can be fed to the secondary separator and steam condensed in a direct contact condenser, or directly discharged into the large tank. On the primary separators the

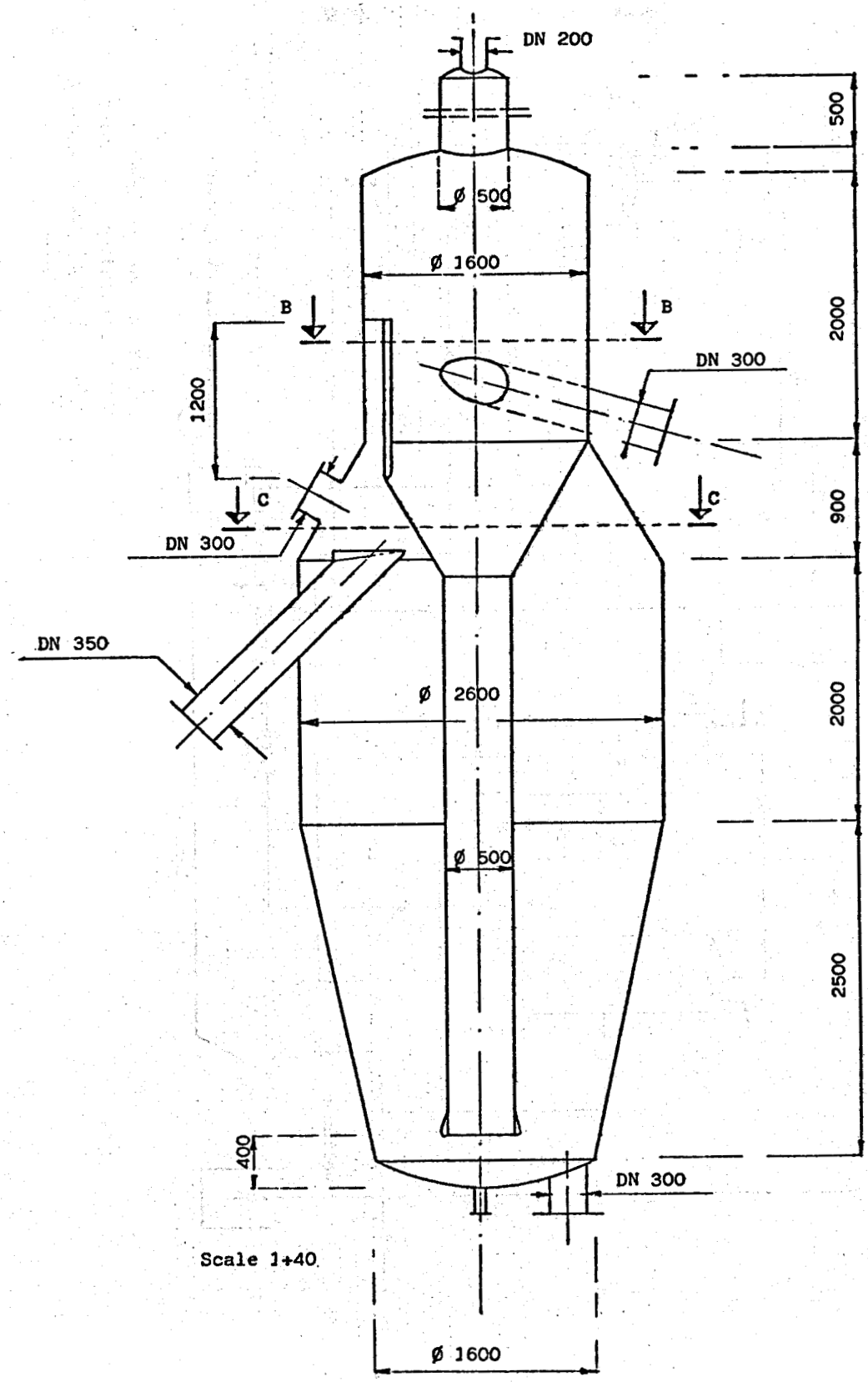

Fig. 8. Crystallizer.

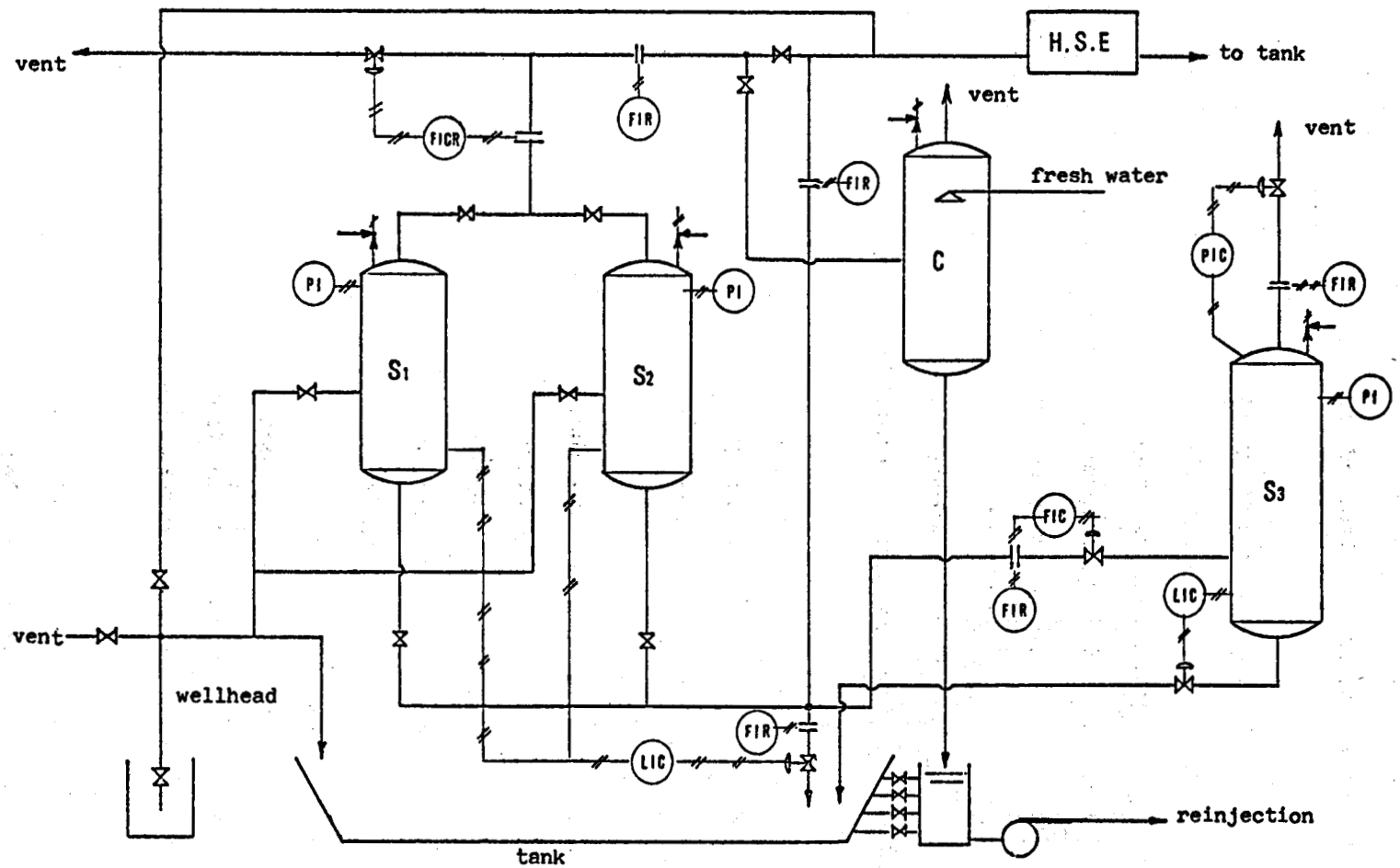

S1, S2 primary separators
S3 secondary separators
H.S.E. helical screw expander
C condenser

Fig. 9. Equipment flow sheet.

venting system of the steam is controlled by the overall flow rate of the rising up steam. Such a choice has been made taking into account the well characteristic curve which, in the adopted operative conditions, is flat. In this case the classical venting controlled by pressure does not assure a constant flow rate.

Liquid level in S1 and S2 is automatically controlled discharging part of the brine into the tank; this amount is little in comparison with the main quantity which is fed to the successive stages.

As calcium carbonate scale will clog frequently the regulation valves, these have been chosen of self cleaning type and two units put in parallel and working alternatively have been provided.

The level control of S3 separator is accomplished by a regulation valve put on the bottom outlet and the pressure is controlled by a valve put on the venting pipe.

As surely glaserite and other salts crystallise on the floor of the tank, this is connected by five pipes, placed at different levels from the floor, with an external vessel; reinjection pump is connected with this one, where dilution water is also added.

For pressure and temperature measurements there are not particular problems and normal instrumentation has been provided: the same for the choice of calibrated orifices in vapour flow measurement. On the contrary these instruments cannot be used for measurement of flow rate of boiling brines as they give large errors due to vaporization inside the orifice; in this case magnetic inductive flowmeters with removable electrodes have been chosen. The metering tube is made by P.T.F.E. and resist up to 180°C and 40 bar.

For level measurements a buoyancy type instrument has been chosen; it has provided a continuous washing of the tube where the floating element is placed.

A complete system of washing is provided in order to maintain as clean as possible pipes, valves, instruments, nozzles, etc.

Literature

1) Cornec E., Krombach M., Caliche 10, 59 (1928)

2) Hering E. - University Thesis - Srasbonrg (1926)

3) Chretien A. - An. Chim. (101), 12, 9, (1929)

4) Blasdal W.C. - J. Ind. Eng. Chem. 10, 334 (1918)

5) Anosov V., Bysova E.A., - I.Z.V., Sectora Fiz. - Khim. Analiza Inst-Obshch. Neorgan. Khim. Akad Nauk USSR 15, 118 (1947)

6) Campbell A.N. et al. - J. Chem. Soc. 56, 2507 (1934)

7) Linke F.W. - Solubilities of Inorganic and Metal Organic Compounds 4th Edition (1958)

8) Shull'gina K., Yanasteva O.K. - Zhui. Obachei Khim. 25, 234 (1955)

9) Gilliot A. - Bull. Soc. Chim. 992 (1951) France

10) Rustamov P.G. - Isv. Akad. Nauk. Azerb. 4, 33, 5, 45 (1957)

11) Pel'sh A.D. - Tr. Vses. Nauch. Iss. Led. Inst. Galurgii 145, 160 (1949)

12) Zaslavsky A.T. et at. Izv. Akad. Nauk. Su Khim 47 (1938)

13) Problemi per lo sfruttamento di F. Giovannini et al.
"Problemi per lo sfruttamento di soluzioni geotermiche ad alta temperatura ed alta salinità per la produzione di energia elettrica".
Relazione finale - University of Pisa 1978 March.

14) F. Giovannini, F. Nasti - Thesis - University of Pisa - 1977 July

15) G. Magozzi et al.
"Studio e sviluppo del processo e progettazione di un impianto pilota per un ciclo di sfruttamento di salamoie ad alta temperatura ed alta salinità".
Relazione finale - University of Pisa 1979 October.

HIGH SALINITY GEOTHERMAL ENERGY CONVERSION BASED UPON THE OPERATING EXPERIENCE AT THE SAN DIEGO GAS & ELECTRIC-DOE GEOTHERMAL LOOP EXPERIMENTAL FACILITY LOCATED AT THE NILAND RESERVOIR, IMPERIAL VALLEY, CALIFORNIA, U.S.A.

Presented By George Anastas

Research at the Geothermal Loop Experimental Facility (GLEF), co-funded by San Diego Gas & Electric (SDG&E) and the U.S. Department of Energy (DOE), was successfully concluded in September of 1979. In 13,000 hours of operation during a three and one-half year period, the nominal 10 megawatt electrical-equivalent GLEF provided engineers and researchers from SDG&E, national laboratories, government agencies and industry the opportunity to identify problems in working with highly saline geothermal fluids and to develop solutions that could be applied to a commercial geothermal power plant producing electricity.

Figure 1 shows the location of the site of the GLEF in relation to the other geothermal anomolies in the Imperial Valley. Figure 2 sets forth, in a concise fashion, the history of the GLEF.

The Niland Reservoir, which supplied fluid to the facility, has a high total dissolved solids (TDS) content of about two hundred fifty thousand (250,000) parts per million (ppm), but has a high downhole temperature between 500-600°F.

Figure 3 shows the constituents of the solids in the brine. Note that the silica content is approximately 200 ppm and that the chloride concentration is well over 100,000 ppm. Figure 4 shows a generalized range of non-condensable gas content of the brine that was used at the facility.

During the period 1976-1977, the facility was operated in a four-stage, flash binary cycle operation. The Final Report of the Geothermal Loop Experimental Facility discusses the operation of the facility in this manner. However, in 1978-1979, the facility was operated in a two-stage flash cycle

configuration is shown in Figure 5. Figure 6 is an aerial photograph of the facility at the time the effluent brine clarifier filter was being constructed.

One of the largest obstacles to constructing a power plant at the Niland Reservoir is related to the reservoir brine. The solids that precipitate from the brine upon cooling not only form scale in the brine piping, but most of the solids are carried through the plant and are injected into the reservoir. This causes the reinjection capability of the wells to decline.

In February, 1978, Imperial Magma and Lawrence Livermore Laboratory began conducting a separate series of tests of equipment to remove suspended solids efficiently from the effluent brine prior to injection. One of the problems that had to be overcome was the relatively slow evolution rate of the silica in solution in the brine. This dissolved silica precipitated so slowly that quick removal of suspended solids from the effluent brine was not sufficient to preclude the brine from containing a degree of silica supersaturation. This silica tended to precipitate in the injection well or in the reservoir itself, causing potentially irreparable damage to the well or the reservoir.

The process that was decided upon and extensively tested by Imperial Magma (with the cooperation of the Envirotech Corporation) is similar to that used in water and sewage treatment industries. To verify the pilot test on a larger scale, the decision was made in mid-1978 to build a full-scale treatment facility at the GLEF, based on this process. The system consists of a reactor clarifier (Figure 7), media sand filter (Figure 8) and thickener (Figure 9). The period of operation of the clarifier/filter system was limited to less than 1000 hours, prior to project termination. Figures 10 and 11 are schematic representations of the operation of the clarifier filter system. Important conclusions derived from the GLEF Project are summarized as follows:

- Supersaturation of silica in the effluent brine can be quickly removed by a reactor/clarifier.
- Most of the resulting suspended solids can be removed by settling/filtering.
- Oxygen must be carefully excluded in order to prevent further reaction and generation of suspended solids.
- Solid waste, predominantly silica, separated via the filter press, is readily transportable.

- The clarification process is relatively stable.
- Injection capability of the processed brine appears feasible if atmospheric oxygen can be excluded from the process.

- Reservoir injection capability and production evaluations were accomplished and the reservoir appears to be capable of supporting commercial power production.
- No induced subsidence was detected.
- Steam of acceptable quality, with further treatment, can be produced (See Figures 12 and 13).

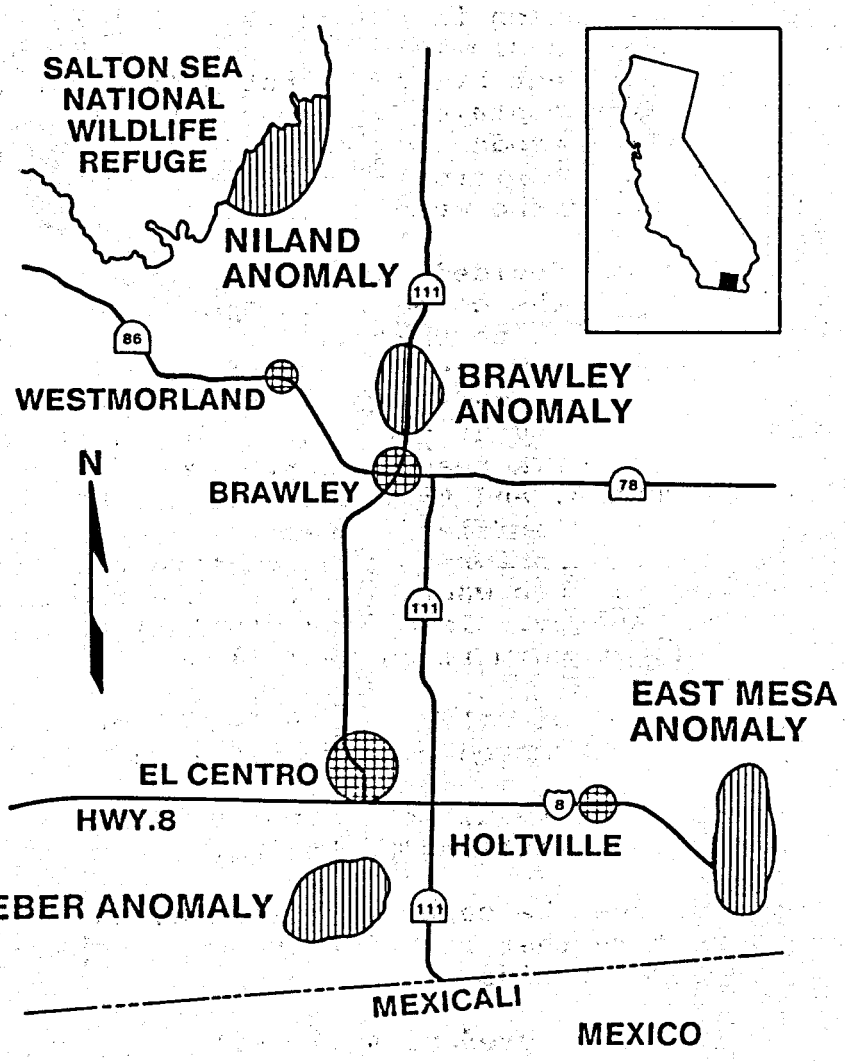

Fig. 1. Location of Imperial Valley geothermal reservoirs.

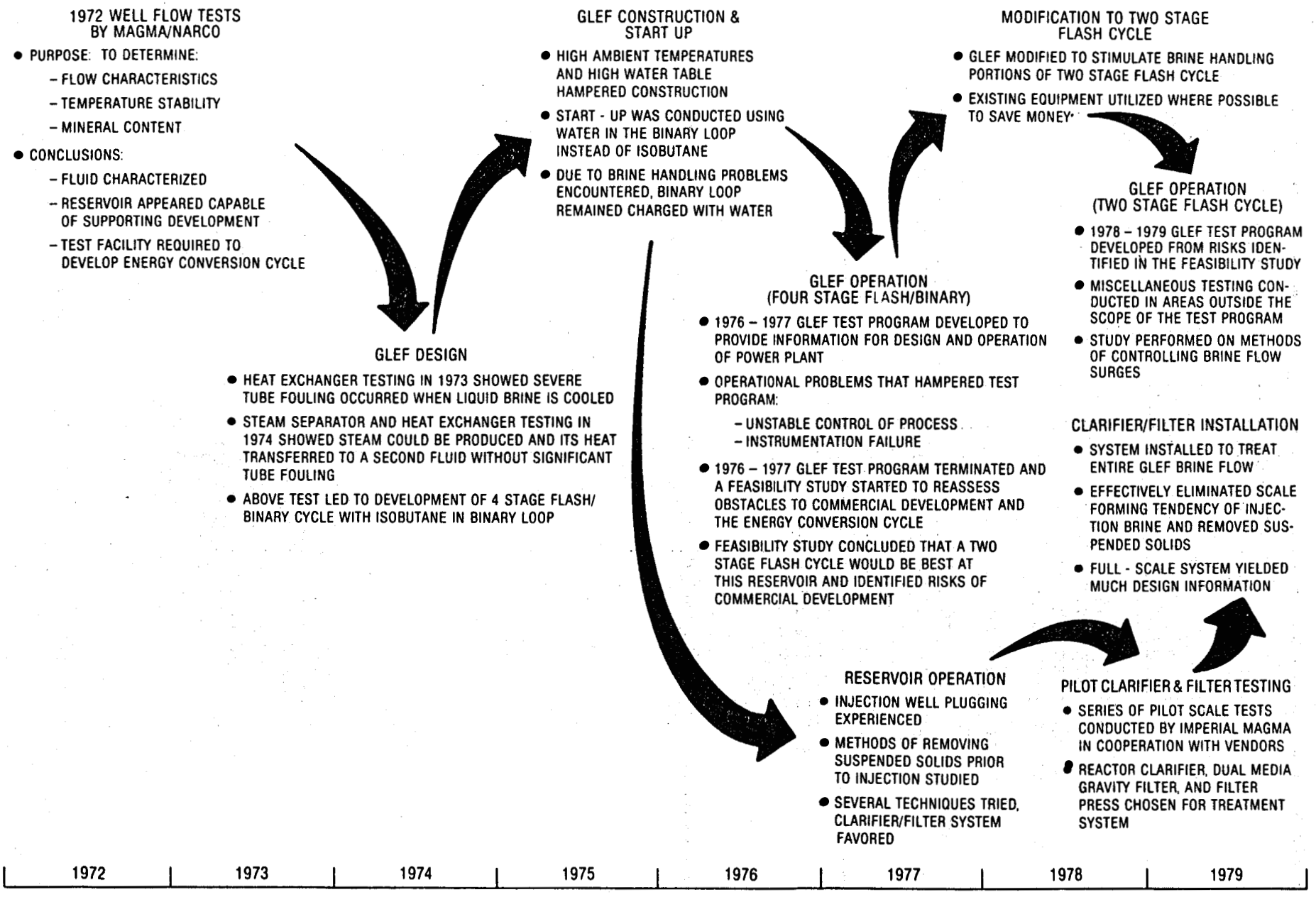

Fig. 2. GLEF history.

ELEMENT	HIGH	LOW	AVERAGE
Cl	146,000	94,000	121,000
Na	54,600	29,600	42,700
Ca	28,300	16,700	22,900
K	14,100	5,830	10,200
Mn	903	498	718
Sr	472	292	382
Zn	313	172	256
Si	236	152	204
Ba	195	79	142
Li	197	122	162
Fe	320	152	236
Mg	116	67	87
Pb	68	24	49

Note: All measurements are ppm

Fig. 3. Elemental range for generalized brine.

	DECEMBER 1976 % OF TOTAL GAS	AUGUST 1979 % OF TOTAL GAS
CO_2	98.14	98.92
CH_4	0.68	0.51
N_2	0.02	0.57
O_2	*ND	*ND
H_2	*ND	*ND

*ND implies none detected

Fig. 4. Generalized range of noncondensable gases in brine.

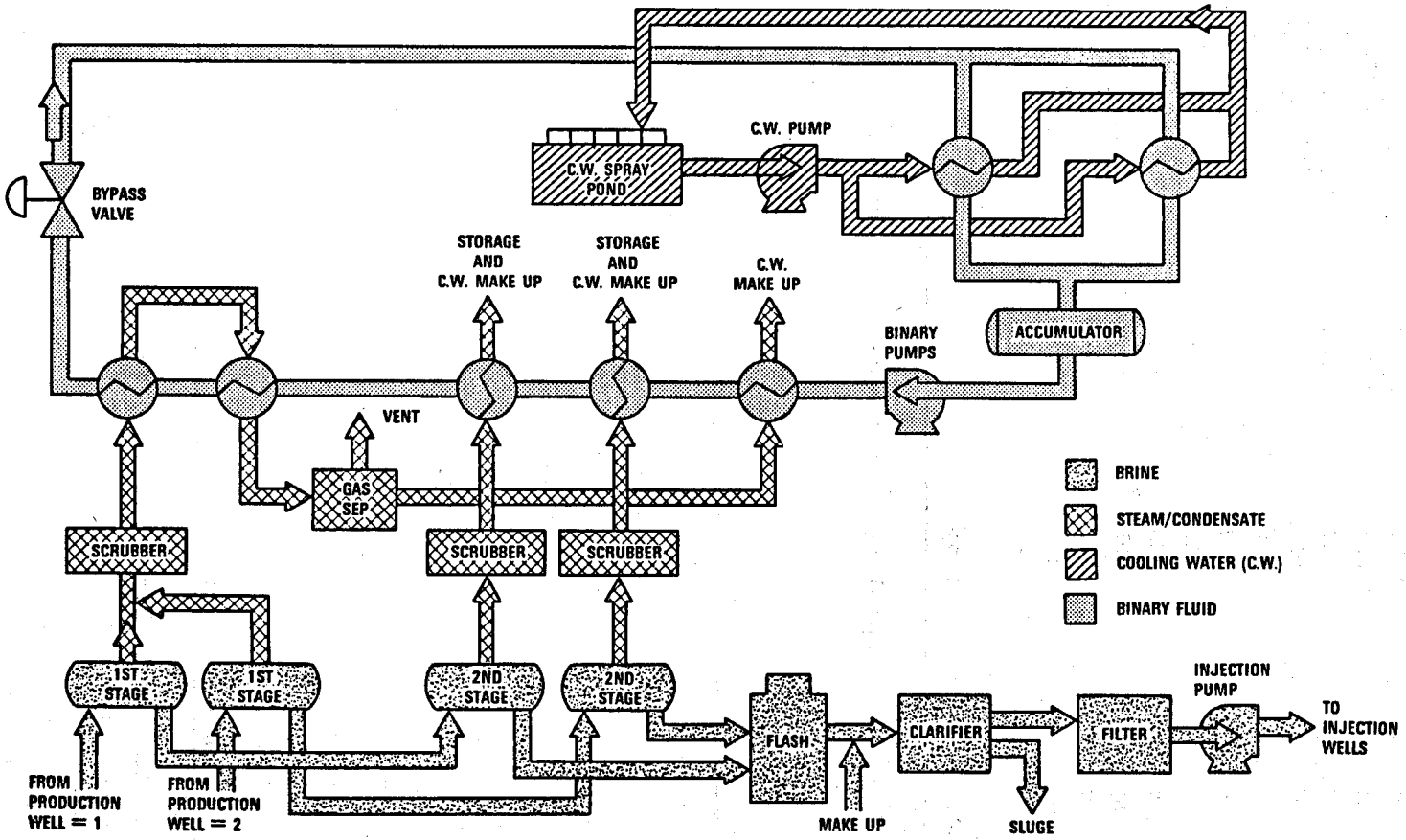

Fig. 5. GLEF process flow diagram.

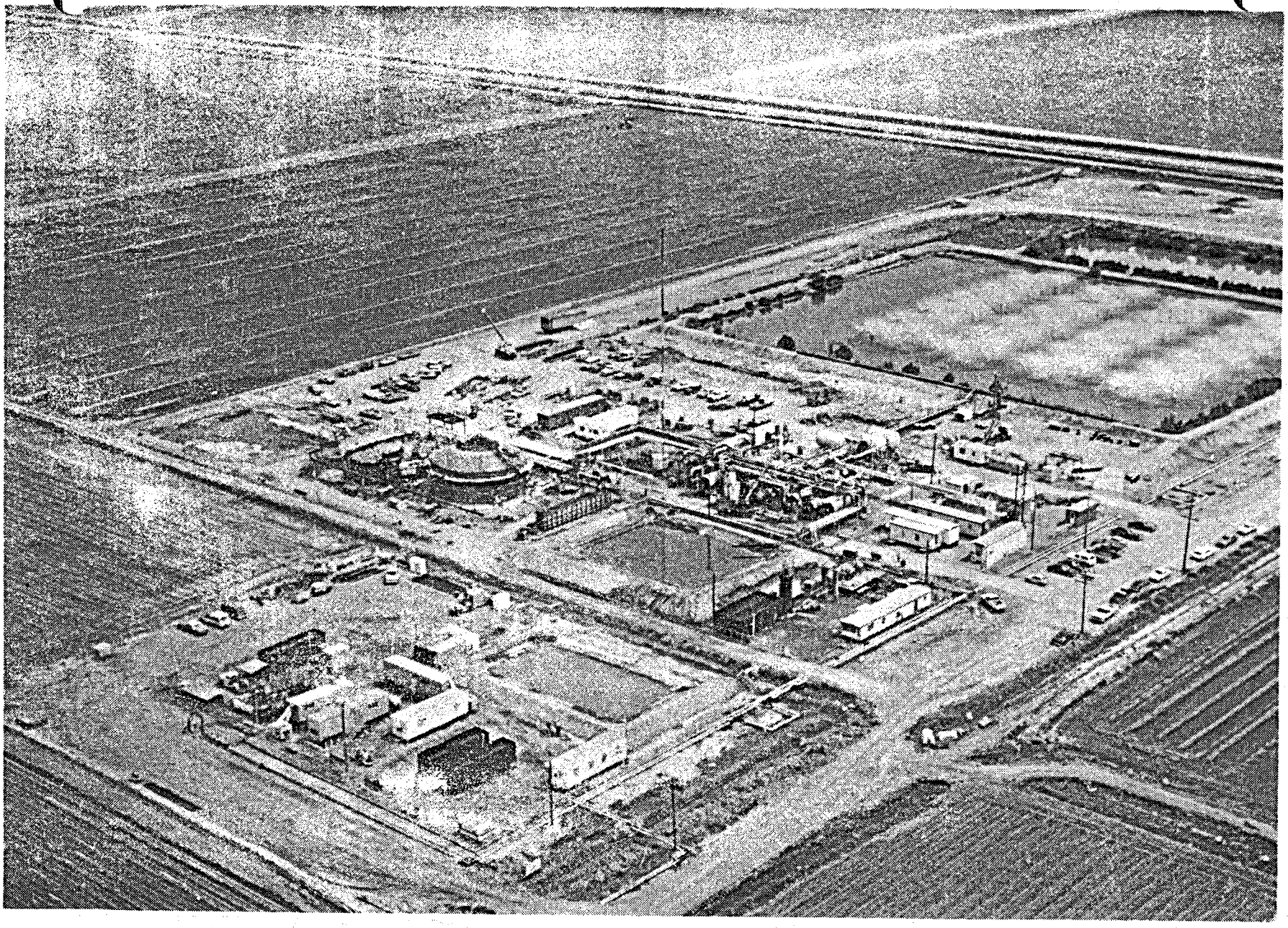

Fig. 6. Aerial photograph of Geothermal Loop Experimental Facility (GLEF).

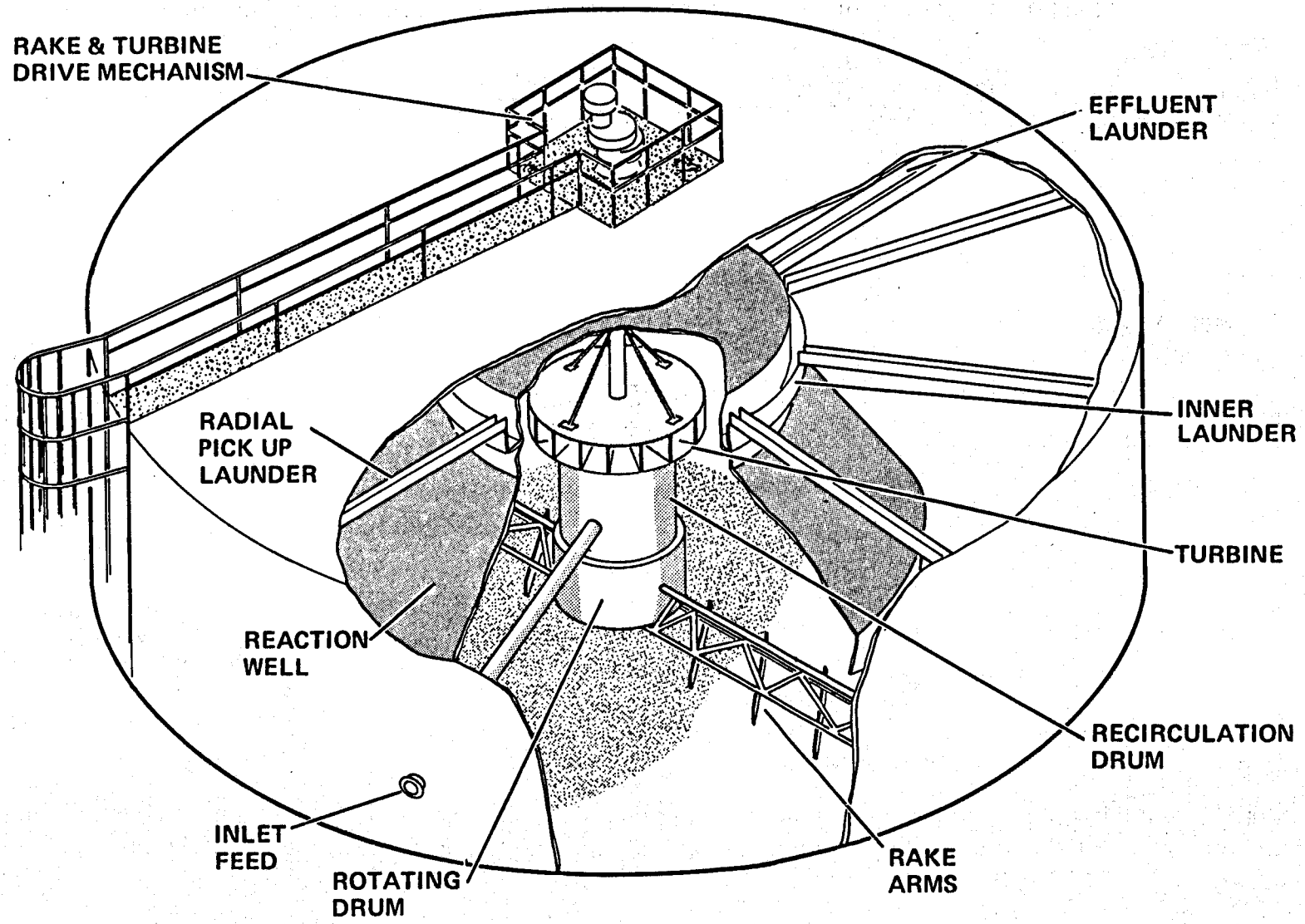

Fig. 7. V-17 Reactor/Clarifier.

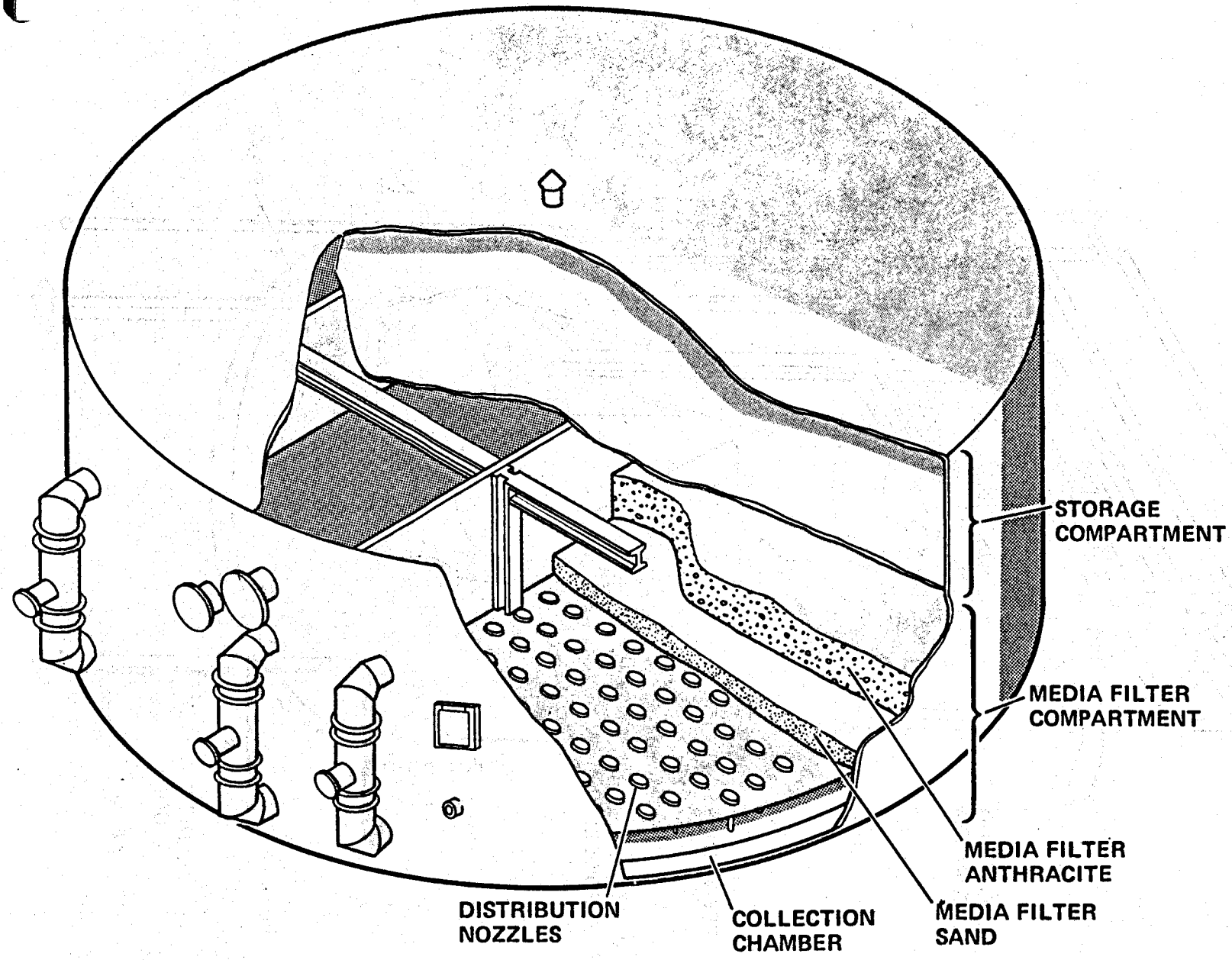

Fig. 8. V-18 SVG Sand filter.

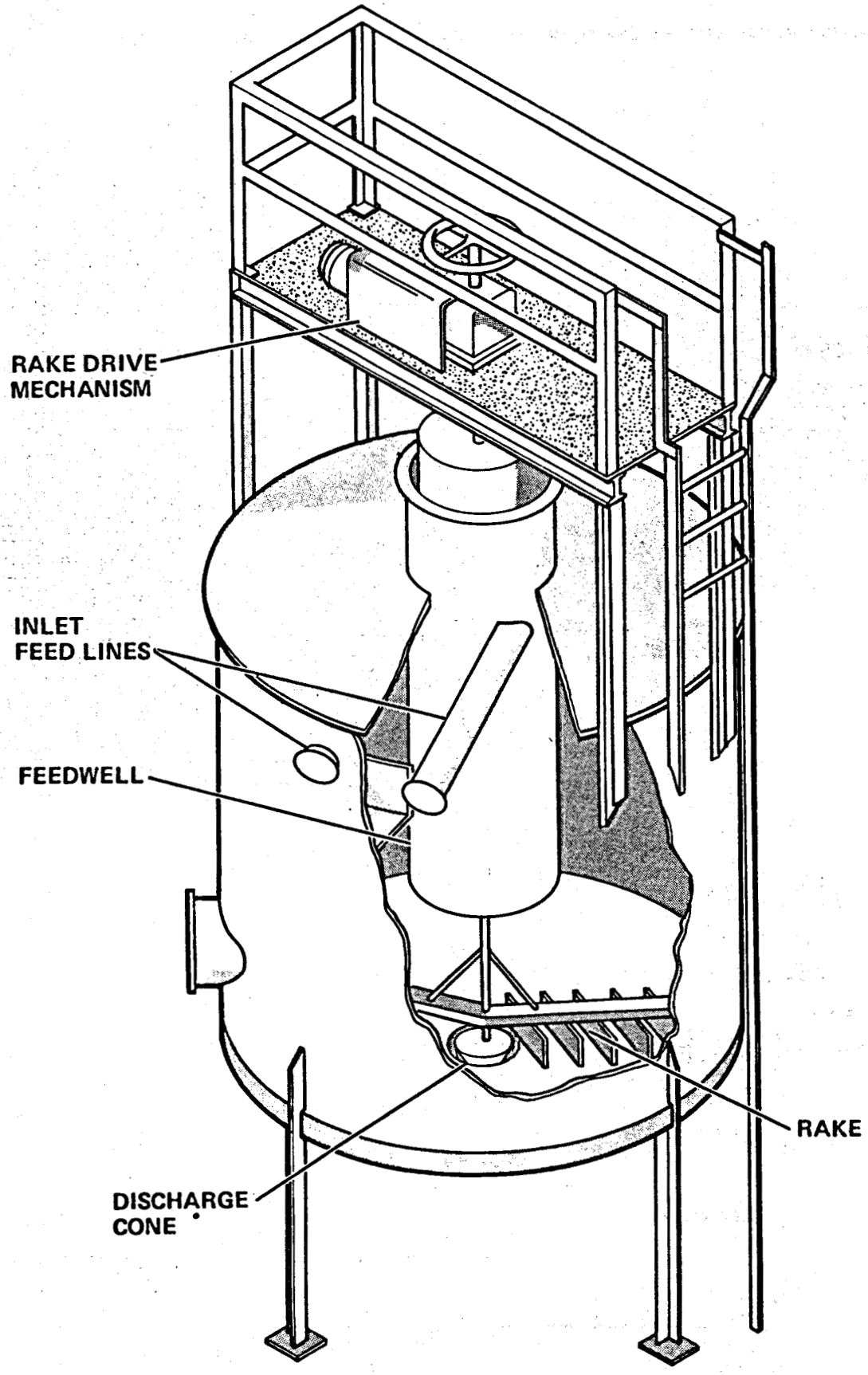

Fig. 9. V-22 Thickener.

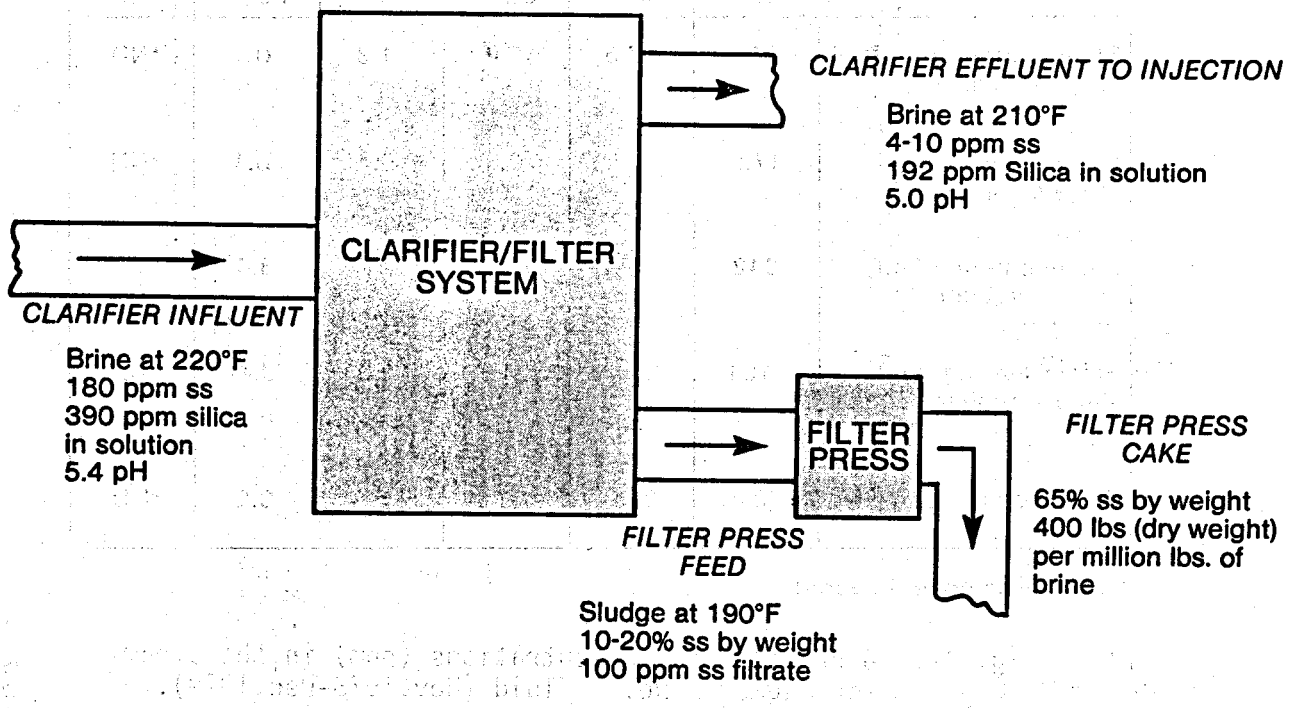

Fig. 10. Clarifier/filter system operation.

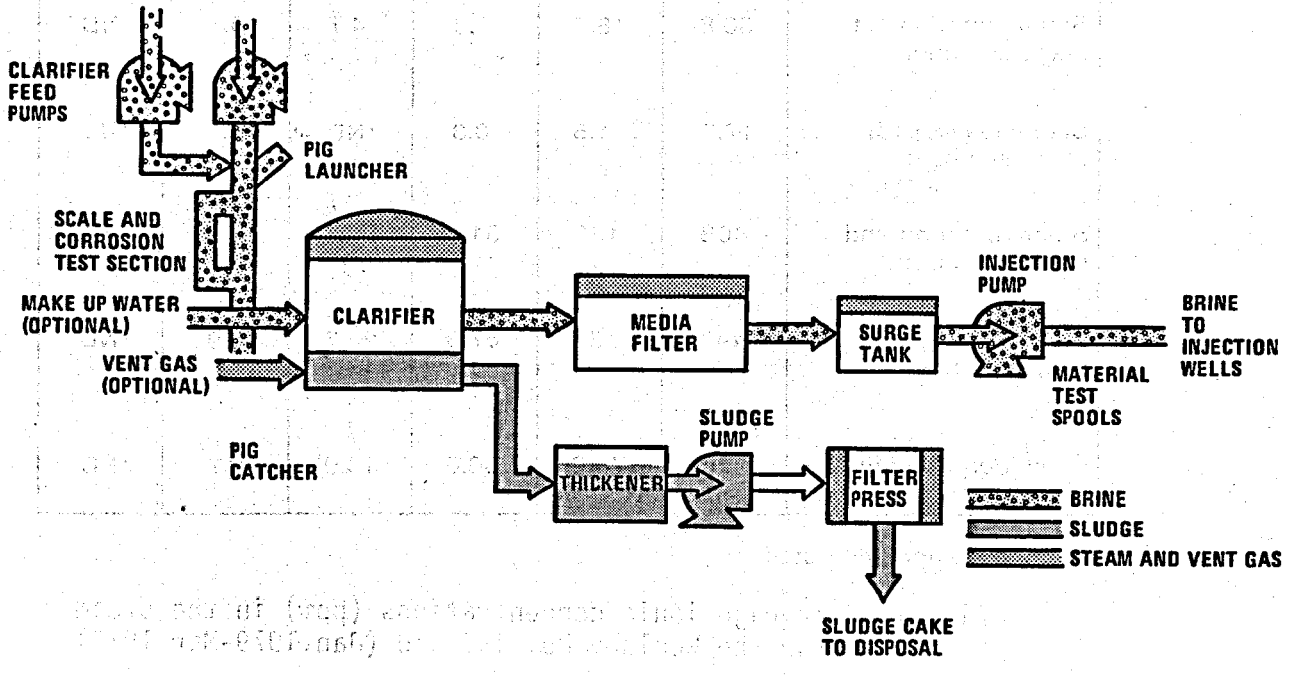

Fig. 11. GLEF process flow diagram.

	Cl^-	Na^+	Ca^{++}	K^+	Fe^{++}	Si
Steam entering 1st stage scrubber	37.1	7.5	3.4	1.3	0.1	*ND
Steam leaving 1st stage scrubber	17.2	1.8	0.6	0.4	0.1	*ND
Steam entering 2nd stage scrubber	342	171	63.6	32.7	3.4	1.5
Steam leaving 2nd stage scrubber	131	51.7	21.5	12.0	0.4	0.1
Combined Condensate	89.5	22.0	10.0	5.1	0.2	*ND

*ND implies none detected

Fig. 12. Average ionic concentrations (ppm) in the steam for Magmamax No. 1 fluid (Nov.1978-Dec.1978).

	Cl^-	Na^+	Ca^{++}	K^+	Fe^{++}	Si
Steam entering 1st stage scrubber	60.8	18.7	9.3	4.7	0.7	*ND
Steam leaving 1st stage scrubber	17.7	1.5	0.3	*ND	0.1	*ND
Steam entering 2nd stage scrubber	408	160	61.1	20.7	0.5	2.5
Steam leaving 2nd stage scrubber	447	136	67.3	25.7	0.9	*ND
Combined Condensate	225	78.2	30.0	14.0	0.7	*ND

*ND implies none detected

Fig. 13. Average ionic concentrations (ppm) in the steam for the Woolsey No. 1 fluid (Jan.1979-Mar.1979).

COOPERATIVE RESEARCH AND DEVELOPMENT IN GEOTHERMAL ENERGY

R. Cataldi
ENEL, Pisa, Italy

P. Witherspoon
Lawrence Berkeley Laboratory
Berkeley, California, USA

1. FOREWORD

During the last few days we have heard that the DOE/ENEL Agreement on Cooperative Research and Development in Geothermal Energy, signed in June 1975, encouraged the implementation of joint activity in five projects. One of these projects deals with the various aspects of 'RESOURCE ASSESSMENT AND RESERVOIR PHYSICS AND ENGINEERING' and is referred to as Project DOE/3.

2. OBJECTIVES

The general objective of Project 3, as defined in the DOE-ENEL Agreement, is to "seek procedures for optimizing the techniques required in the resources assessment and reservoir engineering of geothermal systems." However, when drawing up the Program Outline for Project 3 it was decided that, in view of the multiplicity and variety of problems that might arise, and to simplify the operative side, the activity of the Project should be divided into three separate areas of research. These are:

(1) resource assessment
(2) reservoir physics and engineering
(3) reservoir modelling

2.1

The first of these areas of research includes the specific tasks relative to exploration methodology problems, (geological geophysical

and geochemical), as well as the problems involved in evaluating the regional and local geothermal potential.

With regard to the latter, in particular, the objective was to develop the methodological approach of an "a priori" estimation of geothermal energy, at the same time attempting a general classification of geothermal potential in terms of "resources" and "reserves."

2.2

The second area consists of the study of the problems connected with defining the physical properties of the geothermal reservoirs. The main objective in this case was to develop appropriate processing techniques for the physical and thermodynamic data from the wells. Starting with the methods tried and tested in the oil industry, the aim was to extend these to geothermal research in general and to the long-term forecasting of the behaviour of productive wells in particular.

2.3

The third area of research consisted of the investigation of geothermal systems by means of physical and mathematical models, directed at developing a reference base for a better understanding of the nature and behaviour of these same systems. The model approach, besides representing a generalized means of studying exploited geothermal systems, was also regarded as a useful tool for defining the natural physical parameters of these systems in their pre-drilling undisturbed conditions. In other words, one of the objectives of this area of research of Project 3 was to model natural geothermal systems with a view to understanding how they can form and persist within the earth's crust.

3. TASK OF PROJECT 3

With these objectives in mind, the following 12 specific technical tasks (shown in Table 1) were devised for the three areas of research. Most of them have, by the way, already been completed.

Table 1. TASKS COMPLETED OR IN PROGRESS UNDER PROJECT 3

A) "RESOURCE ASSESSMENT AND EXPLORATION METHODOLOGY"

*	/DEA-3/1	Methods for regional assessment of geothermal resources.
*	/DEA-3/2	Assessment of geothermal potential of Central and Southern Tuscany
†	/DEA-3/11	Helium prospecting in geothermal areas.

B) "RESERVOIR PHYSICS AND ENGINEERING"

*	/DEA-3/3	Analysis of reservoir pressure and decline curves in Serrazzano zone.
*	/DEA-3/4	Well-testing in Travale-Radicondoli geothermal field.
*	/DEA-3/5	Thermodynamic study of Bagnore field.
†	/DEA-3/9	A depletion model of the Gabbro zone - North Larderello.
†	/DEA-3/10	Reservoir engineering studies of the Travale-Radicondoli Reservoir.
§	/DEA-3/15	Study of water influx and variation of fluid composition in the Bagnore field.

C) "RESERVOIR MODELLING"

†	/DEA-3/5	Study of effects of re-injection with a mathematical model.
†	/DEA-3/7	Modelling vapor-dominated geothermal reservoirs.
§	/DEA-3/12	Numerical investigation of geothermal production and injection of fluids.

OTHERS

*	/DEA-3/8	Workshop on Geothermal Resource Assessment and Reservoir Engineering.

---

* Presented at the 1st DOE-ENEL Workshop (Larderello, September 1977).

† Presented at the 2nd DOE-ENEL Workshop (Berkeley, October 1980).

§ Preliminary results.

The first DOE-ENEL Workshop represented another non-technical task. The final results of the tasks indicated by an asterisk in Table 1 were presented and discussed during the first Workshop, held in Larderello in September 1977 and are now published in a special issue of the journal Geothermics.

The results of the other tasks (indicated by a dagger in the Table) are detailed in the following pages (Project 3).

4. MAN-POWER REQUIREMENTS

All the tasks of Project 3 were devised and implemented in close collaboration between Italian and US researchers. This collaboration necessitated frequent working visits of American scientists to the ENEL offices in Pisa and Larderello and of Italian researchers to the USGS (in Menlo Park and Denver), to Stanford University and to Lawrence Berkeley Laboratory.

Without speaking of the engagements of personnel that were necessary to implement these joint tasks, to give some idea of the close techno-scientific 'rapport' created by Project 3, we need only say that there were approximately 20 visits of US scientists to Italy and about 15 of ENEL persnnel to the USA, totaling about 550 and 400 man/day spent abroad for strictly scientific reasons.

5. CONCLUSIONS

The Project Leaders, that is the writers of this Introduction, will not presume to draw conclusions on the validity of the scientific results obtained until now by Project 3.

My colleagues along with the international geothermal community, having read the 20 odd papers already in print on the Proceedings of the first and second DOE-ENEL Workshops, will be able to draw their own conclusions.

What we would like to say is that the type of collaboration adopted for Project 3, with its joint implementation of the defined tasks, has resulted in an extremely prolific exchange and comparison of know-how and experience. We wish also to add that the joint

undertaking of these tasks has generated a strong spirit of emulation and close ties of friendship between all those contributing to Project 3. To these contributors, the Project Leaders want to address their thanks and deep appreciation for the work carried out.

MODELING VAPOR DOMINATED SYSTEMS - SERRAZZANO LUMPED PARAMETER MODELS

R. Celati, R. Marconcini, G. Neri,
K. Pruess, R. Schroeder and O. Weres

1 - Introduction

Task 3/7 of the ENEL-DOE collaboration agreement has been devoted to numerical simulation of two-phase geothermal reservoirs. The work has been conducted by the National Geothermal Unit of ENEL, Italy and the Lawrence Berkeley Laboratory of University of California, USA. The National Research Council of Italy also contributed to the research.

The main objectives of the research were identified in improving the understanding of physical processes, investigating the theoretical bases of some simple reserve estimation methods and testing the feasibility of numerical simulation of a real vapor-dominated reservoir.

Natural geothermal reservoirs are found in a large variety of geologic and hydrogeologic conditions and are characterized by different distributions of the phases in the pore volume and fluid compositions.

The distribution of the phases in the reservoir affects to a large extent the production mechanism and the characteristics of the fluid produced (Refs. 1,2).

The presence of noncondensable gas (mainly CO_2) also can be important in the control of reservoir performance (Refs. 3,4).

The fact that a reservoir delivers dry or even superheated steam does not exclude the possibility that the reservoir may also contain fluid in a liquid phase. In effect mass balance calculations for known vapor-dominated reservoirs show that the existence of a condensed phase must be admitted in order to justify the cumulative fluid production from the estimated reservoir volume (Refs. 2,5,6,7).

The experience of several exploited geothermal fields of New Zealand, Mexico and Italy show that fluid extraction can induce boiling inside reservoirs which were water-dominated in their undisturbed initial con

ditions. Thus it is likely that two-phase zones develop as a result of exploitation in the majority of exploited geothermal reservoirs.

Two major approaches have been followed in the mathematical modelling of geothermal reservoirs: lumped parameter and distributed parameter models.

Lumped parameter models assume reservoirs and fluid properties uniform in space. Although such hypothesis represents a good approximation only for a few geothermal reservoirs, these models have been successfully applied in several reservoir engineering studies (Refs. 3,4,8,9,10,11).

Simple lumped parameter models are preferred when detailed reservoir information is not available or scarce, as it is for the majority of existing geothermal reservoirs.

Distributed parameter models can take into account complex reservoir shapes, etherogeneity, anhysotropy, irregular initial and boundary conditions ecc.

Although their use requires data which are generally difficult to obtain, they offer the possibility to study field behaviour well per well and carefully investigate phenomena controlled by fluid flow.

Distributed parameter models have been applied to Wairakei geothermal field by several authors (Refs. 12,13,14), but up to date there has been no application to the simulation of the production history of an exploited vapor-dominated reservoir.

This paper presents some general results that can be obtained from lumped parameter models (PART 1) and the simulation of the vapor-dominated reservoir of Serrazzano (PART 2) in Larderello field (Italy).

2 - Thermodynamic behavior of vapor dominated reservoirs

The most simple way to conceive a geothermal reservoir is to hypothesise a "hot box", possibly adiabatic, containing three different components: rocks, water and noncondensable gas, assuming all the properties uniform through the box volume - Let us assume that thermal equilibrium persists between the three components with every process which may occur in the system, that no chemical reaction exists between the components and that the gas is dissolved in the liquid phase according to Henry's law. Thus the changes of state are defined by the energy and mass conservation equations as follows.

(1) $$\frac{d}{dt}\left(\mathcal{E}_a + \mathcal{E}_r + \mathcal{E}_g\right) = H_a G_a + H_i G_i + H_g G_g$$

(2) $$\frac{d}{dt}\mathcal{M}_a = G_a + G_i$$

(3) $$\frac{d}{dt}\mathcal{M}_g = G_g$$

Equations (1), (2) and (3) have been numerically integrated assuming T, ρa and Pg as independent variables and assigning the total flow of the fluid extracted or injected. The liquid and steam production rates have been calculated on the basis of their relative permeabilities K_ℓ, Kv, defined analytically using a Corey's equation

$$K_\ell = (S_\ell^*)^4$$
$$K_v = (1 - S_\ell^{*2})(1 - S_\ell^*)^2$$

where

$$S_\ell = 1 - S$$
$$S_\ell^* = (S_\ell - S_{\ell r})/(1 - S_{\ell r} - S_{vr})$$

$S_{\ell r}$ = residual immobile liquid saturation

S_{vr} = residual immobile vapor saturation

Capillary pressure and any adsorption phenomena have not been taken into consideration even though they could play an important role in the reservoir dynamics and in the reserve estimation.

Fig. 1 illustrates an ideal reservoir. This reservoir initially contains a large volume of vapor and a small volume of liquid water at boiling point. The fluid delivery is 40 Kg/sec and the water is presumed to be immobile.

Fig. 2 shows the change over a period of time of the total pressure and of the cumulative steam production.

The main characteristic of the pressure decline curve is given by the rapid decrease occurring in the first period of production due to the extraction of the noncondensable gas. This fast decrease ends when the gas pressure is very small and total pressure is close to that of saturation.

The variation of gas content and steam saturation are shown in Fig. 3.

The reservoir temperature decreases very slowly and obviously determines the vapor pressure as long as two phases are present in the reservoir. The slow decline in temperature signifies that the heat reserves are much greater than the heat required to vaporize the liquid contained in the reservoir.

It can be seen that after 5400 days (approx. 15 yrs) of production, 28% of the water stored in the reservoir has been produced causing a lowering in the temperature of only 3 °C. In the same period, the vapor saturation has changed from .80 to .86.

In practice, the reservoir engineer can never have complete information on the initial state of the reservoir. Thus, he will never have all the information that he needs to build a numerical model of the reservoir in order to predict its future evolution. However, after the reservoir has been in production for a certain period, infor

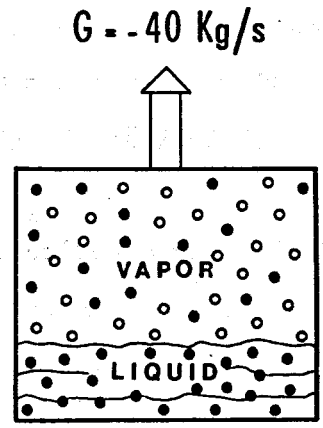

RESERVOIR VOLUME	$V = 4 \cdot 10^9\ m^3$
POROSITY	$\Phi = .07$
SPECIFIC HEAT OF ROCK	$C_R = 1200\ J/Kg°C$
ROCK DENSITY	$\rho_R = 2500\ Kg/m^3$
INITIAL STEAM SATURATION	$S_o = .8$
INITIAL GAS PRESSURE	$P_{go} = 14.8$ Bar
INITIAL RESERVOIR TEMPERATURE	$T = 173°C$
INITIAL STEAM PRESSURE	$P_{vo} = 8.5$ Bar

Fig. 1. Initial and boundary conditions for the reservoir considered in this study.

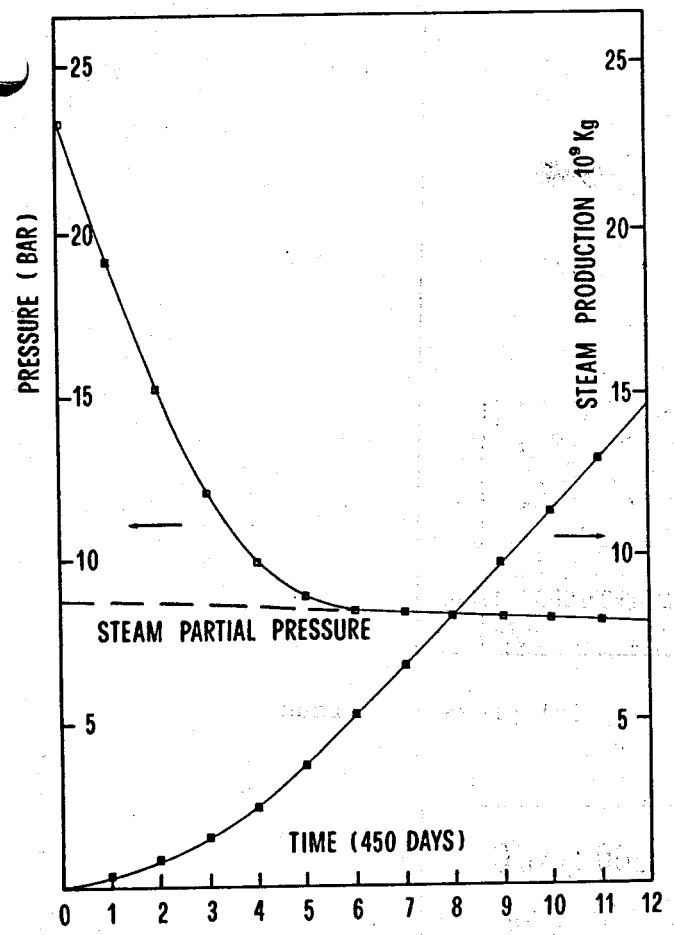

Fig. 2.

Time behavior of the total pressure and of the steam production.

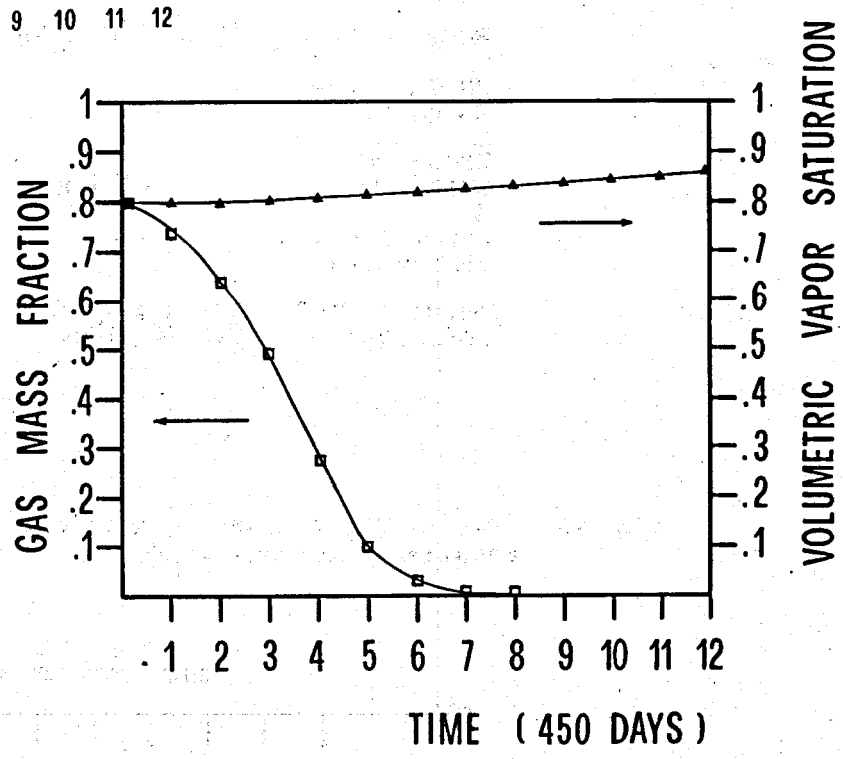

Fig. 3. Evolution of the gas mass fraction in the produced fluid and of the volumetric steam saturation during the reservoir depletion.

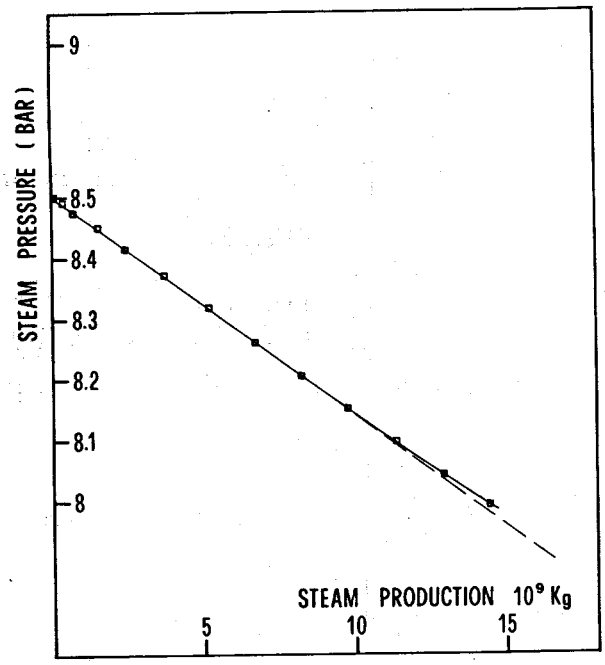

Fig. 4. Graph of the steam partial pressure versus steam production.

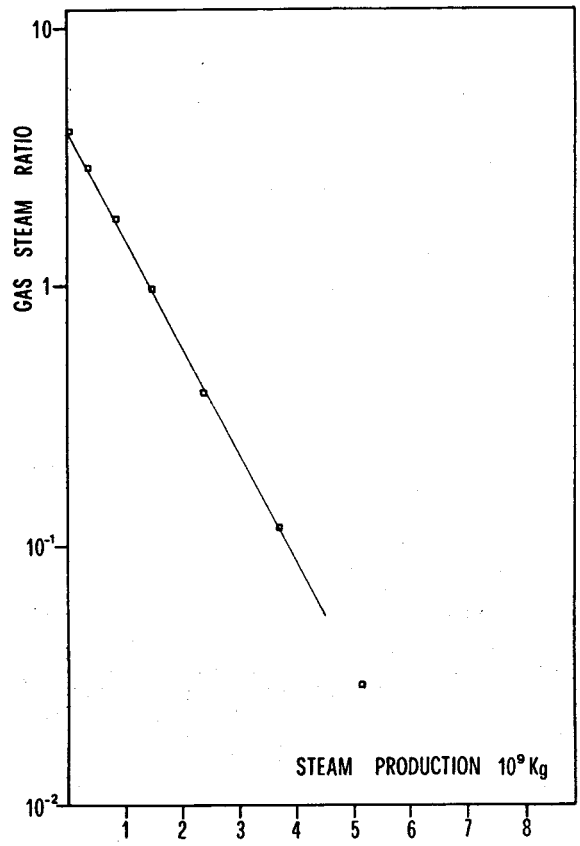

Fig. 5. Graph of the gas steam ratio versus steam production.

mation will be available for the flow rate and pressure which can be used to characterize the reservoir and maybe to estimate the reserves.

Figs. 2 and 3 show graphs that contain almost all the information necessary to evaluate the fluid reserves, once it has been established that the reservoir being studied can be considered zero-dimensional.

The rock energy decrease corresponding to a temperature decrease ΔT is

$$\Delta \mathcal{E}_r = (1-\phi) V c_r \rho_r \Delta T$$

As most of the energy is contained in the rock rather than in the fluid, we can assume with a good approximation that this value must balance the energy spent to vaporize the fluid produced and the work performed on the fluid leaving the system

$$G_a (E_v - E_\ell) \Delta t + G_a (P/\rho_v) \Delta t$$

The result is

$$\Delta T = G_a \Delta t (H_v - E_\ell) / [(1-\phi) c_r \rho_r V]$$

or even

$$\Delta P = \left(\frac{dP}{dT}\right)_s \frac{G_a (H_v - E_\ell) \Delta t}{(1-\phi) c_r \rho_r V}$$

A more precise calculation, which still presumes that the energy of the fluid is negligible with respect to the rocks, gives the equation

$$\Delta P = \left(\frac{dP}{dT}\right)_s \frac{G_a (H_v - h(P))}{(1-\phi) c_r \rho_r V} \Delta t$$

where

$$h(p) = \frac{E_\ell \rho_\ell - E_v \rho_v}{\rho_\ell - \rho_v} \qquad K(p) = \left(\frac{dP}{dT}\right)_s$$

This equation in practice gives the same results as the previous equation, as the vapor density is generally irrelevant compared with that of the liquid.

Finally, given that Hv, El and h (p) are functions which vary slightly with respect to p, the significance of the previous equation is that pressure is almost a linear function of the mass produced. The slope of the plot of the pressure vs the cumulative steam production is approximately proportional to the inverse of the heat capacity of the rock. In practice, for a reservoir of this type, it is possible to evaluate the rock volume (if the density and specific heat are known) by measuring the decrease in pressure or temperature corresponding to a given mass of vapor produced.

Using the results given in Fig. 1 and applying these concepts, the graph shown in Fig. 4 is obtained. Estimating that the average K (p) is between 8.5 and 8 bar and assuming for Hv-El, the value for the initial reservoir conditions, we obtain:

$$(1-\phi)V = 37.44 \; 10^8 m^3$$

which is in good agreement with the actual value of $37.20 \; 10^8 m^3$.

3 – Gas content decline

The previous thermodynamic considerations do not allow the calculation of fluid reserves.

However the gas, which is also present in the reservoir, at equilibrium conditions is much more concentrated in the vapor phase than in the liquid.

Thus, if fluid production also derives from boiling of the liquid present in the reservoir, the variation of gas content in the steam produced clearly depends on the amount of liquid initially in place.

Let Mgv be the mass of gas in the vapor phase.

Assuming the temperature of the system to be almost constant, we have

$$\eta = \frac{\rho_{gv}}{\rho_v}$$

but

$$\frac{d}{dt}\eta = \frac{1}{\rho_v}\,\frac{1}{\phi V S}\,\frac{d}{dt}M_{gv}$$

where $M_{g\ell}$ is the mass of gas dissolved in the liquid.

Introducing the distribution coefficient K_D which is dependent on temperature, and considering also that the vapor saturation varies very little during the time period being considered, we obtain

$$\frac{d}{dt}M_{g\ell} = (1-S)\phi V\,\frac{1}{K_D}\,\frac{\rho_\ell}{\rho_v}\,\frac{d}{dt}\rho_{gv} = (1-S)\phi V\,\frac{\rho_\ell}{K_D}\,\frac{d}{dt}\eta$$

or

$$\left[\phi V S\,\rho_v + (1-S)\phi V \rho_\ell \frac{1}{K_D}\right]\frac{d}{dt}\eta = \eta G_v = G_g$$

Therefore, for short time periods, there is a linear relationship between the logarithm of the gas/steam ratio and the cumulative steam production. Fig. 5 gives graph of $\ln \eta$ in function of the vapor produced. If the value of the quantity ϕ V is known, we can estimate S from the slope of the straight line shown in the figure, obtaining

$$S = .803$$

For vapor-dominated system in which S is quite large, usually the expression $(1-S)\rho_e / K_D$ can be ignored with respect to $\rho_v S$ and the product ϕ VS can thus be calculated directly.

In the example above, where S is quite large we obtain

$$\phi VS = .239\ 10^9\ m^3$$

while the actual value is $.224\ 10^9\ m^3$

Therefore, if the products ϕ VS and $(1 - \phi)$ V are known, it is possible to estimate $(1-S)\phi V \rho_e$ i.e. the fluid reserves, evaluating V or ϕ by other methods, e.g. geophysical.

4 - Conclusions

The evolution of the temperature of a homogeneous two-phase geothermal reservoir is controlled exclusively by the vaporisation process. In vapor dominated system, the gas content of the fluid produced depends mainly on the volume fraction of the reservoir which was initially occupied by vapor.

Adopting these two concepts in the analysis of the evolution of the reservoir temperature and the gas/steam ratio it is possible to evaluate the fluid reserves.

Actually these concepts can only be applied in particular circumstances (Ref. 4). Normally the liquid water in a reservoir is not uniformly distributed, the reservoir is not homogeneous or isotro

pic, fluid properties are different from place to place and probably the assumptions concerning the gas are incomplete.

These factors can be taken into consideration with distributed parameter models.

Nomenclature

$\mathcal{E}$	= Energy	Joule
H	= Specific enthalpy of fluid	Joule/Kg
$\mathcal{M}$	= Mass	Kg
G	= Flow rate (> 0 for injection, < 0 for production)	Kg/s
S	= Volumetric vapor saturation	
P	= Pressure	N/m^2
T	= Temperature	°K
Δt	= Time step	s
ϕ	= Rock porosity	
C_R	= Specific heat of the reservoir rock	J/Kg°K
E	= Specific energy of fluid	J/Kg
ρ	= Fluid density	Kg/m^3
η	= Gas - steam ratio	
M_{gv}	= Mass of the gas in the vapor phase	Kg
M_{gl}	= Mass of the gas in the liquid phase	Kg

Subscripts

a	= Water	ℓ	= Liquid water
r	= Rock	v	= Steam
g	= Gas	gv	= Gas in vapor phase
i	= Injection	gl	= Gas in liquid phase

References

1 - White D.E., Muffler L.J.P. and Truesdell A.H. (1971) - Vapor dominated hydrothermal systems compared with hot water systems. Econ. Geol. 66,75-97

2 - Truesdell A.H. and White D.E. (1973) - Production of superheated steam from vapor-dominated geothermal reservoirs. Geothermics 2,3-4, 145-164

3 - Grant M.A. (1977) - Broadlands-a gas-dominated geothermal field Geothermics 6,1/2, 9-29

4 - Atkinson P.G., Celati R., Corsi R. and Kucuk F. (1978) - Behavior of two-component vapor-dominated geothermal reservoir - SPE paper 7132, presented at the Annual California Regional Meeting of the Society of the Petroleum Engineers of AIME, San Francisco, California 12-14 April.

5 - Nathenson M. (1975b) - Some reservoir engineering calculations for the vapor-dominated system at Larderello, Italy. U.S. Geol. Survey Open-File Rept. 75-142, 38 pp.

6 - Celati R., Manetti G., Marconcini R., Neri G., (1976) - A reservoir engineering study in Gabbro zone (Northern part of Larderello field) 2nd Workshop Geothermal Reservoir Engineering, Dec.1-3, 1976, Stanford University, Stanford, California.

7 - Weres O., Tsao K. and Wood, B. - Resource, Technology and Environment at The Geysers, Lawrence Berkeley Laboratory Report LBL 5231, (July 1977).

8 - Whiting R.L. and Ramey H.J.Jr. (1969) - Application of material and energy balances to geothermal steam production. J.Pet. Technol. pp. 893-900.

9 - Brigham W.E. and Morrow, W.B. (1977) - P/z behavior for geothermal steam reservoirs, Society of Petroleum Engineers Journal 17,6 (December 1977), 407-412.

10 - Pruess K., Bodvarsson G., Schroeder R.C., Witherspoon P.A., Marconcini R., Neri G., and Ruffilli C. - Simulation of the Depletion of Two-Phase Geothermal Reservoirs paper SPE-8266, presented at the 54th Annual Fall Technical Conference and Exhibition of the SPE of AIME, Las Vegas, Nevada, 1979.

11 - Sorey M.L., and Fradkin L.T. (1979) - Validation and comparison of different models of the Wairakey Geothermal Reservoir. 5th Workshop Geothermal Reservoir Engineering, Stanford University, Stanford, California, pp. 215-220.

12 - Mercer J.W., Pinder G.F. and Donaldson I.G. (1975) - A Galerkin finite-element analysis of the hydrothermal system at Wairakei, New Zealand.
Journal of Geophysical Research, 80 (17), 2608-21.

13 - Pritchett J.W., Garg S.K. and Brownell, D.H., Jr. (1976) - Numerical simulation of production and subsidence at Wairakei, New Zealand. Summaries Second Workshop Geothermal Reservoir Engineering, Dec 1-3, 1976, Stanford University, Stanford, California, pp. 310-23.

14 - Mercer J.W. and Faust C.R. (1979) - Geothermal reservoir simulation. 3. Application of liquid-and vapour-dominated hydrothermal modeling techniques to Wairakei, New Zealand.
Water Resources Research 15,3, 653-671

PERFORMANCE MATCHING AND PREDICTION FOR SERRAZZANO GEOTHERMAL RESERVOIR BY MEANS OF NUMERICAL SIMULATION

K. Pruess, O. Weres, R. Schroeder, R. Marconcini, and G. Neri

1. Introduction

Serrazzano geothermal reservoir is one of the distinct zones of the extensive geothermal area near Larderello in central Tuscany, Italy. Natural manifestations and utilization of steam and hot water from shallow holes in this region have occurred for centuries. Deep drilling was begun after 1930, and since 1939 electric power has been generated at Serrazzano from geothermal steam (with an interruption in World War II, when the wells were destroyed).

We have developed a distributed-parameter history-match simulation of the performance of Serrazzano reservoir from 1959 to 1975. The reservoir model obtained from this was subsequently used for predicting the future performance of Serrazzano reservoir through 1990. To our knowledge, no such simulation has ever been attempted for a producing vapor-dominated geothermal reservoir. Serrazzano was chosen as a case study for developing and evaluating the methodology for two reasons: (1) detailed production data and much geological and hydrological information is available for the reservoir; (2) for environmental reasons surface disposal of produced brines is no longer acceptable in Italy, and numerical studies are needed to aid in developing an appropriate injection program.

The numerical simulations presented in the present paper were carried out with a computer program called SHAFT79. This program was developed at Lawrence Berkeley Laboratory, and is briefly reviewed in Chapter 2. Data base and elements of a conceptual model for Serrazzano are discussed in Chapter 3. Subsequently we explain the method used in developing a history

match simulation, and present results for our current "best" model of Serrazzano reservoir. Several effects which could cause a more rapid reservoir decline are examined in Chapter 6, and Chapter 7 presents the extrapolation of reservoir performance through 1990.

2. The Simulator SHAFT79

SHAFT79 solves coupled mass- and energy-transport equations for two-phase flow in a porous medium, using an integrated finite difference method. This method allows a very flexible one-, two-, or three-dimensional description of reservoirs, and is easily applicable to irregular shapes and geological features. Methodology and applications of SHAFT79 have been discussed in References 1-3. The main assumptions and approximations can be summarized as follows: (1) Geothermal reservoirs are approximated as systems of porous rock saturated with one-component fluid in liquid and vapor form. (2) Porosity can vary with temperature and pressure, with all other rock properties being constant. (3) Liquid, vapor, and rock matrix are in local thermodynamic equilibrium, i.e., at the same temperature and pressure, at all times. (4) Capillary pressure is negligible.

SHAFT79 includes an accurate description of thermophysical properties of water substance, based on the steam table equations as given in Reference 4. Time is discretized fully implicitly, and the coupled non-linear finite difference equations for mass- and energy-transport are solved simultaneously, using Newton/Raphson iteration. The linear equations arising in the iteration are solved with an efficient sparse solver.[5]

Accuracy of the program has been verified by comparison with numerical simulations published in the literature, and by comparison with the quasi-analytical similarity solution method developed by O'Sullivan.[6,7] Table 1 summarizes the performance of SHAFT79 in simulating our present "best" model

of Serrazzano geothermal reservoir on LBL's CDC-7600 computer.

3. The Data Base

At the present time, Serrazzano field has 19 producing wells and 18 wells which are shut in because they are dry or nearly dry. The produced fluid is

simulated time	number of time steps	average time step	total CPU-time	CPU-time per time step	typical throughput
15.5 years	243	23.3 days	2267 sec	9.3 sec	12.7

Table 1: SHAFT79 - Performance for Serrazzano Simulation. Throughput is the ratio of mass produced in a time step to mass initially in place in the producing element (the figure given is for well Pozzaie 2 at element N4, see Figure 1).

approximately 96.5% superheated steam, and 3.5% non-condensable gases (mainly CO_2). Liquid water has never been encountered at Serrazzano. However, mass balance considerations demonstrate convincingly that most of the fluid reserves in Serrazzano are in place in liquid form.[8] From the drill logs it has been possible to identify the permeable strata of the reservoir, and to map the geometry of the system.[9,10] The reservoir is an anticlinal horst-and-graben structure, with thickness varying from some ten meters near the intensely fractured structural high to more than 500 meters in areas with thick layers of "evaporite" rocks (see Figure 1). The "evaporite" complex consists of highly permeable and porous anhydrite, limestones, and radiolarites. The location of impermeable boundaries is somewhat open to question.

Formations underlying the structural high may have non-negligible permeability and porosity. Fractures are known to play an important role in fluid transport in Serrazzano.[11,12] It appears possible that significant amounts of steam are brought through fractures into the main reservoir from great depth (> 2 km).

Geochemical and hydrological work has shown that Serrazzano field is a rather isolated section of the Larderello geothermal region; no significant recharge is believed to occur.[13]

Average properties of the rock matrix are subject to large uncertainty. Laboratory tests on cuttings have given consistent values for specific density, specific heat, and heat conductivity. However, average porosity and permeability cannot be determined from core samples on a laboratory scale. These parameters are very poorly known. A few drawdown- and buildup-tests have been conducted in the past, from which a rough picture of the kH-distribution has been inferred.[14,15] Interpretation of these tests is questionable due to 2-phase conditions in parts of the reservoir.

Wellhead temperature and pressure measurements in flowing wells, and pressure measurements in shut-in wells, provide a basis for determining average thermodynamic conditions in the reservoir. Interpretation of these data is complicated by substantial variations on a local scale, sometimes due to deep fractures, sometimes due to shallow cold aquifers.

Operating conditions in Serrazzano approximate production with constant pressure p = 5 bars. Many wells have rather small flow rates, and estimation of downhole conditions is uncertain because of unknown and possibly large effects from heat losses to shallow aquifers.[8]

Important work on average pressure distributions in Serrazzano was done by Atkinson et al. (ref. 16). Using somewhat subjective judgment in evaluating field data with their sometimes large fluctuations and local variations, these authors were able to construct several contour maps of average reservoir pressures between 1960 and 1975. These pressure maps, when combined with temperature data, show that superheated conditions prevail throughout the main well field, near the structural high.

No direct information exists regarding the distribution of pore water in the reservoir. A rough hint is available from a conceptual model of Serrazzano as developed by Weres et al.[17,18] Postulating hydraulic continuity with surrounding aquifers, and using a plausible value of T = 275°C for initial (pre-exploitation) reservoir temperature at depth, the steam/two-phase interface is estimated near 500 m depth.

Positions, producing horizons, and time-dependent flow rates are known for all wells.

In summary: Although much data and qualitative information is available for Serrazzano, the data base falls very much short of the detailed and

complete definition required as input for distributed parameter simulation. Moreover, available data reflect actual field conditions to varying degrees, and are subject to various degrees of confidence. As indicated in Table 2, the most significant deficits with regard to data availability exist in the areas of permeability, distribution of pore water, and porosity. Partially unavailable or uncertain are data defining geometry and boundary conditions of the reservoir, and the detailed distribution of temperatures and pressures.

4. Method of Simulation

The simulation is carried out using the geologically accurate mesh as developed by Weres (ref. 18,19). Figure 1 gives an areal view of the reservoir, with the positions of the geological cross-sections employed in the mesh generation indicated by straight lines labeled A to Z. Figure 2 shows the computer-generated mesh in two different (rotated) views. The mesh represents a reservoir that is a curved thin sheet approximately 1 km from top to bottom, and areally covers about 25 km^2. It has 234 polyhedral elements with 679 polygonal interfaces between them. There are up to 10 interfaces per element.

Our initial attempts to model the pre-exploitation phase were soon abandoned when it became apparent that the almost complete lack of data would leave us with a multitude of rather meaningless parameter choices. Subsequently, we endeavored to model the post-1959 period, for which rather detailed field data are available.

The data (Table 2) have to be grouped into those which are provided as input to the simulation, and those against which simulated results are compared. The division between the two groups is to some extent arbitrary. We noted before that operating conditions in Serrazzano approximate production with

PARAMETERS	RATING Availability	Sensitivity	HANDLING
geometrical definition of reservoir	A-B	β	Essentially fixed (minor adjustments where imperative)
rock properties: density ρ ; specific heat C_R; heat conductivity K_R	A	α	fixed (ρ = 2600 kg/m^3; C_R = 775 J/kg^oC; K_R = 2.1 W/m^oC)
permeability: k	B	β	adjustable
porosity: ϕ	B	α	fixed at somewhat arbitrary ϕ = 10%
boundary conditions	A-B	α-β	fixed (no flow)
initial conditions: temperature T; pressure p;	A-B	β	adjustable within a range
vapor saturation S	B	β	adjustable
wells: locations	A	β	fixed } as measured
flow rates	A	β	fixed } as measured
pressures p as function of time	A-B	-	to be matched by simulation

Table 2: Serrazzano Data Base. The various parameter groups needed for a simulation are rated on scales of availability (A: rather good definition from field data; B: not well defined from field data, hence susceptible to rather arbitrary adjustments; A-B: intermediate) and sensitivity (α: parameter variations have little impact on simulated field performance; β: parameter variations have strong impact on simulated field performance; α-β: intermediate). Availability ratings apply to period after 1960.

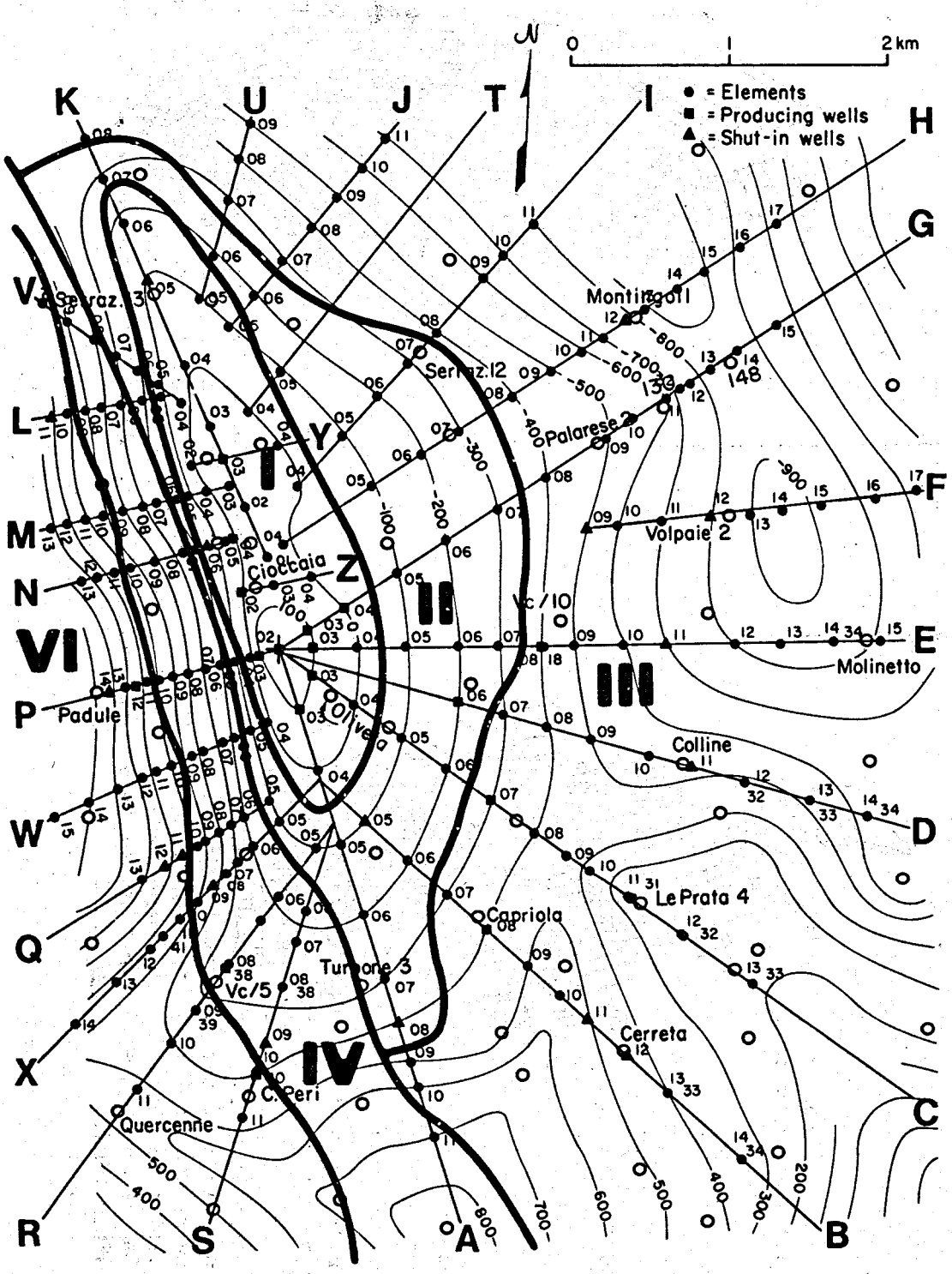

Fig. 1. Areal map of Serrazzano geothermal reservoir. (Thin lines—contours of caprock elevations; straight lines—geological cross sections; thick lines—boundaries of zones with different permeability) (XBL 797-7591B)

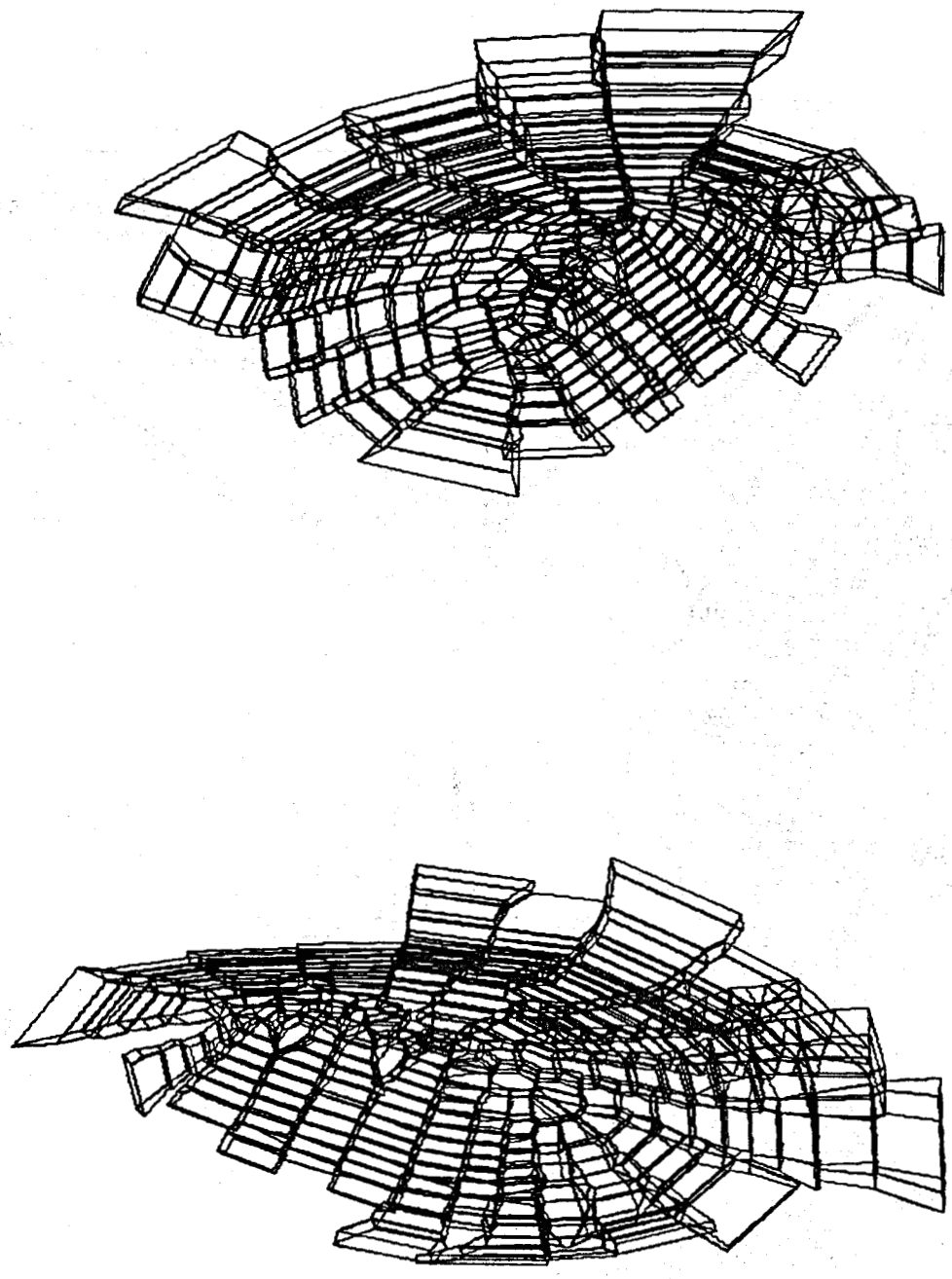

Fig. 2. Serrazzano mesh in rotated perspective views. (XBL 787-9570)

constant (well head) pressure. For modeling purposes, this could be imposed as a (mathematical) sink condition. The objective then would be to match observed production flow rates.

We chose a different approach, which makes a more sensitive use of the observed flow rate data. (These data are measured with good accuracy.) Namely, we impose observed flow rates on the simulated reservoir model. The task of the history match simulation then becomes one of (i) sustaining the observed flow rates over the period from 1959 to 1975, for which production data are available, and (ii) doing so under conditions of relatively mild pressure fluctuations near the main well field.

The history match simulation proceeds in trial-and-error fashion. We make certain assumptions for those parameters which are not well known, or are unknown, compare simulated field performance with observed performance, and then modify our parameter estimates so as to reduce discrepancies between simulated and observed performance. The limited availability of data (see Section 3) confronts us with a multitude of choices. It would appear that one could invoke a large variety of assumptions ad hoc, which may not be too meaningful, yet could not be refuted. The actual situation is, however, not anywhere near that ambiguous. The seemingly rather trivial requirement of sustaining observed flow rates at nearly constant pressures turns out to be very restrictive, due to the long duration of the simulation (15.5 years). The main well field near the structural high contains superheated steam, and therefore has a rather small mass content. The mass produced over 15.5 years is several hundred times larger than the mass in place in the main well field. Only through very subtle fine-tuning of certain parameters was it possible to avoid a premature catastrophic decline of pressures in the

main well field. Table 2 summarizes the handling of the various parameters during development of the history match.

Most important among the adjustable parameters is the permeability distribution. It determines the "dynamic" response of the reservoir; i.e., the way in which time-dependent production rates q(t) give rise to time-dependent pressures p(t). The permeability along the 1-phase flow path determines the short-term (days or weeks) "elasticity" of well field pressure response to fluctuations in production rates. Permeability distributions in the two-phase (boiling) region determine the extent to which pressure at the two-phase/steam interface can be maintained over periods of substantial depletion (years).

Under favorable circumstances, boiling rates away from the interface can be sufficiently large (equal to or larger than at the interface) to supply enough hotter steam to sustain temperature (hence pressure) at the interface. Then, the interface remains approximately stationary and at approximately constant pressure, while pressures decline away from the interface at the margins of the reservoir. The maps of average pressures as developed by Atkinson et al. (ref. 16) suggest that this type of behavior is present in Serrazzano.

A pattern of depletion with approximately stationary two-phase/steam interface at approximately constant pressure can prevail as long as the reserves of liquid water last. Reservoir performance during this period depends little on ultimate fluid reserves, and the simulation is not very sensitive to variations of those parameters which determine ultimate fluid reserves. These are mainly porosity ϕ and vapor saturation S in the two-phase zone. Therefore we have kept ϕ constant at a "best guess" of 10%.

Initial vapor saturation was chosen as follows. We compute relative

permeabilities from a version of Corey's equations:

$$k_{steam} = \begin{cases} (2r-S)\ S^3/r^4 & \text{for } S \leq r \\ 1 & \text{for } S \geq r \end{cases}$$

$$k_{liquid} = \begin{cases} (r-S)^4/r^4 & \text{for } S \leq r \\ 0 & \text{for } S \geq r \end{cases}$$

with the residual immobile water saturation taken as a somewhat arbitrary $1-r = 40\%$.

The pressure maps of Atkinson et al. show that pressure gradients at depth are less than 1/3 the hydrostatic gradient, from which we conclude that no mobile liquid water is present in the reservoir. Thus, initial liquid water saturation 1-S should not exceed 40%. We have taken S = 60% as initial conditions (summer of 1959), while adjusting the location of the two-phase/steam interface in the course of development of the history match.

During the development of the simulation, adjustments were also made to the assumed initial conditions for summer 1959. It was necessary to relinquish some detail (local variations) in order to model successfully overall field behavior. E.g., the well VC/10 (near element E8, Figure 1) is an exceedingly strong producer ($q \approx 25$ kg/sec) with wellhead temperatures in excess of 260°C. The well VC/2 (near element C7, see Figure 1) at about 1 km distance from VC/10, has a low well head temperature of approximately 180°C. Such large variations, which translate into large pressure differences between the (two-phase) steam sources, cannot be accommodated within the mesh. It is likely that VC/10 is fed through a large fracture from depth, which is only poorly connected to the mesh, and that VC/2 is affected by shallow cold

aquifers. We connected VC/10 to a large element representing a deep boiling aquifer, and adopted smoothly varying initial conditions throughout the mesh.

Apart from the inevitable adjustment in the case of VC/10, geometry and no-flow boundary conditions were kept fixed during the simulation. This was done chiefly because modifications based on simulation alone, without independent evidence, would seem rather arbitrary and speculative. Simulation results provide indirect evidence, however, that some cold water recharge is occurring near the margins, and that some steam reaches the main well field from outside the mesh (presumably through deep fractures.)

5. Results of History Match

Our current "best" model of the Serrazzano reservoir was arrived at, in its qualitative (conceptual) and quantitative features, through a large number of simulations. Parameters had to be adjusted again and again to rectify deficits in the simulated reservoir performance. It turned out to be very difficult to sustain observed flow rates throughout the entire modeling period (1959-1975), without "overshooting" pressures in the main well field for the first few years. This difficulty gives important clues to what is happening in the field (see below).

Our model cannot resolve all of the uncertainties about parameters characterizing Serrazzano field. It remains in part speculative, and needs to be further checked and refined as more data become available. We do believe, however, that the model is plausible in view of general ideas about Serrazzano. And it appears reasonable in that it accounts for important trends and features observed in the field.

Qualitatively, the reservoir model is that of a steam cap overlying a boiling aquifer. There is dry steam in the center, near the structural high

(where the main well field is located). Pore water (i.e., two-phase zones) is confined to the margins. Water is immobile throughout. It boils in place as steam flows to the wells. The two-phase/steam interface, located at approximately -500 m (see Figure 1) acts as a nearly constant pressure boundary for the dry steam region. Gravity effects are small as only steam is mobile.

In order to sustain field production over the entire 15.5-year period modeled, we had to introduce 6 zones of different permeability (see Figure 1 and Table 3). Zone I includes the main well field. Its very high permeability is necessitated by the observation that production rates at individual wells can fluctuate appreciably without very strong pressure response. Zones II and IV are essentially regions of dry steam flow, with permeabilities adjusted such as to provide proper resistance to steam flowing from the two-phase margins toward the main well field at the center of the reservoir. Zones III and VI are essentially two-phase regions, with permeabilities such as to obtain a pattern of nearly uniform boiling and hence good pressure maintenance at the two-phase/steam interface during depletion. Zone V is the deep boiling aquifer. The time-dependence of simulated average steam pressures is shown in Figure 3. Values for the slope of pressure decline versus cumulative production (dp/dQ) deduced from this figure are given in Table 4 for the entire simulated period as well as for the post-1967 period. Average simulated pressure decline in the reservoir is somewhat slower than the value $dp/dQ = -1.9 \times 10^{-10}$ bar/kg as deduced from field data by Atkinson et al.[16]

Table 5 gives mass balances for the various zones, as well as for the entire reservoir. It is seen that Zones III and VI contribute roughly equal amounts to cumulative field production. Over 15 years the field loses 18.2% of the mass present on 1/1/60. Total mass reserves are approximately

ZONE	PERMEABILITY (milliDarcy)
I	4000
II	90
III	85
IV	25
V	85
VI	40

Table 3 : Permeability Distribution. The zones are defined in Figure 1.

REGION	$-dp/dQ$ (10^{-10} bar/kg) 1960-75	1967-75
III	.74	1.10
VI	1.91	2.29
entire reservoir	.75	1.35

Table 4 : Simulated Pressure Decline

REGION	Vapor Saturation (%) 1960	1975	Mass Content (10^8 kg) 1960	1975	Mass Loss 10^8 kg	%
I	100	100	1.89	1.84	.05	2.6
II	99.9	100	6.37	4.97	1.40	22.0
III	69.0	73.8	1108.8	950.3	158.5	14.3
IV	83.9	86.5	87.2	74.3	12.9	14.8
VI	60.7	72.6	464.3	333.3	131.0	28.2
R	73.3	78.5	1668.7	1364.8	303.9	18.2

Table 5 : Simulated Mass Balances

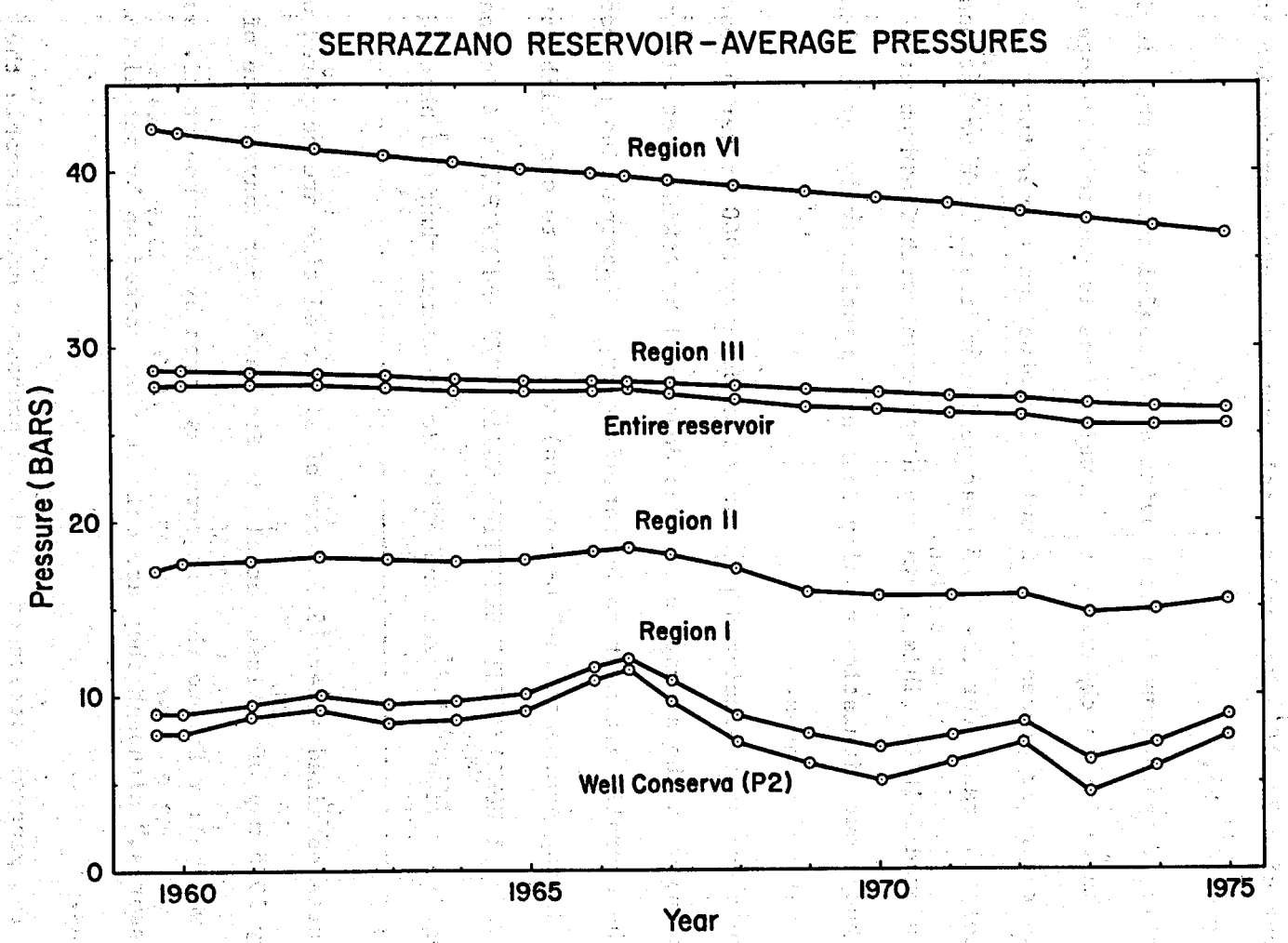

Fig. 3. Simulated average pressures. (XBL 807-1402)

1.7×10^{11} kg in 1960, and 1.4×10^{11} kg in 1975. These values are entirely consistent with Weres' estimate of an initial (pre-exploitation) mass content of 2.3×10^{11} kg, and a total cumulative steam production to date of 0.9×10^{11} kg.[18]

Production temperatures do not provide a meaningful test of the simulation, as much of the variation observed at the well heads is due to well-bore effects rather than reservoir processes.[8] Simulated production temperatures are approximately constant over the 15.5 year period modeled, with variations typically around 5-10°C. This is in rough agreement with field observations, although our simulation usually does not quantitatively agree with the small observed changes.

Figure 4 compares simulated pressures for January 1960 (after 6 months of simulation) with the average pressures developed by Atkinson et al.[16] We consider the overall agreement to be satisfactory. Discrepancies are most pronounced in the southeast (A-B-C-D-region) and are due to our deliberate choice of initial conditions: data from wells VC/2 and Le Prata 4 indicate that the entire region is cooler and at lower pressures than was assumed in reference 16.

Pressures obtained after 15.5 years of simulated time are compared with the January 1975 map of Atkinson et al. in Figure 5. For convenience of discussion we shall refer to the pressures as given by Atkinson et al. as "field pressures," although they are only in part backed up by actual field observations.

While the general pattern of simulated pressures does resemble the "field pressures," for the most part there is no quantitative agreement in detail. Overall, simulated pressures are somewhat high. This is particularly

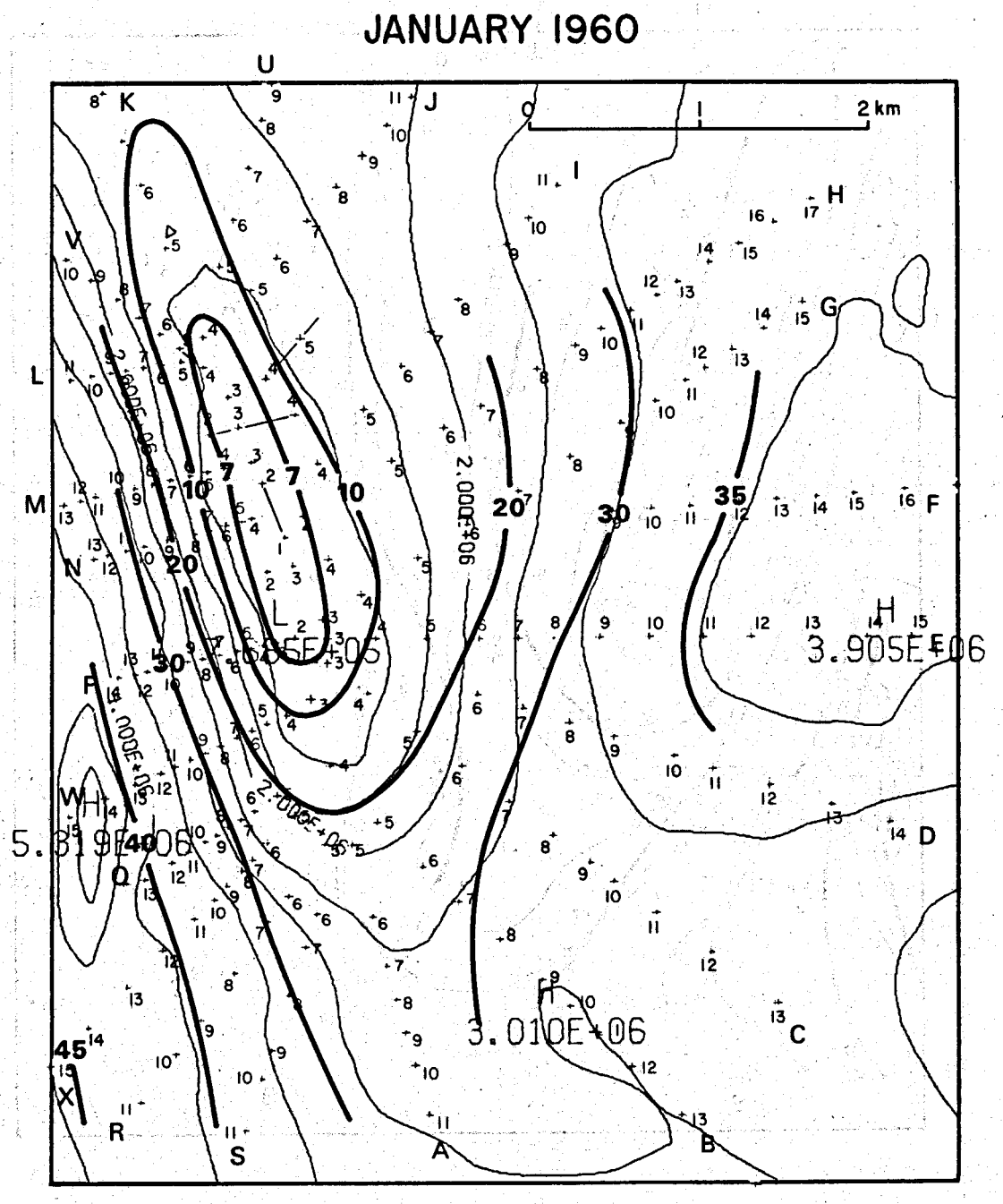

Fig. 4. Pressure distribution for January 1960. The thick contours are based on field observations (units: bars), whereas the thin contours are simulated results (units: Pascals). The simulated results refer to the lowest layer of the reservoir model. Simulated vertical pressure variations are small (≈1 bar). Pressure increments between contour lines are 5 x 10^5 Pascal ≡ 5 bar. (XBL 807-1401A)

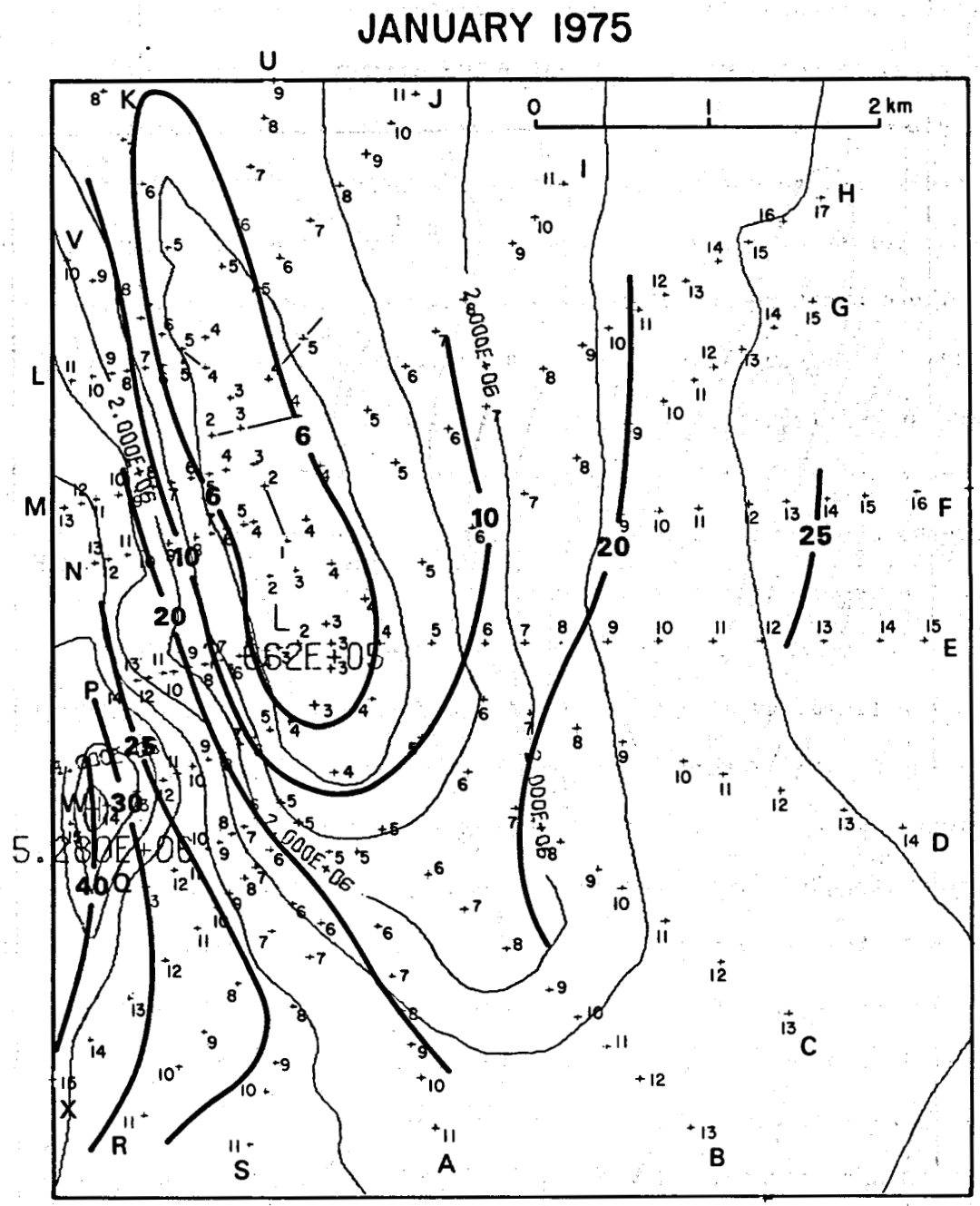

Fig. 5. Pressure distribution for January 1975. (XBL 807-1401B)

evident for pressures in the two-phase region, roughly corresponding to $p > 20$ bars, in both the eastern and western margins of the field. In our model, pressures in the two-phase regions decline solely as a consequence of temperature decline due to heat loss of the rock in boiling water. As we do impose proper steam production rates, we should obtain correct overall heat loss. There are three possible reasons why for a given overall heat loss pressures in the two-phase region could decline more rapidly in the field than in our model: (i) intrusion of some colder water into depleting two-phase zones would lower temperatures, hence pressures; (ii) the volume of the two-phase zone may be somewhat smaller than assumed in our model, either because the reservoir may be somewhat thinner, or because the two-phase/steam interface may be at a depth greater than 500 m ; (iii) heat transfer from the rock to the fluid may be inhibited because some of the permeability may be due to isolated fractures rather than the rock matrix. These effects are further investigated in Chapter 6. Pressures are also somewhat high near the main well field (N4-A3-G4-area). This is probably not entirely due to too high pressures in the two-phase region. The 20 bar contour, which roughly coincides with the two-phase/steam interface, agrees fairly well with the field pressures in the west, without overshooting excessively in the east. Thus, in order to make simulated pressures smaller near the main well field, we would need to diminish permeability along the 1-phase flow path. This, however, would make it impossible to sustain the higher flow rates of the early 1960's. We believe that this difficulty may indicate that some of the steam supply to the main well field originates from deep fractures, rather than from that portion of the reservoir which is simulated in our present model.

Additional support for this hypothesis is provided by the peculiar depletion pattern observed during the simulation. Although simulated pressure decline in the reservoir margins is somewhat slower than observed in the field, we found it quite difficult to sustain the observed flow rates in the main well field. This could only be achieved by fine-tuning the permeability distribution carefully in the two-phase regions such as to optimize pressure maintenance at the two-phase/steam interface. This was achieved by making permeabilities in the two-phase regions rather "large," so that boiling would easily spread all the way to the hotter margins rather than being concentrated near the two-phase/steam interface. Resulting boiling rates are almost uniform throughout, and are actually increasing somewhat away from the interface toward the margins. During the entire simulation period, vapor saturations increase almost uniformly throughout the two-phase region, and the two-phase/steam interface remains stationary. These simulated results support some of the choices made with regard to initial distribution of pore water in 1959, namely, to place the two-phase/steam interface near 500 m depth, where it is believed to have been in the pre-exploitation state, and to take initial vapor saturation to be constant (S = 60%) throughout the two-phase zone. Thus, the model evolves in a way which is consistent with our assumptions for initial distribution of pore water. The extent to which we had to fine-tune the permeability distribution to achieve uniform boiling (and actually going somewhat beyond) in order to sustain production may indicate that in actuality not all production is generated through boiling in the two-phase zone modeled. The results seem to suggest that an as yet undetermined amount of steam enters the main well field through fractures from depth, perhaps at a rate of a few kg/sec.

6. Additional Temperature Decline

We noted before that simulated average pressure decline is slower than observed in the field. In order to obtain a pressure decline of $dp/dQ = -1.9 \times 10^{-10}$ bar/kg, as suggested in ref. 16, an additional average pressure drop of $\delta p \approx 3.5$ bar is required in the two-phase regions. At an average initial temperature $T \approx 240\ ^{o}C$ this corresponds to an additional temperature decline of $\delta T \approx 5\text{-}6\ ^{o}C$. We shall now examine the effects mentioned in Chapter 5 to see which could be likely candidates for producing such a temperature decline.

6.1 Intrusion of Cold Water

In order to assess this effect we compute mixing temperatures for cold water and a hot rock/water/steam reservoir. We start with a reservoir temperature of $T = 240\ ^{o}C$ and a vapor saturation of $S = 67.5\%$, corresponding to the average vapor saturation in the two-phase region obtained after 15.5 years of simulation for the Serrazzano model. Results for additional temperature decline δT as a function of cold water recharge are plotted in Figure 6 for the cases of recharge water temperature $T_w = 20\ ^{o}C$ and $T_w = 80\ ^{o}C$. If recharge is equal to discharge, the system ends up at a vapor saturation $S = 60\%$, equal to the initial value, with an additional temperature decline $\delta T = 2\ ^{o}C$. Recharge would have to exceed twice the discharge in order to yield a δT of $5\ ^{o}C$.

These estimates and the curves in Figure 6 are based on a model of "uniform mixing," i.e., with the recharge waters being uniformly distributed throughout the boiling volume. This model may not be very realistic, because

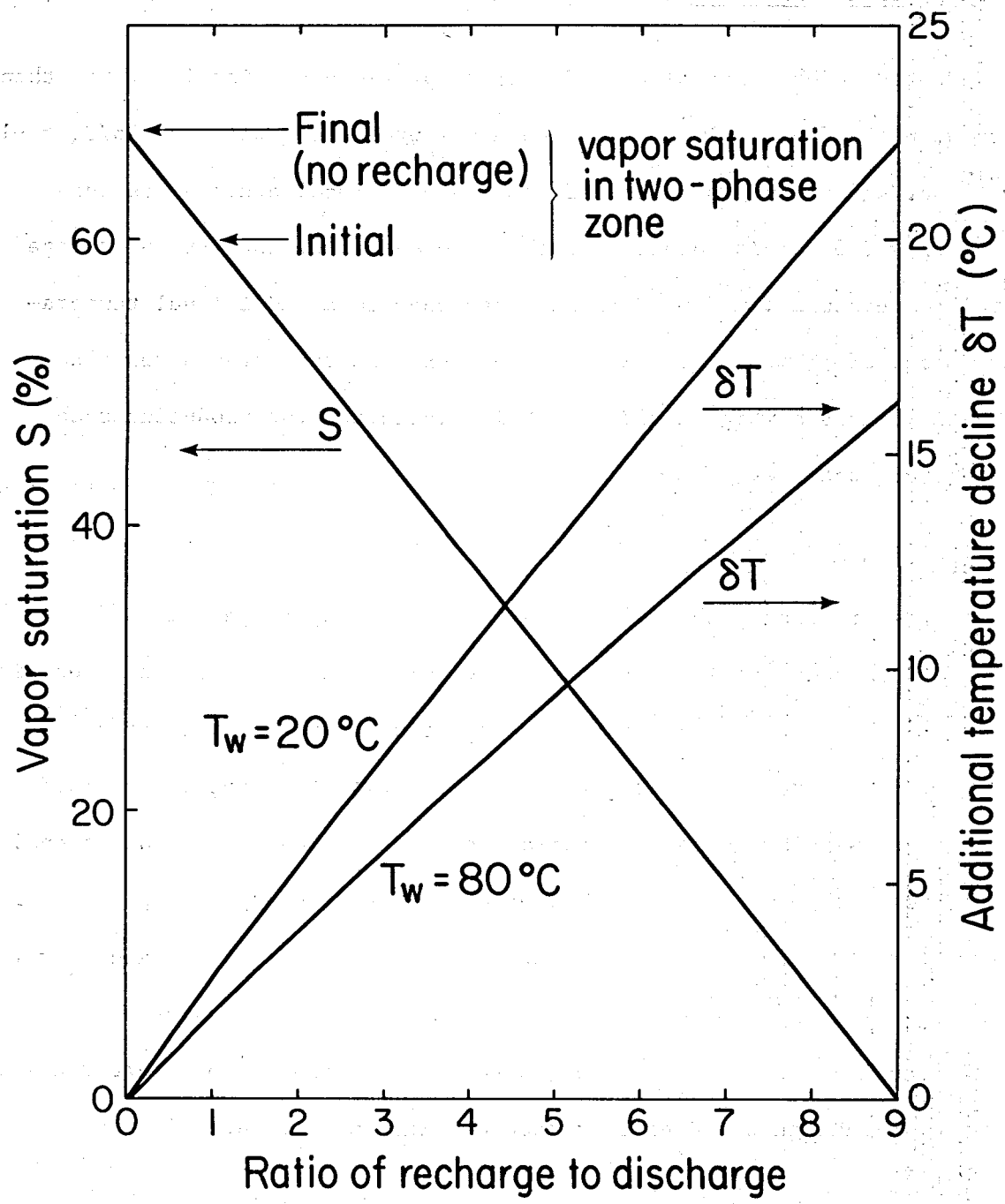

Figure 6. Effects of Cold Water Intrusion. (XBL 808-2725)

recharge waters may instead move from the reservoir margins inward as rather sharp fronts. In the latter case the water flowing into the boiling zone would have been heated up to original reservoir temperature, so that our model, above, would overestimate temperature decline. This suggests that, while recharge could make a significant contribution, it is in all likelihood not a major source of the additional temperature decline.

6.2 Lower Two-Phase/Steam Interface

The total amount of steam produced from the two-phase region in 15.5 years (1959-75) is $Q = 2.94 \times 10^{10}$ kg. Virtually all of this is generated through boiling, in which the rock transfers a total amount of 5.36×10^{16} J of heat to the fluid (corresponding to an average vaporization enthalpy of $h_{vap} = 1.82 \times 10^{6}$ J/kg). If the 1959 initial conditions were modified such as to extend the region of large vapor saturation to greater depth, boiling would be confined to a smaller volume. In order to supply the same amount of heat for vaporization, the rock temperature would have to decline by a larger amount.

In Figure 7 we have plotted the reservoir volume V_D below depth D as a function of depth. The two-phase zone has a volume of 4.94×10^{9} m^3, corresponding to an average depth of the two-phase/steam interface of -479 m. Figure 7 also shows the additional temperature decline δT that would result from a lowering of the two-phase/steam interface. In order to yield a δT of 5-6 ^{o}C, the interface would have to be lowered to a depth of -680 to -700 m. Such a value, while somewhat large, is not incompatible with Weres' model of hydraulic continuity between the pre-exploitation reservoir and surrounding aquifers. With a typical elevation of +100 m for the water table, the vapor pressure at the two-phase/steam interface would have to balance a column of

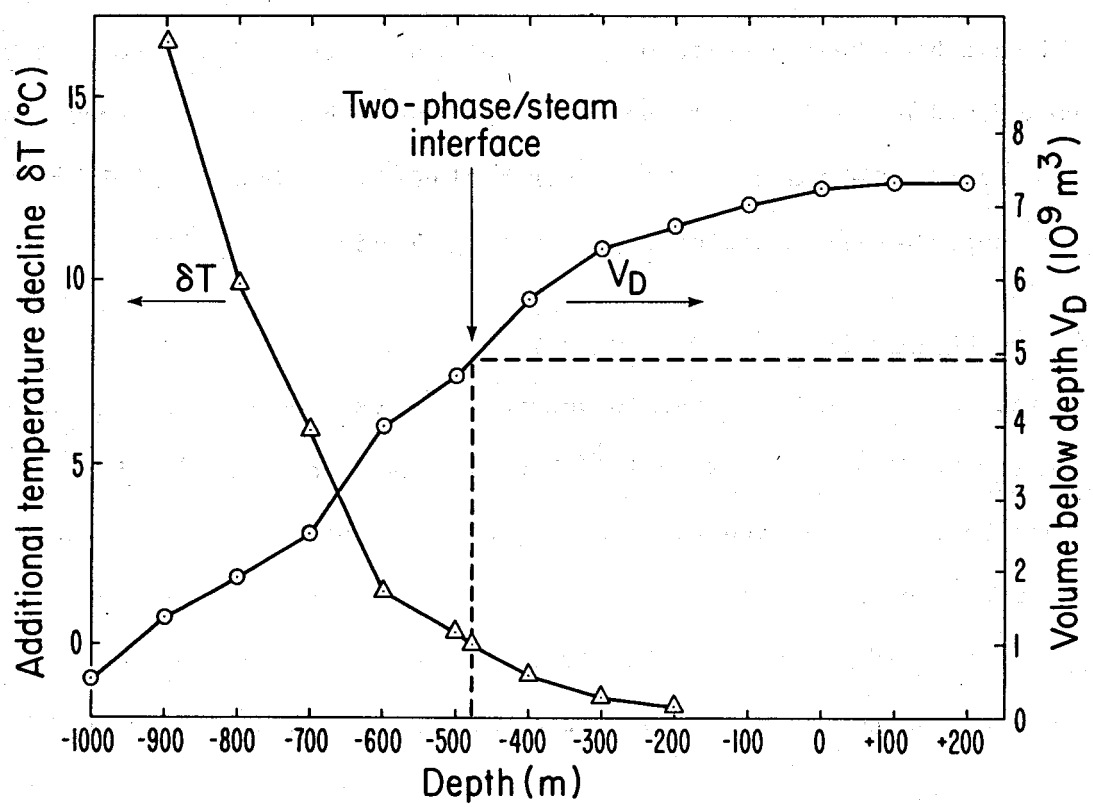

Figure 7. Temperature Decline in Dependence of Assumed Depth of Two-Phase/Steam Interface. (XBL 808-2727)

800 m water. Assuming a linear dependence of water temperature and density upon depth, the required pressure is 69 bars, corresponding to a pre-exploitation temperature at the two-phase/steam interface of 285 ^{o}C. A closely related possibilitiy is that the top of the two-phase zone may have a rather small liquid saturation in 1959, and dry up during subsequent production.

It is to be noted that the effect discussed above comes about from a reduction of the volume of the boiling zone. An alternative to reducing the volume by lowering the two-phase/steam interface would be to decrease the thickness of the reservoir by an appropriate amount (about 50% for a $\delta T \approx 6$ ^{o}C, see Figure 7). The data available to us do not allow to distinguish between these alternatives.

6.3. Incomplete Thermal Equilibration between Rock and Fluid

Fractures are known to play an important role in fluid transport in Serrazzano. It appears possible that parts of the reservoir have low matrix permeability. As steam is produced, the water in the more permeable regions boils, extracting heat from the rock matrix and lowering its temperature. Subsequently heat will flow mainly by conduction from the less permeable rock into the flow regions. The temperature decline in the boiling region will be more rapid, and in the impermeable rock less rapid, than would be observed if water and rock were mixed throughout the entire volume. The additional temperature decline δT occurring in the flow region because of incomplete temperature equilibration between flow- and no-flow-regions will increase with (i) boiling rate, (ii) fraction of impermeable rock volume, and (iii) size of the embedded low-permeability reservoir regions.

We have applied SHAFT79 to make a parametric study of these effects. The model reservoir consists of a large number of identical "elementary units" (see Figure 8). The elementary unit is a cube, the outer part of which consists of porous (or highly fractured) and permeable material, whereas the inner part is a (centered) cube of solid impermeable rock (see Figure 9). As we are interested in a process of slow and very nearly uniform depletion, flow between elementary units is negligible and only one elementary unit needs to be modeled. Initial conditions were chosen as $T = 240\ ^{o}C$, $S = 60\%$, representative of initial conditions (1959) in the two-phase zone of the Serrazzano reservoir. At the surface of the elementary unit a constant production rate of $1.75 \times 10^{-8}\ kg/m^3s$ is applied. This gives rise to a boiling rate of very nearly the same magnitude, which corresponds to what is observed in the Serrazzano simulation. Calculations were done for impermeable rock volumes of 90%, 80%, and 50%, respectively, of the elementary unit volume. Average porosity is held fixed at 10%, so that the porosity in the flow region is 100%, 50%, and 20%, respectively, in the three cases.

Figure 10 shows the dependence of additional temperature decline upon length L of the elementary unit. The side length of the impermeable rock cube is $L \times .9^{1/3}$, $L \times .8^{1/3}$, and $L \times .5^{1/3}$ for the cases of 90%, 80%, and 50% impermeable rock volume, respectively. The case with 90% impermeable volume, corresponding to 100% porosity in the flow region, provides an upper bound for temperature decline. The cases with 80% and 50%, respectively, are more plausible and potentially realistic. A length $L \approx 200$ m produces temperature declines of the magnitude needed to make simulated reservoir performance agree on average with observed performance. 200 m is to be considered a characteristic length of our model. In actuality , of course,

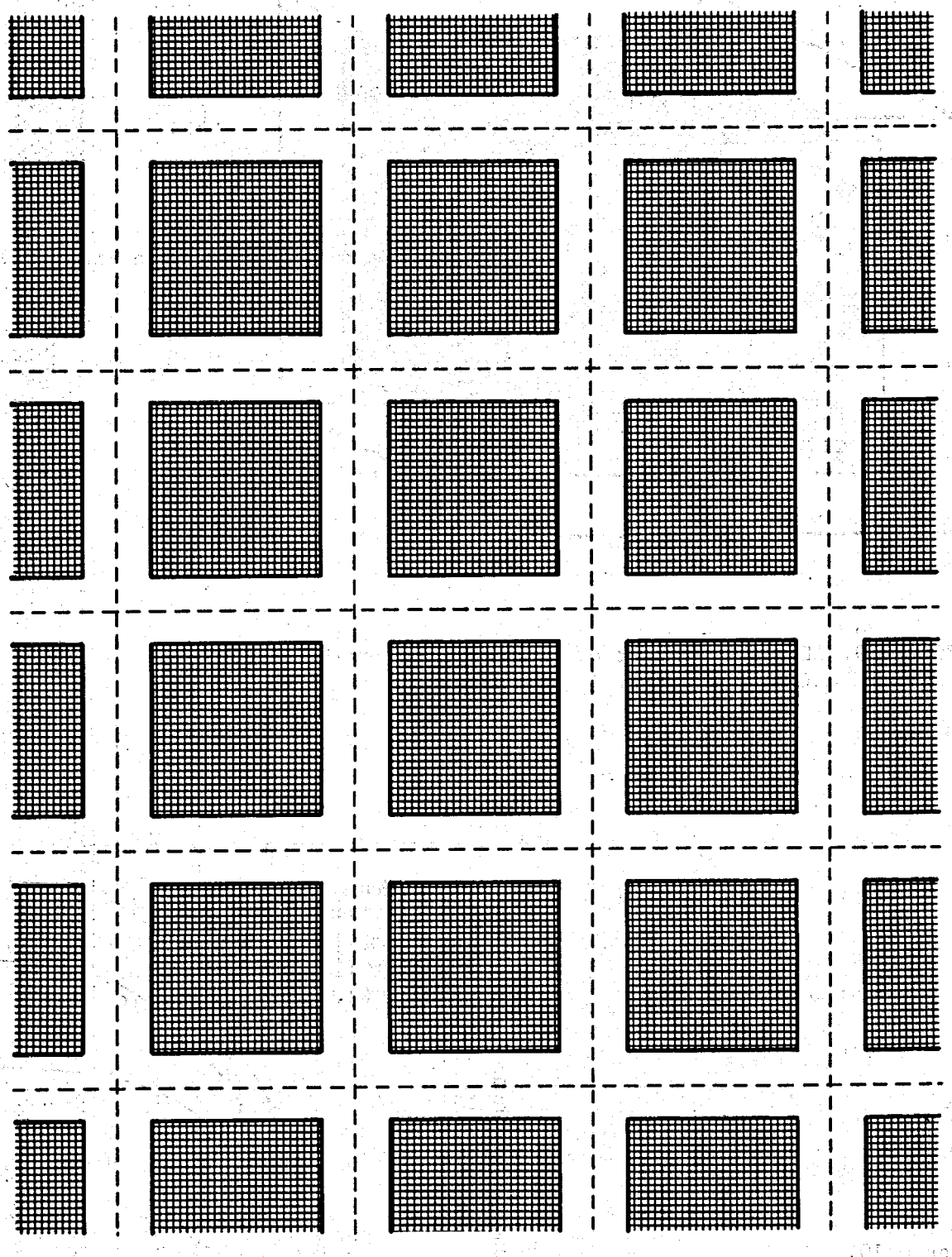

Figure 8. Areal View of Fractured Reservoir Model. (XBL 808-2723)

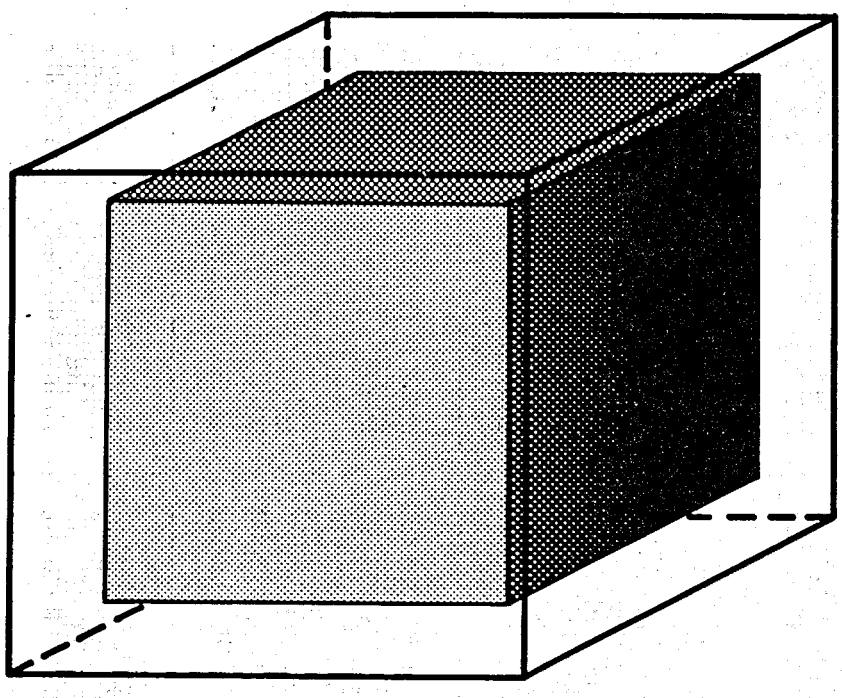

Figure 9. Elementary Unit of Fractured Reservoir. (XBL 808-2724).

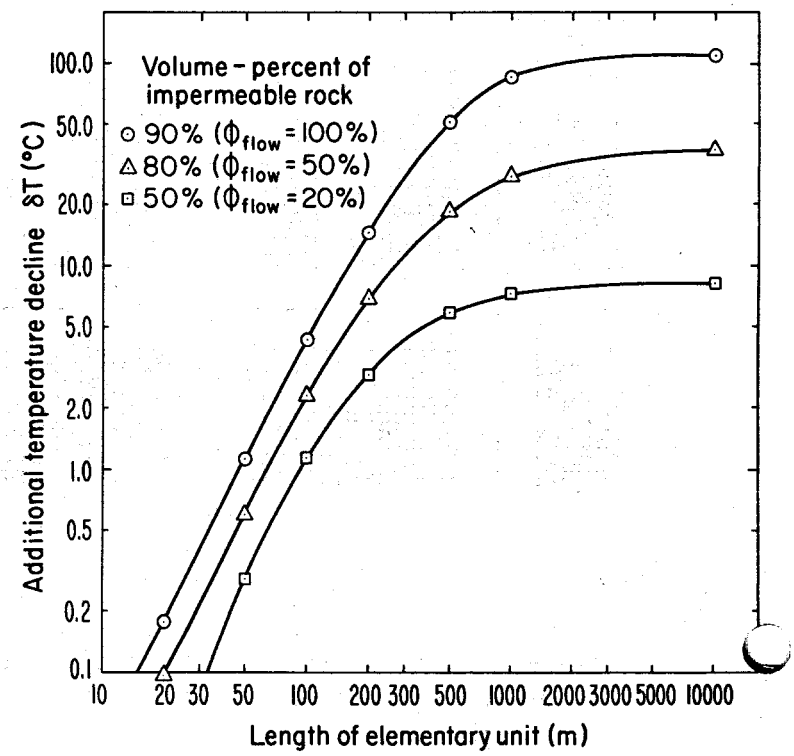

Figure 10.

Effects of Incomplete Thermal Equilibration between Rock and Fluid. (XBL 808-2726)

the reservoir rock need not be regular, and sizes of impermeable regions could vary throughout the reservoir. It appears entirely possible, particularly in view of the large number of unproductive wells, that such large impermeable rock masses could be present interspersed with permeable regions in the reservoir. We suggest, therefore, that incomplete temperature equilibration could well be a major source of additional temperature decline in the field.

In conclusion, both a diminished volume of the two-phase zone or incomplete thermal equilibration between vapor and fluid could very significantly increase the rate of temperature and pressure decline. These two effects could separately or combined account for an additional temperature decline of 5-6 ^{o}C over the simulated period of 15.5 years, such as is required to make simulated average pressure decline agree with the value deduced from field data.

7. Reservoir Performance 1975-1990

The history match from 1959 to 1975 provides a model of Serrazzano reservoir which can be used to extrapolate (forecast) production at a later time. For this, we assume constant well head pressure p = 5 bars. Discharge is simulated by connecting all well elements to a very large element with constant pressure p = 5 bars. Interface areas are adjusted such that proper (measured) production rates are obtained for January 1975, which is the most recent time for which digitized production data were available. The simulation has been extended through January 1990, with results given in Figures 11 through 16 and Table 6.

Total simulated mass production from 1975 to 1990 is 29.8×10^9 kg, corresponding to an average rate of 63.0 kg/sec. Average produced enthalpy is

well	location	PRODUCTION RATE (kg/sec) January 1975	January 1990	decline (%)
BCF/3	WCA3	2.90	2.30	20.9
Capriola	WCB8	12.95	10.76	17.0
Oliveta	WCC3	1.41	1.13	19.7
VC/2	WCC7	0.81	0.66	18.6
Le Prata 4	WEC31	5.35	4.62	13.7
Grottitana	WCD6	3.89	2.87	26.0
Soffionissimo 1	WCE3	2.61	2.11	19.3
Le Vasche	WCG3	3.32	2.67	19.7
Vignacce	WCG4	6.18	5.00	19.2
Pozzaie 2	WEN4	5.46	4.47	18.2
Conserva	WCP2	3.51	2.81	20.0
Avalle 2	WCP3	4.44	3.55	20.0
Lustignano	WCP12	9.89	5.69	42.5
VC/5	WER38	2.33	1.70	27.1
Campo ai Peri	WES40	2.42	1.82	24.6
#8	WCY3	1.33	1.09	18.4
Cioccaia	WCZ2	2.99	2.42	19.3
aggregate*		71.8	55.7	22.4

Table 6: Well-by-Well Production Rates for 1975 and 1990.

* does not include well VC/10.

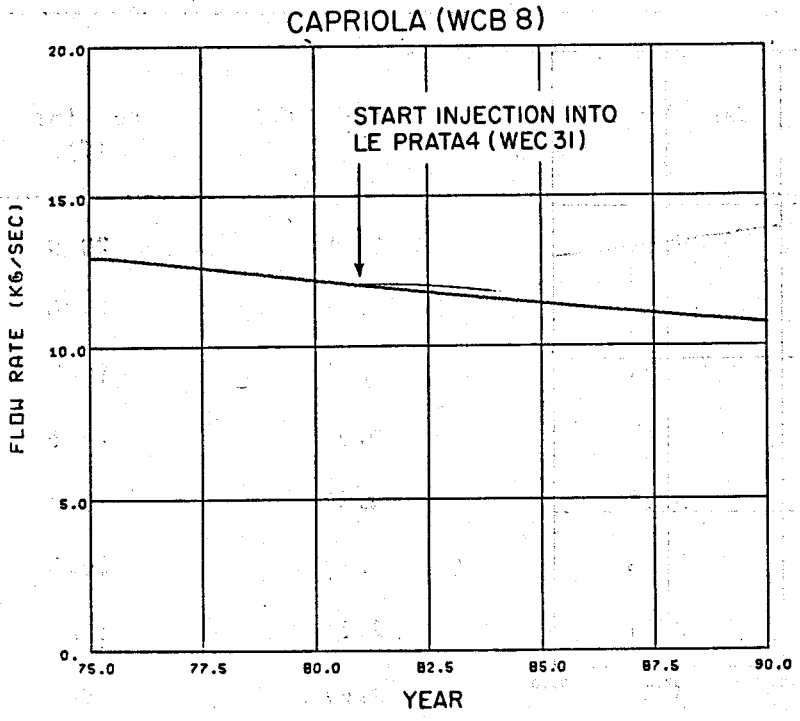

Figure 11. Production Forecast for Well Capriola (WCB8) with and without Injection. (XBL 809-2810)

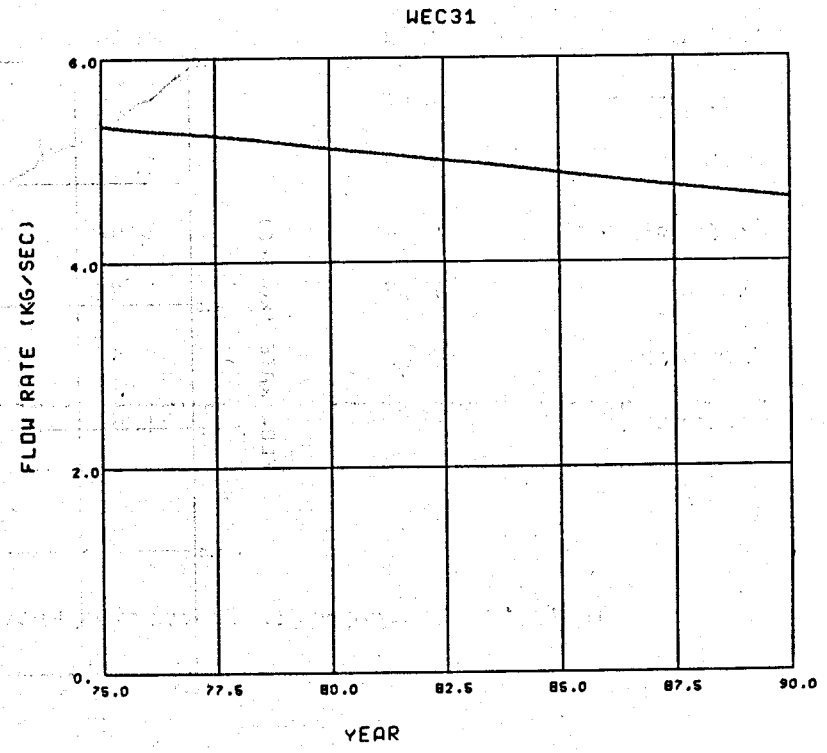

Figure 12. Production Forecast for Well Le Prata 4 (WEC31). (XBL 809-11950).

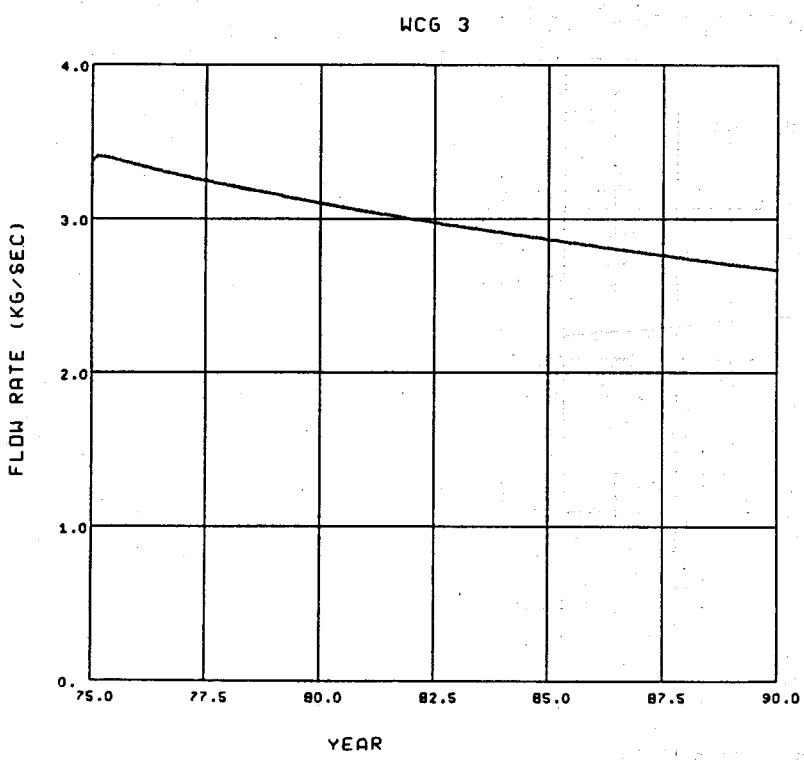

Figure 13. Production Forecast for Well Le Vasche (WCG3). (XBL 809-11949)

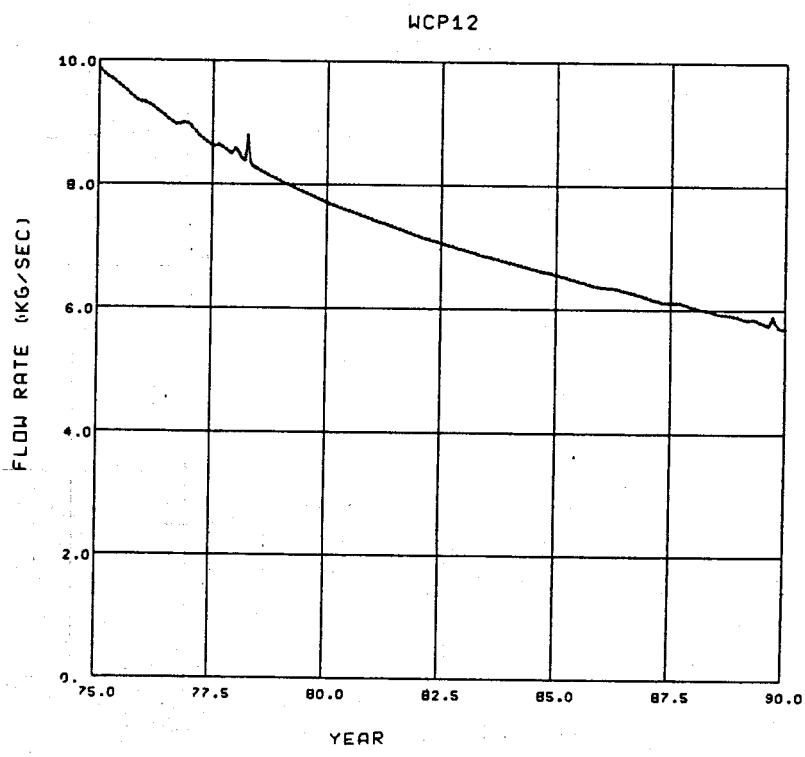

Figure 14. Production Forecast for Well Lustignano (WCP12). (XBL 809-11948)

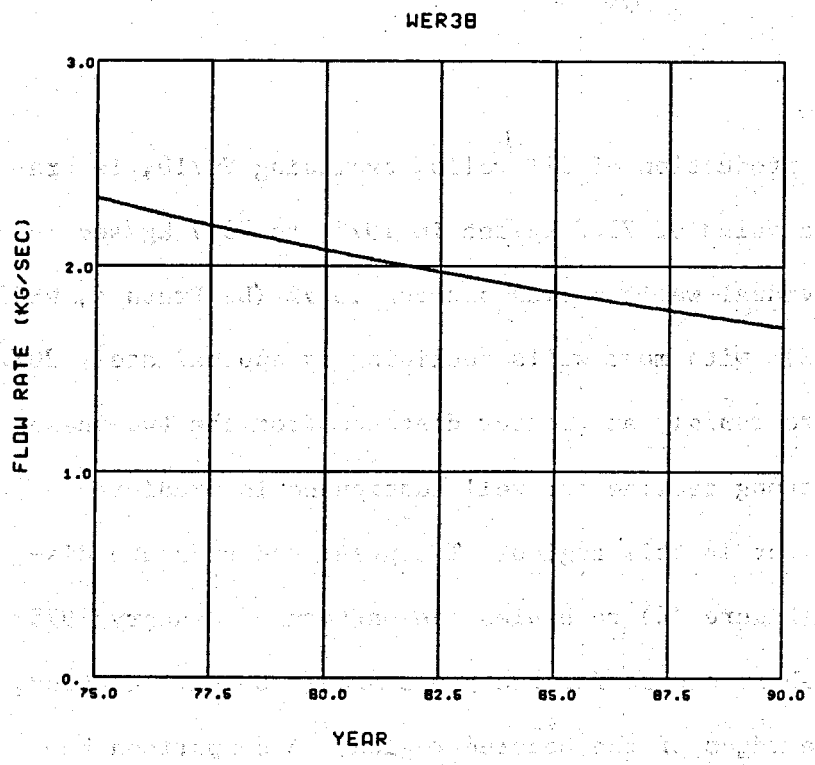

Figure 15. Production Forecast for Well VC/5 (WER38). (XBL 809-11951)

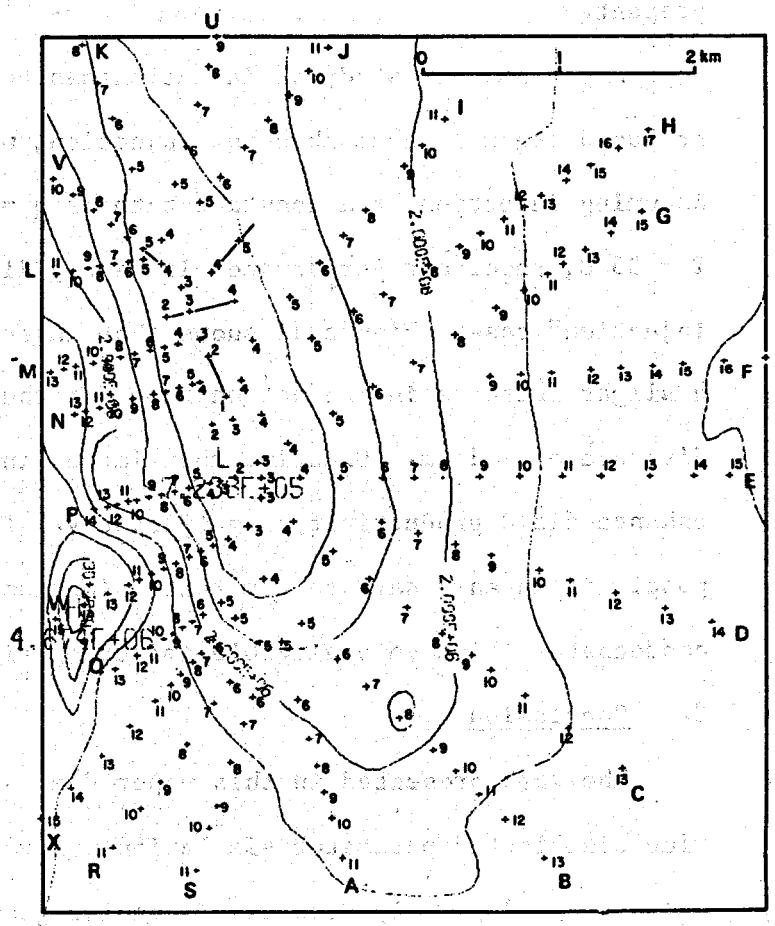

Figure 16. Predicted Reservoir Pressures for January 1990. (XBL 809-2809)

2.851 MJ/kg. The aggregate production of all wells, excluding VC/10, is predicted to drop by 24% from a value of 71.8 kg/sec in 1975, to 55.7 kg/sec in 1990. The decline for individual wells varies between 13.7% (Le Prata 4, WEC31) and 42.5% (Lustignano, WCP12), with most wells declining by approximately 20%. Generally, wells decline more rapidly at greater distance from the two-phase zones. The exceptionally strong decline for well Lustignano is predicted because the reservoir dries out in this region. The predicted pressure distribution for January 1990 (Figure 16) resembles the pattern of January 1975 (Figure 5). The strongest shift occurs for the p = 3 MPa (= 30 bar) contour, which has been pushed to the edges of the modeled region. A comparison between predicted and observed flow rates is planned for the period from 1975 - present.

A preliminary study of injection has been made. Approximately 20% of the produced steam is available for injection, which is a rather small amount. Assuming injection at a constant rate of q = 13 kg/sec, at a temperature of $T = 35^{o}C$, reservoir performance is hardly distinguishable from the "no injection" case. Figure 11 shows that injection into Le Prata 4 (WEC31) causes a slight increase in production rate for the nearest well Capriola (WCB8) at a distance of $\sim$ 1 km. Clearly, much larger injection rates would be required to enhance field productivity significantly. From the point of view of fluid disposal, it appears safe to say that injection of the small amount of available condensate will have negligible impact on field performance.

8. Conclusion

The work presented in this paper demonstrates the feasibility of field-wide distributed parameter simulations of vapor-dominated geothermal reservoirs in geologically accurate irregular geometry. The simulated model is

self-consistent and shows semi-quantitative agreement with field data. We believe that the simulation provides evidence for the validity of the physical model and mathematical methods used in the simulator SHAFT79.

The simulated field behavior substantiates a conceptual model of Serrazzano reservoir as a steam cap overlying a boiling aquifer. Comparison with actual field behavior suggests a smaller volume of the boiling zone than was previously assumed and/or incomplete heat transfer due to fractures at the margins, and significant upflow of steam from depth through fractures.

Application of numerical simulation for well-by-well production forecasting has been demonstrated. A brief study of injection of available condensate indicates negligible impact on field performance.

Acknowledgments

This work was supported by the U.S. Department of Energy under Contract No. W-7405-ENG-48. Thanks are due to N.E. Goldstein and M. J. O'Sullivan for a critical reading of the manuscript.

Nomenclature

C_R	specific heat of rock, J/^oC kg
H	thickness of reservoir, m
K_R	thermal conductivity of rock, W/m^oC
k	absolute permeability, milliDarcy ($\approx 10^{-15} m^2$)
k_{liquid}	relative permeability of liquid, fraction
k_{steam}	relative permeability of steam, fraction
L	length of elementary reservoir units, m
p	pressure, Pascal or bar ($\equiv 10^5$ Pascal)
Q	fluid production, kg
q	rate of fluid production, kg/s
r	parameter for relative permeability functions, dimensionless
S	volumetric vapor saturation, fraction
T	temperature, ^oC
t	time, s
ρ_R	rock density, kg/m^3
ϕ	porosity, dimensionless

References

1. Pruess, K., and Schroeder, R.C.: "SHAFT79 User's Manual," Lawrence Berkeley Laboratory Report LBL-10861 (March 1980).

2. Pruess, K., and Schroeder, R.C.: "Geothermal Reservoir Simulation with SHAFT79," Proc., Fifth Stanford Workshop on Geothermal Reservoir Engineering, Stanford, Ca. (1980), 183-188.

3. Pruess, K., Bodvarsson, G., Schroeder, R.C., Witherspoon, P.A., Marconcini, R., Neri, G., and Ruffilli, C.: "Simulation of the Depletion of Two-Phase Geothermal Reservoirs," paper SPE-8266, presented at the 54th Annual Fall Technical Conference and Exhibition of the SPE of AIME, Las Vegas, Nevada, 1979.

4. International Formulation Committee: "The 1967 IFC Formulation for Industrial Use, A Formulation of the Thermodynamic Properties of Ordinary Water Substance," (February 1967).

5. Duff, I.S.: "MA28 - A Set of Fortran Subroutines for Sparse Unsymmetric Linear Equations," Report AERE-R 8730, Harwell, Oxfordshire, Great Britain (June 1977).

6. O'Sullivan, M.J.: "A Similarity Method for Geothermal Well Test Analysis," Lawrence Berkeley Laboratory Report LBL-10968 (March 1980); submitted to Water Resources Research.

7. O'Sullivan, M.J., and Pruess, K.: "Analysis of Injection Testing of Geothermal Reservoirs," Lawrence Berkeley Laboratory Report LBL-10985 (June 1980); to be presented at the 1980 Annual Meeting, Geothermal Resources Council.

8. Nathenson, M.: "Some Reservoir Engineering Calculations for the Vapor-Dominated System at Larderello, Italy," USGS open file report 75-142, Menlo Park, Ca. (1975).

9. Cataldi, R., Stefani, G., and Tongiorgi, M.: "Geology of Larderello Region (Tuscany): Contribution to the Study of the Geothermal Basins," in: Tongiorgi, E. (ed.), Nuclear Geology on Geothermal Areas, Spoleto (1963), 235-267.

10. Marconcini, R., McEdwards, D., Neri, G., Ruffilli, C., Schroeder, R., Weres, O., and Witherspoon, P.: "Modeling Vapor Dominated Geothermal Reservoirs," Proc., Larderello Workshop on Geothermal Resource Assessment and Reservoir Engineering, Larderello, Italy (Sept. 12-16, 1977), 256-298.

11. Sestini, G.: "Superheating of Geothermal Steam," Geothermics, Special Issue 2 (1970).

12. Celati, R., Squarci, P., Stefani, G.C., and Taffi, L.: "Study of Water Levels in Larderello Region Geothermal Wells for Reconstruction of Reservoir Pressure Trend," Simposio internacional sobre Energia Geotermica en America Latina, IILA-INDE (1976).

13. Celati, R., Noto, P., Panichi, C., Squarci, P., and Taffi, L.: "Interactions between the Steam Reservoir and Surrounding Aquifers in the Larderello Geothermal Field," Geothermics, (1973) 2, 174-185.

14. Barelli, A., Manetti, G., Celati, R., and Neri, G.: "Build-Up and Backpressure Tests on Italian Geothermal Wells," Proc., Second UN Symposium on the Development and Use of Geothermal Resources, San Francisco, Ca., (May 20-29, 1975), 1537-1546.

15. Celati, R., Squarci, P., Neri, G., and Perusini, P.: "An Attempt to Correlate kH Distribution with Geological Structure of Larderello Geothermal Field," Proc., First Stanford Workshop on Geothermal Reservoir Engineering, Stanford, Ca., (1975), 37-41.

16. Atkinson, P., Celati, R., Marconcini, R., Miller, F., and Neri., G.: "Analysis of Reservoir Pressure and Decline Curves in Serrazzano Zone - Larderello Geothermal Field," Proc., Larderello Workshop on Geothermal Resource Assessment and Reservoir Engineering, Larderello, Italy, (Sept. 12-16, 1977), 208-232.

17. Weres, O., Tsao, K., and Wood, B.: "Resource, Technology and Environment at The Geysers," Lawrence Berkeley Laboratory Report LBL-5231, (July 1977).

18. Weres, O.: "A Model of the Serrazzano Zone," Proc., Third Stanford Workshop on Geothermal Reservoir Engineering, Stanford, Ca., (1977), 214-219.

19. Weres, O., and Schroeder, R.C., Documentation for Program OGRE, Lawrence Berkeley Laboratory Report LBL-7060, Berkeley, CA (June 1978).

REINJECTION STUDIES OF VAPOR-DOMINATED SYSTEMS

by

Ronald C. Schroeder, Berkeley Group Inc.
Michael J. O'Sullivan, Lawrence Berkeley Laboratory
Karsten Pruess, Lawrence Berkeley Laboratory
Romano Celati, CNR, Pisa, Italy
Claudio Ruffilli, ENEL, Pisa, Italy

1. Introduction

Reinjection of spent geothermal fluids is becoming a common means of waste disposal. In general, injection of geothermal brine has been accomplished without major problems whenever the fluid is injected into large fractures. Descriptions of long-term injection have been made in numerous reports. Chasteen[1] describes the injection at the Geysers field and at Valles Caldera (Baca). Since 1969, millions of tons of condensate have been injected at the Geysers, and during long-term tests at Baca thousands of tons of produced geothermal fluids have been reinjected. Cuellar[2], Einarsson et al[3], and Witherspoon[4] reported injection of fluids at Ahuachapan, El Salvador, where over seven thousand tons of spent fluid have been injected since 1970. Kubota and Aosaki[5] describe reinjection of spent fluids at Otake, Japan. More than eight million tons had been injected by 1975. Smaller scale disposal of produced brine, or spent condensate has taken place in Hilo, Hawaii; Larderello, Italy; and at the Salton Sea, California[6]. In all of these examples the large-scale injection took place in existing fractures.

When reinjection has been attempted into geological formations that do not have large fractures, the brine disposal has been less successful. At East Mesa considerable problems were encountered, particularly during initial attempts[7]. On the other hand, enormous amounts of brine have been injected into porous aquifers and reservoirs around the world. In the Gulf States,

water that is produced from gas and oil wells is disposed of in relatively shallow aquifers[8]. In numerous cases around the world, oil is recovered using the secondary recovery method of waterflooding[9]. In a single example[10], 4.2 million barrels per day of sea water were injected in a water-flood project in Saudi Arabia. Numerous tertiary steam flooding projects are underway to recover high viscosity crude. Some projects are reclaiming the brine that is produced during oil production, and in one project up to 80 thousand tons per day of brine has been recovered, vaporized, and injected.

Although injection of fluids has been a common practice in both the oil and gas industry, and in the disposal of industrial waste water, the geothermal experience is not as extensive. Temperature effects must be considered in geothermal injection which are not usually important in oil and industrial applications (except steam flooding). Not only are there brine chemistry problems, such as silica deposition, but also significant reservoir problems, such as cold water break-through, which must be resolved prior to geothermal injection.

One of the objectives of task 3/6 was to study the problems encountered and experience required in different geothermal fields.

The data on reinjection in vapor-dominated systems mainly come from Larderello. Reinjection is of utmost inportance in this field because of the decrease in production detected in various productive areas as a consequence of more than 50 years of exploitation. Studies of this field are also of interest as it is considered the only example of an "ageing" steam field, where the problem of maintaining production becomes particularly critical. Reinjection is considered as a means of extracting heat from the geothermal reservoir.

Reinjection has been carried out in peripheral aquifers on the southern margin of the field (Lago, Monterotondo) since 1974, injecting small flow

rates (30-80 m^3/h). No variation was noted in the trend of production rates and fluid characteristics of the wells nearest the injection points. The small quantities of injected water are believed to mix with much larger volumes of cold water flowing toward the steam field. Systematic injection tests over long periods on the inside of the productive areas began only recently; however, several short tests have been run in the past, and occasionally more than 100 m^3/h of water was injected into the reservoir over several months, during drilling operations in the deepest wells. In some cases production was very accurately monitored in the surrounding zone.

The most important points originating from these tests are:

- noteworthy increases in steam production were recorded in the wells nearest the injection well, when injection took place in the upper layers of the reservoir;
- there were no noticeable effects on the quantity and characteristics of the fluid produced when injection took place at depth. The depth limits for this change vary from zone to zone and are not always easy to define; the different injection depths can only be identified when using completed wells of varying depths in the same area or when inserting the casings during drilling operations.

Another characteristic of the Larderello field which is important in connection with the reinjection problem is that large volumes of reservoir seem to contain superheated steam only in the pore volume.

Injection phenomena have been studied theoretically for several years, and most of the basic phenomena are now quite well understood. Numerous theoretical and numerical studies have been made of both fracture flow and production/injection behavior of porous aquifers. Bodvarsson[11,12], Gringarten et al[13], Kasameyer and Schroeder[14], and Bodvarsson and Tsang[15] have all examined the temperature behavior of flow through fractures. Gringarten and

Sauty[16], Kasameyer[17], Tsang and Tsang[18], Lippmann et al[19], and numerous others have studied different aspects of production and injection in porous reservoirs.

Although the basic injection phenomena are known, there are many technical and economic problems still remaining that the geothermal engineer must contend with, in particular for aquifers that are not fracture dominated. For example, the amount of particulates can be a crucial factor in the cost of injection when fractures are not present, as they tend to clog the formation and their removal through the use of sand separators, special well completions, and in-line filtering is expensive. Also the brine utilization scheme can have an important effect on the injection system, since a system that results in oxygenation of the fluid to be injected can result in serious corrosion problems. The necessary treatment to prevent excessive corrosion will again have an important impact on cost.

There are significant environmental factors associated with the injection of fluids, and in a previous session of this meeting some of these factors were discussed. Induced seismicity, control of subidence, geochemical brine incompatibility, chemical treatment methods, and the environmental pollution of groundwater (in the case of shallow aquifer injection) are all questions --although site specific--that require additional study before a full-scale injection project begins.

The problems of injection well testing, particularly in the case of a boiling reservoir fluid or fracture flow, are numerous and mostly unresolved. Recent studies[20,21] have defined some of the important phenomena.

In addition to the problems associated with the brine chemistry, the reservoir environment, and well testing, there are also significant field management problems. These problems are related to the optimization in the utilization of the resource. The number of wells, the well patterns, the

amount of fluid injected, and the temperature of the injected fluid must all be chosen to provide a minimum cost for pipelines, pumps, and wells. At the same time, the reservoir pressure (and vapor saturation for two-phase systems), and heat that is captured from the rocks must be maximized by the injection without premature cool-water breakthrough. The "sweep" of heat from the rocks by fluid injection, and the large potential gain in power production that can be realized has been reported by Gringarten and Sauty[16], Nathenson[21], Kasameyer and Schroeder[14], for example.

The availability of large-scale multidimensional and multiphase numerical reservoir simulators now makes it possible to study the reservoir flow phenomena, well test behavior, field management problems, and some of the environmental problems associated with injection. Recent reports by Mangold, et al[22], Pritchett, et al[23], O'Sullivan and Pruess[20], and others have shown that the application of numerical simulation to geothermal injection is a very fruitful approach.

The purpose of the present work is to review the basic physical phenomena associated with geothermal injection, to discuss problems associated with its numerical simulation and to present the results of some numerical studies. The particular problems chosen for study are:

(1) injection of cold water into a thin (single layer) reservoir;

(2) a five-spot production/injection configuration in a thin (single layer) reservoir;

(3) injection of cold water into a thick (multi-layer) reservoir;

(4) injection of cold water into a one-dimensional vertical column, representing a cross section of Larderello geothermal reservoir.

These four problems by no means include all those of interest and in each case only one set of reservoir parameters is considered. However, they

provide a means of assessing the accuracy of simulators such as SHAFT79[24] in solving injection problems and in quantitatively discussing the most important physical phenomena which occur.

2. Injection Physics

In this section the physics of the flow during injection of fluids is reviewed in two parts. The first part deals with injection into a reservoir that can be approximated as a uniform porous medium for which Darcy's Law is a good approximation, and the second part deals with flow in a reservoir which is dominated by one or more large fractures. The difference between flow in a porous matrix and a fractured matrix is important for both thermal and hydrodynamic phenomena. In a porous material, the temperature of the fluid in the pores is always close to the temperature of the porous matrix. This is not necessarily the case in fractured media. In homogeneous porous media the hydrodynamic flow is slow and often approximately isotropic. In fractured rock, the flow can reach turbulent velocities in the fractures and, in general, fracture flow is not isotropic.

2.1 Porous Matrix

When a fluid of temperature T_1 is injected into a porous rock formation of temperature T_2, two fronts begin to move away from the injection point. The two fronts, shown in Figure 1, are the hydrodynamic front, which occurs at the farthest distance traveled by injected fluid, and the thermal front where temperatures jump from T_1 to T_2.

Bodvarsson[12] solved this problem for linear one-phase flow very elegantly, and several others have done so for radial flow.

Kasameyer[17] showed that in a liquid saturated reservoir a particle of the injected liquid remains at temperature T_1 for an interval of time given by

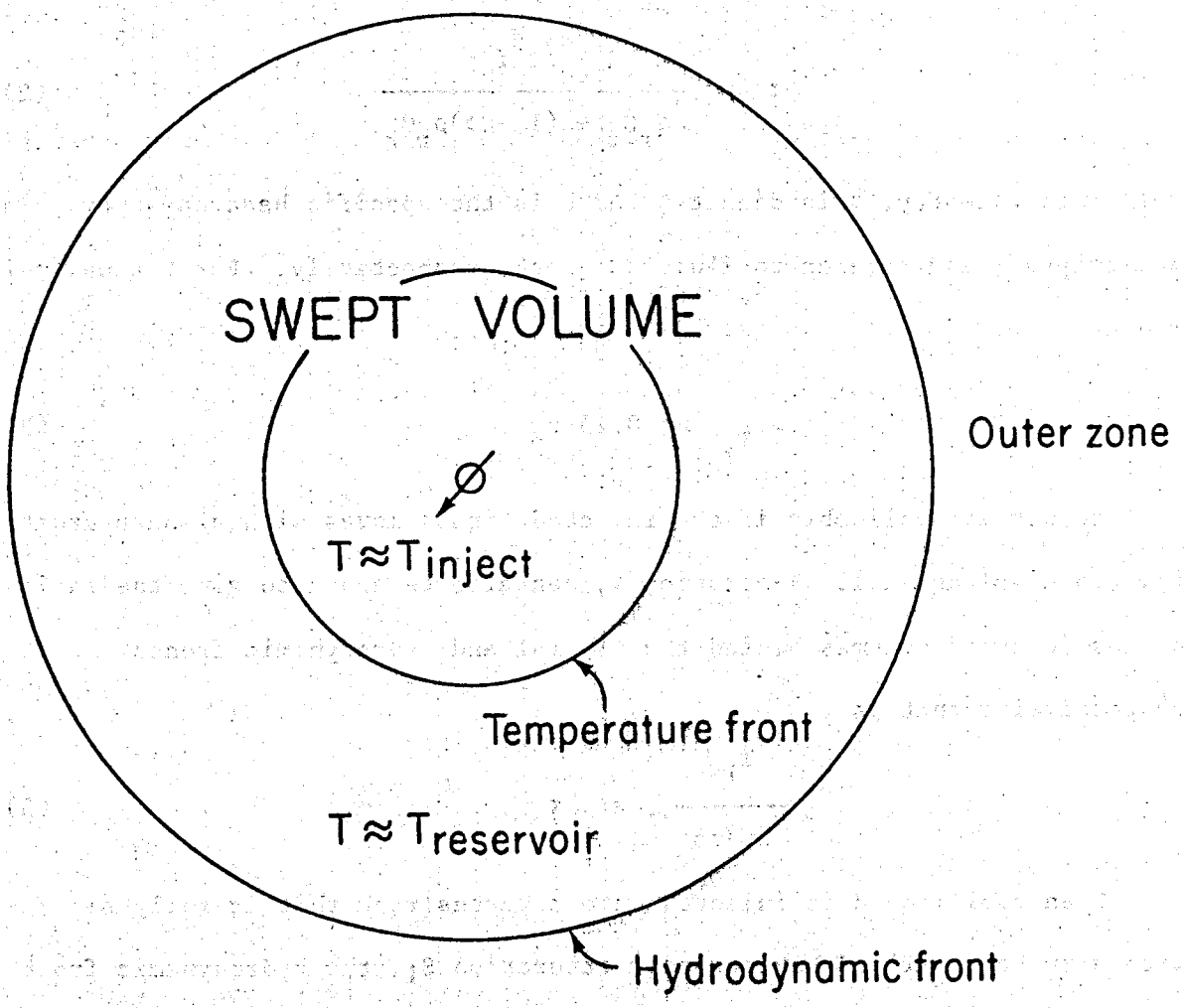

Figure 1. Fronts in a typical injection problem. (XBL 8010-2863)

$$\Delta t_{T_1} = \frac{\tau}{1 - \tau} t_p \tag{1}$$

where t_p is the time (after the injection began) that the particle was injected and τ is the ratio of "thermal masses" given by

$$\tau = \frac{\phi \rho_f C_f}{\phi \rho_f C_f + (1 - \phi) \rho_r C_r} \tag{2}$$

Here ϕ is porosity, ρ is density, and C is the specific heat capacity. The subscripts f and r refer to fluid and rock, respectively. For typical porous media,

$$\Delta t_{T_1} \approx 0.25\ t_p \tag{3}$$

This result is applicable if the injected liquid moves with a sharp front (piston displacement). The ratio, τ, can also be shown to give the ratio of the injected volumes behind the thermal and hydrodynamic fronts respectively, that is

$$\frac{V_{T_1}}{V_{hydro}} = \tau \tag{3}$$

When cool liquid is injected into a porous rock that is fully saturated with a two-phase fluid having steam saturation S_1, the hydrodynamic front can be rather broad. The injected fluid causes steam compression, condensation, and pressure increase in the two-phase zone, giving rise to outward flow of mobile water outside of the swept volume.

In a particular problem studied by O'Sullivan and Pruess[20], the thickness of the zone where liquid water saturation changes from 1 to the undisturbed value of .8 turned out to be about half an order of magnitude in the similarity variable t/R^2. A formula analogous to (3) above for injection into a two-phase reservoir is derived in the appendix.

The viscosity of fluids--including water--is strongly dependent upon temperature. This results in several important phenomena when the injection temperature, T_1, differs significantly from the temperature of the country rock, T_2. Tsang[18,25] has made several numerical studies of the effects of injection, and Lippmann et al[19] used reservoir simulation to study single-phase viscosity effects. O'Sullivan and Pruess[20] have obtained similar results for a two-phase example. The results obtained by Tsang and Lippmann show that at early times during injection of cold water the pressure response at the injection well is determined by the viscosity of the reservoir fluid at temperature T_2. The response then quickly undergoes a transition to a steeper growth rate determined by the much higher viscosity of the cold injected fluid. Recent results for the two-phase case are reported below.

In addition to the viscosity effects there are also effects due to the different fluid densities at temperatures T_1 and T_2. In the discussion above we have assumed that the flow is radial away from the injection well, and uniform with depth in the reservoir. The effect of different densities of the fluids with temperatures T_1 and T_2 is to have the heavier fluid gravitate to the bottom of the reservoir. During injection this results in a front that becomes more and more inclined. As shown in Figure 2, injection of cool fluid in a thick reservoir results in a thermal front which moves faster at the bottom of the reservoir. Nathenson[21] approximated the case of cold water injected into a hot liquid-saturated reservoir. Lippmann[19], and Tsang[22] and co-workers have conducted several numerical studies of injection including the gravity segregation effects.

The effects of gravity segregation when cool liquid is injected into a two-phase reservoir are even more important due to the larger difference in density of the liquid and steam. These effects have also been investigated numerically for two-phase reservoirs and will be covered in detail below.

The effects of the thermal conductivity of rocks and water have been a subject of study by numerous modelers. The consensus opinion is that the conductivity of the rock is so low--even when fully saturated with liquid--that in most cases the broadening of the thermal front due to heat flow in front of the invading cold water can be neglected. That does not mean that thermal conductivity does not play an important role in geothermal processes, however. The heat losses over large boundaries--particularly from a thin aquifer (reservoir)--can be appreciable. The vertical temperature profile near the ground surface in a very thick geothermal reservoir is governed by conduction effects. We will not discuss this special consideration further.

There are two additional physical phenomena that play an important part in the development of hydrodynamic and thermal fronts. One is the "fingering" effect that develops when the invading fluid and in situ fluid are miscible[26]. In the case of a cool brine invading hot brine, this consideration has importance only with respect to the fluid chemistry of the liquids. This is due to the fact that the mixing occurs at the hydrodynamic front, and hence has only chemical not thermal significance.

However, in the case of liquid injection into a two-phase fluid the miscibility and phase interaction of water and steam might result in considerable broadening of the boiling zone ahead of the hydrodynamic front. In Figure 3 we show an example of fingering taken from Blackwell, et al[26].

Although the fluids in this example are not water and steam, the phenomenon is common to any miscible fluids and becomes more significant as the densities and relative permeabilities of the two miscible fluids become increasingly different (e.g., water and dry steam). The fact that water and steam are interacting phases obviously complicates the analysis of this effect.

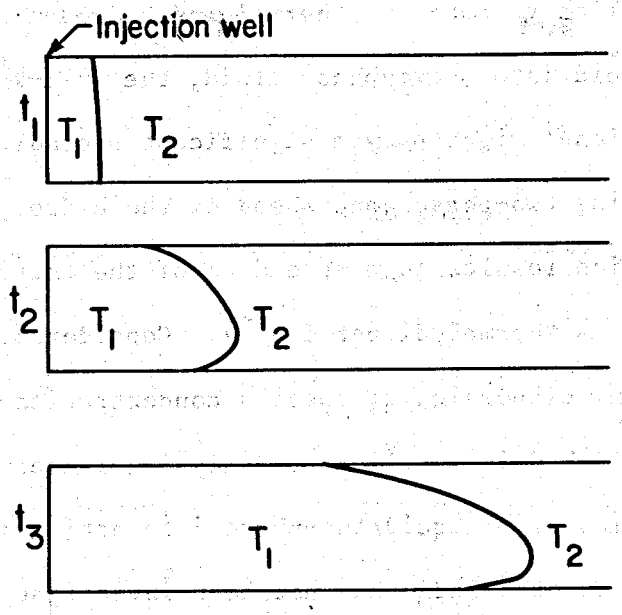

Figure 2. Injection of cold fluid into a thick reservoir.

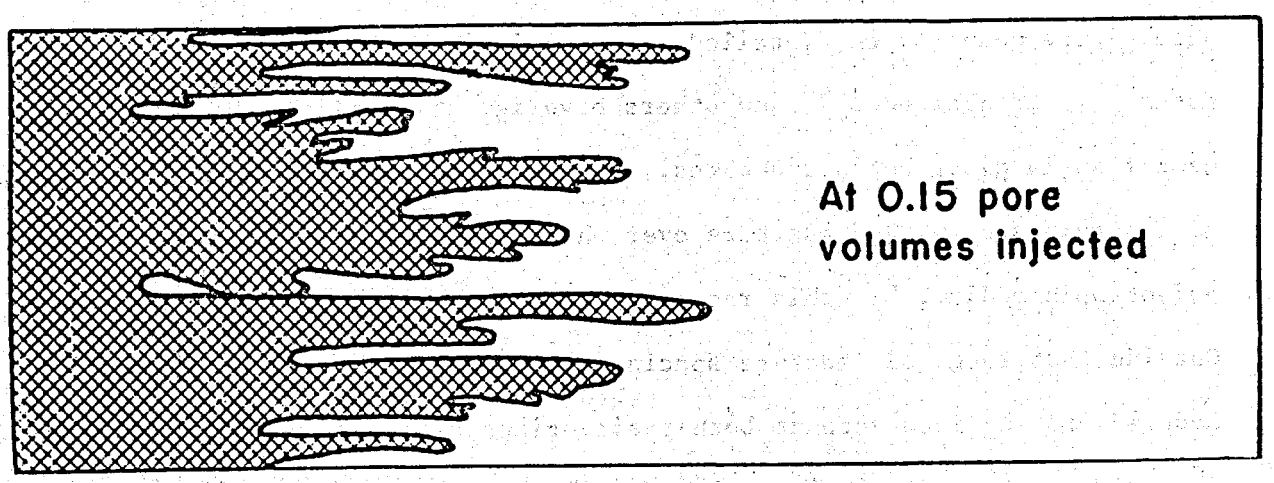

Figure 3. Fingering as observed in an injection problem.

The second consideration, with regard to frontal advance, is hydrodynamic dispersion which applies to both the thermal and hydrodynamic fronts. For the advance of a liquid into a two-phase fluid, the well-known phenomenon of hydrodynamic dispersion[27] might play a significant secondary role in the spreading of the moving two-phase zone ahead of the hydrodynamic front. Hydrodynamic dispersion results in a spreading of the thermal front also (usually referred to as thermal dispersion[28]). Considerable effort has been spent in studying dispersion of species concentration[29]. But much less has been accomplished in modeling or analysis of thermal dispersion. Hydrodynamic dispersion of a liquid/two-phase interaction is a totally new consideration and to our knowledge has not been investigated.

2.2 Fractured Matrix

Some of the effects discussed above are applicable for injection into fractures. However, there are a number of special considerations that are peculiar to hydrothermal flow in fractures. The most important fracture phenomenon is the anisotropy of the flow that is related to fracture orientation. It should be noted that the presence of fractures does not necessitate modeling the detailed anisotropic flow. Warren and Root[30], Kasameyer and Schroeder[14], and others have investigated the fluid and heat flow in distributed fractures. They have shown that there is a range of fracture spacing and aperture over which the rock behaves like a porous anisotropic medium. In this range the fracture orientation is irrelevant. Outside that range of fracture spacing and aperture the fractures must be modeled, taking into account both their orientation and hydrothermal response. For example, the numerical results for plane, parallel fractures indicate that for typical geothermal rocks the fractures can be very widely spaced, >50 m say, while still displaying the thermal behavior of an equivalent

porous medium. The material parameters--porosity and permeability--for the equivalent porous rock are very difficult to estimate or verify, which reduces the practical value of these observations. If the average fracture spacing and aperture can be estimated from drilling, coring, and testing, then the appropriate modeling approach can be chosen.

When the fractures must be modeled as discrete channels, both the fluid flow and heat flow from the rock to the fluid must be modeled accurately. The fluid flow in parallel smooth planar channels was shown to follow the relationship

$$Q = 2\pi \left[\frac{w^2}{12} \frac{w}{\mu} \right] \frac{\Delta p}{\ln r_e/r_w} \qquad (4)$$

for radial flow. Witherspoon et al[31] have shown that this relationship holds for rough, irregular fractures even for different effective applied stresses across the fracture faces. Here w is the fracture aperture, μ is viscosity, p is pressure, r is radius, and Q is flow rate. The subscripts e and w refer to a reference radius and to the wellbore radius, respectively. This result suggests that a "fracture permeability" should be defined to be $w^2/12$. Equation (4) holds only for relatively impermeable rock. If the rock has some matrix permeability and "leaks" fluid into the fracture, equation (4) no longer holds true.

The heat flow from the rock to the fluid moving between plane parallel plates has been approximated in studies of the heat transfer properties of geothermal fractures by numerous investigators. The important observation is that a hydrodynamic and thermal front will not move out radially from an injection well when flow is predominantly through fractures. Bodvarsson and Tsang[32] have begun numerical studies of these phenomena for both liquid flow and two-phase flow. When flow is through vertical fractures the gravitational effects will be important while the effects of miscibility and dispersion are not.

3. Numerical Simulation of Injection

3.1 "Front-Dominated" Problems

From the point of view of numerical modeling, the problem of the injection of cold water into two-phase or steam zones is dominated by the movement of fronts (see Figure 1). As discussed in section 2, there is a hydrodynamic front, which separates the more distant parts of the reservoir from those swept by the injected water, and trailing behind this is a thermal front where the injected fluid makes a transition from reservoir temperature to injection temperature. It is near these fronts where the significant changes occur. The methods of spatial discretization and volume averaging, which are employed in numerical simulators, have inherent limitations for front-dominated problems. The shortcomings of these methods are now discussed in some detail. Subsequently it is shown, by way of numerical experiments as well as analytical methods, that simulation nonetheless yields satisfactory results if executed carefully.

For one-dimensional radial injection into a two-phase reservoir the situation is characterized at all times by a cold zone around the injection well, surrounded by a swept zone close to original reservoir temperature. Outside of this swept zone, some condensation takes place which is accompanied by slight temperature and pressure increases and outward flow. The basic flaw of finite-discretization modeling of this process is caused by the fact that for some period of time the separation between hydrodynamic and thermal fronts is less than the grid spacing. Therefore, the hydrodynamic front is modeled as having a lower temperature. This causes a spurious flow from the outer zone inward, toward the hydrodynamic front. Actually, the flow induced by cold water injection into a two-phase system is outward, away from the injection well at all times (see below).

In mathematical terms, the difficulties arise from the fact that the applicable mass-and-energy-transport equations are usually predominantly

diffusive (parabolic) in nature, but display strongly convective (hyperbolic) character in the vicinity of the fronts. It is well known that hyperbolic equations, when solved on a discrete spatial mesh, are subject to much stronger numerical dispersion.

3.2 Radial Flow

The simplest and most basic injection problem involves one-dimensional radial flow in a thin reservoir. We have used various grid spacings to simulate the problem defined in Table 1. (ΔR = 0.5 m, 1 m, 2 m, 4 m.) Figures 4 and 5 compare simulated results with semi-analytical solutions obtained from the similarity solution method (reference 20). There is very good agreement for vapor saturations and pressures. The numerical simulation does less well for the temperature front, which is predicted in the proper location, but has been smeared out considerably. The grid spacing used in these simulations is ΔR = 1 m. Figure 6 shows that a significant improvement is obtained for a grid spacing of .5 m.

The satisfactory agreement of the numerical simulation with the similarity-solution method shows that, in spite of the problems noted above, the simulation seems to "work." We shall now examine the numerical simulation in some more detail, in order to develop a better understanding of the operating mechanisms.

After injection starts, the temperature and pressure in the well block decline due to mixing with colder water. This causes a (spurious) flow inward in the reservoir, towards the well block. (Note that water is mobile at initial vapor saturation of 20 %.) After a while a phase transition occurs in the well block. Further injection causes pressure to increase rapidly, and water begins to flow outward into the second grid block. This water has a temperature intermediate between the injection temperature and the original reservoir temperature. The second grid block experiences a sequence

TABLE 1: Parameters used in Injection Simulation

PARAMETER	PROBLEM		
	1-D RADIAL	FIVE-SPOT	2-D VERTICAL
Rock density ρ_r (kg/m^3)	2600	2600	2600
Rock specific heat C_r (J/kg^{o}C)	770	755	755
Rock heat conductivity K_r (W/m^{o}C)	2.0	2.1	2.1
Porosity ϕ (%)	15	10	10
Permeability k (10^{-15} m^2)	240	40	40
Residual immobile water saturation S_{wc} *	.30	.40	.40
Residual immobile team saturation S_{gc} *	.05	0.0	0.0
Reservoir thickness (m)	1	10	100
Initial reservoir temperature (^{o}C)	233.8	240	240
Initial vapor saturation (%)	20	75	75
Injection enthalpy (J/kg)	421938	147000	138300
Injection temperature (^{o}C)	100.1	40.0	33.0
Injection rate (kg/sec)	.40358	0.0, 0.025, 0.05	6.0, 15.0
Production rate (kg/sec)	---	0.025	---

*Corey's equations as given in Equation 5 were used for relative permeabilities

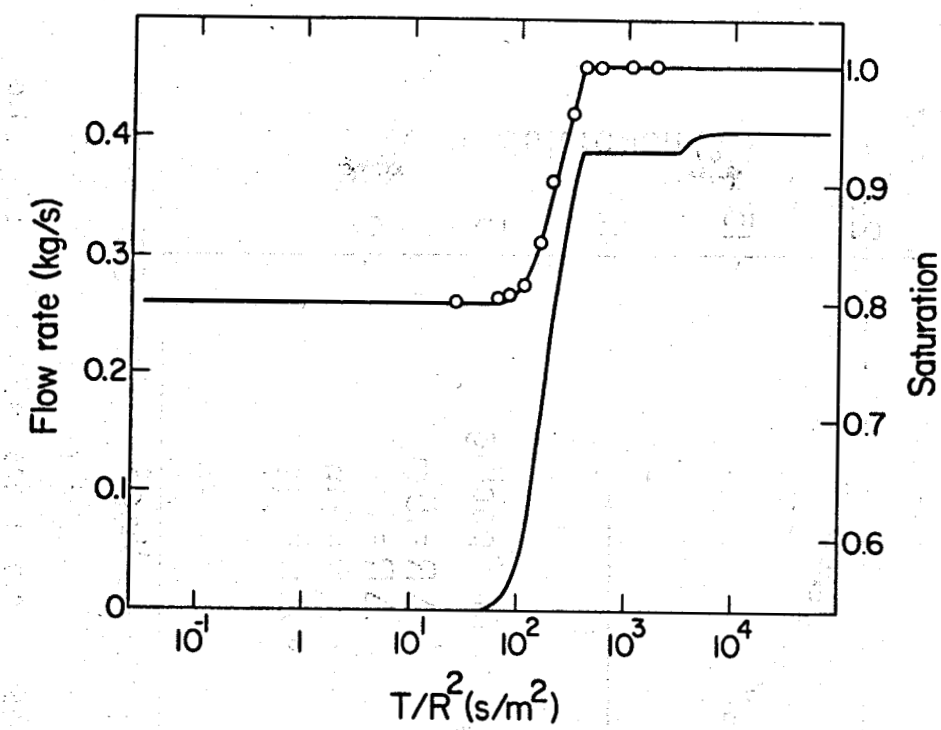

Figure 4. Flowrate and saturation profiles for injection of cold water into a two-phase reservoir. Similarity method results[20] are shown —— and SHAFT79 results as o.

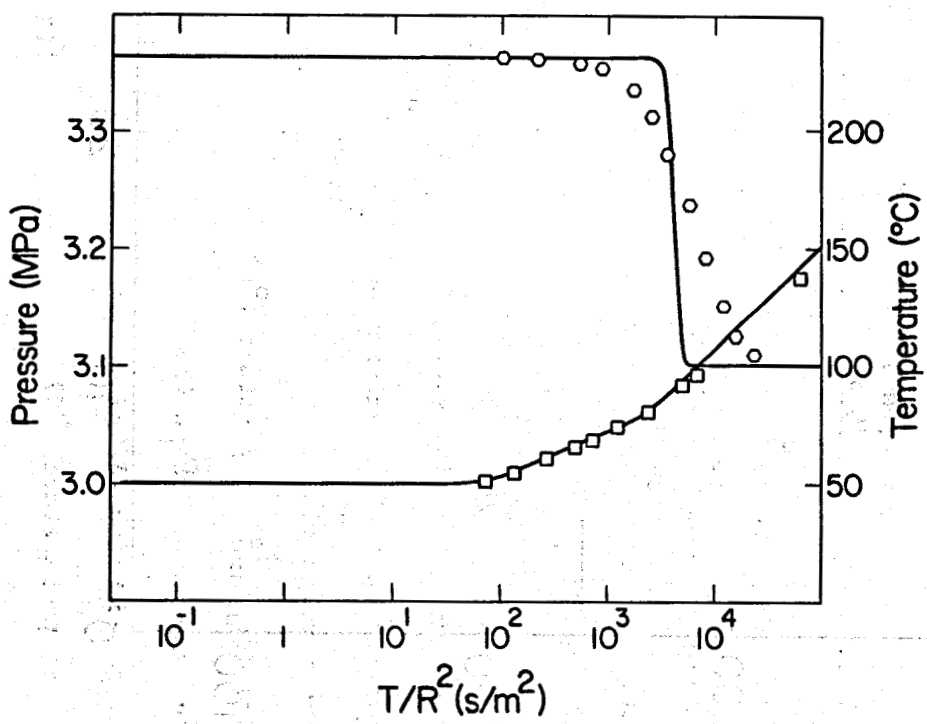

Figure 5. Temperature and pressure profiles for injection of cold water into a two-phase reservoir. Similarity method results[20] are shown as —— and SHAFT79 results as □ for pressures and ⬡ for temperatures.

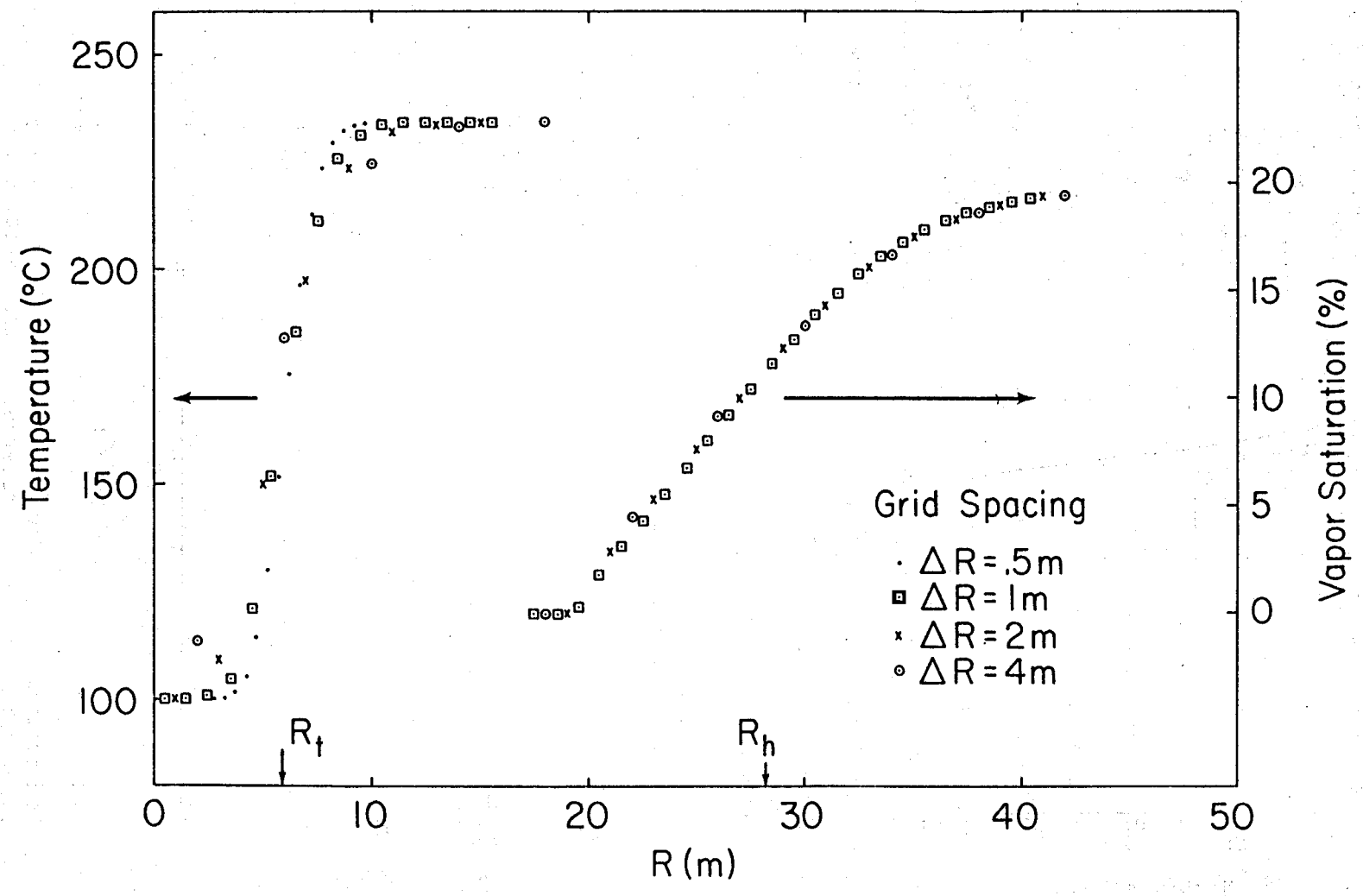

Figure 6. Thermal and hydrodynamic fronts for the radial injection problem at t = 160,000 seconds. (XBL 8010-2862)

of events similar to the first grid block: the water inflow from the well block occurs at somewhat lower temperature, causing temperature and pressure in the second grid block to drop and inducing inward flow from the third grid block. Flow reverses after the second grid block makes a phase transition to liquid conditions, and the process continues in the third grid block. Due to repeated contact with the rock and mixing with fluid of original reservoir temperature, the temperature of the hydrodynamic front increases as it moves on from grid block to grid block. The amplitude of the spurious inward flow diminishes in the process, until it finally disappears entirely. The advancing hydrodynamic front causes some steam to compress and condense, thus increasing temperatures slightly above original reservoir temperature. In the simulation, we observe that the hydrodynamic front at late times experiences a temperature increase of $\Delta T = .374\ ^{o}C$. Assuming complete condensation of the steam present in the swept volume a simple heat balance calculation gives a temperature increase of $\Delta T = .381\ ^{o}C$, in very good agreement with the simulated value. We believe that the outward flow (mostly water) caused by the condensation process is responsible for the very diffuse hydrodynamic front seen in the simulation. Comparison with the similarity solution, Figure 4, shows that this represents a "real" effect, not an artifact of the simulation. Because the hydrodynamic front is so diffuse, good results can be obtained, even for a large grid spacing of $\Delta R = 4$ m. The temperature front on the other hand is very sharp, and subject to much stronger numerical dispersion (see Figure 5). For completeness, we mention that a rather sharp hydrodynamic front will occur in the case where there is no mobile liquid water in the reservoir.

Further insight into the simulation can be obtained from a consideration of t/R^2 invariance. Consider a grid with spacing ΔR_i. It is easy to see from the discretized mass- and energy-transport equations that the entire simulation calculation for radial geometry is invariant under the transformation:

$$\Delta R_i \rightarrow \Delta R_i' = \varepsilon \Delta R_i$$
$$\Delta t_k \rightarrow \Delta t_k' = \varepsilon^2 \Delta t_k$$

If all radii in the grid are scaled by a factor ε, and all time steps are scaled by a factor ε^2, the numerical simulation produces identical results, element for element and time step for time step. The reason for this is that in the finite difference equations time steps and volumes appear only in the combination $\Delta t/V_i$, and that the flow terms contain geometrical factors in the form $A_{ij}/(d_i + d_j)$. Here A_{ij} is the interface area between grid blocks i and j, and d_i and d_j are the respective distances of the nodal points from the interface. Whereas the solution to the differential equations is strictly dependent upon t/R^2, the solution of the difference equations has this property only approximately. At different mesh points the solutions at times chosen to give the same t/R^2 value are not identical because of the time dependence of numerical dispersion. However, as explained above, simultaneous scaling of both the time steps and the grid produces a "discrete" t/R^2 invariance.

We have verified the above mentioned invariance properties of the difference equations explicitly by means of numerical simulation. Simulated results at t = 160,000 sec for a grid with spacing ΔR = 4 m are identical, element for element, with results at t = 40,000 sec for a grid with spacing ΔR = 2 m. This property was then used to obtain simulations for the finer grids, in the following way. Simulated results at t = 160,000 sec for a grid with ΔR = 2 m were used to initialize the simulation with the ΔR = 1 m grid at t = 40,000 sec, and similarly for the ΔR = .5 m grid.

The appendix presents a simple lumped model for computing the movement of hydrodynamic and thermal fronts. From Equations (A.4, A.3) we compute, for $t = 1.6 \times 10^5$ sec, a radius of the swept zone, R_h = 28.31 m. At this

radius, simulated steam saturation is 11.3 % (see Figure 6), which is close to the mean of 0 % and 20 %. The slight deviation occurs because the hydrodynamic front is spread out in an asymmetric way, with the inner part being steeper than the outer part. The spreading is a "true" physical phenomenon, not included in our lumped model, which is caused by water flowing outward outside of the swept volume, as a consequence of condensation-induced pressure increase. From Equation (A.4) the lumped model predicts a radius of the cold zone, R_{cold} = 6.14 m. At this radius, simulated temperature is 167 °C (ΔR = 0.5 m grid), which is the exact mean between injection temperature and original reservoir temperature.

In summary we conclude that comparisons with the similarity solution method and use of various grid spacings demonstrate that numerical simulation of injection can produce accurate results. Further insight into the workings and applicability of numerical simulation for injection problems is obtained from a lumped parameter approximation, and from the invariance properties of the governing equations in finite difference form.

4. Analysis of Injection Well tests

The results given in Figures 4 - 7 apply to a simple constant rate injection test. The semilog plot of the pressure build-up curve shows two straight line sections (Figure 7). The first corresponds to movement of hot water and the second to the movement of cold water. In either case, the mobility of the water can easily be calculated. This is not generally possible for production tests in two-phase reservoirs since the mobility changes during the course of the test and depends in a non-obvious way on the relative permeabilities.

From the straight line portions of the pressure plot the kinematic mobilities can be calculated from the formulas given by Garg[33] as

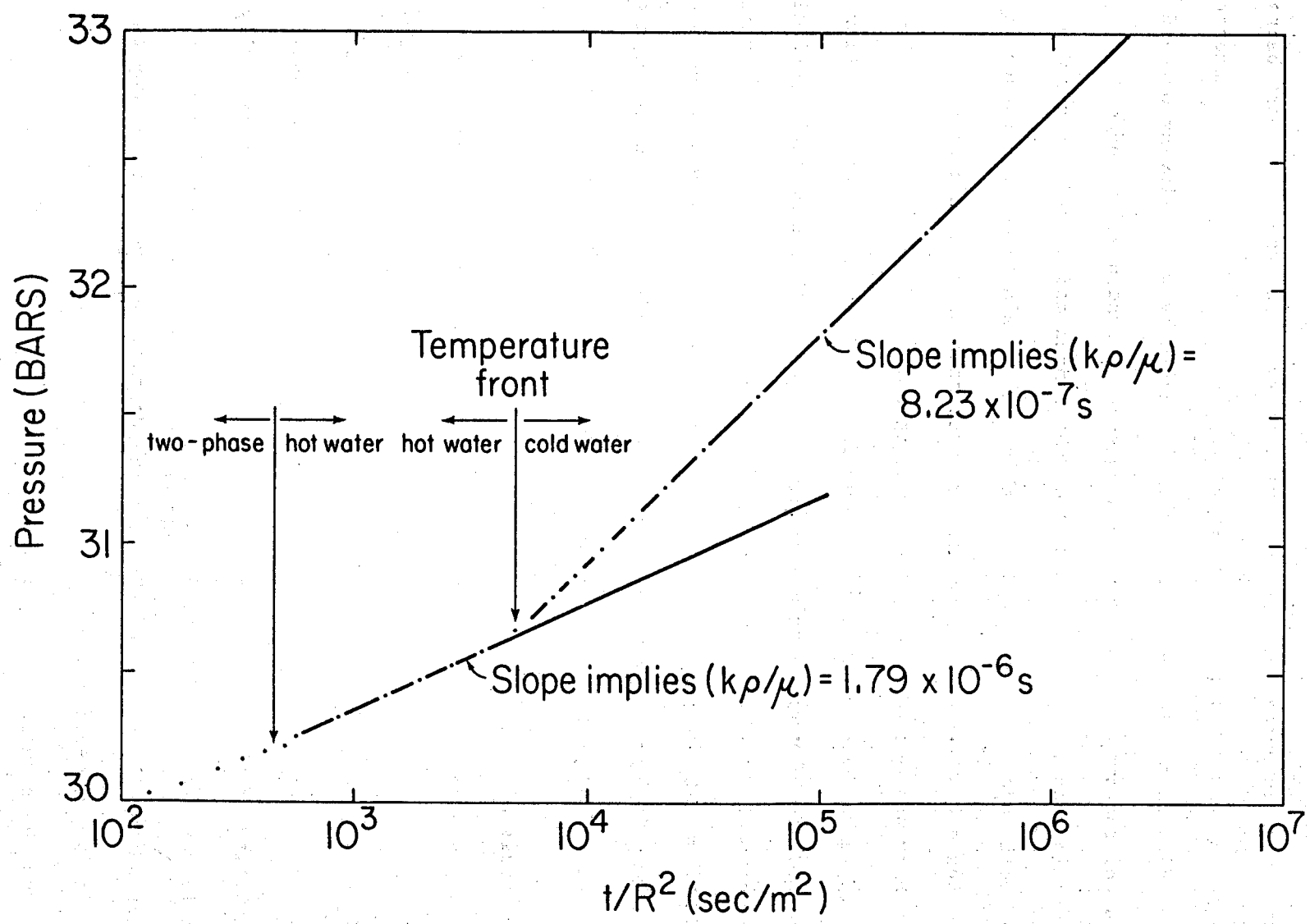

XBL 8010-2864

Figure 7. Simulated pressures for radial injection problem. (XBL 8010-2864)

8.23×10^{-7} s for the 100 °C water and 1.79×10^{-6} s for the 234 °C water. These values compare very well with the exact values of 8.24×10^{-7} s and 1.73×10^{-6} s respectively. It is worth mentioning that the wellblock pressure, if referred to a radius of .56 R_w (R_w = well block radius) as suggested by Garg, yields a point on Figure 7 which is within line thickness of the "cold" straight line.

It is shown in the appendix that the location of the thermal front can be used to estimate porosity. Inserting R_c = 6.14 m for t = 1.6×10^5 sec (corresponding to t/R_c^2 = 4244.1 s/m^2), as read off from Figure 6 into Equation (A.7), yields a very accurate value of ϕ = 15.05 %. However, taking t/R_c^2 from Figure 7 at the intersection of the two straight lines, t/R_c^2 = 4600 s/m^2, gives ϕ = 24.5 %. Small inaccuracies in t/R_c^2 translate into large inaccuracies for ϕ, because in the numerator of Equation (A.7) two large numbers of equal order of magnitude are being subtracted. Field application of this method of porosity estimation has to use the intersection of the two straight lines, and one can not expect very accurate results from this approach.

The excellent agreement between the semi-analytic results and the SHAFT79 results gives confidence in the ability of the simulator, with careful mesh design, to analyse more complicated injection tests including inhomogeneities in the reservoir (skin), constant pressure boundaries (fractures), and variable injection rates.

5. Five-spot Results

In order to investigate the optimal use of reinjection in a vapor-dominated geothermal reservoir, a five-spot configuration of production and injection wells (see Figure 8) was studied. A production well spacing of 1000 m was assumed and reservoir parameters typical of the Italian reservoirs

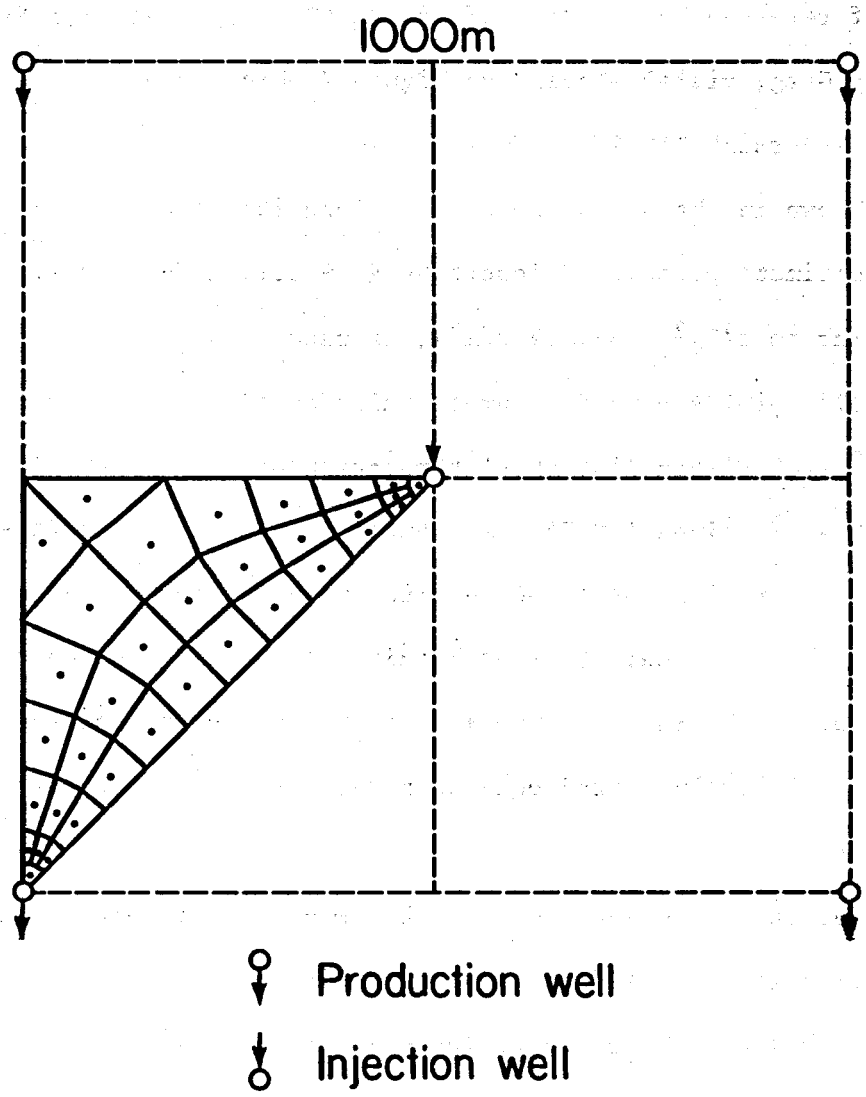

Figure 8. The configuration of production and injection wells and the computational grid for the five-spot problem.

were used (see table 1). The production rate of 0.025 kg/sec was chosen to give a supply of fluid in the reservoir sufficient to sustain approximately thirty years of production.

Because of the symmetry of the configuration only one eighth of a typical five-spot has to be considered. The mesh used in the SHAFT79 calculations is shown in Figure 8. Three cases were considered:

(i) no injection,

(ii) an injection rate equal to the production rate,

(iii) an injection rate double the production rate.

The vapor saturation in the reservoir is sufficiently high so that water is immobile and therefore vigorous boiling is required to maintain the required production rate from steam alone. Therefore the pressure must decline as a consequence of boiling. The permeability in the reservoir is sufficiently high to allow comparatively rapid spreading of boiling and the associated pressure decline. As can be seen in Figure 9, the pressure drops almost uniformly across the reservoir as time progresses, with a corresponding near uniform temperature drop and vapor saturation increase. Once the reservoir has completely superheated (dried out) the amount of mass left in the reservoir is very small and the pressure declines very rapidly (see Figure 10). At this stage the reservoir temperature is still high ($\approx 220\ ^{o}C$), that is, plenty of heat remains in place. In its unexploited state the reservoir contains 57.4×10^{13} J of energy of which only 3×10^{13} J are contained in the fluid. Clearly not all of this energy is available for exploitation. There is a lower limit to the temperature of the reservoir at which production is likely to be useful. For reference, a simple calculation gives the energy contained in the rock matrix at $180^{o}C$ as 39.8×10^{13} J. At the end of its useful life the reservoir still contains 50.0×10^{13} J. Some 4.4×10^{13} J have been transferred from the rock to the fluid to sustain the boiling.

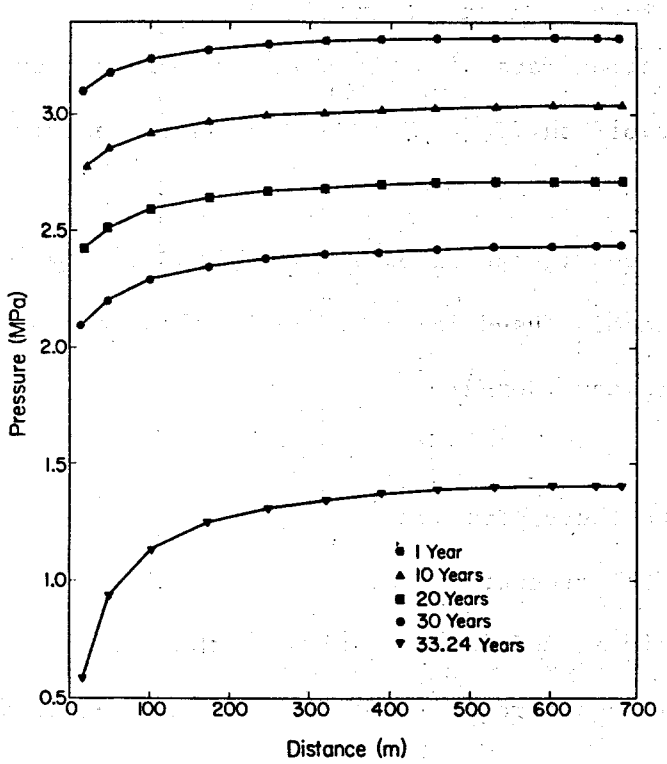

Figure 9a. Pressure profiles along a line joining production and injection wells for the five-spot problem. Injection rate 0.0 kg/sec.

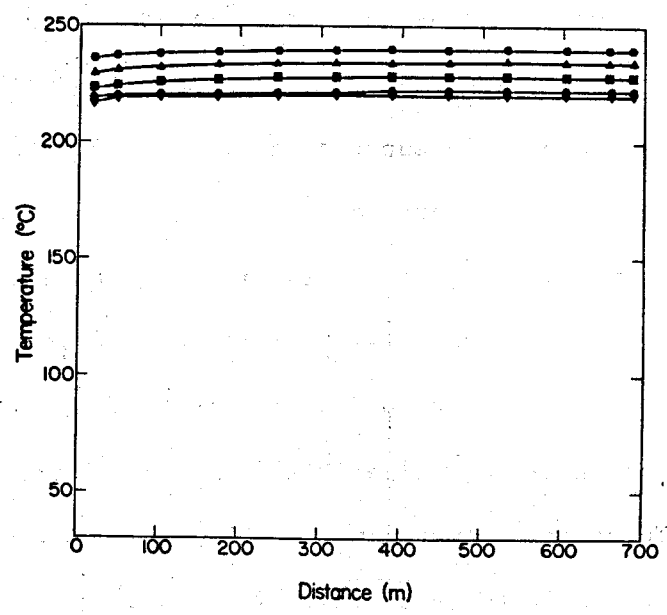

Figure 9b. Temperature profiles along a line joining the production and injection wells for the five-spot problem. Injection rate 0.0 kg/sec.

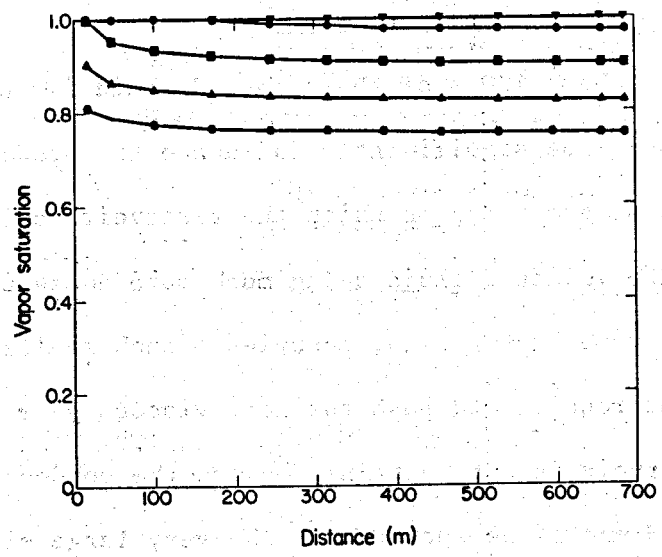

Figure 9c. Vapor saturation profiles along a line joining the production and injection wells for the five-spot problem. Injection rate 0.0 kg/sec.

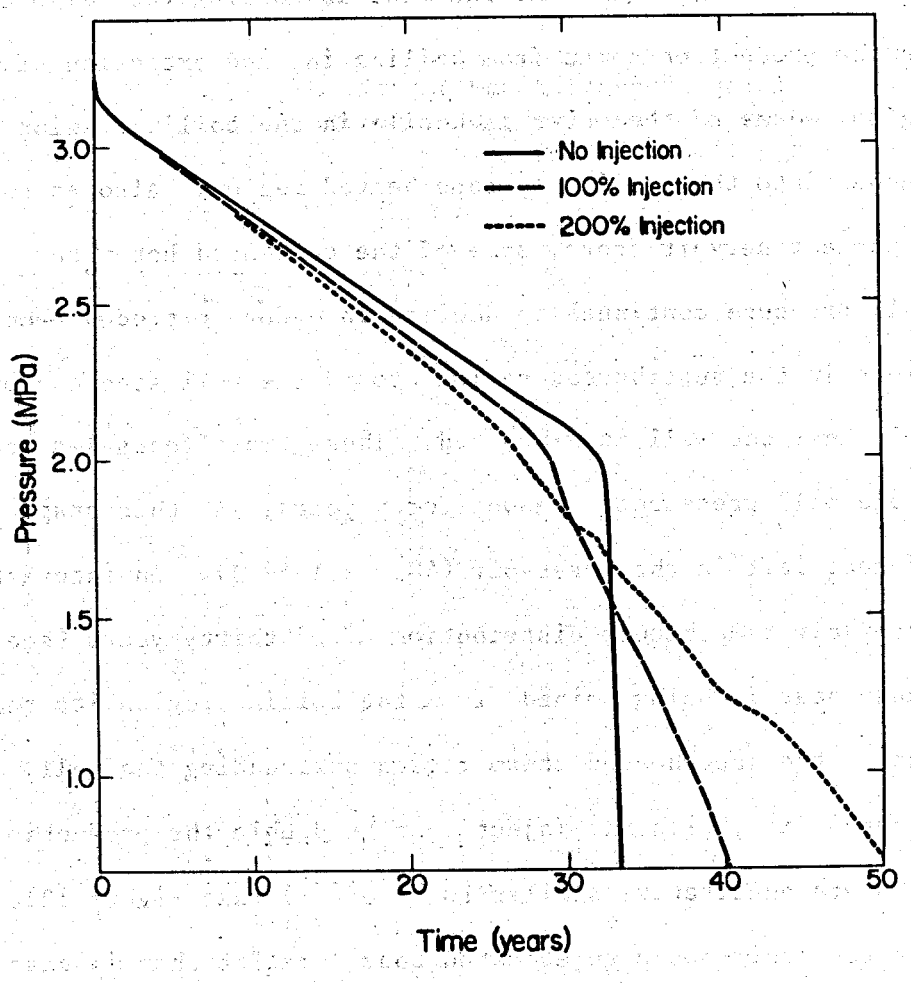

Figure 10. Pressure decline in the production block for the five-spot problem.

In case (ii) where 100 % of the produced fluid is reinjected, the injected fluid does not significantly influence the production until after about thirty years, the stage at which the reservoir would be exhausted with no injection. The injected fluid being much more dense than the original fluid, with 75 % vapor saturation, occupies a much smaller volume. The pressure gradient required to push the more viscous warm or hot water through the reservoir is not sustained beyond the condensation point where the boiling fluid meets the hot water. The very large effective compressibility in the two-phase region prevents pressure changes at the injection well from influencing the production well.

At thirty years about 50 % of the reservoir has dried out, a small fraction is completely liquid and the rest is boiling (see Figure 11). After this time the production comes from boiling in, and extension of, the two-phase region. Some of the water is mobile in the boiling region and therefore it encroaches into the previously superheated region. Also as the pressure over the whole reservoir drops, some of the condensed hot water starts boiling. The overall pressure continues to decline in order to produce enough steam and the gradient in the superheated region around the well steepens once all the mass supply near the well is exhausted. These two effects lead to unacceptably low downhole well pressures at about forty years. At this stage there is still plenty of heat left in the reservoir (48.9×10^{13} J). An interesting feature of the reservoir temperature distribution after thirty years (see Figure 9) is that because heat is being "mined" from the boiling region its temperature drops below that of the superheated steam region surrounding the well.

For case (iii), with the injection rate double the production rate, the results are qualitative similar to case (ii) (see Figure 12). At thirty years, the reservoir has a superheated zone (smaller than in case (ii)), a boiling zone and a large liquid zone. Production is possible for a further

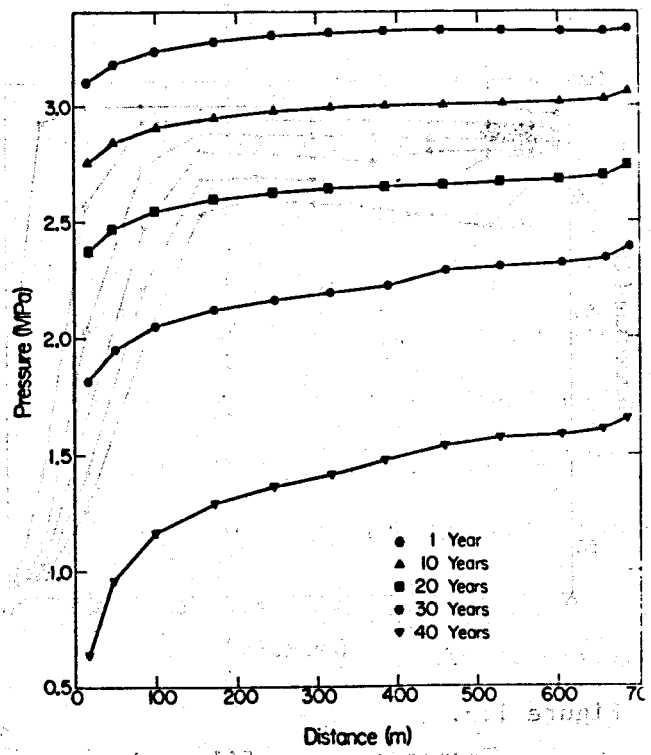

Figure 11a. Pressure profiles along a line joining the production and injection wells for the five-spot problem-injection rate 0.025 kg/sec (100% of production).

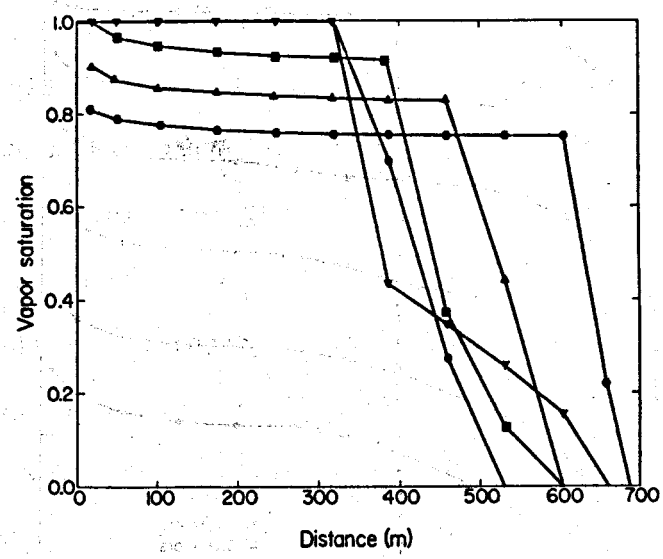

Figure 11b. Temperature profiles along a line joining the production and injection wells for the five-spot problem. Injection rate 0.025 kg/sec (100% of production).

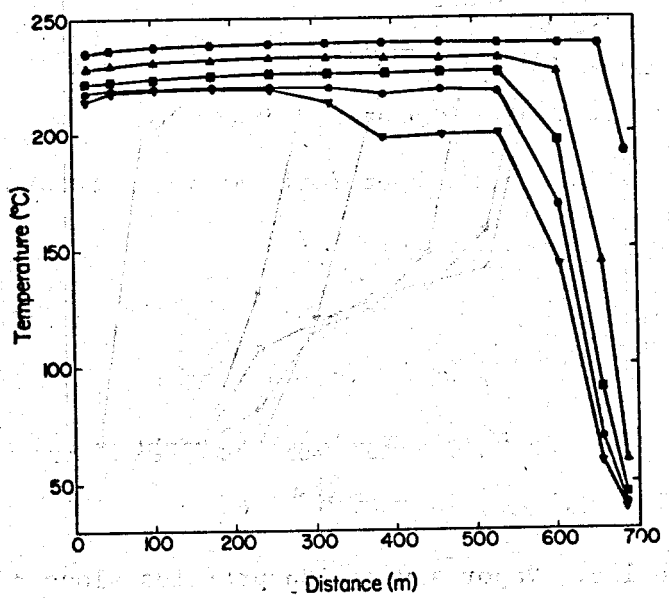

Figure 11c. Vapor saturation profiles along a line joining the production and injection wells for the five-spot problem. Injection rate 0.025 kg/sec (100% of production).

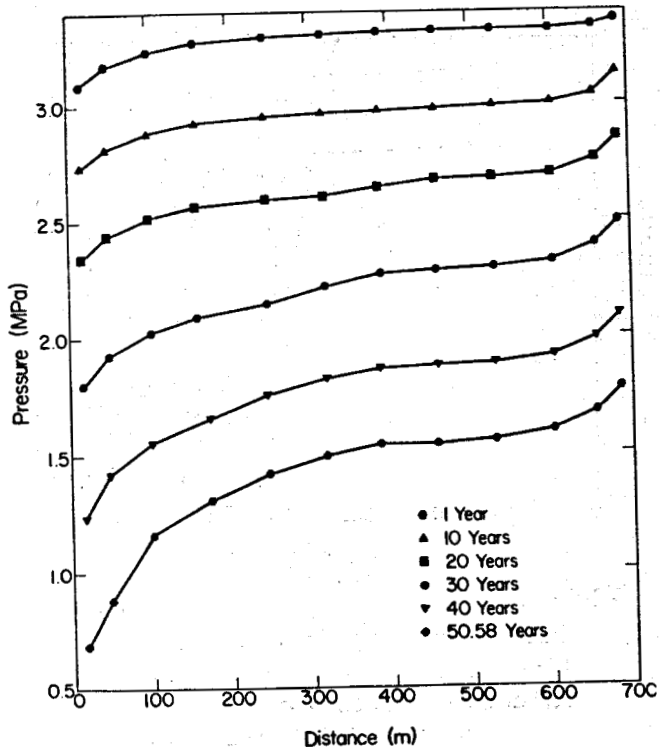

Figure 12a. Pressure profiles along a line joining the production and injection wells for the five-spot problem. Injection rate 0.05 kg/sec (200% of production).

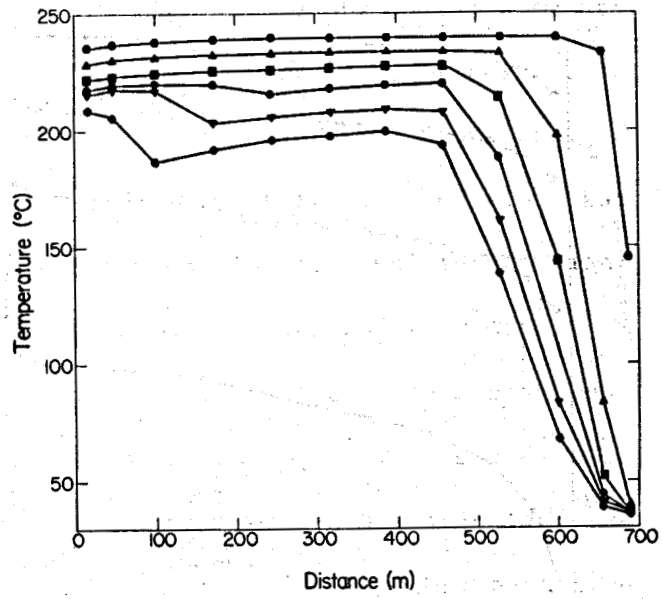

Figure 12b. Temperature profiles along a line joining the production and injection wells for the five-spot problem. Injection rate 0.05 kg/sec (200% of production).

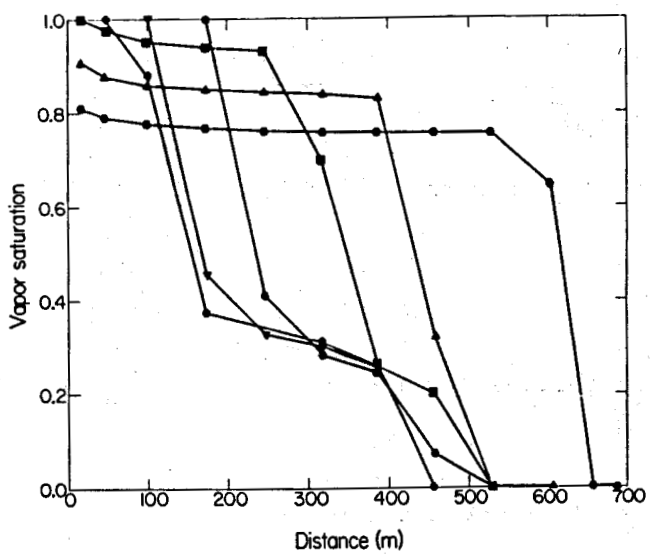

Figure 12c. Vapor saturation profiles along a line joining the production and injection wells for the five-spot problem. Injection rate 0.05 kg/sec (200% of production).

twenty years during which the boiling zone extends into both the superheated region and the condensed region. The pressure throughout the reservoir declines steadily while the temperature declines most rapidly in the two-phase, boiling zone. At the end of useful production, the energy remaining in the reservoir is still 46.9×10^{13} J and clearly higher injection rates would increase the longevity of the field still further.

From these cases it is clear that reinjection can extend the life of a two-phase system considerably but it does not increase power output. In fact, because the injected fluid reduces the volume of the boiling zone available for steam production, the production pressure drops slightly faster when more fluid is injected (see Figure 10).

The results obtained here are for an idealized homogeneous, isotropic, thin reservoir. In real reservoirs, fractures and gravity will lead to a preferential movement, with respect to direction or depth, of the injected fluid. The effect of gravity is studied in the next section.

6. Gravity Segregation

A numerical study of gravity segregation effects has been completed for a single choice of injection temperature and reservoir saturation. Several different cases were examined for a relatively thick (100 meter) plane parallel reservoir. Water at $\approx 33^{\circ}C$ was injected in a single well with the reservoir initially at a steam saturation of $S = 0.75$. Table 1 and 2 summarize the initial conditions for the different problems. The results of the computations are presented in several figures showing some of the most important points. Figure 13 shows the results from Problems 1 and 2 described in Table 2. The figure shows a comparison of the gravity and no gravity cases, and demonstrates dramatically how important gravity segregation effects are when an appreciable amount of steam is present in the reservoir. In these calculations the absolute permeabilities were the same in the horizontal and

TABLE 2: Injection Parameters

Case number	1	2	3	4	5	6
Gravity (m/sec^2)	0	9.81	9.81	9.81	9.81	9.81
Open interval	100m	100m	top 40m	top 40m	bottom 40m	bottom 40m
Injection rate (kg/sec)	15	15	15	6	15	6

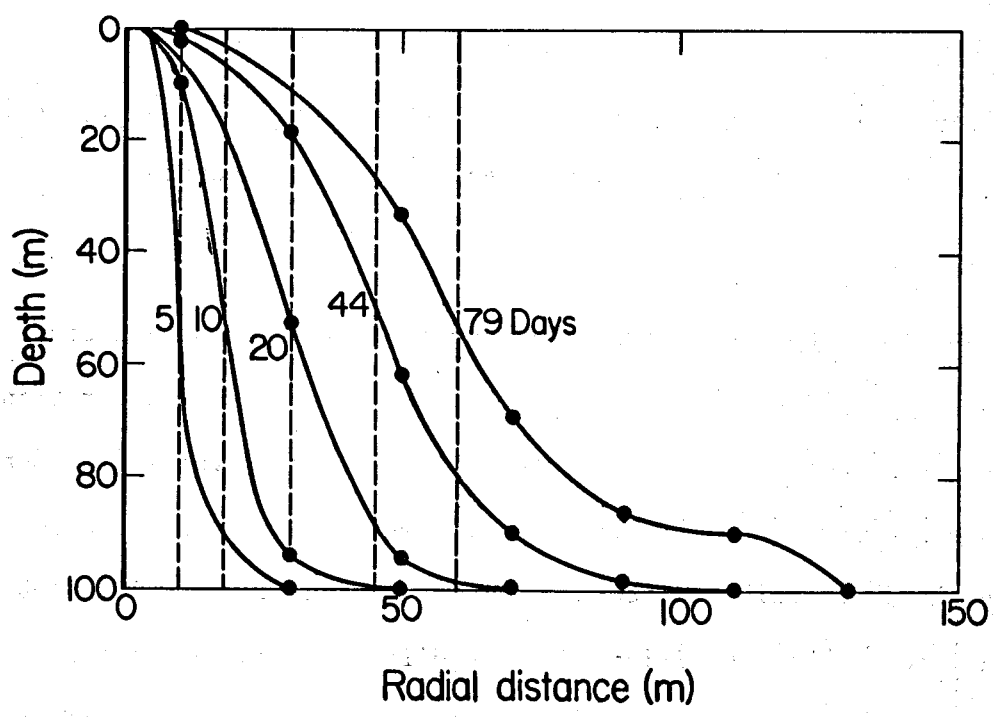

Figure 13. Locations of the hydrodynamic front for injection into a thick reservoir. Case 1, no gravity, ----; Case 2, gravity, ——.

vertical directions. In many cases, the vertical permeability will be considerably less than the horizontal, and will reduce the tendency of the injected fluid to slump to the bottom of the reservoir. Figures 14 and 15 show the corresponding temperatures for Problem 1. The spreading of the thermal front is a numerical effect due to the coarse mesh (20 m).

In Figures 16 through 18 the results for Problems 5 and 6 are presented. The calculations show that the injected fluid initially plumes upward, but then the motion is outward and downward through the remainder of the injection period of about 120 days. Obviously there is a relationship between the vertical height of the leading edge and the injection flow rate. At the higher rate the hydrodynamic front is much more spread out with an apparent "second pulse" forming near the well. At the lower rate the liquid simply slumps into the reservoir with a large gravitational effect. This results in a leading edge of liquid at about 3/4 the distance of the higher rate, even though the higher rate is more than twice as great (15 compared to 6 kg/sec of injected water). Although the liquid advances very quickly near the bottom of the aquifer, the thermal fronts--as shown in Figure 18--lag far behind. These observations have important implications for production/injection well fields.

Figures 19 and 20 show the results for Problems 3 and 4. These results, although not carried out as far as the others, show a significant downward migration of fluid, and suggest that the hydrodynamic front will eventually develop more nearly like the full injection case described above.

Due to the large compressibility in the two-phase portions of the reservoir, we do not see a significant pressure increase beyond the hydro-dynamic front. In the case of injection at the top of the reservoir an interesting, but relatively unimportant, pressure effect occurs. Due to the slumping, condensing liquid, the pressure decreases slightly at the top of the reservoir near the hydrodynamic front, which results in a few percent increase in steam saturation locally.

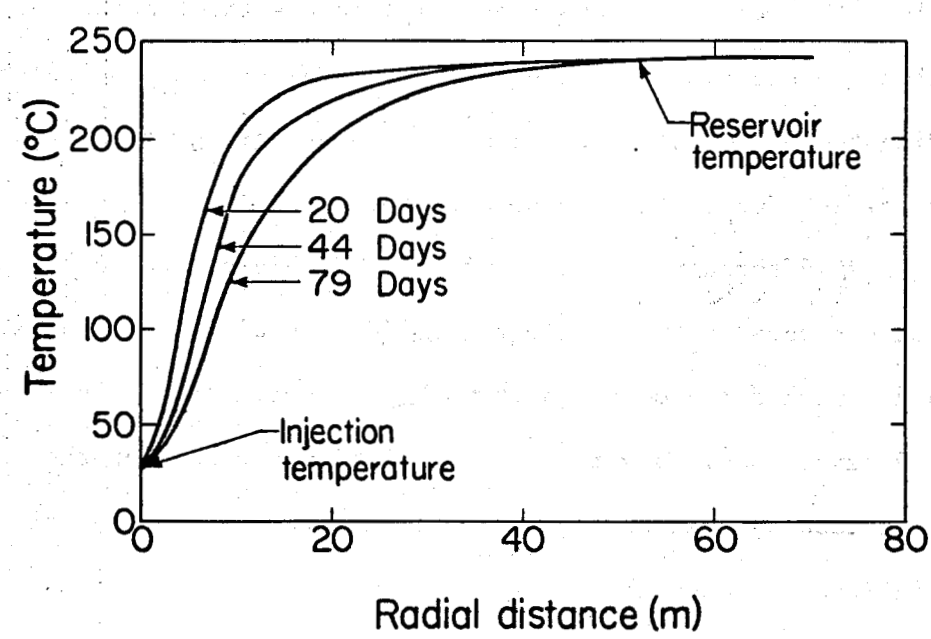

Figure 14. Temperature profiles for injection into a thick reservoir (case 1) along a line in the horizontal central plane (50 m depth).

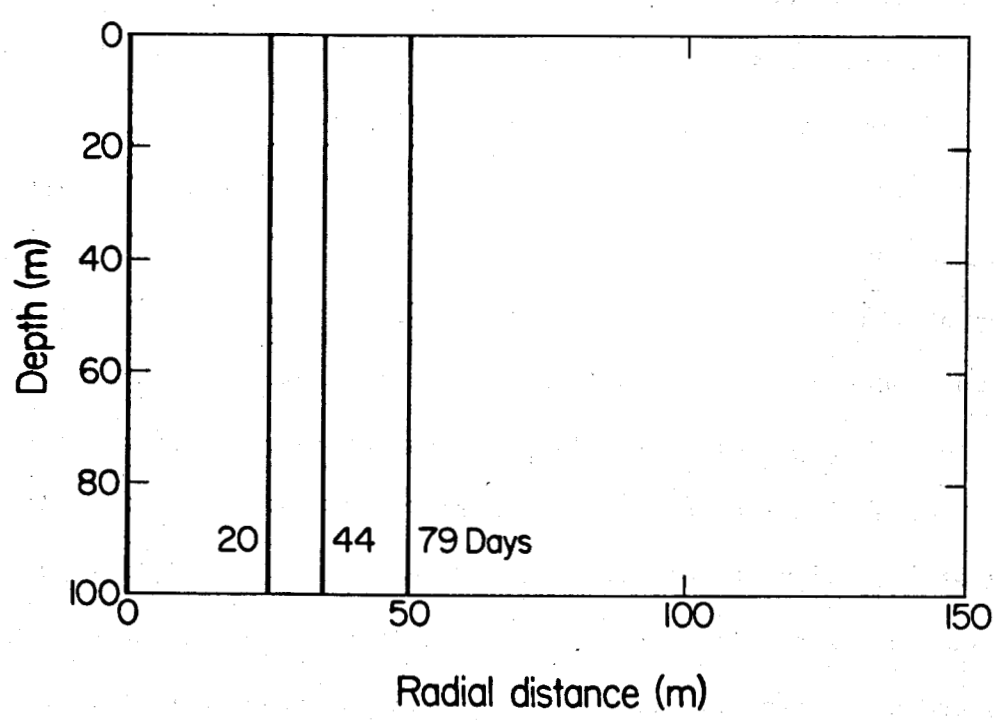

Figure 15. Locations of the thermal front for injection into a thick reservoir (case 2).

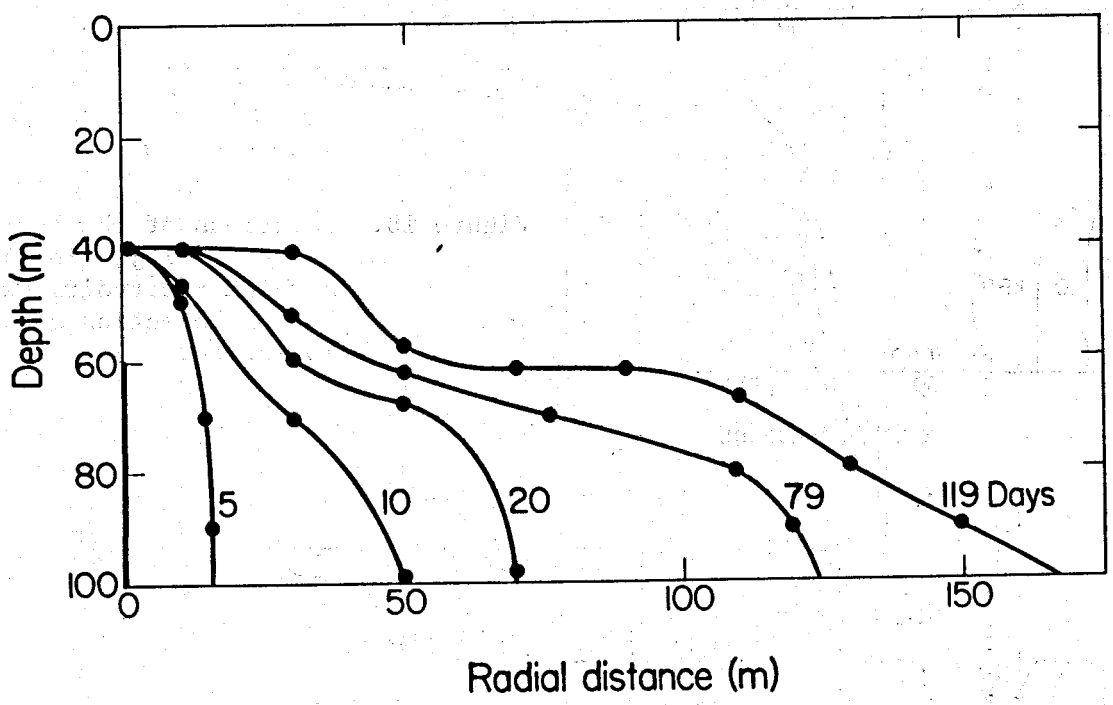

Figure 16. Locations of the hydrodynamic front for injection into a thick reservoir. Case 5, bottom injection at 15 kg/sec.

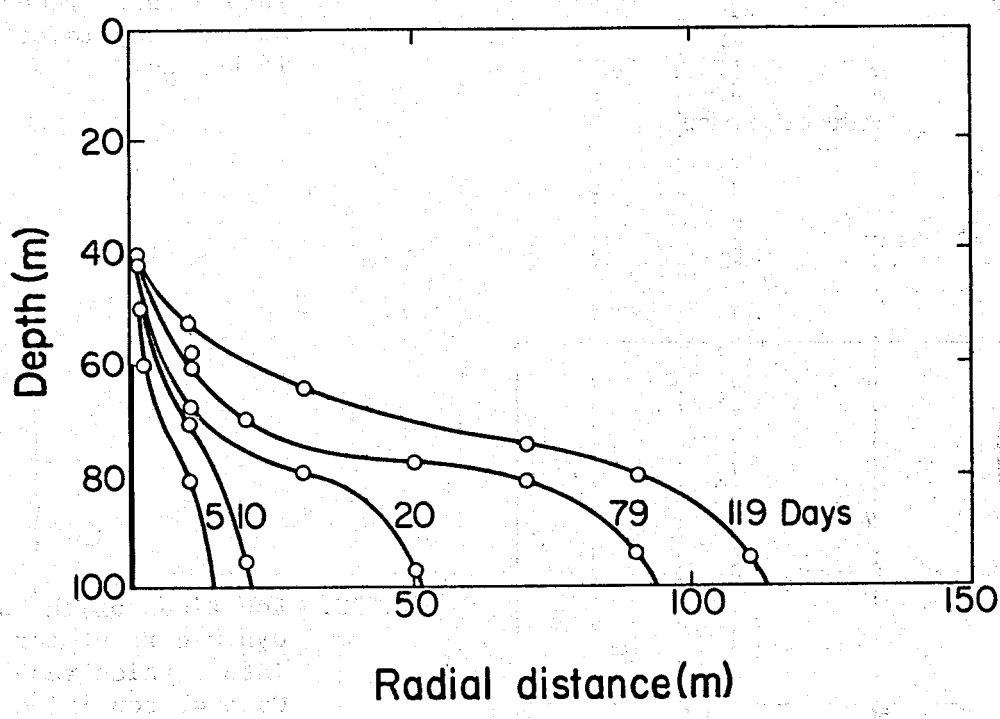

Figure 17. Locations of the hydrodynamic front for injection into a thick reservoir. Case 6, bottom injection at 6 kg/sec.

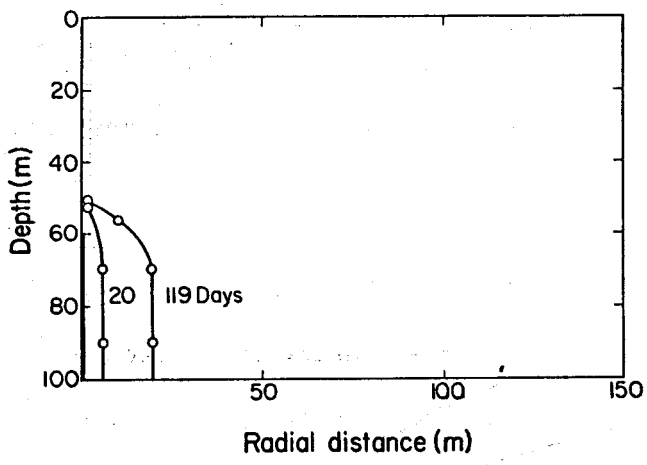

Figure 18. Locations of the thermal front for injection into a thick reservoir. Case 5, bottom injection at 15 kg/sec.

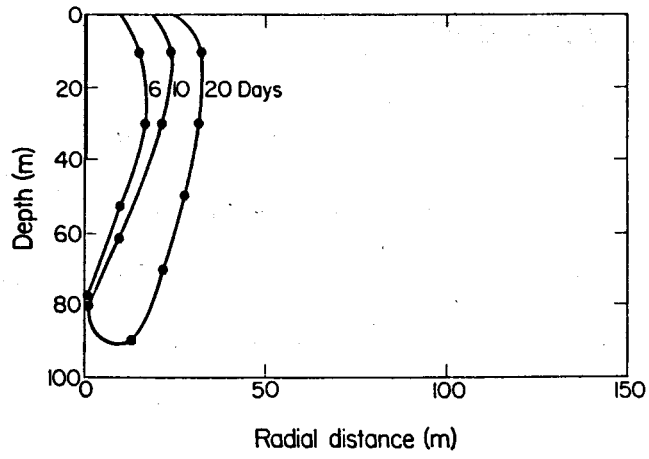

Figure 19. Locations of the hydrodynamic front for injection into a thick reservoir. Case 3, top injection at 15 kg/sec.

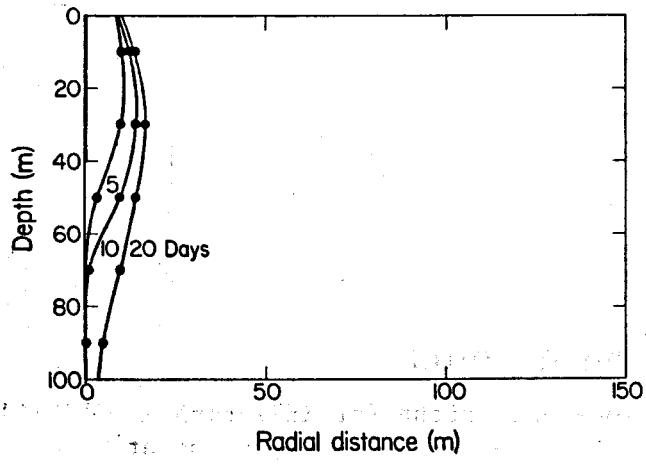

Figure 20. Locations of the hydrodynamic front for injection into a thick reservoir. Case 4, top injection of 6 kg/sec.

Since a coarse grid was used for these calculations (20 x 20 m), a number of questions remain regarding numerical effects on the detailed front propagation. These questions were outside the scope of these investigations.

7. One-Dimensional Approximation of Larderello

We consider a one-dimensional vertical system with porosity. Figure 21 shows our idealized system and the corresponding real reservoir. Reservoir properties and thermodynamic conditions are similar to those encountered in the most depleted zones of Larderello.

The wells produce from a fracture system at the top of the reservoir. The fracture system is presumed to make the pressure uniform at the top and equal to bottomhole values in the productive wells. The steam produced by the boiling water in the deeper layers rises vertically to collect in the fractures at the top of the reservoir. Initial conditions are given in Figure 22. Pressure is maintained practically constant at the top and bottom boundaries by connecting the system with fictitious elements having very large volumes. The system remains practically steady in these conditions with a steam production rate of 17 $kg/(sec \cdot km^2)$. An injected flowrate of 20 $kg/(sec \cdot km^2)$ of water at 30 ^oC was simulated at different depths (Figure 23).

It has already been noted that in problems involving sharp fronts and phase transitions, simulation produces oscillating trends of a certain size and that these oscillations are a consequence of finite space discretization.[34] These oscillations occur in all our examples of water injection into regions of the reservoir where $P < P_{sat}$. They derive from finite discretization and from the hypothesis that, in each point of the reservoir, the rock and fluid are at all times in thermal equilibrium.

Figure 24 shows the trend of the production flow rate and some quantities in the grid elements near the injection point. This refers to case a) of

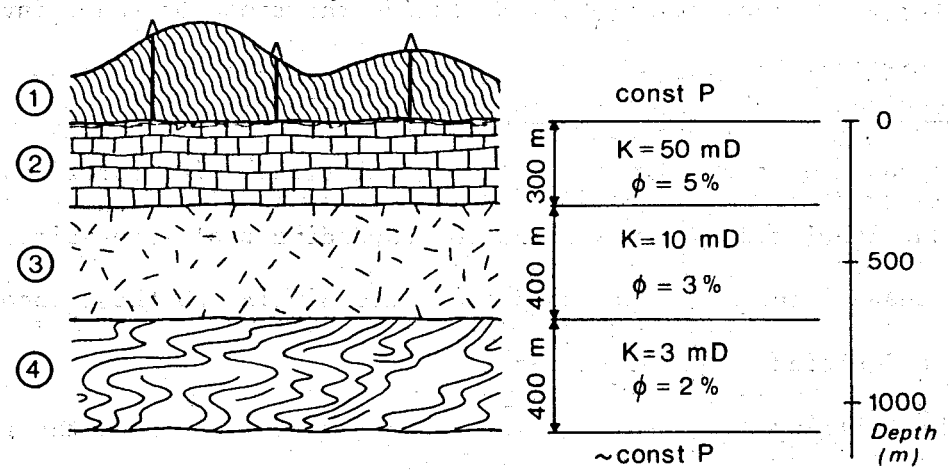

Figure 21. Linear flow model for reinjection studies. Rock and thermodynamic characteristics are similar to those existing in some zones of Larderello: 1-caprock, 2-carbonate formations, 3-fractured quartzites and phyllites, and 4-phyllites. (XBL 8012-12874)

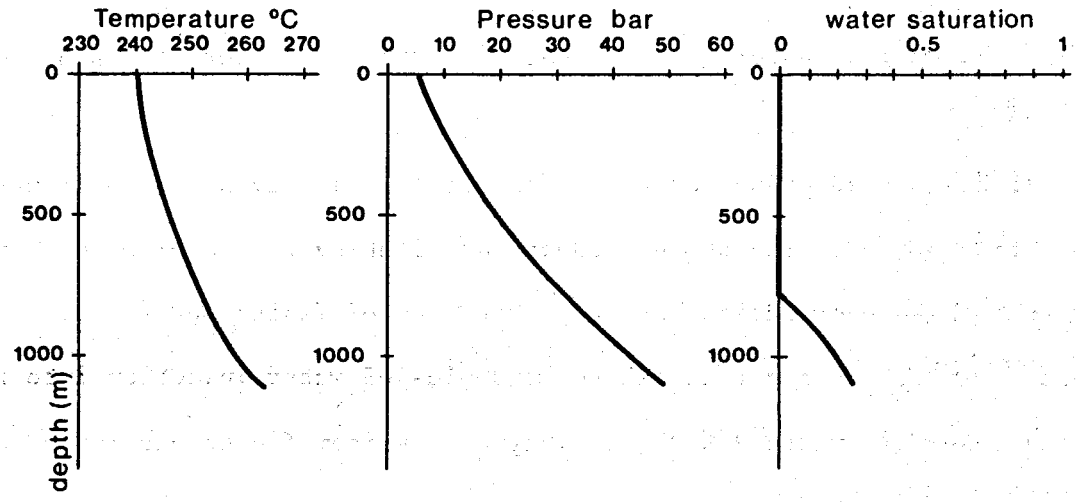

Figure 22. Initial conditions for the model of Figure 21. (XBL 8012-12875)

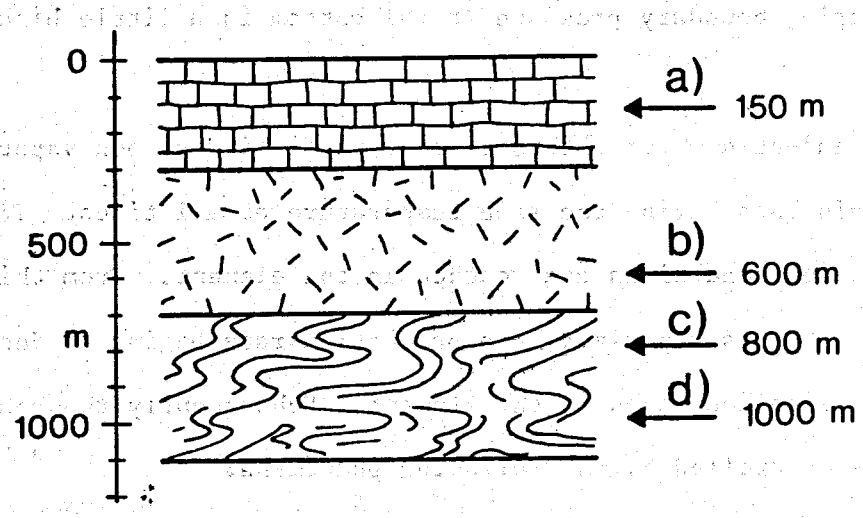

Figure 23. Depths of injection for cases a), b), c), d). (XBL 8012-12872)

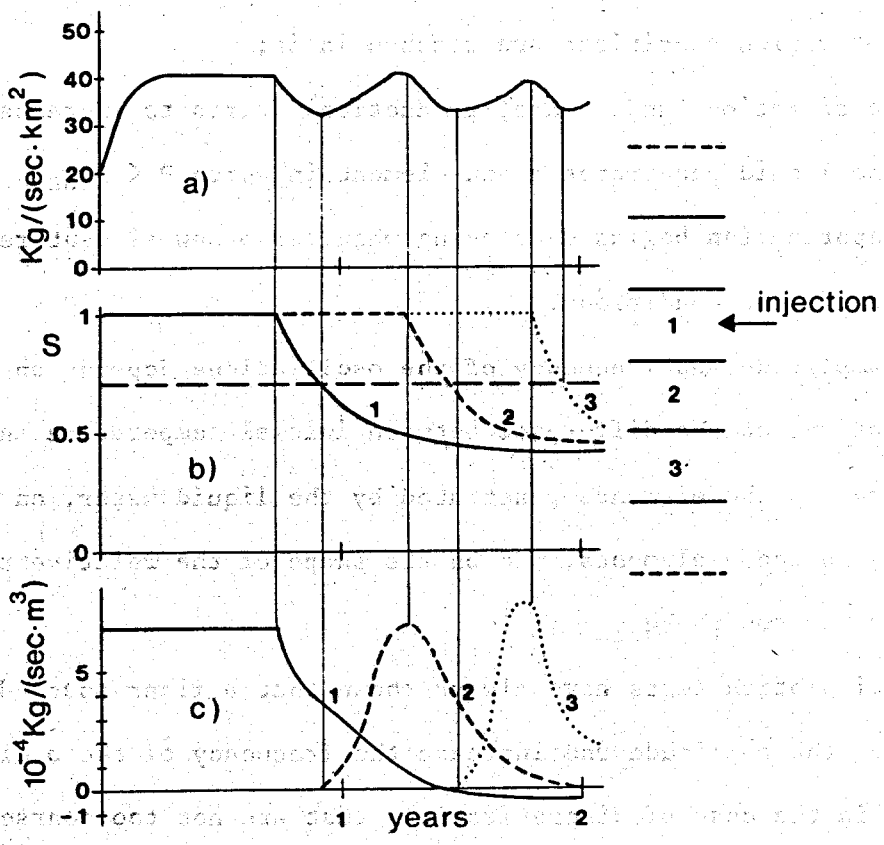

Figure 24. Discretization effects in simulations of the injection of cold water in superheated steam zones of the reservoir. a)production rate, b) steam saturation (immobile water saturation is 0.7), and c) boiling rate. (XBL 8012-12877).

Figure 23 where the thickness of the elements around the injection point is 3 m. In this example, boundary pressure at the bottom is a little higher than in Figure 22.

As the injected water enters element no. 1, it is soon vaporized, the rock and fluid both having the same temperature at all times. This continues until saturation conditions are reached in the element. From this moment on not all the water is vaporized, the production rate begins to decrease, and liquid saturation increases in the element. Subsequently the behavior of the model is controlled by the following phenomena:

- liquid water flows gravitationally (in this case) from one element to the underlying one each time the immobile water saturation is exceeded in the former;
- all the liquid water entering an element is vaporized until saturation conditions are reached in it;
- vaporization (and, hence, production) starts to increase whenever the liquid penetrates a new element in which $P < P_{sat}$.
- vaporization begins decreasing whenever a new element reaches saturation conditions.

The amplitude and frequency of the oscillations depends on space discretization, on the difference between initial temperature and saturation temperatures in the elements penetrated by the liquid water, on the pressure variations in these elements, and on the shape of the relative permeability curves for the two phases.

Our simulation tests have always shown that a finer space discretization will reduce the amplitude and increase the frequency of the oscillations. Moreover, in the case of discretizations that are not too coarse, the oscillations all occur around an average curve; the result of numerical simulation gradually approaches this curve as the space discretization becomes finer (see Figure 25, relative to the same case as Figure 24).

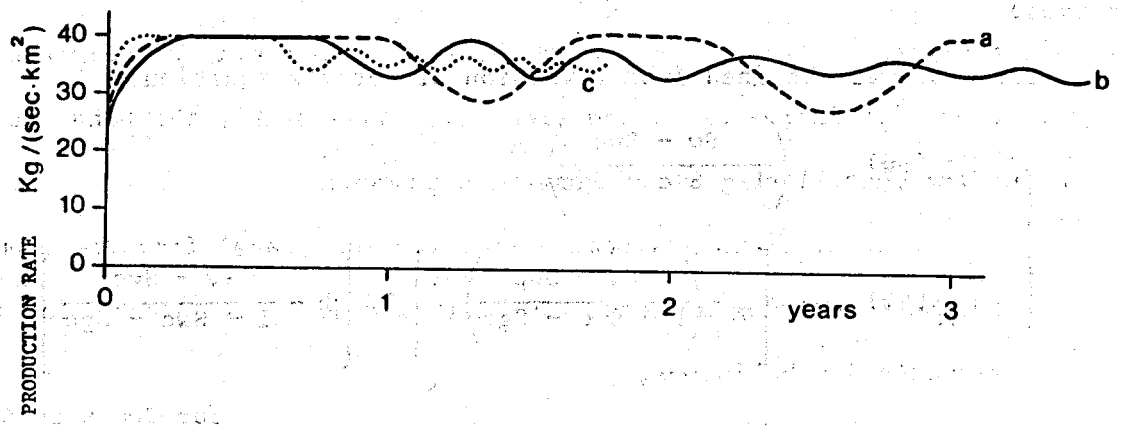

Figure 25. Results of simulations with different sizes of the grid elements in the linear flow model. a) ΔZ = 6.66 m, b) ΔZ = 3m, and c) ΔZ = 1 m. (XBL 8012-12876)

The relative permeability of the two phases is a very important parameter for reinjection as it affects both the pressure gradient and liquid propagation through the rock volume. Unfortunately, there would appear to be no safe criteria at present for attributing one given relative premeability curve to the various reservoir rocks. Figure 26 shows some theoretical and empirical curves.

Curve a) was obtained from a version of Corey's equation.

$$\begin{cases} K_{rw}(Sw) = \left(\dfrac{Sw - Swc}{1 - Swc - Sgc}\right)^4 \\ K_{rs}(Sw) = \left[1 - \left(\dfrac{Sw - Swc}{1 - Swc - Sgc}\right)^2\right] \cdot \left[1 - \dfrac{Sw - Swc}{1 - Swc - Sgc}\right]^2 \end{cases} \quad (5)$$

for $Swc < Sw < 1 - Sgc$

$$\left.\begin{matrix} K_{rw} = 0 \\ K_{rs} = 1 \end{matrix}\right\} \quad \text{for } Sw \leq Swc$$

$$\left.\begin{matrix} K_{rw} = 1 \\ K_{rs} = 0 \end{matrix}\right\} \quad \text{for } Sw \geq 1 - Sgc$$

with $Swc = 0.3$, $Sgc = 0$.

This is the parametrization generally used in our one-dimensional model.

Curve b) is derived from Wairakei production data. The parabolic curves in Figure 26c were used by some authors to simulate two-phase reservoirs[35], while curves d) were based on preliminary laboratory results obtained at Stanford University.[36] These curves were taken as an example of just how varied they can be.

The model's behavior is strongly affected by the choice of relative permeabilities. Usually a high K_{rw} for low water saturation values attenuates the discretization effects mentioned earlier. Figure 27, relative to the case

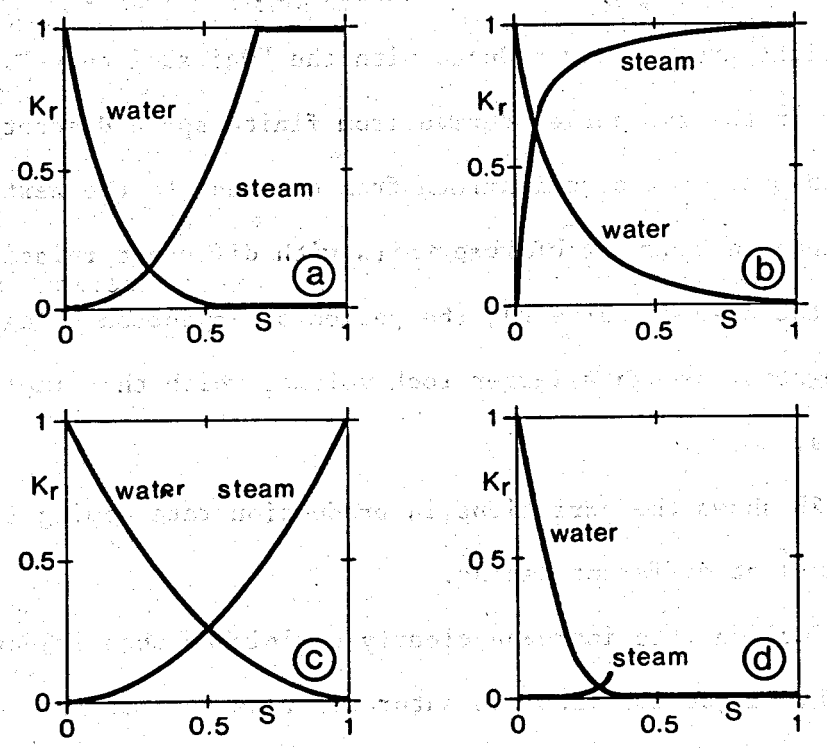

Figure 26. Examples of relative permeability curves for water and steam. (XBL 8012-12871)

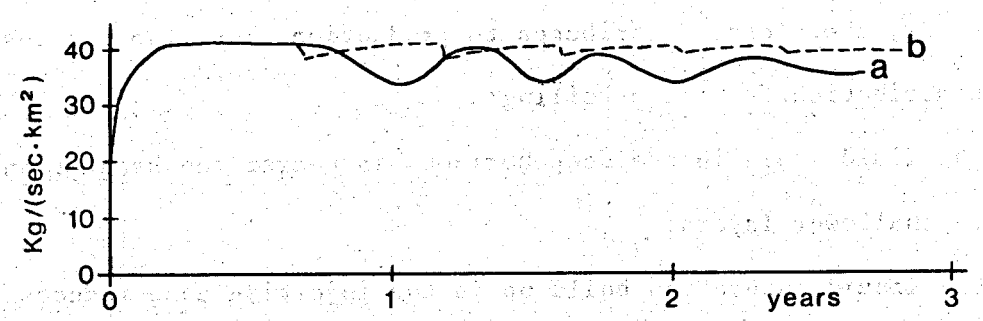

Figure 27. Results of simulation with different relative permeabilities. a)Corey's equation Swc = .3, Sgc = 0 (Figure 26a), b) Relative permeability from Wairakei production data (Figure 26b). (XBL 8012-12873)

of Figure 24 with a 3 m space discretization in the injection zone, shows that the oscillations are greatly reduced with the "Wairakei curve". While the oscillations in the two curves derive from finite space discretiztion, the difference in average production rate from one case to the next is a result of a difference in behavior of reservoirs with different relative permeability curves. In the case of curve b), the period of injection being equal, the liquid propagates through a larger rock volume, which thus implies higher boiling rates.

Figure 28 shows the variations in production rate coming from injecting 20 kg/(sec·km^2) at different depths.

The production rate increase clearly diminishes when injection is made at greater depth. Injection into the saturated zone even brings about a slight production decrease.

Considering cases a), b), and c) only, the variation of production with depth of injection is due to the following facts:

- vaporization of the injected water produces a pressure increase in the injection zone, with a consequent increase in the gradient above and reduction in that below this zone. Vaporization of injected water, therefore, contributes to production, but also reduces the contribution from deep boiling;
- the fluid state in the deep horizons is nearer the saturation then in shallower layers;
- the liquid saturation build-up in the injection zone reduces the relative permeability to steam;
- the pressure increases below the injection horizon. In the parts of the reservoir containing two-phase fluid even a small pressure increase can stop boiling and start condensation.

Figure 29 shows the evolution of saturation around the injection point in cases a) and c). In the latter, more liquid accumulates in the injection

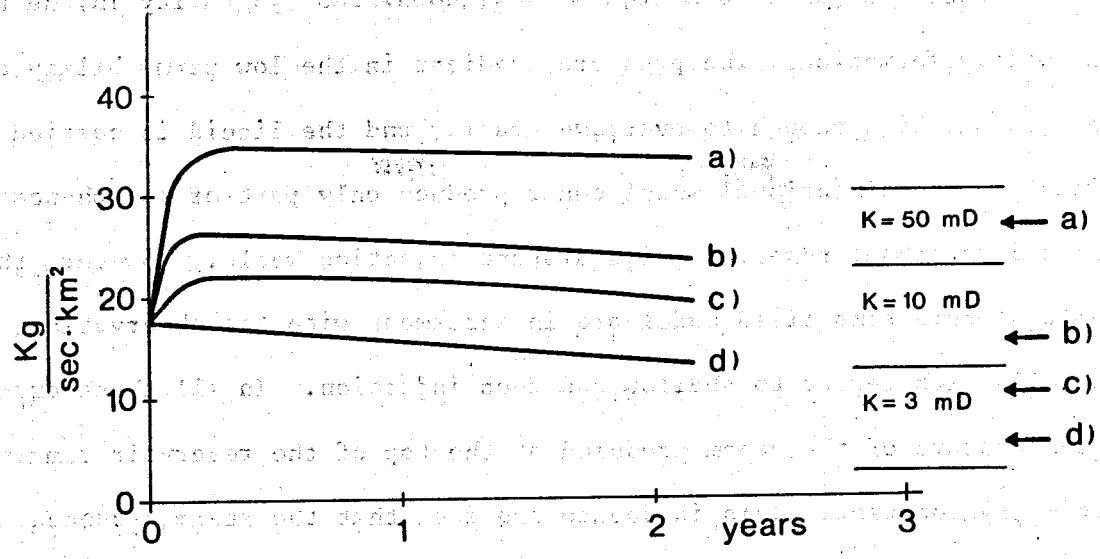

Figure 28. Effect of injection depths in the linear flow model (smoothed curves). (XBL 8012-12870)

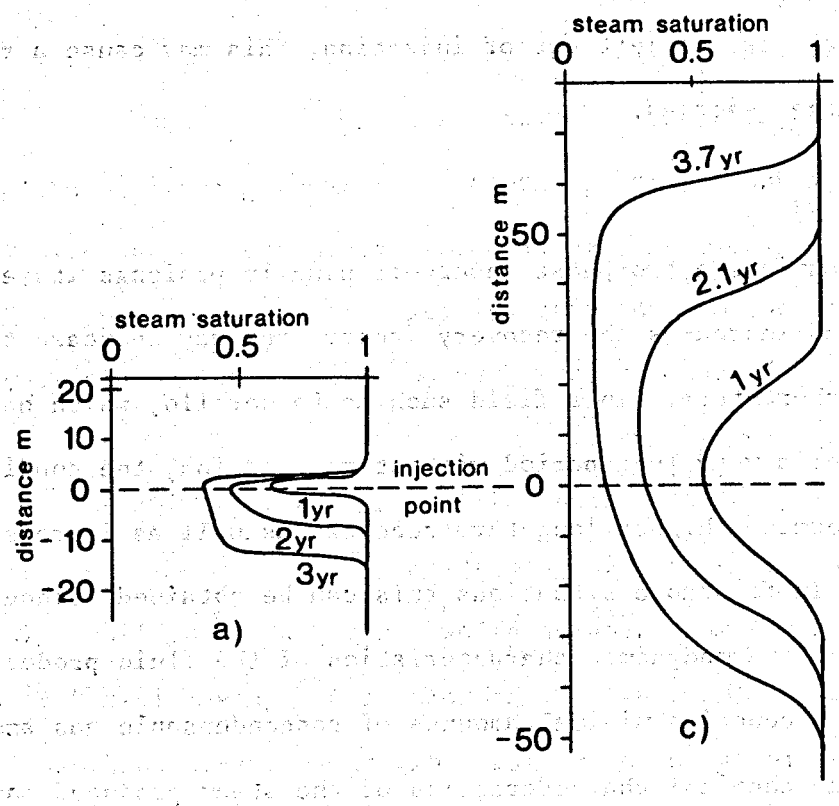

Figure 29. Saturation around the injection point in cases a) and c) of Figure 23. (XBL 8012-12878)

zone. Furthermore, while the liquid flows downwards by gravity in the higher permeability formations, the pressure gradient in the low permeability deep formations is high enough to overcome gravity and the liquid is carried upwards. Obviously a one-dimensional model can reproduce only part of the phenomenology of a three-dimensional reservoir with distant injection wells. However, the results of this simplified model are in agreement with the observations made at Larderello with regard to shallow and deep injection. In all these examples, the temperature of the steam produced at the top of the reservoir remains practically constant. This is due to the fact that the steam produced from injected water (after mixing with steam from deep boiling) crosses a hot rock layer unaffected by boiling. Usually it is desirable that the steam produced from injected water crosses a certain interval of hot rock before reaching the producing wells. If the injection point is too near the extraction point, the thermodynamic characteristics of the fluid are adversely affected, with the risk of efficiency reduction in the conversion phase. On the other hand, if too large rock volumes are left out of injection, this may cause a reduction in recovery of the reserves.

8. Conclusions

Injection into a two-phase reservoir usually prolongs its economic production and increases the recovery factor, but may decrease the production rate in the short-term. In a field such as Larderello, which has been exploited over a very long period without reinjection, the conditions are now such as to permit a higher long-term recovery as well as increased short-term production. In favorable situations this can be obtained without detrimental effects on the thermodynamic characteristics of the fluid produced. As the injected water contains minimal amounts of noncondensable gas and is quickly vaporized, the chemical characteristics of the steam produced may even improve, to the advantage of conversion efficiency.

The application of numerical simulation to the study of reinjection problems reveals how useful this approach can be, even though it is confined for the moment to ideal systems or particular problems. There have been too few field data available so far to show whether the model of the porous medium is capable of simulating fractured reservoirs in which rock-fluid heat exchange is the dominating phenomenon.

Similarly the lack of information on relative permeability, which also has a strong influence on the phenomena, prevents formation of fully reliable models. Field and laboratory tests will consequently play an important role in the near future. Particularly important is to identify, in the geothermal field, the zones in which $P < P_{sat}$, the volumes involved, and the reservoir characteristics. Injection itself could be used for this purpose. Simulation of injection in a reservoir whose fluid is superheated steam poses some problems: a very fine space descretization must be used and the time step must also be shortened when crossing the saturation line in the water equation of state diagram. However, it is felt that approximate results acceptable to the engineer can be achieved even in these circumstances at a reasonable cost.

Finally, it should be noted that $P < P_{sat}$ does not always imply that only superheated steam exists in the porous medium. Vapor pressure lowering can be produced by salinity, capillarity, and adsorption phenomena. These phenomena also require more detailed study.

In summary, our investigations to date result in the following general conclusions:

1. Numerical simulation is a valid and viable tool for studying injection into two-phase reservoirs.
2. Injection well tests in thin formations can be analyzed by means of single-phase pressure transient techniques.
3. Injection into a producing two-phase reservoir may enhance

ultimate energy recovery by large amounts, with small effects on power output.

4. Gravity effects can be very strong in thick reservoirs.

5. Injection into superheated steam zones may increase production rates as well as energy recovery.

It is suggested that future work on modeling injection should investigate the effects of fractures. Also, efforts should be made for modeling actual field cases rather than idealized problems.

References

1. A.J. Chasteen, Geothermal Steam Condensate Reinjection, Vol. 2, Proceedings Second United Nations Symposium, San Francisco, California (May, 1975).

2. G. Cuellar, Behavior of Silica in Geothermal Waste Waters, Ibid.

3. S.S. Einarsson, A. Vides R., and G. Cuellar, Disposal of Geothermal Waste Water by Reinjection, Ibid.

4. P.A. Witherspoon, Unpublished reports.

5. K. Kubota, K. Aosaki, Reinjection of Geothermal Hot Water at the Otake Geothermal Field, Vol. 2, Proceedings Second United Nations Symposium, San Francisco, California (May, 1975).

6. R. Schroeder, Unpublished data.

7. S.M. Benson, C.B. Goranson, D. McEdwards, and R.C. Schroeder, Well Tests, In: Geothermal Resource and Reservoir Investigation of U.S. Bureau of Reclamation Leaseholds at East Mesa, Imperial Valley California, Report #LBL-7094 (October 1978).

8. C.F. Knutson and C.R. Broadman, An Assessment of Sub-Surface Salt Water Disposal Experience on the Texas and Louisiana Gulf Coast, Report No. EY-77-C-08-1531 (1977).

9. J.S. Aronofsky and H.J. Ramey, Jr., Mobility Ratio -- Its Influence on Injection or Production Histories in Five-spot Waterflood, Petroleum Transactions, AIME Journal, Vol. 207, p. 205 (1956).

10. J.S. Brown and H.W. Engelhardt, A Case Study of Startup Management for a Large Seawater Injection Project, SPE Paper 8409, presented at the 54th Annual Fall Technical Conference, Las Vegas, Nevada, September, 1979.

11. G. Bodvarsson, Thermal Problems in the Siting of Reinjecting Wells, Geothermics Vol. 1, no. 2 (1972).

12. G. Bodvarsson, On the Temperature of Water Flowing through Fractures, J. Geophys. Res., Vol. 74, No. 8 (April, 1969).

13. A.C. Gringarten, P.A. Witherspoon, and Y. Onishi, Theory of Heat Extraction From Fractured Hot Dry Rock, J. Geophys. Res., Vol. 80, No. 8 (March, 1975).

14. P. Kasameyer and R. Schroeder, Thermal Depletion of Liquid-Dominated Geothermal Reservoirs with Fracture and Pore Permeability, UCRL-77323 preprint (December, 1975).

15. G.S. Bodvarsson, C.F. Tsang, Injection Into a Fractured Geothermal Reservoir, Transactions, Vol. 4, Geothermal Resources Council (September, 1980).

16. A.C. Gringarten, J.P. Sauty, The Effect of Reinjection on the Temperature of a Geothermal Reservoir Used for Urban Heating, Proceedings, Second United Nations Symosium, San Francisco, California (May, 1975).

17. P.W. Kasameyer, Thermal History of Reinjected Effluents (Unpublished), (August, 1976).

18. T.W. Tsang and C.F. Tsang, An Analytical Study of Geothermal Reservoir Pressure Response to Cold Water Reinjection, Proceedings Fourth Workshop Geothermal Reservoir Engineering, Stanford University (1978).

19. M.J. Lippmann, C.F. Tsang, and P.A. Witherspoon, Analysis of the Response of Geothermal Reservoirs under Injection and Production Procedures, SPE-6537, Presented at the 47th Regional Meeting of the SPE, Bakersfield, California (1977).

20. M.J. O'Sullivan and K. Pruess, Analysis of Injection Testing of Geothermal Reservoirs, Vol. 4, Geothermal Resources Council (September, 1980).

21. M. Nathenson, Physical Factors Determining the Fraction of Stored Energy Recoverable from Hydrothermal Convection Systems and Conduction-dominated Areas, U.S. Geological Survey Open-file Report 75-525 (October, 1975).

22. D. Mangold, C.F. Tsang, M.J. Lippmann and P.A. Witherspoon, A Study of Thermal Effects in Well Test Analysis, SPE Paper 8232, presented at 54th Annual Fall Meeting SPE, Las Vegas (September, 1979).

23. J.W. Pritchett, S.K. Garg, and T.D. Riney, Numerical Simulations of the Effects of Reinjection on Performance of a Geopressured Geothermal Reservoir, Geothermal Resource Council Transaction, Vol. 1 (1977).

24. K. Pruess and R.C. Schroeder, Geothermal Reservoir Simulations with SHAFT79, Proceedings Fifth Workshop Geothermal Reservoir Engineering, Stanford University (December 1979).

25. L.D. Mlodinow and C.F. Tsang, The Effect of Radially Varying Transmissivity on the Transient Pressure Phenomenon, Proceedings Third Workshop Geothermal Reservoir Engineering, Stanford University (December, 1977).

26. R.J. Blackwell, J.R. Rayne, and W.M. Terry, Factors Influencing the Efficiency of Miscible Displacement, Petroleum Transactions Reprint Series, No. 8, Miscible Processes, SPE.

27. T.K. Perkins and O.C. Johnston, A Review of Diffusion and Dispersion in Porous Media, Ibid.

28. J.P. Sauty, A.C. Gringarten, and P.A. Landel, The Effect of Thermal Dispersion on Injection of Hot Water in Aquifers. Proceedings of the Second Invitational Well Testing Symposium (October, 1978).

29. J.P. Sauty, An Analysis of Hydrodispersive Transfer in Aquifers, Water Resources Research, Vol. 16, No. 1, p. 145-158 (February 1980).

30. J.E. Warren and P.J. Root, The Behavior of Naturally Fractured Reservoirs, S.P.E.J., Vol. 3, p. 245-255 (1963).

31. P.A. Witherspoon, J.S.Y. Wang, K. Iwai, and J.E. Gale, Validity of the Cubic Law for Fluid Flow in Deformable Rock Fracture, Report #LBL-9557 (1979).

32. G.S. Bodvarsson and C.F. Tsang, Injection Into Geothermal Fractures, Proceedings of the Third Invitational Well Test Symposium (to be published, 1980).

33. S.K. Garg, Pressure Transient Analysis for Two-phase (Liquid Water/-Steam) Geothermal Reservoirs, paper SPE-7479, presented at the 53rd Annual Fall Technical Conference and Exhibition of the Society of Petroleum Engineers, Houston, Texas (October, 1978).

34. K. Pruess, G. Bodvarsson, R.C. Schroeder, P.A. Witherspoon, R. Marconcini, G. Neri, and C. Ruffilli, Simulation of the Depletion of Two-Phase Geothermal Reservoirs, Paper SPE-8266, presented at the 54th Annual Fall Technical Conference and Exhibition of the SPE, Las Vegas, Nevada (September 1979).

35. S.R. Aydelotte, Transient Well Testing in Two-Phase Geothermal Reservoirs, Lawrence Berkeley Laboratory Report LBL-10562, Berkeley, California (March 1980).

36. J.R. Counsil and H.J. Ramey, Jr., Drainage Relative Permeabilities Obtained from Steam-Water Boiling Flow and External Gas Drive Experiments, Transactions, Geothermal Resources Council, Vol. 3 (September 1979).

37. C.R. Faust and J.W. Mercer, Geothermal Reservoir Simulation, 2. Numerical Solution Techniques for Liquid - and Vapor - Dominated Hydrothermal Systems, Water Resources Research, Vol. 15, No. 1, p. 31-45 (February 1979).

APPENDIX

Consider injection of cold water with temperature T_{in} at constant rate q into a thin infinite two-phase reservoir with uniform initial conditions (temperature T_{res}, vapor saturation S). We postulate that the process will give rise to a sharp temperature front, where reservoir temperature changes from T_{in} to T_{res}, and proceed to estimate total swept volume V_s and volume of the cold zone, V_c.

Neglecting the density of steam in comparison to that of liquid water, we have for the total injected mass:

$$M = qt = V_s \phi S \rho_w' + V_c \phi (\rho_w - \rho_w') \tag{A.1}$$

where ρ_w and ρ_w' are liquid water densities at injection temperature T_{in} and reservoir temperature T_{res}, respectively.

For the total internal energy of the swept volume we have:

$$E = V_c \left[\phi \rho_w C_w + (1 - \phi) \rho_R C_R \right] T_{in} + (V_S - V_c) \left[\phi \rho_w C_w + (1 - \phi) \rho_R C_R \right] T_{res} \tag{A.2}$$

This is approximately equal to the total internal energy present in swept volume and injection fluid separately (neglecting small steam contributions):

$$E \simeq V_S (1 - \phi) \rho_R C_R T_{res} + M C_w T_{in} + V_S \phi (1 - S) \rho_w' C_w T_{res} \tag{A.3}$$

from which:

$$\frac{V_c}{V_S} = \frac{S \phi \rho_w' C_w}{\phi \rho_w' C_w + (1 - \phi) \rho_R C_R} \tag{A.4}$$

also,

$$V_s = \frac{M}{\phi S \rho_w' + (V_c / V_S) \phi (\rho_w - \rho_w')} \tag{A.5}$$

The location of the thermal front can be used to estimate porosity, in the following way. At time t, the total amount of injected fluid is qt. Of this, an amount $V_c\phi\rho_w$ is still at injection temperature, while an amount $(qt - V_c\phi\rho_w)$ has moved on and has been heated up to T_{res}. Assuming that the energy transferred to the fluid was supplied by the cooled rock, we have:

$$(qt - V_c\phi\rho_w)C_w(T_{res} - T_{in}) = V_c(1 - \phi)\rho_R C_R(T_{res} - T_{in}) \qquad (A.6)$$

from which, using $V_c = \pi R_c^2 H$:

$$\phi = \frac{\dfrac{qC_w}{\pi H}\,\dfrac{t}{R_c^2} - \rho_R C_R}{\rho_w C_w - \rho_R C_R} \qquad (A.7)$$

A DEPLETION MODEL FOR THE GABBRO ZONE
(Northern Part of Larderello Field)

by

William E. Brigham, Stanford University
Guiseppi Neri, ENEL-Larderello, Italy

Introduction

Task DEA-3,19 of the ENEL/DOE joint agreement is directed toward the development of simple reservoir models which will match past performance data and can be used to predict future production rates and ultimate reserves. To this end, in 1979 the authors studied the pressure and production data available from the Gabbro Zone - a small producing interval north of the main producing area of the Larderello Field. Production began in this field in 1961. A new type of lumped parameter model was developed to match these data. This report summarizes the results of this modeling effort, including projections into the future.

RESERVOIR PRESSURE - PRODUCTION DATA

Four wells provide most of the production from the Gabbro Zone; Wells G-1, G-3, G-6 and G-9. Three additional wells produce minor volumes; Wells G-7, SD-2 and N-155. The detailed monthly production data from these wells were summed and are shown by six month intervals in Table 1. In this table the six month average production rate data are also listed, as well as the average pressures in the Gabbro Zone producing interval.

The reservoir pressure data in the Gabbro Zone deserves special comment. The paper by Celati et al[1] mentions that the original reservoir pressures found at Gabbro indicated a pressure trend toward the main Larderello producing zone. A study was made of the original pressures found in Wells G-1, G-3, G-4, G-6, G-7, G-8, G-9, SD-2, SD-4, SV-9 and N-115. These initial pressures were extrapolated back in time to an equivalent starting date, and it became clear that an original pressure trend existed in the reservoir. The pressure decreased in the south-southeast direction.

TABLE 1

Detailed Production Data, Gabbro Zone

Date	Average Flow Rate ($10^3 T/M_o$)	Cumulative Production (10^6 Tons)	Average Pressure (Kgm/cm^2)
1960	0.0	.0	30.0
1961	41.2	0.49	
1962	81.8	1.48	26.6
1963	100.7	2.08	
	154.2	3.01	
1964	198.2	4.20	
	232.2	5.59	24.85
1965	244.8	7.06	
	243.0	8.52	22.28
1966	247.3	10.00	
	228.5	11.37	21.27
1967	216.7	12.67	
	221.7	14.00	20.03
1968	271.7	15.63	
	261.7	17.20	18.79
1969	263.3	18.78	
	270.0	20.40	18.02
1970	255.0	21.93	
	248.3	23.42	17.45
1971	240.0	24.86	
	238.3	26.29	17.08
1972	231.7	27.68	
	228.3	29.05	16.52
1973	223.3	30.39	
	223.3	31.73	16.07
1974	220.0	33.05	
	225.0	34.40	15.85
1975	213.3	35.68	
	213.3	36.96	15.18
1976	205.0	38.19	
	215.0	39.48	15.28
1977	206.7	40.72	
	218.3	42.03	14.97
1978	197.0	43.21	
	193.0	44.37	

To average the pressure data, it was necessary to take this reservoir pressure trend into account. To this end we mapped the Gabbro Zone initial pressures including well locations and drew initial pressure contours. From this map it appeared that the pressure in Wells G-4, G-9 and SD-2 were very close to the average reservoir pressure, Wells G-1 and G-7 were about 0.6 Kgm/cm^2 above the average, and Well SD-4 was about 3.4 Kgm/cm^2 above the average. Wells G-3 and G-8 were about 1.9 Kgm/cm^2 below the average pressure, and Well 155 was about 3.8 Kgm/cm^2 below the average.

There is a long history of pressure data from Wells G-4, G-8 and SD-4 and the differences in pressure listed above have persisted throughout the producing life of the Gabbro Zone. These three wells supplied most of the pressure data used to determine the average pressures listed in Table 1. In addition there were 8 data points from Well G-7, 3 points from Well G-9, 11 points from Well SD-2 and one data point from most of the remaining wells. Two wells, B-3 and S. Michele, contain a high CO_2 content, thus their indicated pressures are not reliable and were not included in the calculations.

The pressure versus time data from Table 1 are graphed in Fig. 1. Notice that after 1965 the average pressure drops smoothly with production. However, early in the life, from 1960 to 1965, the three data points behave in an erratic manner. It appears there is some error in these data. Also very little data is available during this period. Unfortunately, we could find no logical basis to use to decide which of these three data points are reliable and which are not. As will be seen later, the paucity of data during this early low-production-rate period makes it difficult to decide which of the reservoir model equations we develop later is the most reliable.

RESERVOIR MODELING

The paper by Celati et al[1] clearly shows that the producing interval at Gabbro is brecciated carbonates associated with evaporitic deposits, with a flysh cap rock. Beneath this permeable horizon lies quartzites and phyllites which are somewhat fractured. This sequence of rock types is similar to the geology seen in the main part of the Larderello field.

The volume of steam that has been produced from Gabbro is far greater than could exist in the reservoir as steam alone, thus there must be boiling

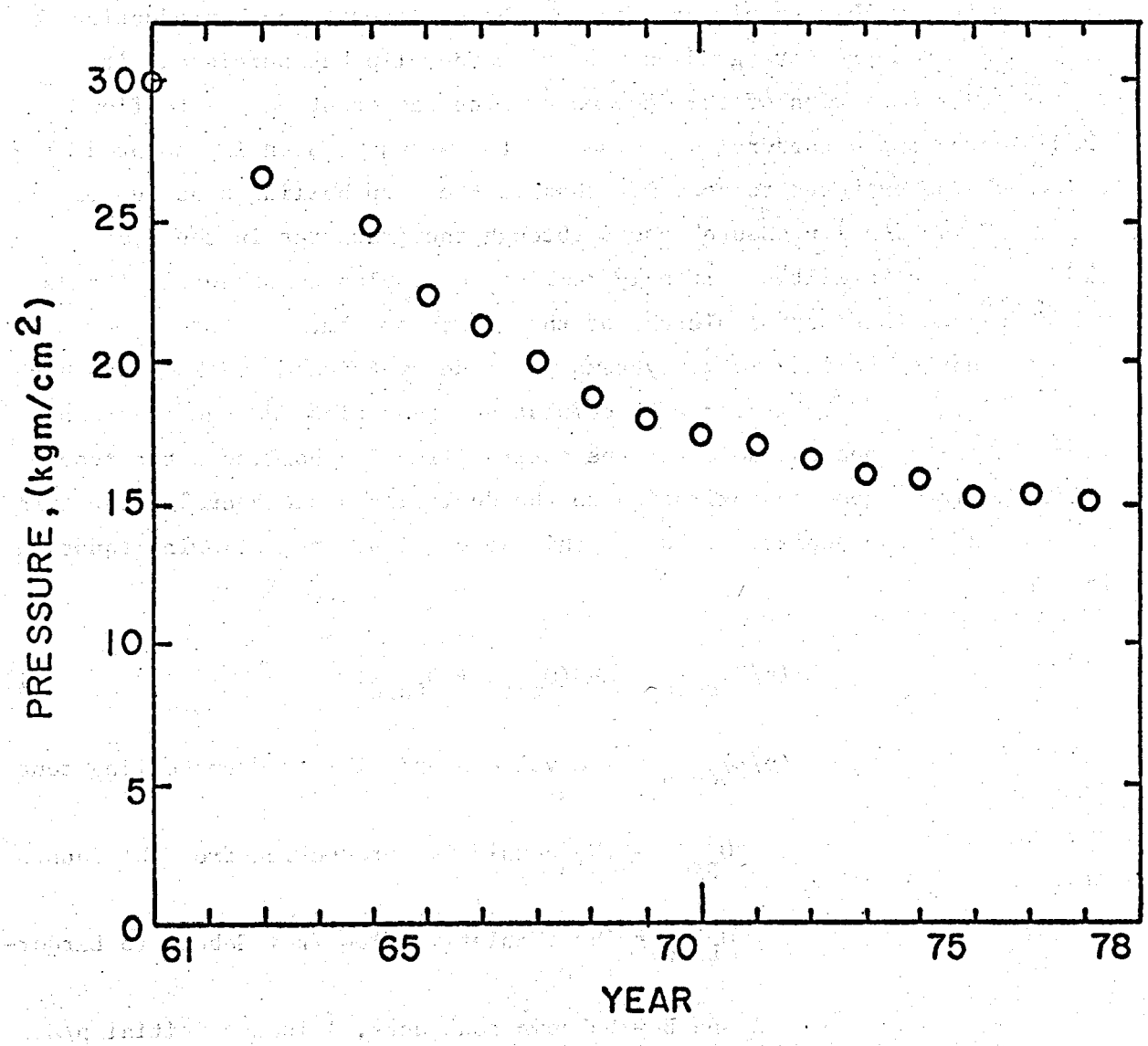

Figure 1. Gabbro zone average reservoir pressure (year end).

water supplying most of the steam to the producing interval. It seems reasonable to assume this water lies somewhere deep within the quartzites and phyllites. This supply of water can be depleted through production. Also, since the pressure gradient toward Larderello has persisted, it appears that depletion of the deep water zone has occurred due to flow from Gabbro toward Larderello. Finally, the pressure seen in the producing zone would be expected to be lower than in the deep boiling zone due to vertical frictional pressure losses through the fractures in the deep quartzites and phyllites. It only remains to develop a mathematical model which matches this verbal picture of the Gabbro system.

A study of boiling water systems was made by Brigham and Morrow[2] which indicated that p/Z is linear with cumulative production for such systems. This linearity does not hold for the entire life of a boiling water reservoir, but it is good approximation to the depletion history during the first 1/3 to 1/2 of the depletion. Using this assumption, the following equation is valid

$$(p/Z)_{deep} = A - B(Q_{prod} + Q_{Lard}) \tag{1}$$

where $(p/Z)_{deep}$ = The value of p/Z in the deep boiling zone

Q_{prod} = The cumulative production from the Gabbro Zone

Q_{Lard} = The cumulative flow from Gabbro to Larderello

A and B = Unknown constants, A is the initial p/Z, B is inversely proportional to the volume of the boiling water zone

The flow to Larderello can be treated as steady state flow, as follows:

$$Q_{Lard} = C' \int (p_{Gabbro} - p_{Lard})\, dt \tag{2}$$

where p_{Gabbro} = The pressure in the Gabbro zone

p_{Lard} = The pressure in Larderello

C' = An unknown constant which is inversely proportional to the permeability of the flow path between Gabbro and Larderello

Further, since the pressure data are all available in one year intervals, the integral in Equation 2 can be shown as a summation,

$$Q_{Lard} = C'\Sigma(p_{Gabbro} - p_{Lard}) \tag{2a}$$

A study of the main Larderello producing zone shows that its pressure has remained nearly constant at 8 Kgm/cm^2 for the past 15 years. Using this concept, Equation 2a can be combined with Equation 1 to arrive at the following equation:

$$(p/Z)_{deep} = A - B\,Q_{prod} - C\Sigma(p-8) \tag{3}$$

Equation 3 is for the p/Z in the deep boiling horizon. The pressure seen in the producing zone is less than in the deep zone due to frictional pressure losses. This can be expressed as follows:

$$(p/Z)_{top} = (p/Z)_{deep} - \Delta(p/Z)_{flow} \tag{4}$$

where $(p/Z)_{top}$ = the value of p/Z seen in the producing zone. The values associated with Figure 1

$\Delta(p/Z)_{flow}$ = the drop in p/Z due to vertical flow through a deep fractured zone

It only remains to develop an analytic expression for the drop in p/Z due to flow of steam through the fractured zone.

Pressure Drop Due to Linear Flow

To derive an equation for the pressure drop from the deep boiling zone through the fractured zone to the producing horizon, we can envision that the flow geometry is approximately linear. This is transient flow; thus the magnitude of the pressure drop will depend on the terms in the p_d function for linear flow, and the timing of the pressure transient will depend on the terms in the t_d function. Analytic solutions for such problems have been published by Miller[3] and by Nabor and Barham.[4] Nabor and Barham's solutions are summarized in Fig. 2, where their term $F(t_d)$ is the p_d function for linear flow at a constant rate.

The three functions shown in Fig. 2 depend on the outer boundary condition; that is, the boundary condition at the boiling water interface. The $F_1(t_d)$ curve is for a system with a closed outer boundary, the $F_{1/2}(t_d)$ curve is for an infinite system, while the $F_o(t_d)$ curve is for a system with a constant pressure outer boundary. The system that most closely approximates Gabbro is the constant pressure boundary, the $F_o(t_d)$ curve. This is marked more heavily in Fig. 2.

A boiling water system is not an exact constant pressure boundary, for as the system depletes the pressure must decline. However, it is a good approximation to treat this system as constant pressure when the pressure in the boiling zone declines slowly with time - as it must for any reservoir with a reasonably long producing life.

Whenever the flow rate varies, it is necessary to use superposition to calculate the transient pressure drop. If equal time increments are used, the superposition equation is,

$$\frac{kA\Delta p}{\mu L} = q_1 p_d(t_d) + (q_2-q_1)p_d(t_d-\Delta t_d) + (q_3-q_2)p_d(t_d-2\Delta t_d) + (q_4-q_3)p_d(t_d-3\Delta t_d) + (q_{n+1}-q_n)p_d(t_d - n\Delta t_d) \qquad (5)$$

Let us study the $F_o(t_d)$ curve of Fig. 2 in detail. A good approximation to this curve is to assume that p_d is proportional to the square root of time until $t_d = 0.785$ and to assume it is a constant equal to 1.00 after $t_d = 0.785$. The maximum error using the approximation is only about 10%.

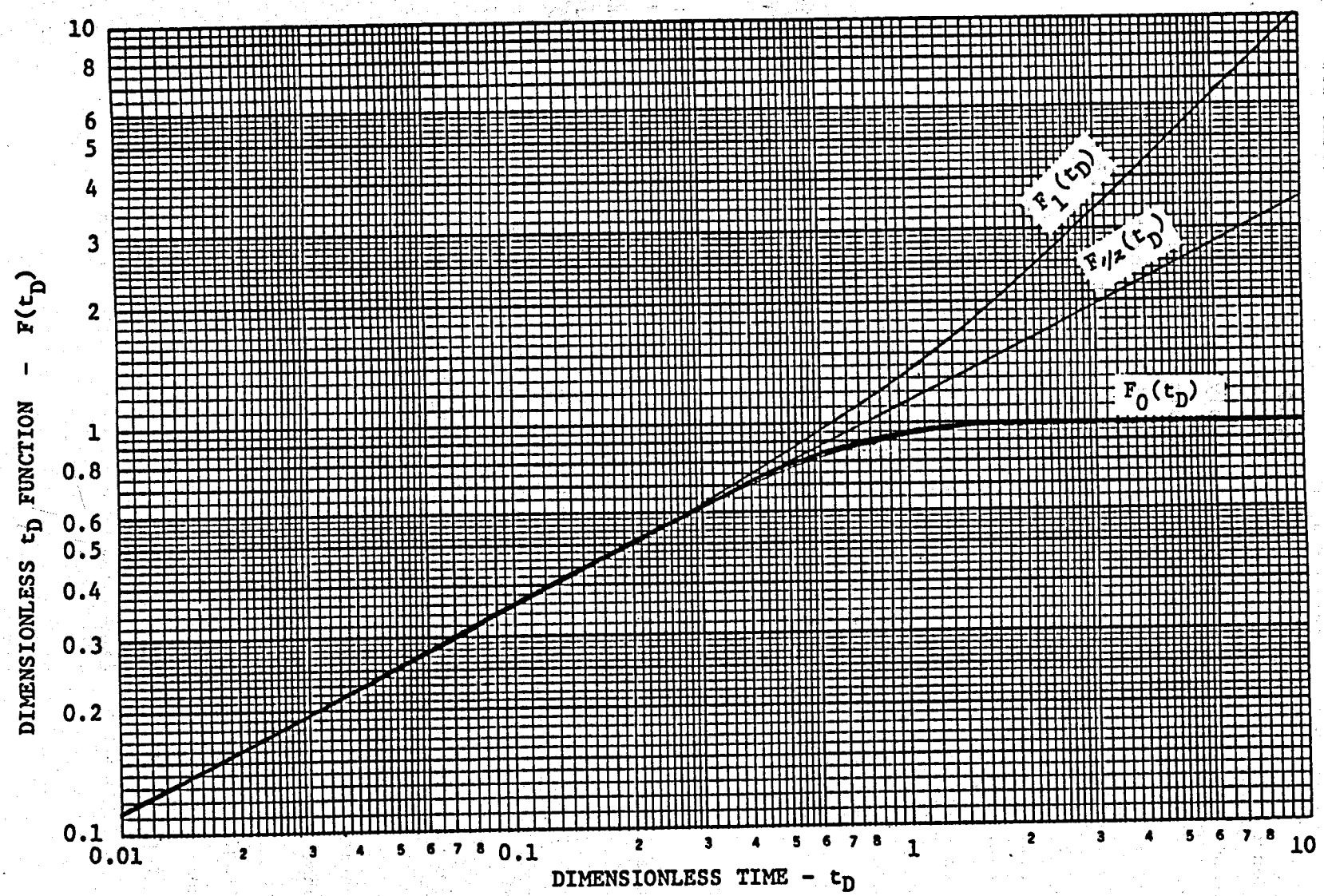

Figure 2. Dimensionless pressure change and efflux functions - linear aquifers.

Ref: Nabor and Barham
<u>Trans</u> AIME (1964) 231, 561

In most real systems we do not know the parameters in t_d well enough to be able to relate real time to t_d; however, we can assume a value for the real time that is equivalent to $t_d = 0.785$ and observe how this affects Eq. 5. Hence forth in this paper we will refer to this time as the "lag time." This phrase was chosen for it is meant to imply the time required to reach effective steady state flow. It is somewhat similar to the common concept of "readjustment time" that is seen in the well test literature; but it is not quite the same, for the readjustment time occurs at $t_d \simeq 1.7$ to 2.0 in Figure 2 where $F_o(t_d)$ is more nearly equal to 1.00.

To determine the effect of the lag time and the above approximations on the superposition equation, let us assume there has been production for six time periods ($6\Delta t$) and let us also assume that the lag time is four time periods ($4\Delta t$). Using the approximations to the $F_o(t_d)$ curve, Equation 5 becomes:

$$\frac{kA\Delta p}{\mu L} = q_1(1) + (q_2-q_1)(1) + (q_3-q_2)(1) + (q_4-q_3)\sqrt{\frac{3\Delta t}{4\Delta t}} + (q_5-q_4)\sqrt{\frac{2\Delta t}{4\Delta t}} + (q_6-q_5)\sqrt{\frac{\Delta t}{4\Delta t}} \qquad (6)$$

Notice the left hand side of Eq. 6 is equal to the flow rate if we had linear steady state flow; thus we can call this term the equivalent steady state flow rate, $q_{eq.}$. The right hand side contains a number of terms that cancel each other, so the equation can be simplified as follows,

$$q_{eq} = q_3\left(1-\sqrt{\frac{3}{4}}\right) + q_4\left(\sqrt{\frac{3}{4}}-\sqrt{\frac{2}{4}}\right) + q_5\left(\sqrt{\frac{2}{4}}-\sqrt{\frac{1}{4}}\right) + q_6\sqrt{\frac{1}{4}} \qquad (7)$$

Equation 7 tells us that any flow that occurred at a time further in the past than the lag time has no effect on the pressure drop that is occurring today. Further, Eq. 7 gives us a basis for a general formulation for the equivalent flow rate as a function of the lag time. For example suppose that the lag time is equal to five time periods. The equation for the equivalent steady date flow rate will be,

$$q_{eq} = q_{n-4}\left(1-\sqrt{4/5}\right) + q_{n-3}\left(\sqrt{4/5}-\sqrt{3/5}\right) + q_{n-2}\left(\sqrt{3/5}-\sqrt{2/5}\right) + q_{n-1}\left(\sqrt{2/5}-\sqrt{1/5}\right) + q_n\sqrt{1/5} \tag{8}$$

The flow rate data from Gabbro were averaged over six month time periods, thus it was logical to use multiples of six months for the unknown lag times. These flow rates are shown in Table II and also the equivalent steady state flow rates are listed for lag times ranging up to 48 months. We also calculated equivalent flow rates for 54 and 60 month lag times, but these are not included in the table for they were found to give unrealistic results, as will be discussed later.

Relating $\Delta(p/Z)$ to Flow Rate

Equations 7 and 8 relate the equivalent steady state flow rate to the actual rates; however, Equations 5 and 6 were written for liquid flow rather than steam flow. The correct equation for the equivalent steady state linear flow of steam is

$$q_{eq} = D'' \int_{p_1}^{p_2} \frac{2pdp}{\mu Z} = D'' \Delta m(p) \tag{9}$$

where

$$m(p) = \int_{p_o}^{p} \frac{2pdp}{\mu Z}$$

D'' = an unknown constant inversely proportional to the permeability in the deep fractured zone

TABLE II

Equivalent Flow Rates at Various Lag Times (10^3T/Mo)

Date	lagtime 0 Mo	lagtime 12 Mo	lagtime 18 Mo	lagtime 24 Mo	lagtime 30 Mo	lagtime 36 Mo	lagtime 42 Mo	lagtime 48 Mo
61	41.2							
	41.2							
62	81.8							
	81.8							
63	100.7							
	154.2							
64	198.2							
	232.2							
65	244.8							
	243.0	243.5	241.4	235.7	227.0	216.0	206.1	198.0
66	247.3							
	228.5	234.0	235.7	236.9	236.4	233.1	227.2	219.0
67	216.7							
	221.7	220.2	221.8	225.2	227.1	228.6	228.9	226.9
68	271.7							
	261.7	264.2	256.7	251.4	249.0	248.8	248.4	248.2
69	263.3							
	270.0	268.0	266.9	267.5	262.7	258.7	256.4	255.8
70	255.0							
	248.3	250.3	253.9	255.1	255.8	257.2	254.6	252.1
71	240.0							
	238.3	238.3	240.5	242.5	245.4	246.9	248.0	249.6
72	231.7							
	228.3	229.3	231.0	232.2	233.9	235.7	238.3	239.9
73	223.3							
	223.3	223.3	224.2	225.2	226.6	227.8	229.3	231.0
74	220.0							
	225.0	223.5	223.5	223.5	224.0	224.6	225.7	226.6
75	213.3							
	213.3	213.3	215.5	216.1	216.8	217.4	218.2	219.1
76	205.0							
	215.0	212.1	212.3	212.4	213.8	214.3	215.0	215.5
77	206.7							
	218.3	214.9	214.9	213.6	213.6	213.5	214.4	214.8

Atkinson and Mannon[5] have shown that m(p) is almost exactly proportional to p^2 for steam reservoirs. Thus Eq. 9 can be simplified to,

$$q_{eq} = D''\Delta(p^2) \tag{10}$$

Note that Eq. 10 relates flow rate to $\Delta(p^2)$, while Eq. 4 requires that the flow rate be related to $\Delta(p/Z)$. There is no theoretical basis whereby these terms can be related, however an empirical power law equation was attempted which is of the following form

$$\Delta(p/Z)_{flow} = D' \frac{\left[\Delta(p^2)\right]^n}{(p/Z)^m_{top}} \tag{11}$$

The applicable pressure and Z factor data are listed in Table 3. To test this empirical equation, pressures ranging from 12 Kgm/cm^2 to 30 Kgm/cm^2 were assumed, with $\Delta(p/Z)$ values ranging from 2.71 to 11.60. These pressure and $\Delta(p/Z)$ values were chosen to cover the range of data seen in the Gabbro history and likely to be seen in the next 15-20 years. These data were fit to Eq. 11 using a lest-square formulation, and the maxiumum error was 2.5%. Most of the errors were less than 1.0%. The values found for the constants were: n = 0.911 and m = 0.519.

It is now possible to write a single equation which combines the concepts discussed above. We can combine Equations 3, 4, 10 and 11 to get,

$$(p/Z)_{top} = A - BQ_{prod} - C\,\Sigma(p-8) - \frac{D(q_{eq})^{0.911}}{\left[(p/Z)_{top}\right]^{0.519}} \tag{12}$$

This is the equation used to match the history of the Gabbro zone and also to extrapolate the producing rate to the future.

Some comments on Eq. 12 seem appropriate at this time. To the best of our knowledge, this is the first time such a depletion material balance model has been used in a geothermal reservoir such that transient flow within the reservoir is coupled with a lumped parameter material balance. In oil reservoir with water influx, a somewhat similar concept has occasionally been used[6], but with a different equation form. Also, as far as we know, this is the first time anyone has shown that $\Delta(p/Z)$ can be simply and accurately related to $\Delta m(p)$. The beauty of Eq. 12 is that it can

TABLE III

Values of Pressure and Gas Deviation Factor, Z, for the Gabbro Zone
(T = ^{o}C)

p, Kgm/cm^2	Z	p/Z, Kgm/cm^2
10.0	0.96150	10.40
12.0	0.95360	12.58
14.0	0.94560	14.81
16.0	0.93690	17.08
18.0	0.92800	19.40
20.0	0.91930	21.76
22.0	0.90974	24.18
24.0	0.90002	26.67
26.0	0.88996	29.21
28.0	0.87935	31.84
30.0	0.86836	34.55

be solved using standard least-squares equations and a programmable calculator, or alternatively a standard regression analysis package can be used on a digital computer.

HISTORY MATCHING

As mentioned earlier there was some doubt about the validity of the first three pressure data points in the pressure/production history. For history matching we assumed the first data point at the end of 1960 was valid, and ignored the two data points at the end of 1962 and 1964. All other data were included in the history matches.

Since we did not know what lag times would be valid for this reservoir, seven lag times were assumed ranging from 18 months to 54 months. The 18 month and 54 month fits of Eq. 12 to the data were quite close; however, the least squares constants were not positive as they must be to be physically realistic. Thus these results are not reported herein. The results from the other five lag time assumptions are shown in Tables IV and V.

In Table IV are listed the pressures calculated from the least-square equation fits for all five lag times. At the bottom of each column is shown the standard deviation of each of the equations. It is clear from this table that any one of the time lag assumptions fits the data quite closely. The standard deviations range from 0.37 to 0.21 Kgm/cm^2. There is a trend toward a lower standard deviation as a longer lag time is assumed, but the reader is cautioned not to place too much emphasis on this trend. When a lag time of 54 months was assumed, the standard deviation was even smaller; but, as mentioned before, one of the constants in the resulting equation was of the wrong sign which is physically unrealistic.

TABLE IV

Calculated Values for p/Z in Gabbro
Compared to Measured Values
(Various Assumed Lag Times)

Date	Measured p/Z Kgm/cm^2	Calculated p/Z for various lag times				
		t_{lag} 24 Mo	t_{lag} 30 Mo	t_{lag} 36 Mo	t_{lag} 42 Mo	t_{lag} 48 Mo
1960	34.55	34.67	34.65	34.62	34.58	34.57
1965	24.55	23.95	24.08	24.29	24.46	24.53
1966	23.40	22.86	22.86	22.90	22.97	23.06
1967	21.76	22.07	22.11	22.08	22.00	21.93
1968	20.40	20.61	20.61	20.55	20.48	20.42
1969	19.40	19.44	19.41	19.41	19.39	19.38
1970	18.80	18.91	18.79	18.66	18.67	18.74
1971	18.40	18.45	18.35	18.25	18.18	18.13
1972	17.70	17.96	17.92	17.86	17.77	17.73
1973	17.20	17.45	17.44	17.43	17.40	17.35
1974	16.95	16.88	16.91	16.92	16.92	16.92
1975	16.20	16.40	16.43	16.46	16.48	16.49
1976	16.30	15.98	16.02	16.07	16.13	16.15
1977	15.90	15.39	15.44	15.51	15.57	15.63
Standard deviation Σ, kgm/cm^2		0.37	0.34	0.29	0.24	0.21

TABLE V

Best Fit Equations to Gabbro Data
Using Various Lag Times

General Equation Form

$$(p/Z)_{top} = A - BQ_{prod} - C\,\Sigma(p-8) - \frac{D(q_{eq})^{0.911}}{\left[(p/Z)_{top}\right]^{0.519}}$$

lag time (Months)	Constants in Best Fit Equations A	B	C	D
24	36.174	0.01027	0.06823	0.16866
30	35.772	0.05872	0.05098	0.21025
36	35.484	0.08818	0.03949	0.23994
42	35.398	0.08888	0.03697	0.25109
48	35.565	0.05825	0.04535	0.23662

Probably the only valid conclusion that can be reached from these results is that any of the five equations and lag times fits the data quite satisfactorily, and we have no valid method of picking one over another.

Table V shows the equations that were generated from the least-squares fits. A study of these equations constants shows that a broad range of reservoir parameters could be used to fit the Gabbro data. For example compare the constants for the 24 month lag time equation with the constants for the 42 month equation. The 24 month equation has the highest initial pressure (A = 36.174), the largest liquid reservoir volume (B = 0.01027), the greatest pressure loss due to flow toward Larderello (C = 0.06823) and the smallest frictional pressure drop (D = 0.16866). For the 42 month equation all these constants are at the opposite extreme; the lowest initial pressure (35.398), the smallest liquid reservoir volume (B = 0.08888), the smallest loss due to flow toward Larderello (C = 0.03697) and the greatest frictional pressure drop (D = 0.25109). These differences are quite significant; for example, the relative reservoir volumes between these two cases are 8.65/1, and the relative flow towards Larderello for these two cases are 16/1. If the results for the 24 month lag time are not considered we find that the ranges of parameters narrows considerably. The maximum range of reservoir size is from the 42 month to the 48 month equation and it is 1.53/1; the maximum range of loss to Larderello is from the 30 month to the 42 month equation, and it is 2.09/1.

In brief, these results tell us that we can match the past data very well indeed using Eq. 12; however, because a number of lag times match the data almost equally well, we do not have an accurate picture of the size of the system, the amount of loss toward Larderello nor the frictional pressure drop.

Fortunately this problem may not be as serious as we might first expect. Often when we achieve a good history match, we find that the projections into the future are realistic even if the specific parameters used to make that match are not. We will test this hypothesis in the next section.

FUTURE PRODUCING RATE

Before projecting the producing rate into the future it was necessary to predict the reservoir flow rate as a function of the average reservoir pressure. In general for gas flow from a reservoir it is possible to calculate the flow rate based on a version of the Forchheimer equation, as follows

$$\bar{p}^2 - p_{tf}^2 = aq + bq^2 \qquad (13)$$

where $\bar{p}$ = the average producing zone pressure, Kgm/cm^2

p_{tf} = the flowing wellhead pressure, Kgm/cm^2

q = the producing rate, $10^3 T/Mo$

a & b = unknown constants

Equation 13 is commonly used for gas flow. The constant, a, expresses the Darcy resistance to flow in the reservoir. The constant, b, expresses the sum of non Darcy effect in the reservoir plus the flowing friction within the well from the bottom to the wellhead.

The historical production rate data at Gabbro were tested against this equation. Individual well data were studied as well as overall reservoir flow data. We found that the past reservoir rate could be matched with a maximum error of 13% and a standard deviation of 5.7%. The best fit equation was,

$$\bar{p}^2 - p_{tf}^2 = 0.00436q^2 \qquad (14)$$

The Darcy term in Eq. 13, the constant, a, was found to be negligible.

The producing rates and pressures were projected in the future assuming the producing wellhead pressure would remain constant at 6 Kgm/cm^2 absolute. This projection requires a trial and error calculation each year, for the flow rate and the reservoir pressure are interdependent in Equations 12 and 14. We always found rapid convergence to the answers in 2 to 4 interactions.

The flow rates were projected for 18 years through the year 1995 using all five lag time equations. These projections are shown in Table VI where both production rate and cumulative production projections are shown.

A study of this table shows that all the projections are quite similar even though the parameters in the equations differed markedly. The greatest differences are between the 24 month and the 30 month projections. But even they differ by only 6% in flow rate by 1995, and only differ by 3% in cumulative production at that time.

There is a sound reason to consider the 24 month lag time projections invalid, for the actual production rate from Gabbro at the end of 1978 was 193 x 10^3T/Mo while the 24 month equation projection was 210.9 x 10^3T/Mo. Thus all the later projected rates may be too high for this case.

TABLE VI

Projections of Gabbro Production to the Future
Various Lag Times

Year	t_{lag} = 24 END YR q	t_{lag} = 24 END YR Q	t_{lag} = 30 END YR q	t_{lag} = 30 END YR Q	t_{lag} = 36 END YR q	t_{lag} = 36 END YR Q	t_{lag} = 42 END YR q	t_{lag} = 42 END YR Q	t_{lag} = 48 END YR q	t_{lag} = 48 END YR Q
1978	210.9	44.52	195.7	44.43	196.9	44.44	198.2	44.44	199.2	44.45
1979	204.1	47.01	191.1	46.75	192.0	46.77	193.0	46.79	194.1	46.81
1980	198.2	49.42	186.8	49.02	187.6	49.05	188.4	49.08	189.4	49.11
1981	193.2	51.77	181.7	51.23	182.7	51.27	184.3	51.32	185.3	51.36
1982	188.2	54.06	176.9	53.38	178.0	53.43	179.7	53.50	180.9	53.56
1983	183.4	56.29	172.4	55.48	173.4	55.54	175.2	55.63	176.6	55.70
1984	178.9	58.46	168.1	57.52	169.2	57.60	171.0	57.71	172.6	57.80
1985	174.5	60.58	164.0	59.51	165.0	59.60	166.9	59.73	168.7	59.84
1986	170.2	62.65	160.0	61.45	161.0	61.56	163.0	61.71	164.9	61.85
1987	166.2	64.67	156.2	63.35	157.1	63.47	159.3	63.65	161.3	63.80
1988	162.3	66.64	152.5	65.20	153.4	65.33	155.6	65.54	157.9	65.72
1989	158.6	68.57	149.0	67.01	149.9	67.15	152.1	67.38	154.5	67.59
1990	155.0	70.45	145.7	68.78	146.5	68.93	148.7	69.19	151.3	69.43
1991	151.5	72.29	142.5	70.51	143.1	70.67	145.5	70.95	148.2	71.22
1992	148.2	74.08	139.4	72.20	140.0	72.36	142.3	72.68	145.2	72.98
1993	145.0	75.84	136.4	73.86	136.9	74.03	139.3	74.37	142.4	74.71
1994	141.9	77.57	133.6	75.48	134.0	75.65	136.4	76.02	139.6	76.40
1995	139.0	79.25	130.8	77.06	131.1	77.24	133.5	77.64	136.9	78.06

If only the remaining four projections are considered, the lowest is for a lag time of 30 months and the highest is for a lag time of 48 months. In 1995 these differ by only 5% in producing rate and only by 1.3% in cumulative production. Thus our earlier speculation, that the various equations will give similar projections into the future, appears valid. Thus there is considerable reason to assume these projections will be realistic.

The history matches and projections to the year 1995 are shown for three cases in Figures 3, 4 and 5. Figure 3 is for a lag time of 30 months. This is the case which predicts the greatest decline during this period. Figure 5 is for a lag time of 48 months; it predicts the least decline. Figure 4 is for a lag time of 42 months. This is the case which predicts the greatest depletion due to production, the smallest depletion due to flow toward Larderello and the greatest drop in pressure due to transient vertical flow. In spite of the large differences in the parameters used in these equations, the future projections from all three are very similar.

These figures also indicate the times when the four major wells started to produce. Note in particular, that when Well G-9 started producing in 1967, the average reservoir pressure declined more rapidly for a period of time and gradually tended to level off. This can be seen both in the reservoir data and in the equation curve fits. This behavior is a direct result of the transient linear flow assumed in the model.

It would have been possible to extrapolate these production rates further into the future using Equations 12 and 14. Instead we chose to study the possibility of using decline curves for extrapolation. The Fetkovich[7] decline curves were tried, but we met with only limited success. The problem was that we found it difficult to differentiate between the various hyperbolic decline constants due to the scatter in the data at early time.

Another approach was tried, which, as far as we know, has not been used before. We will discuss this new method in the following paragraphs. The general decline equation has the following form

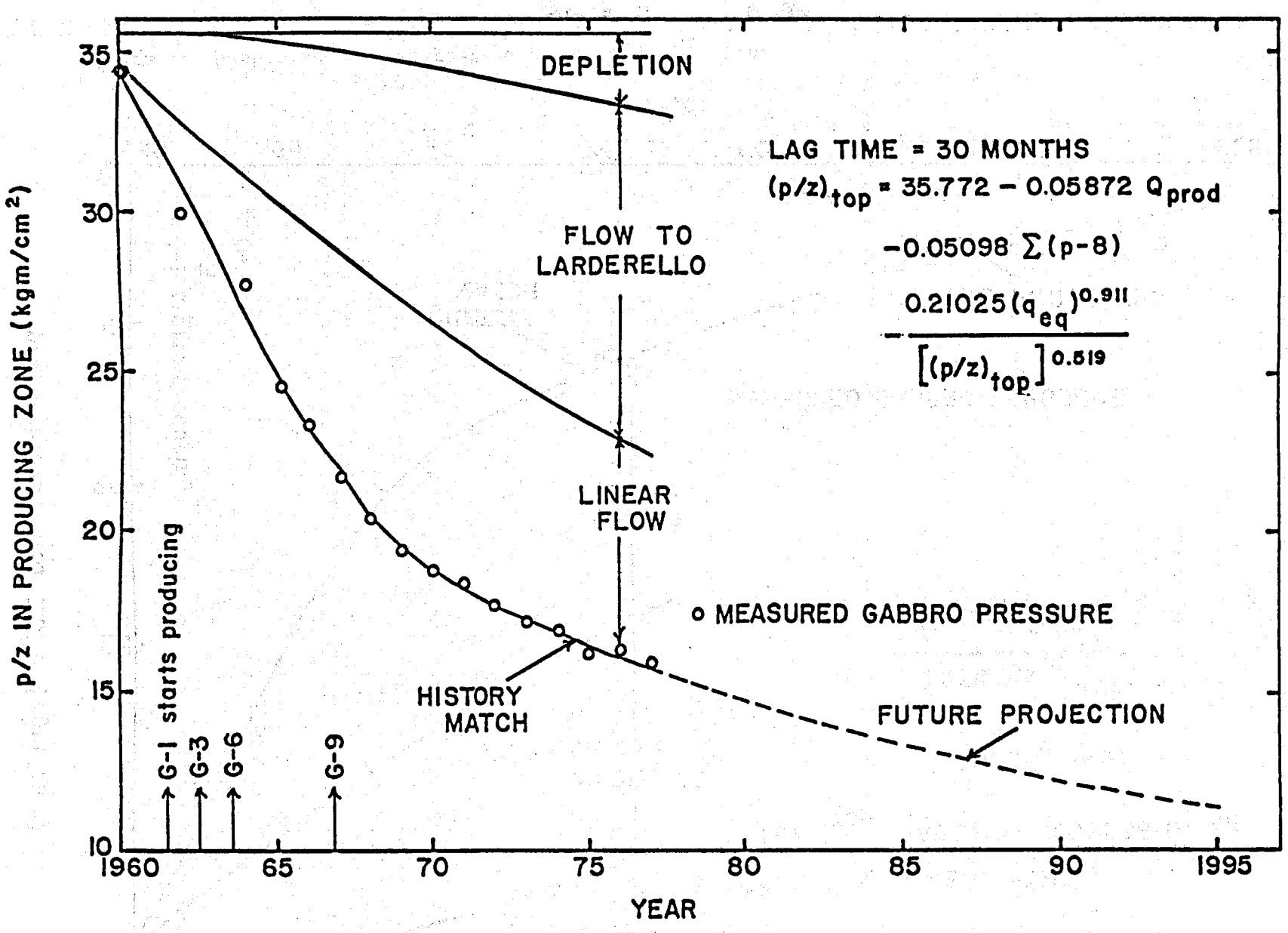

Figure 3. Gabbro zone pressure-production history match.

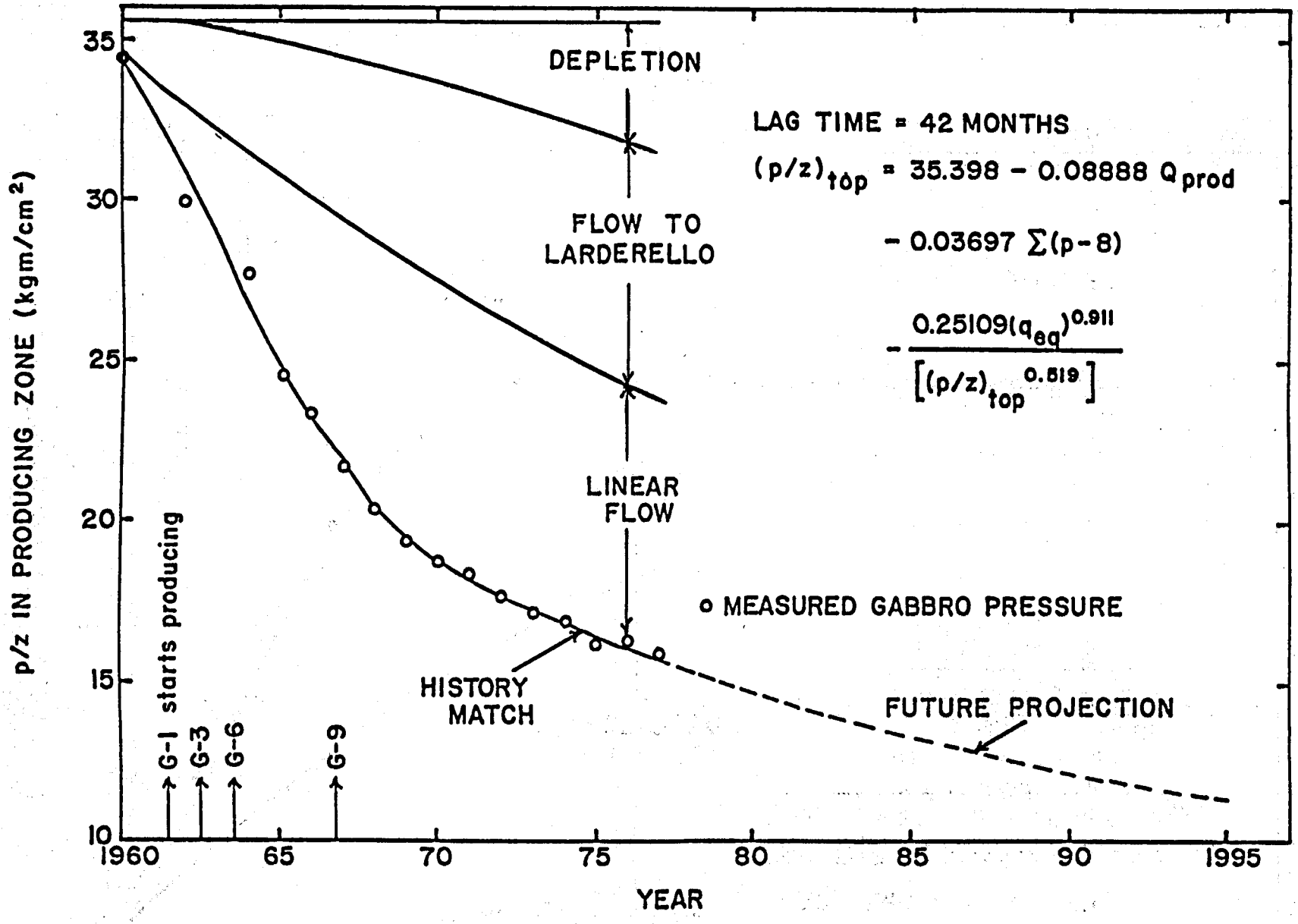

Figure 4. Gabbro zone pressure-production history match.

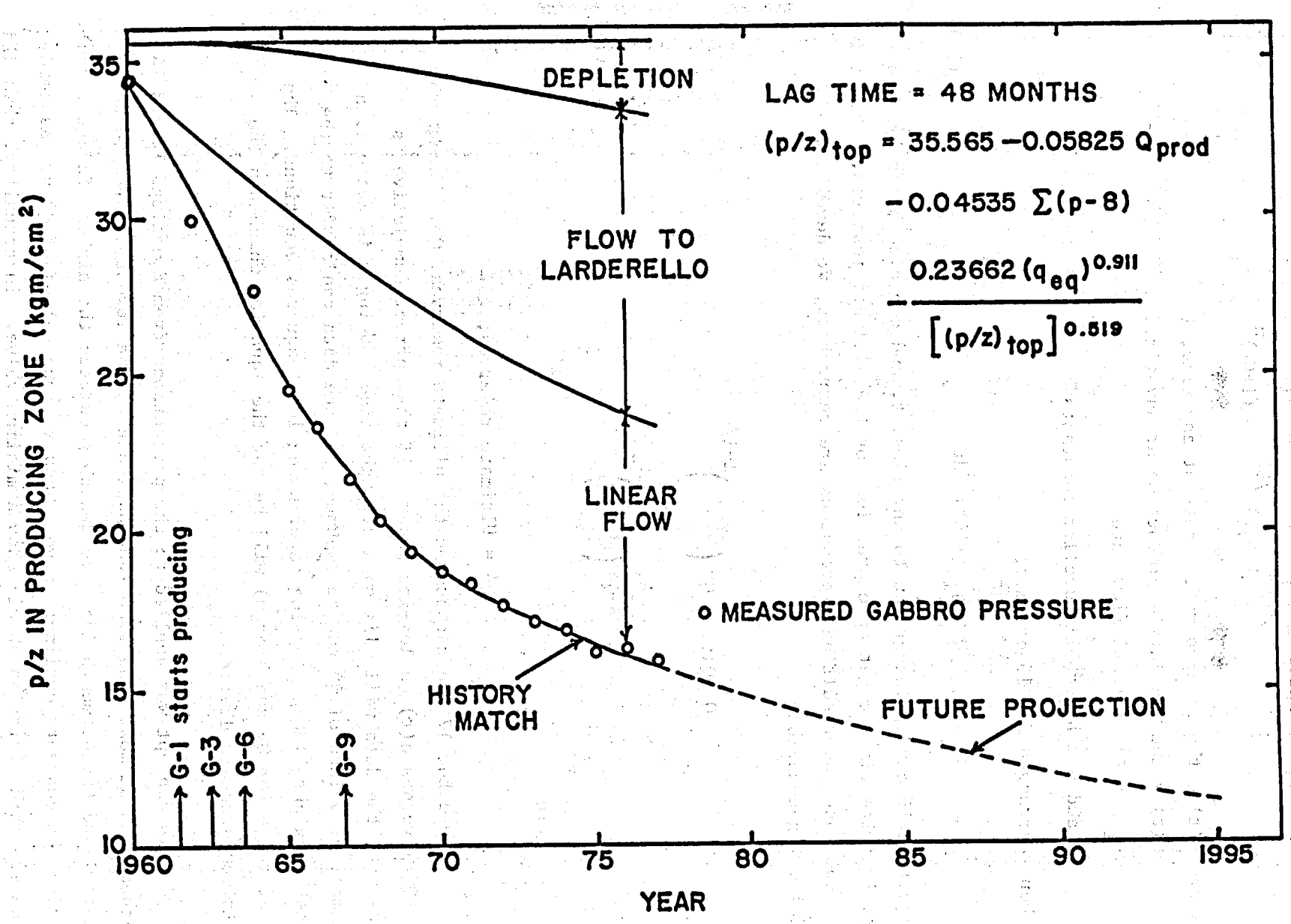

Figure 5. Gabbro zone pressure-production history match.

$$q(t) = \frac{dQ(t)}{dt} = \frac{q_i}{(1+bD_i t)^{1/b}} = \frac{q_i}{(1+Ct)^n} \tag{15}$$

where $q(t)$ = the reservoir flow rate at any time, t

$Q(t)$ = the cumulative production at any time, t

q_i = the initial flow rate

c and n = hyperbolic decline constants

when rearranged Eq. 15 becomes,

$$dQ = q_i\ (1+Ct)^{-n} dt \tag{16}$$

Equation 16 can be integrated to any time, t, and can also be integrated to infinite time to get an expression for the ultimate reserves. When this is done and the resulting expressions are rearranged, we develop the following equation,

$$Q^*-Q(t) = Q^* \left(\frac{q(t)}{q_i}\right)^{1-1/n}$$

$$= Q^* \left(\frac{q(t)}{q_i}\right)^{1-b} \tag{17}$$

where

Q^* = Ultimate reserves, 10^6 Tons

To use Eq. 17 one can assume the ultimate reserves, Q^*, then graph $Q^*-Q(t)$ versus $q(t)$ on log-log paper. If the correct cumulative is assumed, the data will lie on a straight line. Using this concept, a number of values of Q^* can be assumed, and the data can be fit to the best straight line on log-log paper using least-squares equations. The best value for Q^* and b(or n) will be for the equation which has the minimum standard deviation.

This concept was applied to the projections from Equations 12 and 14 assuming a 30 month lag time (which predicted the lowest future producing rates) and the 48 month lag time (which predicted the highest future rates). Using the concepts outlined above, when various values of Q^* are assumed, the standard deviation should show a minimum value. In actuality, this did not occur; the greater the value of Q^* assumed, the smaller was the standard

deviation. When a detailed study was made of the data it became clear that this strange behavior was caused by the scatter in the early producing rate data. Figure 6 shows a graph of the producing rate versus cumulative production data which shows this scatter. It is also clear from this figure that the projections into the future, using Equations 12 and 14, decline quite smoothly.

A compromise technique was developed. Best least-squares fits of the data and projections were calculated using Equation 17, and then the standard deviations were calculated based only on the projections into the future. When this technique was used, a range of minimum error was found, but this minimum was very shallow, thus the answer was not exact. For example, the optimum result using the 30 month lag time equation gave an ultimate reserves value, Q*, ranging from 250 to 300 million tons. The optimum using the 48 month lag time equation gave a value of Q* ranging from 350 to 400 million tons.

Such an inexact result is reasonable when one looks in detail at the future projections of producing rate. All the equations predict a very long producing history with a continuing gradual decline in rate. The exact nature of that decline cannot be forecast accurately. It is interesting that this projected behavior is quite similar to that seen in Larderello, which is in a much later stage of depletion than Gabbro.

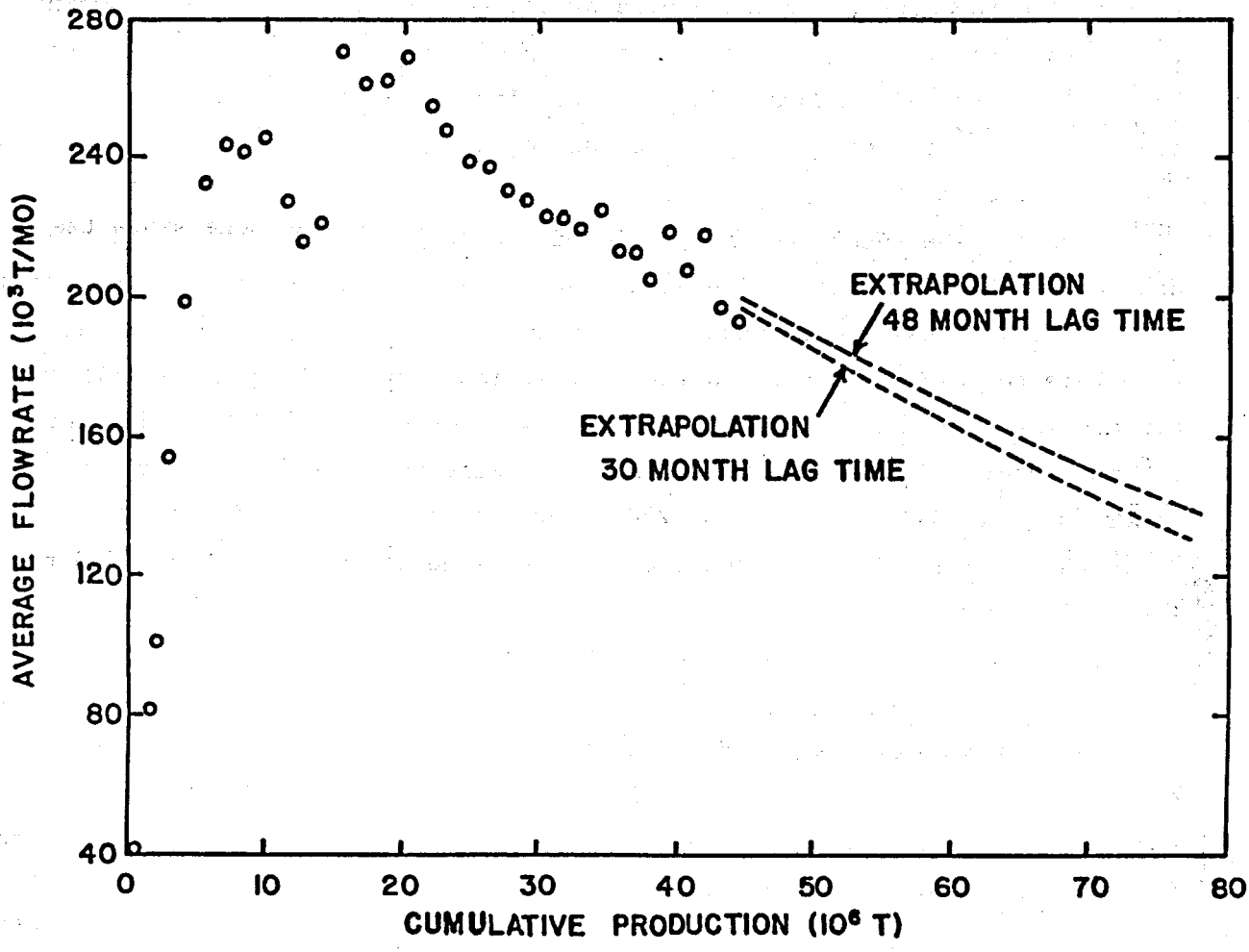

Figure 6. Gabbro zone decline curve.

ANOTHER RESERVOIR MODEL

To be complete in this report we should discuss an attempt to match the data with a slightly different model of the Gabbro system. As formulated in Eq. (12), the model assumes that the depletion from the deep zone due to flow toward Larderello is due to liquid flow (since we are using $\Sigma\Delta p$).

Further, the model assumes the flow is only within the deep zone since the frictional pressure drop term to the shallow zone only includes the actual Gabbro production.

It would be equally logical to assume that the loss to Larderello is steam which first must rise to the shallow zone and then move on the Larderello. If such a model is assumed then the flow to Larderello will be proportional to $\Sigma(p^2-64)$ rather than $\Sigma(p-8)$. In addition we would need a frictional loss term which will include an equivalent Δp^2 term which has been adjusted for the lag time. Such a model can be formulated as follows:

$$(p/Z)_{top} = A - B\,Q_{prod} - C\,\Sigma(p^2-64)$$

$$\frac{-D(q_{eq})^{0.911}}{(p/Z)_{top}^{0.519}} - \frac{E(p^2-64)^{0.911}}{(p/Z)_{top}^{0.519}} \qquad (19)$$

Equation 19 was tested against the data using a lag time of 36 months. As might be expected, due to the additional constant, the resulting equation fit the data very well indeed. However, the resulting constants were completely unrealistic, sometimes giving negative values when they must be positive from physical considerations. Therefore, further work on this model was abandoned.

CONCLUSIONS

The reservoir pressure data in the Gabbro Zone clearly show a pressure trend toward Larderello which has persisted throughout the productive life of this reservoir. During the past ten years the number of producing wells in the Gabbro Zone has remained constant, and during this time both the producing rate and the Gabbro Zone pressure have declined continuously. Thus there is strong evidence that the Gabbro Zone is exhibiting depletion.

A reasonable hypothesis of the Gabbro Zone production dynamics is to assume that deep within the reservoir is a zone of boiling water which is supplying steam to the upper producing interval in which the wells are completed. Depletion of this deep zone can occur due to production from the Gabbro Zone and also due to flow from the Gabbro reservoir toward the main part of the Larderello Field. Further, since the deep zone seems to be connected to the producing zone by a system of relatively tight fractures, an additional transient pressure drop will occur in the producing zone due to frictional losses as the steam flows vertically.

The above concepts have been successfully incorporated into a reservoir model of the Gabbro Zone production history. This is a lumped parameter model which includes transient flow. The boiling water zone depletion is assumed to fit linearly with p/Z. A steady state flow formulation is assumed for the dynamics of flow from Gabbro to Larderello. The transient linear vertical flow is calculated using a lag time concept to change the transient flow terms to an equivalent steady state flow rate. Various lag times were studied and included in this part of the model is a new empirical equation which accurately relates $\Sigma\Delta p^2$ to $\Delta(p/Z)$.

The resulting predictive equation is linear and thus least-squares equations could be used to match the model to the reservoir data. Several combinations of reservoir size, lag time, linear flow pressure drop, and flow rates to Larderello were found to fit the data equally well. Thus, there is a uniqueness problem associated with these fits of the data. Lag times ranging from 30 to 48 months appear to fit the data equally well. The equation for a 24 month lag time predicted a somewhat higher producing rate in 1978 than actually occurred. Lag times less than 24 months and greater than 48 months were also attempted. The resulting equations fit the data quite well; but some of the constants were negative, which is physically unrealistic.

A study of the extrapolations of these various equations into the future showed that the projections to the year 1995 differ by only 6% in that year. Thus, although the reservoir parameters in the equations varied widely, the projected producing rates were quite similar.

Further projections of these flow rates were made using a revised formulation of the standard hyperbolic decline equations. These projections predicted a long producing life with a gradually declining rate. This is similar to the history seen in Larderello. The calculations project an ultimate reserve ranging from 250 to 400 million tons of steam. This rather large range of predictions is caused by the uncertainty of the decline predictions in the next century.

REFERENCES

1. Celati, R., Manetti, G., Marconcini, R. and Neri, G.: "A Reservoir Engineering Study in Gabbro Zone (Northern Part of Larderello Field)" ENEL and CNR Report, 1976.

2. Brigham, W.E. and Morrow, W.B.: "P/Z Behavior for Geothermal Steam Reservoirs", Soc. Pet. Engr. Jour., Vol. 17, No. 6 (Dec. 1977), pp. 407-412.

3. Miller, F.G.: "Theory of Unsteady-State Influx of Water in Linear Reservoirs," Journal Institute of Petroleum (Nov., 1962) 48, 365.

4. Nabor, G.W. and Barham, R.H.: "Linear Aquifer Behavior", Jour. Pet. Tech. (May 1964), Trans. AIME Vol. 231, pp. 561-563.

5. Mannon, L.S. and Atkinson, P.G.: "The Real Gas Pseudo-Pressure for Geothermal Steam-Summary Report," Proceedings 3rd Workshop, Geothermal Reservoir Engineering, SGP TR-25, Stanford, CA, Dec. 14-16, 1977, pp. 29-35.

6. Craft, B.C. and Hawkins, M.F.: "Applied Petroleum Reservoir Engineering", Prentice-Hall Inc. (1959), pp. 240-248.

7. Fetkovich, M.J.: "Decline Curve Analysis Using Type Curves", paper SPE No. 4629, presented at the 48th Fall Mtg. SPE of AIME, Las Vegas, Sept. 30-Oct. 3, 1973.

RESERVOIR ENGINEERING STUDIES OF THE TRAVALE-RADICONDOLI RESERVOIR

A. Barelli, M. Economides, G. Manetti, and F.G. Miller

1. INTRODUCTION

Initial reservoir engineering studies of the Travale-Radicondoli steamfield in the Larderello region of Italy were begun in late 1976, with the ultimate objective of estimating energy reserves. Research centered on pressure transient (well test) studies. Reasonable success was attained in studying mathematical models of the reservoir in an attempt to duplicate the pressure buildup behavior of Travale Well 22 as observed in the field. A well interference test[1] was later designed and implemented, involving Well T-22 as the test well, and seven other nearby observation wells. Results of analysis of the test appeared to be conclusive. They indicated the direction of the main fracture in the reservoir which is penetrated by Well T-22, the steam flow pattern in the reservoir, and that the reservoir can be represented by a parallelepiped model.

Following this study, it was believed that a better concept of the Travale reservoir structure and the flow behavior of its fluids could be developed through analysis of the pressure-production history of Well T-22 over a period of two years and seven months, beginning just after construction of a power plant in 1973.

2. METHODOLOGY

The data available (Fig. 1) consist of a long wellhead pressure history from July 1973 to July 1975. During this period, flowrates, wellhead temperatures, and noncondensable gas composition were recorded once a month. By means of this information, bottomhole pressures were calculated.

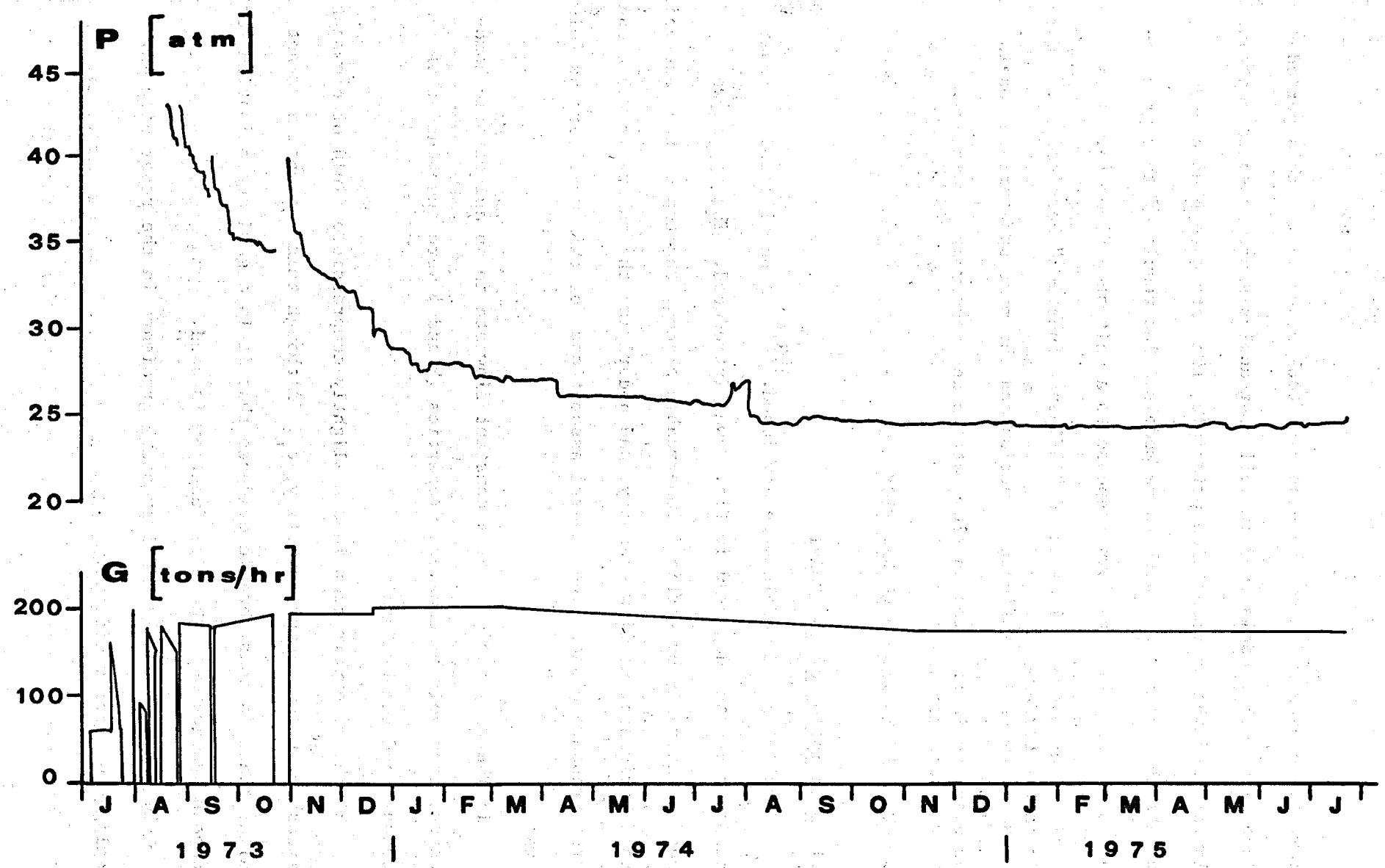

FIG. 1 - Wellhead pressure history

Flowrate changes and many shut-ins also took place during this period. Since almost all models used in well test analysis are based on constant flowrate and the superposition principle, the data have been processed to make them comparable with these models. The result of this processing is the pressure drawdown response to a unit step flowrate. This idealized drawdown will be named "influence function" hereinafter.[6] Comparison between the influence function and the most appropriate models can disclose information on flow pattern and reservoir parameters.

3. PARALLELEPIPED INTERPRETATION

3.1 Description of the Model

Parallelepiped models were developed.[2,3,4] A parallelepiped reservoir such as that depicted in Fig. 2 was introduced. The system was bounded laterally by vertical impermeable planes, the top of the reservoir was a horizontal no-flow boundary, and underlying the reservoir was a constant pressure plane. The general assumptions for this model are as follows:

1) The well produced at a constant flowrate in an anisotropic homogeneous reservoir of constant properties (k and ϕ were independent of pressure and temperature).

2) The reservoir contained a slightly compressible fluid of constant viscosity, μ, and compressibility, c_t. Although this assumption is not valid, there is considerable evidence that it is a good approximation for gaseous systems when the $m(p)$ function is used.

3) There were only small pressure gradients in the reservoir, and negligible gravity effects.

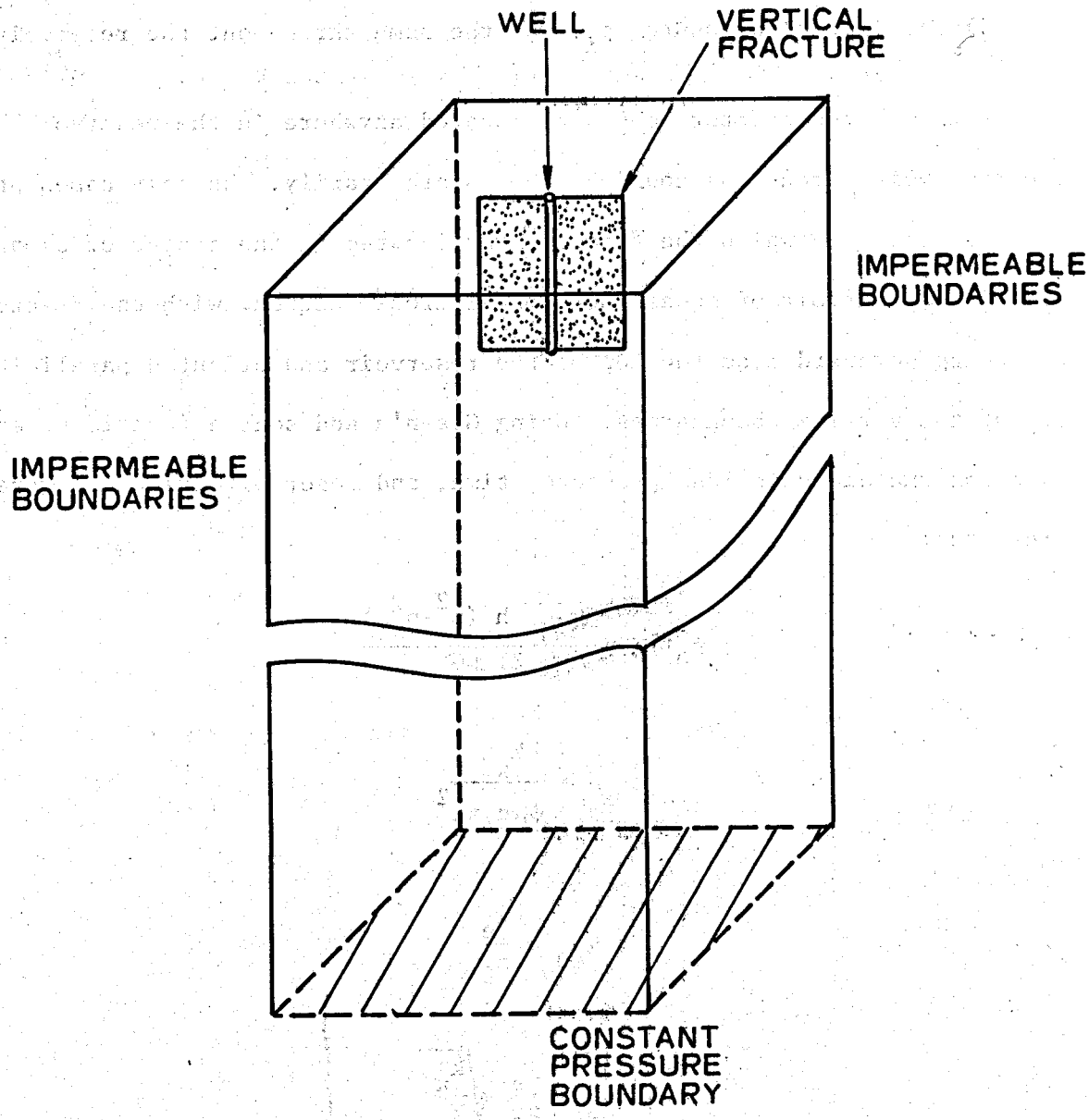

FIG. 2 - Parallelepiped model for a well intersected by a partially penetrating vertical fracture

4) Well fluid production was via a vertical fracture which partially penetrated the reservoir. The top of the fracture could be located at any elevation, and the fracture could extend to any depth.

5) The initial pressure, p_i, was the same throughout the reservoir.

Although the fracture could be located anywhere in the reservoir and the reservoir dimensions could be chosen arbitrarily, the only cases studied were those in which the fracture was located in the center of a parallelepiped reservoir of square horizontal cross-section, with the fracture extending downward from the top of the reservoir and oriented parallel to two of the vertical boundaries. Using Green's and source functions, equations of the dimensionless pressure, time, and reservoir thickness were presented:

$$p_D = \frac{\pi M \sqrt{k_x k_y}\ h\ (p_i^2 - p_{wf}^2)}{R\ ZT\ \mu G} \tag{1}$$

$$t_{Dx_f} = \frac{k_x t}{\phi \mu c_t x_f^2} \tag{2}$$

$$\left.\begin{aligned} x_{eD} &= \frac{x_e}{x_f} \\ y_{eD} &= \frac{y_e}{x_f}\sqrt{\frac{k_x}{k_y}} \\ h_D &= \frac{h}{x_f}\sqrt{\frac{k_x}{k_z}} \end{aligned}\right\} \tag{3}$$

A computer program was written to calculate the pressure drop at any point in the system at any dimensionless time, t_{Dx_f}. Several runs were made by considering different values of dimensionless formation thickness, h_D, fracture penetration ratio, x_e/x_f, and dimensionless fracture height, h_f/x_f. The dimensionless formation thickness varied from 2 to 20, the fracture penetration from 2 to 10, and the dimensionless fracture height was assumed to be unity.

All cases exhibited a unique one-half slope straight line for small values of time. This behavior was caused by the linear flow behavior in the vicinity of the fracture. At large values of time, the wellbore pressure drop stabilized, indicating steady-state flow in the system. Figures 2 and 3 show that over a large region of the graph, the curves for pressure response at a fractured well in a parallelepiped reservoir were similar in slope to the infinite conductivity vertical fracture solution for an infinite reservoir.

3.2 Data Manipulation and Type-Curve Matching

The first major task was to manipulate the physical data. First, since there were no accurate pressure data during the initial 47 days, a widely practiced method of averaging was used. All cumulative production prior to the 47th day was added and then divided by the last flowrate (150 tons/hour). Thus a "pseudo" time of roughly 16 days was obtained. This has theoretical basis in superposition in time, as can be found in Horner and other sources. Therefore, "day zero" in the long drawdown data is day 16. The second "data manipulation" concerned the three shutdowns that appear on the data. Since no pressure data were collected during the shutdown, they were "hand smoothed." A simple influence function,

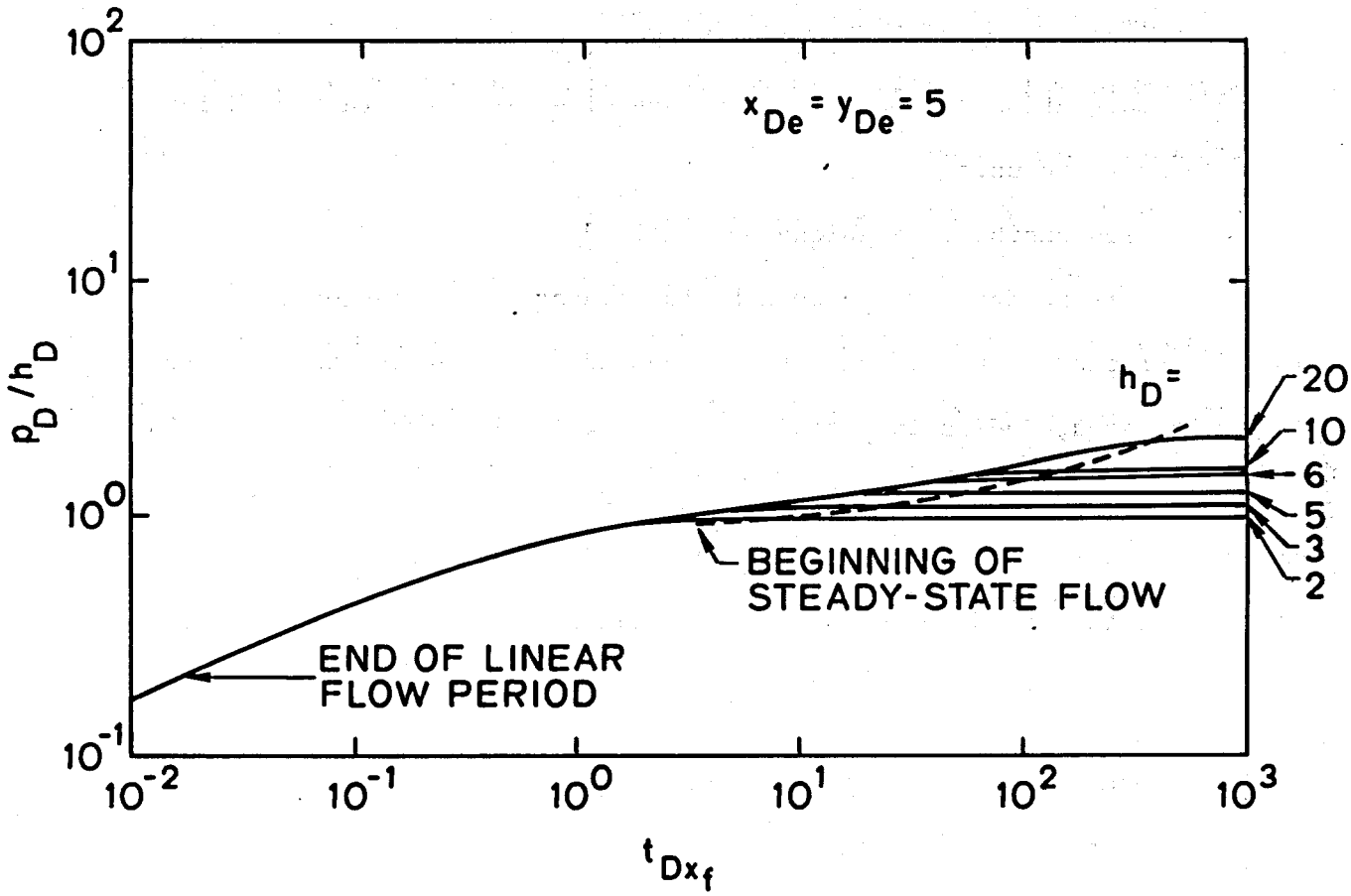

FIG. 3 - Log p_D/h_D vs log t_{Dx_f} for a fractured well in a parallelepiped reservoir (x_e/x_f=5).

$\Delta p^2/q$, was used. The graph appears on Fig. 4. A Cartesian graph was used to show the influence function (bottomhole pressures were used throughout the calculations).

The next task was to graph the influence function on log-log paper, matched on a type-curve prepared for a "parallelepiped reservoir" penetrated by a vertical fracture (Fig. 5). Several interim calculations were done in order to facilitate the type-curve matching. If the parallelepiped assumptions are to be accepted, then the flattening of the pressure curve that appears on Fig. 5 should be interpreted as the result of boiling subformation water. This breakpoint appears to be about day 475. The type-curve matching resulted in the following set of points:

$$x_{eD} = x_e/x_f = 5$$

$$\Delta p^2/q = 10$$

$$p_D/h_D = 0.94$$

$$t = 100 \text{ days}$$

$$t_{Dx_f} = 8$$

$$h_D = 9$$

$$y_{eD} = 5$$

From $x_{eD} = 5$, $y_{eD} = 5$, and their definition, we obtain:

$$k_x = k_y$$

Since the reservoir lateral extent is known (1 km in each direction), then:

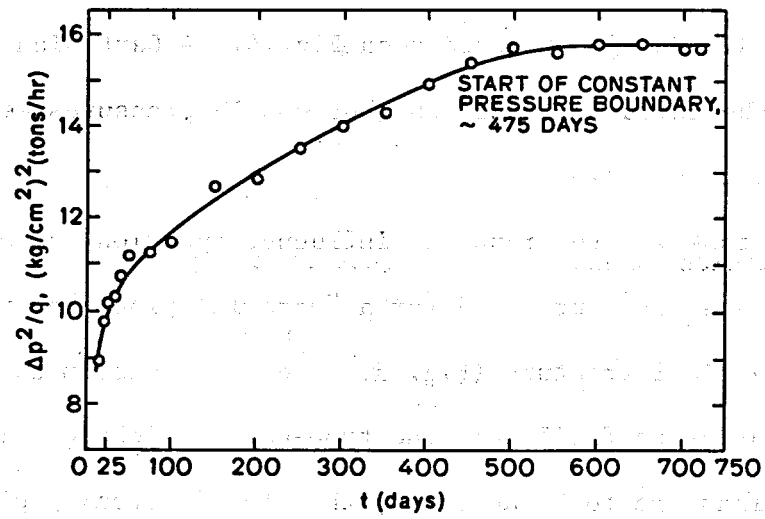

FIG. 4 - Cartesian graph of drawdown of T-22.

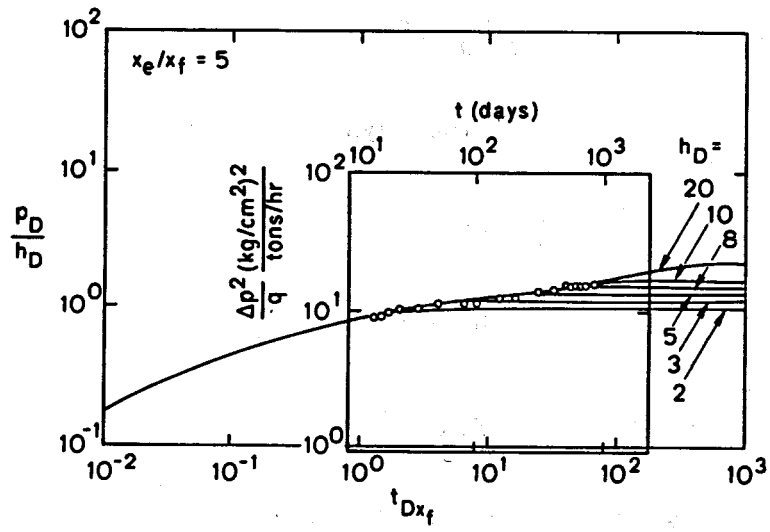

FIG. 5 - Type-curve matching of T-22 drawdown data. Type-curve for a parallelepiped reservoir with a vertical fracture.

$$x_e = 500 \text{ m}$$

$$x_f = 100 \text{ m}$$

From the definition of the dimensionless pressure:

$$\frac{p_D}{h_D} = \frac{\pi M\sqrt{k_z k_y}\, x_f}{RzT\mu} \; \frac{(p_i^2 - p_{wf}^2)}{G}$$

and substituting the known variables:

$$(k_z k_y)^{1/2} = 3.34\text{x}10^{-2} \text{ darcy} \tag{4}$$

From the definition of dimensionless time:

$$t_{Dx_f} = \frac{k_x t}{\phi \mu c_t x_f^2}$$

and substituting the known variables:

$$\frac{k_y}{\phi} = \frac{k_x}{\phi} = 7\text{x}10^{-2} \text{ darcy} \tag{5}$$

Combining Eqs. 4 and 5 and remembering that $k_x = k_y$, we obtain two equations:

$$\frac{k_x^2 k_z}{\phi} = 7.8\text{x}10^{-5} \text{ darcy}^3 \tag{6-a}$$

$$\sqrt{\frac{k_z}{k_x}} \cdot \phi = 0.47 \tag{6-b}$$

Combining Eqs. 5 and 6-b, then:

$$\phi k_z = 1.5\text{x}10^{-2} \text{ darcy}$$

Introducing the definitions of h_D in Eq. 6-b:

$$\frac{h}{h_D} \phi = 47.7 \text{ m}$$

and hence:

$$h\phi = 430 \text{ m}$$

The pore volume is then:

$$V\phi = 4\ y_e x_e\ h\phi \simeq 4\text{x}10^8 \text{ m}^3$$

Another interpretation using the same match can be made by following Grant's approach[8] which considers the thermodynamics related to phase changes. He shows that for small pressure changes, the diffusion equation is still valid in the two-phase zone if ϕc_t is replaced by an "effective compressibility," the value of which is on the order of 0.06 atm^{-1} in this case.

Calculations have been repeated starting from Eq. 4 downwards. The main results are:

$$k_x = k_y \simeq 10^{-1} \text{ darcy}$$

$$k_z \simeq 10^{-2} \text{ darcy}$$

$$h \simeq 0.3 \text{ km}$$

$$V = 0.3 \text{ km}^3$$

4. AN ALTERNATE APPROACH

4.1 Bottomhole Pressure Calculations

Bottomhole pressure history was calculated by Rumi's method.[7] Adiabatic flow of pure steam was considered.

4.2 Influence Function: Calculations and Results

Using the calculated bottomhole pressure history, the drawdown due to a unit step flowrate (influence function) was calculated according to ref. 5, assuming only that the superposition in time is valid.

The influence function was calculated in terms of $(p_i^2-p_{wf}^2)/G$. Squared p's were used because steam is considered to be a perfect gas (Figs. 6 and 7). The drawdown pressure history match based on Δp^2 is shown on Fig. 8. The calculated influence function is graphed on log-log paper on Fig. 6. A certain scatter is evident, probably due to uncertainties in the data (especially in the first period). Nonlinear phenomena in the reservoir may also invalidate the superposition principle.

Type-curve matching has been attempted with models considering fractured reservoirs. Satisfactory matches were obtained, but reservoir parameters such as fracture height, fracture length, and reservoir volume are in contrast with the size of the known reservoir, probably because the models do not consider phase changes.

Since the interference test conducted in April 1977 revealed the presence of linear flow in the reservoir, the influence function was graphed vs the square root of time (Fig. 7) to identify a possible linear flow regime. The main portion of the data (from 45 days to 2.5 years) seems to lie on a straight line, suggesting linear flow.

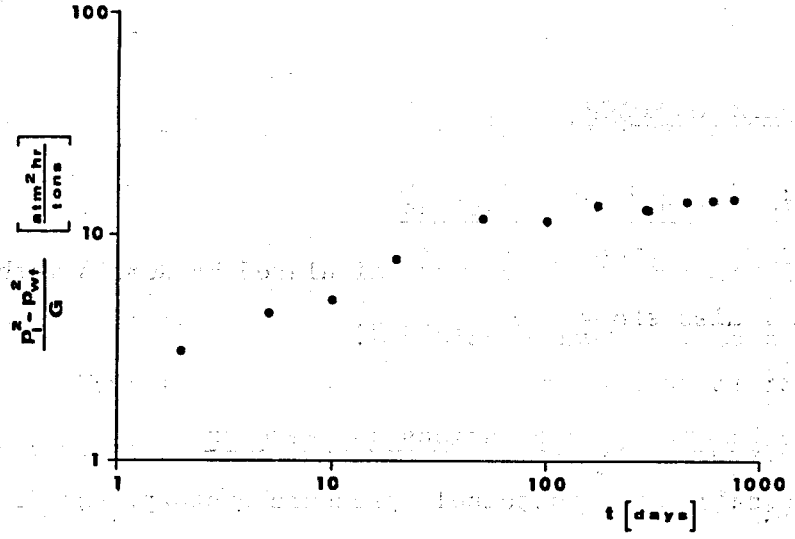

FIG. 6 - T-22 influence function.

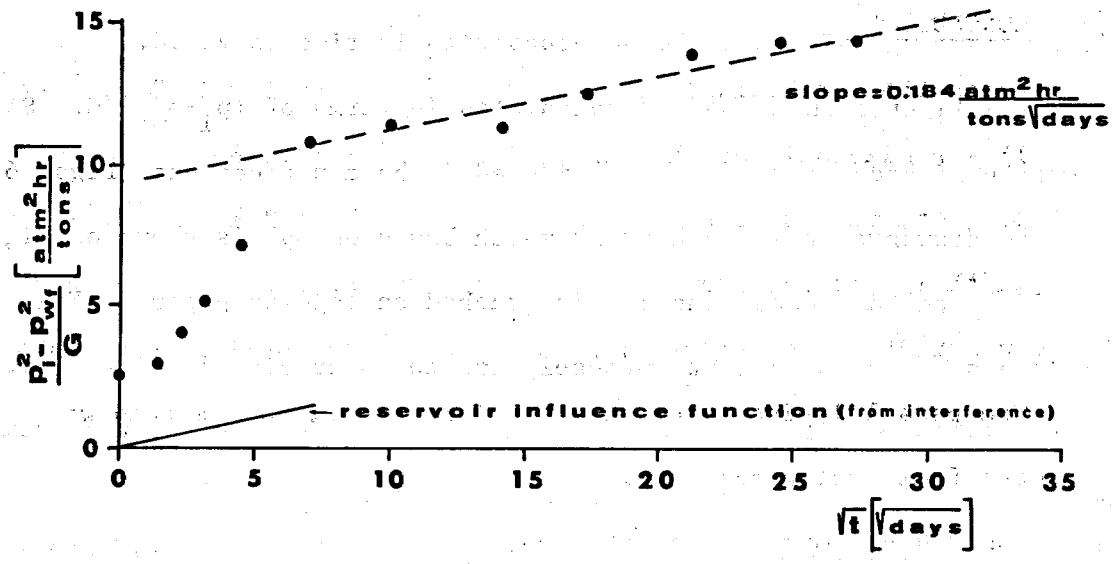

FIG. 7 - Drawdown T-22--influence function.

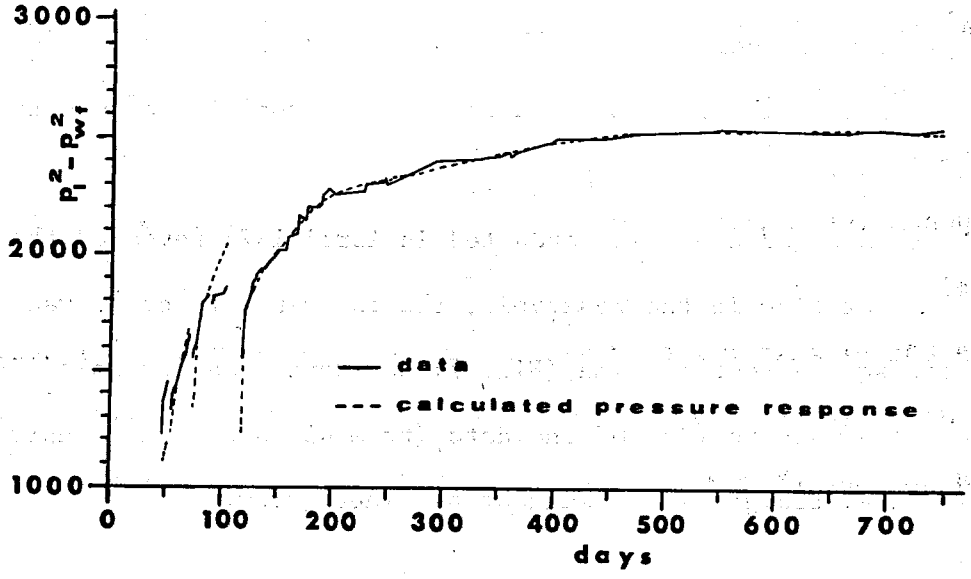

FIG. 8 - Drawdown pressure history match.

The slope of this straight line is (0.184 atm^2) / ($t/h/\sqrt{day}$). We do not know why this line does not intersect the origin, since in linear flow, pressure drops are proportional to the square root of time.

Figure 7 also shows the result of the interference test. The two slopes appear to be the same despite the fact that different ranges of time were investigated. The earlier data are difficult to understand, but are unreliable since the flow pressure history of the first 45 days is unknown.

5. CONCLUSIONS

Using the parallelepiped model, two major benefits can be extracted:

1) - a diagnosis of the shape of the reservoir and

2) - the values of the directional permeabilities.

In this case unfortunately the data scatter prevents a unique match and consequently the reservoir parameters are not well determinable.

The parallelepiped model gives a larger pore volume than would be expected from geological knowledge; this observation leads to the hypothesis of phase changes with strong thermodynamic implications, as suggested by Grant.[8]

An alternate approach to the problem was also made and an "influence function" generated postulating only that the principle of superposition in time is valid. This influence function permits calculation of the pressure response for a given flow rate history independently of the type of model used.

Both the parallelepiped model and the alternate approach reveal the presence of a linear flow pattern as indicated by the interference test and buildups, but they differ from each other at later times.

NOMENCLATURE

c_t = isothermal compressibility

G = mass flowrate

h = pay thickness

h_f = fracture height

k = permeability

m(p) = real gas potential

M = molecular weight

p = pressure

p_i = initial pressure

p_{wf} = flowing pressure

p_{ws} = shut-in pressure

R = universal gas constant

T = absolute temperature

t = flowing time

x_f = half-fracture length

x_e = boundary location

y_e = boundary location

V = reservoir bulk volume

z = gas deviation factor

μ = viscosity

ϕ = porosity

Subscript

D = dimensionless

REFERENCES

1. Atkinson, P., Barelli, A., Brigham, W.E., Celati, R., Manetti, G., Miller, F.G., Neri, G., and Ramey, H.J., Jr.: "Well Testing in Travale-Radicondoli Field," Proc., ENEL-ERDA Workshop, Larderello, Italy, Sept. 12-16, 1977; Geothermics (1978), 7, No. 204, 145-184.

2. Cinco-Ley, H., Brigham, W.E., Economides, M.J., Miller, F.G., Ramey, H.J., Jr., Barelli, A., and Manetti, G.: "A Parallelepiped Model to Analyze the Pressure Behavior of Geothermal Steam Wells Penetrating Vertical Fractures," Paper SPE 8231, presented at the 54th Annual Fall Meeting, SPE of AIME, Las Vegas, Nevada, Sept. 23-26, 1979.

3. Barelli, A., Celati, R., Manetti, G., and Neri, G.: "Progress Report on a Mathematical Model of a Parallelepiped Reservoir with No Penetrating Wellbore and Mixed Boundary Conditions," presented at the Workshop on Geothermal Reservoir Engineering, Stanford, California, Dec. 1975.

4. Economides, M.J., Ogbe, D., Miller, F.G., Cinco-Ley, H., and Fehlberg, E.L.: "Pressure Buildup Analysis of Geothermal Steam Wells Using a Parallelepiped Model," Paper SPE 8886, presented at the 50th Annual California Regional Meeting, SPE of AIME, Los Angeles, Apr. 9-11, 1980.

5. Barelli, A., and Palama, A.: "On Some Computation Methods of Unit Response Functions from Varying Rate Data," Geothermics (1980), 9.

6. Economides, M.J., Brigham, W.E., Cinco-Ley, H., Miller, F.G., Ramey, H.J., Jr., Barelli, A., and Manetti, G.: "Influence Functions and Their Application to Geothermal Well Testing," Geothermal Resources Council (1979), III, 177.

7. Rumi, O.: "Some Considerations on the Flowrate-Pressure Curve of the Steam Wells of Larderello," Geothermics (1973), 2, Nos. 3-4, 154-173.

8. Grant, M.A.: "Water Content of the Kawah Kamojang Geothermal Reservoir," Geothermics (1979), 8, 21-30.

ACKNOWLEDGMENTS

This work was carried out as a part of Project 3 of the DOE-ENEL Agreement on Cooperative Research and Development in Geothermal Energy. The authors thank their sponsoring agencies for the opportunity to participate in this binational cooperative effort.

STUDY OF WATER INFLUX AND FLUID COMPOSITION IN THE BAGNORE FIELD

(Progress report and plan of future action for Task 3/15)

Romano Celati, Franco D'Amore, Michael J. Economides,
and Giuseppe Neri

Abstract

The purpose of Project 3/15 is to study water influx and variations of fluid composition in the Bagnore field. As this field contains large amounts of noncondensable gases it is an ideal candidate for studying the relationship of these gases with the flow performance of geothermal wells. An additional asset is that a posteriori models can be deduced because the field is depleted. The ultimate goal, of course, is to extract technology applicable to other reservoirs at an early stage in their development.

Introduction

Short-term as well as long-term models are to be considered.

1. Pressure transient analyses can be utilized to estimate reservoir variables such as permeability, porosity, and extent of drainage areas. Thermal effects are usually ignored in such analyses if isothermal operation is assumed, but this can affect the reliability of estimates. Other factors complicating geothermal rock formations are boiling interfaces, fractures in otherwise impermeable matrices, and nonhomogeneities. For the Bagnore field, large quantities of noncondensable gases also complicate analyses.

   From preliminary work it appears that pressure analyses can be facilitated by use of the "real gas pseudopressure," m(p), defined by:

$$m(p) = \int_{p_o}^{p} \frac{p}{\mu Z}\, dp$$

   in which p is the pressure of interest, p_o a base pressure, μ absolute viscosity, and Z the gas deviation factor. A calculation of the real gas pseudopressure or potential for the Bagnore field is now under way. Additionally, a more general form of this function is currently being

generated for various noncondensable gas compositions. However, one must consider also that classic techniques of pressure transient analysis presume single-phase fluid reservoirs.

An approximation of what is believed to be a typical geothermal-reservoir configuration is the recently published "parallelepiped model." Even this configuration with its assumption of vapor- and liquid-dominated zones, may yield only gross-approximation results. Laboratory research just completed at Stanford University indicates that significant amounts of fluid can be adsorbed on the surfaces of geothermal rocks. Boiling off of this adsorbed fluid can account for as much as ten times the amount of steam that would otherwise be present in the pore space.

A solution of applicable partial differential equations using the adsorbed water mathematically as a source function is planned for early attention.

2. A more sophisticated approach to the Bagnore reservoir study and for an extension to other geothermal reservoirs, is to use M. O'Sullivan's two-phase model, recently discussed in the Society of Petroleum Engineers Journal.

   The O'Sullivan model has already been modified in the present research to include the effect of carbon dioxide. This modification can be extended easily to include other gases, methane for example. The model consists of a numerical simulator which is designed to interpret the long-term behavior of the Bagnore field. This simulator includes both dynamic and thermal effects; with the introduction of the gas factor, Z, it can also account for thermodynamic vapor-liquid equilibria. Further, the recent Stanford findings on water adsorption can easily be incorporated. An effort toward this goal is now under way.

3. While pressure transient analysis may provide values for reservoir parameters such as permeability, porosity, and length and height of fractures, it fails to yield estimates of the liquid reserves of geothermal reservoirs. Whether fluid is adsorbed or whether it exists as "subformation brine" it is often the major source for steam production at the surface.

   A guide method utilizing a "black box" Rayleigh distillation also has been developed in the present work. The distribution coefficients necessary for the distillation calculation can be both functions of pressure and

temperature. The method can give an approximation of the liquid reserves provided that no water influx or generation of CO_2 is evident.

4. An all encompassing verification of the above methods can be represented by the results of a geochemical study currently under development. A conceptual model able to explain initial distribution of CO_2, CH_4 and possibly H_3BO_3 and NH_3, utilizing equilibrium calculations, will be investigated.

   Temperature of the depleting reservoir can be calculated using appropriate H_2 and H_2S geothermometers currently under development.

   The geochemical study could confirm the decreasing height of the vapor-dominated zone, the lowering of temperature by water-table influx, and possibly could reveal coning phenomena as well as determine whether appreciable amounts of carbon dioxide are entering the brine either by lateral influx or by generation in place. Answers to these questions will aid evaluation of the other models mentioned earlier in this report.

Future work

The continuation of Task 3/15 will be accomplished partly in Italy and partly at Stanford.

In Italy the model developed under Task 3/15 will be further improved and applied to the Bagnore field.

Gas behavior will be investigated applying the already modified model of O'Sullivan.

At Stanford the major effort will be devoted to developing simple techniques for analyzing pressure transients, taking into account the real gas potential for the Bagnore field, while long-term gas behavior will be studied by means of the Rayleigh distillation calculation.

Acknowledgments

This work was carried out as a part of Project 3 of the DOE-ENEL Agreement on Cooperative Research and Development in Geothermal Energy. The authors thank their sponsoring agencies for the opportunity to participate in this binational cooperative effort.

HELIUM PROSPECTING IN GEOTHERMAL AREAS

Preliminary Data on Larderello-Travale and Cesano Geothermal Fields

R. Bertrami[1], A. Ceccarelli[1], I. Friedman[2], W. Doering[2], and S. Lombardi[3]

Introduction

One of the objectives in geochemical prospecting for geothermal research is that of individuating, in the surface manifestations, indicators of buried geothermal reservoirs. Many chemical species present in gases, natural waters and soils have been proposed for this purpose (e.g., F. Tonani, 1970; A. Koga and T. Noda, 1975; H.R. Bowman et al., 1975; J.S. Matlick, III and P.R. Buseck, 1975).

Recently the helium present in the soil's gas was also proposed as an indicator in geothermal prospecting (A.A. Roberts et al., 1975; I. Friedman et al., 1976). This method has the advantages of being extremely simple and applicable even in areas with no natural manifestations. It has, however, never been experimented with on wide scale in known geothermal fields.

As part of a study which includes helium prospecting of a wide region of the pre-Appennine belt of Italy, this paper presents and discusses the data obtained in the geothermal fields of Larderello-Travale and Cesano.

Brief Geological Outline

- Larderello - Travale

Many papers describe in detail the geological and tectonic features of Tuscany's geothermal fields (e.g., R. Mazzanti, 1966; A. Lazzarotto, 1967;

---

1. ENEL-UNG, Pisa, Italy
2. USGS - Federal Center, Denver, CO USA
3. Istituto di Geologia, Università di Roma, Rome, Italy

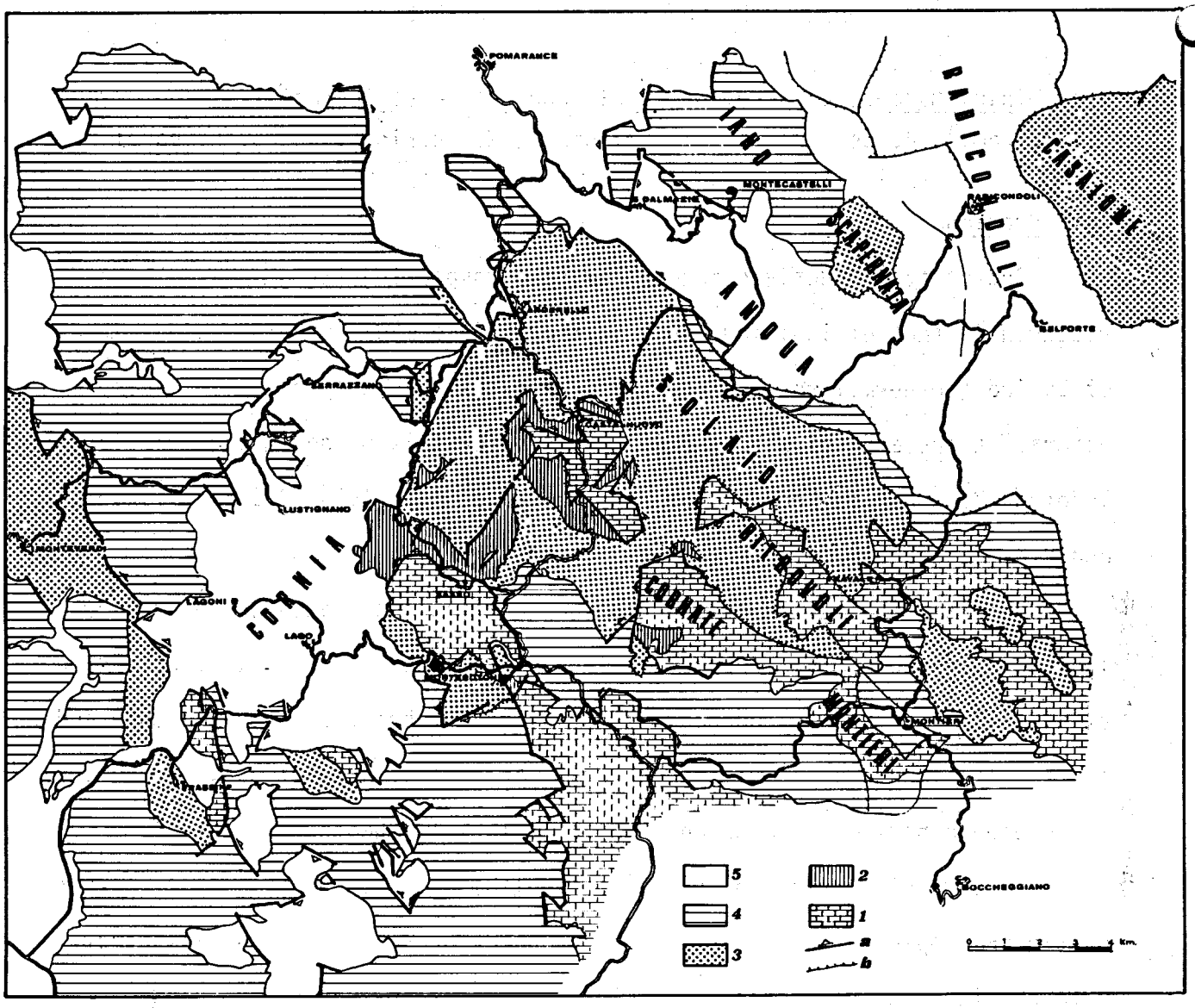

Fig. 1 - Geological-structural sketch of the Larderello-Travale region (from G.P. Brandi et al., 1968; A. Lazzarotto and R. Mazzanti 1976; redrawn).

1: Tuscanides: basal terrigenous complex, carbonate complex, upper terrigenous complex (Upper Triassic-Oligocene).

2: Ligurides: shale and limestone complex (Eocene).

3: Ligurides: marly limestone complex (Cretaceous-Upper Paleocene).

4: Ligurides: ophyolitiferous complex (Lower Cretaceous).

5: Lacustrine and marine sediments (Upper Miocene-Pliocene).

a: Faults, with triangle in the dipped side.

b: Overthrusts.

R. Cataldi et al., 1963; R. Celati, et al., 1978).

The geological history can be summarized as follows (Fig. 1):

- the oldest formations belong to a metamorphic Paleozoic basement, made up by phyllites and quartzites with intercalations of dolomites, marbles and anhydrites.

- A complex series of nappes lying on the basement were implaced during the last phases of alpine orogeny (Upper - Middle Miocene). From the bottom to the top it can be distinguished as: a) "Tuscanides" (Upper Triassic-Oligocene) constituted by a sequence of basal terrigenous complex, a carbonate complex and an upper terrigenous complex. The Tuscanides and the upper part of the basement represent the geothermal reservoir; b) "Ligurides" (Upper Jurassic - Eocene) which include three main flysch-facies units thrust one over the other, from bottom upwards: shale and limestone complex (Eocene), marly limestone complex (Cretaceous - Upper Paleocene), ophyolitiferous complex (Lower Cretaceous).

- Lacustrine and marine formations overlie the whole series with unconformity (Upper Miocene - Pliocene). These formations and the "Ligurides" are assumed to represent the impermeable cover of the geothermal reservoir.

-<u>Cesano</u>

The Cesano geothermal field, described by many papers (e.g., E. Locardi et al., 1975; P. Baldi et al., 1976a; P. Baldi et al., 1976b; R. Funiciello et al., 1976; R. Funiciello et al., 1979), is located about 20 km north of Rome, in the Sabatini Mts.

It corresponds to a minor structural high, bordered by normal faults, inside a large graben that developed beginning in the Upper Miocene on the pre-Appenine belt.

Phreatomagmatic activity occurred between approximately 200,000 and 100,000 years ago, corresponding to the youngest volcanic activity of the Sabatini Mts. The Sabatini activity (mainly fissured-type) started around 500,000 years ago. The first products were acidic trachytic pyroclastic flows followed by markedly alkaline lavas and pyroclastics. The thickness of pyroclastic products may reach 1000 meters.

The sedimentary deposits beneath the volcanic cover are described below (see Fig. 2):

- a) discontinuous post-orogenic sedimentary activity, including lithotypes ranging in age from Lower Pleistocene to Upper Miocene, mainly clay, occasionally silty, with conglomeratic horizons.

- b) Flysch-facies complex, 200-900 meter thick: numerous lithotypes are represented (shaly argillites, marls, sandstones and limestones), the age of which range from Middle Cretaceous to Lower Miocene.

- c) Carbonate basal sequence including marls, marly limestones, and limestones, ranging in age between Oligocene and Upper Trias. The Upper Trias is present both as dolomitic limestone and as calcareous-anhydritic formations.

Experimental Work

The survey consisted of a grid sampling in the Larderello-Travale and Cesano fields, with a density of one sample per square kilometer. The work took place in July, August and September 1980, when climatic conditions were quite uniform with little precipitation.

A total of more than 1000 samples were collected, out of which 800 in Larderello-Travale and 280 in Cesano. In the latter area, some profiles were made with a sampling density roughly of 3 points per square kilometer.

Three samples were taken at each sampling point by inserting a metallic

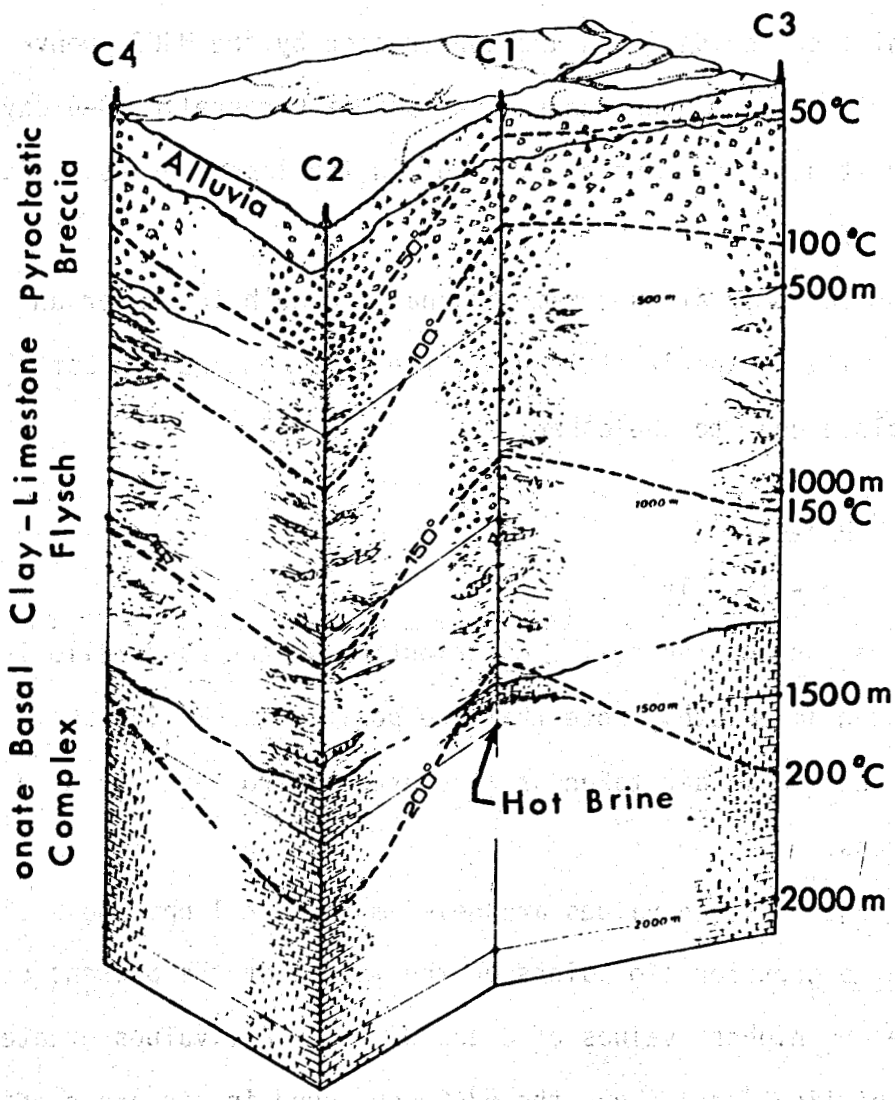

Fig. 2 - Block diagram showing the relationship between volcanic cover and sedimentary cycle on Cesano geothermal field (from P. Baldi et al., 1976b).

probe in the ground, according to the technique used by the USGS laboratories at Denver (G.M. Reimer and G.C. Bowle, 1975). The samples were collected in evacuated glass containers (VACUTAINER®, VENOJECT®), fitted with rubber caps.

The measurements were made using a Dupont 120 SSA-leak detector, fitted with an inlet device designed and constructed by the USGS, Denver, (G.M. Reimer, 1976). Part of the measurements were made at Larderello, 3-4 days after sampling, although most of these were carried out in the laboratories at Denver about 15-20 days after.

The results of aliquot samples analysed both in Denver and Larderello show that, within experimental error, the data obtained in both laboratories are very close one to the other.

Results and Discussion

Larderello - Travale

Figure 3 shows the helium distribution in the Larderello-Travale area.

One can immediately note that the positive anomalies above the concentration of helium in air taken as a reference zero, are found in rather well-defined areas.

The concentration values are never more than 1 ppm above that in the atmosphere, except for two points on the margin of the present study area which have the highest values of 8 and 33 ppm. All values greater than 50 parts per billion (ppb) above the 5240 ppb found in air are considered anomalous.

The main characteristics of this distribution are:

1. Practically no anomalous helium concentrations were found in a wide zone in the north (Micciano-Pomarance).
2. Some anomalous concentrations were recorded near the productive

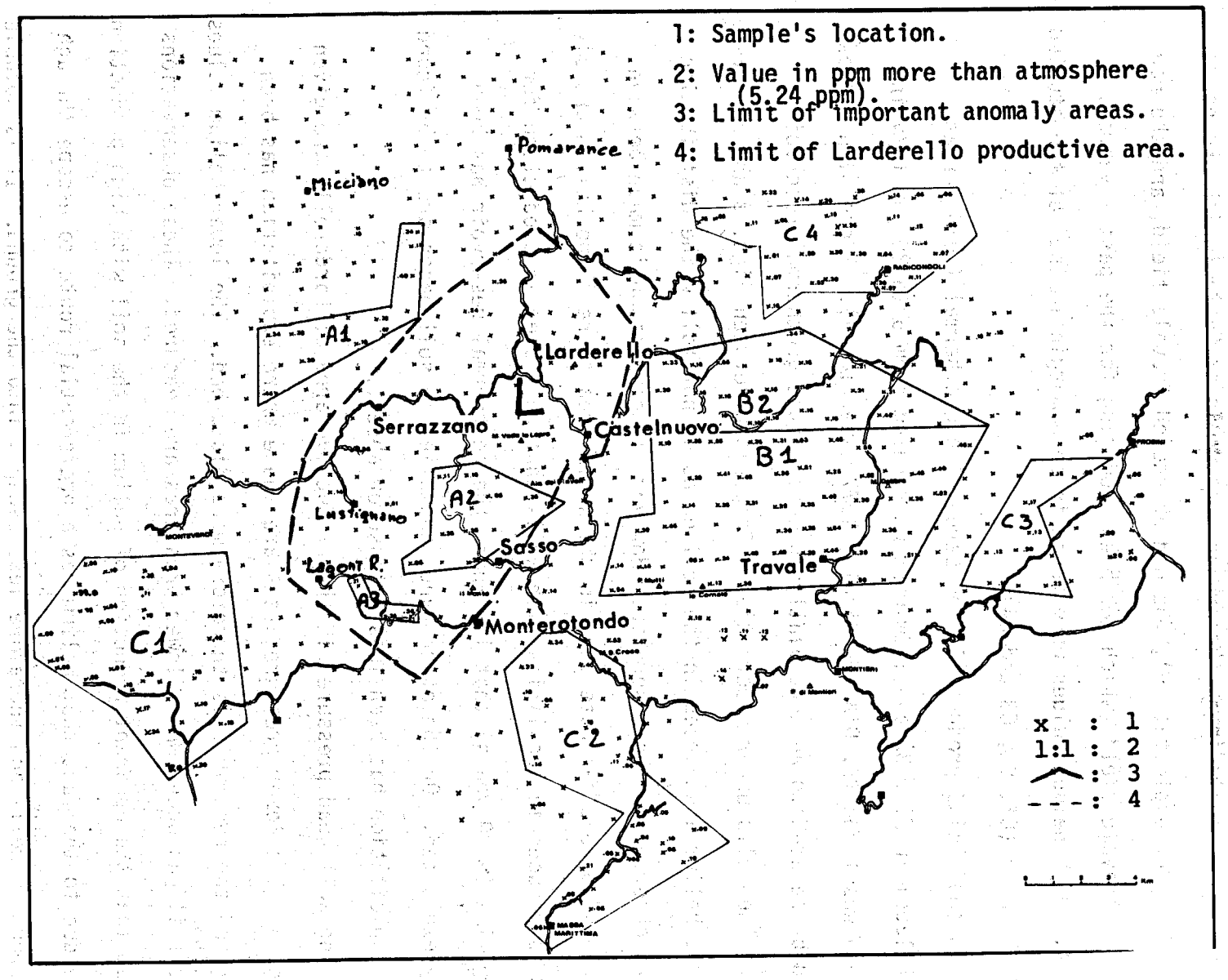

Fig. 3 - Distribution of the helium in the soil gases in the Larderello-Travale geothermal field.

fields in the Larderello zone (A1, A2 and A3 in Fig. 3).

3. An anomaly zone extends between Larderello and Travale (B1 and B2), including: the area of gas wells at Sesta (which are not under exploitation), the old abandoned Travale field, and the new Travale field (which has been producing for the past 7 years).
4. High helium values were found in some marginal zones of the studied area (C1, C2, C3 and C4).

In the fluids produced in the Larderello geothermal field (areas with L label in Fig. 3) a helium content ranging from 5 to 20 ppm (v/v in the gas) was found (F. D'Amore et al., 1977; see Fig. 4). These high values should be related to an accumulation process in the geothermal reservoir feeding the wells under observation. Comparison between Figs. 3 and 4 shows that the helium abundances in the soil gases do not follow the distribution pattern observed in the reservoir. However, if comparison is made between Figs. 3 and 5, one can note that in the whole area there is no helium anomaly or it is reduced in localities with wells that have been in production for a long time ($\gtrsim$ 30 years) that is, where the geothermal reservoir has been highly exploited. On the other hand, anomalies in soil gases are to be found where exploitation has been less intense or absent.

The well head pressures in the productive area of Larderello are given in Fig. 6. The lower pressure areas are those where exploitation has been higher and the reservoir is therefore more disturbed. The lower helium values in the soil gas occur where lower pressures are measured. These observations suggest that the apparent reduction of helium in the soil with high production may be due to the fact that helium has a preferential route to escape through the producing wells and therefore less escapes into the ground. It is notable that many of the surface manifestations have disappeared in the Larderello area with the onset of exploitation.

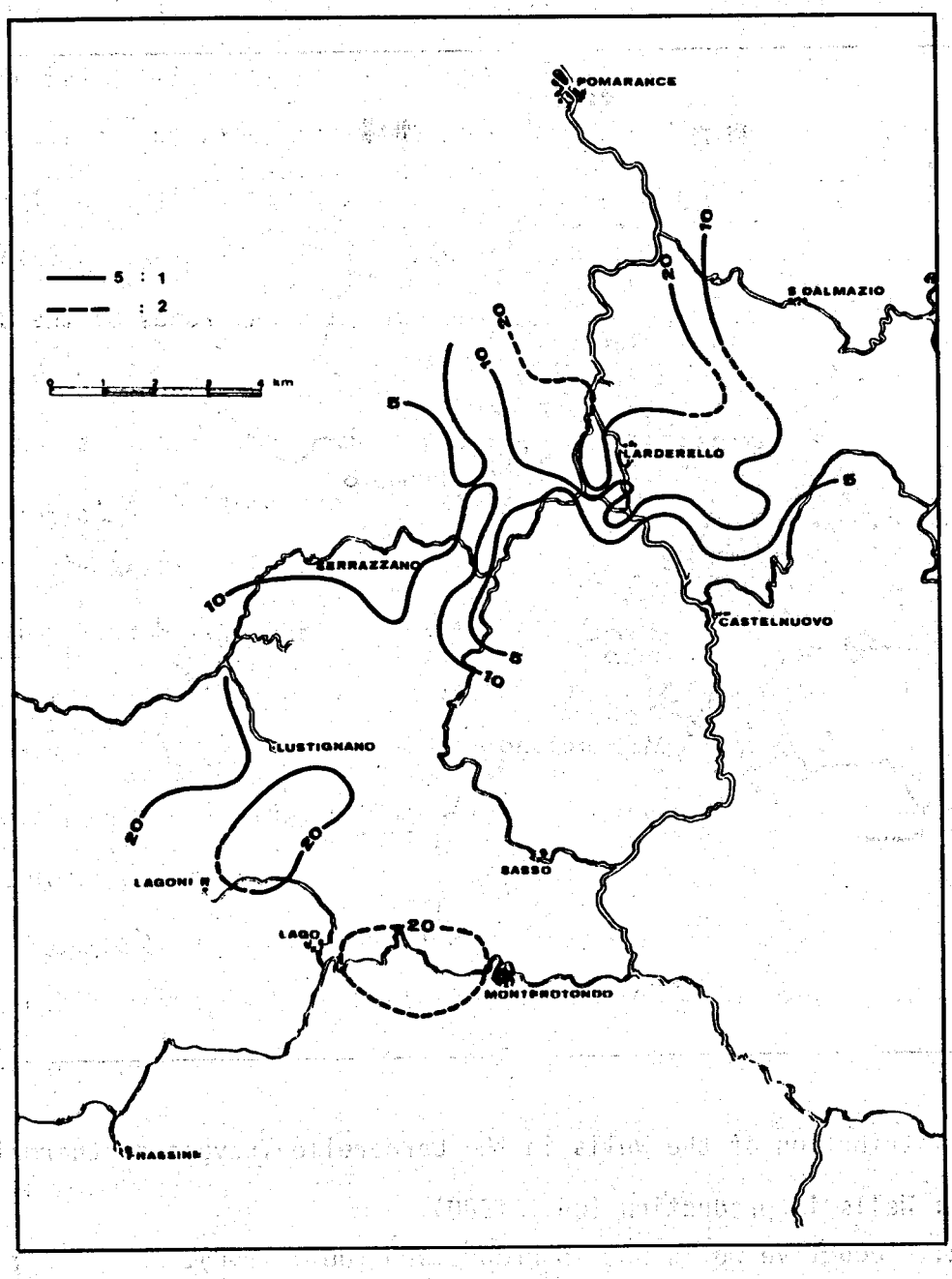

Fig. 4 - Helium concentrations in the wells in the Larderello geothermal field (from D'Amore et al., 1977).

1: Interpolated isoconcentration lines with values in ppm.

2: Isoconcentration lines for areas with few wells surveyed.

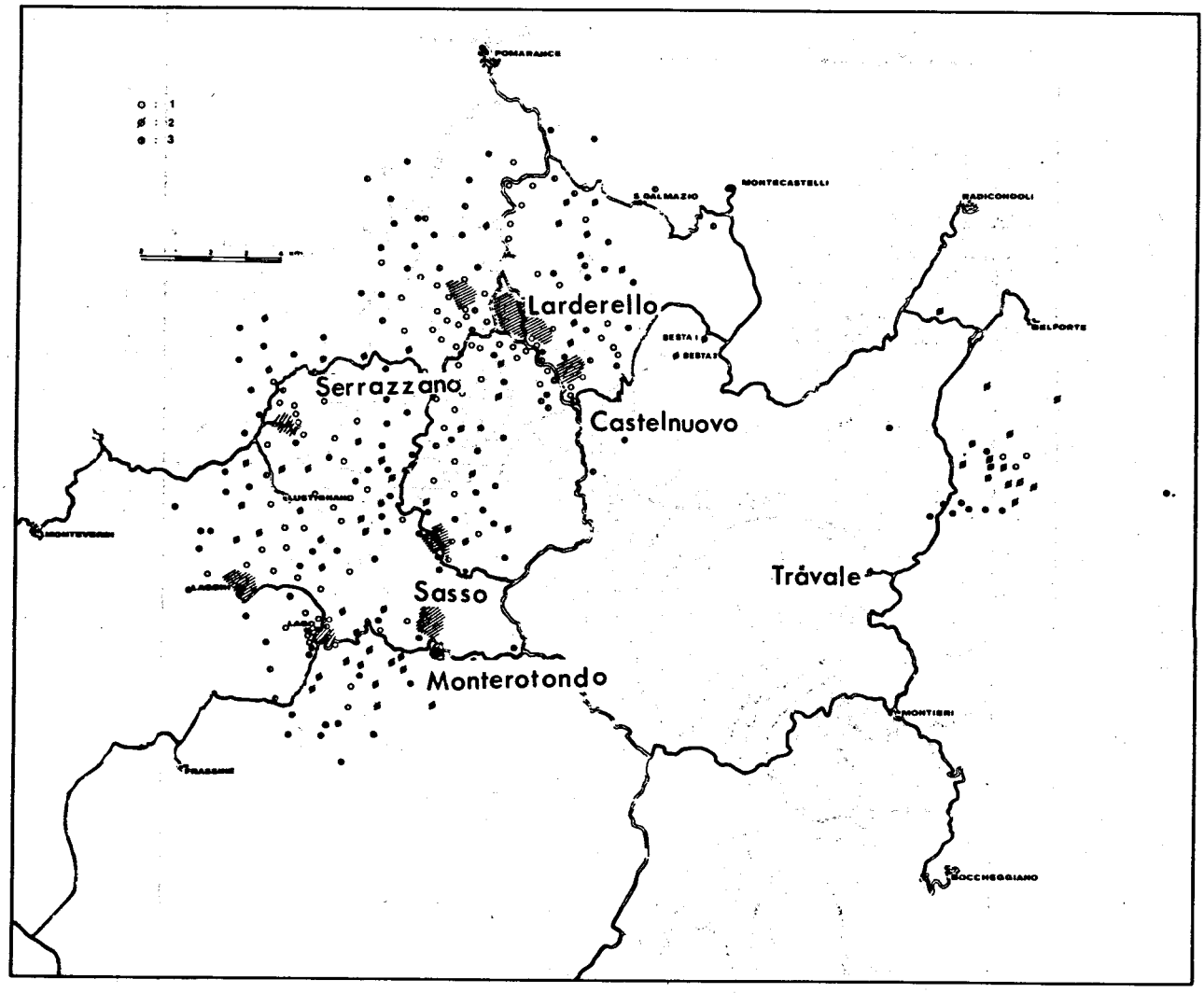

Fig. 5 - Distribution of the wells in the Larderello-Travale geothermal field.

1: Wells in production (July 1980).

2: Productive wells not in production (July 1980).

3: Not productive wells.

Dashed areas: intensively drilled areas with most of the wells in production.

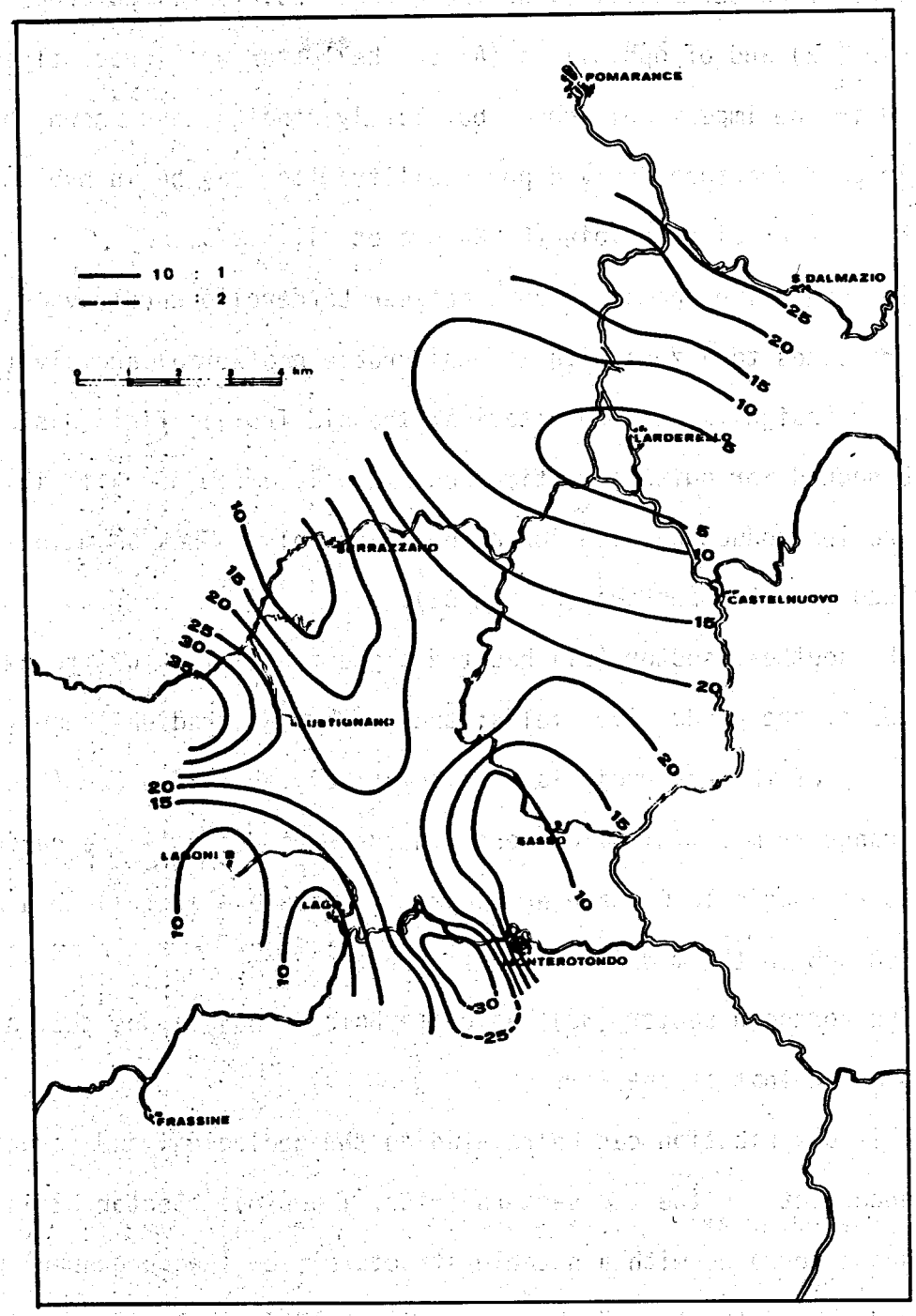

Fig. 6 - Well shut-in pressures in the Larderello geothermal field.

1: Interpolated isopressure lines with values in Kg/cm^2.

2: Extrapolated isopressure lines.

However, the anomalies of areas A1, A2 and A3 (Fig. 3) may be controlled by a higher rock permeability, as these zones have small outcrops of the reservoir (A2) and of ophyolites (A1). The latter until recently were included in the impermeable cover but lately studies have shown that, due to their good fracture-derived permeability, they may be in hydraulic contact with the geothermal reservoir (C. Calore et al., 1979).

The extensive anomalous zone between Larderello and Travale (B1 and B2) corresponds to a zone with a considerable geothermal anomaly (Fig. 7) and relatively insignificant exploitation; the old Travale field has, in fact, been abandoned for quite some time now and only a few of wells in the new field are in production, and for a few years only. This anomalous zone can be divided into two sectors (B1 and B2).

The southern sector (B1) has the highest helium values found on the perimeter of the productive fields; the geothermal gradient here reaches 0.1^{o}C/m and the top of the reservoir is at a relatively shallow depth (Fig. 8). The values range from a minimum of zero (in correspondence to the carbonatic outcrops at Poggio le Cornate and south of Travale - Fig. 1) to a maximum of about 600 ppb in the middle of the sector.

The northern sector (B2) has quite homogeneous values that are about 160 ppb above that of the air.

This distribution can be related to the geological and structural differences between the two sectors (Figs. 1 and 8). Sector B2 is an area of Neogenic terrains with a notable structural low (Anqua graben) where the maximum depth of the top of the reservoir is 1200 m below sea level (R. Cataldi et al., 1977).

It would appear from this that certain major tectonic factors, such as the faults and uplifted structures of the Anqua-Salaio zone (Fig. 1), have

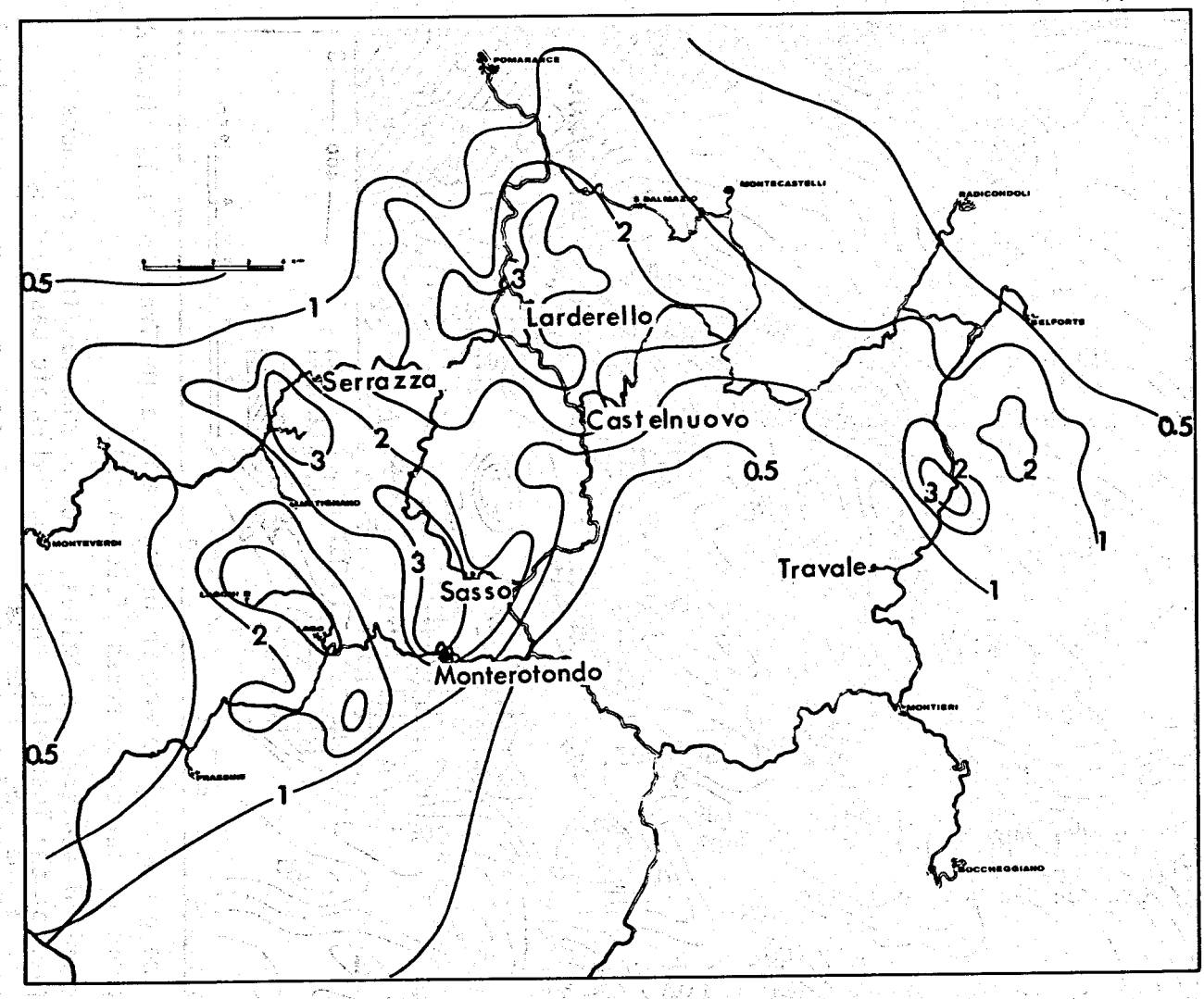

Fig. 7 - Trend of the geothermal graident on the inside of the Larderello-Travale field.
Values are in ^{o}C per 10 m depth.

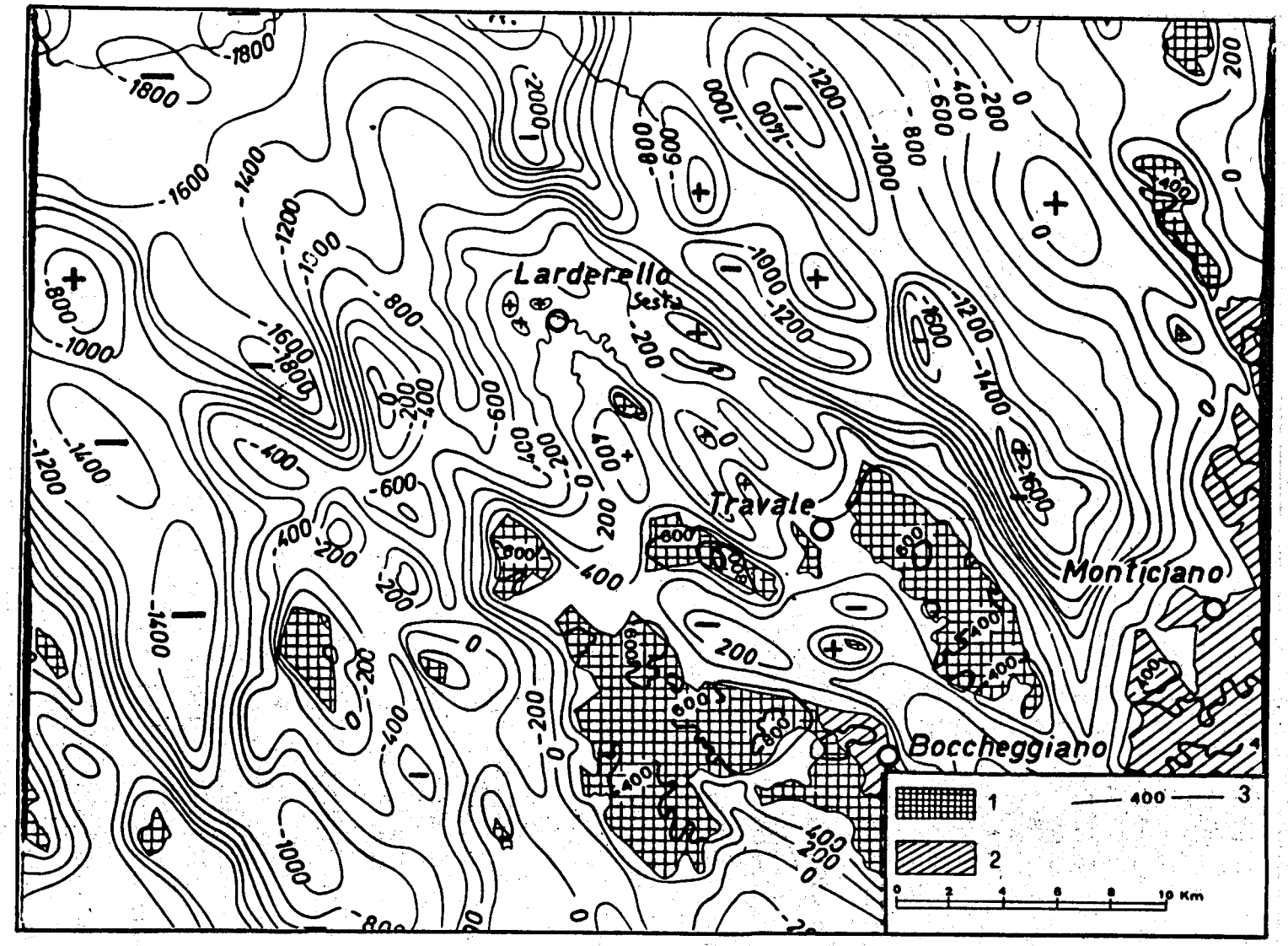

Fig. 8 - Isobaths of the top of the geothermal reservoir in the Larderello- Travale field (from R. Cataldi et al., 1977). 1: Outcrops of carbonate rocks (Tuscanides).

2: Outcrops of schists, quartzites, etc. of the basalt terrigenous complex of the Tuscanides and of the Paleozoic basement.

3: Contours on top of the main reservoir in meters relative to sea level datum.

an influence on the presence of helium anomalies on the surface.

It should, however, be noted that the great thickness of sedimentary cover (mostly in excess of 1000 meters thick in sector B2) is unable to block the escape of helium in this area.

The tectonic structures of Anqua-Salaio extend towards Pomerance, which is a zone with no recorded helium anomalies. The top of the reservoir in this zone plunges downward and is more than 2000 meters below the ground surface.

The anomalies recorded on the margins of the study (C1, C2, C3 and C4) are generally near important fault systems and where the top of the reservoir is within a few hundred meters from the surface (C1, C3, C4) or even outcrops (C2). The large quantities of helium present in the geothermal reservoir presumably find an easy escape route through these areas which are characterized by carbonate and evaporitic Mesozoic formation and Triassic-Paleozoic quartzitic-phyllitic formations. In addition, tectonics plays an important role in facilitating the helium leakage as all four areas are near the borders between horst and graben structures.

The presence of granitic bodies at shallow depth near the area C2 (Niccioleta) and west of C1 (Campiglia) could have a bearing on the helium anomalies in these zones.

- Cesano

Fig. 9 shows the location of sampling sites and the helium anomalies in the Cesano area.

The positive anomalies are located mainly in two belts, east and south of Bracciano lake. The helium enrichment found in soil gases compared with air composition is fairly high. The positive values range from 50 to 150 ppb and a few are even higher, reaching a maximum of 400 ppb. The anomalous values are represented in Figs. 10 and 11.

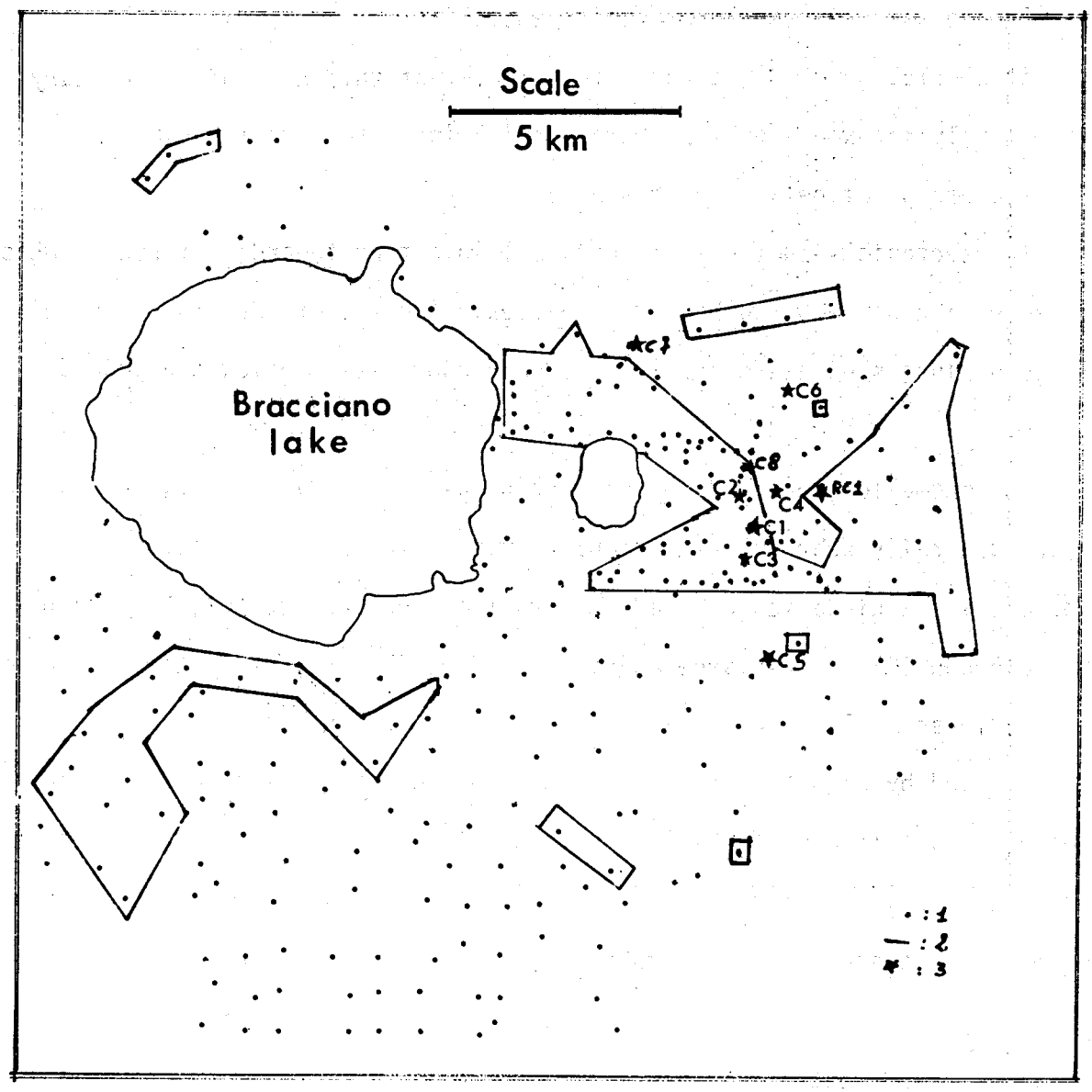

Fig. 9 - Distribution of the helium anomalies in the soil gases in the Cesano geothermal field.

1: Sample's location.

2: Limit of important anomaly areas.

3: Geothermal wells.

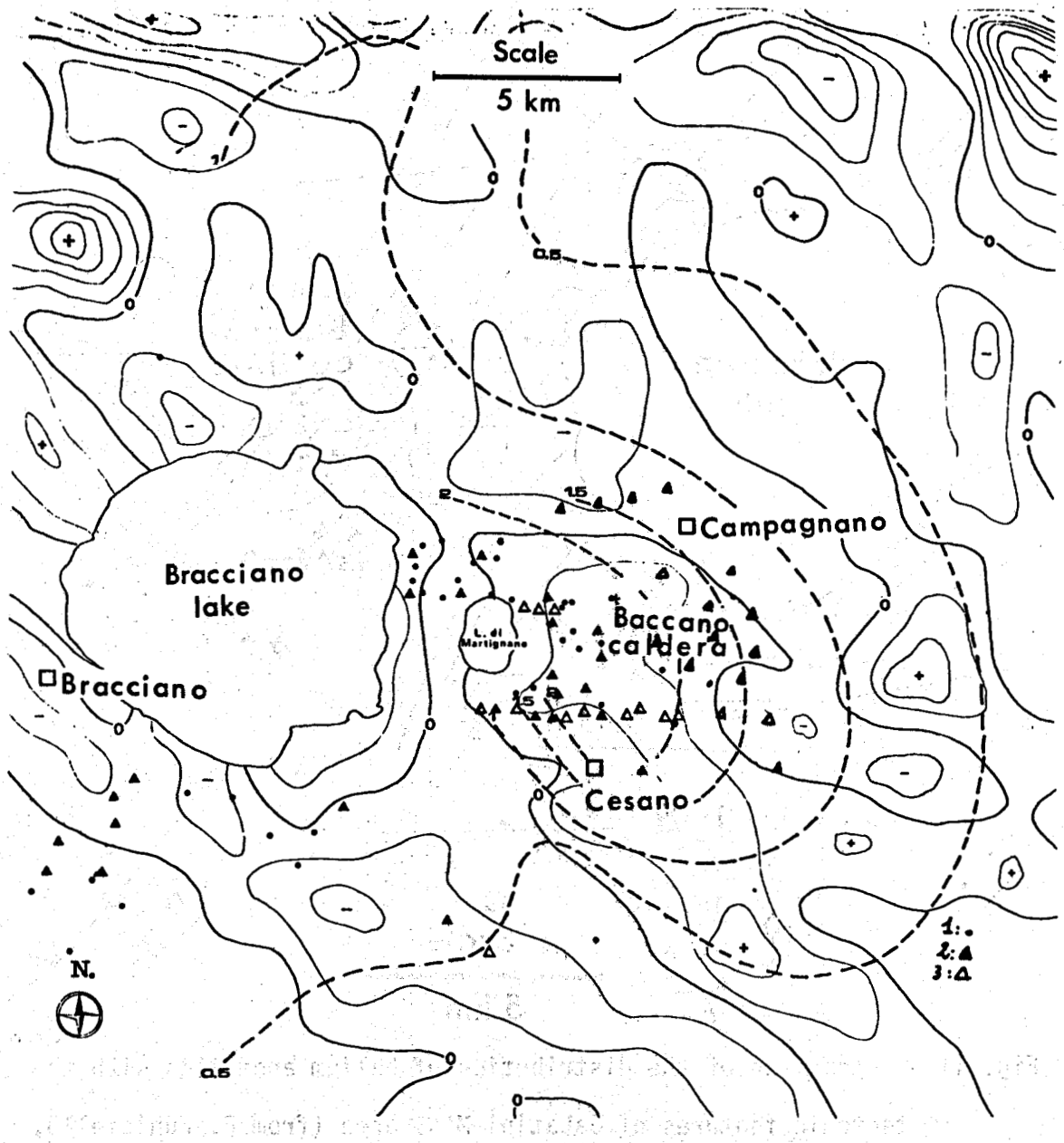

Fig. 10 - Comparison of the distribution of helium anomalies with the gravimetric profiles (from G. Buonasorte and A. Fiordelisi, 1979). The geothermal gradient east of Bracciano lake is also shown.

1: Anomalies between 50 and 100 ppb;

2: Anomalies between 100 and 150 ppb;

3: Anomalies exceeding 150 ppb.

Solid lines: gravimetric contours (m gal.)

Dashed lines: geothermal gradient contours (^{o}C per 10 m. depth).

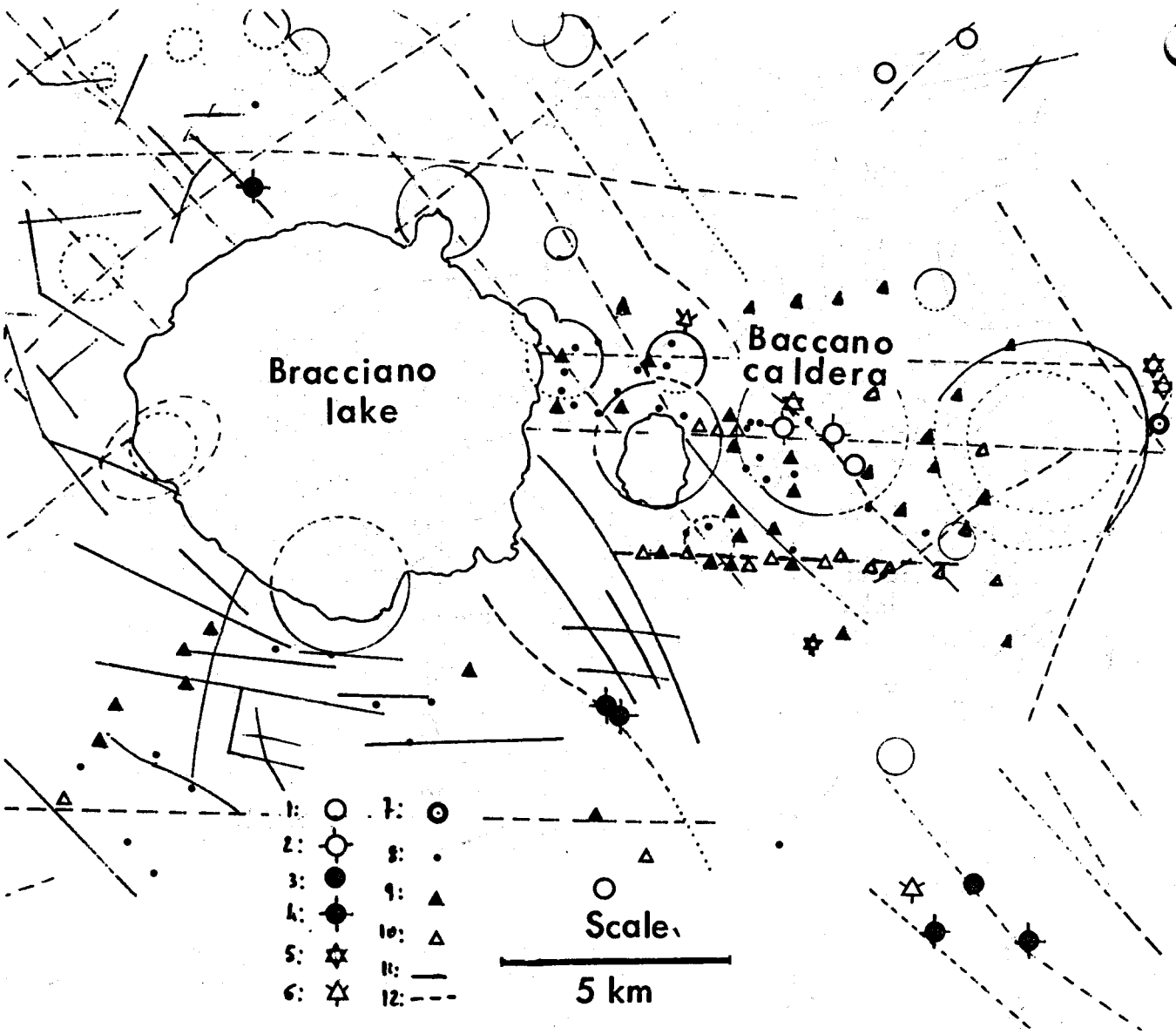

Fig. 11 - Comparison of the distribution of helium anomalies with the tectonic features of Sabatini Mts. area (from R. Funiciello, personal communication).

1: Helium in soil gas from 50 to 100 ppb.
2: Helium in soil gas from 100 to 150 ppb.
3: Helium in soil gas over 150 ppb.
4: Mineral springs.
5: Mineral springs with gas.
6: Hot mineral springs.
7: Hot mineral springs with gas.
8: Mineral wells
9: Mineral wells with gas.
10: Gas manifestation.
11: Faults.
12: Inferred faults.

In the former they are superposed on a gravimetric map, which also shows geothermal gradient in the east zone of Bracciano lake. It can be noted that the most striking helium values do correspond to a gravimetric high where the geothermal gradient reaches its maximum value ($0.2^{o}C/m$).

In Fig. 11 a comparison is made with the alignment of the main fault systems (mostly normal faults) and the location of the craters produced by recent phreatomagmatic activity of the Sabatini Mts. Both faults and craters are in line with the main tectonic trends of the pre-Apennine belt. It can be seen that the distribution of the helium anomalies is related to these main trends and, in particular, to the distensive tectonics which have been active in the area during successive phases from Early Neogene to present.

The anomalies, at least in part, are located in the zone of the younger phreatomagmatic calderas ($\approx$100,000 years), which moreover are related to the recent distensive tectonics.

Finally, it is worth stressing that in the area where we find the higher anomalous helium values in soil gases, drilling has proved the existence of a peculiar geothermal field.

First Conclusions

The results of this study show that a large helium anomaly exists in the Larderello-Travale geothermal field. However, since the productive wells provide a preferential escape route from the reservoir, the helium can be detected in the soil gases where the reservoir is relatively undisturbed and the rock permeability is favorable.

The depth of the top of the reservoir is probably a controlling factor for the existence of positive helium anomalies on the surface: where the cover is of the type found in the study areas, the helium probably can no longer escape if the roof of the reservoir lies below 2000 m from ground level.

The tectonic framework has also an important role in controlling helium leakage, and fracture systems are clearly delineated by this gas.

Furthermore helium tends to escape from the water recharge zones. The only exception to this rule is Poggio le Cornate (with outcrops of the reservoir and no helium anomalies) which is located near the Castelnuovo productive area, where the exploitation has brought about a strong decrease in the reservoir pressure and in helium abundance.

In the Cesano area, the helium anomalies correlate well with the high geothermal gradient and with the structure.

In this area the highest helium anomaly is located east of Bracciano lake, where a peculiar geothermal field has been discovered in recent years.

It is worth noting that, contrary to Larderello, the Cesano field has not yet been affected by intensive exploitation.

Future Development

Considering the results obtained so far, the study will proceed along the following lines:

- completing the case histories by prospecting of the whole region between Larderello and Rome and in particular other known fields where exploitation has been less intense than at Larderello (Alfina, Latera) or the reservoir still undisturbed (Colli Albani);
- more detailed surveys in correspondence to particular tectonic features;
- isotopic analyses of the helium found near the geothermal fields, both on the surface and in the reservoir, to obtain a better definition of its origin and leakage mechanism;
- further study of possible relationships between helium anomalies and seismic activity.

BIBLIOGRAPHY

P. Baldi, R. Funicello, E. Locardi and M. Parotto, 1976 a. VOLCANOLOGIC AND STRUCTURAL STUDY OF CESANO GEOTHERMAL AREA (ROME, ITALY). Int. Cong. on Thermal Waters, Geothermal Energy and Volcanism in the Mediterranean Area, Athens, Proc. Geothermal Energy, V.7, 43-45.

P. Baldi, G. Civitelli, R. Fumicello, G. Lombardi, M. Parotto and L. Serva, 1976b. STUDY OF THE STRATIGRAPHY AND MINERALIZATION OF THE DEEP WELLS IN CESANO GEOTHERMAL FIELD (ROME, ITALY). Int. Congr. on Thermal Waters, Geothermal Energy and Volcanism in the Mediterranean Area, Athens, Proc. Geothermal Energy, V.1, 71-85.

H. R. Bowmann, A. J. Hebert, H. A. Wollenberg and F. Asaro, 1975 TRACE, MINOR AND MAJOR ELEMENTS IN GEOTHERMAL WATERS AND ASSOCIATED ROCK FORMATIONS (NORTH-CENTRAL NEVADA). Second U. N. Symposium on the Development and Use of Geothermal Resources, San Francisco, 20-29 May, V. 1, 699-702.

G. P. Brandi, L. Dallan, A. Lazzarotto, R. Mazzanti, P. Squarci, L. Taffi, L. Trevisan, 1968, NOTE ILLUSTRATIVE DELLA CARTA GEOLOGICA D'ITALIA: F-119. Min. Ind. Comm. Art., Servizio Geologico d'Italia.

G. Buonasorte and A. Fiordelisi, 1979. CARATTERISTICHE GEOLOGICHE E STRUTTURALI DEL CAMPO GEOTERMICO DI CESANO. ENEL-DSR Internal Report.

C. Calore, R. Celati, P. Squarci and L. Taffi, 1979, CARATTERISTICHE IDROGEOLOGICHE E TERMICHE DELLE ZONE PERIFERICHE NORD E OVEST DEL CAMPO DI LARDERELLO. CNR-Progetto Finalizzato Energetica- Atti del I° Seminario Informativo, Roma, 18-21 Dicembre, 248-258.

R. Cataldi, G. Stefani and M. Tongiorgi, 1963. GEOLOGY OF LARDERELLO REGION (TUSCANY): CONTRIBUTION TO THE STUDY OF THE GEOTHERMAL BASIN. Nuclear Geology on Geothermal Areas, Spoleto, Sept. 9- 13.

R. Cataldi, A. Lazzarotto, P. Muffler, P. Squarci and G. Stefani, 1977. ASSESSMENT OF GEOTHERMAL POTENTIAL OF CENTRAL AND SOUTHERN TUSCANY. Proc. of the ENEL-ERDA Workshop, Larderello, Sept. 12-16. ENEL, Studi e Ricerche, 352-412.

R. Celati, P. Squarci and L. Taffi, 1978. GEOLOGICAL, HYDROGEOLOGICAL AND PHYSICAL CHARACTERISTICS OF THE TUSCAN GEOTHERMAL FIELDS. Italian Days of Science, Budapest, April 21-28.

F. D'Amore, G. C. Ferrara, P. Noto and S. Nuti, 1977. TENORI DI ELIO NEI FLUIDI DEL CAMPO GEOTERMICO DI LARDERELLO- PRIME CONSIDERAZIONI SULLE RELAZIONI TRA ELIO ED ALTRI COMPONENTI DEL FLUIDO, ENEL- DSR Internal Report 511-Z 13/B.

I. Friedman, E. H. Denton, A. A. Roberts and G. M. Reimer, 1976. A MOBILE HELIUM SNIFFER FOR PETROLEUM, URANIUM, AND GEOTHERMAL PROSPECTING. Proc. 25tg Int. Geol. Congr., Sydney, N.S.W. V.2, 443-444.

R. Funiciello, E. Locardi, G. Lombardi and M. Paro to, 1976. THE SEDIMENTARY EJECTA FROM PHREATOMAGMATIC ACTIVITY AND THEIR USE FOR LOCATION OF POTENTIAL GEOTHERMAL AREAS. Int. Cong. on Thermal Waters, Geothermal Energy and Volcanism on the Mediterranean Area, Athens, Proc. Geoth. Energy, v. 1, 227-240.

R. Funiciello, G. Mariotti, M. Parotto, M. Preite-Martinez, F. Teccia, R. Toneatti and T. Turi, 1979. GEOLOGY, MINERALOGY AND STABLE ISOTOPE GEOCHEMISTRY OF THE CESANO GEOTHERMAL FIELD (SABATINI MTS. VOLCANIC SYSTEM, NORTHERN LATIUM, ITALY). Geothermics, v. 8, 55-73.

A. Koga and T. Noda, 1975. GEOCHEMICAL PROSPECTING IN VAPOR DOMINATED FIELDS FOR GEOTHERMAL EXPLORATION. Second U.N. Symposium on the Development and Use of Geothermal Resources, San Francisco, 20-29 May, v. 1, 761-766.

A. Lazzarotto, 1967. GEOLOGIA DELLA ZONA COMPRESA FRA L'ALTA VALLE DEL FIUME CORNIA ED IL TORRENTE PAVONE. Memorie della Societa Geologica Italiana, v. 6, 151-197.

A. Lazzarotto and R. Mazzanti, 1976. GEOLOGIA DELL'ALTA VAL DI CECINA. Boll. Soc. Geol. It., 95, 1365-1487.

E. Locardi, R. Funiciello, G. Lombardi and M. Parotto, 1975. THE MAIN VOLCANIC GROUPS OF LATIUM (ITALY): RELATIONS BETWEEN STRUCTURAL EVOLUTION AND PETROGENESIS. Guidebook prepared for the International Colloquium of Planetary Geology, Rome, September 22-30, 1-32.

J.S. Matlick, III and Peter R. Buseck , 1975. EXPLORATION OF GEOTHERMAL AREAS USING MERCURY: A NEW GEOCHEMICAL TECHNIQUE. Second U.N. Symposium on the Development and Use of Geothermal Resources, San Francisco, 20-29 May, v. 1, 785-792.

R. Mazzanti, 1966. GEOLOGIA DELLA ZONA DI POMARANCE - LARDERELLO. Memorie della Societa Geologica Italiana, v. S., 105-138.

G.M. Reimer, 1976. DESIGN AND ASSEMBLY OF A PORTABLE HELIUM DETECTOR FOR EVALUATION AS A URANIUM EXPLORATION INSTRUMENT. U.S. Dept. of Interior, USGS, Open File Report 76-398.

G.M. Reimer and C.G. Bowles, 1975. SOIL GAS HELIUM CONCENTRATIONS IN THE VICINITY OF A URANIUM DEPOSIT, RED DESERT, WYOMING. U.S. Dept. of Interior, USGS, Open File Report 79-975.

A.A. Roberts, I. Friedman, T.J. Donovan and E.H. Denton, 1975. HELIUM SURVEY, A POSSIBLE TECHNIQUE FOR LOCATING GEOTHERMAL RESERVOIRS. Geophysical Research Letters, June, v. 2, 209-210.

F. Tonani, 1970. GEOCHEMICAL METHODS OF EXPLORATION FOR GEOTHERMAL ENERGY. U.N. Symposium on the Development and Utilization of Geothermal Resources, Pisa-Geothermics, Special Issue 2, v. 2, Part 1, 492-515.

Second

DOE-ENEL Workshop for Cooperative Research in Geothermal Energy

Earth Sciences Division
Lawrence Berkeley Laboratory
University of California
Berkeley, California 94720

PROGRAM

Sunday, October 19, 1980

16:30 - 19:30	Registration, Lobby of the Holiday Inn, Emeryville, California

Monday, October 20, 1980

7:00 - 8:45	Registration, LBL Auditorium Lobby, Building 50
8:45	LBL Welcome: *Dr. David A. Shirley, Director*
9:00	Review of Italian Geothermal Program: *Prof. Luigi Paris*
9:30	Review of U.S. Geothermal Program: *J. Salisbury*
10:00	Session I, "Project 5 — Environmental" Introduction: *G. Ferrara and C. Bufe, Co-Chairmen*
10:15	The Distribution of Radon and Radon Daughters in the Geothermal Region of Larderello: *Alfred J. Breslin, Andreas C. George and Giovanni Scandiffio*
10:35	Discussion
10:45	Refreshments
11:00	H_2S Abatement — Focus at The Geysers, California: *Gerald Katz*
11:20	Discussion
11:30	Seismic Monitoring in Italian Geothermal Areas Seismic Activity in the Larderello-Travale Area: *F. Batini, C. Bufe, G. M. Cameli, R. Console, and A. Fiordelisi* Seismic Activity in the Geothermal Fields under Exploration: *F. Batini, G. M. Cameli, E. Carabelli, and A. Fiordelisi*
11:50	Geothermal Induced Seismicity — Bane or Blessing? *C. Bufe and P. Shearer*
12:10	Discussion Closing Remarks: *C. Bufe, Co-Chairman*

12:30	Lunch (No-Host, lower level of LBL cafeteria, Building 54, has been reserved)
13:30	Session II, "Project 1 — Stimulation" Introduction: *M. Smith and P. Ceron, Co-Chairmen*
13:45	Selection of Dry Wells in Tuscany for Stimulation Tests: *P. Baldi, G. Bertini, C. Calore, G. Cappetti, C. Cataldi, R. Celati, and P. Squarci*
14:05	Discussion
14:15	Selection of Fracturing Techniques and Examples of Applications in Italy: Task 1/2: *P. Berry, C. Cataldi, and E. M. Dantini*
15:00	Refreshments
15:15	The DOE Geothermal Well Stimulation Program: *R. J. Hanold and D. A. Campbell*
15:35	Discussion
15:45	The DOE Hot Dry Rock Program; *G. J. Nunz*
16:15	Discussion
16:25	Closing Remarks: *P. Ceron, Co-Chairman*

Tuesday, October 21, 1980

8:00 - 9:00	Registration, LBL Auditorium Lobby, Building 50
9:00	Session III, "Project 4 — Deep Drilling" Introduction: *U. Cigni and S. Varnado, Co-Chairmen*
9:15	Italian Experience and Problems in Deep Drilling (> 3000 m): *U. Cigni*
9:40	Discussion
9:50	Materials Employed in Deep Geothermal Drilling in Italy: *P. Del Gaudio*
10:15	Discussion
10:20	Refreshments
10:35	Geothermal Drilling Practices in The Geysers: *Lou Capuano*
11:00	Discussion
11:10	Materials Used in Drilling Geothermal Wells in The Geysers: *Larry Leet*
11:25	Discussion
11:35	Closing Remarks, *S. Varnado: Co-Chairman*
11:40	Lunch, No-Host (lower level of LBL cafeteria, Building 54, has been reserved)

13:30	Session IV, "Project 2 — Brine Utilization" Introduction: *C. McFarland and G. Allegrini, Co-Chairmen*
13:45	Study of Saline Equilibria; *G. Conti, G. Nardini, G. F. Nencetti, L. Petarca, A. M. Tine, and N. Vatistas*
14:05	Discussion
14:15	Potential Solutions for Geothermal Brine Production Utilization and Reinjection Problems: *O. J. Vetter*
14:30	Discussion
14:45	Production Test Facilities of the Hot Brine of Cesano Geothermal Field: *R. Corsi and R. Di Falco*
15:05	Discussion
15:15	Refreshments
15:30	Production Test Results at the Salton Sea Geothermal Field: *Anthony J. Adduci*
15:50	Discussion
16:00	Design and Construction of a Pilot Plant for Utilization of Cesano Brine: *G. Allegrini and G. Nardini*
16:20	Discussion
16:30	High Salinity Geothermal Energy Conversion Based upon the Operating Experience at the San Diego Gas & Electric-DOE Geothermal Loop Experimental Facility Located at the Niland Reservoir, Imperial Valley, California, U.S.A.: *George Anastas*
16:50	Discussion
17:00	Closing Remarks: *G. Allegrini, Co-Chairman*

Wednesday, October 22, 1980

8:00 - 9:00	Registration, LBL Auditorium Lobby, Building 50
9:00	Session V, "Project 3 — Reservoir Studies" Introduction: *R. Cataldi and P. Witherspoon, Co-Chairmen*
9:15	Modeling Vapor-Dominated Systems — Serrazzano: *R. Celati, R. Marconcini, G. Neri, K. Pruess, R. Schroeder, and O. Weres*
10:00	Discussion
10:10	Refreshments
10:25	Reinjection Studies in Vapor-Dominated Systems: *R. Celati, M. J. O'Sullivan, K. Pruess, C. Ruffilli, and R. Schroeder*
11:05	Discussion
11:15	A Depletion Model for the Gabbro Zone (Northern Part of Larderello Field): *William E. Brigham and Giuseppe Neri*
11:55	Discussion

13:30	Reservoir Engineering Studies of the Travale-Radicondoli Reservoir: *A. Barelli, M. J. Economides, G. Manetti, and F. G. Miller*
13:50	Study of Water Influx and Fluid Composition in the Bagnore Field: *Romano Celati, Franco D'Amore, Michael J. Economides, and Giuseppe Neri*
14:10	Discussion
14:20	Helium Prospection in Geothermal Areas: *R. Bertrami, A. Ceccarelli, I. Friedman, W. Boering, and S. Lombardi*
14:50	Discussion
15:00	Closing Remarks
15:05	Refreshments
15:20	Summary of the Meeting: *J. Salisbury and C. Palmerini*
16:00	Adjourn
18:30 - 19:30	No-host Social Hour Starboard Room, Marriott Inn, Berkeley Marina
20:00	Banquet, Starboard Room, Marriott Inn, Berkeley Marina *P. Witherspoon, Chairman* *P. Ceron and J. Salisbury, Speakers*

Thursday, October 23, 1980

Field trip to The California Geysers *(Werner J. Schwarz, Coordinator)*

7:30	Buses leave Holiday Inn, Emeryville, California
10:30	Tour of California Geysers Geothermal Power Plant
13:00	Depart for Souverain Cellars Winery
13:00 - 15:00	Lunch, tour of winery
15:00 - 17:00	Return to Holiday Inn, Emeryville, California

Friday, October 24, 1980

Trip to Terra Tek Inc., Salt Lake City, Utah (Arranged by Terra Tek)

LIST OF PARTICIPANTS

Anthony J. Adduci
U.S. DOE
1333 Broadway
Oakland, CA 94612

(415) 273-7943

Giovanni Allegrini
ENEL
Larderello, ITALY 56044

(0588) 67372

George Anastas
San Diego Gas & Electric
101 Ash Street
San Diego, CA 92112

(714) 235-7733

Meredith Joan Anguin
EPRI
3412 Hillview Avenue
Palo Alto, CA 94303

(415) 855-2594

Paul Atkinson
Union Oil Company
P.O. BOX 6854
Santa Rosa, CA 95401

(707) 542-9543

Plinio Baldi
ENEL- UNG
Piazza Bartolo da Sassoferrato, 14
Pisa, ITALY 56100

(050) 575005

Giovanni Barbanera
TSMES
Viale G. Cesare 2P
Bergamo, ITALY

Benjamin Barker
Union Oil Company
P.O. BOX 6854
Santa Rosa, CA 95405

(707) 542-9543

Sally Benson
LBL
1 Cyclotron Road
Bldg. 90- 1024B
Berkeley, CA 94720

(415) 486- 5875

Rino Bertrami
ENEL- UNG
P. 7A B. Sassoferrato, 14
Pisa, ITALY 56401

0 (588) 20898

Gudmundur Bodvarsson
LBL
1 Cyclotron Road
Bldg. 90- 1042D
Berkeley, CA 94720

(415) 486-5350

Bill Brigham
Stanford University
Petroleum Engineering Dept.
Stanford, CA 94305

(415) 497-0611

Charles G. Bufe
USGS and DGE/DOE
Federal Building
12th & Pennsylvannia, N.W.
Washington, D.C. 20461

(202) 633-8820

Gian Mauro Cameli
ENEL- Unita Nazionale Geotermica
Piazza Bartolo da Sassoferrato 14
Pisa, ITALY

(050) 571479- 574030

Louis Capuano
ThermaSource
P.O. BOX 1236
Santa Rosa, CA 95402

(707) 523-2960

Edmondo Carabelli
ISMES
V.G. Cesare 29
Bergamo, ITALY

(35) 243-043

Carlo Cataldi
ENEL
Piazza B. da Sassoferrato
Pisa, ITALY 56100

(50) 575005

Raffaele Cataldi
ENEL
Piazza B. da Sassoferrato 14
Pisa, ITALY 56100

Romano Celati
Consiglio Nazionale Ricerche
Via Buongusto
Pisa, ITALY 56100

39 (050) 41503

Pietro Ceron
ENEL
Via B. da Sassoferrato 14
Pisa, ITALY
(050) 575005

G.L. Chierici
AGIP spA
P.O. BOX 12069
Milano, ITALY

(02) 53 53 40 86

Riccardo Corsi
ENEL- UNG Pisa
Piazza Bartolo da Sassoferrato 15
Pisa, ITALY

(050) 576005

Ugo Cigni
ENEL
Larderello, ITALY 56044

(0) 588 67372

Enzomaria Dantini
University of Rome
Via Eudossiana 18
Rome, ITALY 00100

(06) 484536- 4757200

Ken Deakins
Dresser Ind. Inc.
14800 Grove Street
Healdsburg, CA 95405

(707) 539-0129

Paulo del Gaudio
ENEL
Viale San Marco 3
Larderello, ITALY 56044

39 (588) 67109

Michael Economides
University of Alaska
Fairbanks, AK

(907) 4795524

Steven Enedy
Union Geothermal
2099 Range Avenue
Santa Rosa, CA 95401

(707) 542-9543

Gian Carlo Ferrara
ENEL-UNG
Piazza B. da Sassoferrato
Pisa, ITALY 56100

(050) 575005

Irving Friedman
U.S.Geological Survey
M.S. 963-DFC
Denver, CO 80225

(303) 234-5531

George Frye
Aminoil USA
Santa Rosa, CA 95406

(707) 527-5332

Robert M. Galbraith
LBL
Bldg. 90 - 1024
1 Cyclotron Road
Berkeley, CA 94720

(415) 486-6031

Mario Gallardo Alanis
Melchor Ocampo pte #35
Cd. Hidalgo Mich.
Michoacan, MEXICO

Giorgio Gerini
Commission of the European Community
200 Rue de la Loi
Brussels, BELGIUM 1140

(32) 2-735.00.40 Ext. 1216

Norman Goldstein
LBL
Bldg. 90 - 1012B
1 Cyclotron Road
Berkeley, CA 94720

(415) 486-5961

Colin Goranson
BGI
P.O. Box 777
Berkeley, CA 94701
(415) 843-7678

Keshav Goyal
LBL
Bldg. 90 - 1024D
1 Cyclotron Road
Berkeley, CA 94720
(415) 486-5400

M. Guglielminetti
AGIP SpA
San Donato
Milano, ITALY

Mohinder Gulati
Union Oil Co.
P. O. Box 6854
Santa Rosa, CA 95405
(707) 542-9543

Sue Halfman
LBL
Bldg. 90 - 1042B
1 Cyclotron Road
Berkeley, CA 94720
(415) 486-4790

R.J. Hanold
Los Alamos Scientific Lab.
Los Alamos, NM 87545
(505) 667-2631

Thomas Heenan
DOE/SAN
1333 Broadway
Oakland, CA 94521
(415) 273-7943

Earl G. Hoff
Phillips Petroleum Co.
P.O. Box 239
Salt Lake City, UT 84110
(801) 364-2083

William Holman
U.S. Dept. of Energy
1333 Broadway
Oakland, CA 94612
(415) 273-7151

J.H. Howard
LBL
Bldg. 90 - 1042E
1 Cyclotron Road
Berkeley, CA 94720
(415) 447-8560

Arfon Jones
TerraTek
Univ. Research Park
420 Wakara Way
Salt Lake City, UT 84108
(801) 582-2220

Gerald Katz
U.S. Dept. of Energy
1556 Filbert #4
San Francisco, CA 94123
(415) 928-2753

L.W. Leet
Dresser Magcobar
1944 Calavaras Drive
Santa Rosa, CA 95405
(707) 523-3147

Marcelo Lippmann
LBL
Bldg. 90 - 1012E
1 Cyclotron Road
Berkeley, CA 94720
(415) 486-5035

Salvatore Lombardi
Universita di Roma
Istituto di Geologia
p. A. Moro 5
Rome, ITALY 00100
(06) 4856634

Ruth Sara Ludwin
U.S.G.S.
345 Middlefield Road
Menlo Park, CA 94025
(415) 323-8111

Donald Mangold
LBL
Bldg. 90 - 1024F
1 Cyclotron Road
Berkeley, CA 94720
(415) 486-6459

Clifton B. McFarland, Jr.
DOE
12th & Penna. Ave., N.W.
Washington, D.C. 20461

(202) 633-8107

Constance Miller
LBL
Bldg. 90 - 1042D
1 Cyclotron Road
Berkeley, CA 94720

(415) 486-6454

Frank G. Miller
Petroleum Engineering Dept.
Stanford University
Stanford, CA 94305

(415) 497-2938

*
Carlos Miranda Moctezuma
C.F.E.
Melchor Ocampo Pte. 35
Cd. Hidalgo
Michoacan, MEXICO

91-725-40352

Allen Moench
U.S. Geological Survey
M.S. 96
345 Middlefield Road
Menlo Park, CA 94025

(415) 857-7171

Martin W. Molloy
U.S. DOE/SAN
1333 Broadway
Oakland, CA 94612

(415) 273-7943

Charles W. Morris
Republic Geothermal Inc.
11823 E. Slauson Ave., Suite 1
Santa Fe Springs, CA 90670

(213) 945-3661

Patrick Muffler
U.S.G.S.
345 Middlefield Road
Menlo Park, CA 94025

* Leland (Roy) Mink
DOE/ID
520 2nd Street
Idaho Falls, ID 83705

Kent S. Murray
Calif. Energy Commission
1111 Howe Avenue
Sacramento, CA 95825

(916) 920-8885

Giuliano Nardini
University of Pisa
Pisa, ITALY

Gianfranco Nencetti
University of Pisa
via Diotisali 2
Pisa, ITALY

Giuseppe Neri
ENEL
3, via S. Marco
Larderello, ITALY 86044

(58) 8 67531

Gregory J. Nunz
Los Alamos Scientific Lab.
P. O. Box 1663
Los Alamos, NM 87545

(505) 667-3185

David H. Oppenheimer
U.S.G.S.
345 Middlefield Road
Menlo Park, CA 94025

(415) 323-8111 X2791

Jaime Ortiz Ramirez
Melchor Ocampo #35 Pte.
Cd. Hidalgo
Michoacan, MEXICO

M.J. O'Sullivan
LBL
Bldg. 90 - 1024C
1 Cyclotron Road
Berkeley, CA 94720

(415) 486-6457

Rosanne Pagano
LBL
Bldg. 931 - 400
1 Cyclotron Road
Berkeley, CA 94720

(415) 486-4017

John F. Philip
LBL
Bldg. 90 - 1012A
1 Cyclotron Road
Berkeley, CA 94720
(415) 486-6468

Karsten Pruess
LBL
Bldg. 90 - 1042E
1 Cyclotron Road
Berkeley, CA 94720
(415) 486-6106

H.J. Ramey
Stanford University
Petroleum Engr. Dept.
Stanford, CA 94305
(415) 497-1774

Phila Rogers
LBL
Bldg. 931 - 431
1 Cyclotron Road
Berkeley, CA 94720
(415) 486-4015

John W. Salisbury
U.S. Dept. of Energy
Fed. Bldg. MS 3344
12th & Penna., N.W.
Washington, D.C. 20461
(202) 633-9362

Richard Salzbrenner
Sandia Labs.
Albuquerque, NM 87120
(505) 844-5041

Giovanni Scandiffio
ENEL
Piazza Bartolo da Sassoferrato 14
Pisa, ITALY 56100

R. Schroeder
BGI
245 Gravatt Drive
Berkeley, CA 94705
(415) 843-7678

Werner Schwarz
LBL
Bldg. 90 - 1070
1 Cyclotron Road
Berkeley, CA 94720
(415) 486-4706

Peter Shearer
U.S.G.S. MS 77
345 Middlefield Road
Menlo Park, CA 94025
(415) 323-8111 X2180

David Shirley
LBL
Building 50A - 4133
1 Cyclotron Road
Berkeley, CA 94720
(415) 486-5111

Terrance L. Simkin
LBL
Bldg. 90 - 1106
1 Cyclotron Road
Berkeley, CA 94720
(415) 486-6105

Norton C. Smith
LASL
163 El Gancho
Los Alamos, NM 87544
(505) 667-3185

Claudio Sommaruga
AGIP SpA
S. Donato Milanese
Milano, ITALY
(02) 535- 35609

Ray Solbau
LBL
Bldg. 42
1 Cyclotron Road
Berkeley, CA 94720
(415) 486-6092

Luis Antonio Templos M.
C.F.E.
Melchor Ocampo Pte. 35
Hidalgo
Michoacan, MEXICO
91 (725) 40352

Sverrir Thorhallsson
National Energy Authority
Grensasvegur 9
Reykjavik, ICELAND
83600

Chin Fu Tsang
LBL
Bldg. 90 - 1012H
1 Cyclotron Road
Berkeley, CA 94720
(415) 486-5782

Sam Varnado
Sandia Labs.
Albuquerque, NM 87185
(505) 844-6094

Otto Vetter
Vetter Research
3189 C Airway Avenue
Costa Mesa, CA 94626
(714) 751-2945

Stephen Vonder Haar
LBL
Bldg. 90 - 1024D
1 Cyclotron Road
Berkeley, CA 94720
(415) 486-5350

Oleh Weres
LBL
Bldg. 90 - 1140E
1 Cyclotron Road
Berkeley, CA 94720
(415) 486-5625

P.A. Witherspoon
LBL
Bldg. 90 - 1106
1 Cyclotron Road
Berkeley, CA 94720
(415) 486-5082/66

Giuseppe Ziliotto
ISMES V.G. Cesare No. 29
Bergamo, ITALY

NAME INDEX

Adduci, Anthony J. - 272, 503.

Allegrini, G. - 291, 503.

Anastas, George - 311, 503.

Baldi, P. - 98.

Barelli, A. - 464, 504.

Batini, F. - 20, 48, 501.

Berry, P. - 116, 502.

Bertini, G. - 98, 502, 504.

Bertrami, R. - 483.

Boering, W. - 504.

Breslin, Alfred J. - 3, 501.

Brigham, William E. - 434, 503.

Bufe, Charles G. - 20, 86, 501.

Calore, C. - 98, 502.

Cameli, G. M. - 20, 48, 501.

Campbell, D. A. - 164, 502.

Cappetti, G. - 98, 502.

Capuano, Louis E., Jr. - 218, 502.

Carabelli, E. - 48, 501.

Cataldi, C. - 98, 116, 502, 503.

Cataldi, R. - 323.

Ceccarelli, A. - 483, 504.

Celati, Romano - 98, 328, 381, 480, 502, 503, 504.

Ceron, P. - 502, 504.

Cigni, U. - 189, 502.

Console, R. - 20, 501.

Conti, G. - 228, 503.

Corsi, R. - 247, 503.

D'Amore, Franco - 480, 504.

Dantini, E. M. - 116, 502.

Del Gaudio, P. - 205, 502.

Di Falco, R. - 247, 503.

Doering, W. - 483.

Economides, Michael J. - 464, 480, 504.

Ferrara, G. - 501.

Fiordelisi, A. - 20, 48, 501.

Friedman, I. - 483, 504.

George, Andreas C. - 3, 501.

Gianni, P. - 228.

Hanold, R. J. - 164, 502.

Katz, Gerald - 15, 501.

Leet, Larry - 226, 502.

Lombardi, S. - 483, 504.

Manetti, G. - 464, 504.

Marconcini, R. - 328, 342, 503.

McFarland, C. - 503.

Miller, F. G. - 464, 504.

Nardini, G. - 291, 503.

Nencetti, G. F. - 228, 503.

Neri, Guiseppi - 328, 342, 434, 480, 503, 504.

Nunz, Gregory J. - 173, 502.

O'Sullivan, M. J. - 503.

Paris, Luigi - 501.

Petarca, L. - 228, 503.

Pruess, Karsten - 1, 328, 342, 381, 503.

Ruffilli, Claudio - 381, 503.

Salisbury, J. - 501, 503, 504.

Scandiffio, Geovanni - 3, 501.

Schroeder, R. - 328, 342, 503.

Schwarz, Werner J. - 1, 504.

Shearer, Peter M. - 86, 501.

Shirley, David A. - 501.

Sinclair, A. Richard - 164.

Smith, M. - 502.

Squarci, P. - 98, 502.

Tine, M. R. - 228, 503.

Varnado, S. - 502.

Vatistas, N. - 228, 503.

Vetter, O. J. - 245, 503.

Weres, O. - 328, 342, 503.

Witherspoon, P. - 323, 503, 504.

ORGANIZATIONAL ABBREVIATIONS

AGIP - Azienda Generale Italiana Petroli (Italy)

CFE - Comision Federal de Electricidad de Mexico

CRN - Centro Nazionale Ricerca (Italy)

DOE - Department of Energy (USA)

ENEL - Ente Nazional per L'Energia Elettrica (Italy)

EPRI - Electric Power Research Institute (USA)

INEL - Idaho National Engineering Laboratory (USA)

ISMES - Instituto Sperimentale Modelli e Strutture (Italy)

LANL - Los Alamos National Laboratory (USA)

LBL - Lawrence Berkeley Laboratory (USA)

LLNL - Lawrence Livermore National Laboratory (USA)

UNG - Unita Nazional Geotermica (Italy)

USGS - U.S. Geological Survey